Comparison of Experimental Results and Analytical Solutions for the Deflections of Anisotropic Plates

by

Randolph John Notestine

S. B. Massachusetts Institute of Technology
(1989)

Submitted in Partial Fulfillment of the
Requirements for the Degree of

MASTER OF SCIENCE

in

AERONAUTICS AND ASTRONAUTICS

at the

MASSACHUSETTS INSTITUTE OF TECHNOLOGY

June 1991

© Massachusets Institute of Technology, 1991. All rights reserved.

Signature of Author ____________________
Department of Aeronautics and Astronautics
May 17, 1991

Certified by ____________________
Prof. Michael J. Graves
Thesis Supervisor

Accepted by ____________________
Prof. Harold Y. Wachman
Chairman, Department Graduate Committee

MASSACHUSETTS INSTITUTE
OF TECHNOLOGY

JUN 1991

Comparison of Experimental Results and Analytical Solutions for the Deflections of Anisotropic Plates

by

Randolph John Notestine

Submitted to the Department of Aeronautics and Astronautics on May 17, 1991 in partial fulfillment of the requirements for the Degree of Master of Science in Aeronautics and Astronautics.

Abstract

Graphite/epoxy plates with a variety of elastic couplings were tested under three static, transverse loadings and a dynamic transverse vibration to determine their behavior relative to different symmetric combinations of clamped, simply supported, and free boundary conditions. Both tape and fabric material systems were used to create specimens with weak bending-twisting coupling, strong bending-twisting coupling, bending-shearing coupling, and no in-plane or out-of-plane couplings. Aluminum plates were also tested as controls. The three static loadings investigated were uniform pressure, a uniform rectangular pressure patch, and a point load.

Analyses used Mindlin shear deformation plate theory with selected comparisons to Kirchhoff plate theory. Rayleigh-Ritz, Navier, and constrained Navier solutions for most of the static experimental cases were performed. In addition, single mode static solutions for a displacement based potential function solution are presented. Natural mode shapes and frequencies were predicted from the Rayleigh-Ritz solution.

The experimental and analytical results for both static and dynamic loadings exhibit good agreement, except for experimental errors in the clamped boundary condition. It is concluded that the Rayleigh-Ritz solution properly accounts for bending-twisting coupling and that bending-shearing coupling has no observable affect on the experimental stiffnesses for the cases tested where in-plane sliding is allowed.

The single mode potential function results are overly stiff compared to the Rayleigh-Ritz solutions for the majority of the cases investigated. For the plates without bending-twisting coupling, under uniform pressure with four sides simply supported, however, a sixteen term polynomial potential function is 2-4% less stiff than the 81 term Rayleigh-Ritz and Navier solutions used. This example illustrates the solution efficiency that may be obtained through displacement based potential function solutions.

Extensive experimental and analytical results are presented for both the static and dynamic cases investigated.

Thesis Supervisor: Michael J. Graves

Title: Boeing Assistant Professor of
Aeronautics and Astronautics
Department of Aeronautics and Astronautics
Massachusetts Institute of Technology

Acknowledgements

Special thanks to those who everyday go beyond the call of duty and do it with a smile on their face. Thank you, Al Supple, Ping Lee, Deborah Zero, Anne Maynard, Phyllis Collymore, Lisa Sasser, Liz Zotos, Don Weiner, Earl Wassmouth, Dick Perdichizzi, Larry Baltimore, and Eileen Dorschner. All of you helped round out my education and made the experience that much more enjoyable. Al Supple and Ping Lee deserve special thanks for the incredible job they do for TELAC. They may not run the lab, but they keep the lab running!

I'd like to thank all the structures Professors in the Aero Department for their dedication to teaching as well as research. Thank you, Prof. Dugundji, for teaching my the meaning of the words "thorough" and "patience". I hope a little of both have rubbed off on me. Thank you, Prof. Lagace, for sparking my interest in composites and being supportive of my decisions over the years. Thank you, Prof. Michael Graves, for your sincere and unwavering interest in both my research and my personal life. Best of luck with your career.

Thank you, Joe and Kevin, for being there since the very beginning and sharing the joys of Unified. Thanks, Kevin, for teaching me just a little bit of 18.03 and thanks Joe for tolerating the piezzo's.

I am indebted to Kortney Leabourne for all the hard work she put into this thesis. She deserves credit for numerous machining jobs (including the infamous URPP), most of the "stellar" figures in Chapter 3, several impressive electronic feats (±15 V), and for tolerating my "assistance". Oh, and "all sorts of" thanks for "letting" me be "first author".

I'd like to thank all of the graduate students that I had the pleasure of working with at TELAC. Thank you, Pierre, Kevin, and Chris for your support during my formative years. Kiernan, Ken, Adam, and Tom, thank you for your friendship and proving that it could be done. Thank you, Peter, Kim, Wilson, Narendra, Claudia, Teresa, James, Ed, Wai Tuck, Mac, Mary, and Hiroto, for your assistance, and just as importantly your friendship.

Thank you, Wilson, for sharing your Rayleigh-Ritz program and helping me wade through my modifications. Teresa and Mary, thank you for all the help with the job hunt and thanks, Teresa, for sharing the wonderful thesis writing experience.

Thank you, John and Ed, for being such great roommates and tolerating my ups and downs these final months of thesis writing. John, thanks for the understanding ear on all the long runs and for feeding the Mac while I was off looking for a job.

Narendra, whatever did you do, to deserve my acquaintance? Someday, we will work together again. I'll bring the chalkboard. Thank you for being such a good friend. You're not out of the woods yet.

Thank you, Anna Christine, for being who you are and loving me for who I am. Your support means everything to me.

I'd like to thank my parents for the many sacrifices they made to send me to MIT. Someday, I hope to be as unselfish with my own children.

Foreword

This work was performed in the Technology Laboratory for Advanced Composites (TELAC) of the Department of Aeronautics and Astronautics at the Massachusetts Institute of Technology.

Table of Contents

Table of Contents (con't)

Table of Contents (con't)

Table of Contents (con't)

List of Figures

List of Figures (con't)

List of Figures (con't)

List of Figures (con't)

List of Figures (con't)

List of Figures (con't)

List of Figures (con't)

List of Figures (con't)

List of Figures (con't)

List of Figures (con't)

List of Figures (con't)

List of Figures (con't)

List of Figures (con't)

List of Tables

List of Tables (con't)

Nomenclature

A_1	Amplitude of potential function
A_{ij}	Plate extensional stiffness matrix
a	Plate dimension in x direction
B_{ij}	Plate coupling stiffness matrix
b	Plate dimension in y direction
C_{ij}	Transverse shear stiffnesses
D_{ij}	Plate bending stiffness matrix
f_x, f_y, f_z	Body forces in the x, y, and z directions
h	Plate thickness
l_{ij}	Constants which arise from the differential operators
L_{ij}	Differential operators
m_x, m_y	Surface tractions in the x and y directions
M_x, M_y, M_{xy}	Moment resultants
N_x, N_y, N_{xy}	Stress resultants
p_x, p_y	Body force resultants
p_z	Distributed transverse loading
Q_{ij}	Reduced in-plane stiffnesses
Q_x, Q_y	Transverse shear stress resultants
R_0, R_1, R_2	Integrated inertia terms
u	Plate displacement in x direction
u^o	Midplane displacement in x direction
v	Plate displacement in y direction
v^o	Midplane displacement in y direction
w	Midplane displacement in z direction
x, y, z	Plate coordinates

γ	Engineering shear strain
ε	Extensional strain
κ	Shear correction factor
ρ	density
σ	Extensional stress
τ	Shear stress
Φ	Potential function
Ψ_x	Shear rotation of the undeformed normal w.r.t the y-z plane
Ψ_y	Shear rotation of the undeformed normal w.r.t the z-x plane

Chapter 1
Introduction

Composite materials pose rewarding challenges to the structural engineer familiar with isotropic materials. Strength becomes a function of direction in the material, failure occurs in many diverse and sometimes unrelated modes, and bending behavior can be materially coupled with in-plane behavior. Although still the exception rather the the norm, composites are finding their way into an ever increasing number of applications, from high tech sports equipment to primary aircraft structure, where their high strength to weight ratio makes them attractive alternatives to their isotropic predecessors. As the use of composites increases, more and more engineers will discard their anisophobia and open their minds to the wonders of an anisotropic world.

A single ply, or layer, of composite material is orthotropic. By rotating individual plies through different angles and laminating them together, however, complicated material couplings can be created. These material couplings, which arise due to the laminate's anisotropic nature, can significantly affect the laminate's mechanical properties. Engineers should carefully include the effects of these couplings when necessary, in order to fully utilize composites, rather than avoiding all couplings due to a lack of understanding.

This work investigates the effects of bending-twisting and bending-shearing coupling in laminates subjected to three static, transverse loadings and a dynamic transverse vibration. The experimental results are compared with analytical solutions to determine the quality of the modeling and the effect of the couplings for the loadings and boundary conditions considered.

Additionally, a new displacement based potential function solution is presented.

Chapter two provides a general background from the literature on the subject of anisotropic plate bending. Both Kirchhoff and Mindlin plate theories are considered, and typical solution techniques are discussed. The experimental procedures for specimen manufacture and testing are detailed in chapter three. Chapter four describes the analyses used, and explains the displacement based potential function solution.

The extensive experimental results are presented in chapter five, followed by the analytical results in chapter six. Comparisons of the experimental and analytical results are then made in chapter seven. Finally, chapter eight provides a concise summary of the conclusions of this investigation and suggestions for future work.

Chapter 2

Summary of Previous Work

This chapter briefly summarizes previous composite plate analysis techniques. The solution of a plate problem consists of an underlying theory, or model of the plate, and a solution technique, or mathematical procedure, for approximating the response of a plate to a given loading, for a particular set of boundary conditions. In general, a solution technique may be applied to several different theories, and a theory may be solved using any of several solution techniques. The relation is not always this clear cut, however, as some theories lend themselves more readily to some solution techniques than others.

2.1 Plate Theories

Thousands of papers have been written on the topics of plate theories and solutions to plate theories; even hundreds of papers have been written concerning laminated orthotropic and anisotropic plates. Many of these plate theories and solution techniques are highly specialized and are applicable or useful for only a small class of problems. Only those theories which are general enough to be applied to a broad class of engineering problems are discussed here.

2.1.1 Kirchhoff Plate Theory

The "classical" plate theory or Kirchhoff plate theory [1] uses three midplane displacement variables. The in-plane displacements, u^o and v^o, are the midplane displacements in the x and y directions respectively. The out-of-plane displacement, w, is the displacement in the z direction, or the displacement normal to the plane of the plate. The displacement field is as follows:

$$u = u^o(x,y,t) - z\frac{\partial w}{\partial x}; \qquad v = v^o(x,y,t) - z\frac{\partial w}{\partial y}; \qquad w = w(x,y,t)$$

Kirchhoff plate theory assumes that as a plate deforms an imaginary plane originally normal to the midplane will remain planer and normal to the midplane throughout the deformation, see Figure 2.1. This implies that the transverse shear strains will be approximately zero. The negligible transverse shear strain assumption is acceptable for "thin" plates with "moderate" transverse shear stiffness, but becomes less accurate with increasing plate thickness or decreasing transverse shear stiffness. A plate is classified as "thin" if the shorter edge length to thickness ratio is greater than one hundred. Generally, transverse shear stiffness is considered "moderate" if the ratio of in-plane stiffness to transverse shear stiffness is around 2.5.

Kirchhoff plate theory is an integrated plate theory. Quantities are integrated through the thickness, which simplifies the model, but usually results in pointwise breaches of equilibrium. The integrated loadings, or resultants, are defined as:

$$N_x = \int_{-\frac{h}{2}}^{\frac{h}{2}} \sigma_x \, dz; \qquad N_y = \int_{-\frac{h}{2}}^{\frac{h}{2}} \sigma_y \, dz; \qquad N_{xy} = \int_{-\frac{h}{2}}^{\frac{h}{2}} \tau_{xy} \, dz$$

$$M_x = \int_{-\frac{h}{2}}^{\frac{h}{2}} \sigma_x \, z \, dz; \qquad M_y = \int_{-\frac{h}{2}}^{\frac{h}{2}} \sigma_y \, z \, dz; \qquad M_{xy} = \int_{-\frac{h}{2}}^{\frac{h}{2}} \tau_{xy} \, z \, dz$$

$$Q_x = \int_{-\frac{h}{2}}^{\frac{h}{2}} \tau_{xz} \, dz; \qquad Q_y = \int_{-\frac{h}{2}}^{\frac{h}{2}} \tau_{yz} \, dz$$

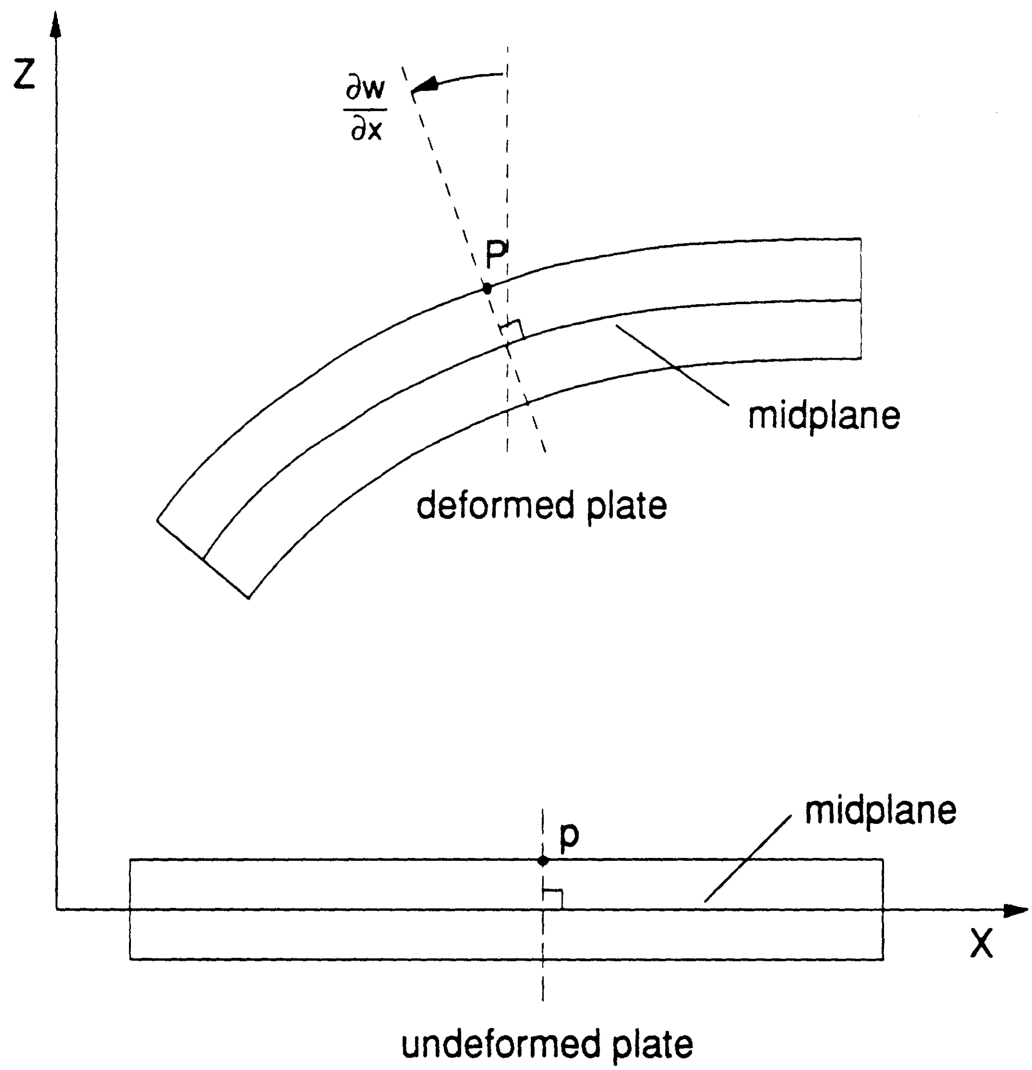

Figure 2.1 Kirchhoff plate theory deformation. Plane sections remain plane and normal to the midplane throughout deformation.

$$p_x = \int_{-\frac{h}{2}}^{\frac{h}{2}} f_x \, dz \; ; \qquad p_y = \int_{-\frac{h}{2}}^{\frac{h}{2}} f_y \, dz \; ; \qquad p_z = \int_{-\frac{h}{2}}^{\frac{h}{2}} f_z \, dz + \bar{p}_z$$

where the N_i's are stress resultants, the M_i's are moment resultants, the Q_i's are transverse shear stress resultants, and p_x and p_y are body force resultants arising from the body forces, f_x and f_y. The distributed transverse load, p_z, is the sum of the applied transverse load, $\bar{p}_z$, and the integrated loading due to a body force, f_z. Additionally, the plate may rest on a frictionless, uniform elastic foundation with stiffness K. The Kirchhoff plate model is depicted in Figure 2.2.

The integrated stiffnesses are defined as:

$$A_{ij} = \int_{-\frac{h}{2}}^{\frac{h}{2}} Q_{ij} \, dz \; ; \qquad B_{ij} = \int_{-\frac{h}{2}}^{\frac{h}{2}} Q_{ij} \, z \, dz \; ; \qquad D_{ij} = \int_{-\frac{h}{2}}^{\frac{h}{2}} Q_{ij} \, z^2 \, dz \; ; \qquad (i,j = 1,2,6)$$

where the Q_{ij}'s are the ply, reduced in-plane stiffnesses [2]. The integrated inertia terms are defined as follows:

$$R_0 = \int_{-\frac{h}{2}}^{\frac{h}{2}} \rho \, dz \; ; \qquad R_1 = \int_{-\frac{h}{2}}^{\frac{h}{2}} \rho \, z \, dz \; ; \qquad R_2 = \int_{-\frac{h}{2}}^{\frac{h}{2}} \rho \, z^2 \, dz$$

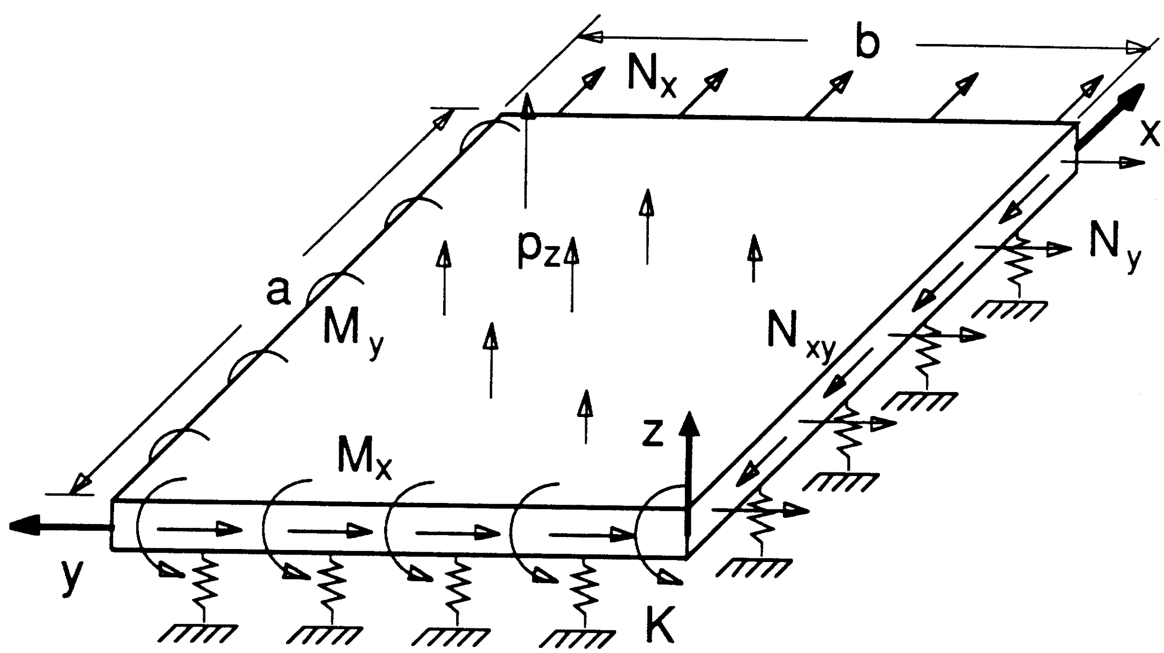

Figure 2.2 Kirchhoff plate model with applied loadings.

The constitutive equations follow as:

$$\begin{bmatrix} N_x \\ N_y \\ N_{xy} \\ M_x \\ M_y \\ M_{xy} \end{bmatrix} = \begin{bmatrix} A_{11} & A_{12} & A_{16} & B_{11} & B_{12} & B_{16} \\ A_{12} & A_{22} & A_{26} & B_{12} & B_{22} & B_{26} \\ A_{16} & A_{26} & A_{66} & B_{16} & B_{26} & B_{66} \\ B_{11} & B_{12} & B_{16} & D_{11} & D_{12} & D_{16} \\ B_{12} & B_{22} & B_{26} & D_{12} & D_{22} & D_{26} \\ B_{16} & B_{26} & B_{66} & D_{16} & D_{26} & D_{66} \end{bmatrix} \begin{bmatrix} \varepsilon_x^o \\ \varepsilon_y^o \\ \gamma_{xy}^o \\ \kappa_x \\ \kappa_y \\ \kappa_{xy} \end{bmatrix}$$

The strain-displacement relations, in accordance with the displacement field, are:

$$\varepsilon_x^o = u^o_{,x}\,; \qquad \varepsilon_y^o = v^o_{,y}\,; \qquad \gamma_{xy}^o = u^o_{,y} + v^o_{,x}$$

$$\kappa_x = -w_{,xx}\,; \qquad \kappa_y = -w_{,yy}\,; \qquad \kappa_{xy} = -2\,w_{,xy}$$

where the comma designates differentiation with respect to the variables that follow.

From the constitutive equations and the strain-displacement relations, we see that the B_{ij} terms, or coupling stiffnesses, couple the in-plane and out-of-plane displacements. Finally, the equations of motion are [3]:

$$\begin{bmatrix} L_{11} & L_{12} & L_{13} \\ L_{12} & L_{22} & L_{23} \\ L_{13} & L_{23} & L_{33} \end{bmatrix} \begin{bmatrix} u^o \\ v^o \\ w \end{bmatrix} = \begin{bmatrix} -p_x \\ -p_y \\ +p_z \end{bmatrix}$$

where the L_{ij}'s are differential operators defined as:

$$
\begin{aligned}
L_{11} &= A_{11}\,L_{xx} + 2\,A_{16}\,L_{xy} + A_{66}\,L_{yy} - R_0\,L_{tt} \\
L_{12} &= A_{16}\,L_{xx} + (A_{12} + A_{66})\,L_{xy} + A_{26}\,L_{yy} \\
L_{13} &= -B_{11}\,L_{xxx} - 3\,B_{16}\,L_{xxy} - (B_{12} + 2\,B_{66})\,L_{xyy} - B_{26}\,L_{yyy} + R_1\,L_{xtt} \\
L_{22} &= A_{66}\,L_{xx} + 2\,A_{26}\,L_{xy} + A_{22}\,L_{yy} - R_0\,L_{tt} \\
L_{23} &= -B_{16}\,L_{xxx} - (B_{12} + 2\,B_{66})\,L_{xxy} - 3\,B_{26}\,L_{xyy} - B_{22}\,L_{yyy} + R_1\,L_{ytt} \\
L_{33} &= D_{11}\,L_{xxxx} + 4\,D_{16}\,L_{xxxy} + 2\,(D_{12} + 2\,D_{66})\,L_{xxyy} + 4\,D_{26}\,L_{xyyy} + D_{22}\,L_{yyyy} \\
&\quad + K + R_0\,L_{tt} - R_2\,L_{xxtt} - R_2\,L_{yytt}
\end{aligned}
$$

where:

$$
L_{xx} = \frac{\partial^2}{\partial x^2}; \qquad L_{xxy} = \frac{\partial^3}{\partial x^2 \partial y}; \qquad L_{xxtt} = \frac{\partial^4}{\partial x^2 \partial t^2}
$$

and the other partial derivatives are defined similarly.

The equations of motion may be solved with sufficient initial and boundary conditions. For example, along an x edge any combination of the following boundary conditions may be prescribed:

$$
\begin{array}{rcl}
u^o & \text{or} & N_x \\
v^o & \text{or} & N_{xy} \\
w & \text{or} & Q_x + M_{xy,y} \\
w_{,x} & \text{or} & M_x
\end{array}
$$

These governing partial differential equations and boundary conditions summarize the Kirchhoff plate theory. For thin plates with moderate transverse shear stiffness these equations are a reasonable model, however, in other cases transverse shear deformation should be accounted for.

2.1.2 Mindlin Plate Theory

For thick plates or plates with a low transverse shear stiffness, rotations of the midplane normals must be included for accurate modeling. Shear deformation plate theory or Mindlin plate theory [4] uses five displacement variables. The midplane displacements are u^o and v^o as before, however, two out-of-plane shear rotations, Ψ_x and Ψ_y, are introduced. The out-of-plane displacement, w, remains defined as in Kirchhoff plate theory. The new displacement field is as follows:

$$u = u^o(x,y,t) + z\ \Psi_x(x,y,t)\ ; \qquad v = v^o(x,y,t) + z\ \Psi_y(x,y,t)\ ; \qquad w = w(x,y,t)$$

Mindlin plate theory assumes that as a plate deforms an imaginary plane originally normal to the midplane will remain planer, but will rotate from the midplane normal during deformation, see Figure 2.3. This allows non-zero transverse shear strains. Mindlin plate theory more accurately models thick plates or plates with low transverse shear stiffness.

Mindlin plate theory is also an integrated plate theory. The integrated loadings, body force resultants, and distributed transverse load are all defined as they were in Kirchhoff plate theory. Distributed surface tractions, m_x and m_y, may also be applied to the upper surface of the plate [5, 6]. Recall that the uniform elastic foundation is assumed frictionless, thus not causing surface tractions on the lower side of the plate. The Mindlin plate model is depicted in Figure 2.4.

The integrated in-plane stiffnesses are defined as in Kirchhoff plate theory, however, additional transverse shear stiffnesses are needed. Traditionally, the transverse shear stiffnesses have been defined as [3]:

$$A_{ij} = \int_{-\frac{h}{2}}^{\frac{h}{2}} C_{ij}\, z\, dz\ ; \qquad (i,j = 4,5)$$

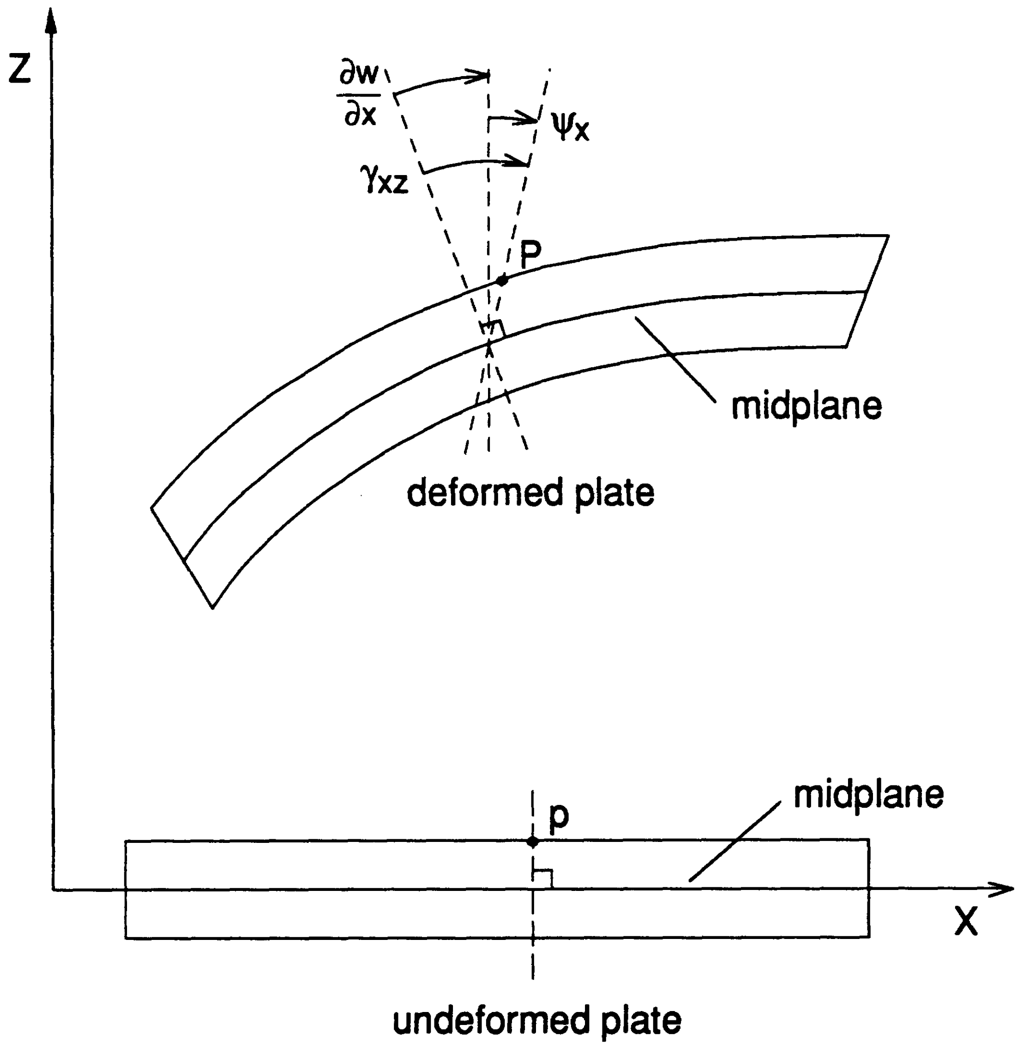

Figure 2.3 Mindlin plate theory deformation. Plane sections remain plane but rotate from the midplane normal throughout deformation.

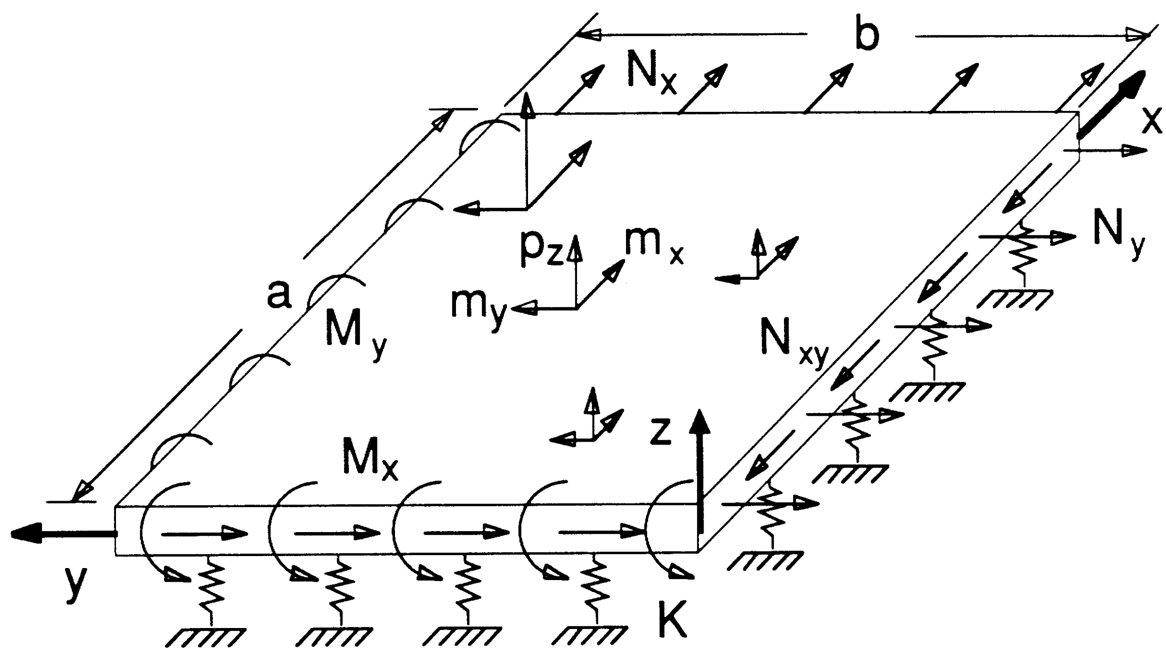

Figure 2.4   Mindlin plate model with applied loadings.

where the C_{ij}'s are the ply transverse shear stiffnesses [2]. Recently, several authors [7, 8] have proposed a different formulation of the transverse stiffnesses for laminated plates. The alternative formulation is based on 3-D elasticity and allows a weighted average, very similar to springs in series, of the individual transverse shear stiffnesses. The alternative transverse shear stiffnesses are defined as follows:

$$\begin{bmatrix} A_{44} & A_{45} \\ A_{45} & A_{55} \end{bmatrix} = h \begin{bmatrix} \overline{S}_{44} & \overline{S}_{45} \\ \overline{S}_{45} & \overline{S}_{55} \end{bmatrix}^{-1}$$

$$\overline{S}_{ij} = \frac{1}{h} \int_{\frac{-h}{2}}^{\frac{h}{2}} S_{ij}\, dz$$

where the S_{ij}'s are the ply compliances [2], and h is the plate thickness. For a plate laminated from layers of the same material the difference in transverse shear stiffness between the two methods is small. If, however, the plate is laminated from materials with significantly different ply transverse shear stiffnesses, the resulting laminate transverse stiffnesses will be very different.

Having defined all the plate stiffnesses, the constitutive equations may be expressed as follows [9]:

$$
\begin{bmatrix} N_x \\ N_y \\ N_{xy} \\ M_x \\ M_y \\ M_{xy} \end{bmatrix} = \begin{bmatrix} A_{11} & A_{12} & A_{16} & B_{11} & B_{12} & B_{16} \\ A_{12} & A_{22} & A_{26} & B_{12} & B_{22} & B_{26} \\ A_{16} & A_{26} & A_{66} & B_{16} & B_{26} & B_{66} \\ B_{11} & B_{12} & B_{16} & D_{11} & D_{12} & D_{16} \\ B_{12} & B_{22} & B_{26} & D_{12} & D_{22} & D_{26} \\ B_{16} & B_{26} & B_{66} & D_{16} & D_{26} & D_{66} \end{bmatrix} \begin{bmatrix} \varepsilon_x^o \\ \varepsilon_y^o \\ \gamma_y^o \\ \kappa_x \\ \kappa_y \\ \kappa_{xy} \end{bmatrix}
$$

$$
\begin{bmatrix} Q_y \\ Q_x \end{bmatrix} = \kappa \begin{bmatrix} A_{44} & A_{45} \\ A_{45} & A_{55} \end{bmatrix} \begin{bmatrix} \gamma_{yz} \\ \gamma_{xz} \end{bmatrix}
$$

The transverse shear stiffnesses have been multiplied by a shear correction factor, κ, following Mindlin [4] and others [3,5,9]. This is to account for the inaccuracies inherent in assuming the shear stress is constant through the thickness, while the boundary conditions guarantee the shear stress goes to zero at the plate surfaces. Care should be taken to differentiate between the shear correction factor which has no subscripts and the curvatures which have subscripts. The strain-displacement relations are found from the displacement field. The in-plane strains remain as defined for Kirchhoff plate theory, however, the curvatures and transverse shear strains are now defined as follows:

$$
\kappa_x = \Psi_{x,x} \, ; \qquad \kappa_y = \Psi_{y,y} \, ; \qquad \kappa_{xy} = \Psi_{x,y} + \Psi_{y,x}
$$

$$
\gamma_{yz} = w_{,y} + \Psi_y \, ; \qquad \gamma_{xz} = w_{,x} + \Psi_x
$$

Finally, the equations of motion are as follows [5]:

$$
\begin{bmatrix}
L_{11} & L_{12} & L_{13} & L_{14} & L_{15} \\
L_{12} & L_{22} & L_{23} & L_{24} & L_{25} \\
L_{13} & L_{23} & L_{33} & L_{34} & L_{35} \\
L_{14} & L_{24} & L_{34} & L_{44} & L_{45} \\
L_{15} & L_{25} & L_{35} & L_{45} & L_{55}
\end{bmatrix}
\begin{bmatrix}
u^o \\ v^o \\ w \\ \Psi_x \\ \Psi_y
\end{bmatrix}
=
\begin{bmatrix}
-p_x \\ -p_y \\ -p_z \\ +m_x \\ +m_y
\end{bmatrix}
$$

where the L_{ij}'s are differential operators defined as:

$$
\begin{aligned}
L_{11} &= A_{11}\, L_{xx} + 2\, A_{16}\, L_{xy} + A_{66}\, L_{yy} - R_0\, L_{tt} \\
L_{12} &= A_{16}\, L_{xx} + (A_{12} + A_{66})\, L_{xy} + A_{26}\, L_{yy} \\
L_{13} &= 0 \\
L_{14} &= B_{11}\, L_{xx} + 2\, B_{16}\, L_{xy} + B_{66}\, L_{yy} - R_1\, L_{tt} \\
L_{15} &= B_{16}\, L_{xx} + (B_{12} + B_{66})\, L_{xy} + B_{26}\, L_{yy} \\
L_{22} &= A_{66}\, L_{xx} + 2\, A_{26}\, L_{xy} + A_{22}\, L_{yy} - R_0\, L_{tt} \\
L_{23} &= 0 \\
L_{24} &= B_{16}\, L_{xx} + (B_{12} + B_{66})\, L_{xy} + B_{26}\, L_{yy} \\
L_{25} &= B_{66}\, L_{xx} + 2\, B_{26}\, L_{xy} + B_{22}\, L_{yy} - R_1\, L_{tt} \\
L_{33} &= \kappa\, A_{55}\, L_{xx} + 2\, \kappa\, A_{45}\, L_{xy} + \kappa\, A_{44}\, L_{yy} - K - R_0\, L_{tt} \\
L_{34} &= \kappa\, A_{55}\, L_x + \kappa\, A_{45}\, L_y \\
L_{35} &= \kappa\, A_{45}\, L_x + \kappa\, A_{44}\, L_y \\
L_{44} &= \kappa\, A_{55} - D_{11}\, L_{xx} - 2\, D_{16}\, L_{xy} - D_{66}\, L_{yy} + R_2\, L_{tt} \\
L_{45} &= \kappa\, A_{45} - D_{16}\, L_{xx} - (D_{12} + D_{66})\, L_{xy} - D_{26}\, L_{yy} \\
L_{55} &= \kappa\, A_{44} - D_{66}\, L_{xx} - 2\, D_{26}\, L_{xy} - D_{22}\, L_{yy} + R_2\, L_{tt}
\end{aligned}
$$

Again the equations of motion may be solved with sufficient initial and boundary conditions. Instead of four boundary conditions per edge, however, there are now five. For example, along an x edge any combination of the following boundary conditions may be prescribed:

$$
\begin{array}{ccc}
u^o & \text{or} & N_x \\
v^o & \text{or} & N_{xy} \\
w & \text{or} & Q_x \\
\Psi_x & \text{or} & M_x \\
\Psi_y & \text{or} & M_{xy}
\end{array}
$$

These governing partial differential equations and boundary conditions summarize the Mindlin plate theory. The Mindlin plate theory is useful in characterizing thick plates or plates with low transverse shear stiffness.

J. N. Reddy [10] has formulated a higher order shear deformation theory based on the same five displacement variables as Mindlin plate theory, but with a higher order displacement field for u and v. This theory is aesthetically pleasing because it allows the transverse shear stress distribution to be parabolic through the thickness, however, it effectively doubles the complexity of the plate bending problem. While Reddy's theory represents an improvement over Mindlin plate theory, this improvement is most significant for plates with a length to thickness ratio less than ten. For plates with a length to thickness ratio greater than ten, i.e. most engineering problems, the improvement is negligible and for that reason Reddy's theory will not be discussed further here.

2.1.3 Symmetric Operator Reduction Method

V. Z. Vlasov observed that a series of partial differential equations describing the equilibrium of elastic solids will always have a symmetric matrix of differential operators. The symmetry is in accordance with Betti's reciprocal theorem and is insured as long as any elimination of higher order terms is done consistently [11].

Simply put, Betti's reciprocal theorem states that the flexibility influence coefficients for a linearly elastic solid will be symmetric [12]. If a unit generalized force at point 1 causes a generalized displacement at point 2 of w_0, then a unit generalized force at point 2 will cause a generalized displacement at point 1, also of w_0. The symmetry of the flexibility influence coefficients is directly related to the symmetry of the differential operator matrix.

For a symmetric operator matrix with constant coefficients, Vlasov found that the system of partial differential equations may be reduced to a single partial differential equation in terms of a potential function, whose order of differentiation is identical to that of the original system. Vlasov derived the eighth order partial differential equation governing the deflection of isotropic shells neglecting transverse shear deformation.

Vlasov's work with isotropic shells was later extended to orthotropic shells by S. A. Ambartsumyan [13]. While the expressions become more cumbersome with the added material complexity, the reduction method remains unchanged. Again Ambartsumyan's reduction used a Kirchhoff type shell theory, neglecting transverse shear. While much of Ambartsumyan's work dealt with anisotropic shells, he never applied the reduction method to the fully anisotropic case. This was done by Graves [14] in his Ph.D. thesis.

The symmetric operator reduction method is neither a plate theory nor a solution technique. Given a set of partial differential equations resulting from any plate theory that obeys Betti's reciprocal theorem, the reduction method allows the system of equations to be recast as a single equation in terms of a potential function. It is hoped that such recasting will promote unique and useful solutions.

2.2 Solution Techniques

Once the equilibrium equations have been found for a particular plate theory, it remains to find a solution for specific boundary conditions and initial conditions. Applicability of solution techniques seems to be more dependent upon the particular boundary conditions of a problem than on the underlying plate theory used to formulate the problem.

2.2.1 Navier Solutions

Navier solutions expand the displacement functions as double Fourier sine and/or cosine series which are selected to explicitly satisfy all the boundary conditions. The solution utilizes the orthogonality of Fourier series by finding the Fourier expansion of the applied loading and then solving for the unknown coefficients through harmonic balance. Completeness of the solution is assured due to the completeness of the Fourier series themselves. Navier solutions are very numerically efficient but are applicable to a limited number of problems.

Navier solutions are possible for plates with all four sides simply supported, but are restricted to plates with no bending-stretching and no bending-twisting coupling. Without bending-stretching coupling the in-plane and out-of-plane problems are uncoupled. For a Kirchhoff plate bending problem this leaves one partial differential equation to be solved subject to two boundary conditions per edge; for a Mindlin plate bending problem this leaves a system of three partial differential equations to be solved subject to three boundary conditions per edge.

For a rectangular Kirchhoff plate of dimensions a by b, simply supported at $x = 0, a$ and $y = 0, b$, the Navier solution assumes the transverse deflection, w, as an infinite double sine series, which satisfies all the boundary conditions explicitly:

$$w(0,y) = w(a,y) = w(x,0) = w(x,b) = 0$$
$$M_x(0,y) = M_x(a,y) = M_y(x,0) = M_y(x,b) = 0$$

When the distributed transverse loading, p_z, is also expanded in an infinite double sine series, the solution may be found directly through harmonic balance [15]. For a plate without bending-stretching and bending-twisting couplings:

$$w(x,y) = \sum_{m=1}^{\infty} \sum_{n=1}^{\infty} a_{mn} \sin\frac{m\pi x}{a} \sin\frac{n\pi y}{b}$$

where:

$$a_{mn} = \frac{p_{mn}}{D_{11}\left(\frac{m\pi}{a}\right)^4 + 2\left(D_{12} + 2\,D_{66}\right)\left(\frac{m\pi}{a}\right)^2\left(\frac{n\pi}{b}\right)^2 + D_{22}\left(\frac{n\pi}{b}\right)^4}$$

$$p_{mn} = \frac{4}{a\,b}\int_0^a \int_0^b p_z \sin\frac{m\pi x}{a} \sin\frac{n\pi y}{b}\, dx\, dy$$

The natural frequencies of vibration may be found by assuming a displacement that is periodic in time:

$$w(x,y,t) = w(x,y)\, e^{i\omega t}$$

Substitution into the governing differential equation then yields the squares of the natural frequencies as follows:

$$\omega_{mn}^2 = \frac{D_{11}\left(\frac{m\pi}{a}\right)^4 + 2\left(D_{12} + 2\,D_{66}\right)\left(\frac{m\pi}{a}\right)^2\left(\frac{n\pi}{b}\right)^2 + D_{22}\left(\frac{n\pi}{b}\right)^4}{R_0}$$

Navier plate bending solutions that include bending-twisting coupling are not possible because these terms multiply odd order differential operators which introduce cosine terms that do not satisfy the homogeneous displacement and moment boundary conditions.

For a rectangular Mindlin plate of dimensions a by b, simply supported at $x = 0, a$ and $y = 0, b$, the Navier solution assumes the following three infinite trigonometric series [5]:

$$w(x,y) = \sum_{m=1}^{\infty} \sum_{n=1}^{\infty} a_{mn} \sin\frac{m\pi x}{a} \sin\frac{n\pi y}{b}$$

$$\Psi_x(x,y) = \sum_{m=1}^{\infty} \sum_{n=1}^{\infty} b_{mn} \cos\frac{m\pi x}{a} \sin\frac{n\pi y}{b}$$

$$\Psi_y(x,y) = \sum_{m=1}^{\infty} \sum_{n=1}^{\infty} c_{mn} \sin\frac{m\pi x}{a} \cos\frac{n\pi y}{b}$$

which satisfy all the boundary conditions:

$$w(0,y) = w(a,y) = w(x,0) = w(x,b) = 0$$

$$M_x(0,y) = M_x(a,y) = M_y(x,0) = M_y(x,b) = 0$$

$$\Psi_y(0,y) = \Psi_y(a,y) = \Psi_x(x,0) = \Psi_x(x,b) = 0$$

When the distributed transverse loading, p_z, is again expanded in an infinite double sine series, the solution may be found through harmonic balance and matrix manipulations. For a plate without bending-stretching and bending-twisting couplings:

$$a_{mn} = \frac{p_{mn}\left(l_{45}^2 - l_{44}\, l_{55}\right)}{\Delta}$$

$$b_{mn} = \frac{p_{mn}\left(l_{34}\, l_{55} - l_{35}\, l_{45}\right)}{\Delta}$$

$$c_{mn} = \frac{p_{mn}\left(l_{35}\, l_{44} - l_{34}\, l_{45}\right)}{\Delta}$$

where the l_{ij}'s are constants, arising from the differential operators, defined as:

$$l_{33} = -\kappa A_{55}\left(\frac{m\pi}{a}\right)^2 - \kappa A_{44}\left(\frac{n\pi}{b}\right)^2$$

$$l_{34} = -\kappa A_{55}\left(\frac{m\pi}{a}\right)$$

$$l_{35} = -\kappa A_{44}\left(\frac{n\pi}{b}\right)$$

$$l_{44} = \kappa A_{55} + D_{11}\left(\frac{m\pi}{a}\right)^2 + D_{66}\left(\frac{n\pi}{b}\right)^2$$

$$l_{45} = \left(D_{12} + D_{66}\right)\left(\frac{m\pi}{a}\right)\left(\frac{n\pi}{b}\right)$$

$$l_{55} = \kappa A_{44} + D_{66}\left(\frac{m\pi}{a}\right)^2 + D_{22}\left(\frac{n\pi}{b}\right)^2$$

$$\Delta = \begin{vmatrix} l_{33} & l_{34} & l_{35} \\ l_{34} & l_{44} & l_{45} \\ l_{35} & l_{45} & l_{55} \end{vmatrix}$$

Again, natural frequencies of vibration may be found by assuming the displacement and rotations are periodic in time:

$$w(x,y,t) = w(x,y)\ e^{i\omega t}$$
$$\psi_x(x,y,t) = \psi_x(x,y)\ e^{i\omega t}$$
$$\psi_y(x,y,t) = \psi_y(x,y)\ e^{i\omega t}$$

Substitution into the governing differential equations yields the following eigenvalue problem:

$$\begin{bmatrix} I_{33} - \omega_{mn}^2 R_0 & I_{34} & I_{35} \\ I_{34} & I_{44} - \omega_{mn}^2 R_2 & I_{45} \\ I_{35} & I_{45} & I_{55} - \omega_{mn}^2 R_2 \end{bmatrix} \begin{Bmatrix} w_{mn} \\ \psi_{xmn} \\ \psi_{ymn} \end{Bmatrix} = \begin{Bmatrix} 0 \\ 0 \\ 0 \end{Bmatrix}$$

which must be solved for the natural frequencies of vibration.

If the rotary inertia term, R_2, is small compared to the displacement inertia term, R_0, the rotary inertia can be ignored with little loss of accuracy. This approximation greatly simplifies the problem of determining the natural frequencies of vibration. When the rotary inertia is set to zero, the natural frequencies may be found as follows:

$$\omega_{mn}^2 = \frac{I_{33}\left(I_{44}\, I_{55} - I_{45}^2\right) + 2\, I_{34}\, I_{35}\, I_{45} - I_{44}\, I_{35}^2 - I_{55}\, I_{34}^2}{R_0\left(I_{44}\, I_{55} - I_{45}^2\right)}$$

Again Navier solutions that include bending-twisting coupling are not possible because these terms multiply differential operators which introduce cosine terms that do not satisfy the homogeneous boundary conditions.

2.2.2 Constrained Lagrange Multiplier Solution

While the double sine series solves the four sides simply supported problem, there is no analogous trigonometric series to solve the four sides clamped problem. The general four sides clamped problem has traditionally been solved approximately using polynomials [1] or hyperbolic and trigonometric functions using the Rayleigh-Ritz technique [16].

Chen and Ramkumar [17, 18] recently solved the four sides clamped problem for a Mindlin plate with the trigonometric series used in the simply supported problem. Because these functions do not satisfy all the boundary conditions for the clamped problem, the Lagrange multiplier method was used to append the unsatisfied boundary conditions as constraints to the energy statement. This solution is only valid for Mindlin plates without bending-stretching and bending-twisting couplings, as was the Navier solution for four sides simply supported.

For a Mindlin plate with four sides clamped, the boundary conditions are:

$$w(0,y) = w(a,y) = w(x,0) = w(x,b) = 0$$
$$\Psi_x(0,y) = \Psi_x(a,y) = \Psi_y(x,0) = \Psi_y(x,b) = 0$$
$$\Psi_y(0,y) = \Psi_y(a,y) = \Psi_x(x,0) = \Psi_x(x,b) = 0$$

where the Navier trigonometric series do not satisfy the four conditions in the second line above. The Lagrange multipliers cause coupling between the harmonics, prohibiting symbolic solutions as have been given in the Navier cases.

2.2.3 Rayleigh-Ritz Method

Rayleigh-Ritz solutions minimize the energy of a system for a given set of trial functions. Because these trial functions need only satisfy the essential, or geometric, boundary conditions, and not the nonessential, or stress, boundary conditions, trial functions are relatively easy to find. In fact, with the Rayleigh-Ritz method all couplings can be accounted for. A Rayleigh-Ritz solution is only approximate, however, and the quality of the solution is dependent upon the insight used in selecting the trial functions.

Since virtually every text on solid mechanics discusses the Rayleigh-Ritz technique, it will not be described here in detail. Whitney [16] discusses the Rayleigh-Ritz method, and applies it to orthotropic plates with various boundary conditions. He uses products of the one dimensional beam functions to create two dimensional plate trial functions. Slightly different beam functions, with a simpler form, were proposed by Dugundji [19]. For a beam along the x axis with length a, the function is described by the general equation:

$$f_n(x) = \sqrt{2}\sin\left(\beta_n \frac{x}{a} + \theta\right) + A\, e^{-\beta_n\left(\frac{x}{a}\right)} + B_n\, e^{-\beta_n\left(1 - \frac{x}{a}\right)}$$

where the mode shape parameters are defined according to the boundary conditions and are given in Table 2.1.

Table 2.1 Dugundji Beam Mode Shape Parameters

B.C.'s	β_n	θ	A	B_n
SS–SS	$n\pi$	0	0	0
CL–FR	$(n-1/2)\pi$	$-\pi/4$	1	$(-1)^{n+1}$
CL–CL	$(n+1/2)\pi$	$-\pi/4$	1	$(-1)^{n+1}$
FR–FR	$(n+1/2)\pi$	$+3\pi/4$	1	$(-1)^{n+1}$
SS–CL	$(n+1/4)\pi$	0	0	$(-1)^{n+1}$
SS–FR	$(n+1/4)\pi$	0	0	$(-1)^{n}$

SS = simply supported; CL = clamped; FR = free

Such trial functions are suitable for the transverse deflection, w(x,y), however, care should be taken in selecting the trial functions for the shear rotations. Inappropriate choice of shear rotation trial functions can result in "shear locking" in thin plates, where the shear stiffness is greatly over estimated. As a plate becomes thin, the Mindlin theory must be able to approach the Kirchhoff theory, i.e. the transverse shear strains should approach zero. In order to avoid "shear locking", Minguet [20] suggests the following set of trial functions where $f_m(x)$ and $g_n(y)$ are the appropriate set of beam functions for the specified boundary conditions:

$$w(x,y) = \sum_{m=1}^{\infty} \sum_{n=1}^{\infty} a_{mn}\, f_m(x)\, g_n(y)$$

$$\Psi_x(x,y) = \sum_{m=1}^{\infty} \sum_{n=1}^{\infty} b_{mn}\, f_{m,x}(x)\, g_n(y)$$

$$\Psi_y(x,y) = \sum_{m=1}^{\infty} \sum_{n=1}^{\infty} c_{mn}\, f_m(x)\, g_{n,y}(y)$$

where once again the commas designate differentiation with respect to the variable that follows. This choice of functions allows the transverse shear strains to go to zero, if the problem so dictates, thus avoiding "shear locking" problems.

Chapter 3

Experimental Procedure

This chapter describes all of the manufacturing and testing procedures used in this investigation. A description of the jig is provided, followed by discussions of nomenclature, specimen selection, and specimen manufacture. The different experiments are discussed individually in terms of instrumentation and experimental procedure. The test matrix for the investigation is given.

3.1 Test Jig Description

A test jig was designed and manufactured for this investigation. The jig allows a variety of boundary conditions and loading scenarios. It may be mounted in the MTS machine or used independently.

The test jig is made of steel and is composed of ten main pieces: two rectangular frames which clamp the laminate, four rails which allow positioning, and four legs. These parts are held together by numerous bolts and nuts. The details of the jig dimensions are shown in Figure 3.1. The jig was designed to support a maximum tensile load of fifty thousand pounds.

Three types of boundary conditions are available: clamped, simply supported, and free. Both the clamped and simply supported conditions require screwing the appropriate pairs of steel bars to the edges of the jig frames. The bars, shown in Figure 3.2, were designed to enforce the appropriate boundary conditions as well as possible, while remaining interchangeable. The free boundary condition is created by the absence of a metal bar. The test plates must be trimmed to different sizes to accommodate the boundary conditions, however, all test sections are 254 mm x 204 mm regardless of the boundary conditions used. The extra plate length required

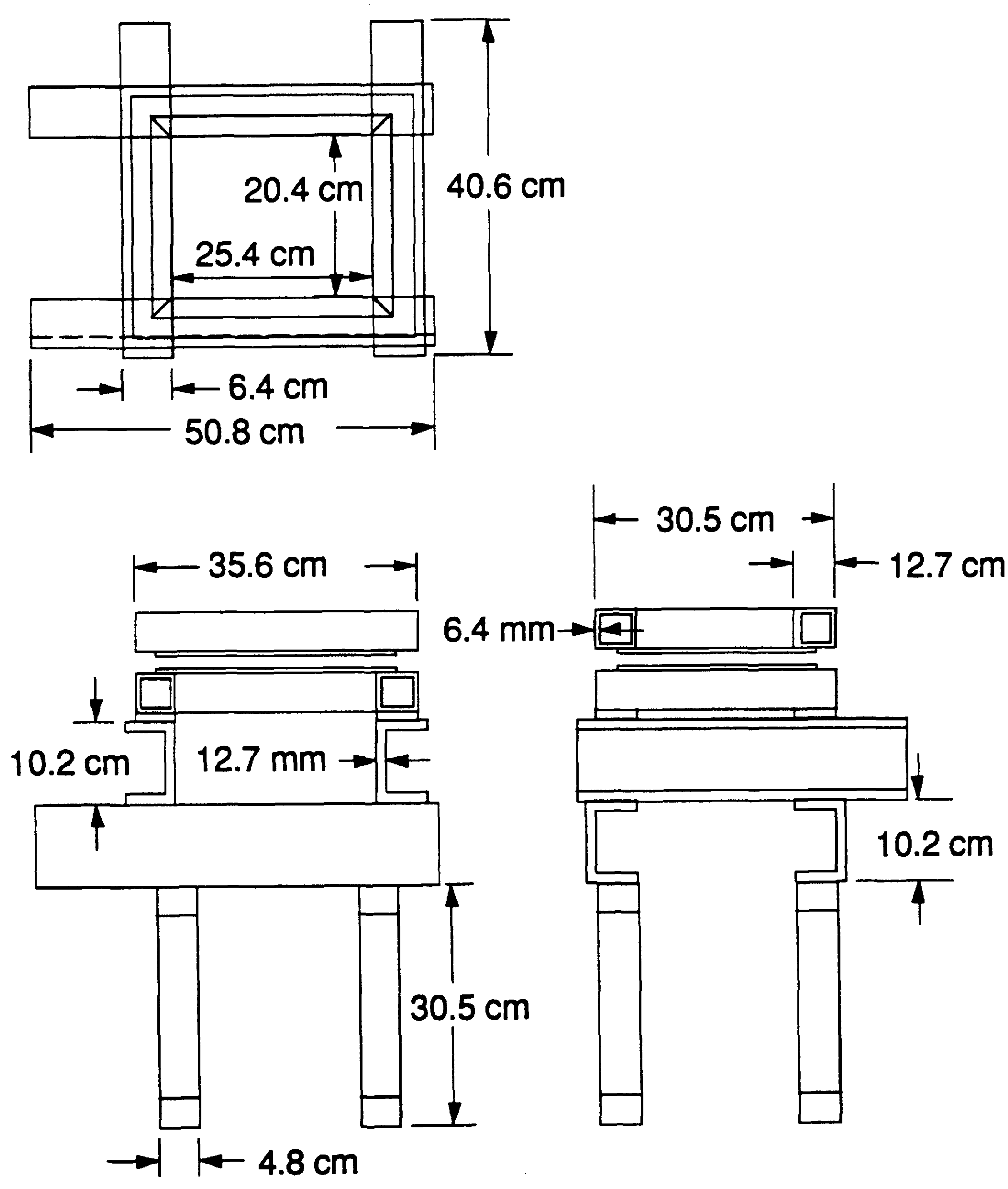

Figure 3.1 Plate jig schematic and dimensions.

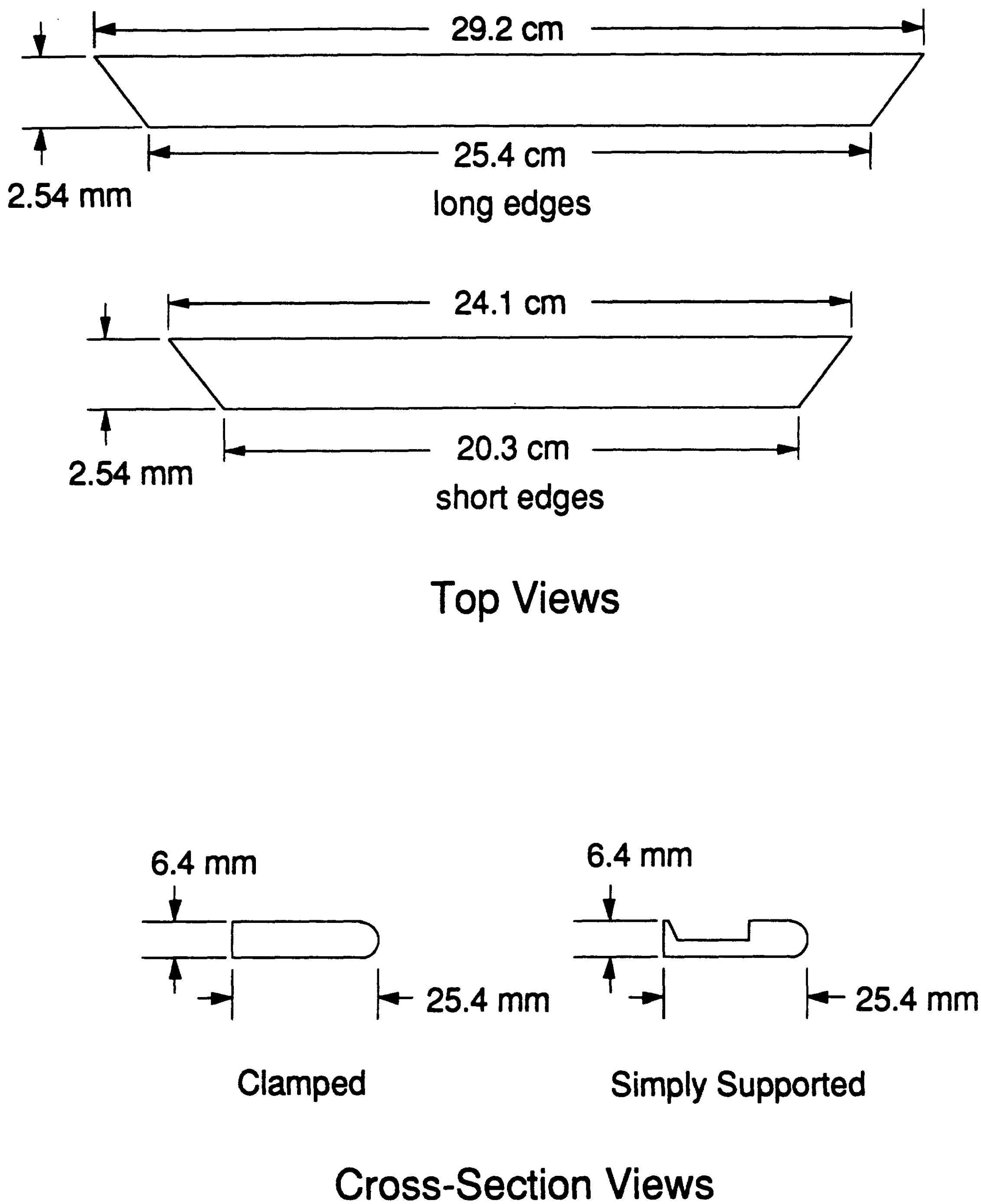

Figure 3.2 Boundary condition bars for plate jig.

per edge for each boundary condition is given in Table 3.1; a summary of plate dimensions used in this investigation is given in Figure 3.3. The jig allows all possible combinations of boundary conditions, except for all four sides free.

Table 3.1 Extra Plate Length per Edge Required for Boundary Conditions

Boundary Condition	Extra Length (mm)
Clamped	25
Simply Supported	6
Free	0

The test jig may be mounted in the MTS machine by screwing its four legs into the base table of the MTS, around the lower grip as shown in Figure 3.4. The two halves of the main jig frame lie upon two sets of rails which run parallel to the edges of the frame. A series of holes, in each set of rails, allows the structure to be bolted in several positions; allowing loading, through the MTS lower grip, to be applied at any one of several locations on the plate. The grid of available loading center locations is shown in Figure 3.5.

3.2 Nomenclature

Fibrous composite material systems are referenced by a fiber/matrix designation. Thus AS4/3501-6 specifies an AS4 (carbon) fiber in a 3501-6 (epoxy) matrix. In addition to varying material systems, fibrous composites also come in different forms: unidirectional tape and bidirectional fabric of different weaves. Laminates are designated by the angular orientation, in degrees, of each ply with respect to the longitudinal axis. Plies are listed from top to bottom and the angular orientation of each ply is measured counterclockwise from the longitudinal axis of the laminate. Each angle

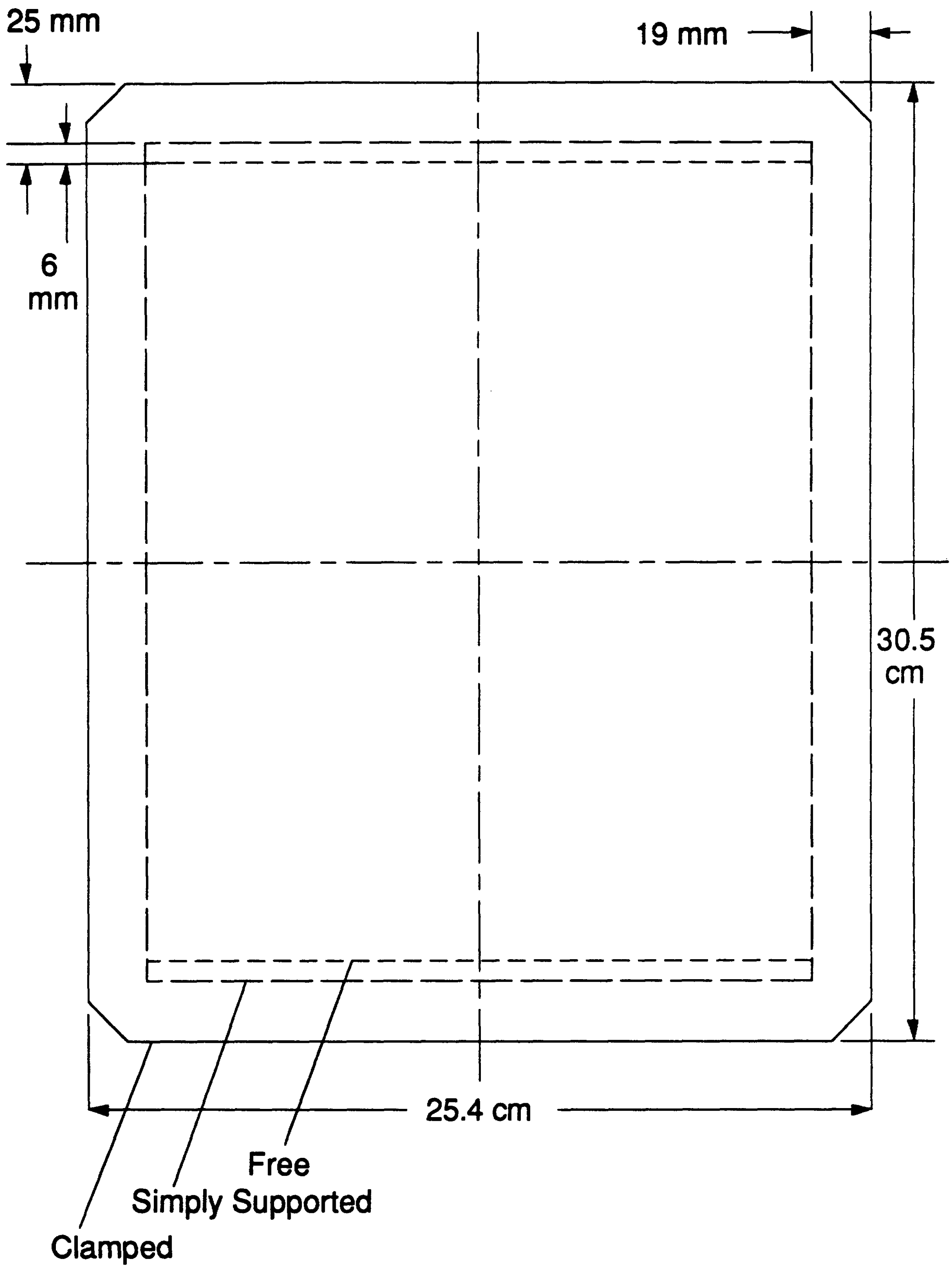

Figure 3.3 Specimen dimensions for different boundary conditions.

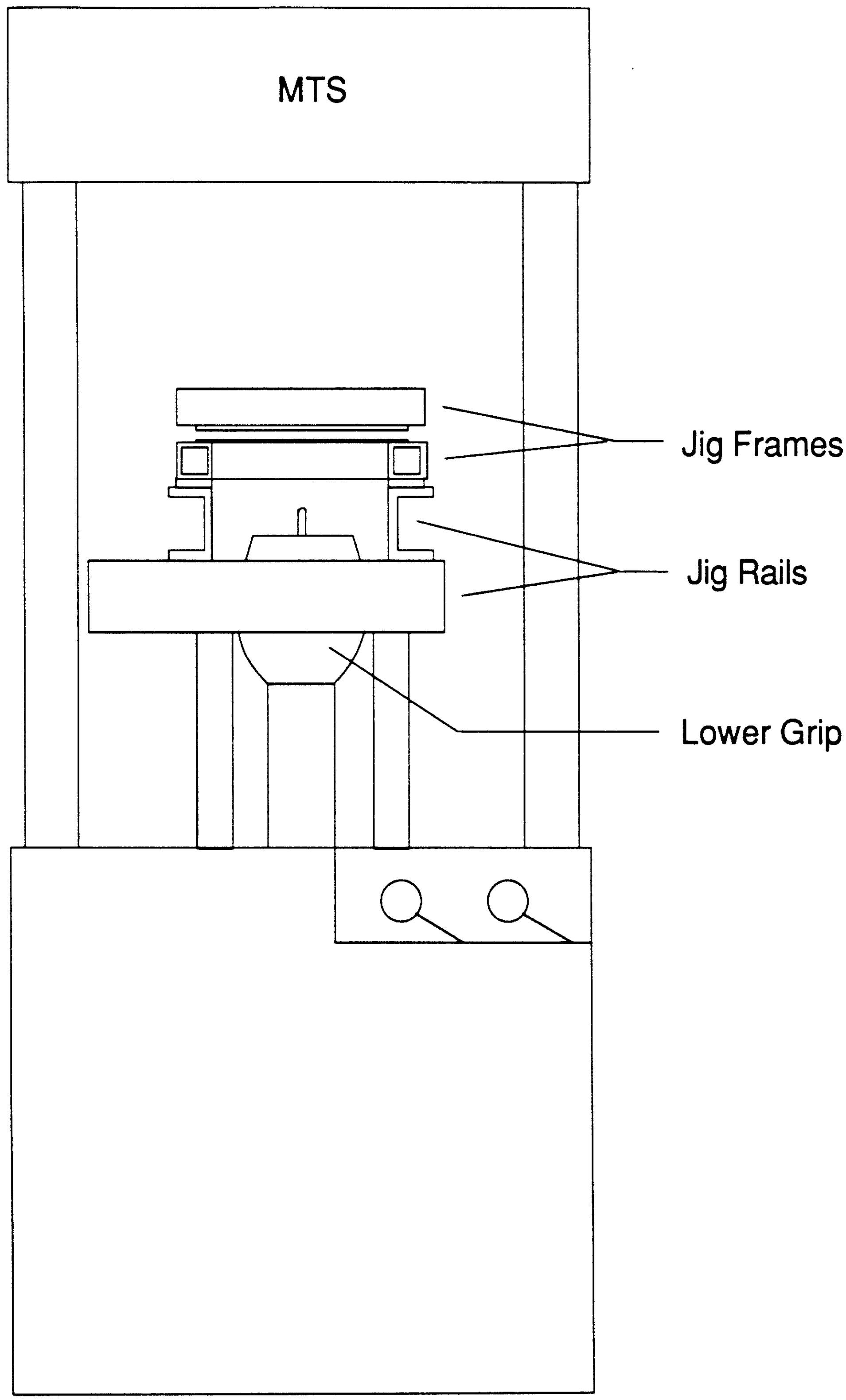

Figure 3.4 Test jig mounted in MTS machine.

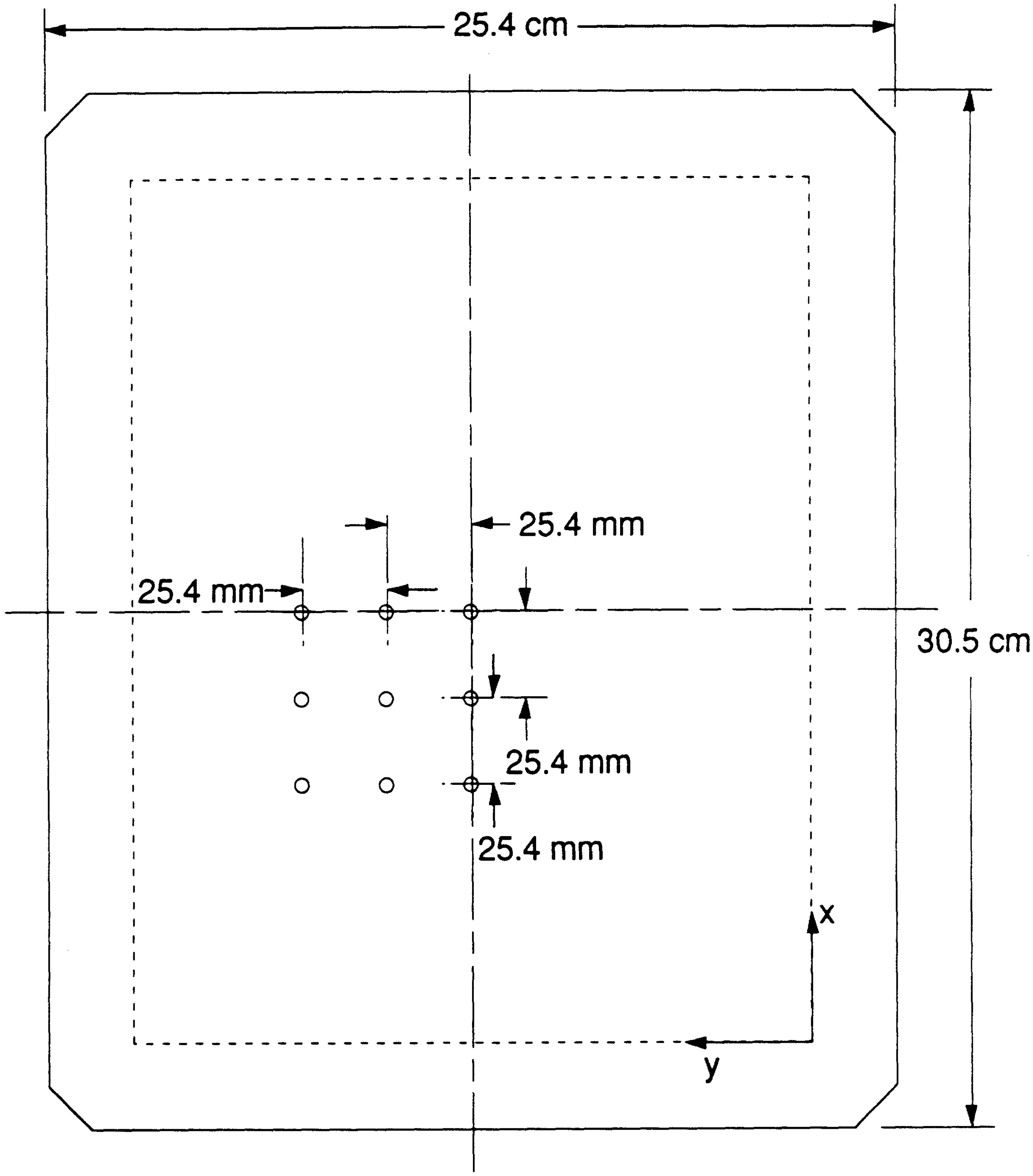

Figure 3.5 Grid of available loading center locations.

specifies one ply of tape, unless subscripted with an "f" to indicate one ply of fabric, and plies are separated by a "/" symbol. Thus [0/90] specifies two layers of tape, while [0_f/90_f] specifies two layers of fabric; in both cases the first ply is oriented at 0° to the longitudinal axis while the second ply is oriented at 90°. In fabric, 0° is defined as the warp direction as illustrated in Figure 3.6.

Additionally, subscripted numbers indicate multiple adjacent plies of the same orientation, a subscripted "S" indicates a layup is symmetric with respect to the laminate's midline, and a subscripted "A" indicates a layup is antisymmetric with respect to the laminate's midline. In both the symmetric and antisymmetric cases, only the upper half of the laminate is listed. An antisymmetric laminate has a minus theta ply in the lower half of the laminate corresponding to every theta ply in the upper half. For example, $[30/\text{-}60]_S$ is equivalent to [30/-60/-60/30] while $[30/\text{-}60]_A$ is equivalent to [30/-60/60/-30]. When a symmetric layup has an odd number of plies a "\" follows the middle ply orientation; $[0/90\backslash]_S$ indicates the three ply laminate, [0/90/0].

3.3 Specimen Selection

Four different specimen layups were selected for this investigation. Each layup was designed to exhibit different types of couplings between extension, bending, twisting, and shearing. The layups were designated A, B, C, and D for simplicity. Table 3.2 shows the laminate layups and the inherent couplings these layups exhibit.

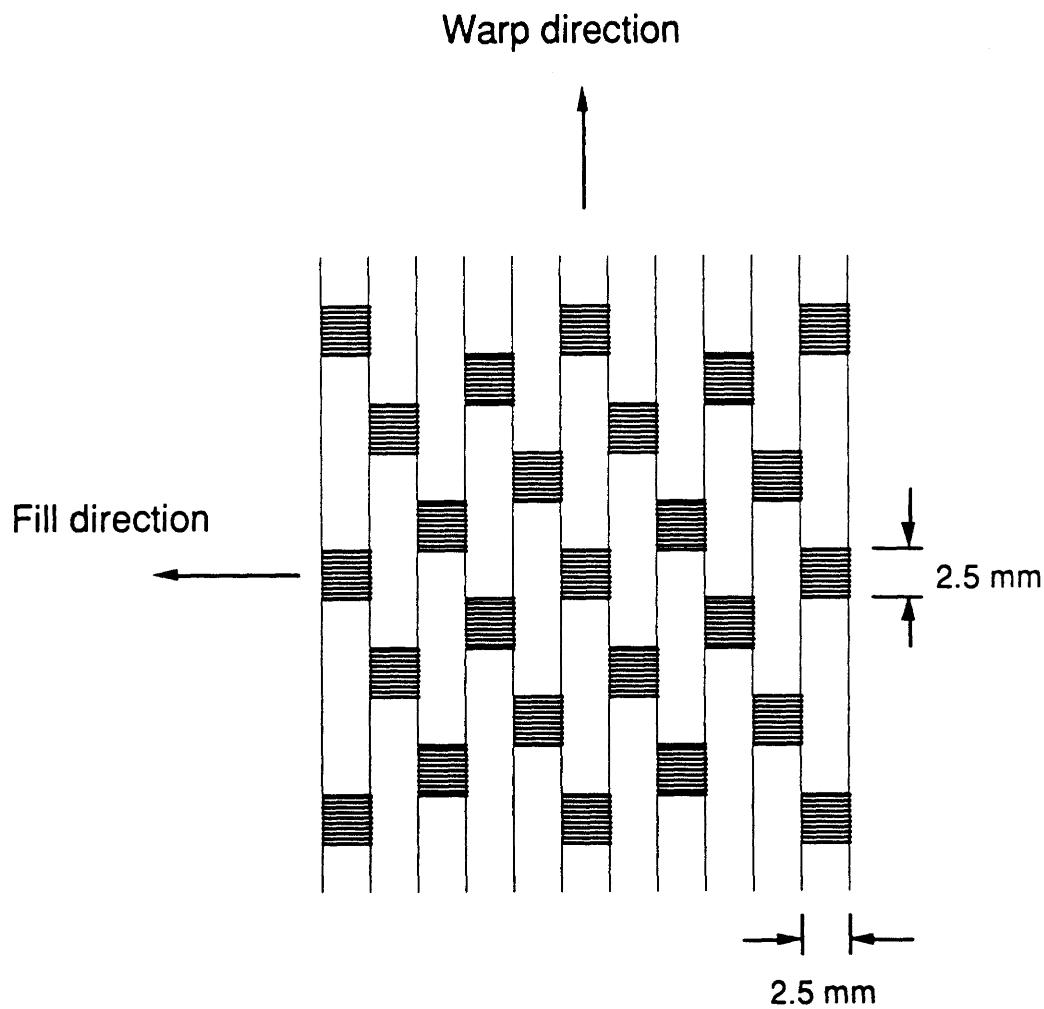

Figure 3.6 Warp direction in five harness weave fabric.

Table 3.2 Laminate Designations and Inherent Couplings

Designation	Layup	Couplings
A	$[45_4/0_3/45_4/(0_3)\backslash]_S$	strong bending-twisting
B	$[(0_2/\pm 45)_2/90_2/0]_S$	weak bending-twisting
C	$[(\pm 45_f)_2/(45_f/-45_f/45_f)\backslash]_S$	none
D	$[-15_3/75_6/-15_3]_A$	bending-shearing

No specimens were selected that exhibit bending-extension coupling due to the difficulty of manufacturing such specimens. Because such specimens are very susceptible to thermal warping due to their lack of symmetry, they must be manufactured through room temperature bonding of autoclaved sublaminates.

Three aluminum plates were used as controls throughout the experimental investigation. The aluminum plates had approximately the same bending stiffness as the composite specimens in the x direction. The aluminum plates were designated by an "I", for isotropic.

3.4 Composite Specimen Manufacture

Twelve composite plate specimens were manufactured for this investigation, three plates of each of the four layups. The C specimens were made of A370-5H/3501-6 Graphite/Epoxy fabric; 5H attached to the fiber designation indicates a five harness satin weave. The other three specimen types, A, B, & D, were made of AS4/3501-6 Graphite/Epoxy tape. Both prepregs were manufactured by Hercules Corporation and were stored at -18°C prior to use to retard the curing process.

The composite plate specimens were manufactured according to TELAC manufacturing specifications [21]. Vinyl gloves were worn whenever uncured graphite/epoxy was handled, and care was taken to avoid contaminating the prepreg. The prepreg was cut with sharp razor blades and templates to insure accurate angle reproduction. The plies were laid up on a layup table which has a raised aluminum right angle to insure accurate ply alignment. The laminate corner that was included by the two aluminum edges was designated the "good" corner. The laminates were stored in sealed vacuum bagging prior to curing.

An intricate setup procedure insured proper laminate consolidation and minimal cleanup effort. An aluminum cure plate was sprayed with mold release and then covered with a sheet of guaranteed nonporous teflon (GNPT). Aluminum "T" dams, also sprayed with mold release, were used to abut two sides of each laminate, while cork dams were placed along the other two edges. An individual oversized sheet of GNPT was placed beneath each laminate and brought up between the laminate and its dams. A sheet of porous teflon was placed on top of each laminate followed by the appropriate number of bleeder sheets. One sheet of bleeder was used for every two plies of prepreg. The bleeder was covered by another sheet of GNPT, followed by an aluminum top plate and a final sheet of GNPT. The cure plate was covered by porous teflon and fiberglass air breather. Vacuum tape and bagging were used to seal off the entire cure plate. The cure plate setup is illustrated in Figure 3.7.

The laminates were cured in an autoclave; the entire cure cycle lasted slightly over five hours. A vacuum of 0.10 MPa was drawn on the cure plate and the autoclave pressure was raised to 0.59 MPa. The temperature was raised to 121°C and held for one hour to allow the resin to flow. The

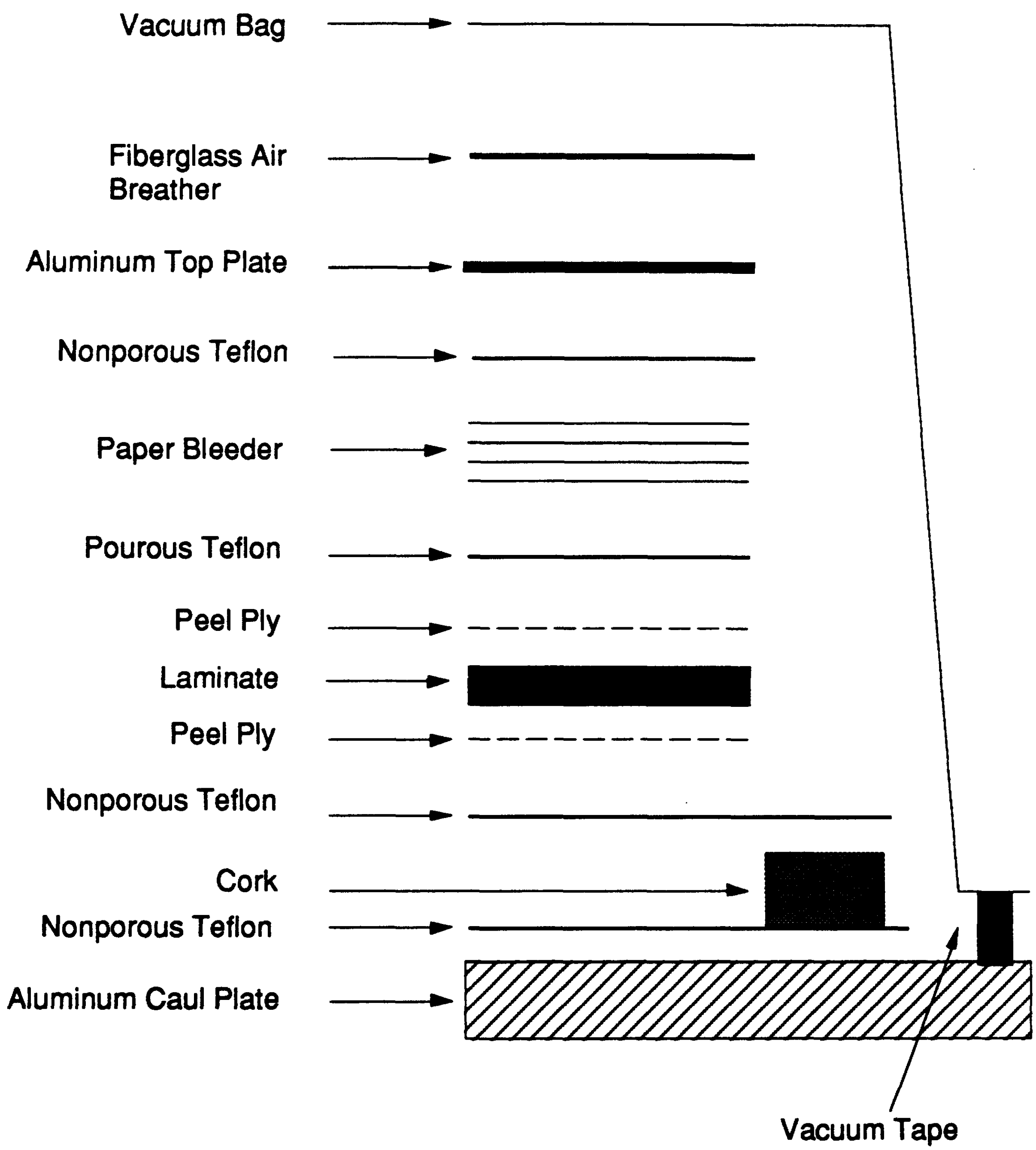

Figure 3.7 Cure plate setup for standard cure.

temperature was then raised to 177°C and held for two hours, to allow the resin's polymer chains to crosslink, before being returned to room temperature. All heating and cooling rates were limited to approximately 3°C per minute. The cure cycle is depicted in Figure 3.8. After being removed from the cure plate assembly, the laminates were post cured for eight hours at 177°C to allow additional crosslinking to occur.

The laminates were milled to the proper size using an automatic feed milling machine that is equipped with a diamond wheel cutter which is cleaned and cooled by a water stream. The laminates were aligned with a carpenter's square and clamped to the table to insure straight cuts. The first cut in each laminate was positioned from one of the edges including the "good" corner. The same cutting procedure was followed for all subsequent laminate trimmings.

Laminate thickness was measured at nine points on each specimen. Figure 3.9 shows the locations of these measurement points; the measurements appear in Appendix A. A weighted average of these measurements was used as the laminate thickness for calculating each specimen's bending stiffness. These average thicknesses appear in Table 3.3, along with the thicknesses of the aluminum plates.

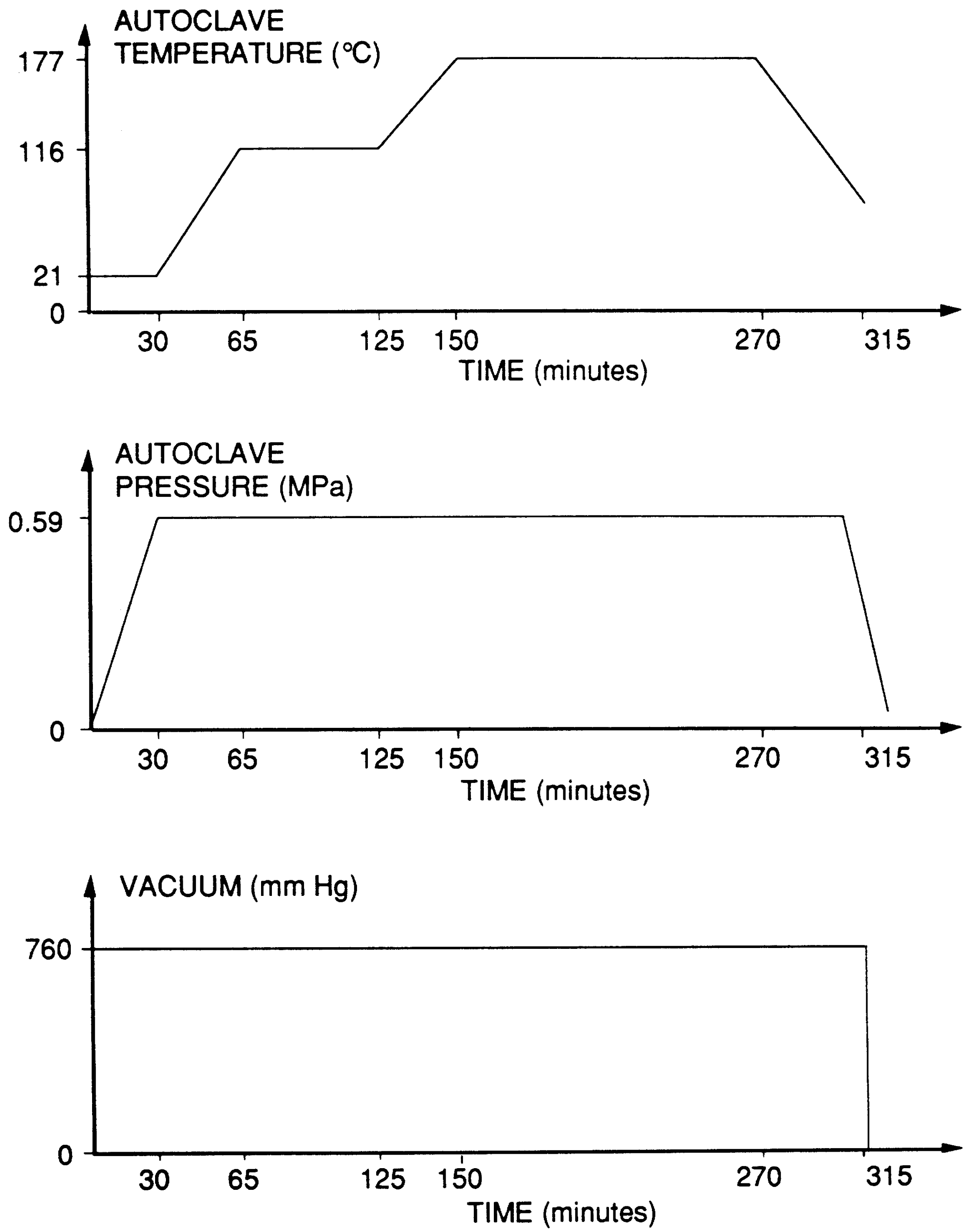

Figure 3.8 Temperature, pressure, and vacuum histories for standard cure.

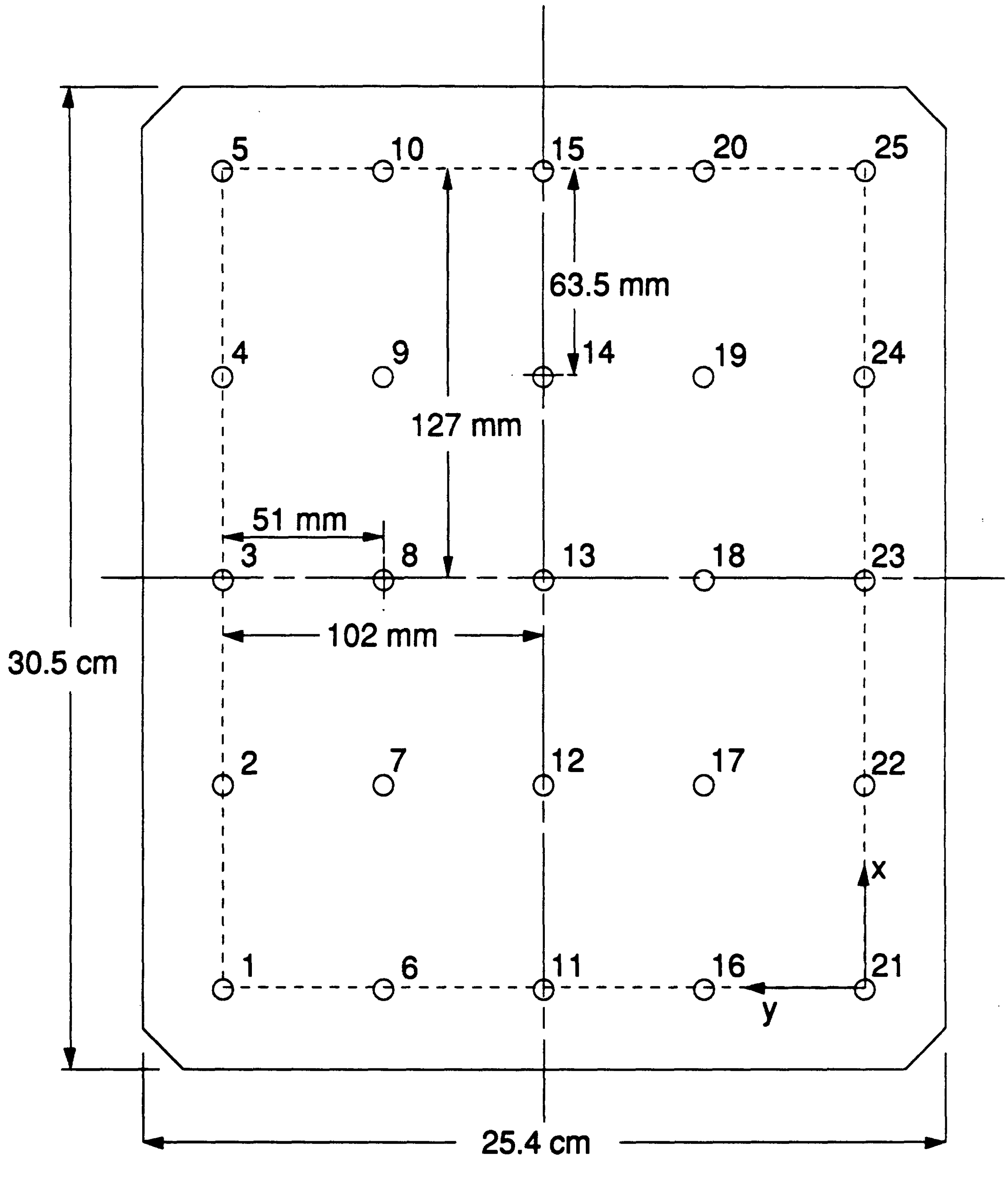

Figure 3.9 Thickness measurement points for composite specimens.

Table 3.3 Test Specimen Average Thicknesses

Specimen	Thickness (mm)
A-1	3.18
A-2	3.20
A-3	3.28
B-1	2.83
B-2	2.84
B-3	2.83
C-1	3.55
C-2	3.55
C-3	3.52
D-1	3.07
D-2	3.02
D-3	3.06
I-1	3.16
I-2	3.16
I-3	3.24

3.5 Point Load Experimentation

A 12.7 mm diameter, hemispherically ended steel tup was used to simulate a point load. The tup had been previously used in TELAC for impact and static indentation tests. Tests were conducted with the tup at the plate center, (x,y) = (127 mm,102 mm), and off-center, (x,y) = (76 mm,127 mm), as shown in Figure 3.10.

3.5.1 Point Load Test Instrumentation

The point load tests were conducted with the jig mounted in the MTS machine. The tup was mounted to a PCB Piezotronics model 208A05 force transducer, in turn mounted to a 60.3 mm diameter steel rod which was clamped in the lower grips of the MTS. The loading device assembly is shown

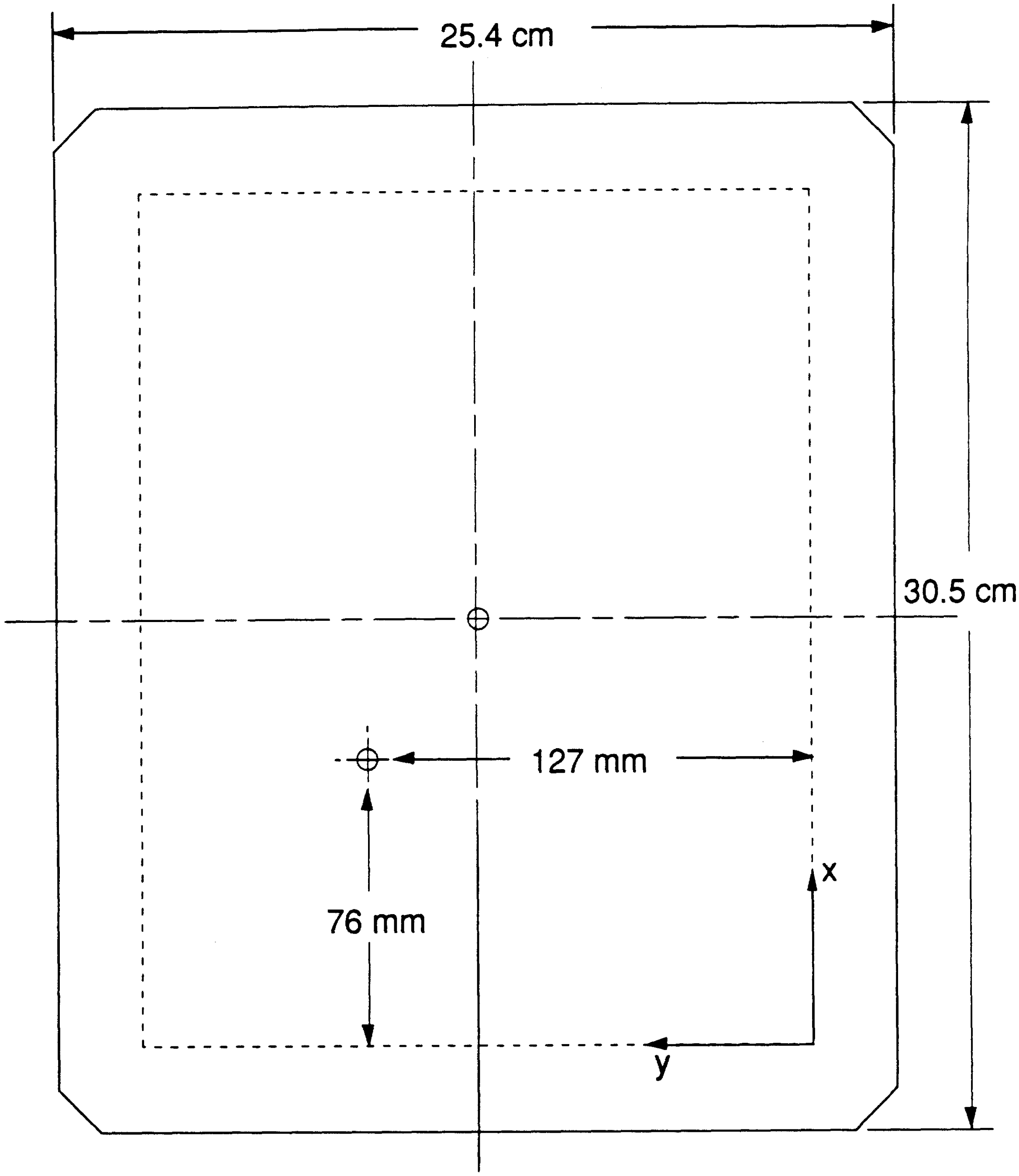

Figure 3.10 Tup locations for point load tests.

in Figure 3.11. The force transducer signal was conditioned with a PCB Piezotronics model 484B signal conditioner; the output was fed to an A/D board.

Trans-Tek model 353-000 displacement transducers were used to measure the plate displacements at five points. The displacement transducer cases were mounted to the upper half of the test jig with a two tier transducer jig, to prevent transducer slippage or rotation. The five transducer locations were picked to provide global insight into the plate deflection shape and are illustrated in Figure 3.12. The displacement transducers had internal signal conditioning and were powered with a ±15 Volt, 200 mA, DC power supply. The transducer signals were fed to an A/D board.

The first three series of tests, those involving only combinations of clamped and simply supported edges, used the MTS's proprietary A/D board for which no information is available. In these tests, the five transducer channels were recorded along with the force transducer and the MTS stroke. The tests involving free edges were conducted after the laboratory had upgraded to a Macintosh based data acquisition system. The system uses a MacAdios board [22] driven with LabVIEW software [23]. The tests were conducted with both the 30 Hz low pass differential mode filter and the 160 Hz low pass common mode filter activated, to minimize the electromagnetic noise that was prevalent in the room. Only five channels of data could be filtered, so transducer number five was not recorded. This allowed the force transducer channel to be filtered and recorded along with transducers number one through four. The MTS stroke was recorded unfiltered.

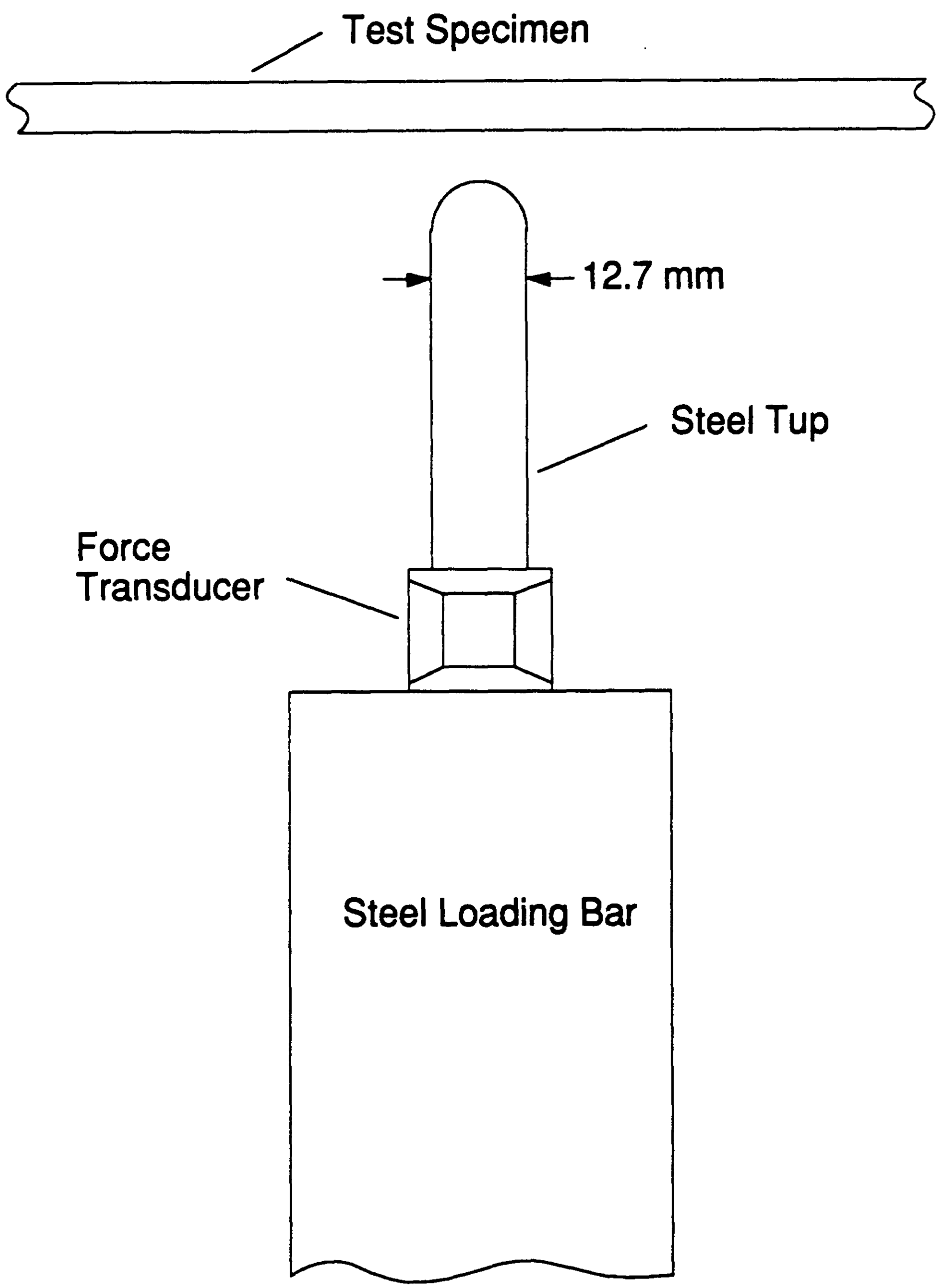

Figure 3.11 Point load test loading device assembly.

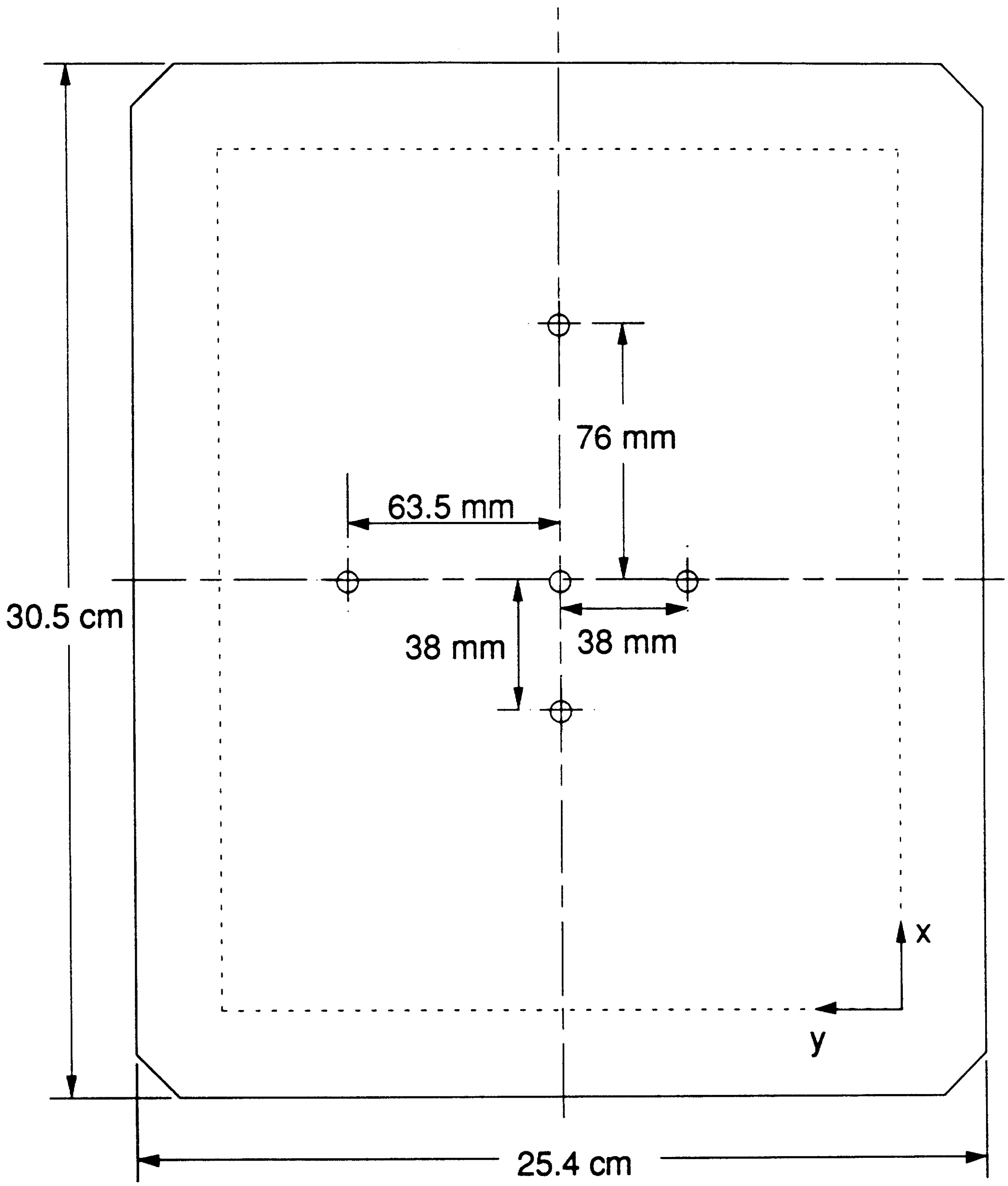

Figure 3.12 Location of displacement transducers.

3.5.2 Point Load Test Procedure

The plates were positioned in the jig with the "good" corner at (x,y) = (0 mm,204 mm). The tup was brought into minimal contact with the plate prior to each test. The MTS was operated in stroke control, at several thousandths of a cm per second, to the specified displacement. Displacements were kept small to avoid damaging any plates, but were large enough to measure the initial load-displacement slope. Tests lasted between 40 and 100 seconds, during which time seven (or six) channels of data were recorded. MTS stroke, force transducer load, and displacements from the five (or four) transducers were recorded at rates varying between one and two hertz, for each test. The different sampling rates were used to obtain significant amounts of data, while minimizing the number of repetitive readings caused by working at the lower end of the equipment's capacity.

3.6 Uniform Rectangular Pressure Patch Experimentation

A device to apply a 51 mm by 63.5 mm rectangular patch of uniform pressure was designed and manufactured for these experiments. The device was a small box with five steel sides and a sixth made of aluminum honeycomb. Over four hundred blunted nails were positioned in the cells of the honeycomb, and rested on a water filled rubber bladder which was contained within the box, see Figure 3.13. The purpose of the sealed bladder was to ensure a uniform loading through each nail, regardless of their displacements relative to one another. The uniform rectangular pressure patch, URPP, was designed to maintain uniform pressure in spite of the plates complicated two dimensional curvatures. Tests were conducted with the URPP device at the plate center, (x,y) = (127 mm,102 mm), and off-center, (x,y) = (76 mm,127 mm), as was done with the point load tests.

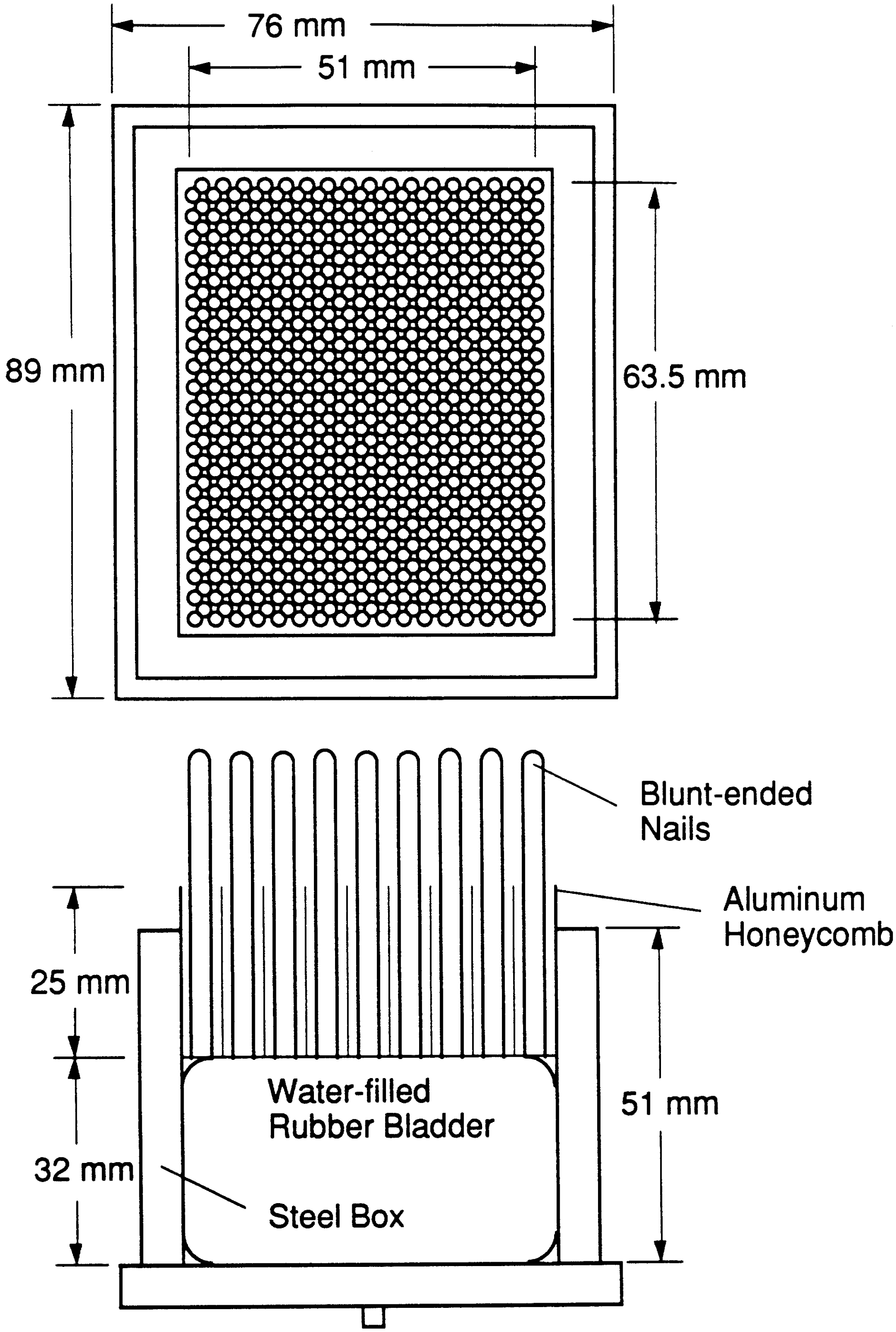

Figure 3.13 Uniform rectangular pressure patch (URPP) device.

3.6.1 Uniform Rectangular Pressure Patch Test Instrumentation

The URPP device mounted on top of the force transducer in place of the tup as shown in Figure 3.14. The URPP tests were also conducted in the MTS machine and used the same instrumentation as for the point load tests.

3.6.2 Uniform Rectangular Pressure Patch Test Procedure

The plates were positioned in the jig with the "good" corner at (x,y) = (0 mm,204 mm). The URPP device was raised until a couple of pounds of load was registered by the force transducer prior to each test. This slight preloading was done to eliminate "dead" time at the beginning of each test, during which time the air and water in the bladder begins to compress but minimal load is transferred to the plate. The MTS was operated in stroke control, at a few thousandths of an inch per second. Unlike the point load tests which were run to a specified stroke, the URPP tests were run to a specified load. Stroke control was stopped manually when the plate reached the same applied load it had been subjected to in the respective point load test. This was done due to the compressibility of the URPP device and the uncertainties thus introduced. Again, tests lasted between 40 and 100 seconds, during which time the seven (or six) channels of data were recorded at rates varying between one and two hertz. Again, different sampling rates were used to obtain significant amounts of data, while minimizing the number of repetitive readings caused by working at the lower end of the equipment's capacity.

3.7 Uniform Pressure Experimentation

A uniform pressure loading was created by drawing a vacuum on one side of the test plates. A 9.52 mm thick aluminum plate was sealed to the bottom half of the jig with vacuum tape and attached with the four, 15.9 mm

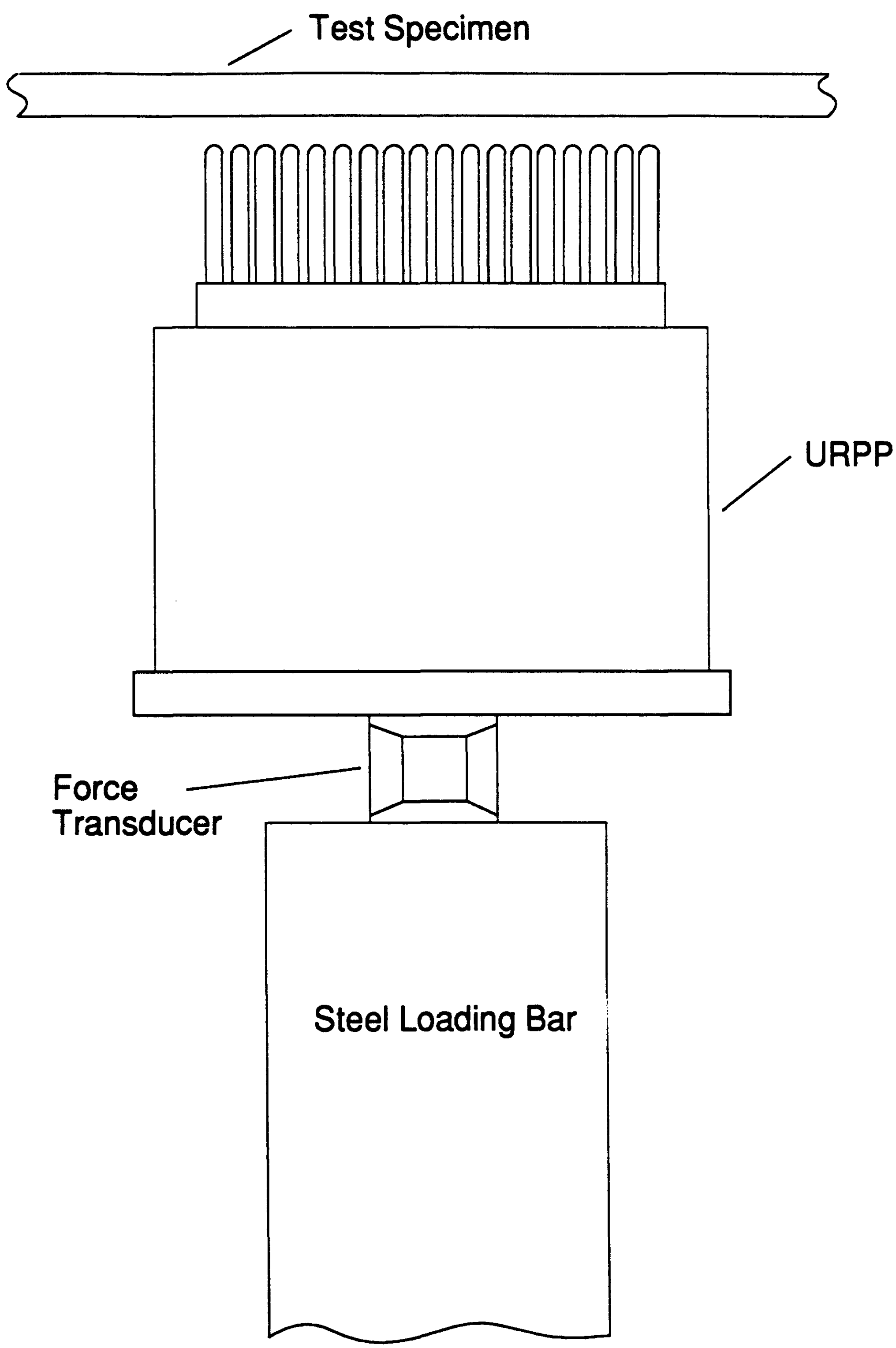

Figure 3.14 URPP test loading device assembly.

corner bolts to create a vacuum chamber. The aluminum plate was plumbed with a vacuum line and a vacuum gage as shown in Figure 3.15.

3.7.1 Uniform Pressure Test Instrumentation

The uniform pressure tests were conducted with the test jig lying on a laboratory table. A Cenco-Megavac vacuum pump was plumbed to the aluminum sealing plate through a needle valve to allow ample control of the vacuum draw rate. A second needle valve served as a vacuum release, see Figure 3.15. A 101.6 kPa WIKA vacuum gage with 1.7 kPa intervals was used to monitor the vacuum. The five displacement transducers were again used to measure the plate displacement. A PDP 11-23 based data acquisition system was used to record the transducer data.

3.7.2 Uniform Pressure Test Procedure

The plates were positioned in the jig with the "good" corner at (x,y) = (0 mm,0 mm). The uniform pressure tests were conducted upside-down with respect to the other tests so that all plate deflections would be "up" with respect to the plate layups. Vacuum tape was placed around the perimeter of the boundary conditions to seal the test specimen and boundary conditions to the lower half of the jig. Care was taken to not allow vacuum tape between the test specimen and the boundary conditions, to prevent "softening" of the boundary conditions. The plates were loaded at approximately 34 kPa per minute, while transducer readings were taken at increments of 1.7 kPa. None of the plates were loaded beyond 101.6 kPa, and many of the seals failed between 67.7 and 101.6 kPa.

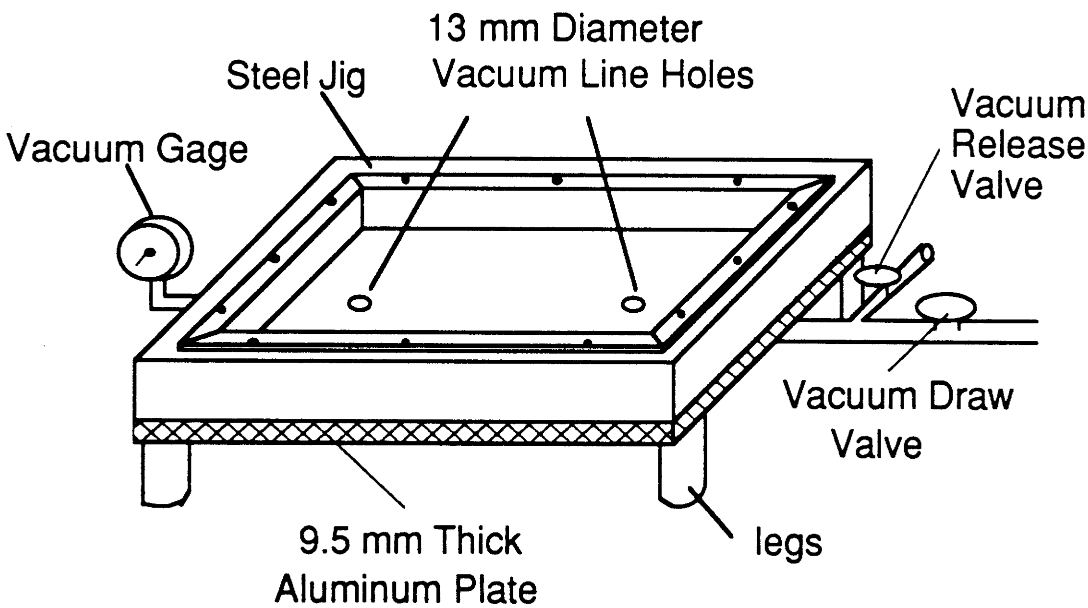

Figure 3.15 Vacuum assembly for uniform pressure tests.

3.8 Forced Vibration Experimentation

Approximate natural frequencies and mode shapes were experimentally obtained for the test specimens by transversely shaking them with a mechanical shaker through a soft spring. Plate response was monitored with an accelerometer mounted near an edge of the plate.

3.8.1 Forced Vibration Test Instrumentation

The plates were shaken with a Ling model 420-1 mechanical shaker. Contact with the plate was made through a soft spring, see Figure 3.16. The shaker was powered by a ALTEC shaker amplifier, which was in turn driven by a Wave Tek 2 MHz function generator. A Fluke 1952B counter-timer was used to more accurately measure the function generator's frequency. An Enderco, model 7701-50 accelerometer along with an Tek Tronic 465 Oscilloscope were used to monitor the test specimen's response. Photographs of the plate's mode shapes, accentuated with salt crystals, were taken on ASA-400 black and white film with a Nikon FM2, 35 mm camera, and a Micro-Nikkor 105 mm 1:4 lens.

3.8.2 Forced Vibration Test Procedure

The plates were positioned in the jig with the "good" corner at (x,y) = (0 mm,204 mm). The accelerometer was mounted to the test specimen with double stick tape, and the plates were lightly sprinkled with salt to accentuate movement. Frequency sweeps were conducted with the shaker in various positions under the plate to aid in forcing all obtainable modes. Shaker amplitude was increased to help identify and sketch mode shapes, however, all frequency measurements were taken at the lowest possible amplitude to minimize nonlinear effects.

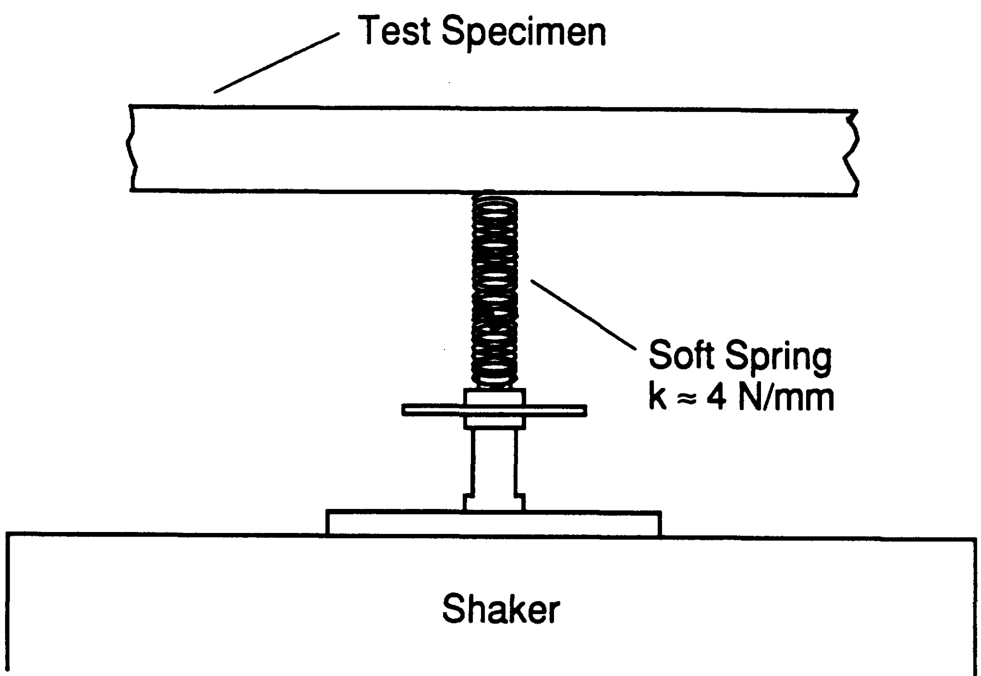

Figure 3.16 Soft spring connection between mechanical shaker and specimen.

3.9 Test Matrix

Five different combinations of boundary conditions were investigated. The combinations were composed of clamped, simply supported, and free edges, however, for all five combinations the pair of x edges and the pair of y edges were each subjected to the same constraint. Table 3.4 shows the test matrix for this investigation. The boundary conditions are listed as x edge condition – y edge condition. The Point Load and URPP tests were conducted at the plate center (C) and off-center (O-C) as described above. The number of specimens tested at each condition is listed.

Table 3.4 Test Matrix

B. C.'s	Spec.	Point Load C	Point Load O-C	URPP C	URPP O-C	Uniform Pressure	Forced Vibration
CL–CL	A	3*	3	3	3	3	3
	B	3	3	3	3	3	3
	C	3	3	3	3	3	3
	D	3	3	3	3	3	3
	I	1	1	1	1	1	1
SS–CL	A		3		3	3	3
	B		3		3	3	3
	C		3		3	3	3
	D		3		3	3	3
	I		1		1	1	1
SS–SS	A	3	3	3	3	3	3
	B	3	3	3	3	3	3
	C	3	3	3	3	3	3
	D	3	3	3	3	3	3
	I	1	1	1	1	1	1
CL–FR	A		3		3		3
	B		3		3		3
	C		3		3		3
	D		3		3		3
	I		1		1		1
SS–FR	A		3		3		3
	B		3		3		3
	C		3		3		3
	D		3		3		3
	I		1		1		1

* Entries indicate number of specimens tested for each condition.
C = centered; O-C = off-center
CL = clamped; SS = simply supported; FR = free;

Chapter 4

Analysis

This chapter describes all of the analysis methods used in this investigation. New material is presented in detail, while previous techniques are merely summarized. Copies of all major code used in this investigation appear in Appendices B, D, and E.

4.1 Specimen Mechanical Properties

Two different graphite/epoxy material systems were used in this investigation in addition to the aluminum specimens used as controls. The nominal cured ply properties for these three material systems are given in Table 4.1.

Table 4.1 Nominal Cured Ply Properties

Property	AS4/3501-6	AW370-5H/3501-6	Aluminum
E_1 (GPa)	142.0	72.5	69.0
E_2 (GPa)	9.81	72.6	69.0
ν_{12}	0.30	0.059	0.30
G_{12} (GPa)	6.00	4.43	26.6
G_{23} (GPa)	3.77	27.2	26.6
G_{31} (GPa)	6.00	27.2	26.6
ρ (kg/m^3)	1570	1560	2700
t_{ply} (mm)	.134	.343	—

Analytical results are normally based on nominal ply thickness. Due to multiple adjacent layers of the same ply angle, however, most of the experimental specimens were thinner than nominal thickness. Since bending stiffness is related to thickness cubed while modulus is a linear function of matrix volume ratio, the nominal ply properties listed above were used with the average measured thickness for each specimen group. Hopefully this leads to better estimates of the laminate bending stiffnesses.

The laminate stiffnesses were calculated from the appropriate formulas given in Chapter 2. In-plane specimen stiffnesses are given in Table 4.2. The code used to generate these values appears in Appendix B.

Table 4.2 In-plane Laminate Stiffnesses

	Specimens				
Stiffness	A	B	C	D	I
A_{11} (10^6 N/m)	260	237	152	209	240
A_{22} (10^6 N/m)	106	134	152	209	240
A_{12} (10^6 N/m)	72.9	40.1	121	32.4	71.9
A_{66} (10^6 N/m)	82.7	48.7	121	41.7	83.9
A_{16} (10^6 N/m)	68.6	0.0	0.0	0.0	0.0
A_{26} (10^6 N/m)	68.6	0.0	0.0	0.0	0.0
B_{11} (10^3 N)	0.0	0.0	0.0	0.0	0.0
B_{22} (10^3 N)	0.0	0.0	0.0	0.0	0.0
B_{12} (10^3 N)	0.0	0.0	0.0	0.0	0.0
B_{66} (10^3 N)	0.0	0.0	0.0	0.0	0.0
B_{16} (10^3 N)	0.0	0.0	0.0	–30.9	0.0
B_{26} (10^3 N)	0.0	0.0	0.0	30.9	0.0
D_{11} (N-m)	190	200	159	188	199
D_{22} (N-m)	105	48.5	159	137	199
D_{12} (N-m)	74.3	26.9	126	25.1	59.8
D_{66} (N-m)	82.8	32.7	127	32.3	69.8
D_{16} (N-m)	71.5	3.43	0.0	0.0	0.0
D_{26} (N-m)	71.5	3.43	0.0	0.0	0.0

Transverse shear stiffnesses were calculated using both methods described in

Chapter 2, and are listed in Table 4.3. The 3-D moduli values for transverse shear stiffness were used in all of the analysis; the "classical" values are listed only for reference. For these specimens the two methods yield similar estimates for the transverse stiffness, because each laminate is made of only one material.

Table 4.3 Transverse Laminate Stiffnesses

Specimen	Method	A_{55} (10^6 N/m)	A_{44} (10^6 N/m)	A_{45} (10^6 N/m)
A	3-D	14.5	17.0	2.30
A	classical	14.1	16.6	2.24
B	3-D	13.0	14.7	0.00
B	classical	12.4	14.0	0.00
C	3-D	96.3	96.3	0.00
C	classical	96.3	96.3	0.00
D	3-D	14.9	14.9	0.00
D	classical	14.1	14.1	0.00
I	3-D	83.9	83.9	0.00
I	classical	83.9	83.9	0.00

The shear correction factor for all of the analyses has been taken as:

$$\kappa = \frac{\pi^2}{12}$$

following Dobyns [5] and Whitney [9].

4.2 Reduction of Tenth Order Mindlin Plate Theory

The full tenth order Mindlin Plate theory discussed in Chapter 2 can be recast into a single tenth order partial differential equation using the reduction technique of Vlasov [11] and Ambartsumyan [13]. For an anisotropic plate this equation is very complicated, however, if the plate is symmetric about its midplane significant simplifications occur. For a midplane symmetric anisotropic plate, the following terms are zero:

$$B_{ij} = 0 \; ; \qquad R_1 = 0$$

The following differential operators defined in Chapter 2 are then zero:

$$\begin{aligned} L_{13} &= 0 \; ; & L_{14} &= 0 \; ; & L_{15} &= 0 \\ L_{23} &= 0 \; ; & L_{24} &= 0 \; ; & L_{25} &= 0 \end{aligned}$$

thus uncoupling the stretching and bending parts of the problem. The stretching problem involves midplane displacements, u^o and v^o, while the bending problem involves transverse displacement, w, and shear rotations, Ψ_x, and Ψ_y. The stretching problem alone is a fourth order system, while the bending problem alone is a sixth order system.

The midplane symmetric anisotropic plate bending problem can now be represented as follows:

$$\begin{bmatrix} L_{33} & L_{34} & L_{35} \\ L_{34} & L_{44} & L_{45} \\ L_{35} & L_{45} & L_{55} \end{bmatrix} \begin{bmatrix} w \\ \Psi_x \\ \Psi_y \end{bmatrix} = \begin{bmatrix} -p_z \\ +m_x \\ +m_y \end{bmatrix}$$

where the differential operators are as defined in Chapter 2. This sixth order system will now be reduced to a single sixth order partial differential equation using the symmetric operator reduction method.

If the plate is only subjected to a transverse loading, p_z, the new equation can be written symbolically as:

$$L^6 \Phi = -p_z$$

where L^6 is a sixth order differential operator, and Φ is the new potential function. The differential operator is defined as the determinant of the symmetric operator coefficient matrix:

$$L^6 = \begin{vmatrix} L_{33} & L_{34} & L_{35} \\ L_{34} & L_{44} & L_{45} \\ L_{35} & L_{45} & L_{55} \end{vmatrix}$$

For the case of transverse loading, the displacement and shear rotations can be expressed as follows:

$$w = \left(L_{44} L_{55} - L_{45}^2\right) \Phi$$

$$\Psi_x = \left(L_{35} L_{45} - L_{34} L_{55}\right) \Phi$$

$$\Psi_y = \left(L_{34} L_{45} - L_{35} L_{44}\right) \Phi$$

If surface tractions are also applied, additional solutions for Φ must be properly accounted for [11].

The sixth order partial differential equation for Φ may be expressed as:

$$P_1 \frac{\partial^6\Phi}{\partial x^6} + P_2 \frac{\partial^6\Phi}{\partial x^5 \partial y} + P_3 \frac{\partial^6\Phi}{\partial x^4 \partial y^2} + P_4 \frac{\partial^6\Phi}{\partial x^3 \partial y^3} + P_5 \frac{\partial^6\Phi}{\partial x^2 \partial y^4} + P_6 \frac{\partial^6\Phi}{\partial x\, \partial y^5} + P_7 \frac{\partial^6\Phi}{\partial y^6} +$$

$$P_8 \frac{\partial^6\Phi}{\partial t^6} + P_9 \frac{\partial^6\Phi}{\partial t^4 \partial x^2} + P_{10} \frac{\partial^6\Phi}{\partial t^4 \partial x\, \partial y} + P_{11} \frac{\partial^6\Phi}{\partial t^4 \partial y^2} +$$

$$P_{12} \frac{\partial^6\Phi}{\partial t^2 \partial x^4} + P_{13} \frac{\partial^6\Phi}{\partial t^2 \partial x^3\, \partial y} + P_{14} \frac{\partial^6\Phi}{\partial t^2 \partial x^2 \partial y^2} + P_{15} \frac{\partial^6\Phi}{\partial t^2 \partial x\, \partial y^3} + P_{16} \frac{\partial^6\Phi}{\partial t^2 \partial y^4} +$$

$$P_{17} \frac{\partial^4\Phi}{\partial x^4} + P_{18} \frac{\partial^4\Phi}{\partial x^3 \partial y} + P_{19} \frac{\partial^4\Phi}{\partial x^2 \partial y^2} + P_{20} \frac{\partial^4\Phi}{\partial x\, \partial y^3} + P_{21} \frac{\partial^4\Phi}{\partial y^4} + P_{22} \frac{\partial^4\Phi}{\partial t^4} +$$

$$P_{23} \frac{\partial^4\Phi}{\partial t^2 \partial x^2} + P_{24} \frac{\partial^4\Phi}{\partial t^2 \partial x\, \partial y} + P_{25} \frac{\partial^4\Phi}{\partial t^2 \partial y^2} +$$

$$P_{26} \frac{\partial^2\Phi}{\partial x^2} + P_{27} \frac{\partial^2\Phi}{\partial x\, \partial y} + P_{28} \frac{\partial^2\Phi}{\partial y^2} + P_{29} \frac{\partial^2\Phi}{\partial t^2} + P_{30} = -p_z$$

where the P_i's are constant coefficients and are defined in Appendix C.

For the case of midplane symmetric plates without bending-twisting coupling the equation simplifies further to:

$$P_1 \frac{\partial^6\Phi}{\partial x^6} + P_3 \frac{\partial^6\Phi}{\partial x^4 \partial y^2} + P_5 \frac{\partial^6\Phi}{\partial x^2 \partial y^4} + P_7 \frac{\partial^6\Phi}{\partial y^6} + P_8 \frac{\partial^6\Phi}{\partial t^6} + P_9 \frac{\partial^6\Phi}{\partial t^4 \partial x^2} + P_{11} \frac{\partial^6\Phi}{\partial t^4 \partial y^2} +$$

$$P_{12} \frac{\partial^6\Phi}{\partial t^2 \partial x^4} + P_{14} \frac{\partial^6\Phi}{\partial t^2 \partial x^2 \partial y^2} + P_{16} \frac{\partial^6\Phi}{\partial t^2 \partial y^4} + P_{17} \frac{\partial^4\Phi}{\partial x^4} + P_{19} \frac{\partial^4\Phi}{\partial x^2 \partial y^2} + P_{21} \frac{\partial^4\Phi}{\partial y^4} +$$

$$P_{22} \frac{\partial^4\Phi}{\partial t^4} + P_{23} \frac{\partial^4\Phi}{\partial t^2 \partial x^2} + P_{25} \frac{\partial^4\Phi}{\partial t^2 \partial y^2} + P_{26} \frac{\partial^2\Phi}{\partial x^2} + P_{28} \frac{\partial^2\Phi}{\partial y^2} + P_{29} \frac{\partial^2\Phi}{\partial t^2} + P_{30} = -p_z$$

where the simplified constant coefficients are:

$$P_1 = \kappa A_{55} D_{11} D_{66}$$

$$P_3 = \kappa A_{44} D_{11} D_{66} + \kappa A_{55}\left(D_{11} D_{22} - D_{12}^2 - 2 D_{12} D_{66}\right)$$

$$P_5 = \kappa A_{44}\left(D_{11} D_{22} - D_{12}^2 - 2 D_{12} D_{66}\right) + \kappa A_{55} D_{22} D_{66}$$

$$P_7 = \kappa A_{44} D_{22} D_{66}$$

$$P_8 = - R_0 R_2^2$$

$$P_9 = \kappa A_{55} R_2^2 + R_0 R_2 (D_{11} + D_{66})$$

$$P_{11} = \kappa A_{44} R_2^2 + R_0 R_2 (D_{22} + D_{66})$$

$$P_{12} = - \kappa A_{55} R_2 (D_{11} + D_{66}) - R_0 D_{11} D_{66}$$

$$P_{14} = - \kappa A_{44} R_2 (D_{11} + D_{66}) - \kappa A_{55} R_2 (D_{22} + D_{66}) + R_0\left(D_{12}^2 - D_{11} D_{22} + 2 D_{12} D_{66}\right)$$

$$P_{16} = - \kappa A_{44} R_2 (D_{22} + D_{66}) - R_0 D_{22} D_{66}$$

$$P_{17} = - D_{11} \kappa^2 A_{44} A_{55} - K D_{11} D_{66}$$

$$P_{19} = - 2 D_{12} \kappa^2 A_{44} A_{55} - 4 D_{66} \kappa^2 A_{44} A_{55} + K\left(D_{12}^2 - D_{11} D_{22} + 2 D_{12} D_{66}\right)$$

$$P_{21} = - D_{22} \kappa^2 A_{44} A_{55} - K D_{22} D_{66}$$

$$P_{22} = - R_0 R_2 \kappa (A_{44} + A_{55}) - K R_2^2$$

$$P_{23} = R_0 \kappa (A_{44} D_{11} + A_{55} D_{66}) + R_2 \kappa^2 A_{44} A_{55} + K R_2 (D_{11} + D_{66})$$

$$P_{25} = R_0 \kappa (A_{44} D_{66} + A_{55} D_{22}) + R_2 \kappa^2 A_{44} A_{55} + K R_2 (D_{22} + D_{66})$$

$$P_{26} = K \kappa (A_{44} D_{11} + A_{55} D_{66})$$

$$P_{28} = K \kappa (A_{44} D_{66} + A_{55} D_{22})$$

$$P_{29} = - R_0 \kappa^2 A_{44} A_{55} - K R_2 \kappa (A_{44} + A_{55})$$

$$P_{30} = - K \kappa^2 A_{44} A_{55}$$

4.2.1 Bending of Clamped Plates

An approximate one mode polynomial solution was investigated for the case of a midplane symmetric anisotropic plate, without bending-twisting coupling, with four edges clamped. The polynomial was chosen such that all boundary conditions were satisfied explicitly; the amplitude was then found by using the Galerkin method.

For simplicity, the single polynomial mode uses only even powers of x and y. For this problem the axes are located at the center of the plate rather than at the corner, so the even function represents a symmetric deformation. The polynomial solution should only be used for symmetric loadings, due to it's even nature.

The approximate polynomial solution is complete through x and y to the tenth power. Unlike the other solutions that have been discussed, this potential function is in general not separable in x and y; it is not a product of a function of x and a function of y. The general form of the polynomial potential function being used is as follows:

$$\begin{aligned}
\Phi_1 = A_1 \Big(1 &+ a_2 x^2 + a_3 x^4 + a_4 x^6 + a_5 x^8 + a_6 x^{10} + a_7 y^2 + a_8 x^2 y^2 \\
&+ a_9 x^4 y^2 + a_{10} x^6 y^2 + a_{11} x^8 y^2 + a_{12} x^{10} y^2 + a_{13} y^4 + a_{14} x^2 y^4 \\
&+ a_{15} x^4 y^4 + a_{16} x^6 y^4 + a_{17} x^8 y^4 + a_{18} x^{10} y^4 + a_{19} y^6 + a_{20} x^2 y^6 \\
&+ a_{21} x^4 y^6 + a_{22} x^6 y^6 + a_{23} x^8 y^6 + a_{24} x^{10} y^6 + a_{25} y^8 + a_{26} x^2 y^8 \\
&+ a_{27} x^4 y^8 + a_{28} x^6 y^8 + a_{29} x^8 y^8 + a_{30} x^{10} y^8 + a_{31} y^{10} + a_{32} x^2 y^{10} \\
&+ a_{33} x^4 y^{10} + a_{34} x^6 y^{10} + a_{35} x^8 y^{10} + a_{36} x^{10} y^{10}\Big)
\end{aligned}$$

The twelve boundary conditions, three per edge, reduce to six independent equations due to the symmetric nature of Φ_1. The six independent boundary conditions are as follows:

$$w(0,y) = 0 \; ; \qquad \Psi_x(0,y) = 0 \; ; \qquad \Psi_y(0,y) = 0$$

$$w(x,0) = 0 \; ; \qquad \Psi_y(x,0) = 0 \; ; \qquad \Psi_x(x,0) = 0$$

These six equations, however, expand to 34 equations upon matching coefficients of the different exponents of the variables. This is the polynomial analogy to harmonic balance. Of the resulting 34 equations, 31 are independent. Since the general function has 35 unknowns, the final four coefficients remain arbitrary and have been set to zero.

Since the polynomial will now explicitly satisfy the boundary conditions, its appropriate magnitude may be found with the Galerkin technique [24]. While the potential function satisfies all the boundary conditions, in general it will not satisfy the governing partial differential equation. When this approximate function is placed into the differential equation some error or residual, R, will result:

$$R = L^6 \Phi + p_z$$

The Galerkin method sets the residual, integrated with respect to a weighting function, W_i, over the domain of the plate, to zero:

$$\int_{\frac{-a}{2}}^{\frac{a}{2}} \int_{\frac{-b}{2}}^{\frac{b}{2}} R \; W_i \; dy \; dx = 0$$

Any weighting function may be used, however, in practice the approximate function itself is most often used [24]. In this case, the first mode of the displacement, w_1, rather than Φ_1 has been used because the product of w and the partial differential equation integrated over the domain has the units of energy. By using the Galerkin method in this way, the work done by the error in the external loads is minimized. This application of the Galerkin method can be represented as follows:

$$\int_{\frac{-a}{2}}^{\frac{a}{2}} \int_{\frac{-b}{2}}^{\frac{b}{2}} \left(A_1 \; L^6\Phi + p_z\right) w_1 \; dy \; dx = 0$$

where A_1 is the unknown amplitude to be determined.

Polynomial potential functions, such as the one above, offer great flexibility in properly accounting for all types of couplings. However, to be generally useful for a variety of problems, a set of functions rather than a single function needs to be developed. This set of functions should include both symmetric and antisymmetric shapes and should be mathematically complete; it should be able to describe all physically possible deflection shapes and converge to the loading function, p_z.

The difficulty is in selecting functions that satisfy all the boundary conditions. Finding such functions is computationally intensive. A routine to find the single approximate potential function described above is included in Appendix D.

4.2.2 Bending of Simply Supported Plates

For a simply supported midplane symmetric plate without bending-twisting coupling a Navier type solution can be found for the potential function. When Φ is taken as an infinite double sine series:

$$\Phi(x,y) = \sum_{m=1}^{\infty} \sum_{n=1}^{\infty} a_{mn} \sin\frac{m\pi x}{a} \sin\frac{n\pi y}{b}$$

all the boundary conditions are satisfied explicitly. When the distributed transverse loading, p_z, is also expanded in an infinite double sine series, the coefficients of Φ may be found through harmonic balance. The transverse deflection, w, may then be found from the equations above as:

$$w(x,y) = \sum_{m=1}^{\infty} \sum_{n=1}^{\infty} \frac{p_{mn}\left(L_{44}\, L_{55} - L_{45}^{2}\right) \sin\frac{m\pi x}{a} \sin\frac{n\pi y}{b}}{L^{6} \sin\frac{m\pi x}{a} \sin\frac{n\pi y}{b}} \sin\frac{m\pi x}{a} \sin\frac{n\pi y}{b}$$

where once again:

$$p_{mn} = \frac{4}{a\,b}\int_0^a \int_0^b p_z \sin\frac{m\pi x}{a} \sin\frac{n\pi y}{b}\, dy\, dx$$

Although appearing slightly different, the expression for w(x,y) above is equivalent to the expression given in Chapter 2 for plates with transverse shear deformation. Again, Navier type solutions that include bending-twisting coupling are not possible because these terms multiply differential operators which introduce cosine terms into w that do not explicitly satisfy the homogeneous boundary conditions.

A polynomial potential function solution, similar to the clamped potential function above, was also found for the four edges simply supported problem for plates without bending-twisting coupling. For this case the polynomial was chosen to be complete through even powers of x and y to the sixth power. Again, due to its even nature, this potential function is only intended for symmetric problems. The general form of the polynomial potential function being used is as follows:

$$\begin{aligned}\Phi_1 = A_1 \Big(1 &+ a_2\, x^2 + a_3\, x^4 + a_4\, x^6 + a_5\, y^2 + a_6\, x^2 y^2 \\ &+ a_7\, x^4 y^2 + a_8\, x^6 y^2 + a_9\, y^4 + a_{10}\, x^2 y^4 + a_{11}\, x^4 y^4 \\ &+ a_{12}\, x^6 y^4 + a_{13}\, y^6 + a_{14}\, x^2 y^6 + a_{15}\, x^4 y^6 + a_{16}\, x^6 y^6 \Big)\end{aligned}$$

Again, the twelve boundary conditions reduce to six independent conditions due to the symmetric nature of Φ_1. The six independent boundary conditions are as follows:

$$w(0,y) = 0\,; \qquad M_x(0,y) = 0\,; \qquad \Psi_y(0,y) = 0$$

$$w(x,0) = 0\,; \qquad M_y(x,0) = 0\,; \qquad \Psi_x(x,0) = 0$$

A polynomial, of the general form above, which is independent of material properties, but explicitly satisfies the boundary conditions has been found to be:

$$\Phi_1 = A_1 \Big(1 - \frac{300}{61\,a^2} x^2 + \frac{240}{61\,a^4} x^4 - \frac{64}{61\,a^6} x^6$$

$$- \frac{300}{61\,b^2} y^2 + \frac{90000}{3721\,a^2 b^2} x^2 y^2 - \frac{72000}{3721\,a^4 b^2} x^4 y^2 + \frac{19200}{3721\,a^6 b^2} x^6 y^2$$

$$+ \frac{240}{61\,b^4} y^4 - \frac{72000}{3721\,a^2 b^4} x^2 y^4 + \frac{57600}{3721\,a^4 b^4} x^4 y^4 - \frac{15360}{3721\,a^6 b^4} x^6 y^4$$

$$- \frac{64}{61\,b^6} y^6 + \frac{19200}{3721\,a^2 b^6} x^2 y^6 - \frac{15360}{3721\,a^4 b^6} x^4 y^6 + \frac{4096}{3721\,a^6 b^6} x^6 y^6 \Big)$$

The amplitude, A_1, may be found for a particular loading by using the Galerkin method as discussed above for clamped plates. Again, to be generally useful for a variety of problems, a set of functions rather than a single mode needs to be developed.

For plates with bending-twisting coupling, other solution forms must be used. Polynomial solutions which explicitly satisfy the boundary conditions could be found, as has been done above for plates without bending-twisting coupling.

4.3 Lagrange Multiplier Solutions

The work done by Ramkumar and Chen [17, 18] can be extended to any combination of simply supported and clamped edges. In fact, typographical errors in both papers resulted in solutions for two adjacent edges clamped with the other two edges simply supported rather than the four sides clamped case for which numerical and graphical data were presented. The two cases of interest for this work are all four sides clamped and two opposite sides clamped with the other pair of edges simply supported.

4.3.1 Four Sides Clamped

The four sides clamped problem requires four series of constraints to be appended to the energy equation. Ramkumar and Chen [17, 18] have inadvertently only listed two. One series of constraints is required for each clamped edge and comes from using harmonic balance to enforce the zero slope boundary conditions. For example, if the two opposing x edges are clamped, the boundary conditions are:

$$\Psi_x(0,y) = \sum_{m=1}^{\infty} \sum_{n=1}^{\infty} b_{mn} \cos\frac{m\pi 0}{a} \sin\frac{n\pi y}{b} = 0$$

$$\Psi_x(a,y) = \sum_{m=1}^{\infty} \sum_{n=1}^{\infty} b_{mn} \cos\frac{m\pi a}{a} \sin\frac{n\pi y}{b} = 0$$

which lead to the following constraints from harmonic balance:

$$\sum_{m=1}^{\infty} b_{mn} = 0 \quad (\text{for } n = 1,2,\ldots\infty)$$

$$\sum_{m=1}^{\infty} (-1)^m b_{mn} = 0 \quad (\text{for } n = 1,2,\ldots\infty)$$

Two similar sets of constraints come from the y edges. Each constraint is appended to the energy expression with a Lagrange multiplier and then the resulting system of equations is solved [17, 18]. The fully clamped case results in 2(M+N) equations and 2(M+N) unknowns. M and N are the number of modes used in the x and y directions respectively, since in practice the infinite series is always truncated at some point. The two adjacent sides clamped and two sides simply supported problem that was inadvertently described by Ramkumar and Chen [17, 18], was only (M+N) by (M+N) in size.

A code was developed for the four sides clamped solution and is listed in Appendix E.

4.3.2 Two Sides Clamped and Two Sides Simply Supported

The case of two opposite edges clamped and the other edges simply supported is very similar to the two adjacent edges clamped problem. Only two sets of constraints are needed rather than four, so the resulting system of equations is only (M+N) by (M+N) in size.

A code was also developed for the two opposite edges clamped and two edges simply supported case. A listing is given in Appendix E, following the four sides clamped code listing.

4.4 Rayleigh-Ritz Solutions

The Rayleigh-Ritz solutions included in this work are from an internal TELAC code written by Wilson Tsang. The program uses Dugundji's beam functions [19] for the transverse displacement and the shear compatible derivatives of the beam functions [20] for the shear rotations, as discussed in chapter two. The Rayleigh-Ritz code is listed in Appendix F along with a post-processor which produced the extensive graphics output included in this work. The Rayleigh-Ritz solution includes the effects of bending-twisting coupling. The code was modified to calculate static displacements as well as natural frequencies of vibration.

Chapter 5
Experimental Results

This chapter contains the results of all the plate tests. Representative plots from the static tests are presented and discussed. Regressions of all the static tests appear in Appendix G. Experimental natural mode shapes and frequencies are presented for all the dynamic tests conducted.

5.1 Static Test Results

The important data from the static tests are the initially linear force-displacement histories of the specimens. In many of the tests non-linear effects eventually became noticeable, but those effects are not modeled by the present analysis and therefore have been truncated in the data reduction.

5.1.1 Data Reduction

For each test, transducer measurements were taken at four or five points on the plate as discused in Chapter 3. Regressions of these displacements against the total applied load were performed to determine "spring constants" or local stiffnesses for the transducer locations on the plate. The stiffnesses have units of force per unit deflection (N/mm). The stiffness represents the magnitude of force that must be applied, through the appropriate mechanism, to achieve one mm of deflection at the transducer location. A stiffness was regressed for each transducer location per test. Only the linear portions of the displacement curves were used in the regressions. Initial contact affects and any large deflection non-linearities were truncated.

The regressed stiffnesses for the static tests appear in Appendix F, along with their respective "goodness of fit" values. The average stiffnesses for each specimen type are also given along with the largest deviation from the average, as a percentage of the average. The deviation term reflects the largest variation in the experimental stiffnesses that contributed to the average.

5.1.2 Representative Load-Deflection Plots

The load-deflection plots for specimen A-1, subjected to the off-center URPP at (x,y) = (76 mm,127 mm), are presented below in Figures 5.1-5.5 for each of the five boundary condition combinations investigated. The force transducer was being used in the lower end of its range and suffers from poor resolution. As a result, the data is clumped along horizontal lines of constant force, creating a "staircase" effect. For clamped boundary conditions, the force transducer data is fairly linear, however, for simply supported and free boundary conditions the data exhibits a strong staircase trend. The linear regressions, with goodness of fit values ranging from 0.981 to 0.997, help filter out the staircase noise. The regressions are overlaid on the plots in Figures 5.1-5.5. These plots are representative of the experimental trends observed for all of the tests, however, more non-linear behavior was evident in some of the other tests.

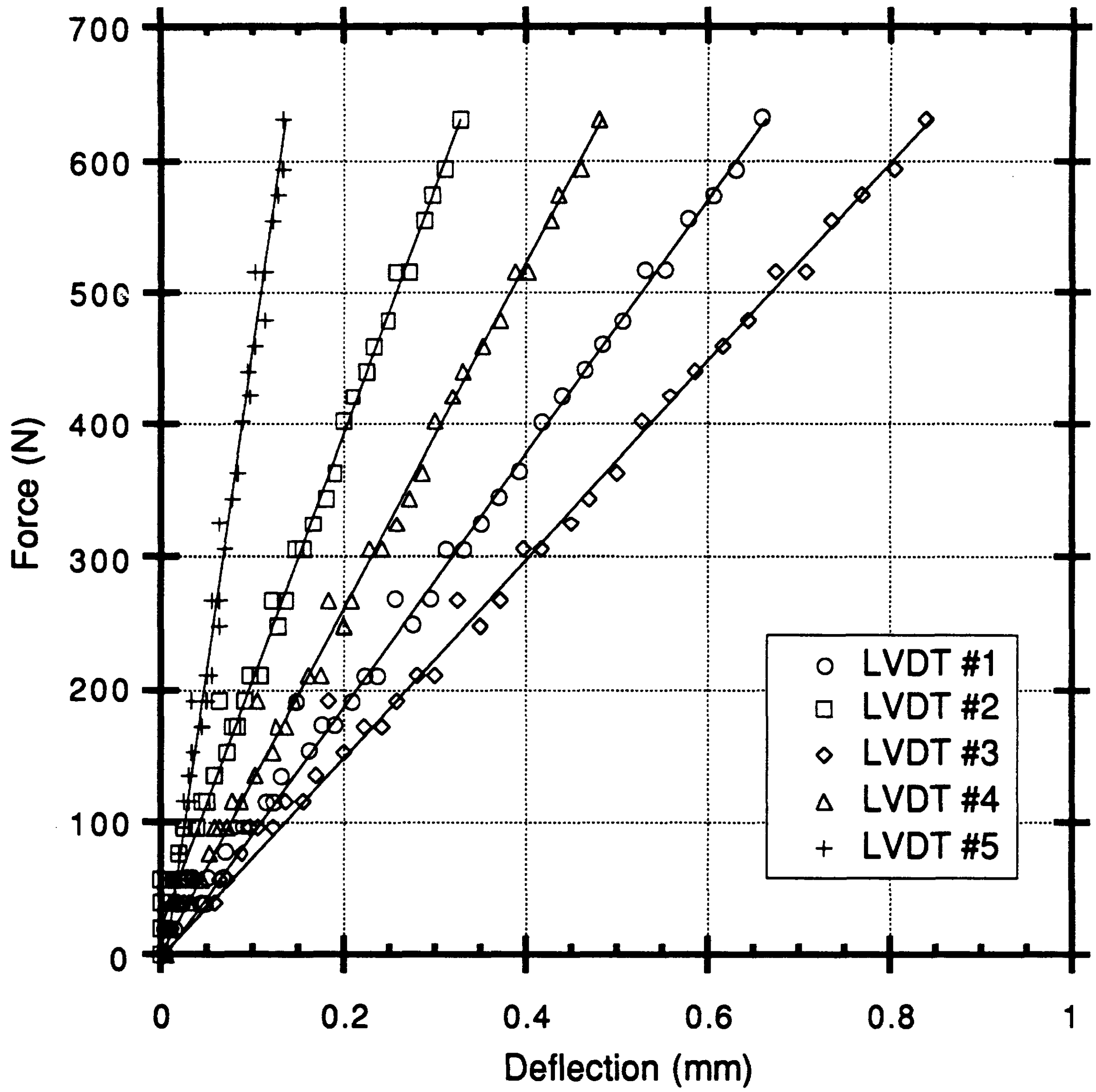

Figure 5.1 Load-deflection data for specimen A-1 loaded off-center by the URPP with all four edges clamped.

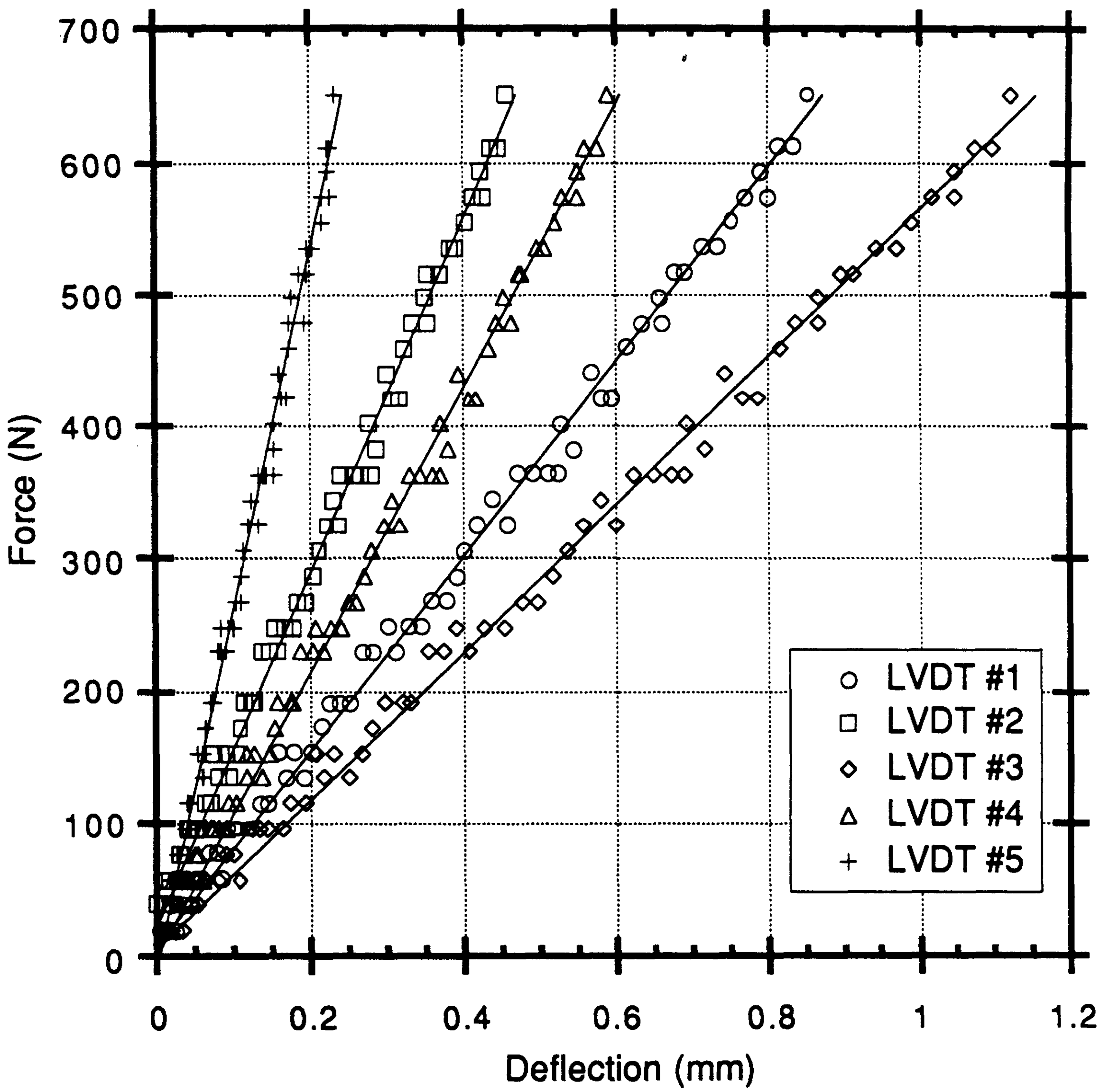

Figure 5.2 Load-deflection data for specimen A-1 loaded off-center by the URPP with x edges simply supported and y edges clamped.

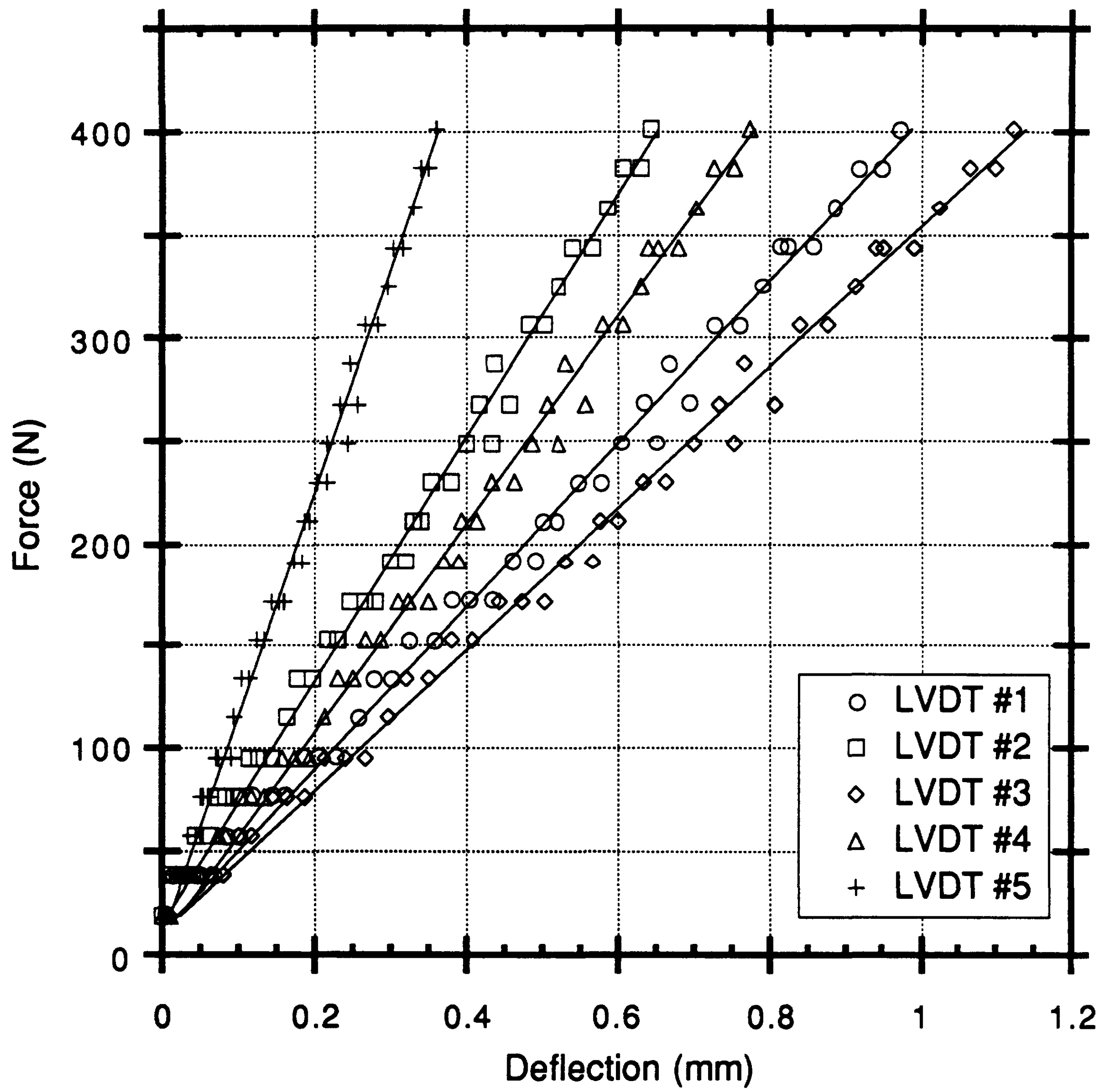

Figure 5.3 Load-deflection data for specimen A-1 loaded off-center by the URPP with all four edges simply supported.

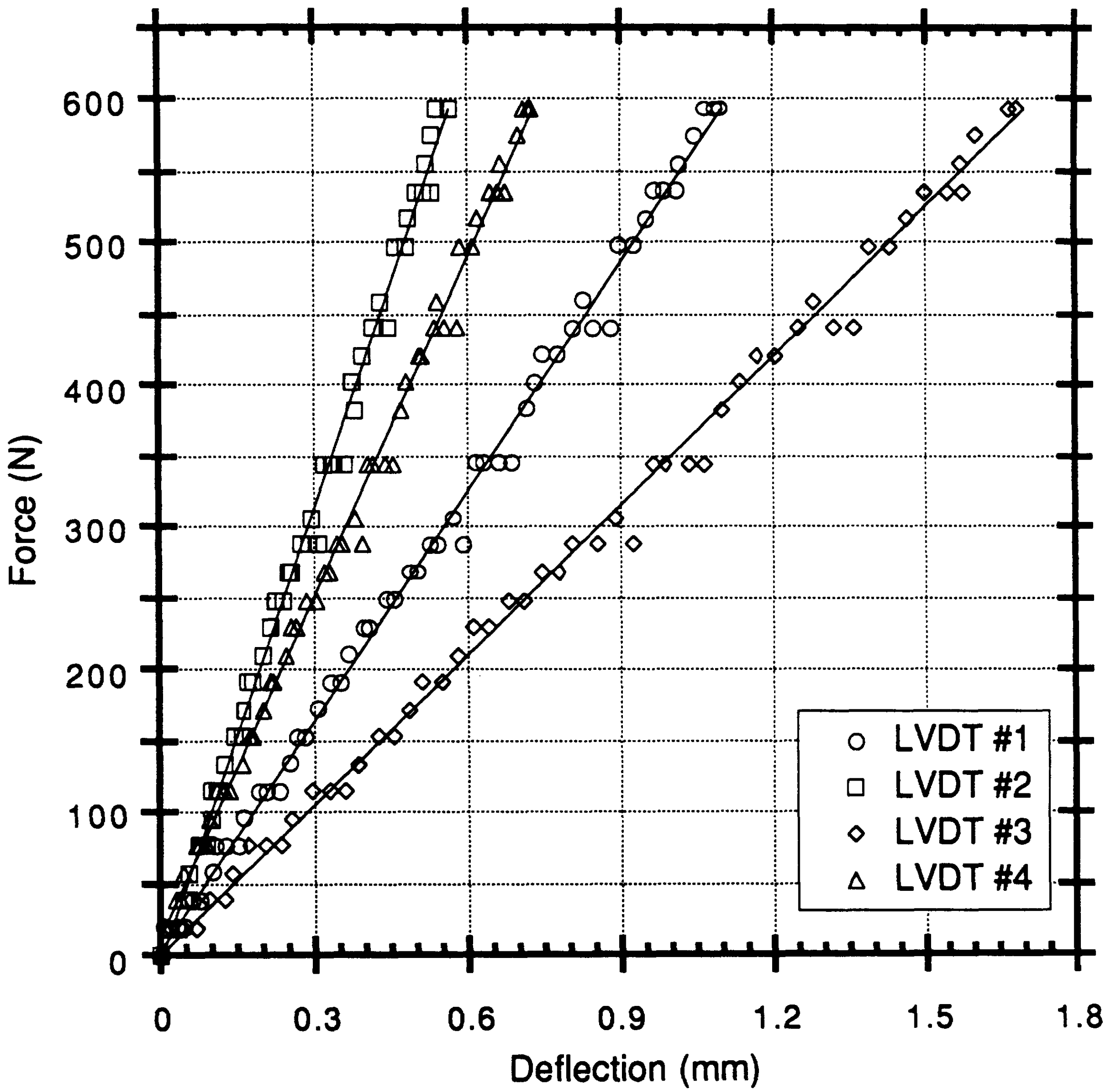

Figure 5.4 Load-deflection data for specimen A-1 loaded off-center by the URPP with x edges free and y edges clamped.

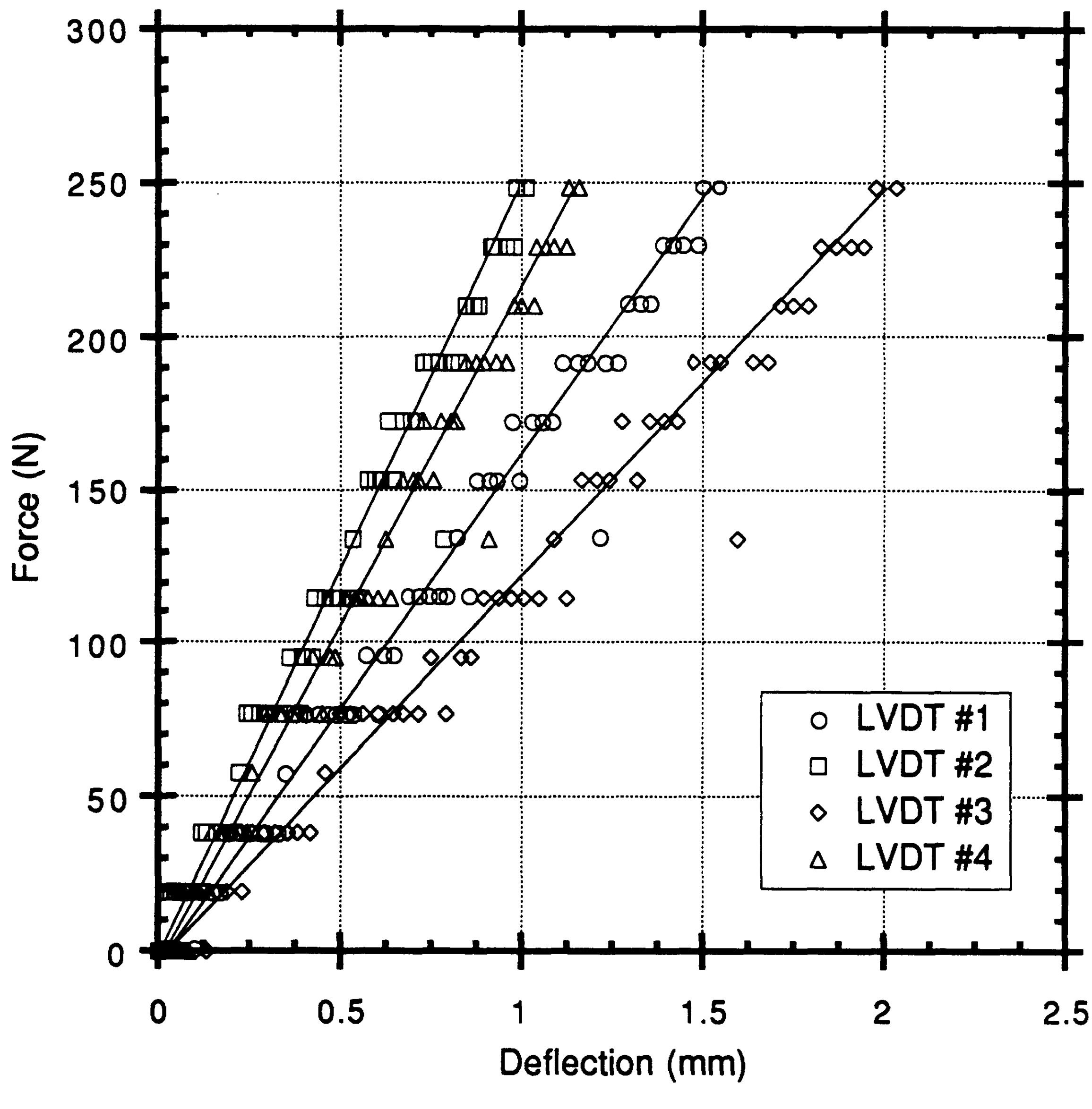

Figure 5.5 Load-deflection data for specimen A-1 loaded off-center by the URPP with x edges free and y edges simply supported.

5.2 Forced Vibration Tests

The forced vibration tests allowed approximate natural mode shapes and frequencies to be determined. During testing, sketches were made of all mode shapes and frequencies and photographs were taken of representative mode shapes for each specimen type.

5.2.1 Data Reduction

Average modal frequencies and the range over which these frequencies occurred, were calculated for each specimen type. The mode shapes documented in the following section occurred in at least two of the three plates for each specimen type. Single occurrences were discarded as manufacturing/testing anomalies. Excitations at 630 and 1200 Hz were found to be common across all the plates, and were discarded as natural frequencies of the jig, shaker, and/or loading spring.

The figures in the following section are reverse video scans of the actual photographs. Thus, the black composite plates appear white and the salt, used to accentuate the mode shapes, appears black. Shadows along the edge of the plate, caused by the sides of the jig, appear lighter than the rest of the plate. The small black rectangles in some of the scans are labels that were placed on the plates and the black dots mark the locations were the plate thickness was measured. Narrow black frames have been placed around the scans to help define the plate edges.

5.2.2 Natural Mode Shapes and Frequencies

Photographs were not taken of the aluminum control plates due to lighting difficulties with the shiny metallic surface. The mode shapes for an isotropic plate are, however, very well understood. It is customary to designate each shape by the respective x and y harmonics. The experimentally obtained frequencies for the aluminum control plates are listed in Table 5.1 following this convention.

Table 5.1 Experimental Modal Frequencies (Hz) for Aluminum Control Plates

		Mode (x direction harmonic – y direction harmonic)				
B. C.'s	Spec.	1–1	2–1	1–2	2–2	3–1
CL–CL	I-2	475	888	1100	x	1588
SS–CL	I-2	490	780	1240	1482	1360
SS–SS	I-3	340	765	768	x	1450
FR–CL	I-2	355	424	x	x	827
FR–SS	I-2	192	280	771	x	525

x = not found experimentally

The reverse video scans for all the composite plate specimens are presented in Figures 5.6 through 5.25. Each figure shows the lowest four modes found experimentally. Higher modes were found for some specimens but have not been included here. The figures are organized by boundary condition and then by specimen type.

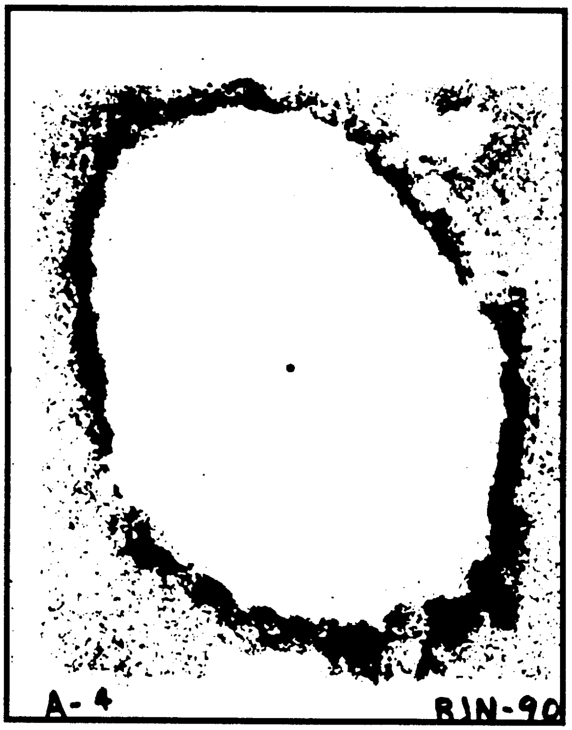

f = 475±7 Hz

f = 885±3 Hz

f = 1432±9 Hz

f = 1867±3 Hz

Figure 5.6 Four lowest experimentally detected mode shapes and frequencies for Specimen A with all four edges clamped.

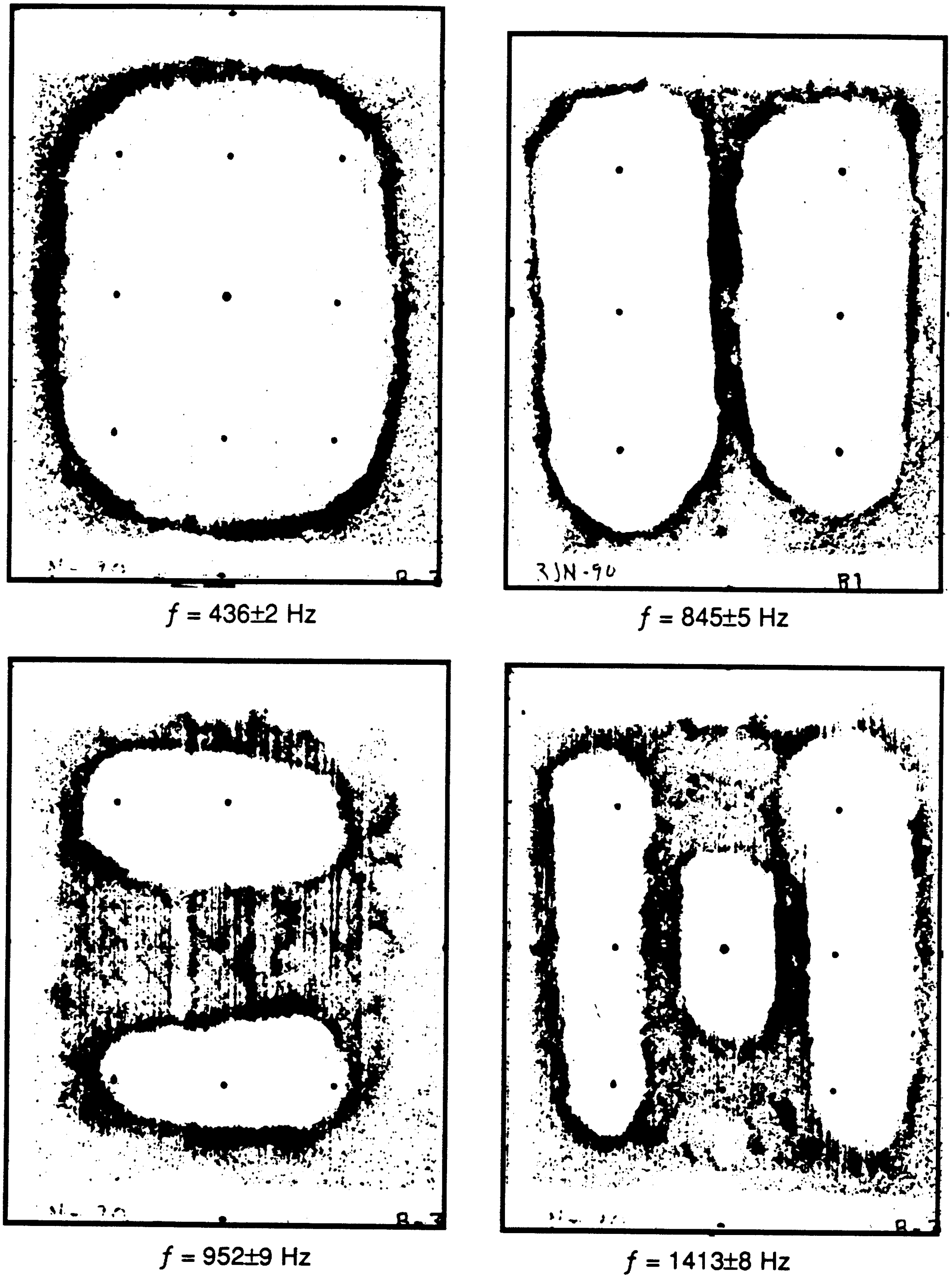

f = 436±2 Hz

f = 845±5 Hz

f = 952±9 Hz

f = 1413±8 Hz

Figure 5.7 Four lowest experimentally detected mode shapes and frequencies for Specimen B with all four edges clamped.

f = 744±2 Hz

f = 1046±19 Hz

f = 1420±20 Hz

f = 1867±2 Hz

Figure 5.8 Four lowest experimentally detected mode shapes and frequencies for Specimen C with all four edges clamped.

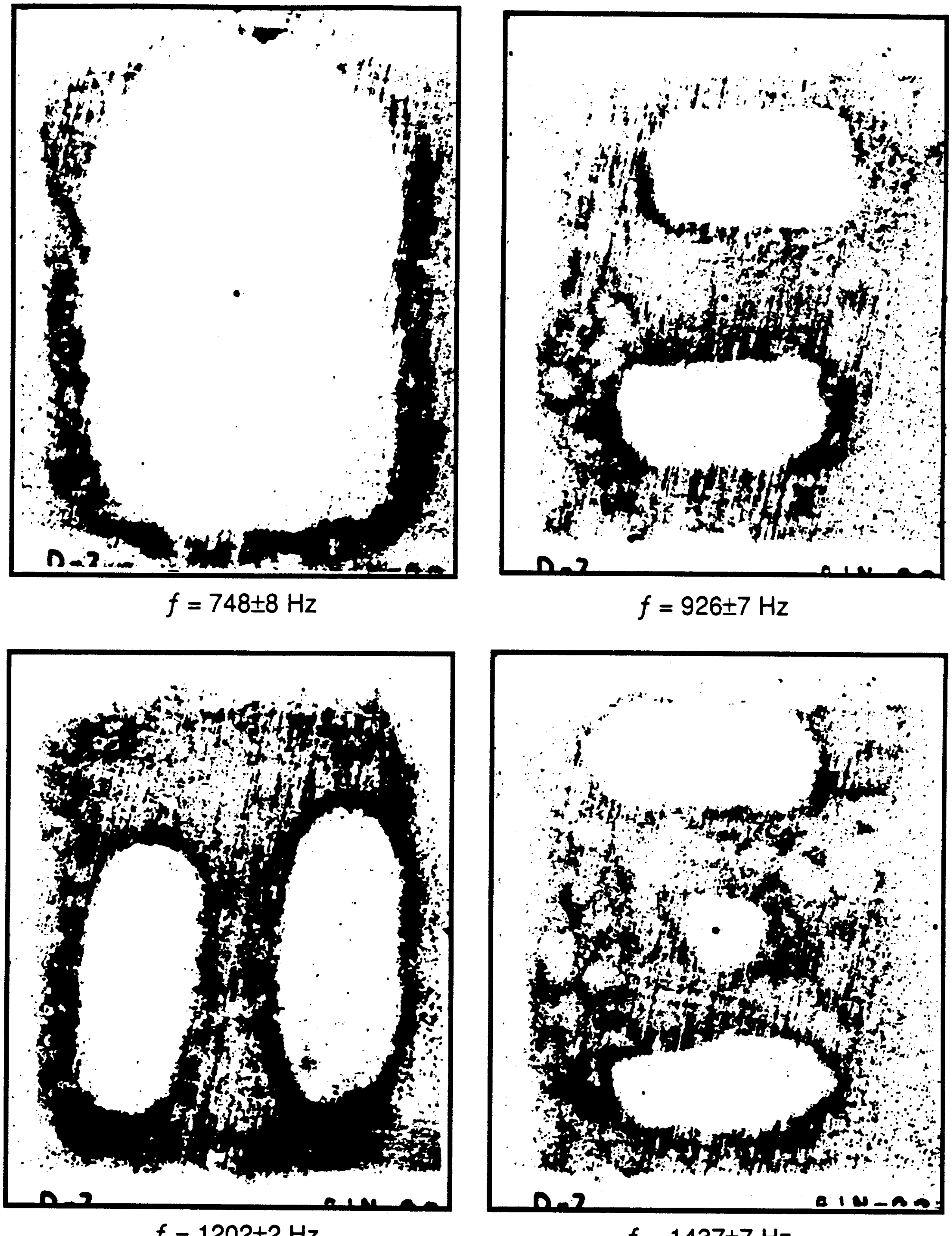

Figure 5.9 Four lowest experimentally detected mode shapes and frequencies for Specimen D with all four edges clamped.

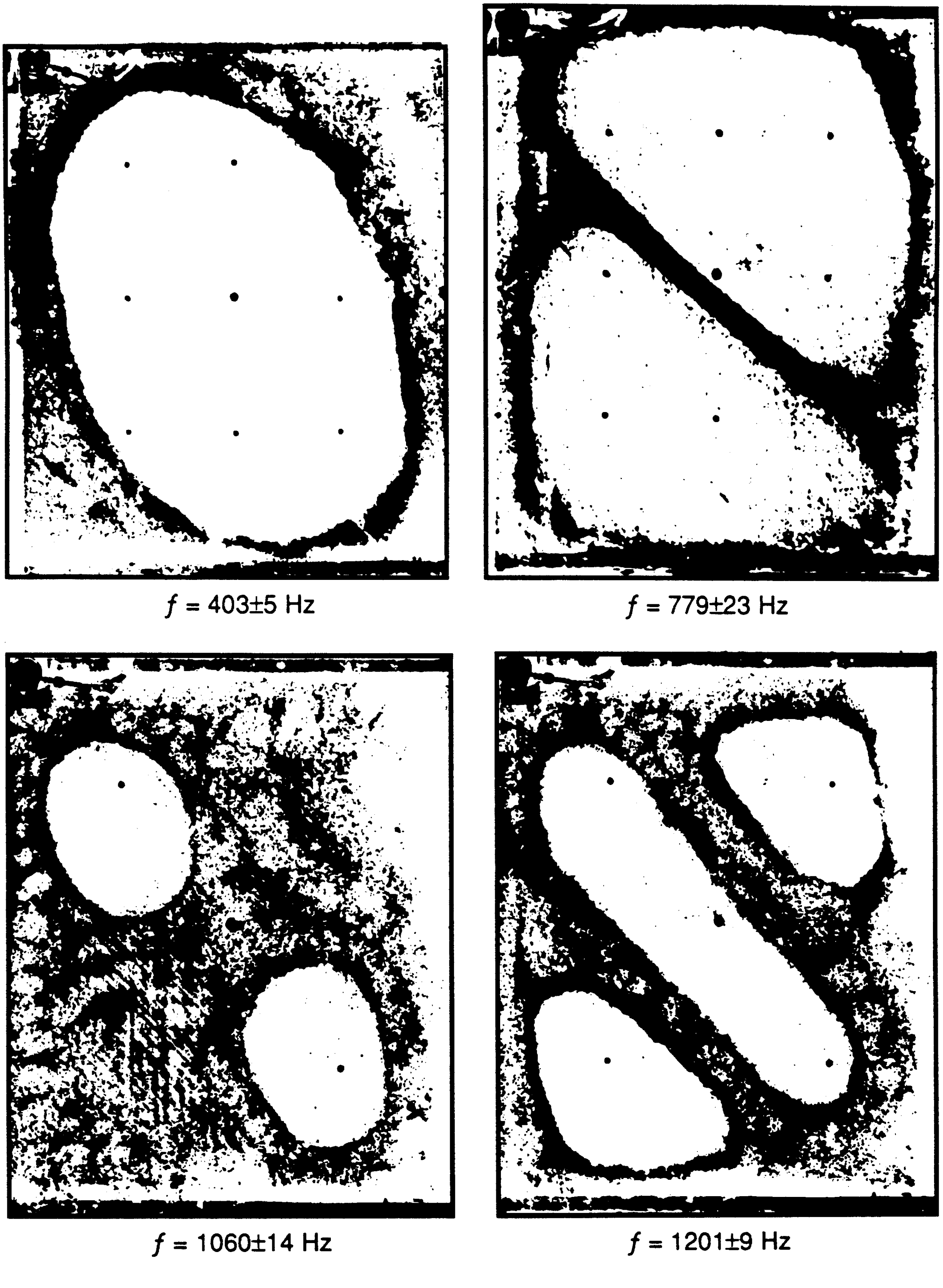

Figure 5.10 Four lowest experimentally detected mode shapes and frequencies for Specimen A with x edges (short edges) simply supported and y edges (long edges) clamped.

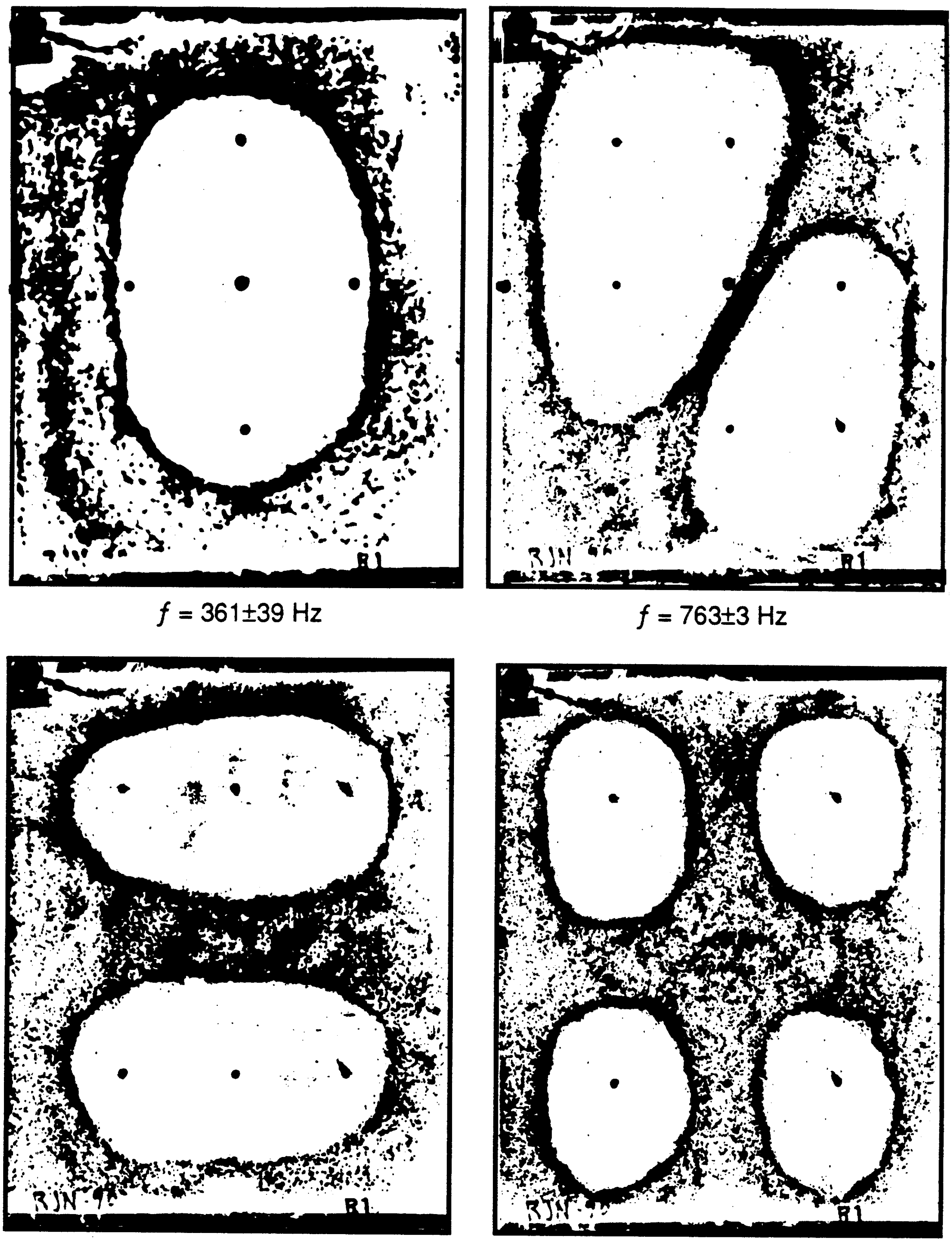

f = 361±39 Hz

f = 763±3 Hz

f = 778±21 Hz

f = 1204±25 Hz

Figure 5.11 Four lowest experimentally detected mode shapes and frequencies for Specimen B with x edges (short edges) simply supported and y edges (long edges) clamped.

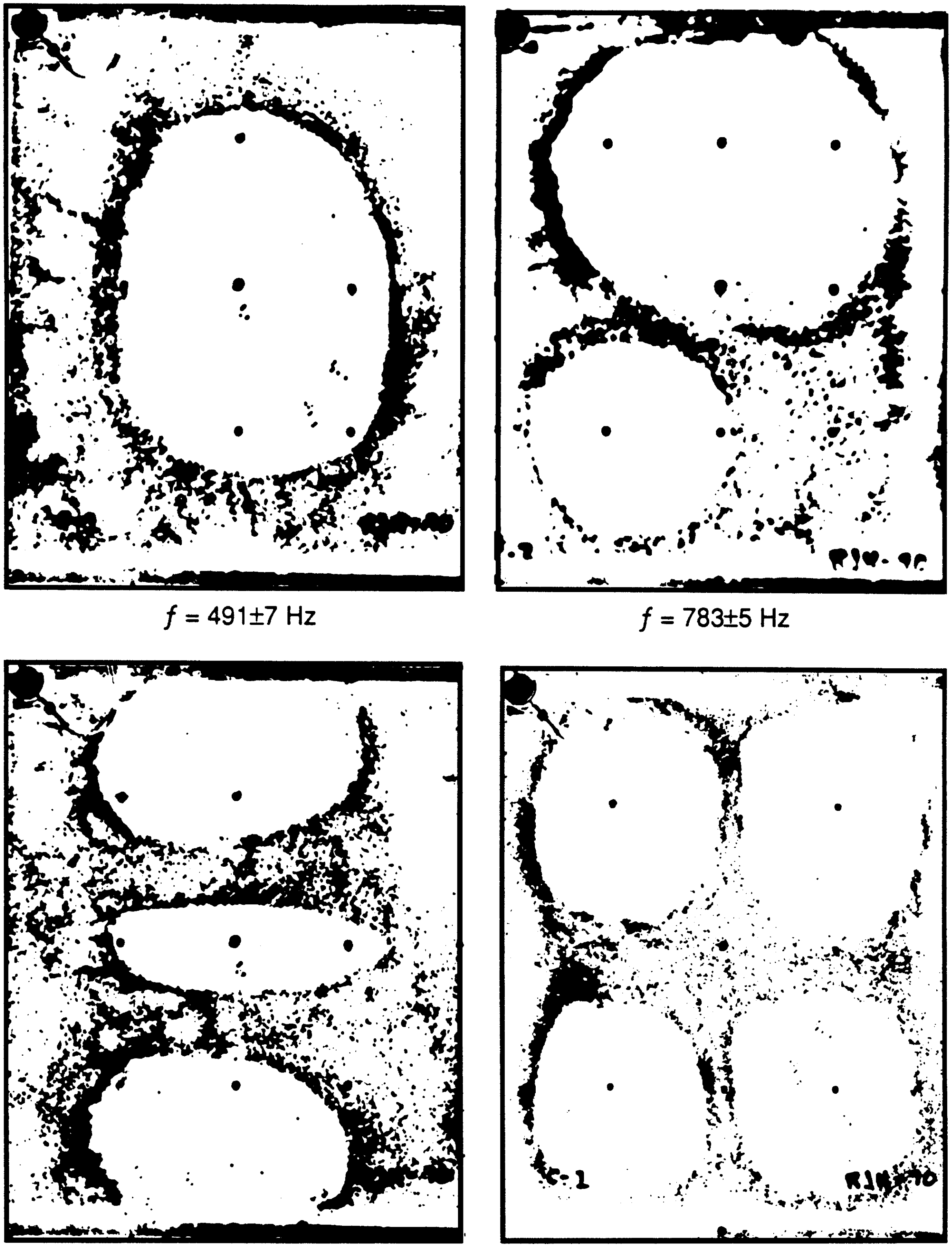

f = 491±7 Hz f = 783±5 Hz

f = 1500±12 Hz f = 1872±4 Hz

Figure 5.12 Four lowest experimentally detected mode shapes and frequencies for Specimen C with x edges (short edges) simply supported and y edges (long edges) clamped.

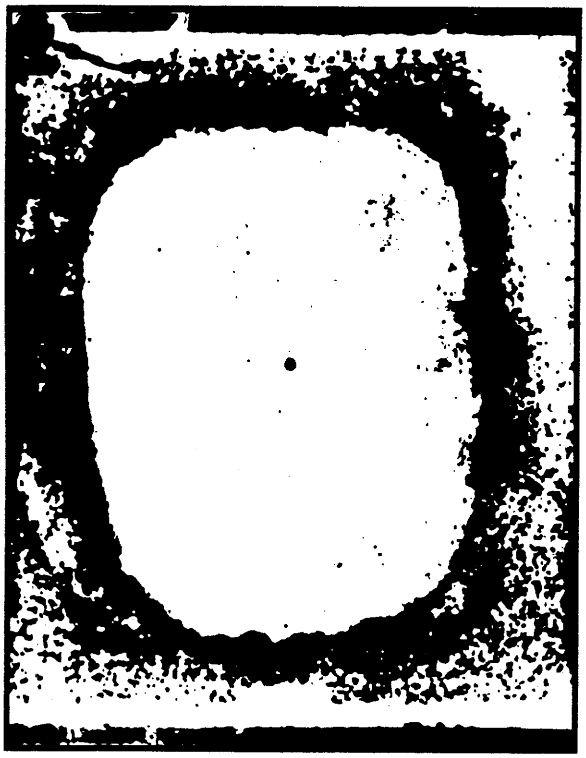

f = 499±3 Hz

f = 733±12 Hz

f = 1517±36 Hz

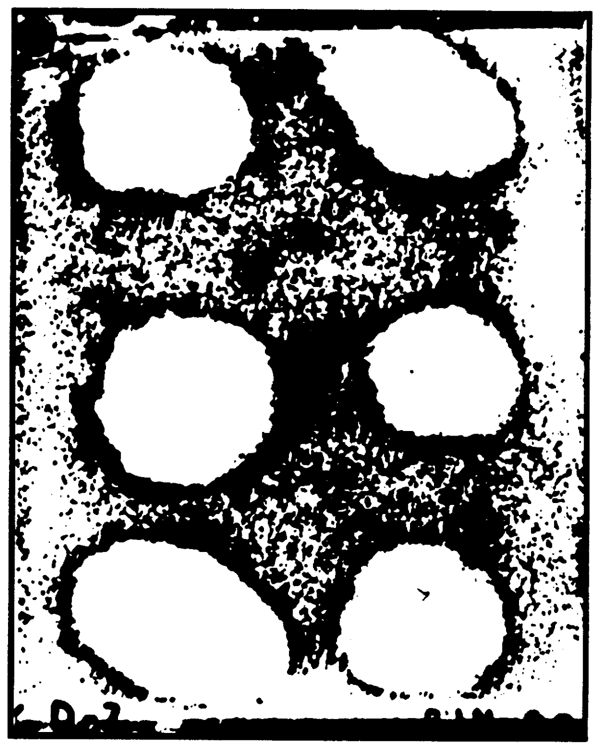

f = 1874±4 Hz

Figure 5.13 Four lowest experimentally detected mode shapes and frequencies for Specimen D with x edges (short edges) simply supported and y edges (long edges) clamped.

f = 319±13 Hz

f = 662±2 Hz

f = 778±5 Hz

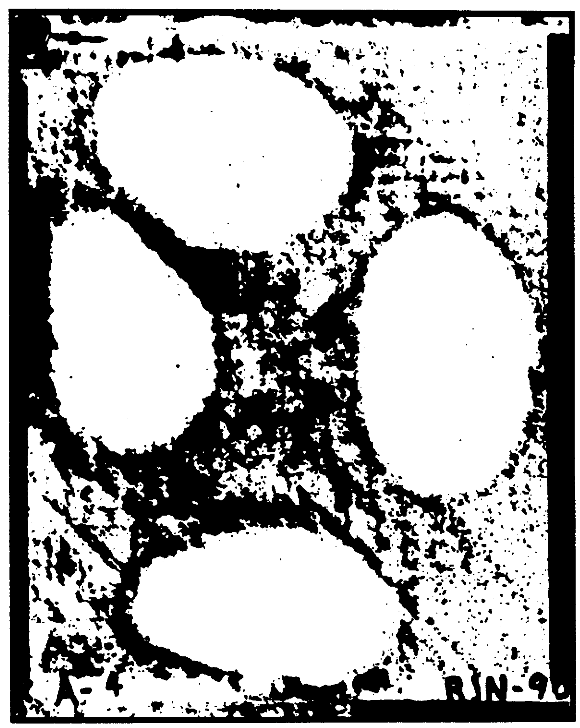

f = 1513±26 Hz

Figure 5.14 Four lowest experimentally detected mode shapes and frequencies for Specimen A with all four edges simply supported.

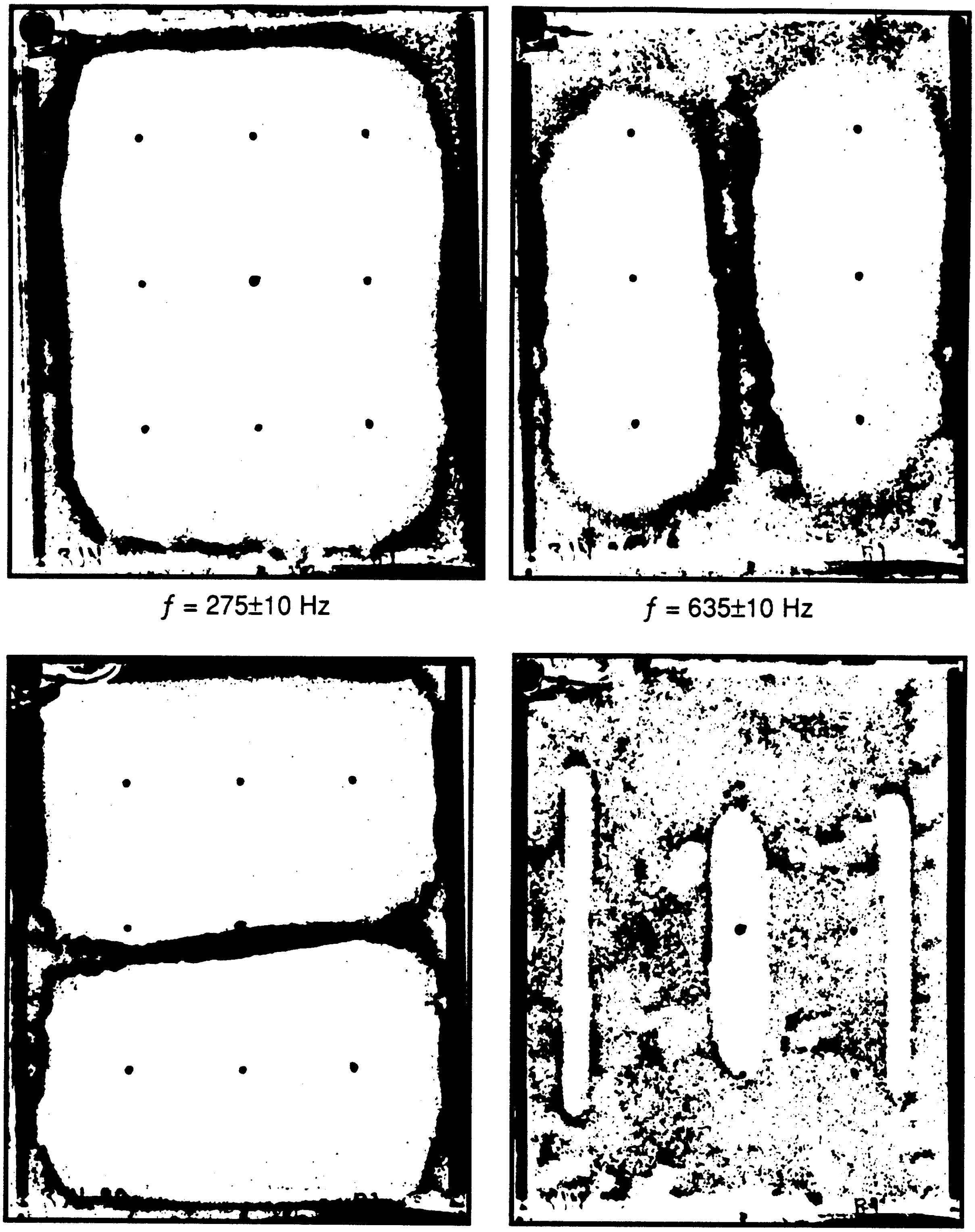

Figure 5.15 Four lowest experimentally detected mode shapes and frequencies for Specimen B with all four edges simply supported.

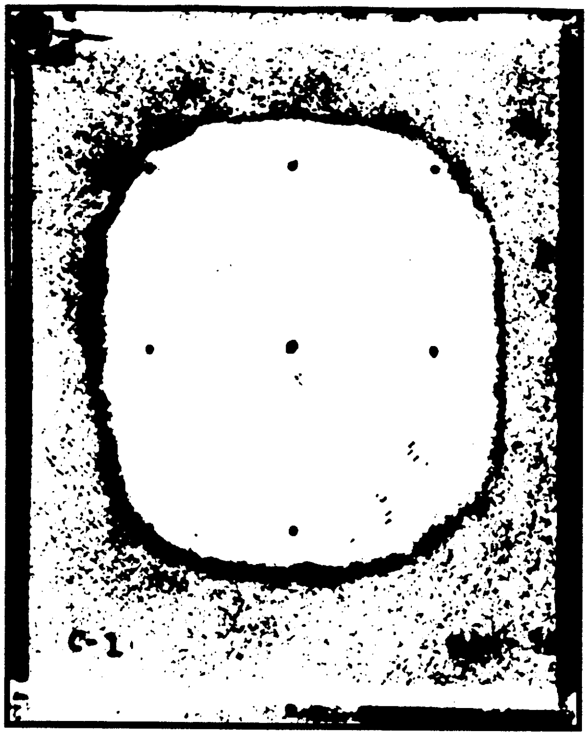

f = 366±16 Hz

f = 779±3 Hz

f = 929±5 Hz

f = 1487±4 Hz

Figure 5.16 Four lowest experimentally detected mode shapes and frequencies for Specimen C with all four edges simply supported.

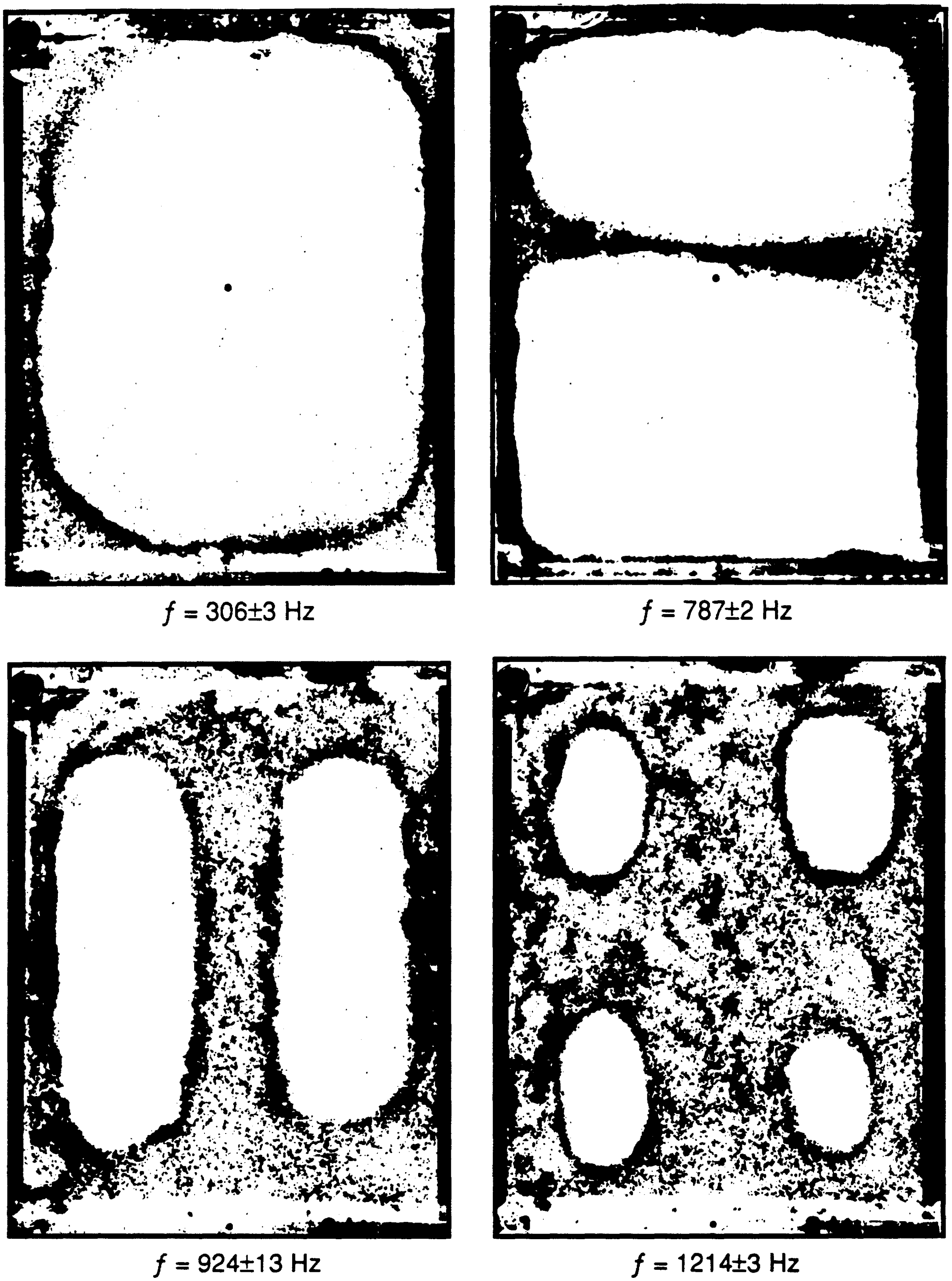

Figure 5.17 Four lowest experimentally detected mode shapes and frequencies for Specimen D with all four edges simply supported.

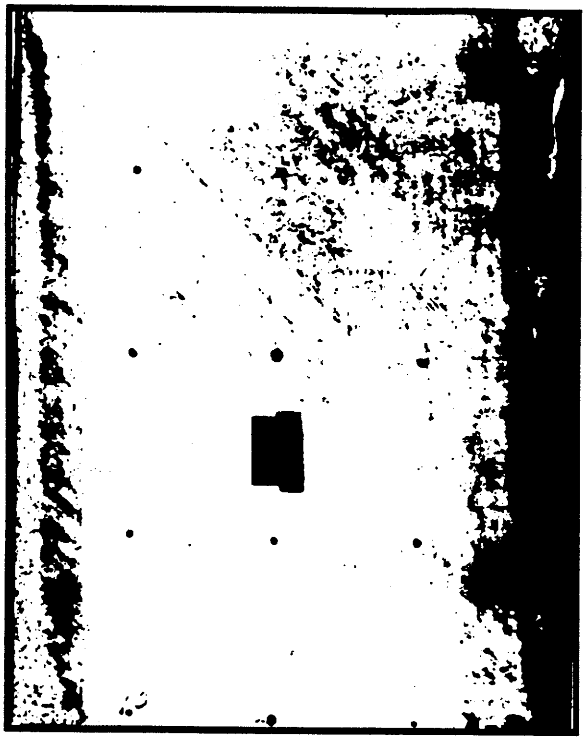

f = 305±3 Hz

f = 352±2 Hz

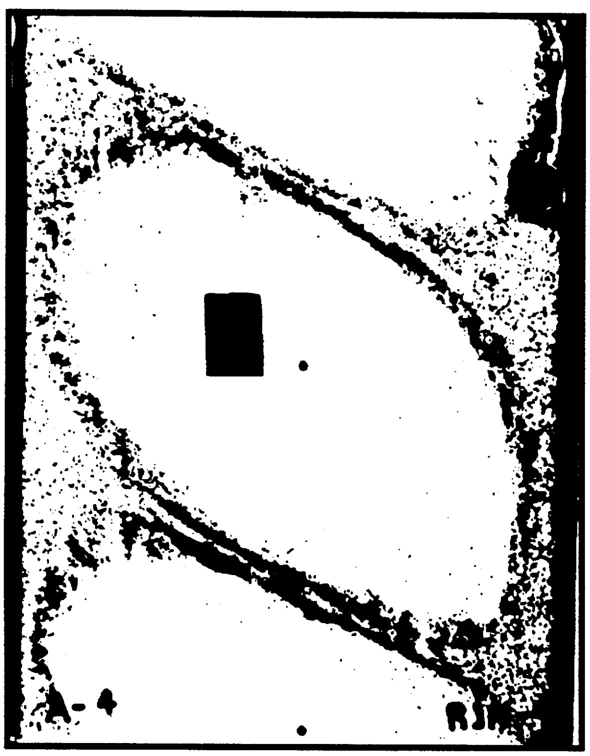

f = 785±2 Hz

f = 774±5 Hz

Figure 5.18 Four lowest experimentally detected mode shapes and frequencies for Specimen A with x edges (short edges) free and y edges (long edges) clamped.

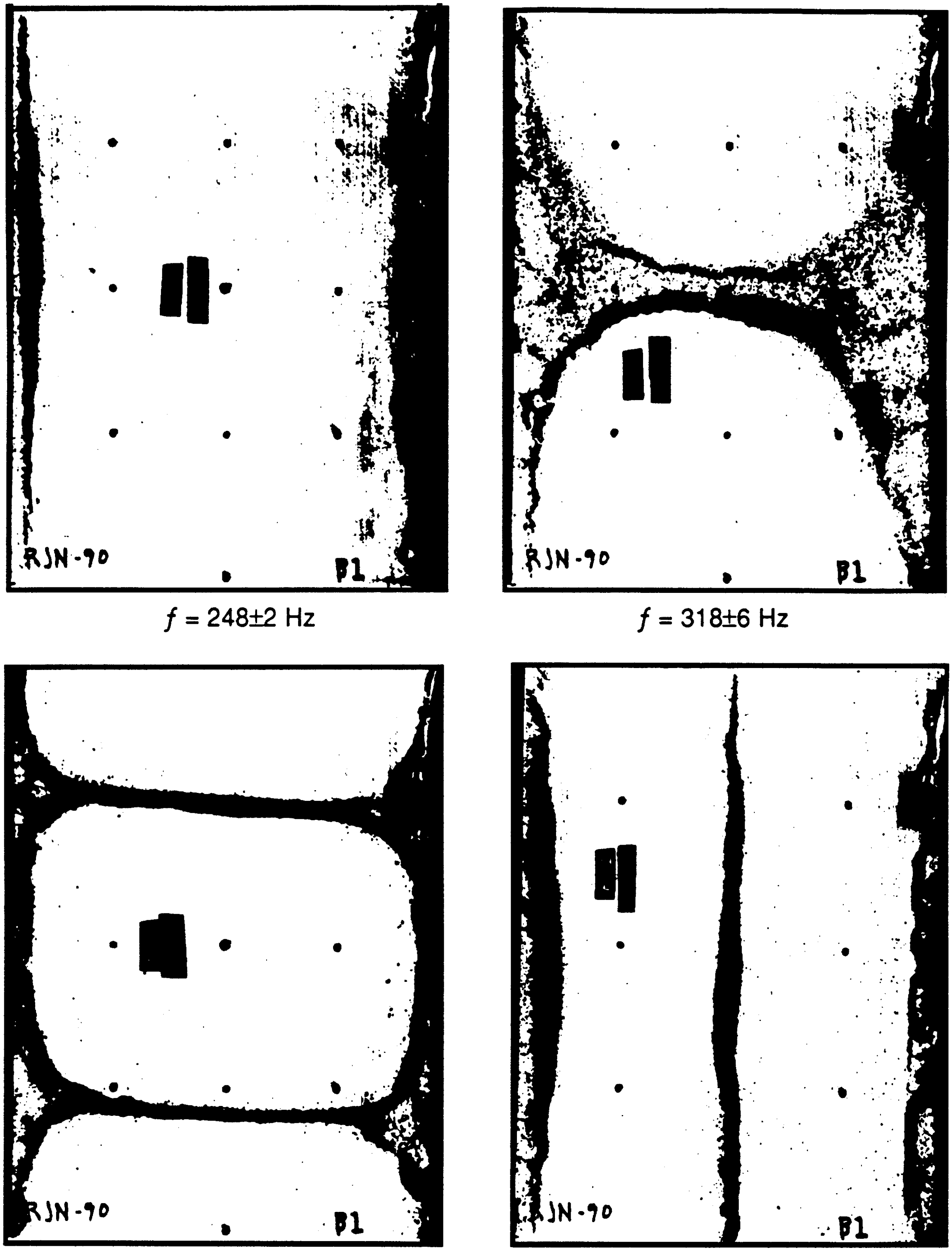

f = 248±2 Hz

f = 318±6 Hz

f = 584±4 Hz

f = 689±7 Hz

Figure 5.19 Four lowest experimentally detected mode shapes and frequencies for Specimen B with x edges (short edges) free and y edges (long edges) clamped.

f = 382±4 Hz

f = 504±3 Hz

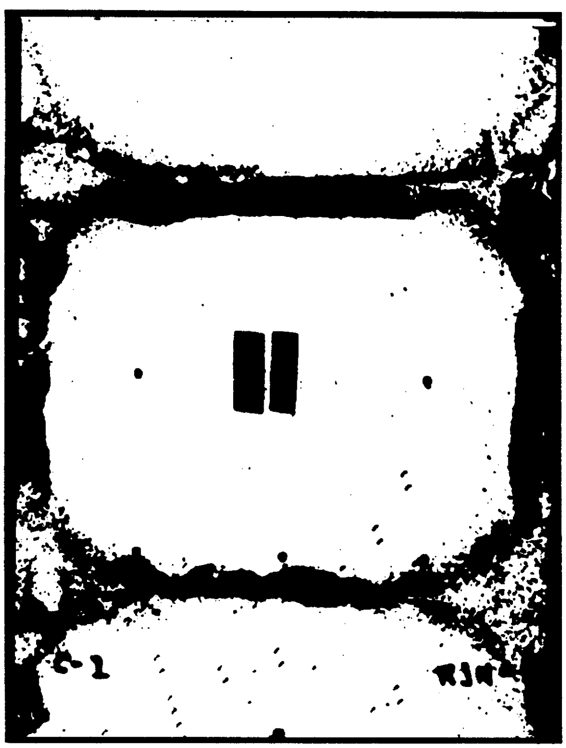

f = 839±4 Hz

f = 1389±48 Hz

Figure 5.20 Four lowest experimentally detected mode shapes and frequencies for Specimen C with x edges (short edges) free and y edges (long edges) clamped.

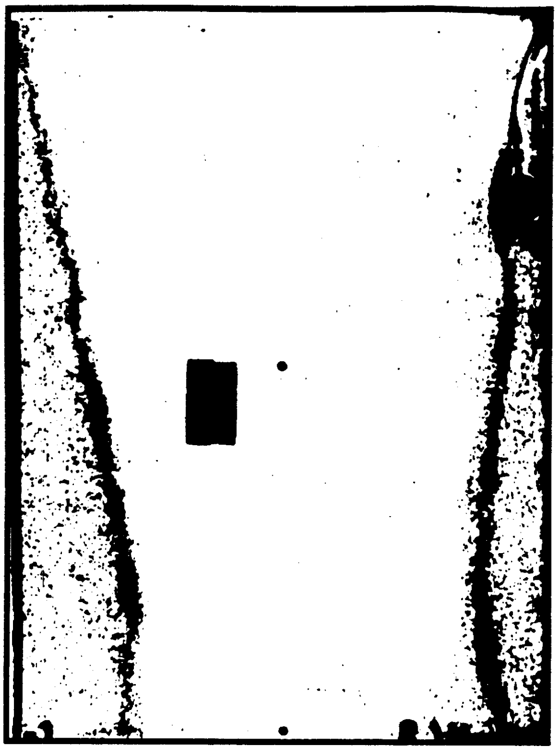

f = 354±2 Hz

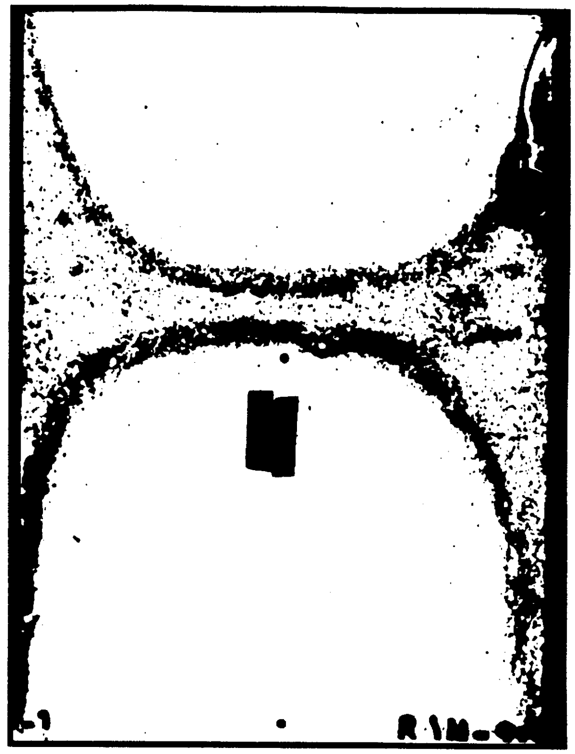

f = 397±3 Hz

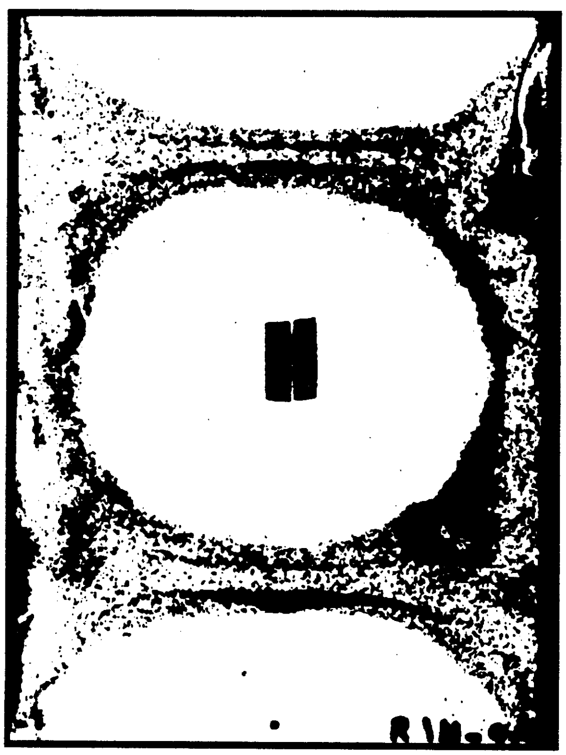

f = 617±26 Hz

f = 917±5 Hz

Figure 5.21 Four lowest experimentally detected mode shapes and frequencies for Specimen D with x edges (short edges) free and y edges (long edges) clamped.

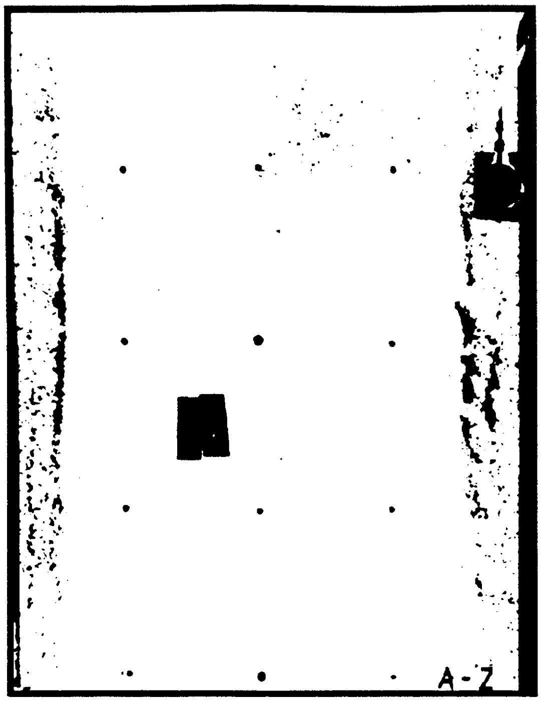

f = 194±3 Hz

f = 248±4 Hz

f = 483±11 Hz

f = 759±7 Hz

Figure 5.22 Four lowest experimentally detected mode shapes and frequencies for Specimen A with x edges (short edges) free and y edges (long edges) simply supported.

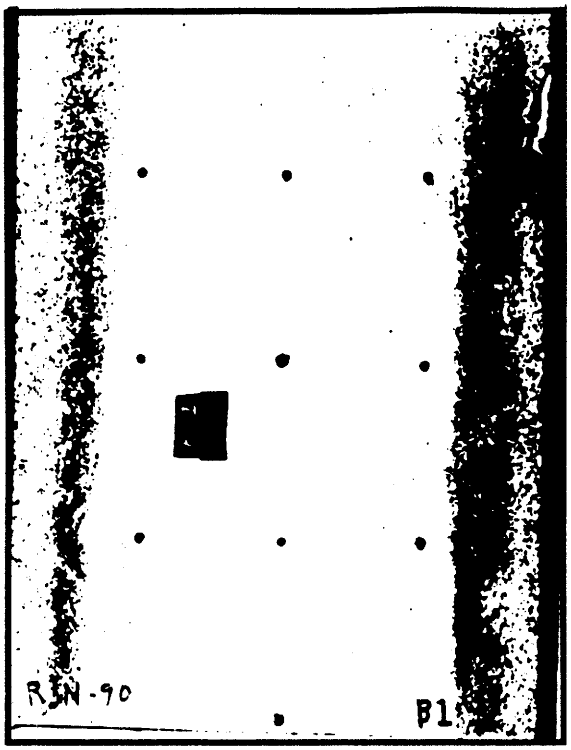

f = 168±3 Hz

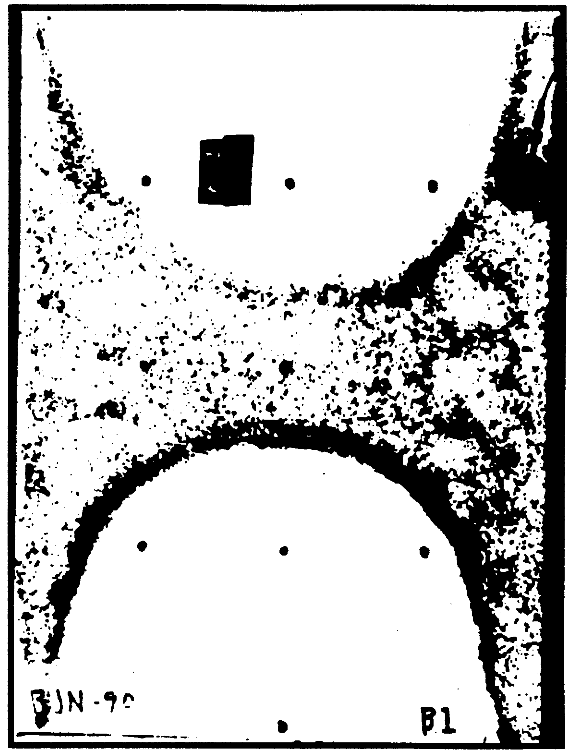

f = 247±3 Hz

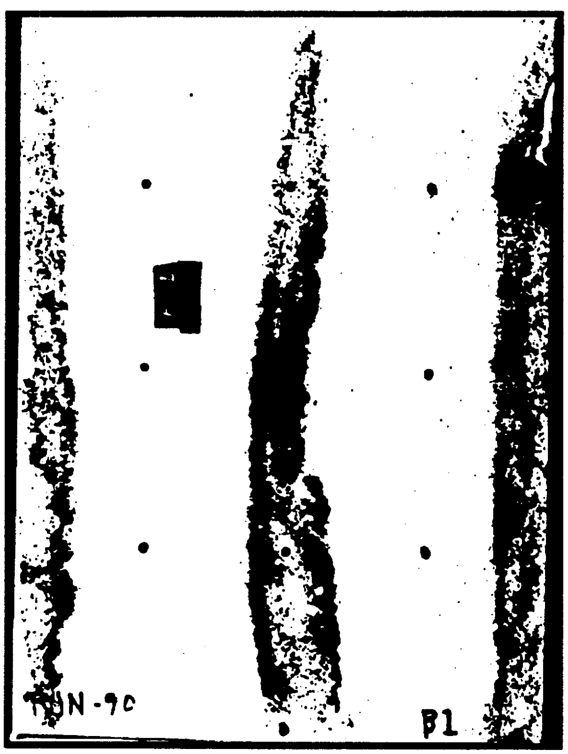

f = 501±9 Hz

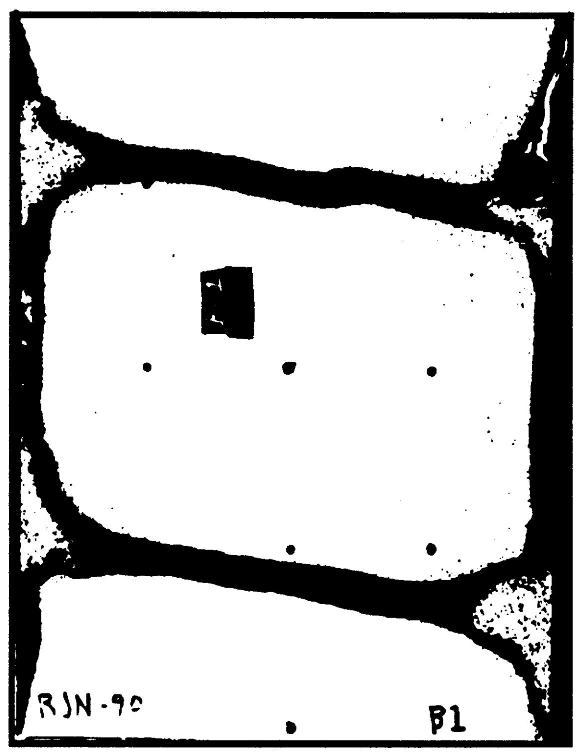

f = 542±2 Hz

Figure 5.23 Four lowest experimentally detected mode shapes and frequencies for Specimen B with x edges (short edges) free and y edges (long edges) simply supported.

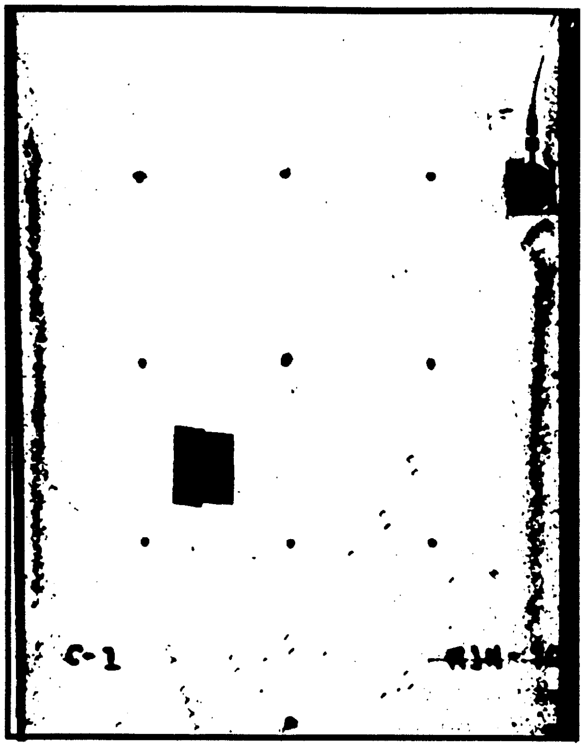

f = 211±9 Hz

f = 390±4 Hz

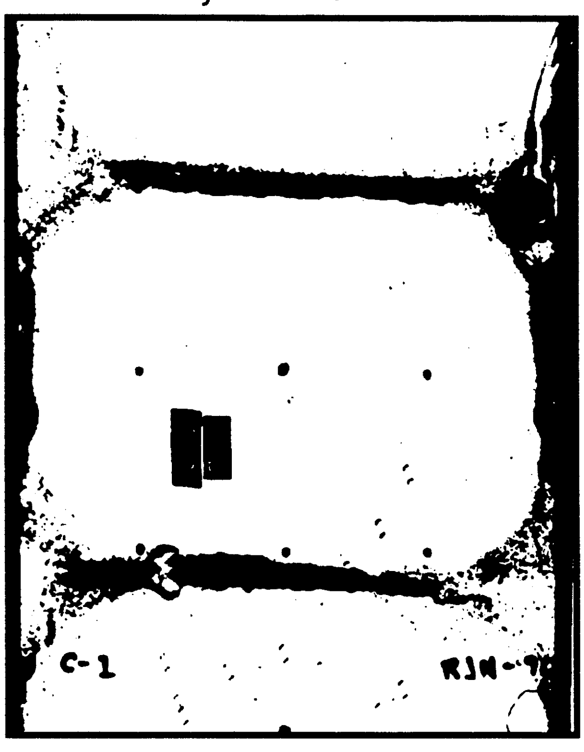

f = 733±6 Hz

f = 776±4 Hz

Figure 5.24 Four lowest experimentally detected mode shapes and frequencies for Specimen C with x edges (short edges) free and y edges (long edges) simply supported.

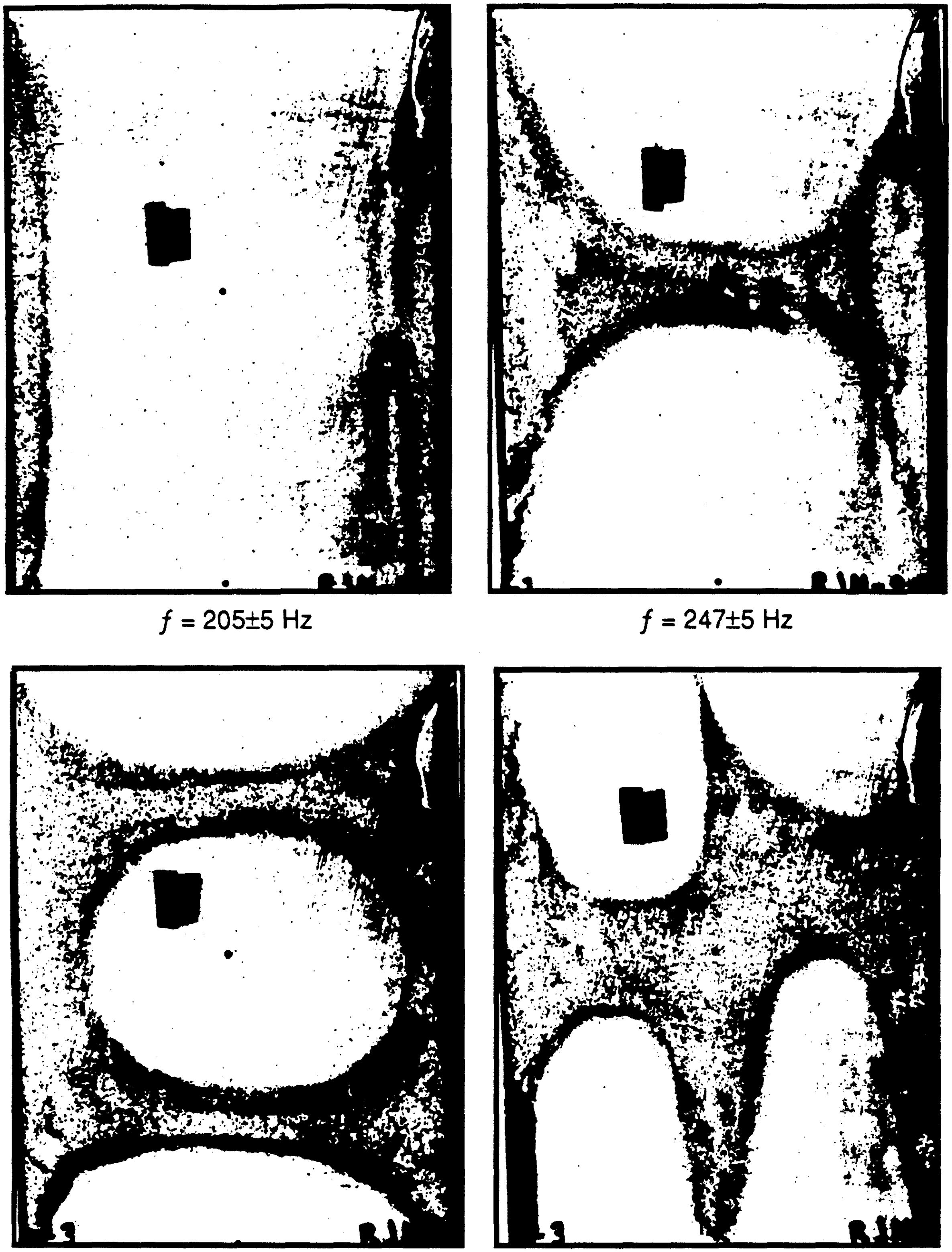

Figure 5.25 Four lowest experimentally detected mode shapes and frequencies for Specimen D with x edges (short edges) free and y edges (long edges) simply supported.

Chapter 6

Analytical Results

This chapter contains the results of all the analysis conducted as part of this investigation. A brief comparison of results from Kirchhoff and Mindlin plate theories is presented and the convergence of solution techniques is discussed. Comparisons of the analytical techniques that include shear deformation are made for most of the conditions investigated experimentally. Natural mode shapes and frequencies, obtained from the Rayleigh-Ritz model, are presented for many of the conditions investigated experimentally. Analytical stiffnesses (N/mm), corresponding to the experimental stiffnesses found for each transducer point, are tabulated in Appendix H.

6.1 Comparison of Kirchhoff and Mindlin Plate Theories

The difference between Kirchhoff and Mindlin plate theory becomes important for thick plates or plates with a low transverse shear stiffness. The thicker the plate or the lower the transverse shear stiffness, the more important this difference will become. Although several of the experimental specimens have a low transverse shear stiffness, they are still relatively thin and therefore exhibit only minor transverse shear deformation.

Figure 6.1 shows the analytical centerline deflections for Specimen B, under a centered point load of 100 Newtons with all four edges clamped, for both Kirchhoff and Mindlin plate theories. Both analyses are based on the 9 x 9 mode Rayleigh-Ritz model. The Kirchhoff curve was produced from the Mindlin solution by raising the transverse shear stiffnesses by three orders of magnitude, effectively causing infinite transverse shear stiffness, in accordance with Kirchhoff plate theory. For reference, the shear stiffness of

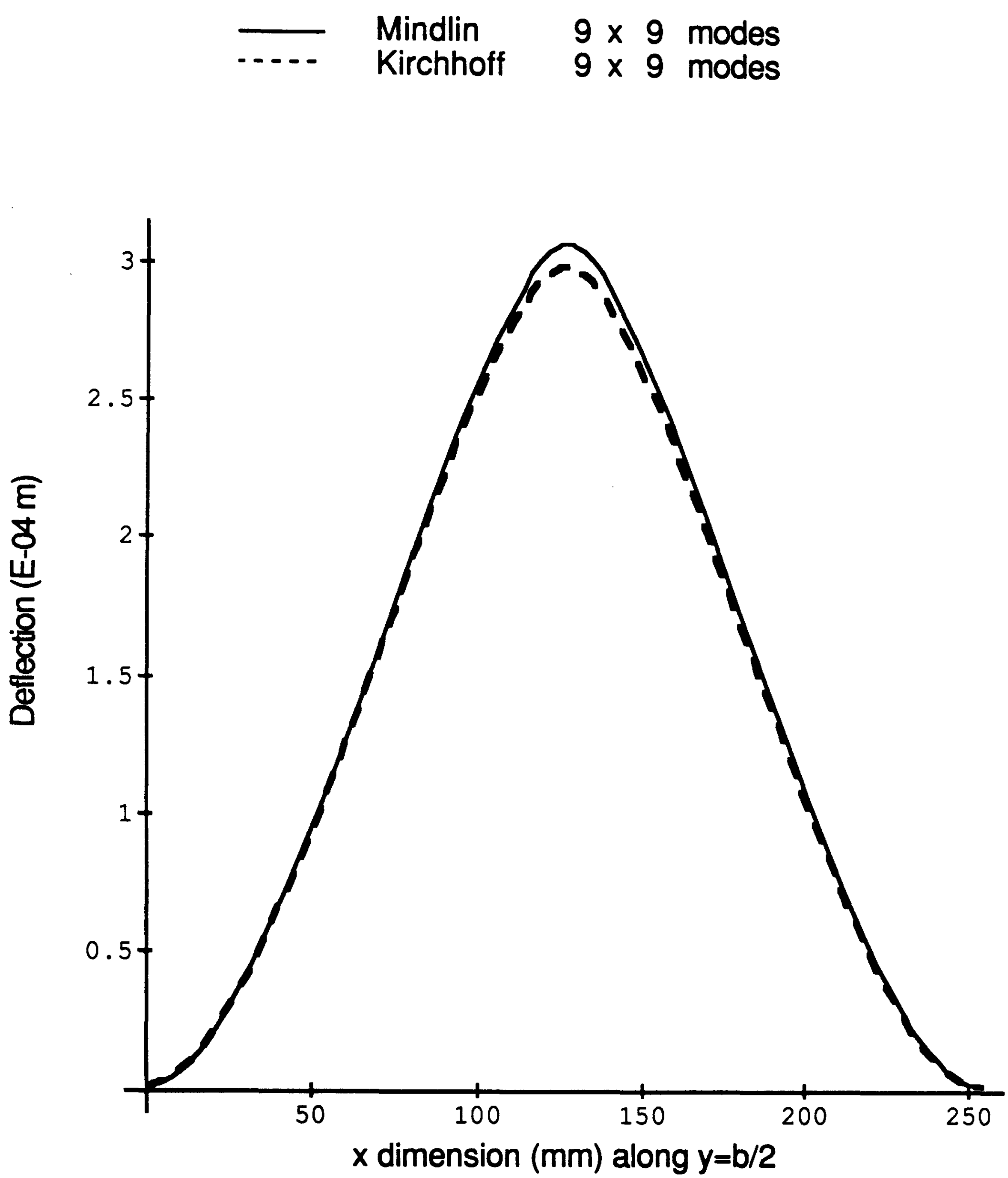

Figure 6.1 Comparison of Kirchhoff and Mindlin deformations for Specimen B under a centered point load of 100 Newtons with all four edges clamped.

aluminum is seven times that of AS4/3501-6 tape. The difference in center deflections between the Kirchhoff and Mindlin curves is 2.8%. For Specimen I, which is isotropic and therefore has a moderate transverse stiffness, the difference is less than 1%, and is not graphically visible.

For the experimental specimens, going to Mindlin plate theory improves the natural frequency predictions by less than 1% for the first four modes, however, greater improvement will occur with higher modes. The analytical frequencies for two specimens for Kirchhoff and Mindlin theory as well as Mindlin theory with the rotary inertia, R_2, set to zero are presented. Table 6.1 shows the analytical frequencies, temporarily neglecting the bending-twisting coupling, for Specimen B with four edges simply supported. The fourth digit accuracy sacrifice for neglecting rotary inertia seems tolerable for the significant computational savings, as discussed in chapter four.

Table 6.1 Comparison of Natural Frequencies (Hz) for Specimen B with Four Edges Simply Supported

Mode	Kirchhoff	Mindlin ($R_2 = 0$)	Mindlin
1st	284.5	284.0	284.0
2nd	658.3	656.0	655.8
3rd	772.4	768.0	767.8
4th	1138.2	1129.9	1129.3

Table 6.2 shows the analytical frequencies for Specimen I with four edges simply supported. Again, the analysis of the isotropic plate benefits less from Mindlin theory than that of the laminated plates due to the difference in their transverse to longitudinal modulus ratio.

Table 6.2 Comparison of Natural Frequencies (Hz) for Specimen I with Four Edges Simply Supported

Mode	Kirchhoff	Mindlin ($R_2 = 0$)	Mindlin
1st	297.7	297.5	297.5
2nd	646.2	645.4	645.2
3rd	842.1	840.8	840.4
4th	1190.9	1188.2	1187.4

Although the specimens under consideration exhibit minor to negligible improvement with Mindlin plate theory, no generalizations should be made. Thicker plates of the same material and layup would exhibit more of a difference between the two theories.

6.2 Convergence of Constrained Navier and Rayleigh-Ritz Solutions

The Rayleigh-Ritz models were always run with 9 "contributing" beam functions in each direction, for a total of 81 modes. Unsymmetric problems used the first 9 modes, while symmetric problems used the first 9 odd modes in each direction. Figure 6.2 shows the convergence trend for Specimen B with four edges clamped and a centered point load. The 9 x 9 mode solution gives a reasonably well converged answer for the cases investigated.

The traditional Navier solution for four sides simply supported follows a convergence trend similar to the Rayleigh-Ritz model. In fact, for a simply supported plate without bending-twisting coupling, the Rayleigh-Ritz and the Navier solutions are identical. Thus, the traditional Navier solutions were also run with 9 x 9 modes.

The constrained Navier solution suffers from very slow convergence. Figure 6.3 compares the convergence trend of the constrained Navier solution with the 9 x 9 mode Rayleigh-Ritz solution for Specimen B, again with four edges clamped and a centered point load. The constrained Navier solutions

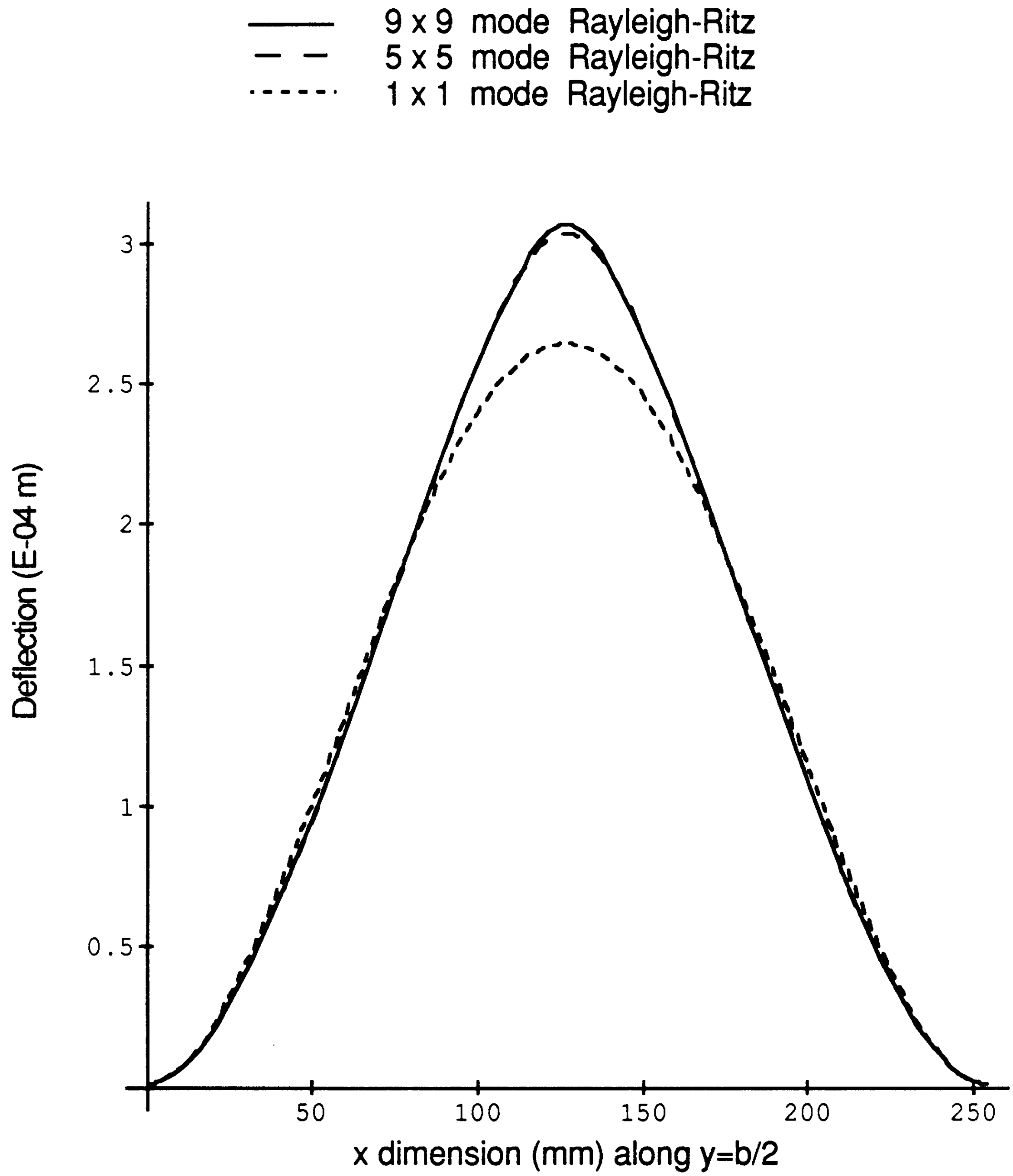

Figure 6.2 Convergence trend of Rayleigh-Ritz solution for Specimen B with four edges clamped and a centered point load.

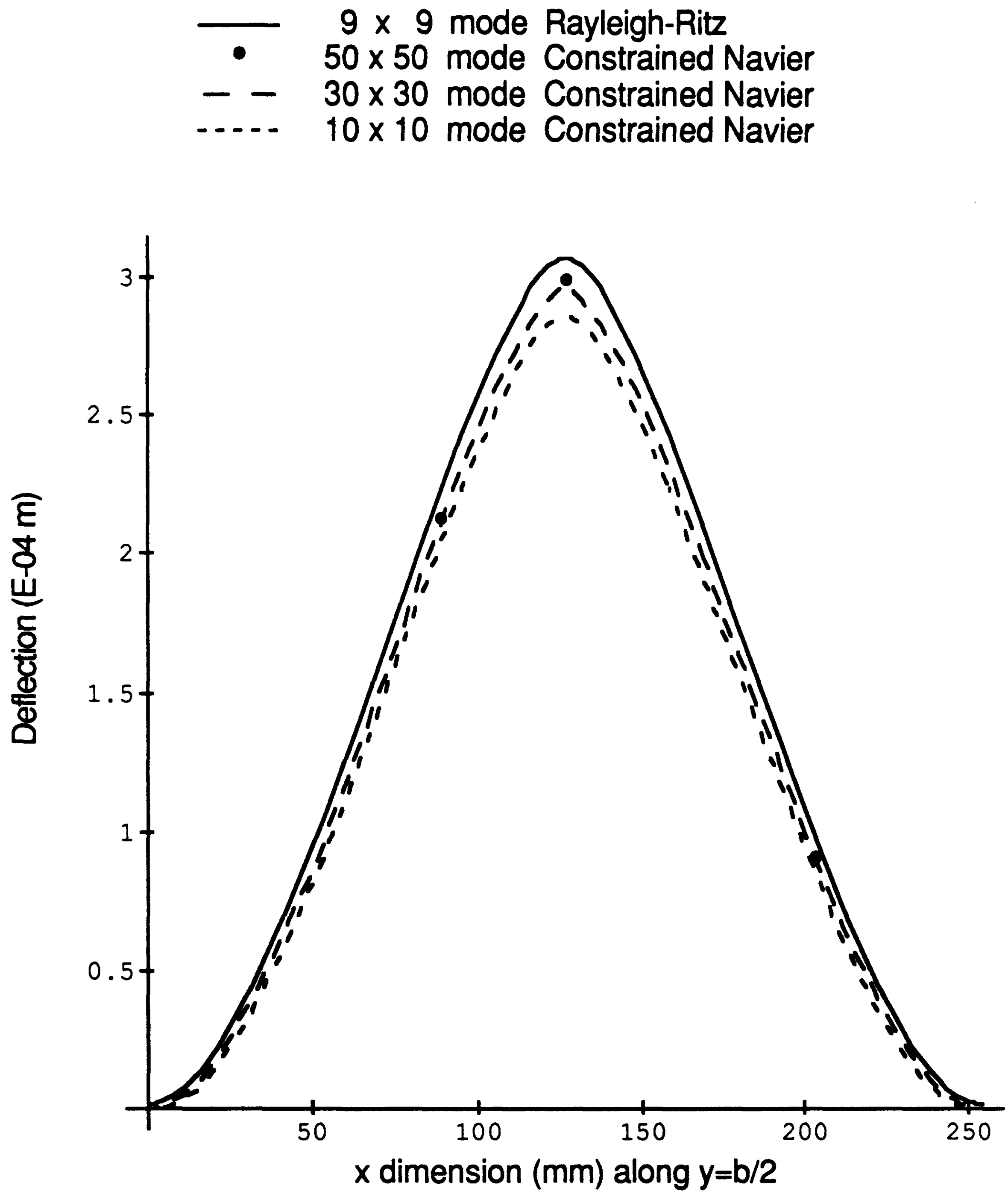

Figure 6.3 Convergence trend of constrained Navier solution for Specimen B with four edges clamped and a centered point load.

were run with 50 x 50 modes, due to computer limitations, although the level of convergence falls short of that achieved with the Rayleigh-Ritz models. In Figure 6.3, the 50 x 50 mode solution is depicted only at three points rather than as a continuous function, due to computer limitations encountered with graphing a function of 2500 terms. The displacement points chosen correspond to transducer locations in the experiments.

Hybrid models, for the x edges simply supported and y edges clamped case, were developed which used 9 Navier modes in the x direction and 50 constrained Navier modes in the y direction. These hybrid models also fall short of the level of convergence achieved with the Rayleigh-Ritz models.

6.3 Results for Centered Point Load

This section presents the analytical results for the centered point load problems that were investigated experimentally. The Rayleigh-Ritz, single mode polynomial potential functions, and Navier solutions are presented for the five specimens, for the boundary conditions four sides clamped and four sides simply supported. The solutions are presented in graphical form, in Figures 6.4 through 6.13, as plots of transverse displacement along the plate centerlines.

The Rayleigh-Ritz solutions use 9 x 9 modes while the potential function solutions are all single mode solutions. The constrained Navier solutions use 50 modes in a direction with clamped boundary conditions, while the traditional Navier solutions use only 9 modes in a direction with simply supported boundary conditions. More modes were used for the constrained Navier solution due to its slower convergence. Both Navier solutions are given only at discrete points.

Again, the constrained Navier, the traditional Navier, and the potential function solutions neglect the bending-twisting coupling that is present in Specimens A and B. This coupling is correctly accounted for in the Rayleigh-Ritz formulation. Specimen A, which has a strong bending-twisting coupling, is poorly modeled by the Navier solutions.

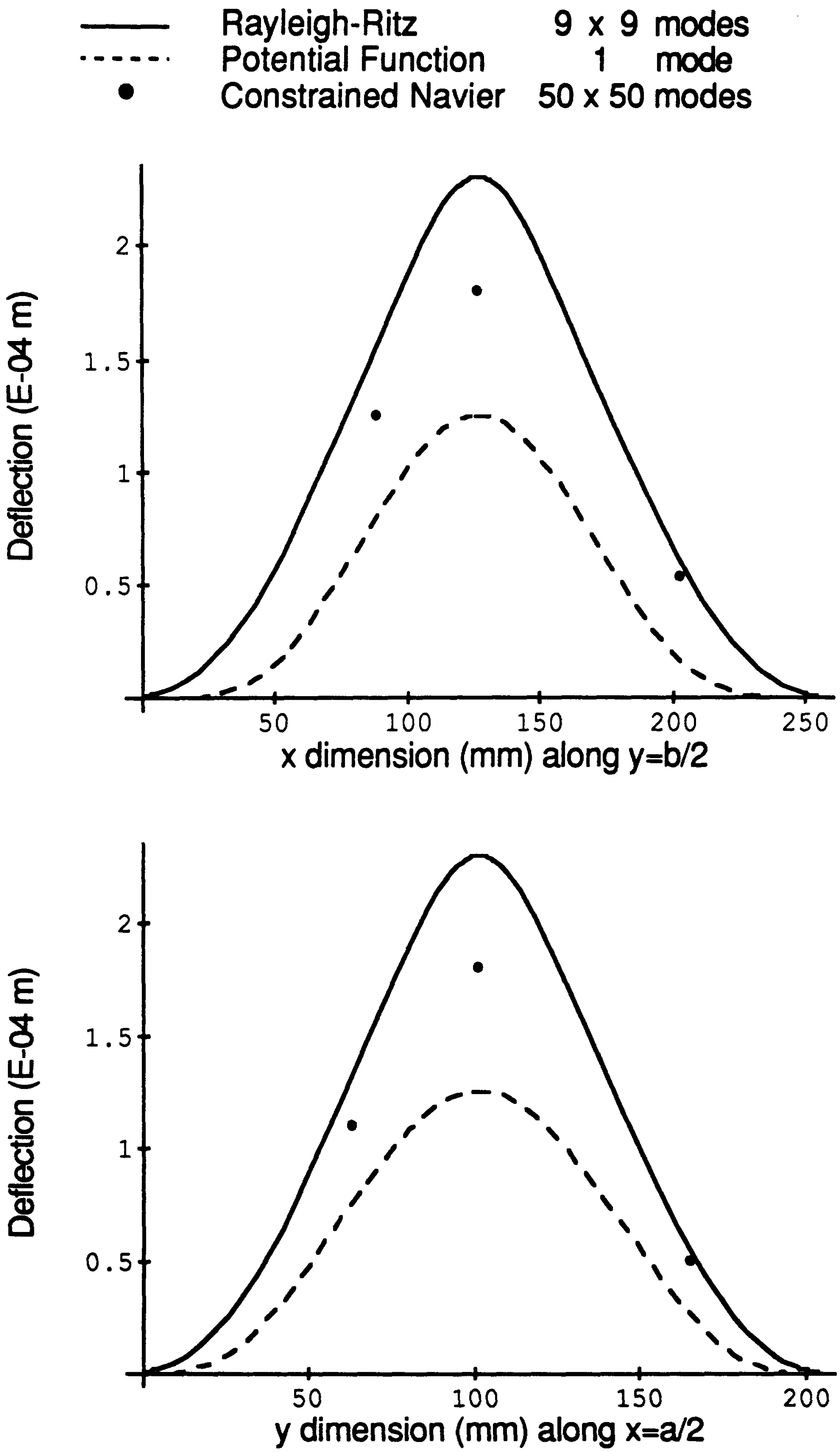

Figure 6.4 Transverse deflection for Specimen A, under a centered point load of 100 Newtons, with all four sides clamped.

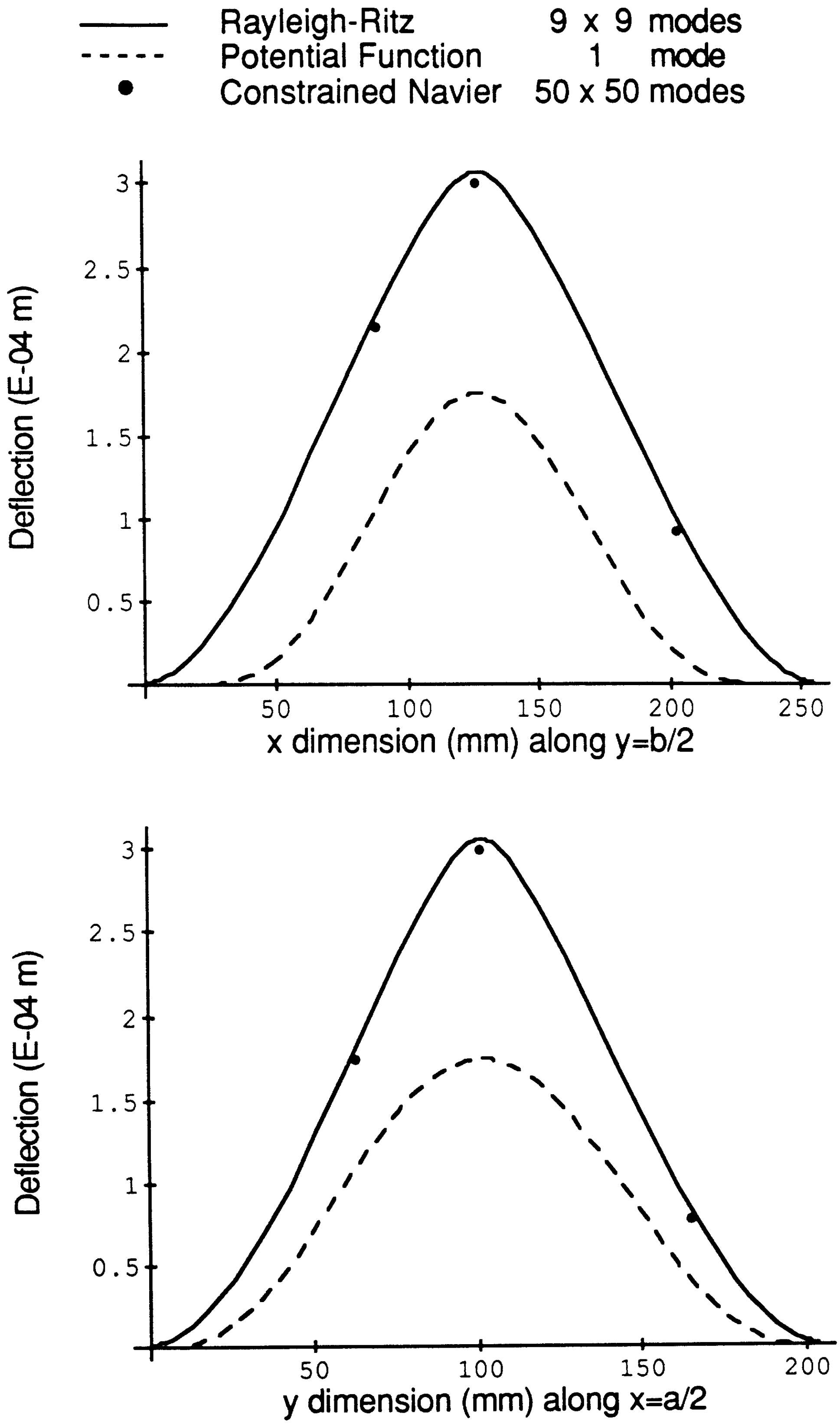

Figure 6.5 Transverse deflection for Specimen B, under a centered point load of 100 Newtons, with all four sides clamped.

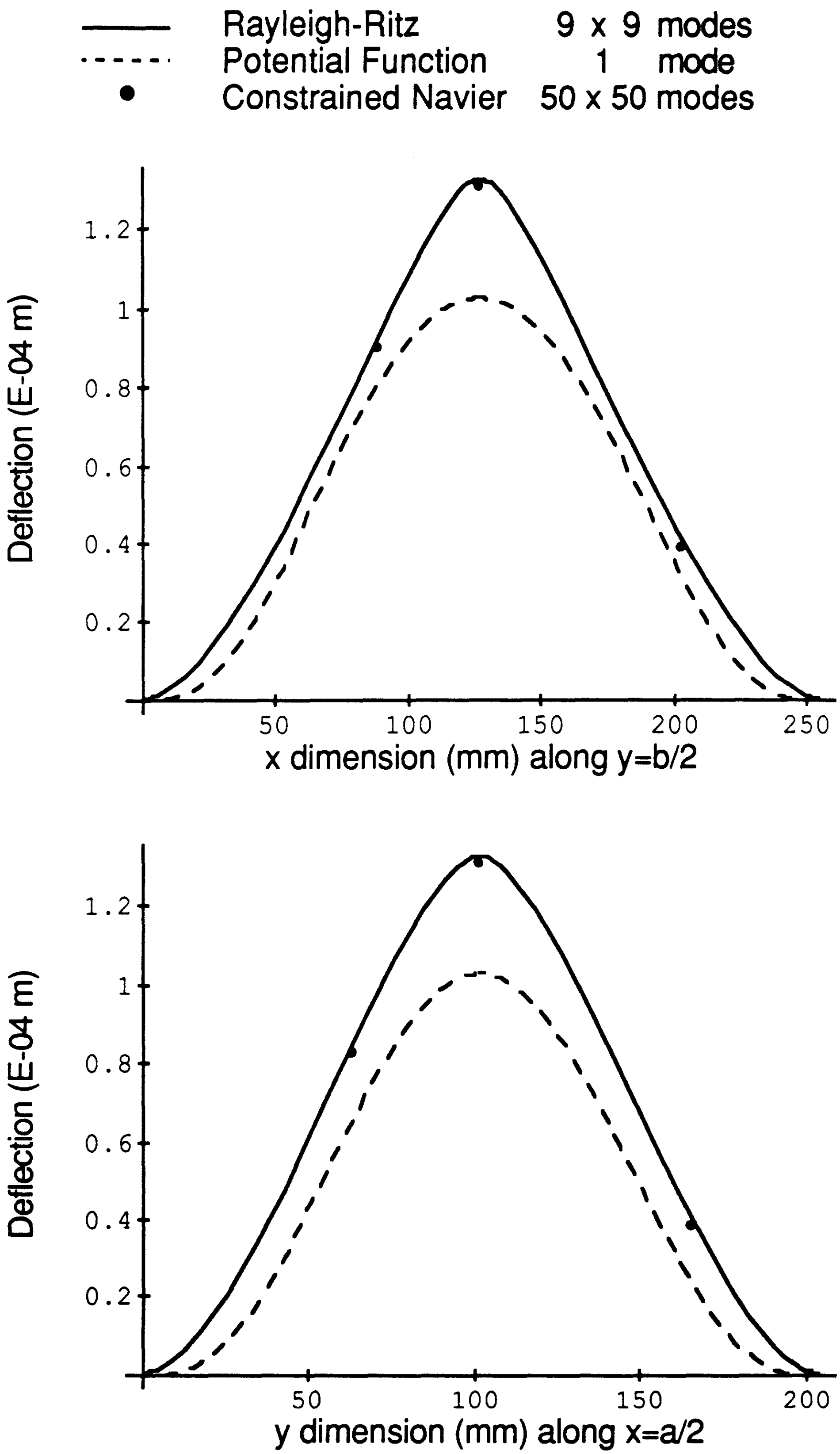

Figure 6.6 Transverse deflection for Specimen C, under a centered point load of 100 Newtons, with all four sides clamped.

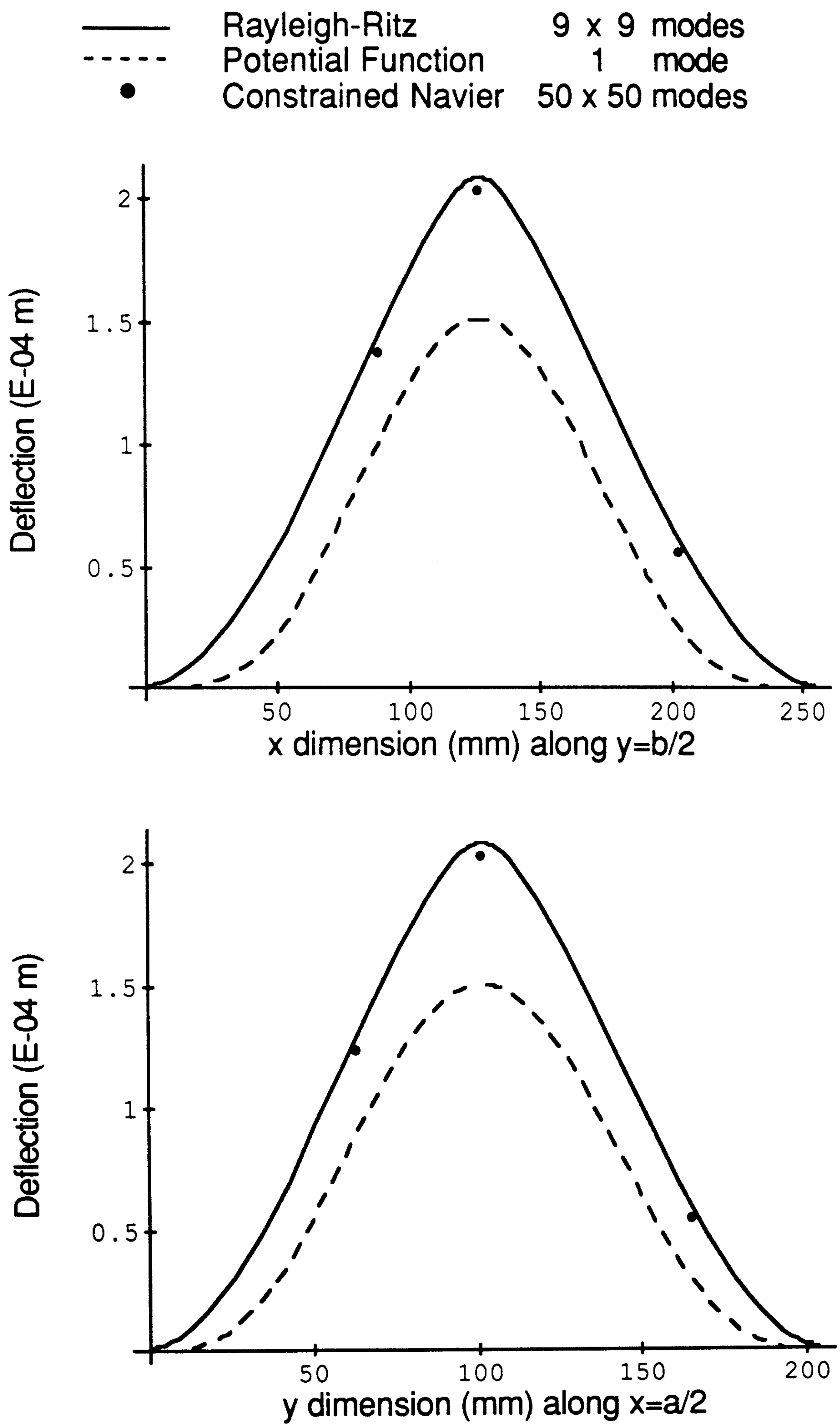

Figure 6.7 Transverse deflection for Specimen D, under a centered point load of 100 Newtons, with all four sides clamped.

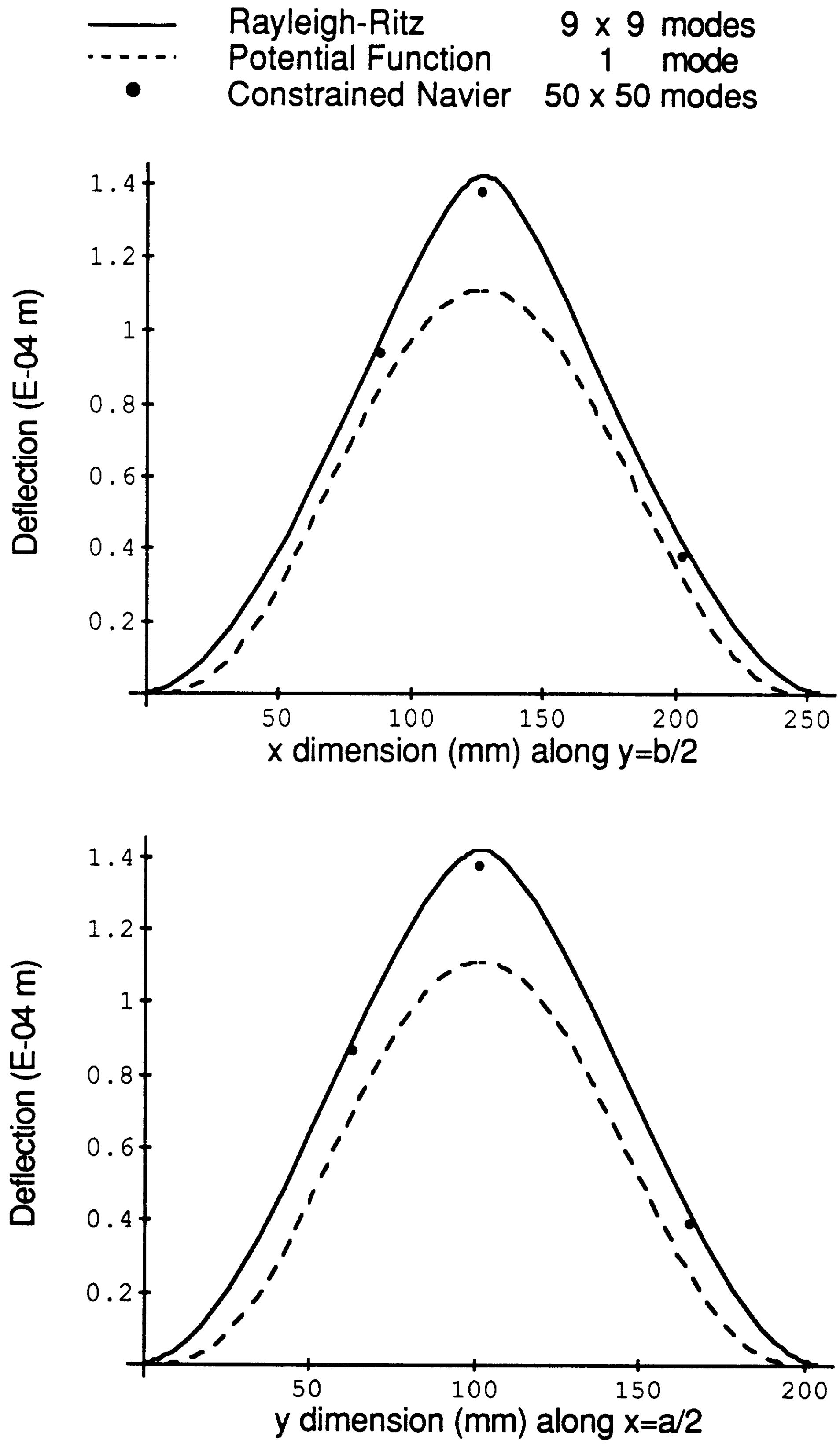

Figure 6.8 Transverse deflection for Specimen I, under a centered point load of 100 Newtons, with all four sides clamped.

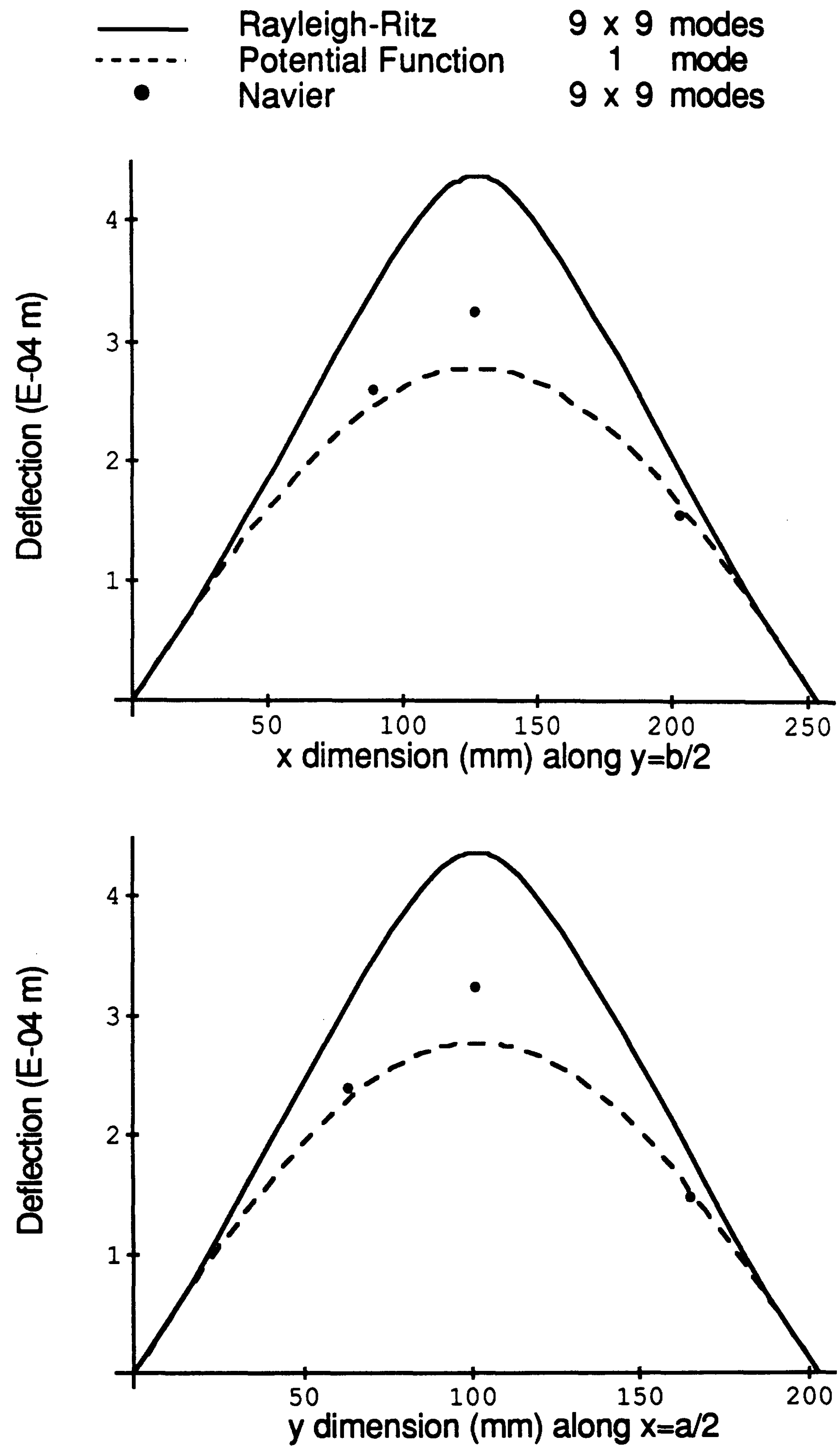

Figure 6.9 **Transverse deflection for Specimen A, under a centered point load of 100 Newtons, with all four sides simply supported.**

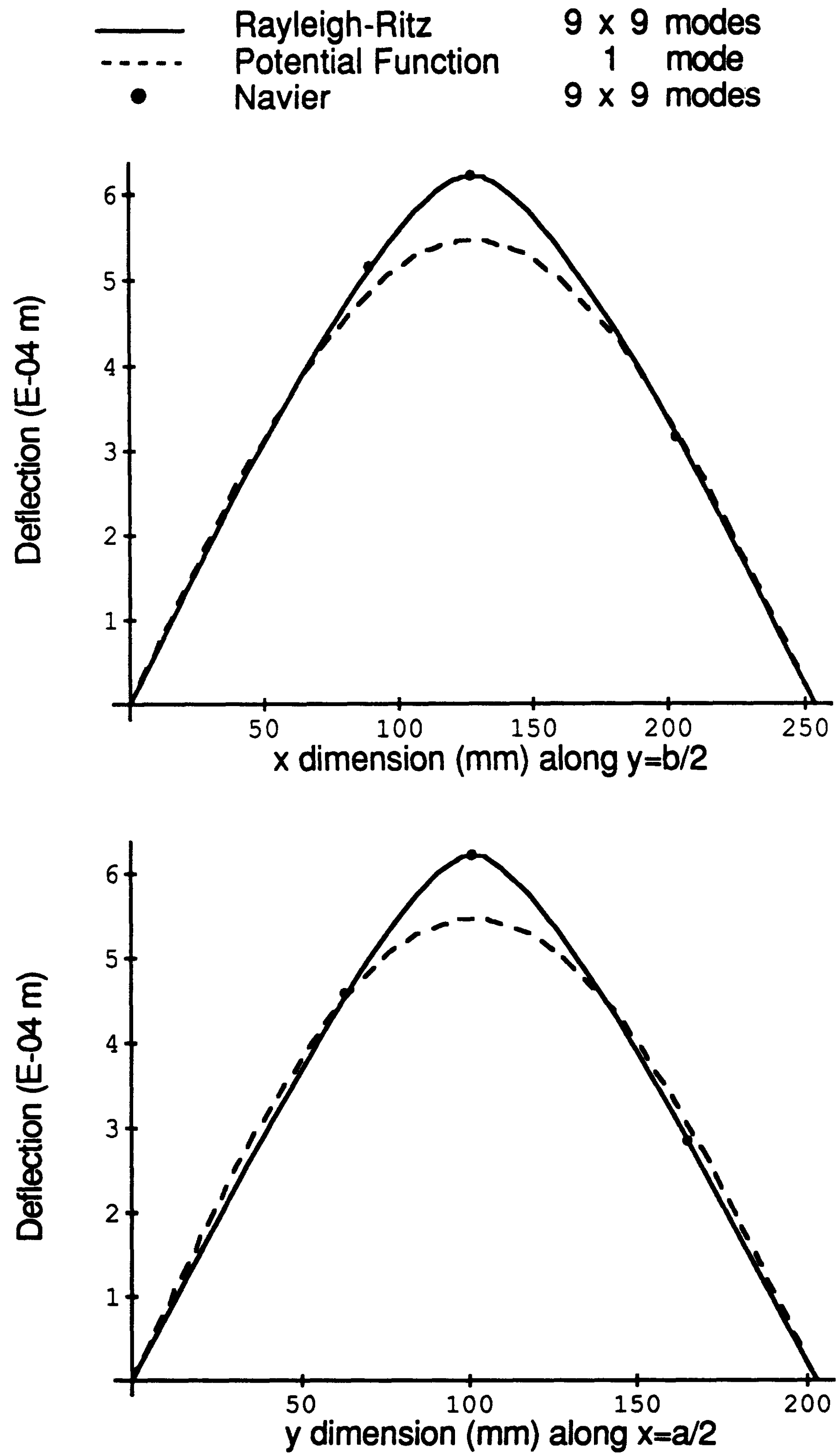

Figure 6.10 **Transverse deflection for Specimen B, under a centered point load of 100 Newtons, with all four sides simply supported.**

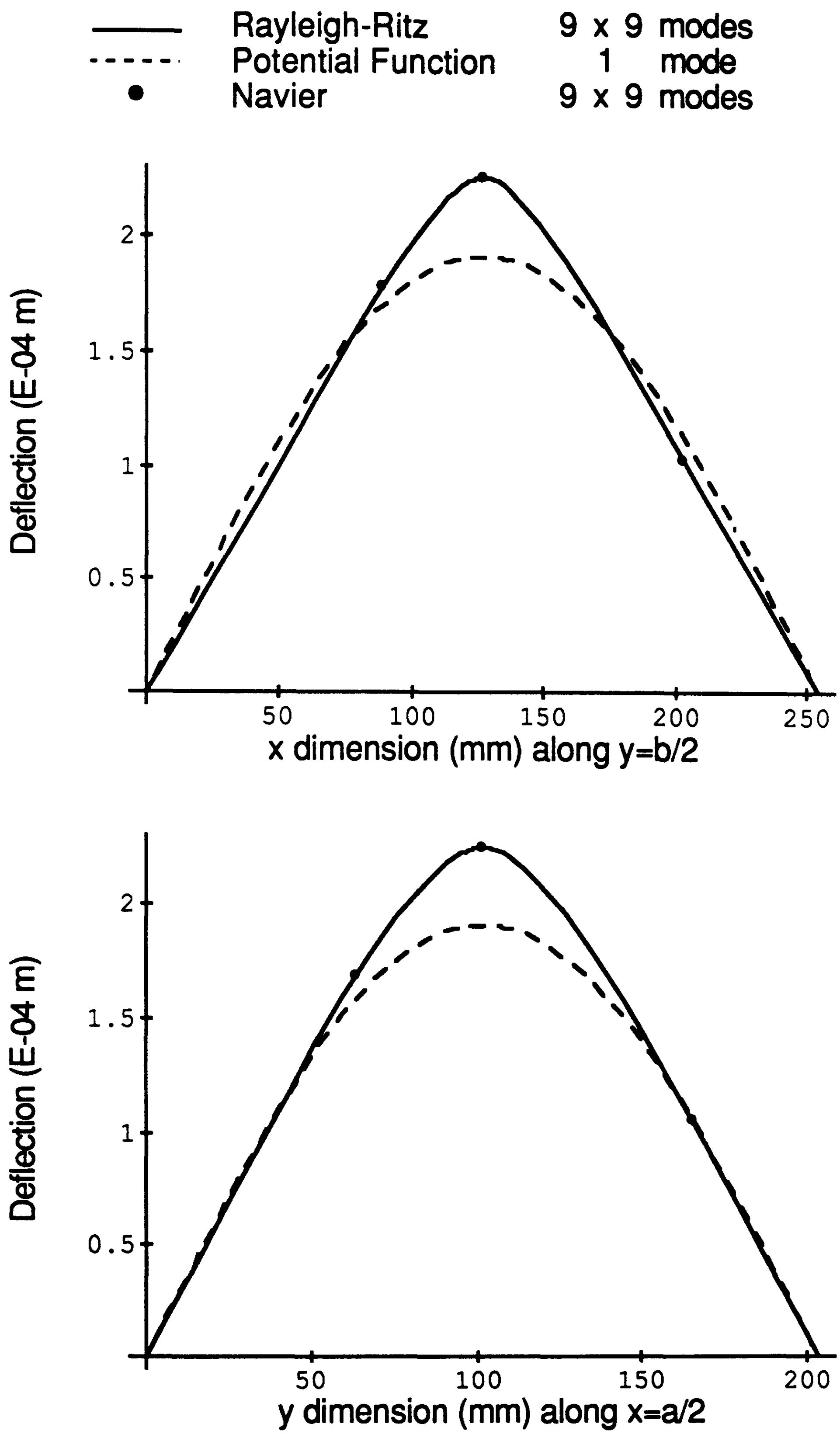

Figure 6.11 Transverse deflection for Specimen C, under a centered point load of 100 Newtons, with all four sides simply supported.

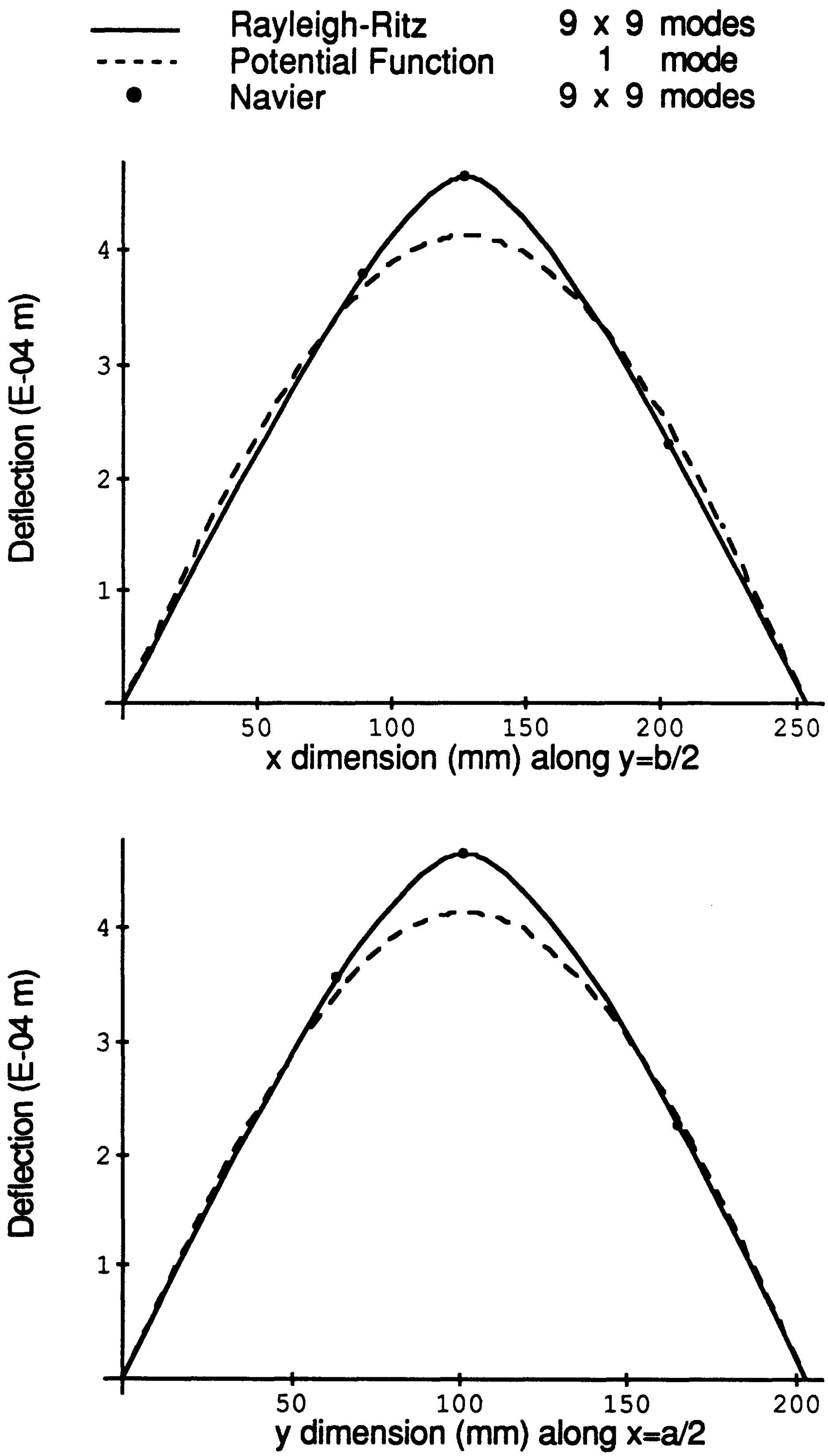

Figure 6.12 Transverse deflection for Specimen D, under a centered point load of 100 Newtons, with all four sides simply supported.

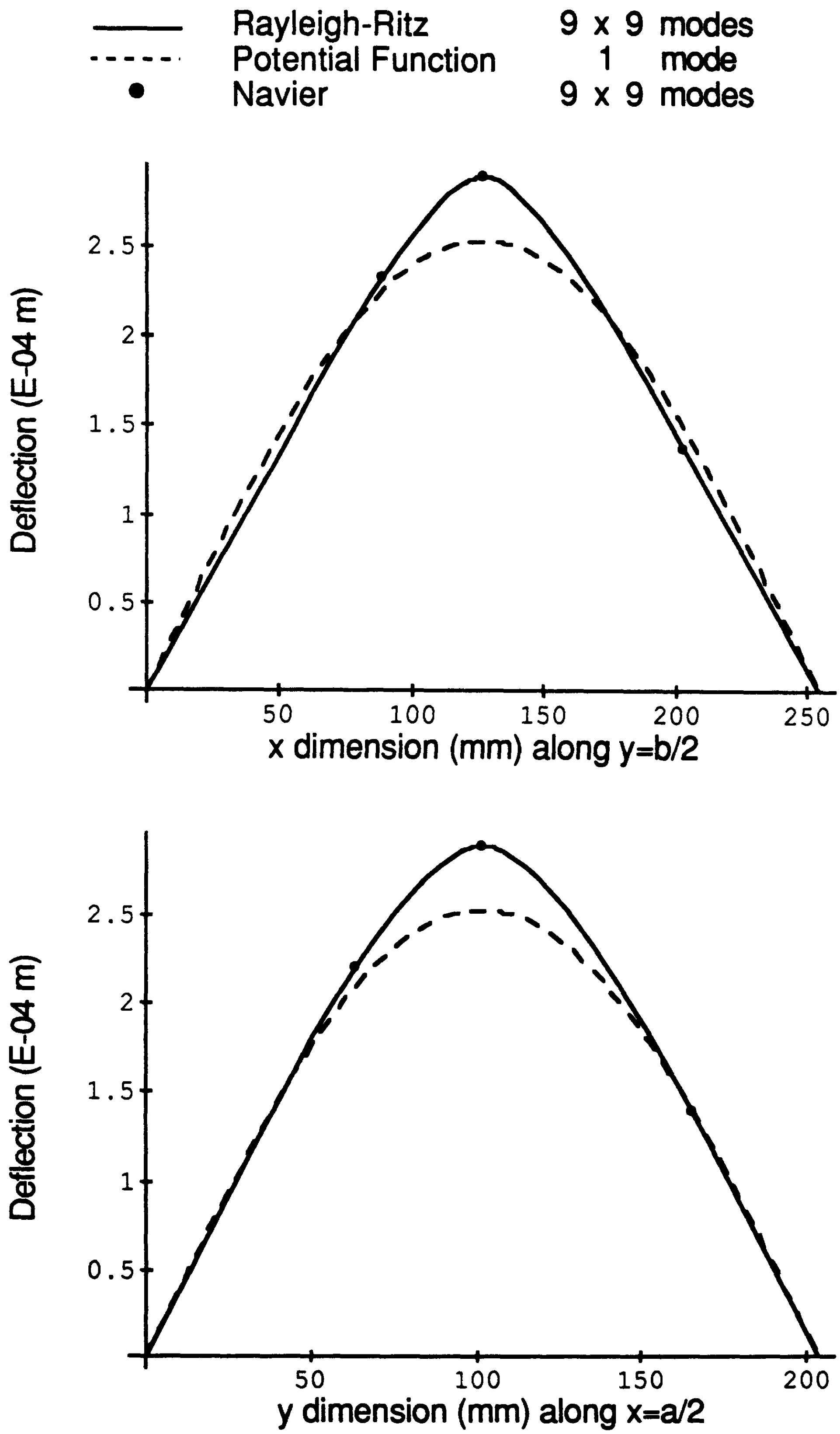

Figure 6.13 **Transverse deflection for Specimen I, under a centered point load of 100 Newtons, with all four sides simply supported.**

6.4 Results for Off-Center Point Load

This section presents the analytical results for the off-center point load problems that were investigated experimentally. For all of the off-center load cases, the loading was applied at (x,y) = (76 mm,127 mm). The Rayleigh-Ritz and Navier solutions are presented for the five specimens, for the boundary conditions four sides clamped, x edges simply supported and y edges clamped, and four sides simply supported. The solutions are presented in graphical form, in Figures 6.14 through 6.28, as plots of transverse displacement along the plate centerlines.

The Rayleigh-Ritz solutions use 9 x 9 modes. The constrained Navier solutions use 50 modes in a direction with clamped boundary conditions, while the traditional Navier solutions use only 9 modes in a direction with simply supported boundary conditions. More modes were used for the constrained Navier solution due to its slower convergence. Both Navier solutions are given only at discrete points, selected to correspond to transducer locations in the experiments, due to the computer time involved with plotting a function which may consist of as many as 2500 terms.

Again, both Navier solutions neglect the bending-twisting coupling that is present in Specimens A and B. This coupling is correctly accounted for in the Rayleigh-Ritz formulation. Specimen A, which has a strong bending-twisting coupling, is poorly modeled by the Navier solutions.

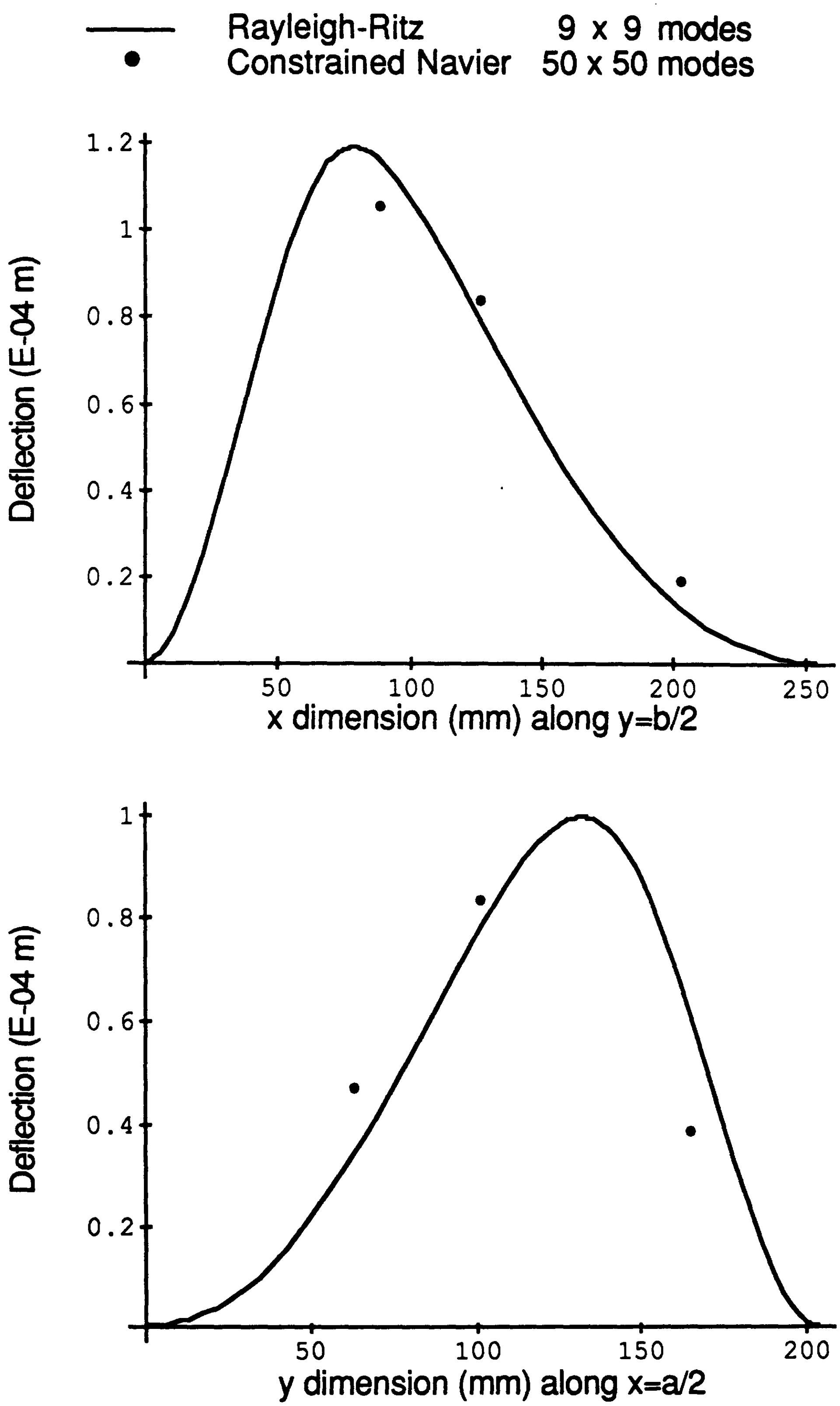

Figure 6.14 Transverse deflection for Specimen A, under an off-center point load of 100 Newtons, with all four sides clamped.

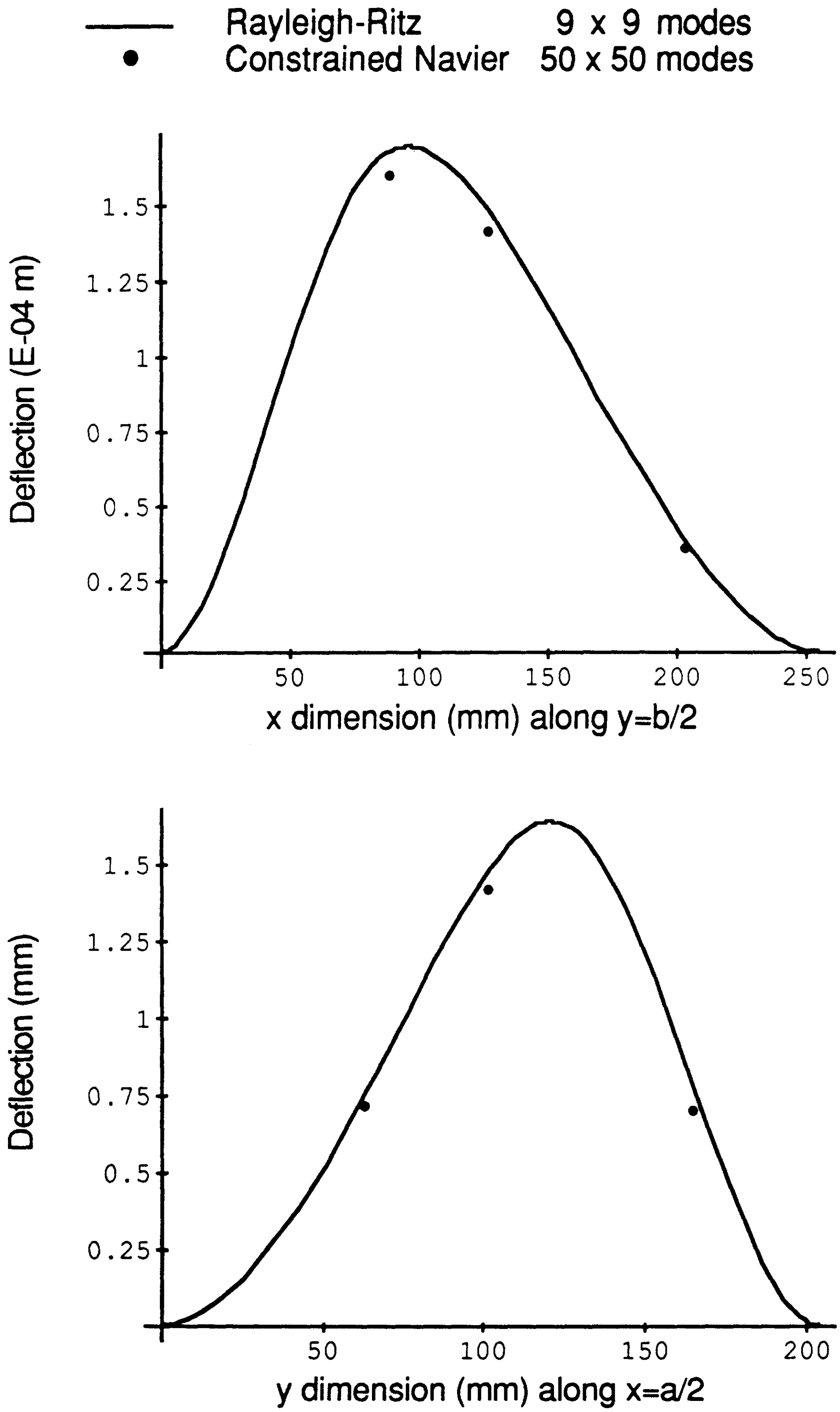

Figure 6.15 Transverse deflection for Specimen B, under an off-center point load of 100 Newtons, with all four sides clamped.

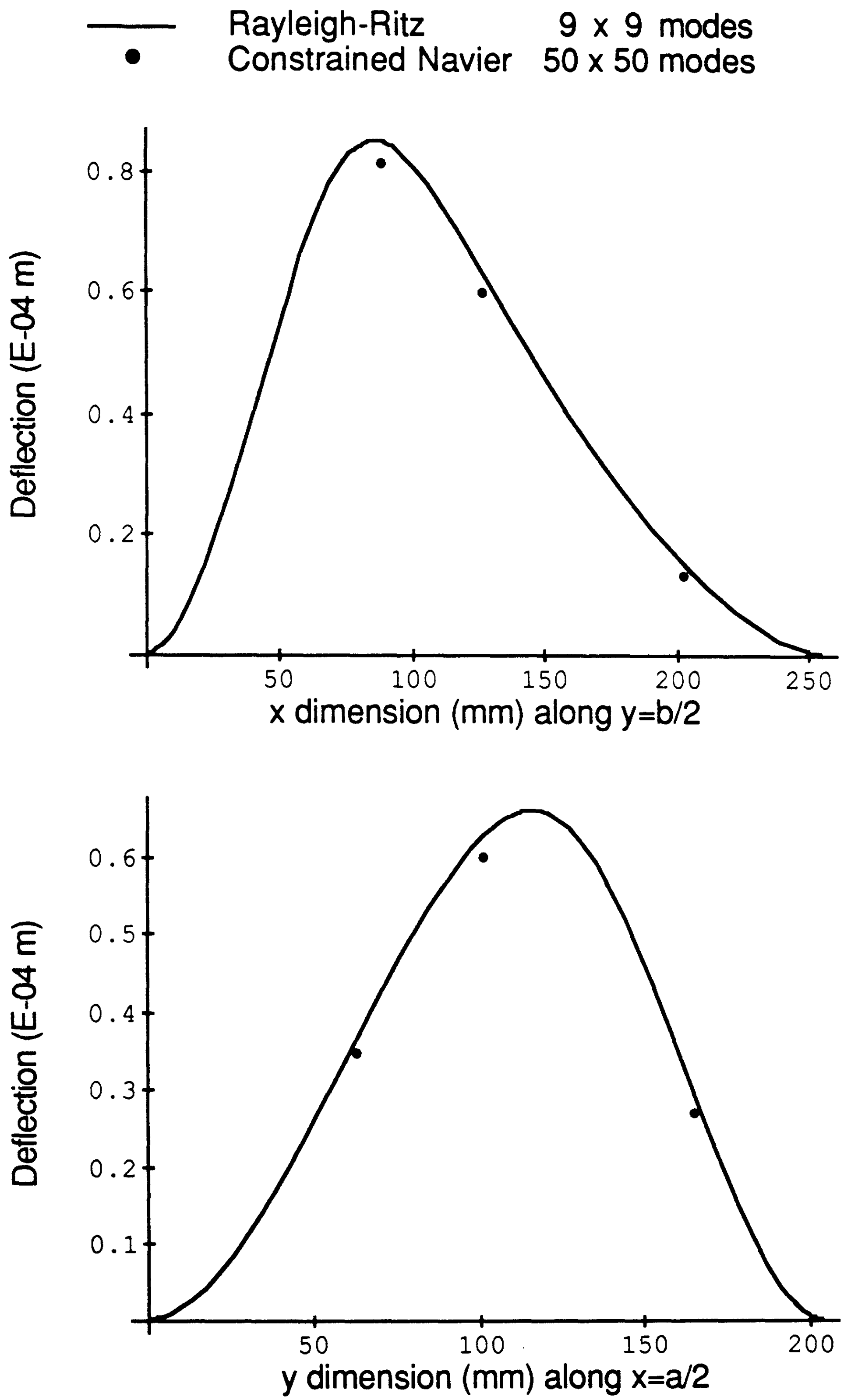

Figure 6.16 Transverse deflection for Specimen C, under an off-center point load of 100 Newtons, with all four sides clamped.

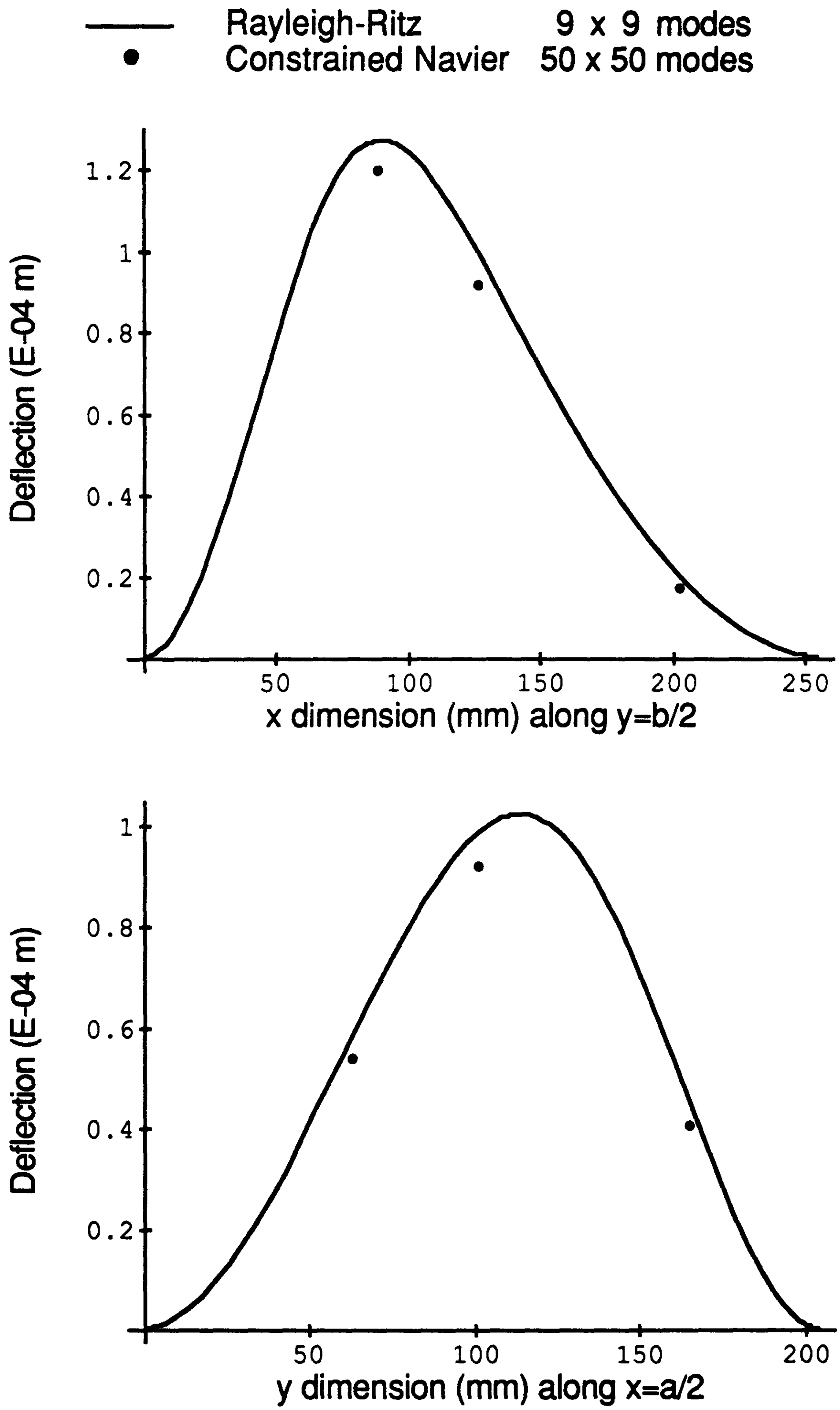

Figure 6.17 Transverse deflection for Specimen D, under an off-center point load of 100 Newtons, with all four sides clamped.

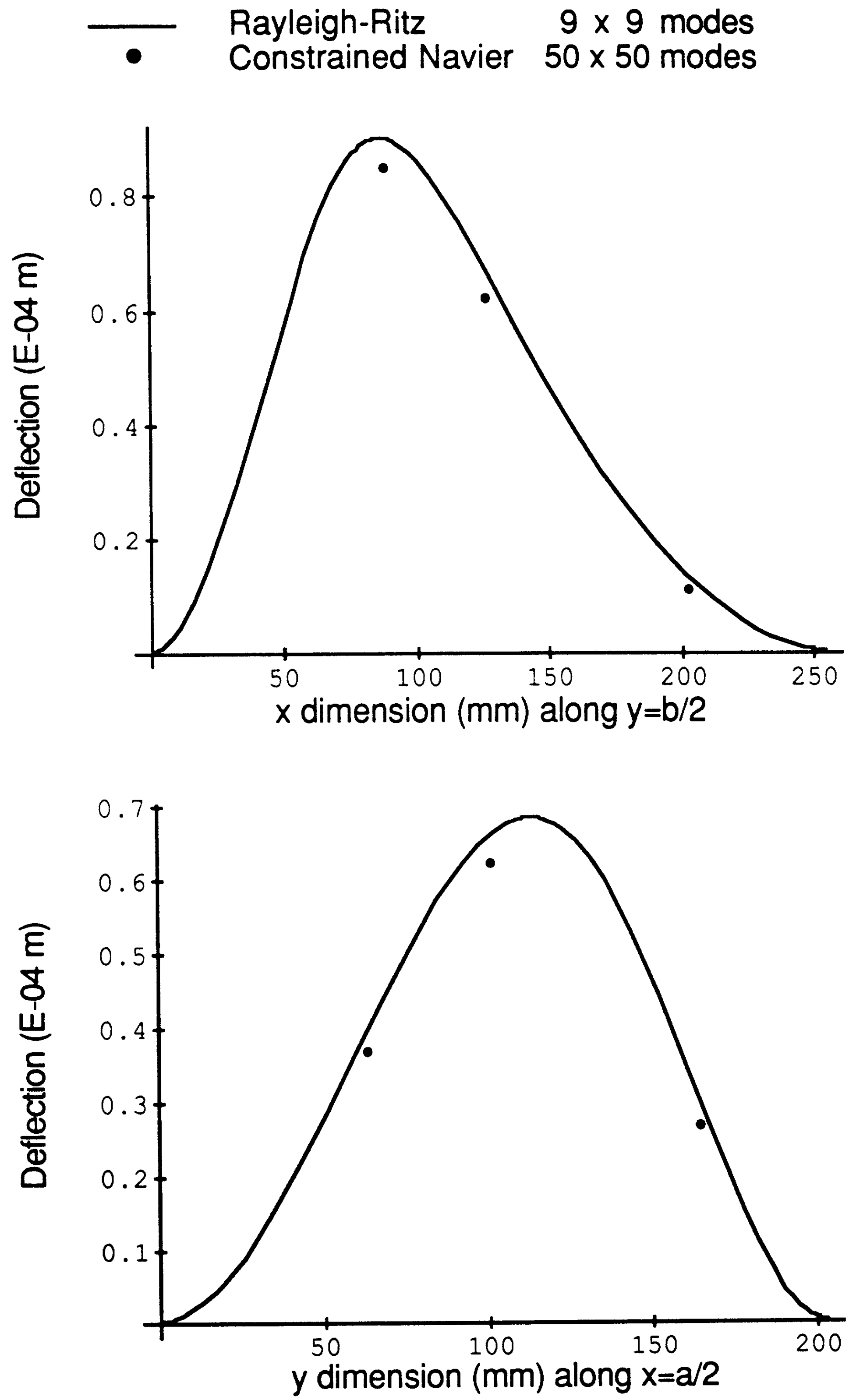

Figure 6.18 Transverse deflection for Specimen I, under an off-center point load of 100 Newtons, with all four sides clamped.

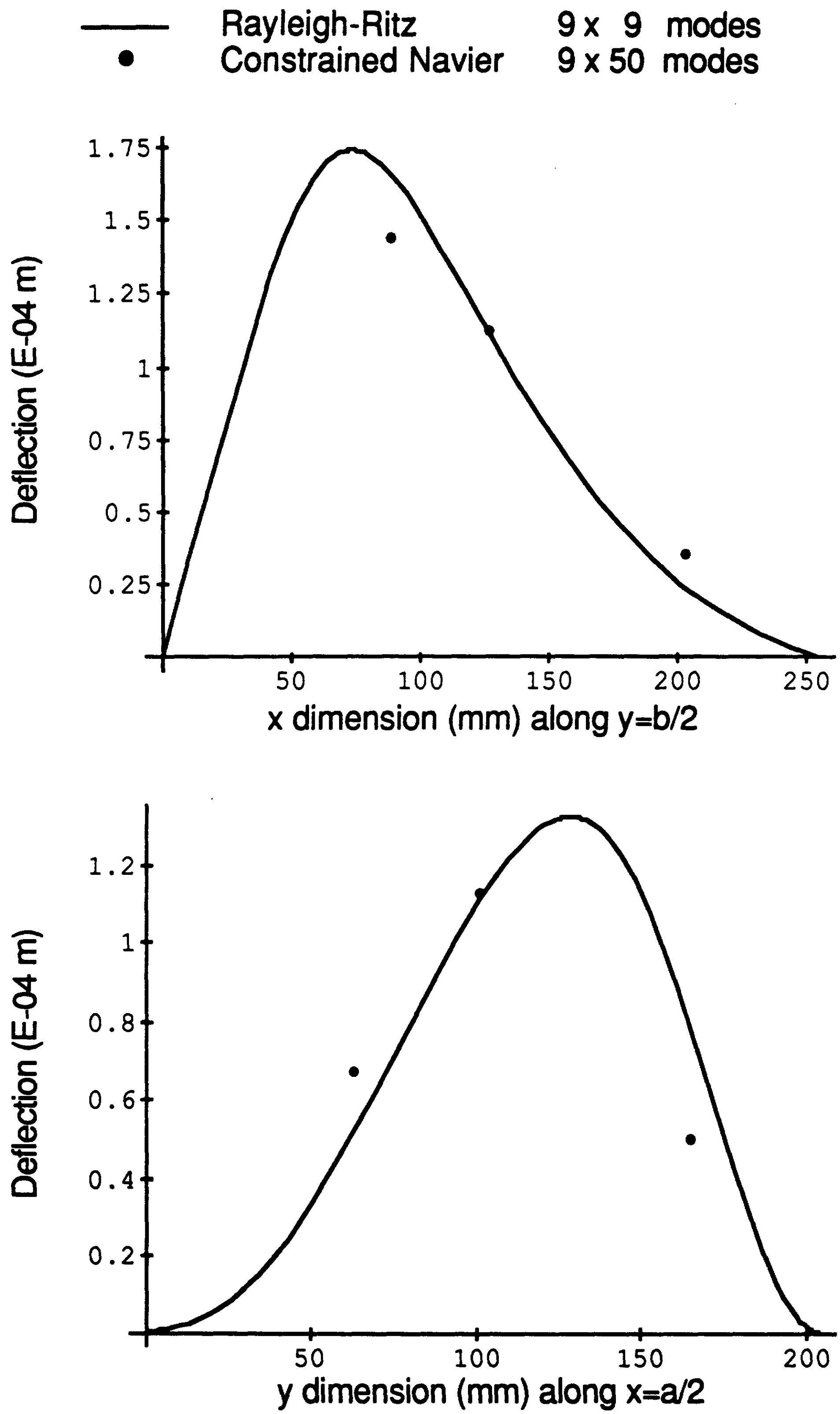

Figure 6.19 Transverse deflection for Specimen A, under an off-center point load of 100 Newtons, with x edges (short edges) simply supported and y edges (long edges) clamped.

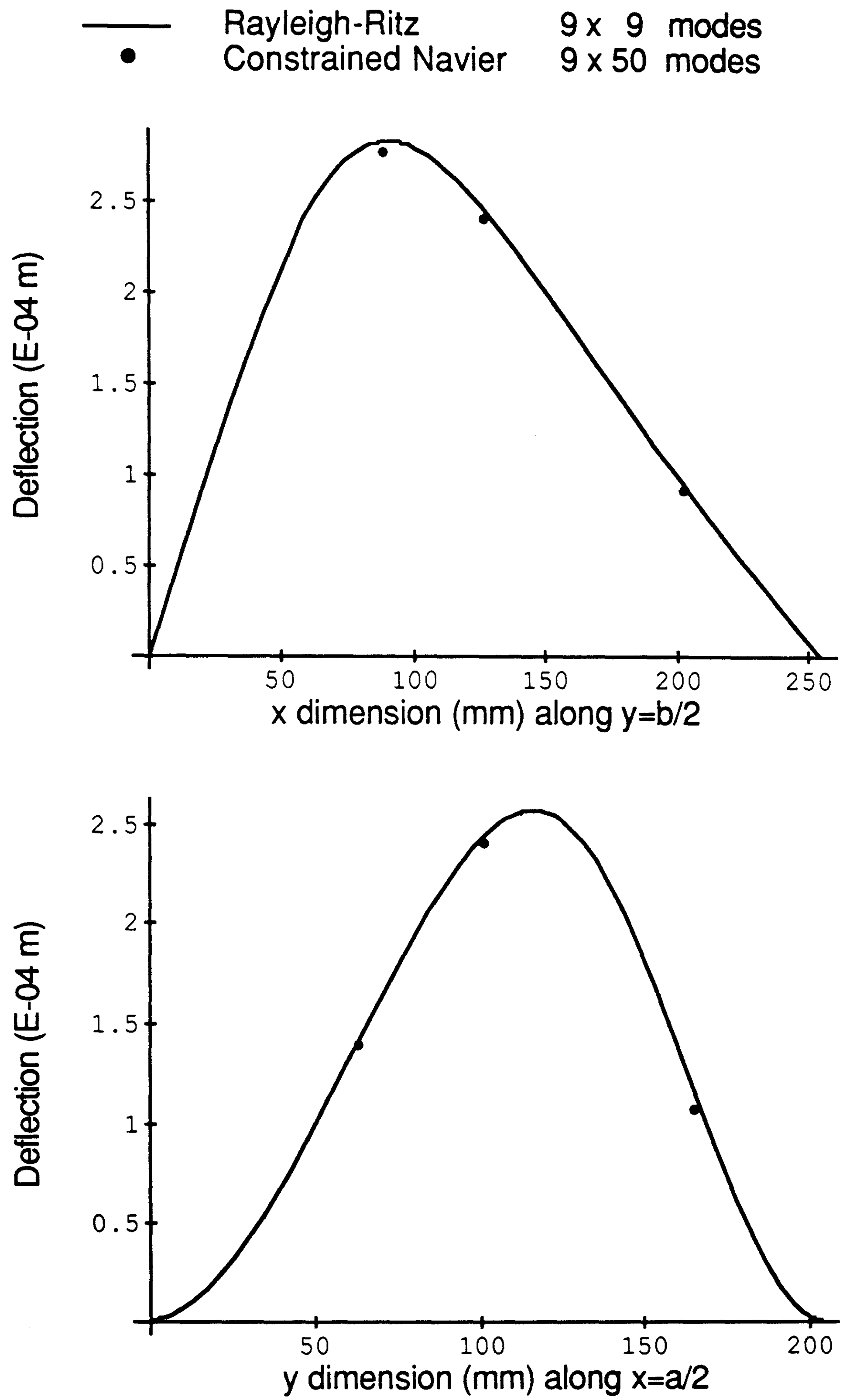

Figure 6.20 Transverse deflection for Specimen B, under an off-center point load of 100 Newtons, with x edges (short edges) simply supported and y edges (long edges) clamped.

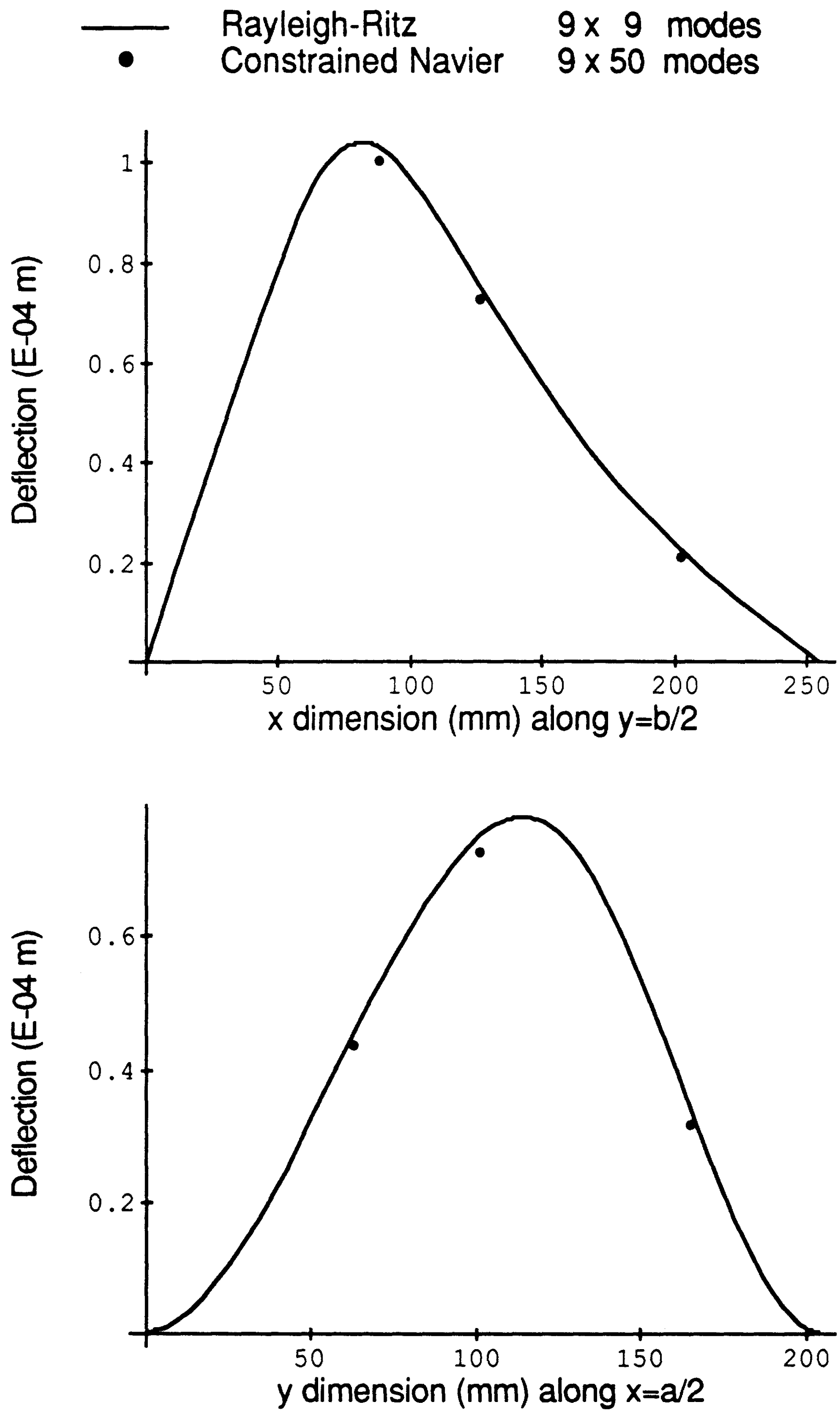

Figure 6.21 Transverse deflection for Specimen C, under an off-center point load of 100 Newtons, with x edges (short edges) simply supported and y edges (long edges) clamped.

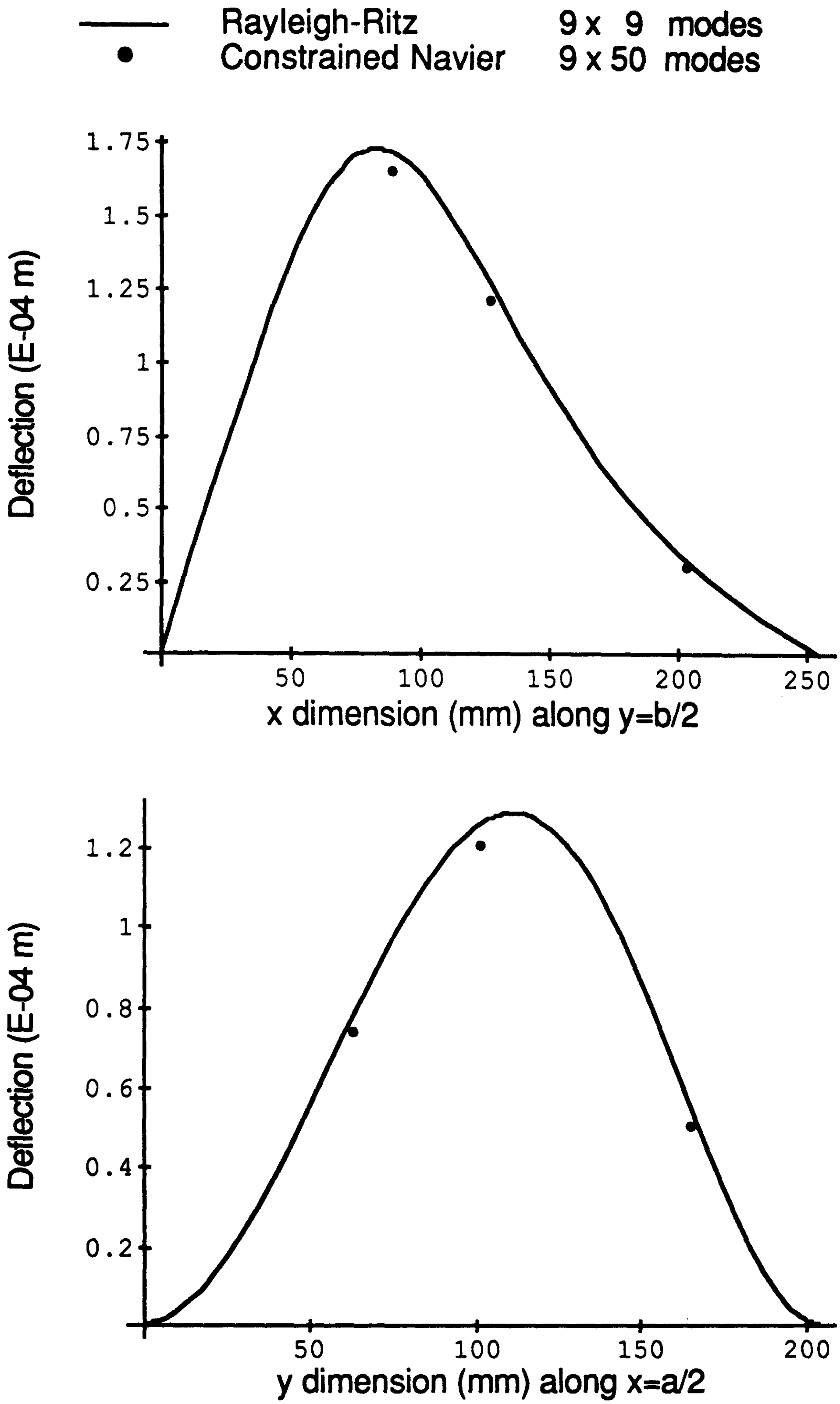

Figure 6.22 Transverse deflection for Specimen D, under an off-center point load of 100 Newtons, with x edges (short edges) simply supported and y edges (long edges) clamped.

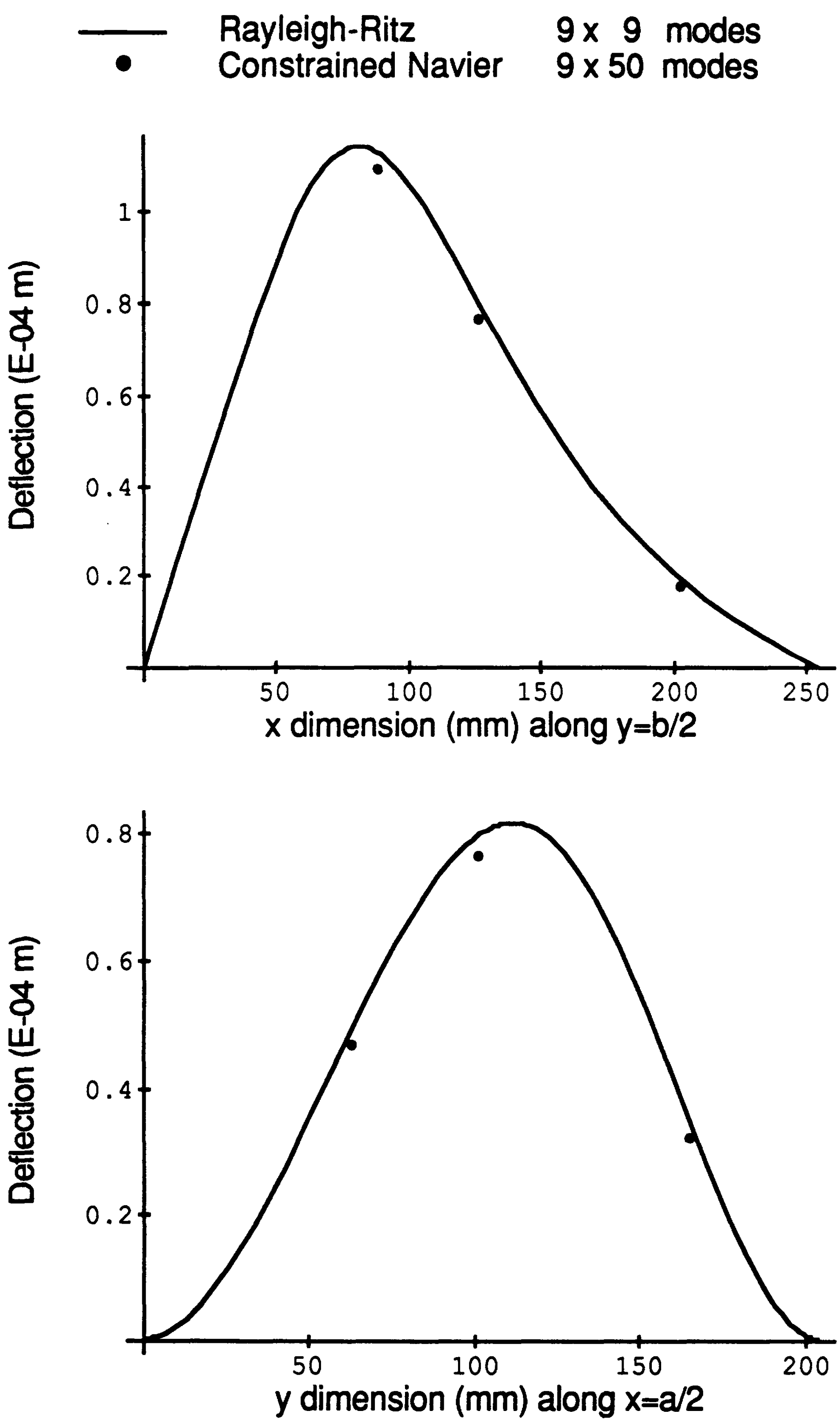

Figure 6.23 Transverse deflection for Specimen I, under an off-center point load of 100 Newtons, with x edges (short edges) simply supported and y edges (long edges) clamped.

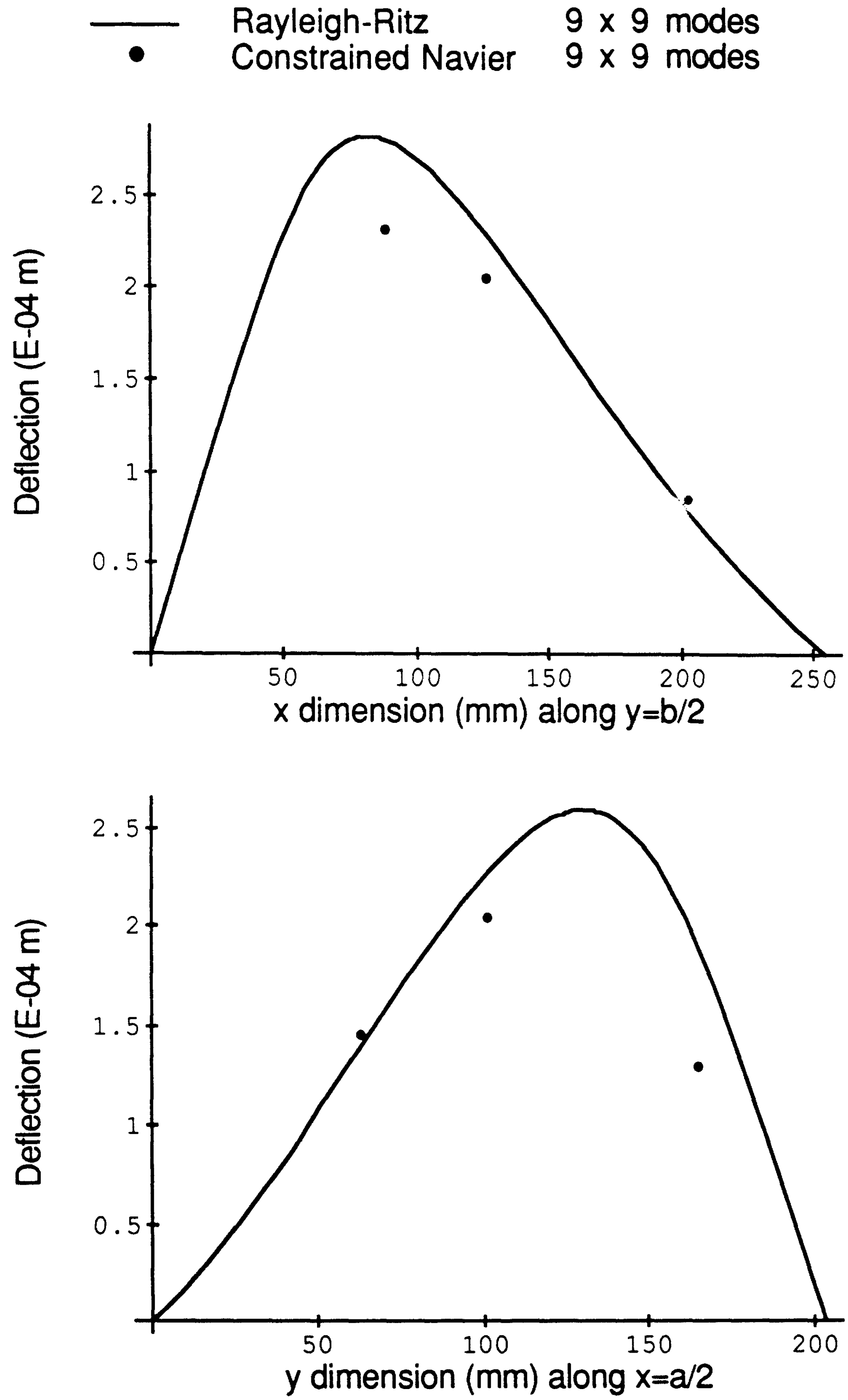

Figure 6.24 Transverse deflection for Specimen A, under an off-center point load of 100 Newtons, with all four sides simply supported.

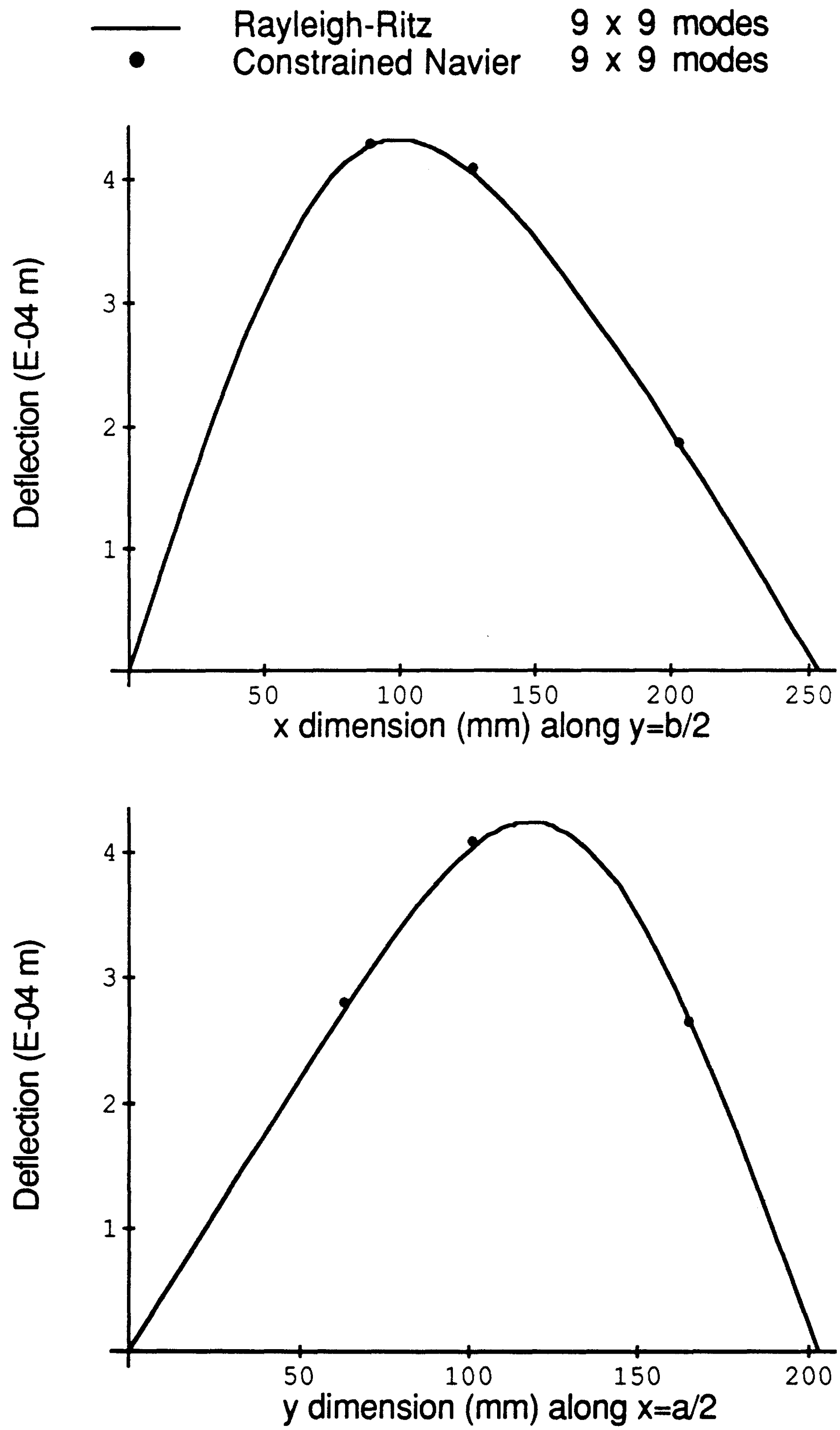

Figure 6.25 Transverse deflection for Specimen B, under an off-center point load of 100 Newtons, with all four sides simply supported.

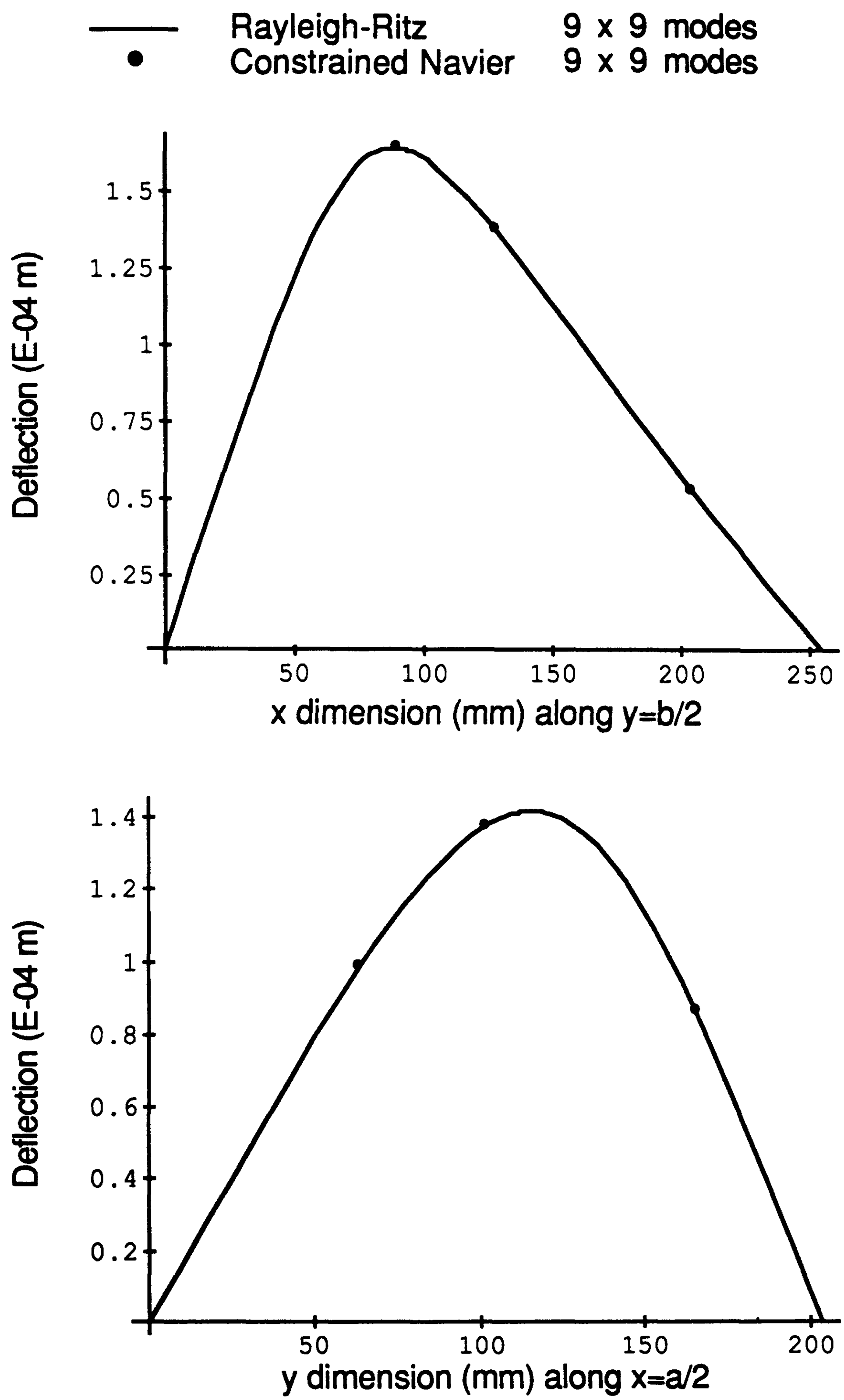

Figure 6.26 Transverse deflection for Specimen C, under an off-center point load of 100 Newtons, with all four sides simply supported.

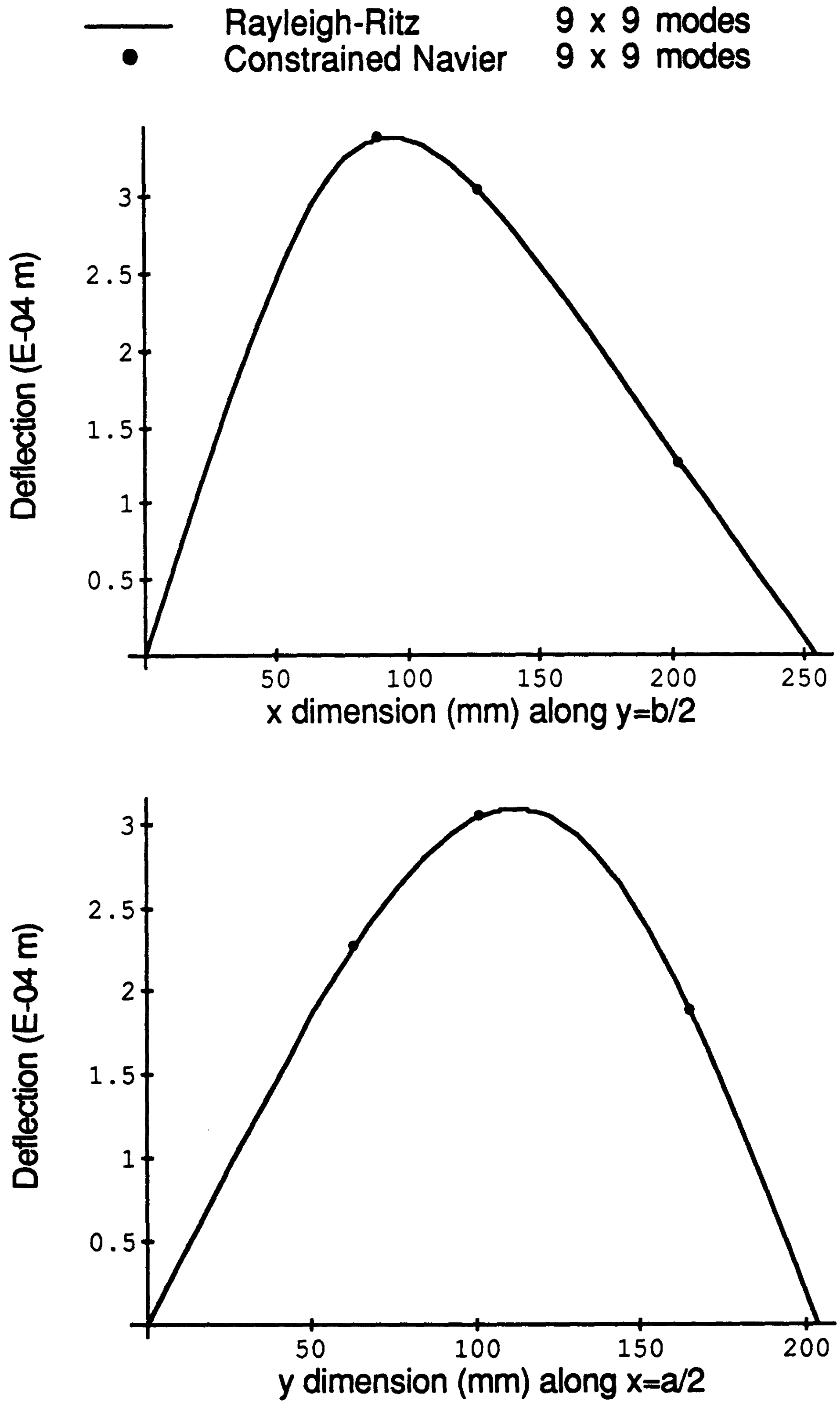

Figure 6.27 Transverse deflection for Specimen D, under an off-center point load of 100 Newtons, with all four sides simply supported.

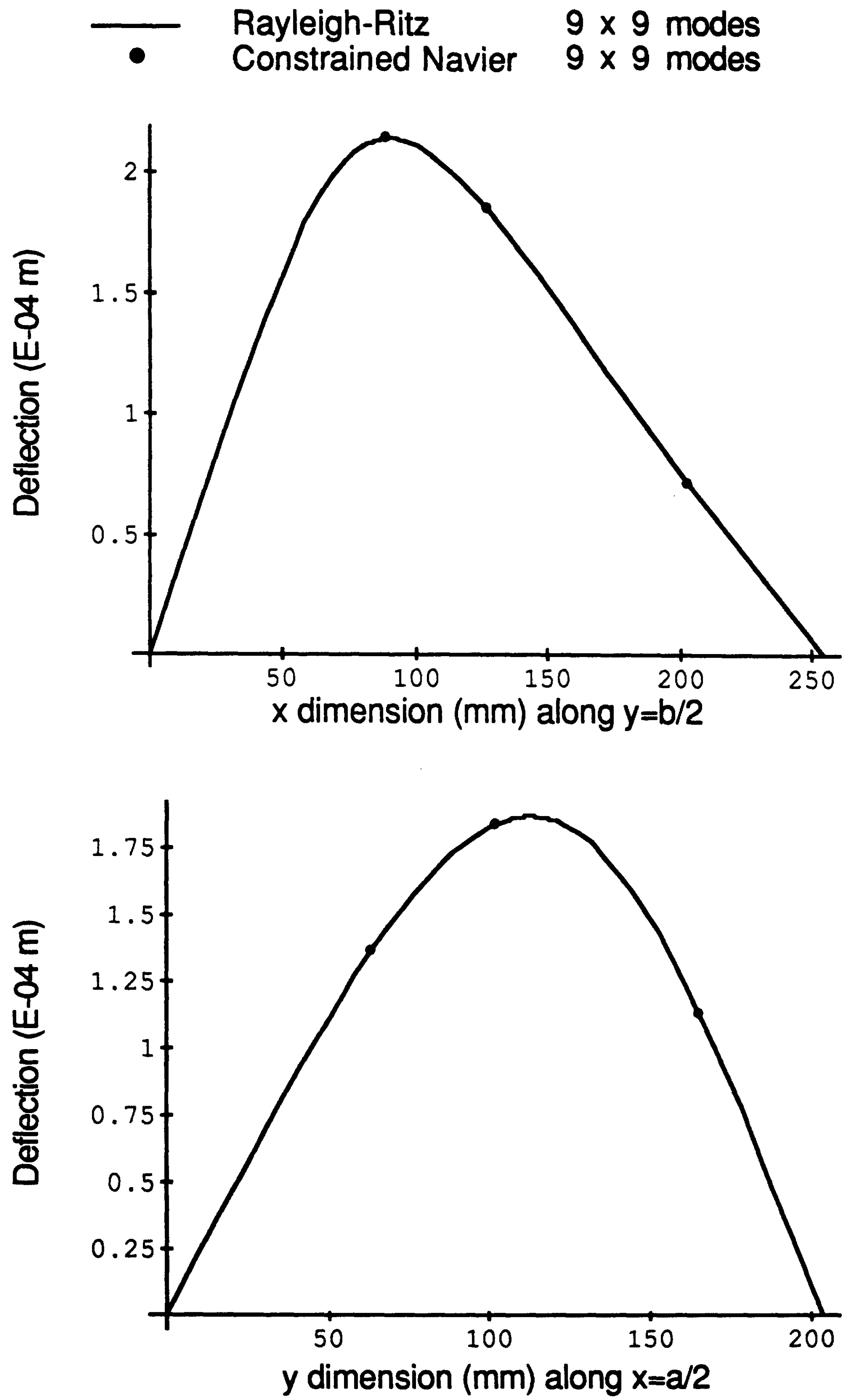

Figure 6.28 Transverse deflection for Specimen I, under an off-center point load of 100 Newtons, with all four sides simply supported.

6.5 Results for Centered Uniform Rectangular Pressure Patch

This section presents the analytical results for the centered uniform rectangular pressure patch (URPP) problems that were investigated experimentally. The rectangular pressure patch was 50.8 cm by 63.5 cm and was aligned with the longer edge parallel to the x axis. The Rayleigh-Ritz, single mode polynomial potential functions, and Navier solutions are presented for the five specimens, for the boundary conditions four sides clamped and four sides simply supported. The solutions are presented in graphical form, in Figures 6.29 through 6.38, as plots of transverse displacement along the plate centerlines.

The Rayleigh-Ritz solutions use 9 x 9 modes while the potential function solutions are all single mode solutions. The constrained Navier solutions use 50 modes in a direction with clamped boundary conditions, while the traditional Navier solutions use only 9 modes in a direction with simply supported boundary conditions. More modes were used for the constrained Navier solution due to its slower convergence. Both Navier solutions are given only at discrete points, selected to correspond to transducer locations in the experiments, due to the computer time involved with plotting a function which may consist of as many as 2500 terms.

Again, the constrained Navier, the traditional Navier, and the potential function solutions neglect the bending-twisting coupling that is present in Specimens A and B. This coupling is correctly accounted for in the Rayleigh-Ritz formulation. Specimen A, which has a strong bending-twisting coupling, is poorly modeled by the Navier solutions.

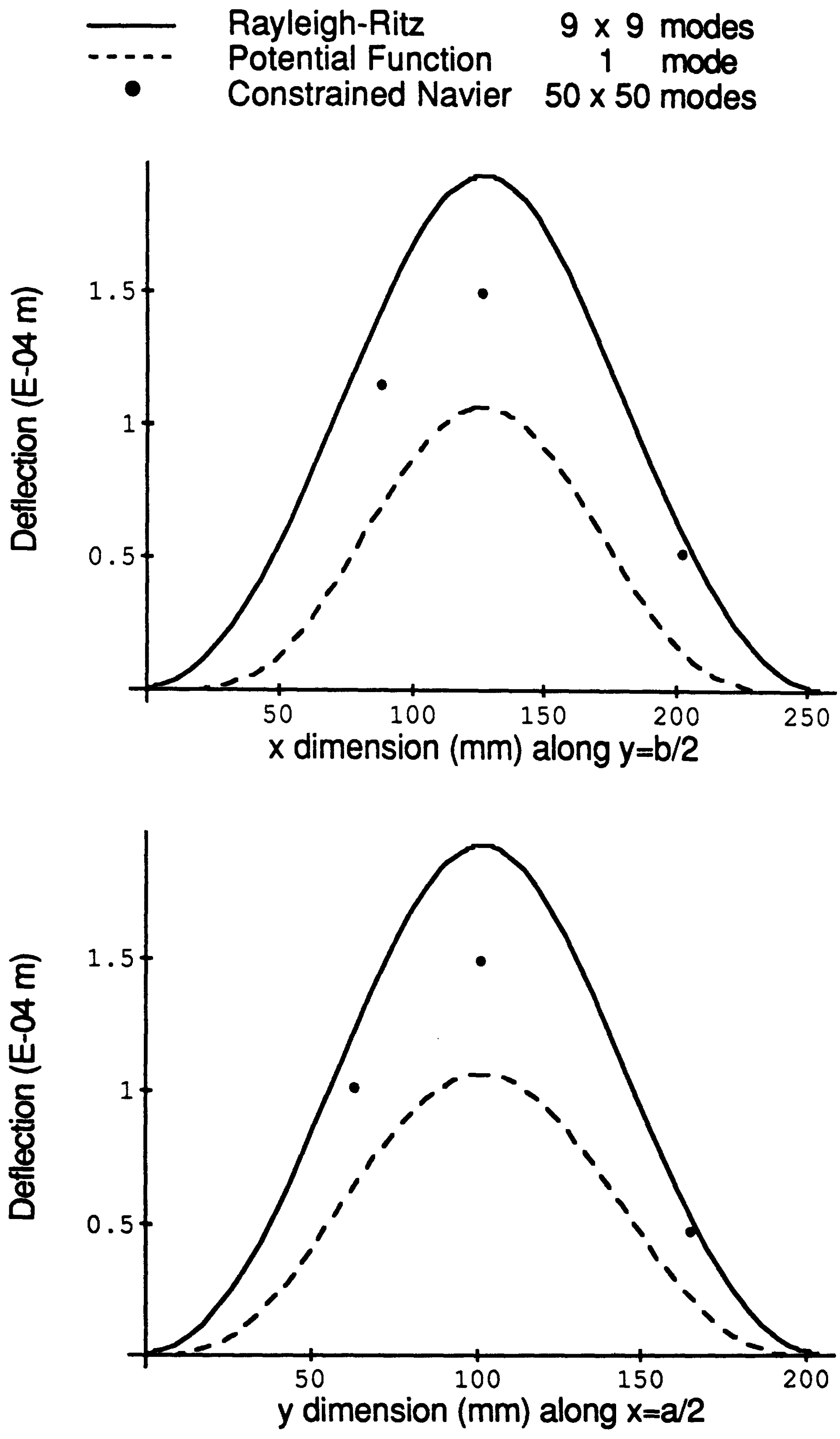

Figure 6.29 Transverse deflection for Specimen A, under a centered URPP load of 100 Newtons, with all four sides clamped.

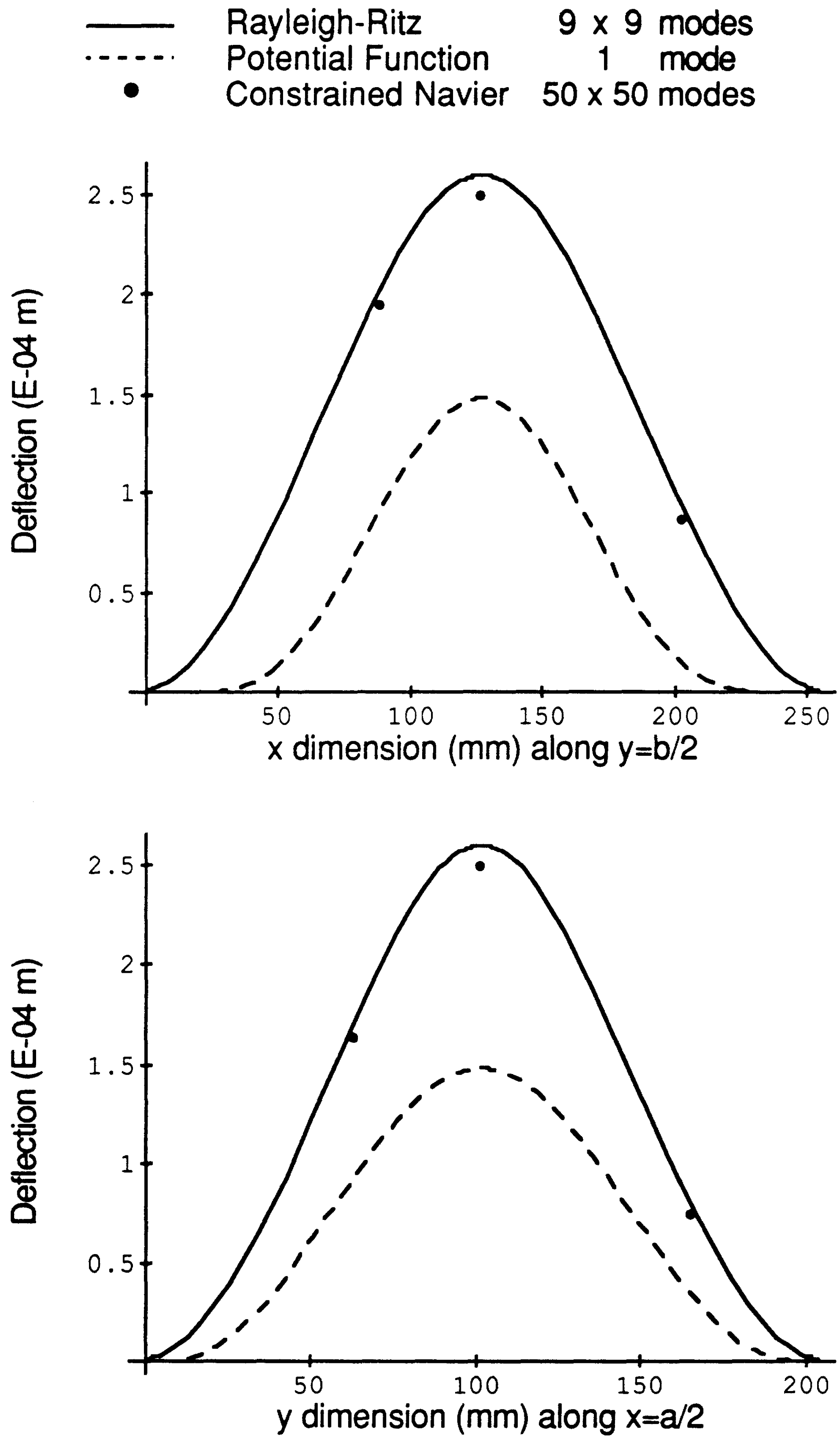

Figure 6.30 Transverse deflection for Specimen B, under a centered URPP load of 100 Newtons, with all four sides clamped.

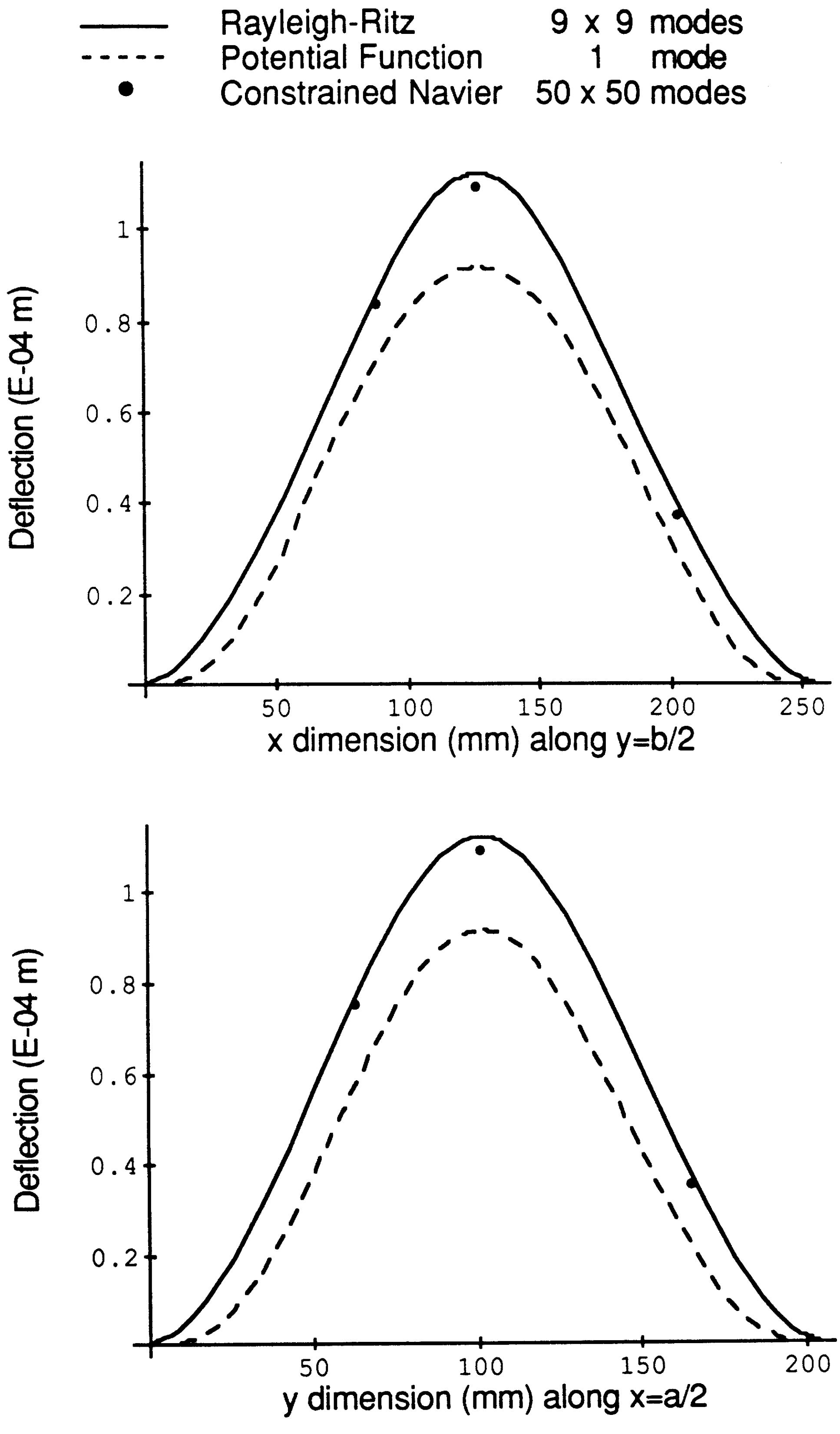

Figure 6.31 Transverse deflection for Specimen C, under a centered URPP load of 100 Newtons, with all four sides clamped.

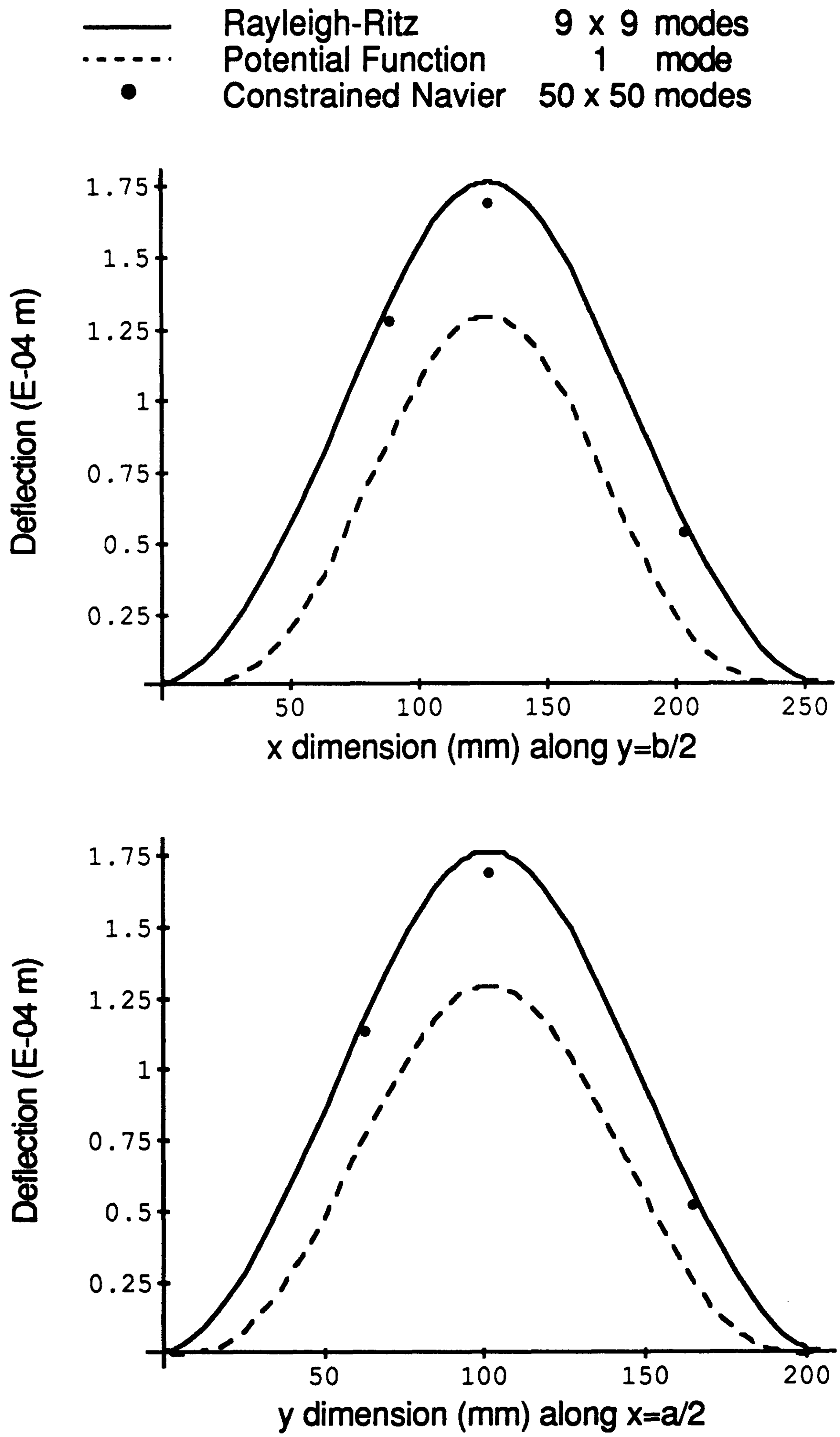

Figure 6.32 **Transverse deflection for Specimen D, under a centered URPP load of 100 Newtons, with all four sides clamped.**

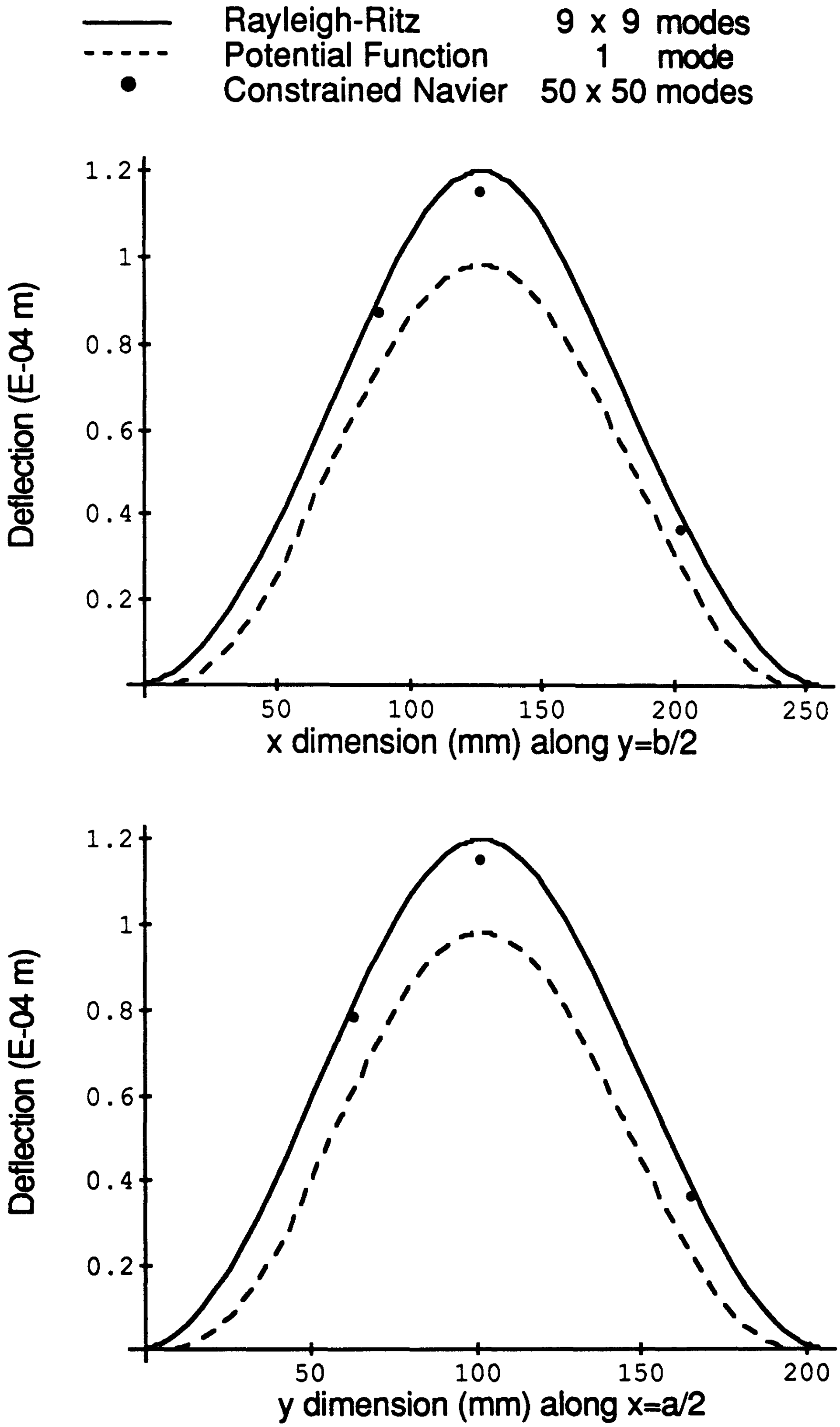

Figure 6.33 Transverse deflection for Specimen I, under a centered URPP load of 100 Newtons, with all four sides clamped.

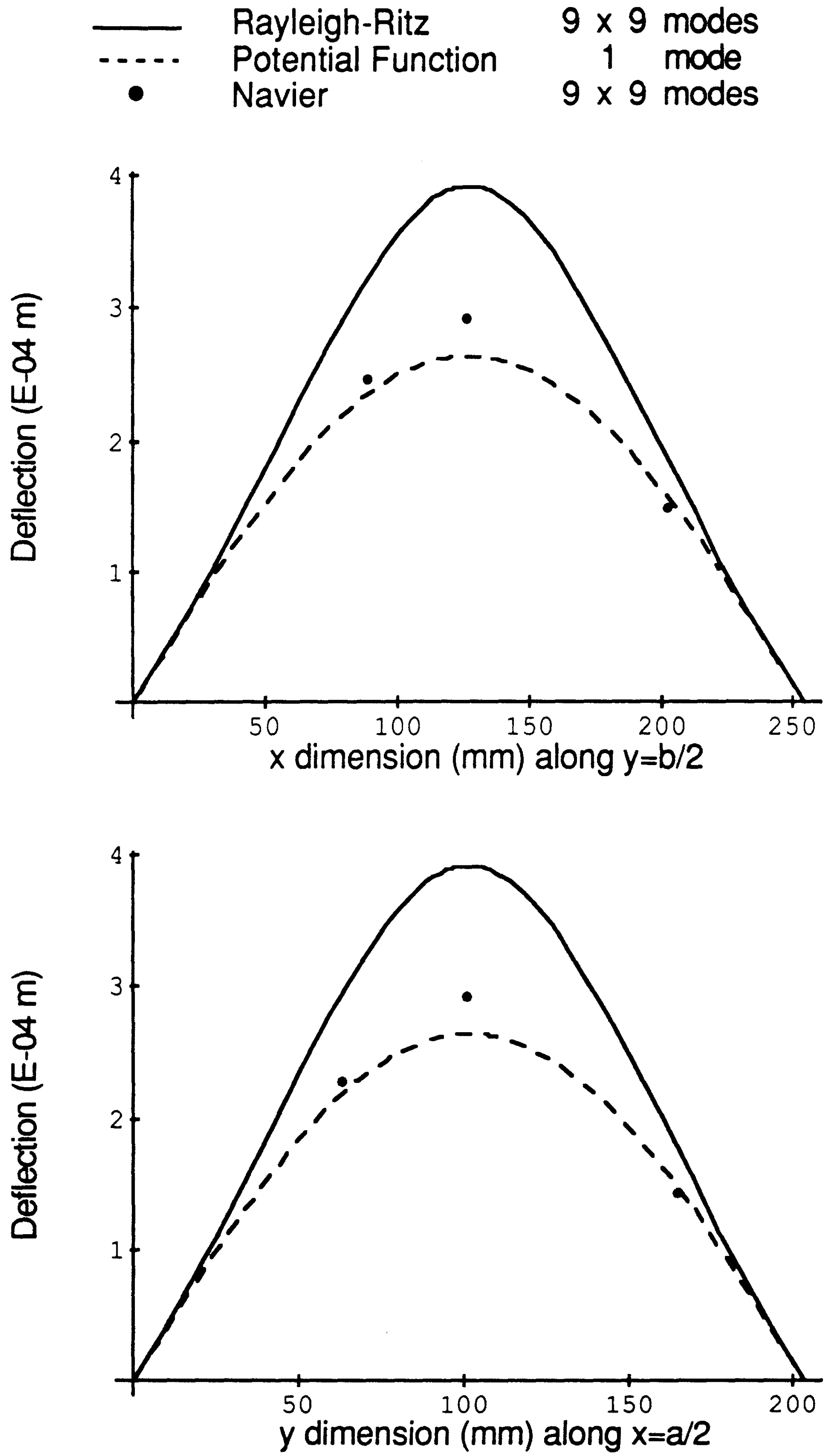

Figure 6.34 Transverse deflection for Specimen A, under a centered URPP load of 100 Newtons, with all four sides simply supported.

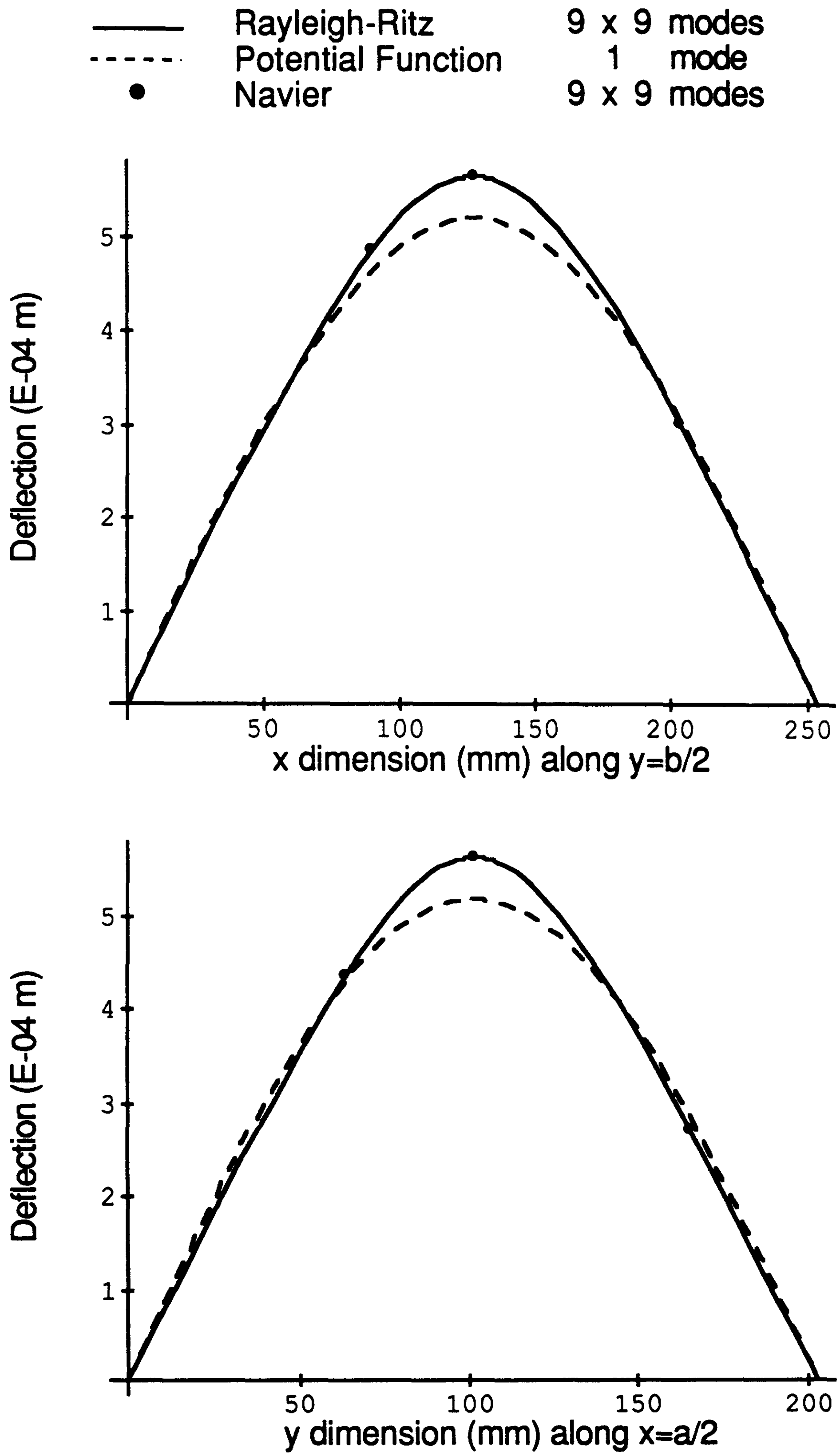

Figure 6.35 Transverse deflection for Specimen B, under a centered URPP load of 100 Newtons, with all four sides simply supported.

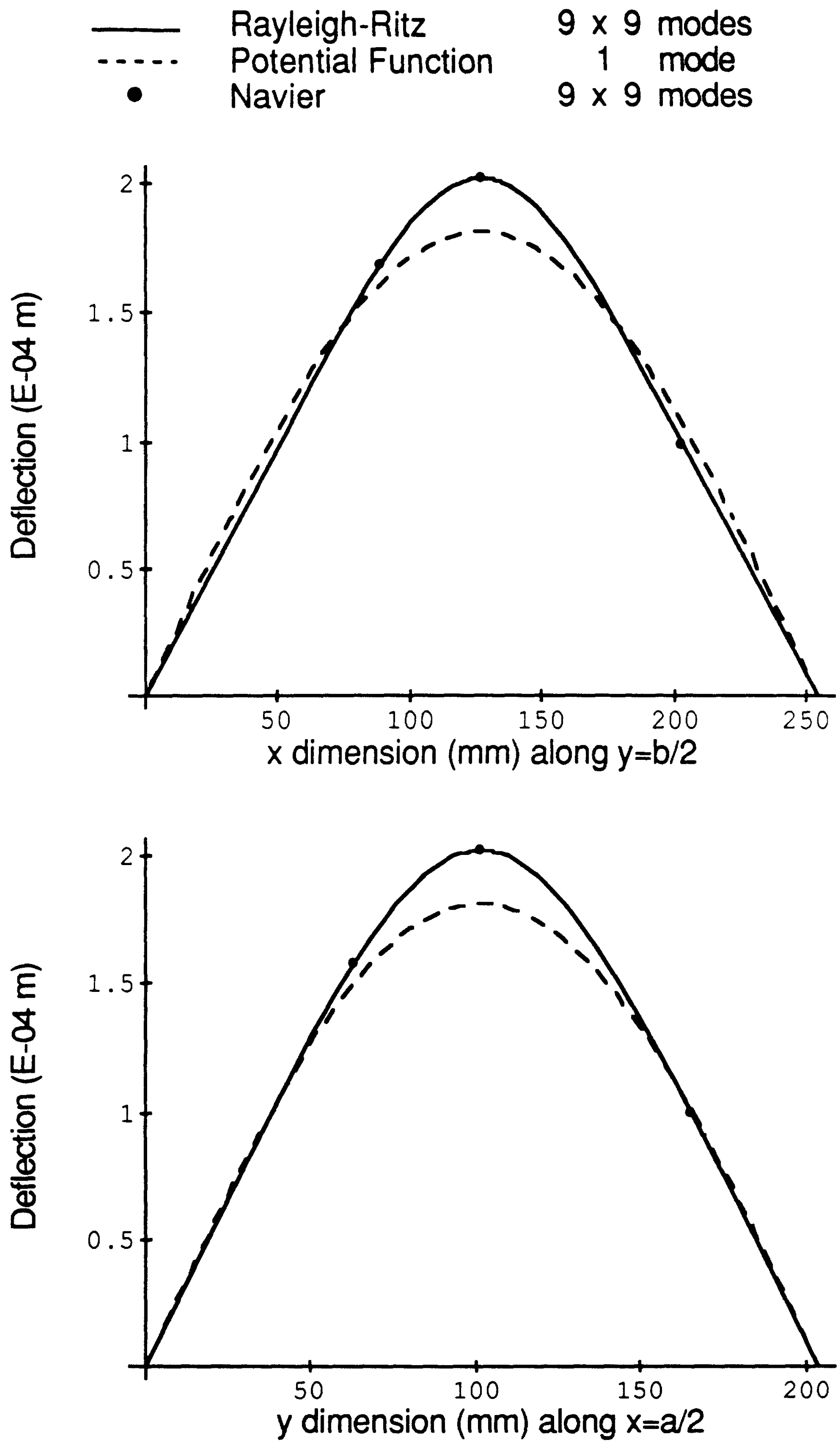

Figure 6.36 Transverse deflection for Specimen C, under a centered URPP load of 100 Newtons, with all four sides simply supported.

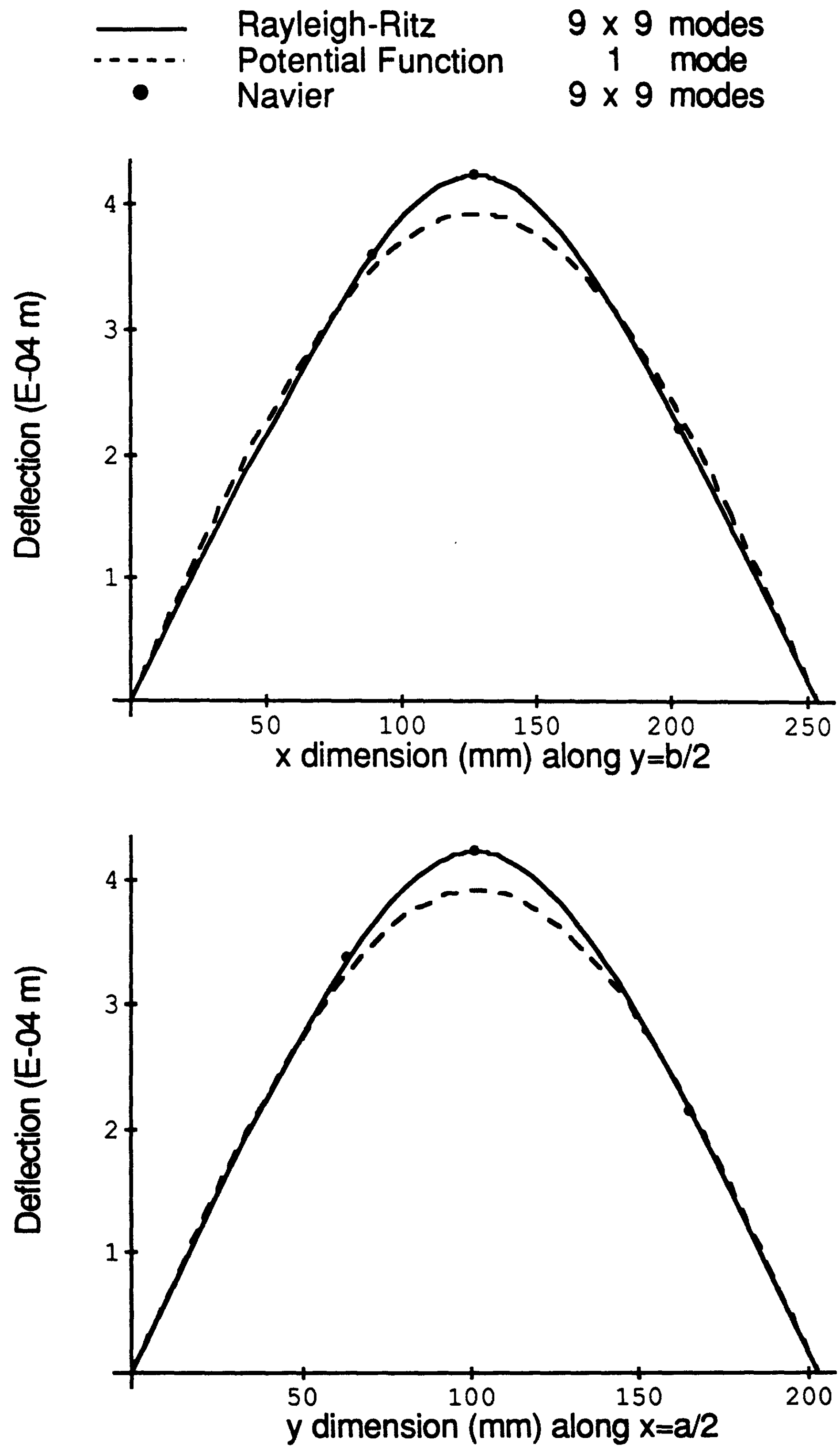

Figure 6.37 Transverse deflection for Specimen D, under a centered URPP load of 100 Newtons, with all four sides simply supported.

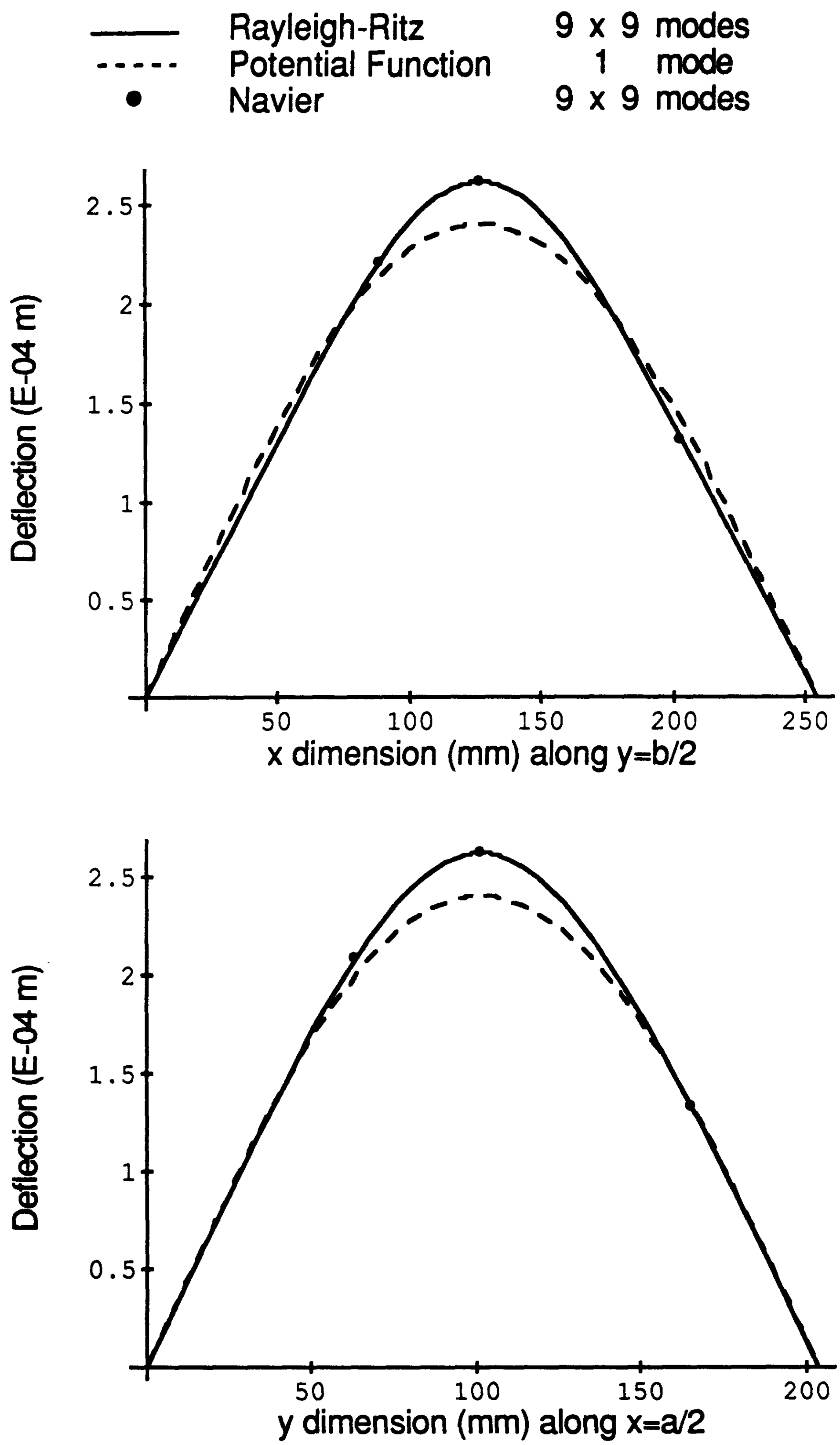

Figure 6.38 Transverse deflection for Specimen I, under a centered URPP load of 100 Newtons, with all four sides simply supported.

6.6 Results for Off-Center Uniform Rectangular Pressure Patch

This section presents the analytical results for the off-center uniform rectangular pressure patch (URPP) problems that were investigated experimentally. For all of the off-center load cases, the loading was centered at (x,y) = (76 mm,127 mm). The rectangular pressure patch was 50.8 cm by 63.5 cm and was aligned with the longer edge parallel to the x axis. The Rayleigh-Ritz and Navier solutions are presented for the five specimens, for the boundary conditions four sides clamped, x edges simply supported and y edges clamped, and four sides simply supported. The solutions are presented in graphical form, in Figures 6.39 through 6.53, as plots of transverse displacement along the plate centerlines.

The Rayleigh-Ritz solutions use 9 x 9 modes. The constrained Navier solutions use 50 modes in a direction with clamped boundary conditions, while the traditional Navier solutions use only 9 modes in a direction with simply supported boundary conditions. More modes were used for the constrained Navier solution due to its slower convergence. Both Navier solutions are given only at discrete points, selected to correspond to transducer locations in the experiments, due to the computer time involved with plotting a function which may consist of as many as 2500 terms.

Again, both Navier solutions neglect the bending-twisting coupling that is present in Specimens A and B. This coupling is correctly accounted for in the Rayleigh-Ritz formulation. Specimen A, which has a strong bending-twisting coupling, is poorly modeled by the Navier solutions.

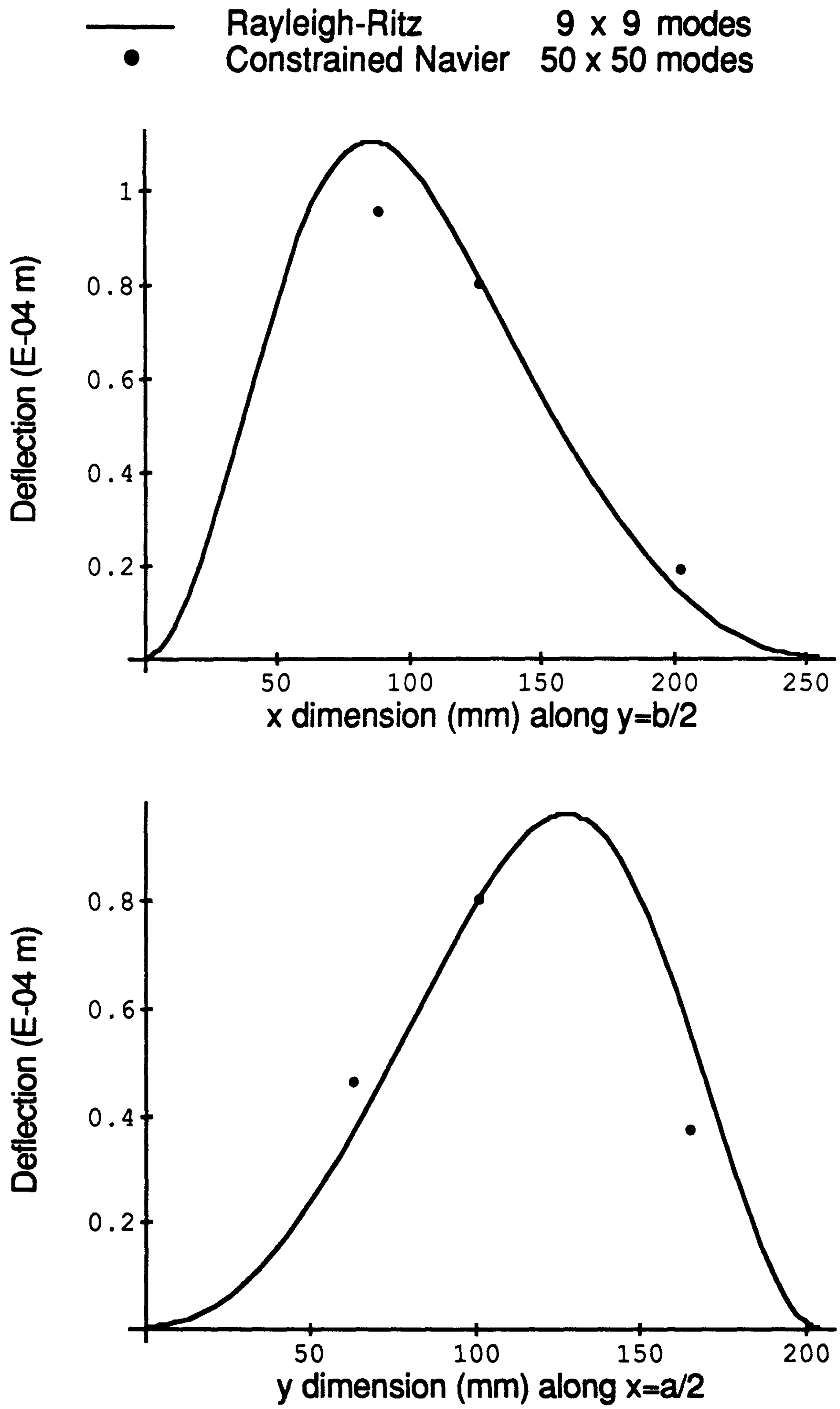

Figure 6.39 Transverse deflection for Specimen A, under an off-center URPP load of 100 Newtons, with all four sides clamped.

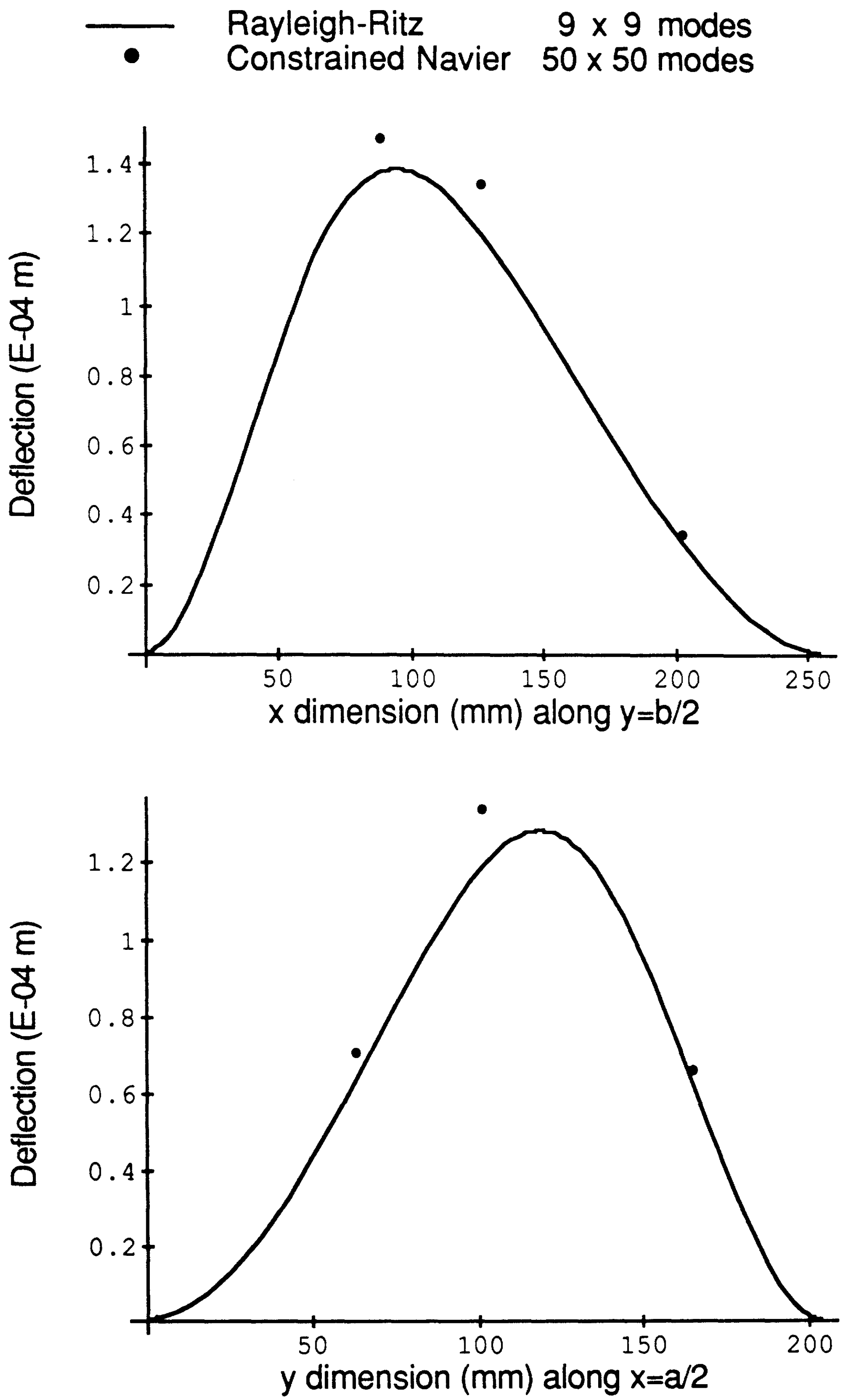

Figure 6.40 Transverse deflection for Specimen B, under an off-center URPP load of 100 Newtons, with all four sides clamped.

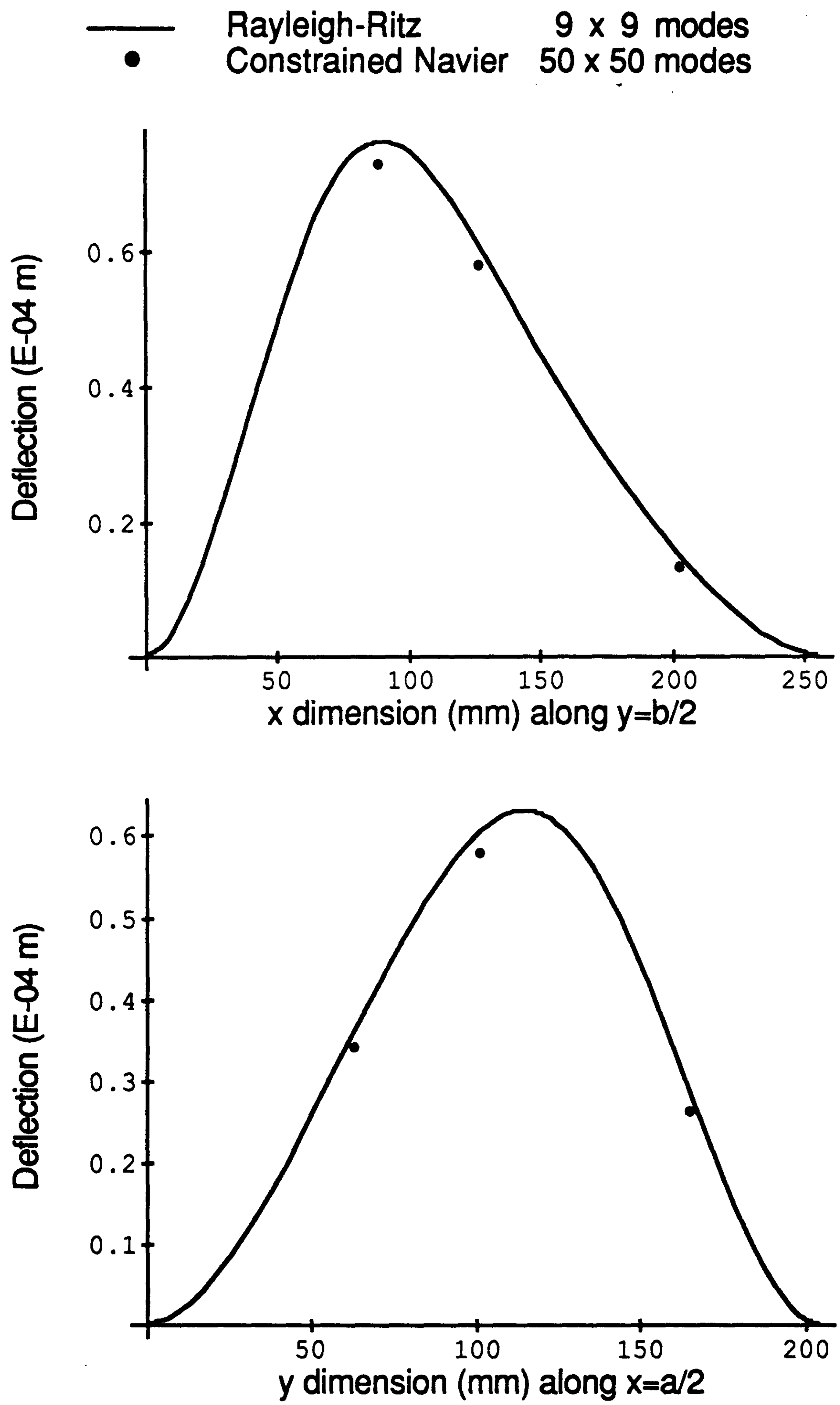

Figure 6.41 Transverse deflection for Specimen C, under an off-center URPP load of 100 Newtons, with all four sides clamped.

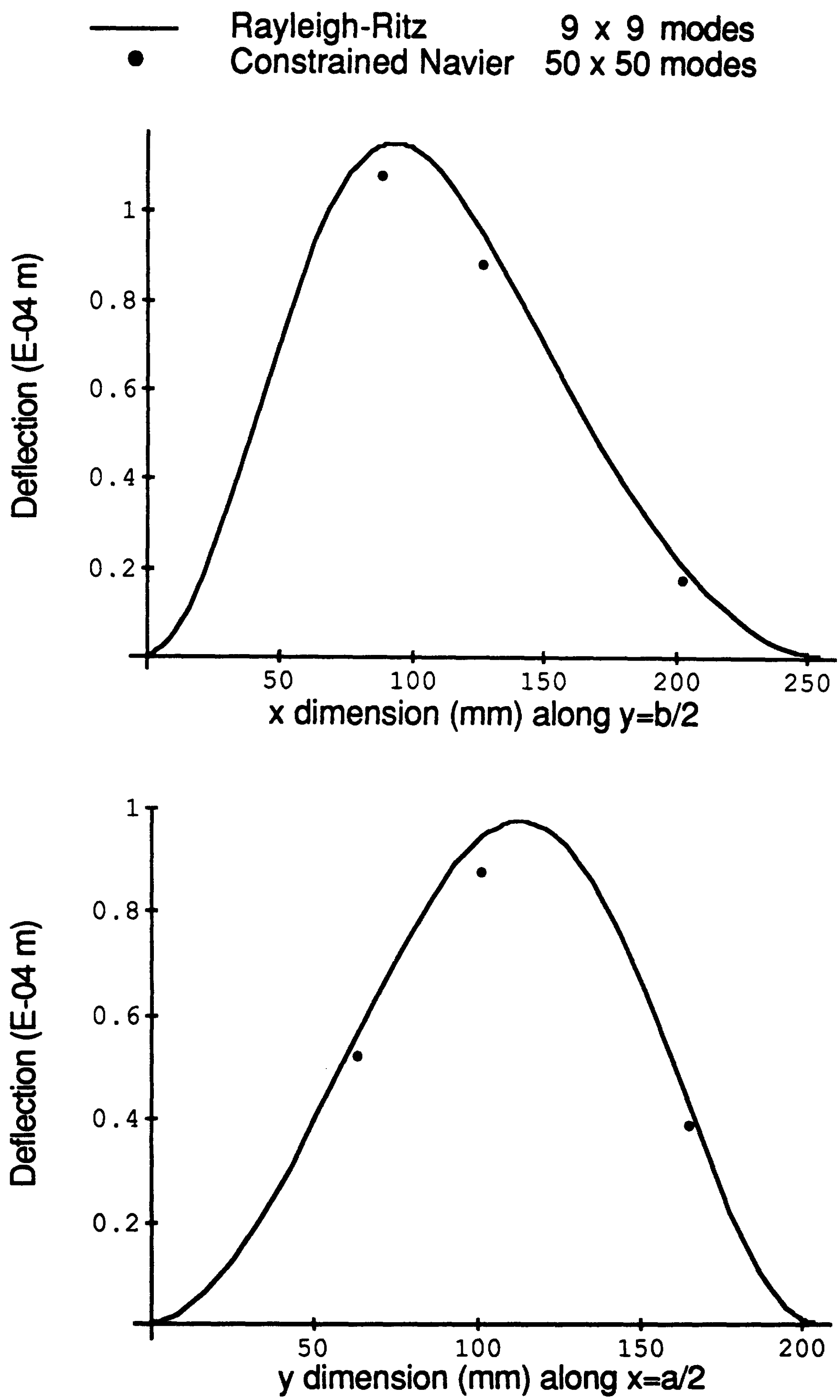

Figure 6.42 Transverse deflection for Specimen D, under an off-center URPP load of 100 Newtons, with all four sides clamped.

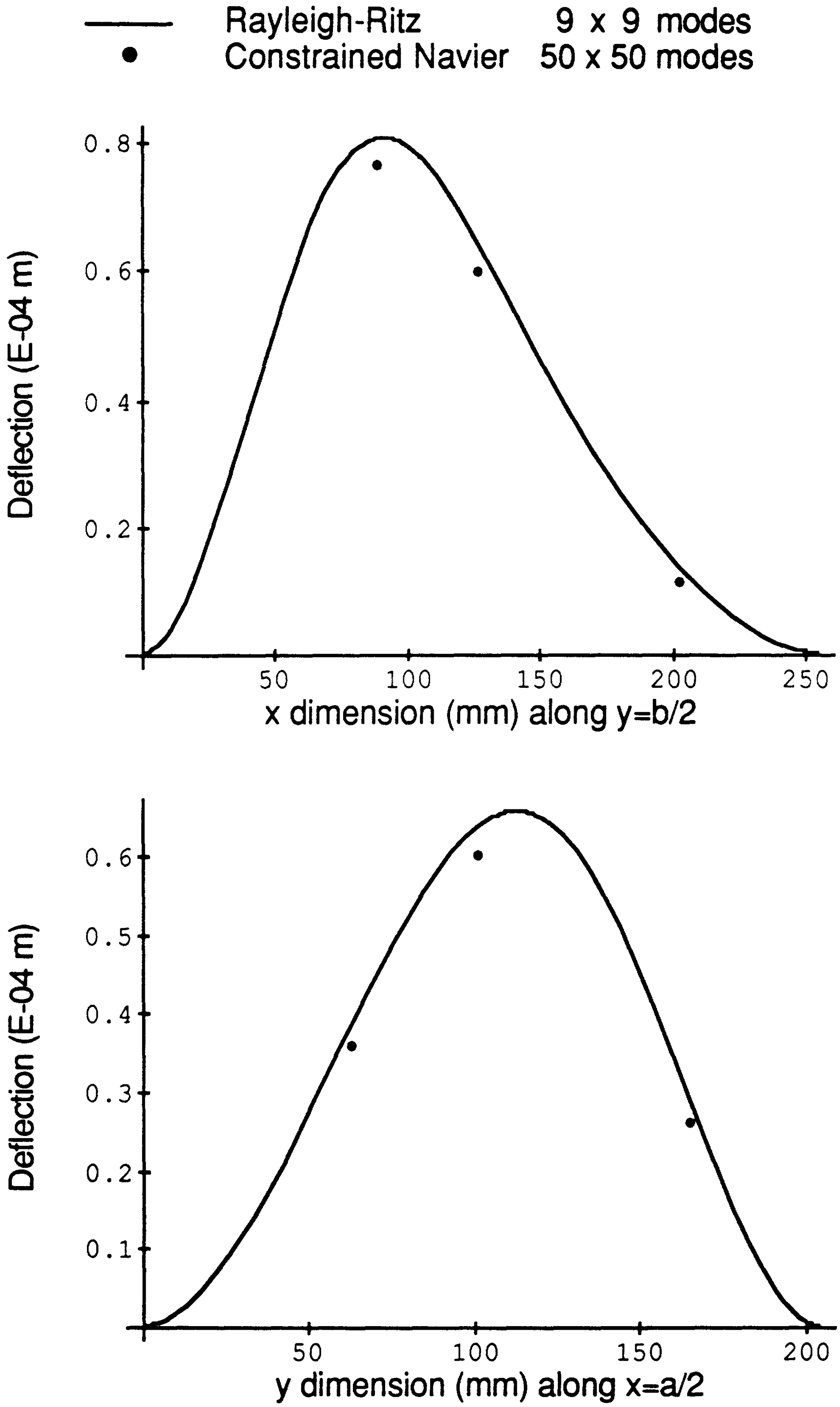

Figure 6.43 Transverse deflection for Specimen I, under an off-center URPP load of 100 Newtons, with all four sides clamped.

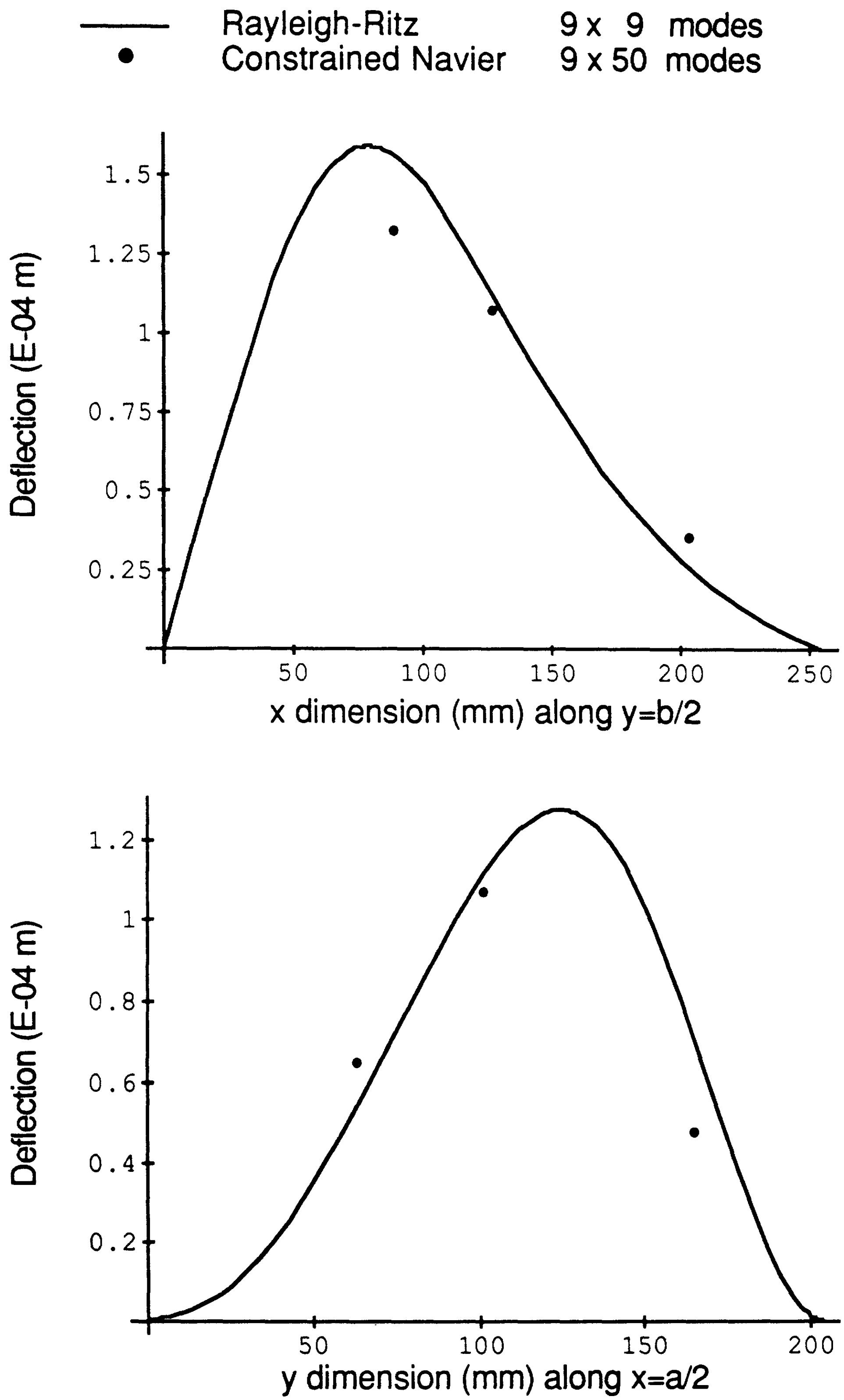

Figure 6.44 Transverse deflection for Specimen A, under an off-center URPP load of 100 Newtons, with x edges (short edges) simply supported and y edges (long edges) clamped.

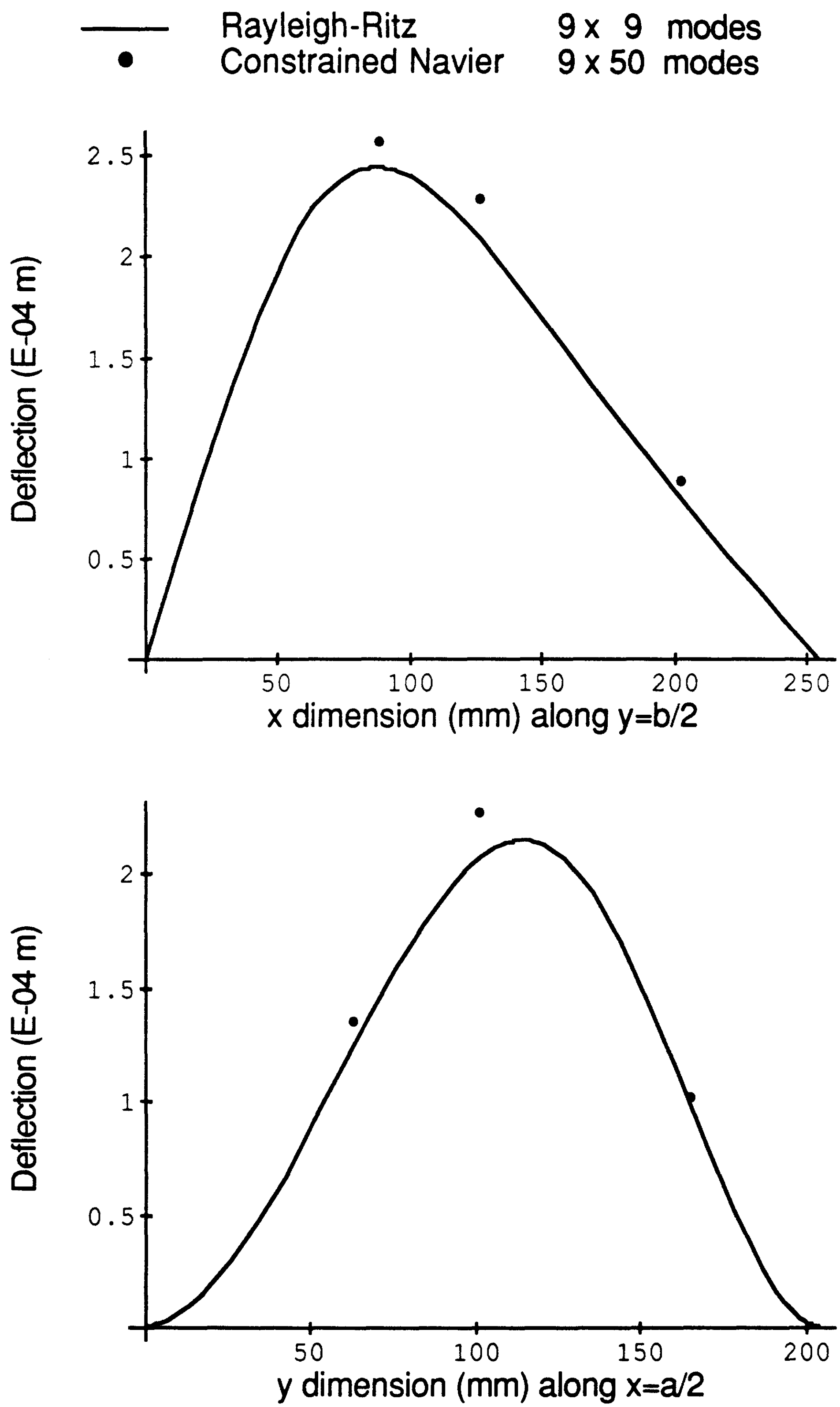

Figure 6.45 Transverse deflection for Specimen B, under an off-center URPP load of 100 Newtons, with x edges (short edges) simply supported and y edges (long edges) clamped.

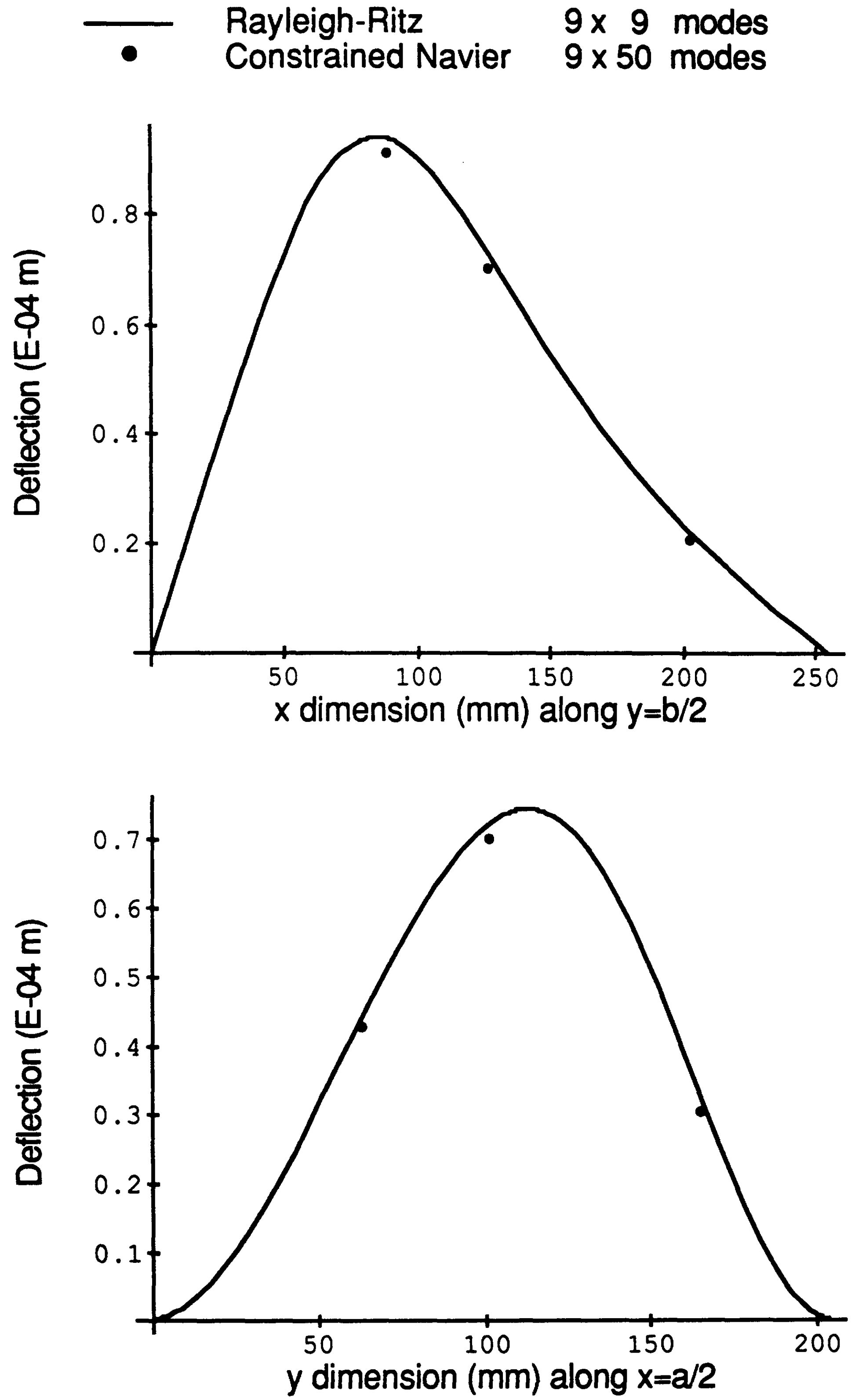

Figure 6.46 Transverse deflection for Specimen C, under an off-center URPP load of 100 Newtons, with x edges (short edges) simply supported and y edges (long edges) clamped.

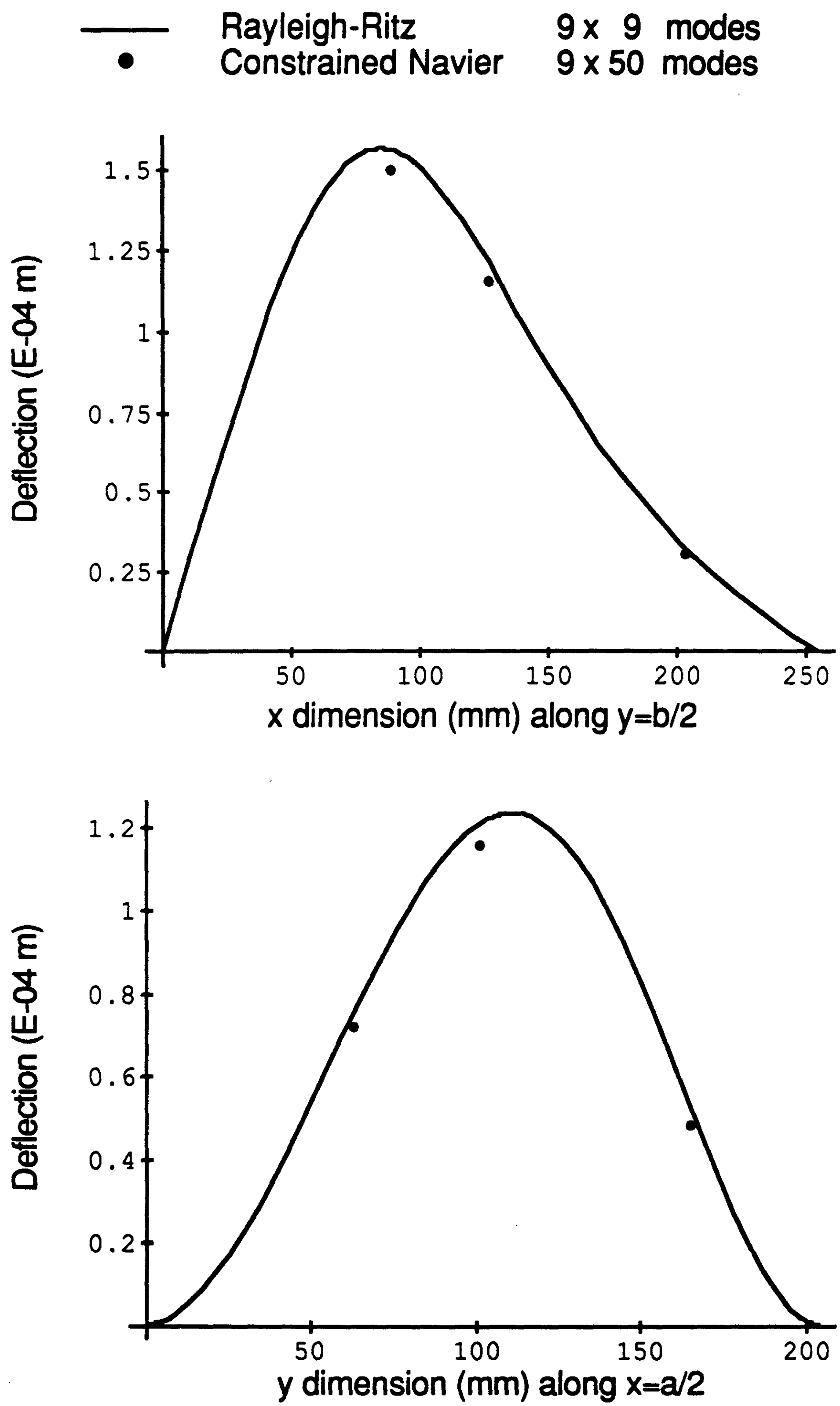

Figure 6.47 Transverse deflection for Specimen D, under an off-center URPP load of 100 Newtons, with x edges (short edges) simply supported and y edges (long edges) clamped.

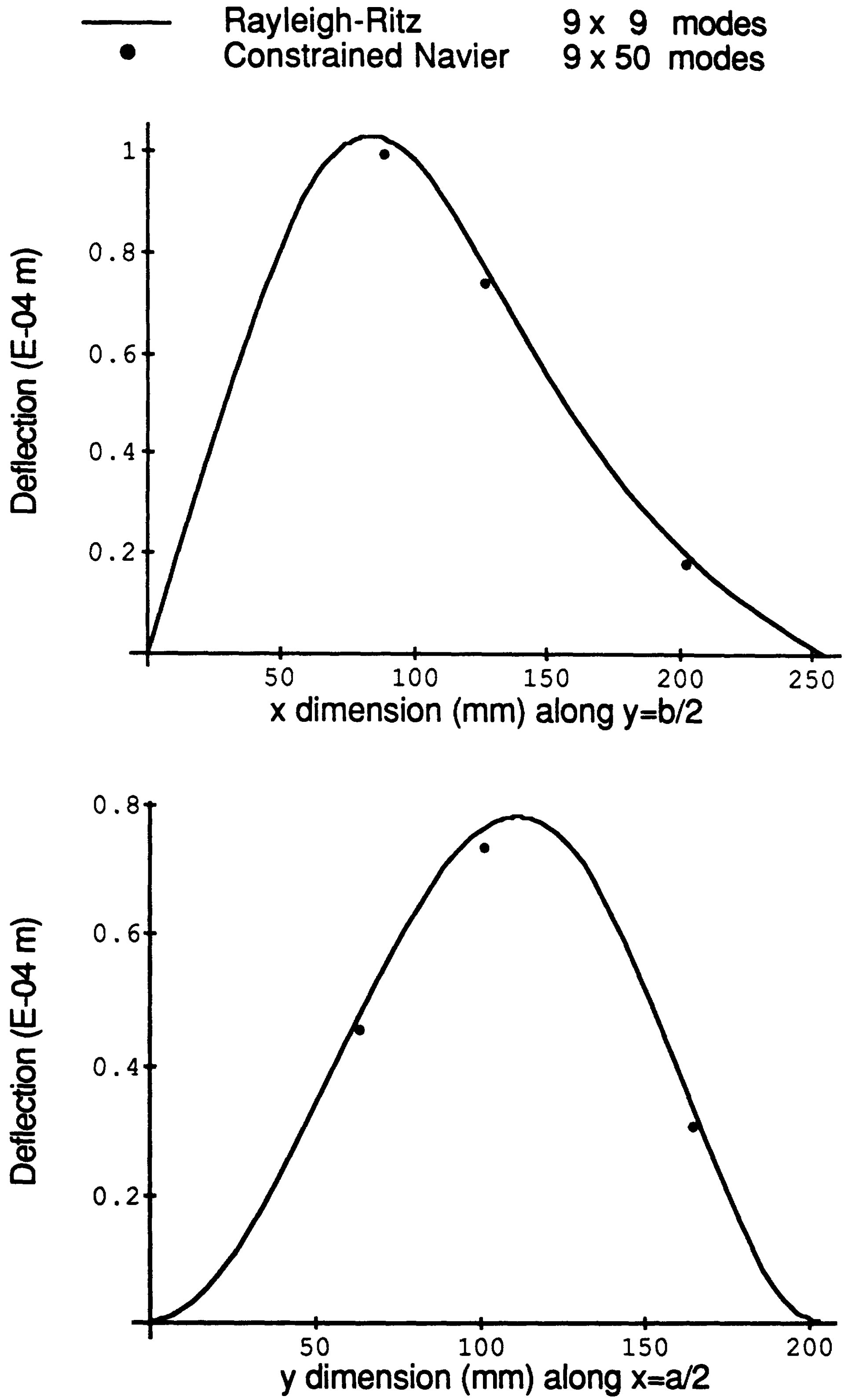

Figure 6.48 Transverse deflection for Specimen I, under an off-center URPP load of 100 Newtons, with x edges (short edges) simply supported and y edges (long edges) clamped.

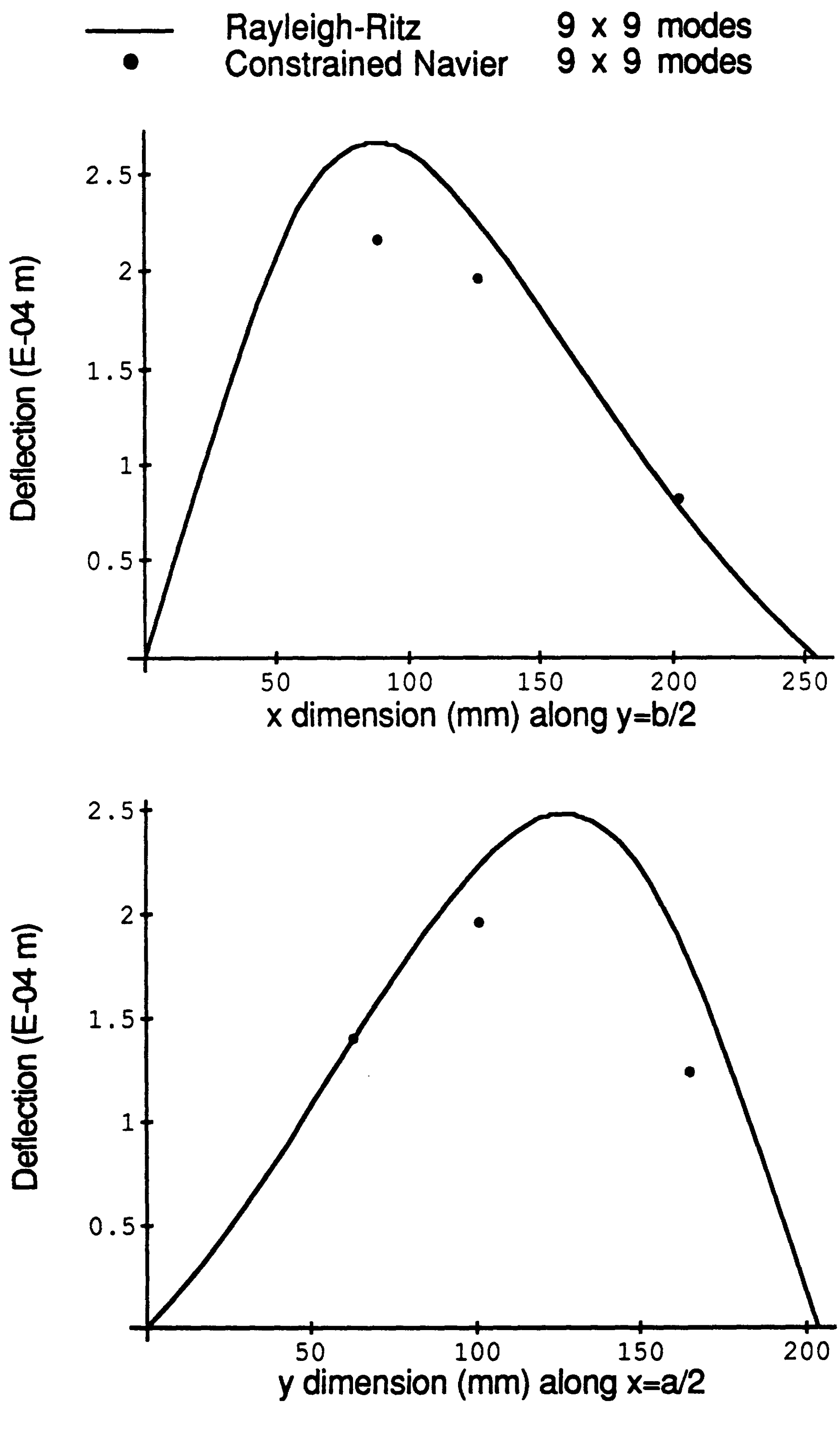

Figure 6.49 Transverse deflection for Specimen A, under an off-center URPP load of 100 Newtons, with all four sides simply supported.

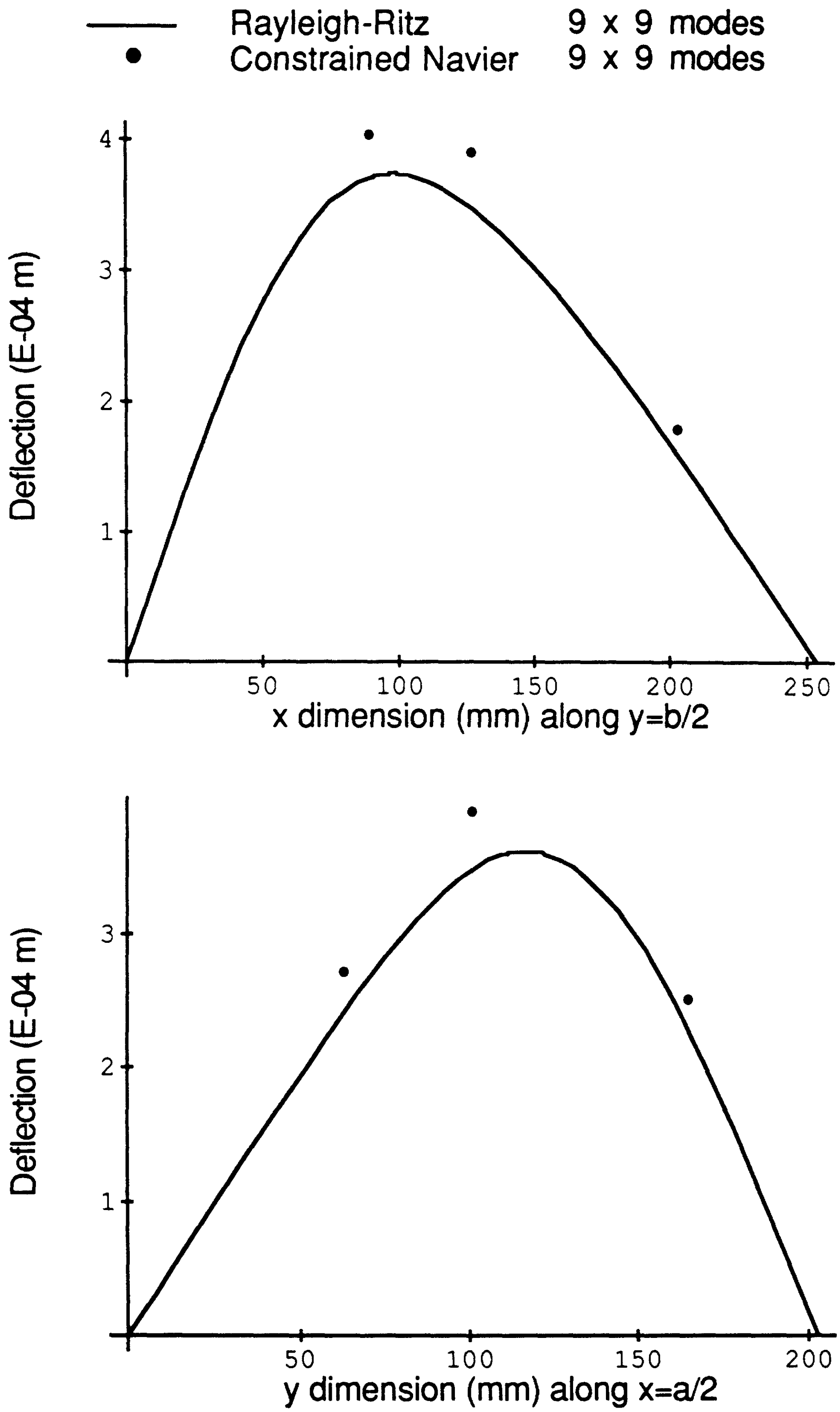

Figure 6.50 Transverse deflection for Specimen B, under an off-center URPP load of 100 Newtons, with all four sides simply supported.

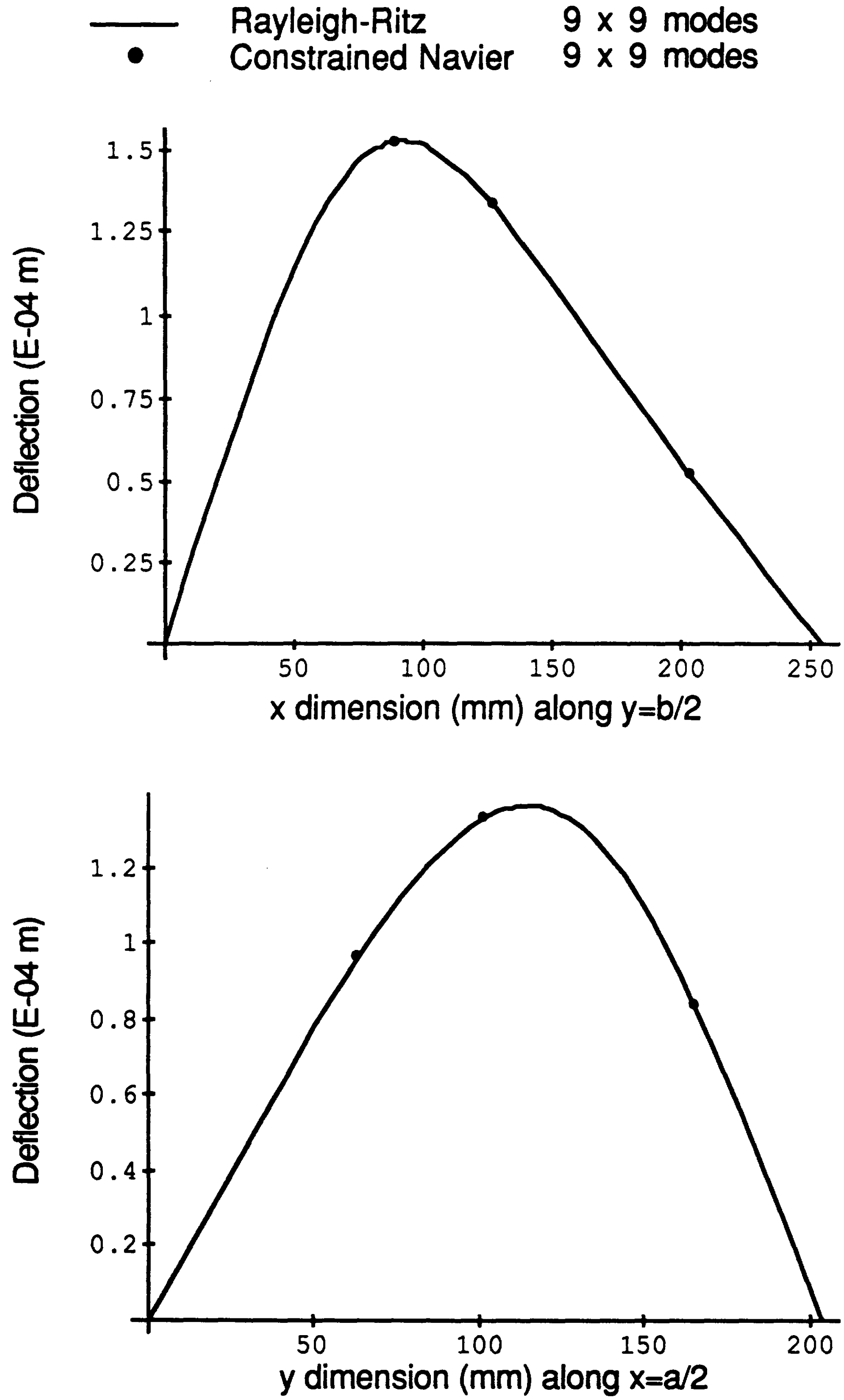

Figure 6.51 Transverse deflection for Specimen C, under an off-center URPP load of 100 Newtons, with all four sides simply supported.

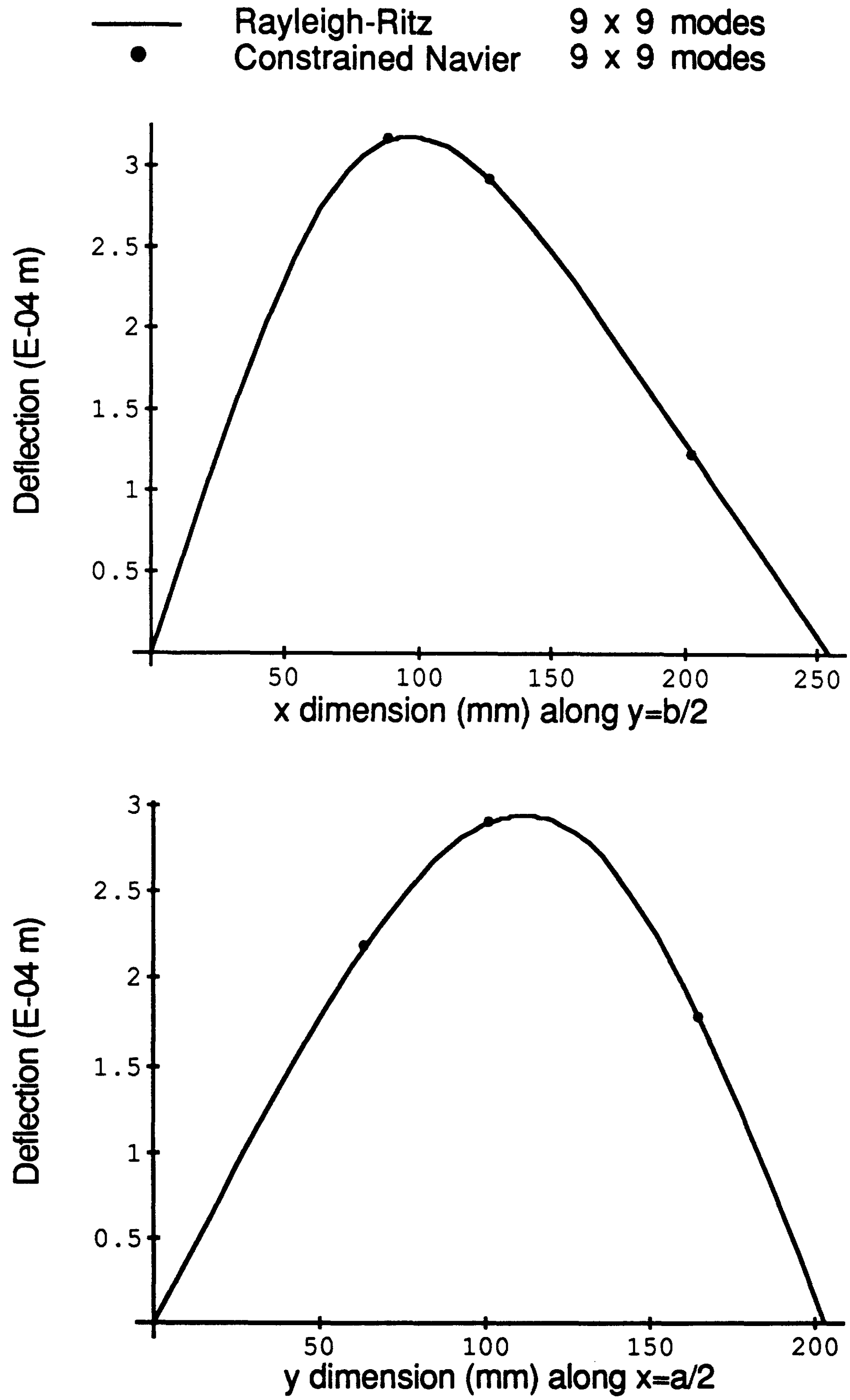

Figure 6.52 Transverse deflection for Specimen D, under an off-center URPP load of 100 Newtons, with all four sides simply supported.

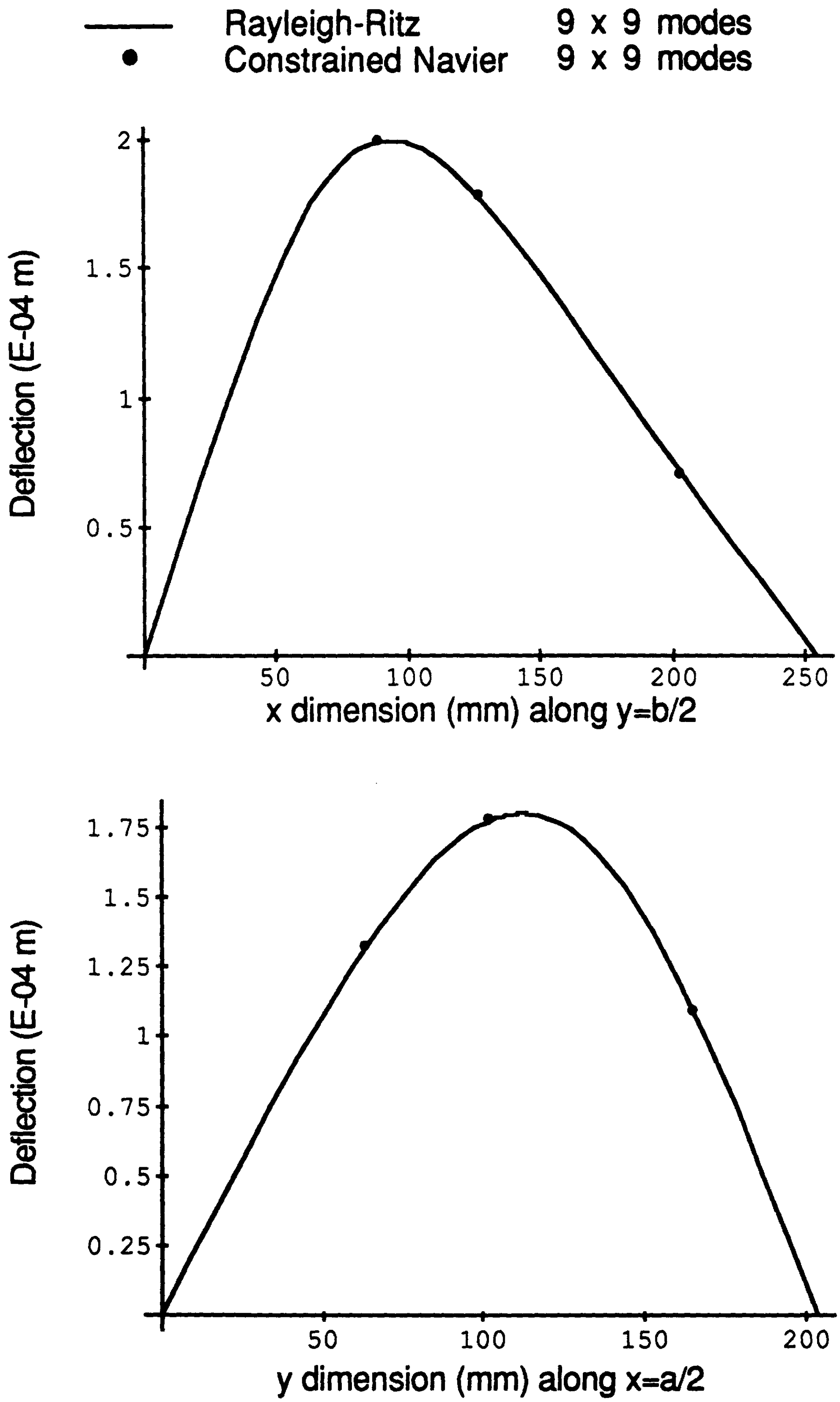

Figure 6.53 Transverse deflection for Specimen I, under an off-center URPP load of 100 Newtons, with all four sides simply supported.

6.7 Results for Uniform Pressure

This section presents the analytical results for the uniform pressure problems that were investigated experimentally. The Rayleigh-Ritz, single mode polynomial potential functions, and Navier solutions are presented for the five specimens, for the boundary conditions four sides clamped and four sides simply supported. Only Rayleigh-Ritz and Navier solutions are presented for the five specimens, for the boundary condition x edges clamped and y edges simply supported. The solutions are presented in graphical form, in Figures 6.54 through 6.68, as plots of transverse displacement along the plate centerlines.

The Rayleigh-Ritz solutions use 9 x 9 modes while the potential function solutions are all single mode solutions. The constrained Navier solutions use 50 modes in a direction with clamped boundary conditions, while the traditional Navier solutions use only 9 modes in a direction with simply supported boundary conditions. More modes were used for the constrained Navier solution due to its slower convergence. Both Navier solutions are given only at discrete points, selected to correspond to transducer locations in the experiments, due to the computer time involved with plotting a function which may consist of as many as 2500 terms.

Again, the constrained Navier, the traditional Navier, and the potential function solutions neglect the bending-twisting coupling that is present in Specimens A and B. This coupling is correctly accounted for in the Rayleigh-Ritz formulation. Specimen A, which has a strong bending-twisting coupling, is poorly modeled by the Navier solutions.

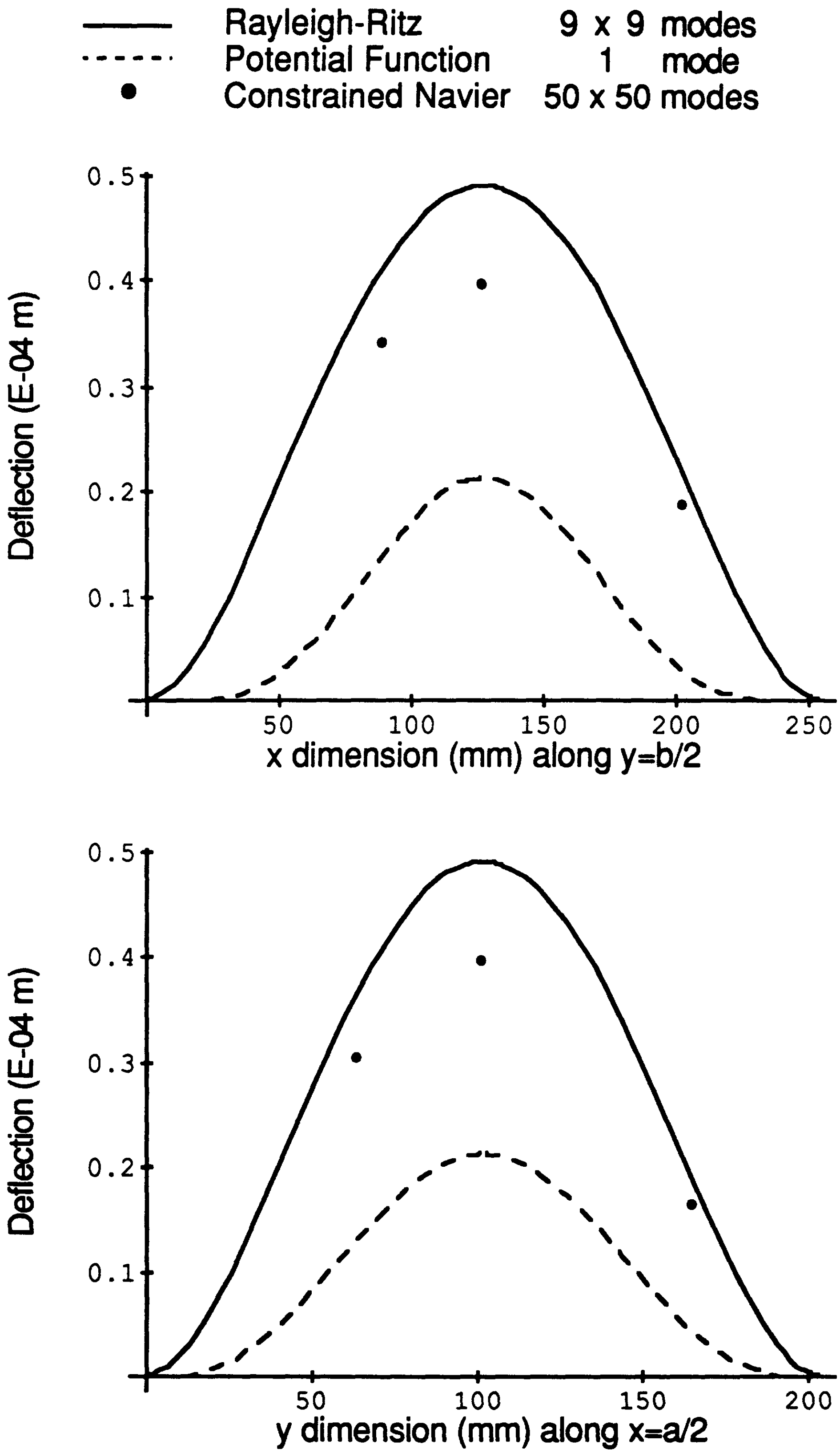

Figure 6.54 Transverse deflection for Specimen A, under a uniform pressure load of 100 Newtons, with all four sides clamped.

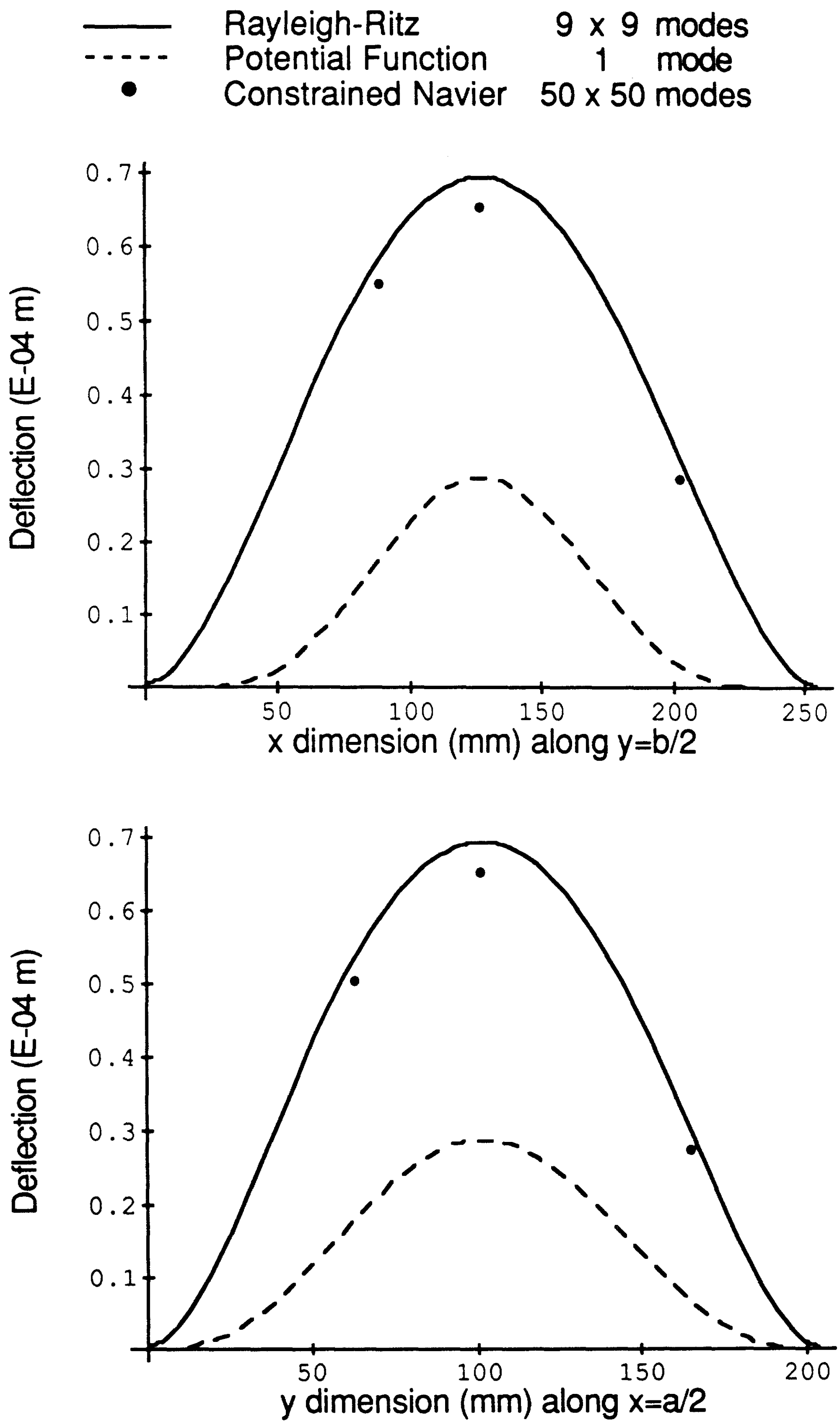

Figure 6.55 Transverse deflection for Specimen B, under a uniform pressure load of 100 Newtons, with all four sides clamped.

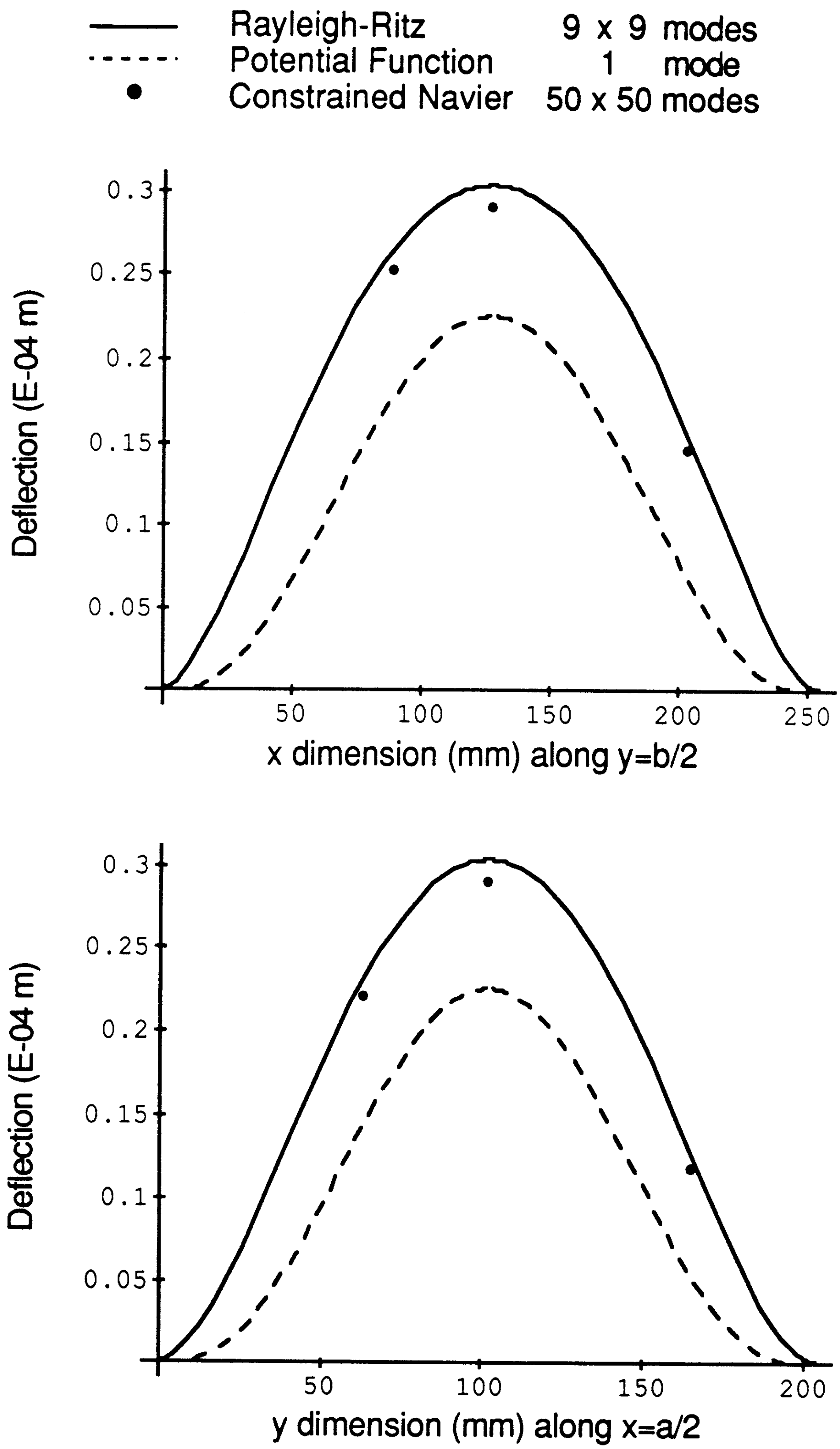

Figure 6.56 Transverse deflection for Specimen C, under a uniform pressure load of 100 Newtons, with all four sides clamped.

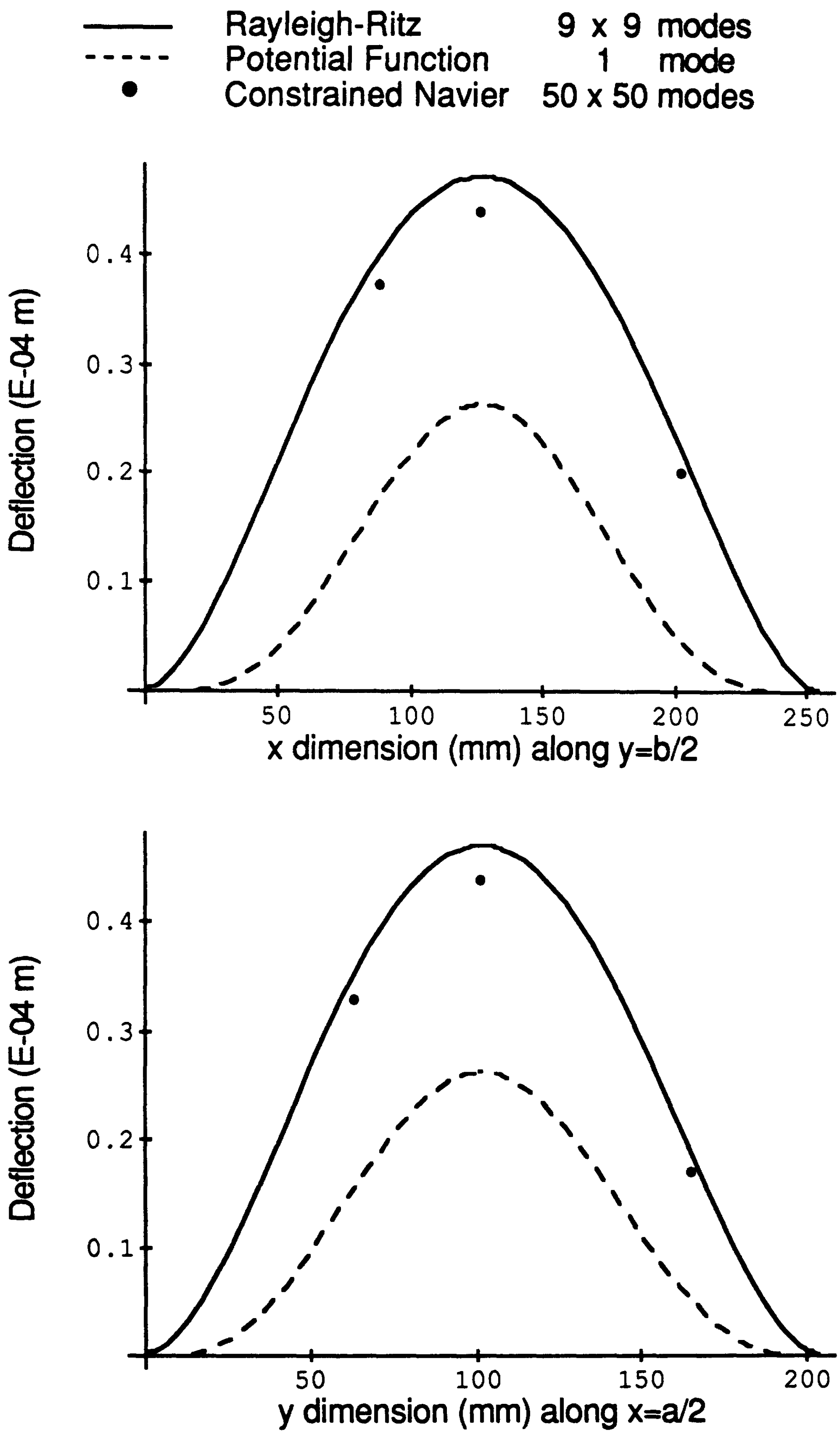

Figure 6.57 Transverse deflection for Specimen D, under a uniform pressure load of 100 Newtons, with all four sides clamped.

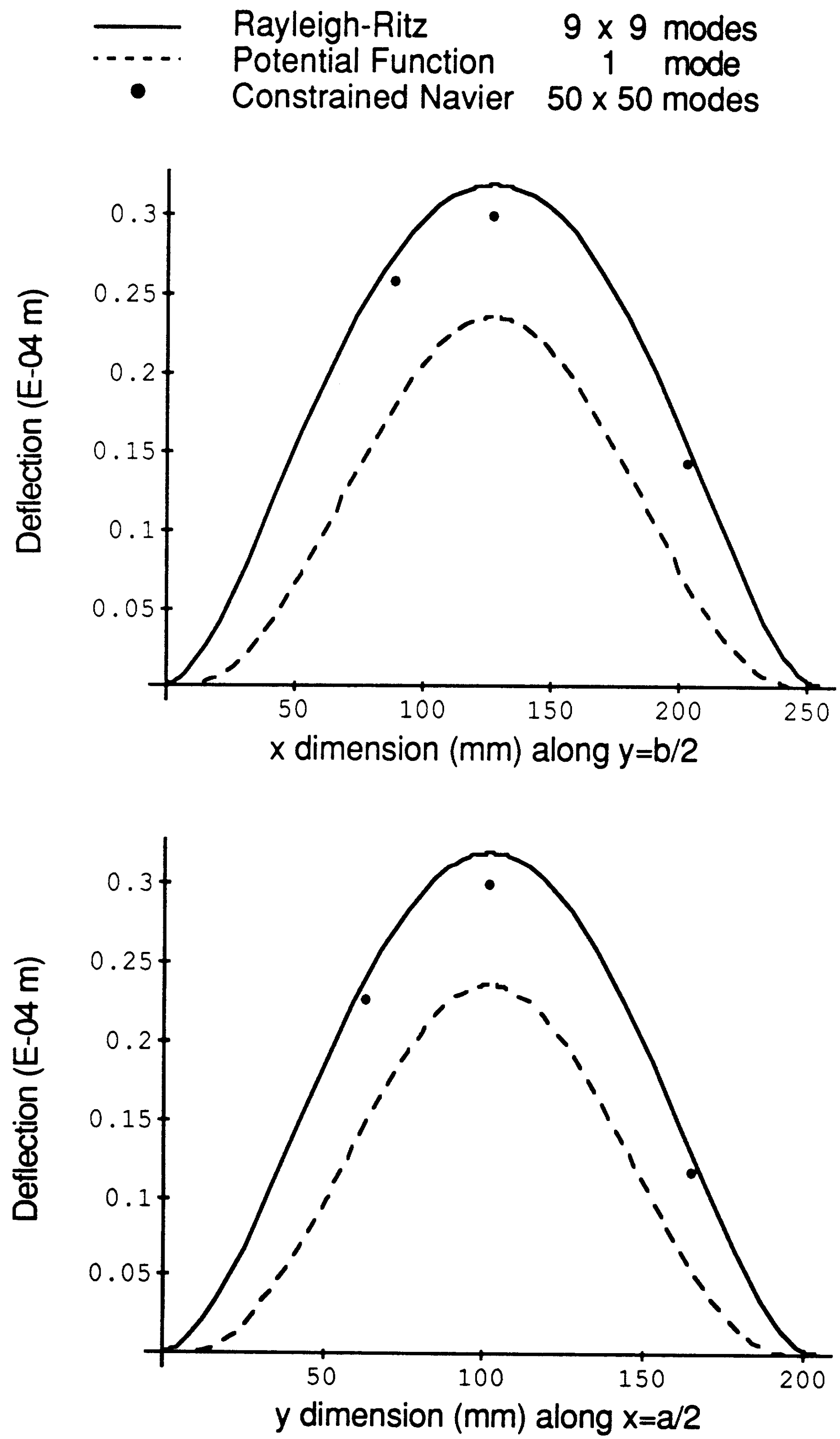

Figure 6.58 Transverse deflection for Specimen I, under a uniform pressure load of 100 Newtons, with all four sides clamped.

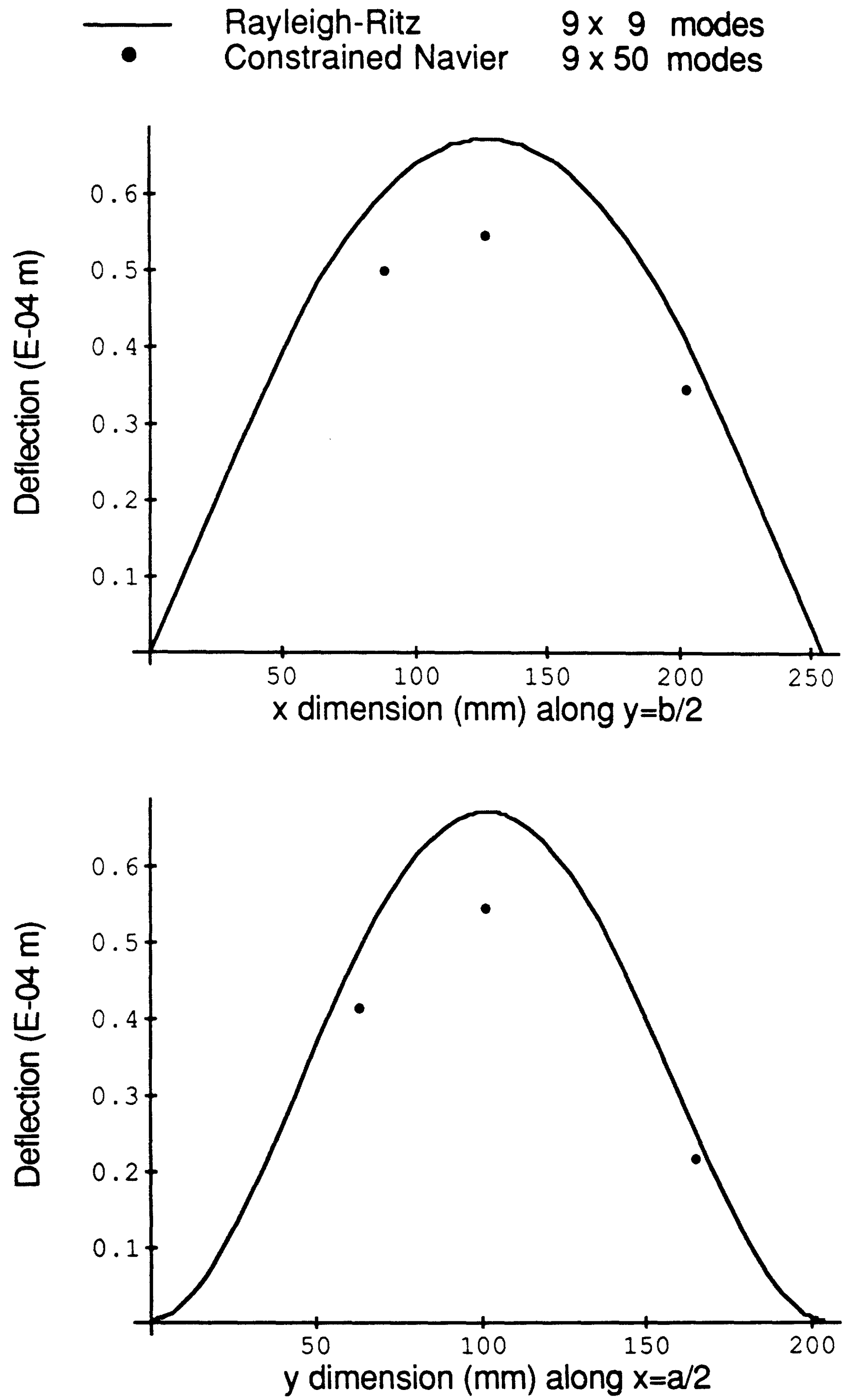

Figure 6.59 Transverse deflection for Specimen A, under a uniform pressure load of 100 Newtons, with x edges (short edges) simply supported and y edges (long edges) clamped.

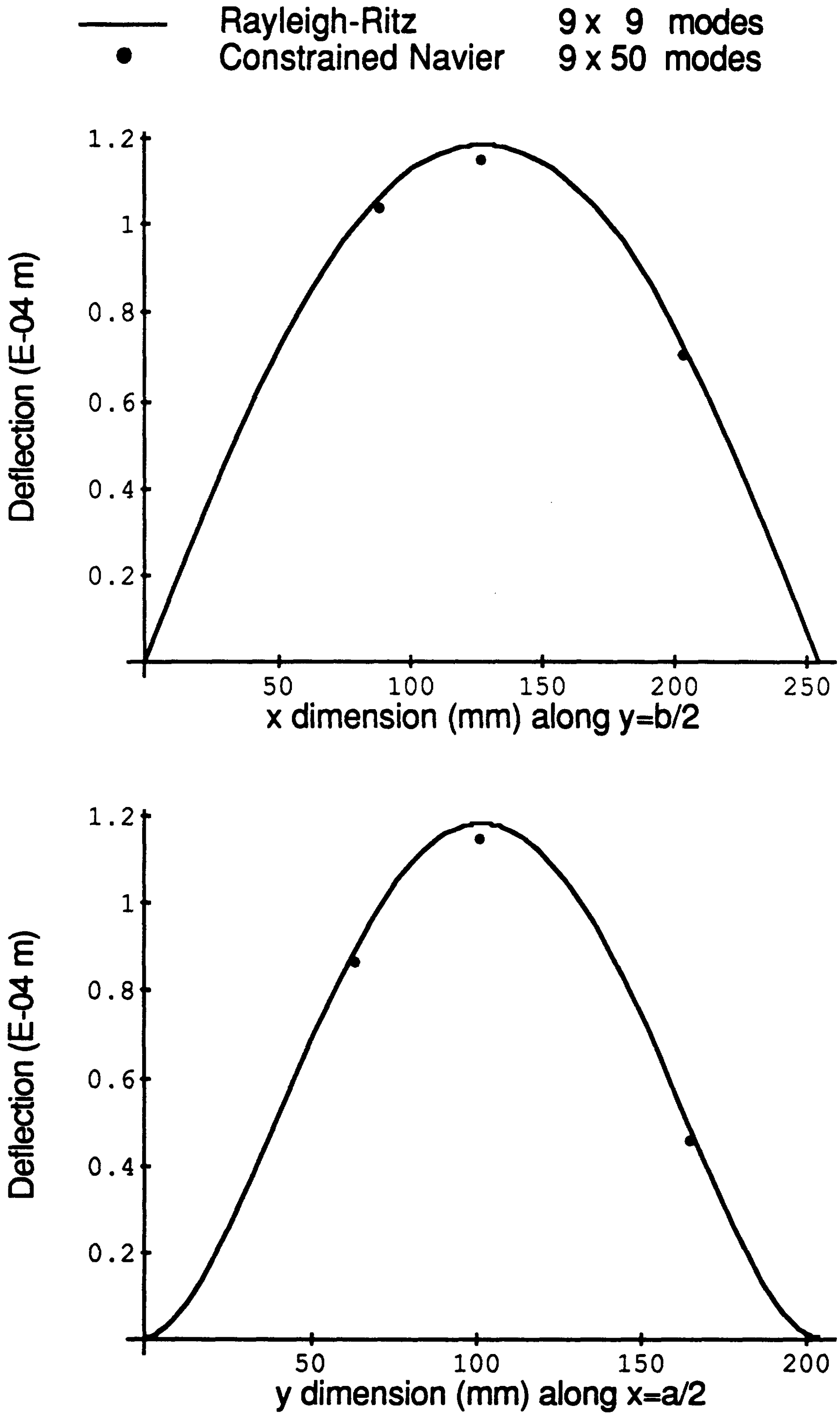

Figure 6.60 Transverse deflection for Specimen B, under a uniform pressure load of 100 Newtons, with x edges (short edges) simply supported and y edges (long edges) clamped.

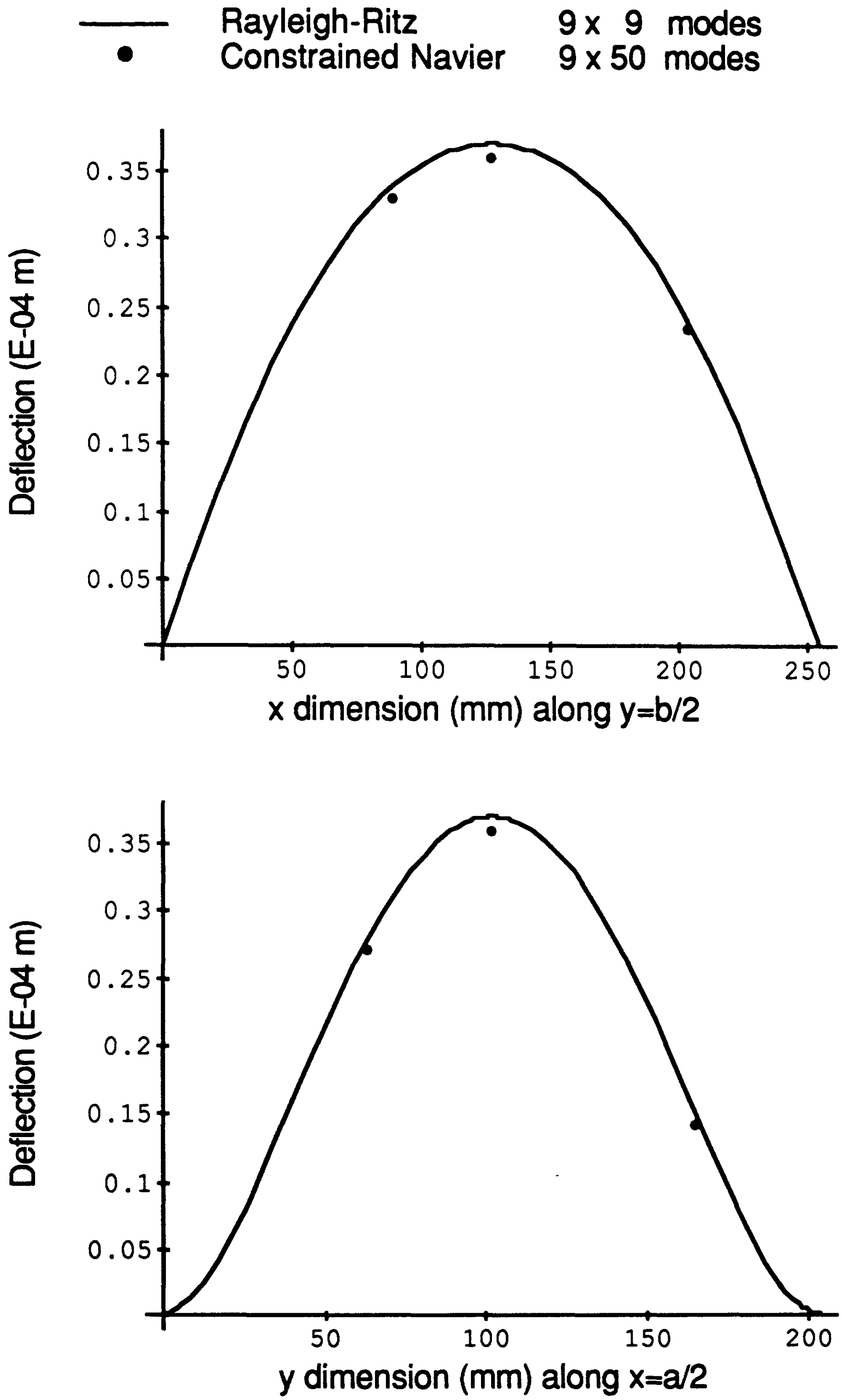

Figure 6.61 Transverse deflection for Specimen C, under a uniform pressure load of 100 Newtons, with x edges (short edges) simply supported and y edges (long edges) clamped.

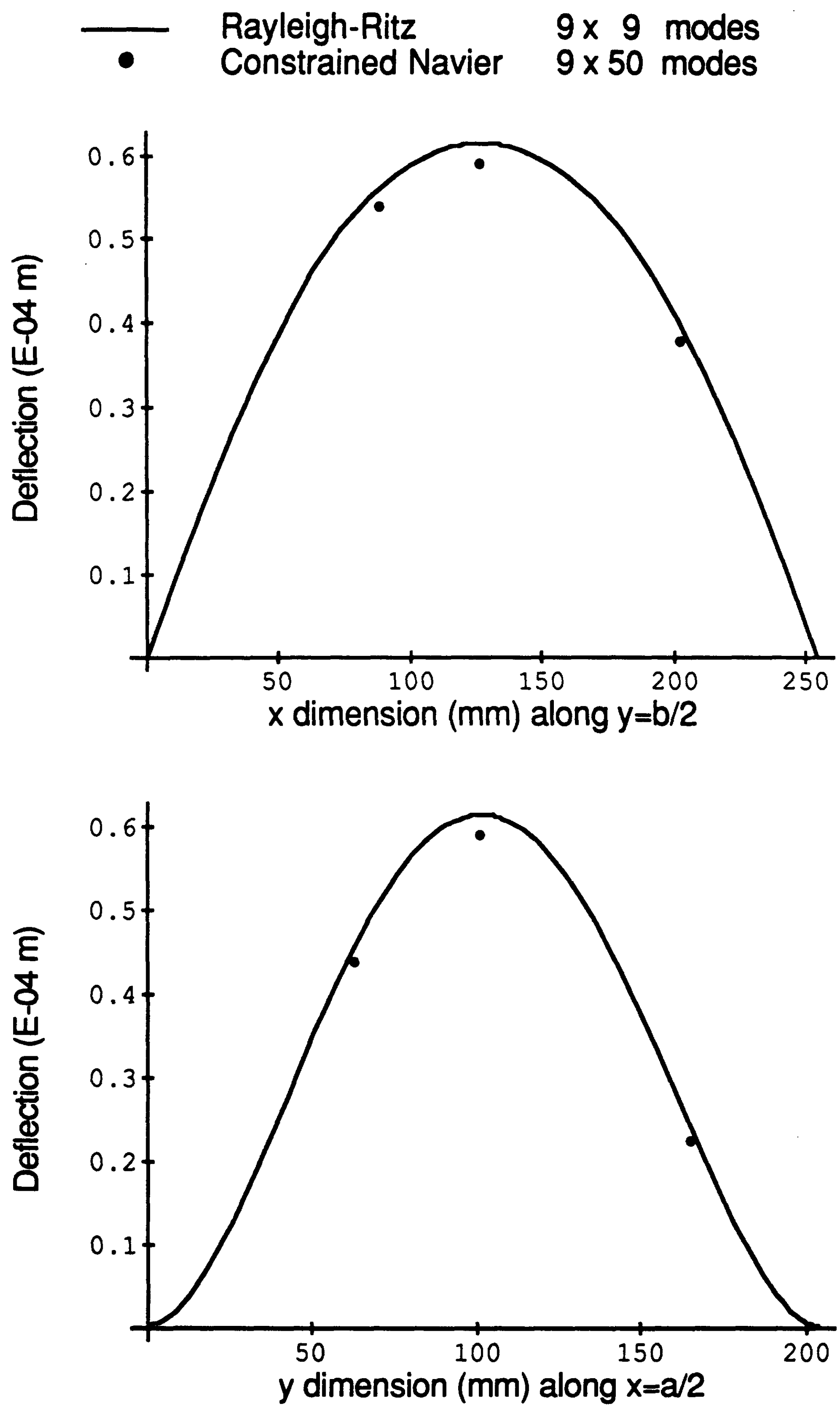

Figure 6.62 **Transverse deflection for Specimen D, under a uniform pressure load of 100 Newtons, with x edges (short edges) simply supported and y edges (long edges) clamped.**

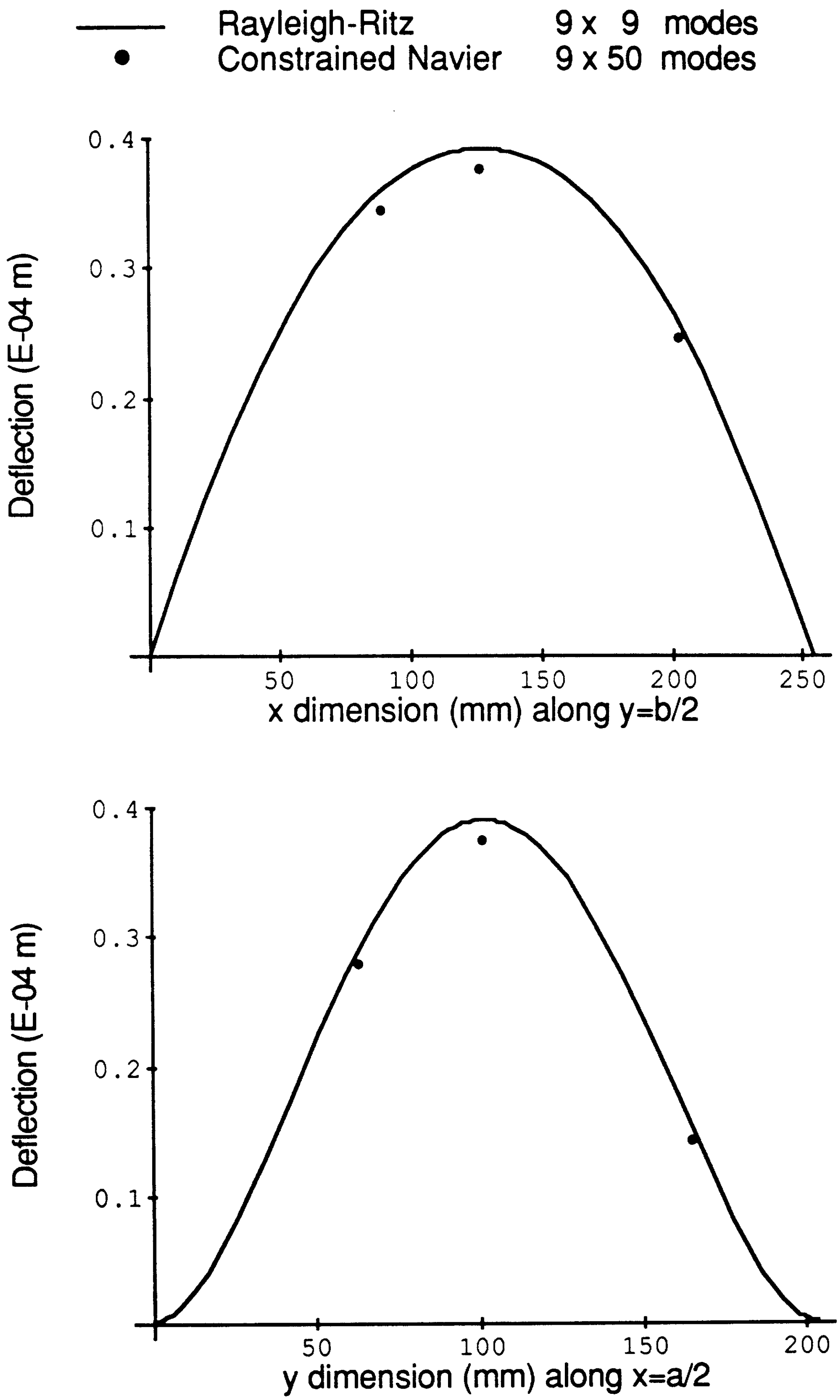

Figure 6.63 Transverse deflection for Specimen I, under a uniform pressure load of 100 Newtons, with x edges (short edges) simply supported and y edges (long edges) clamped.

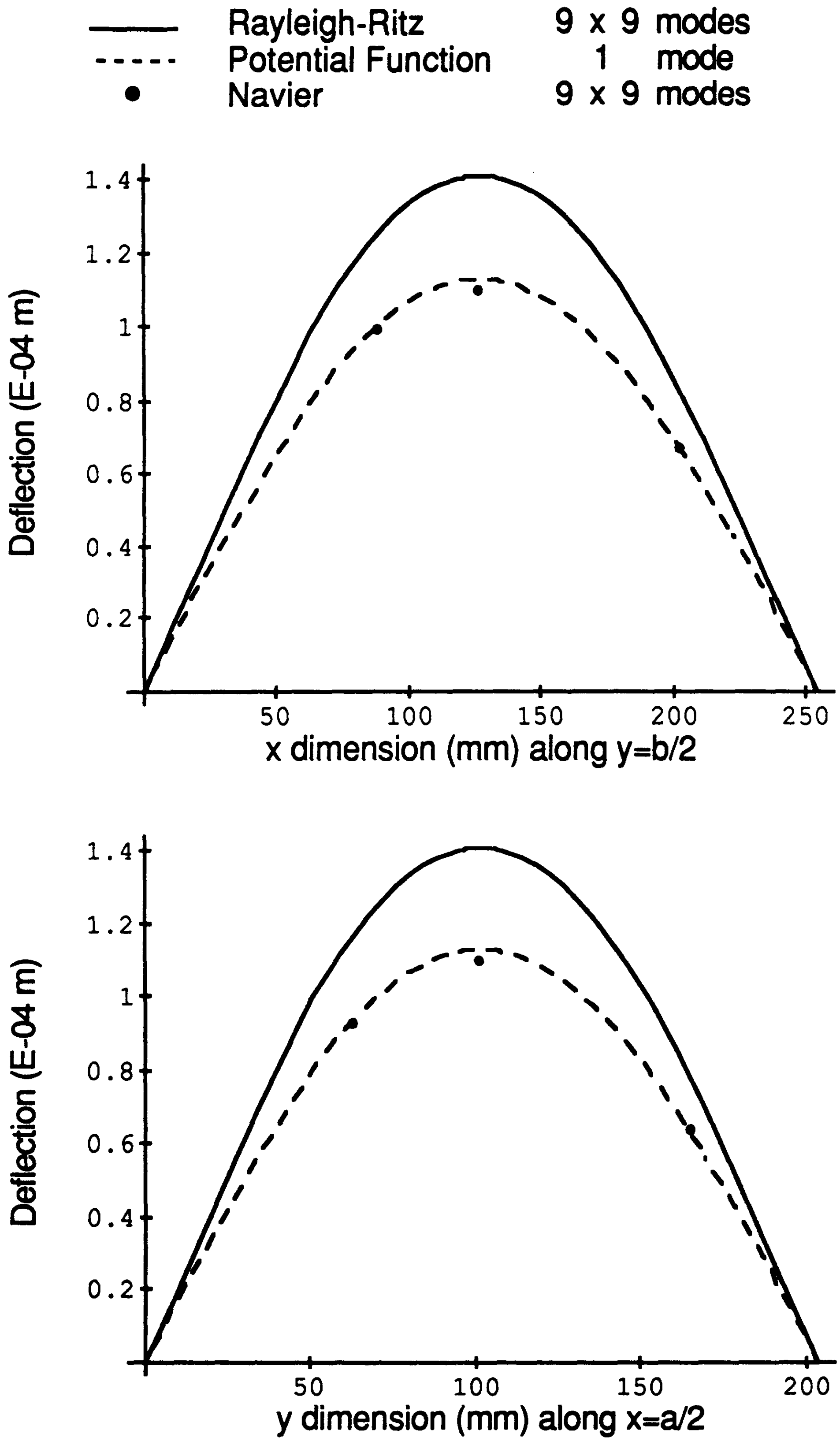

Figure 6.64 Transverse deflection for Specimen A, under a uniform pressure load of 100 Newtons, with all four sides simply supported.

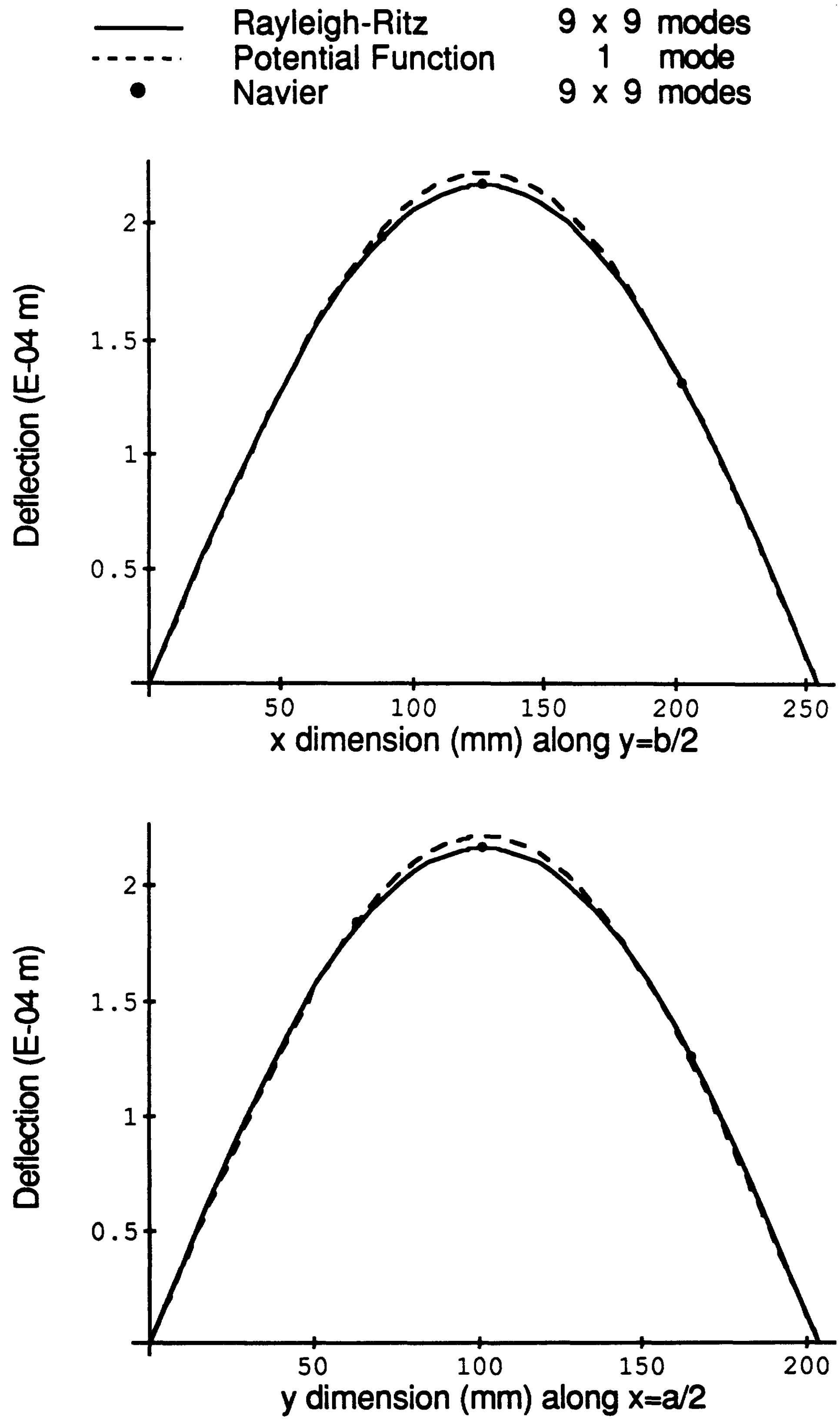

Figure 6.65 Transverse deflection for Specimen B, under a uniform pressure load of 100 Newtons, with all four sides simply supported.

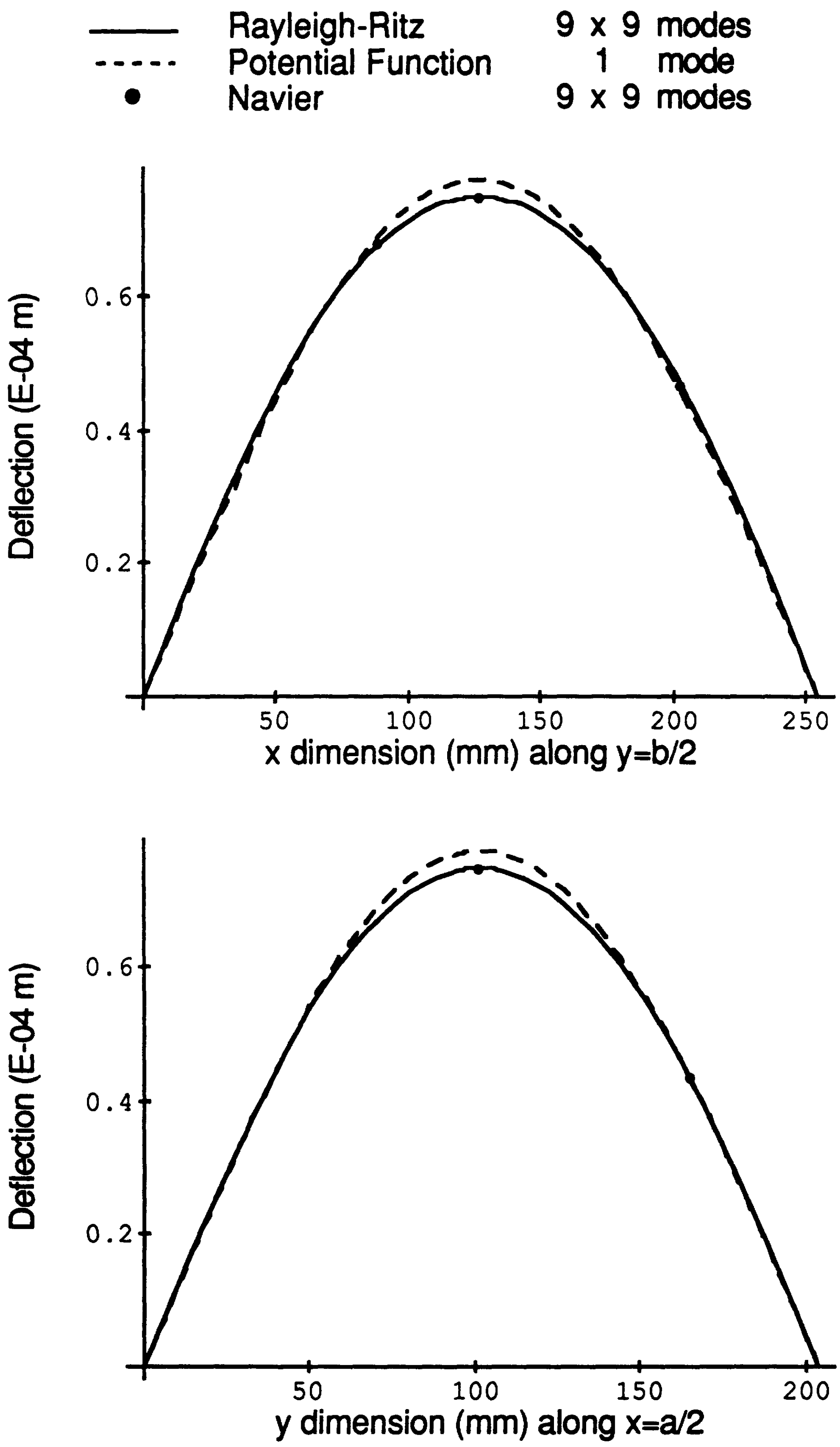

Figure 6.66 Transverse deflection for Specimen C, under a uniform pressure load of 100 Newtons, with all four sides simply supported.

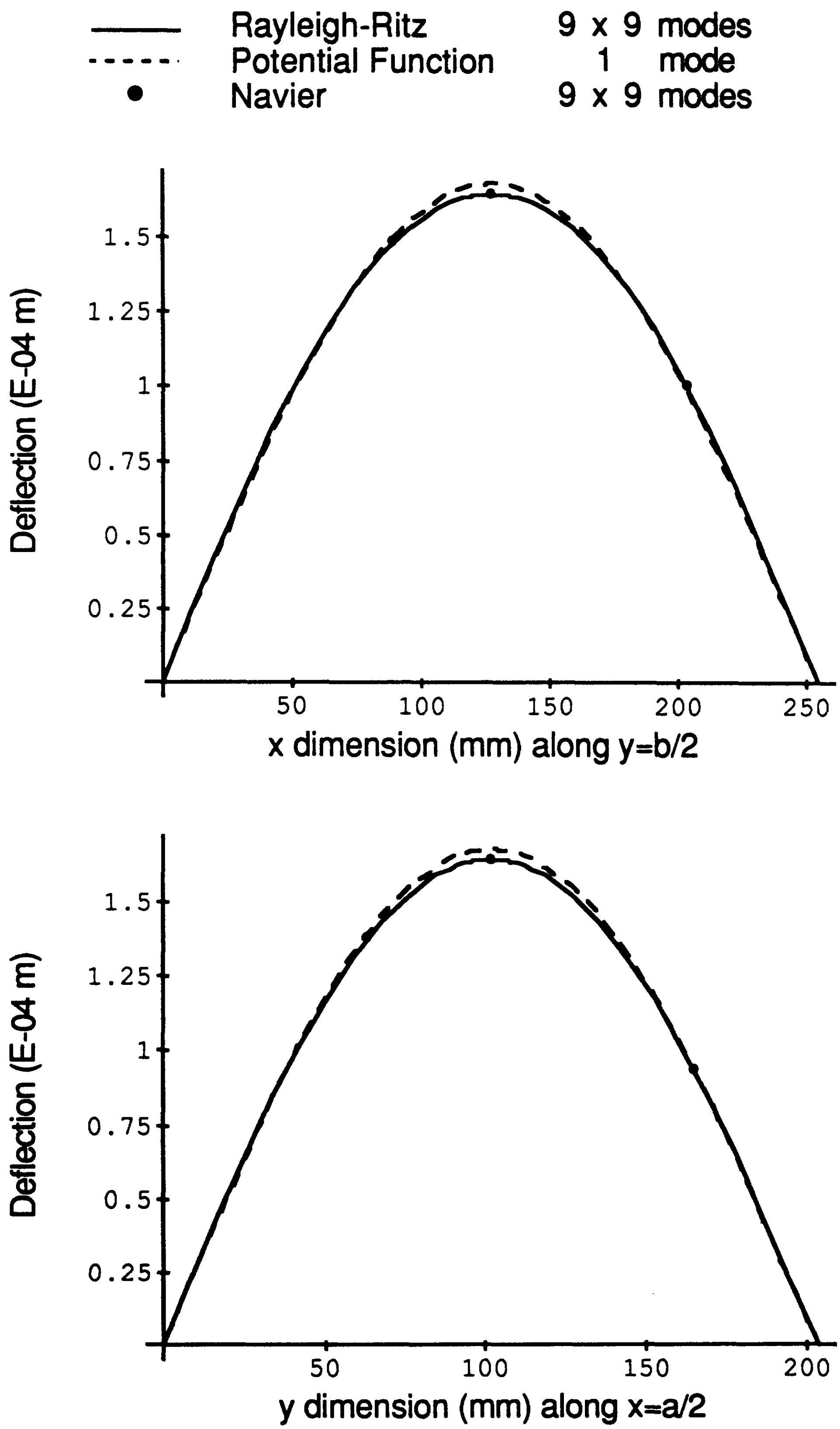

Figure 6.67 Transverse deflection for Specimen D, under a uniform pressure load of 100 Newtons, with all four sides simply supported.

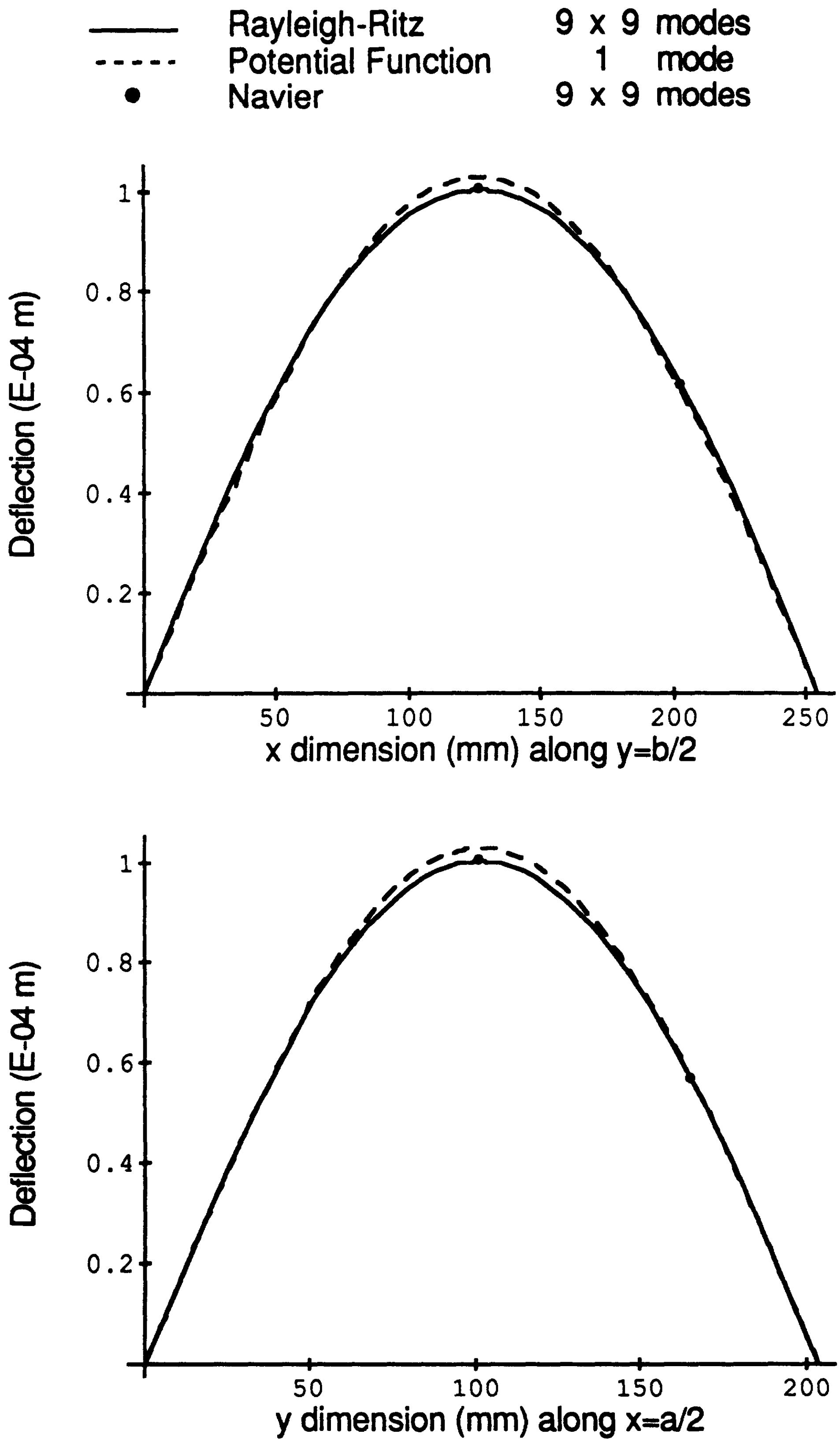

Figure 6.68 Transverse deflection for Specimen I, under a uniform pressure load of 100 Newtons, with all four sides simply supported.

6.8 Results for Free Vibration

Analytical, free vibration mode shapes and natural frequencies were found for each of the five plates for the boundary conditions four sides clamped, x edges simply supported and y edges clamped, and four edges simply supported. The mode shapes and natural frequencies were determined from a Rayleigh-Ritz analysis using 9 x 9 modes. The rotary inertia was ignored, as discussed in section 6.2, to simplify the calculation of the frequencies. Bending-twisting coupling was included in the Rayleigh-Ritz model.

The first four mode shapes and corresponding frequencies for each specimen and boundary condition are presented in Figures 6.69 through 6.83. The strong bending-twisting coupling of Specimen A, which causes the node lines to rotate from the plate axes, is very evident, while the weak bending-twisting coupling of Specimen B is barely noticeable.

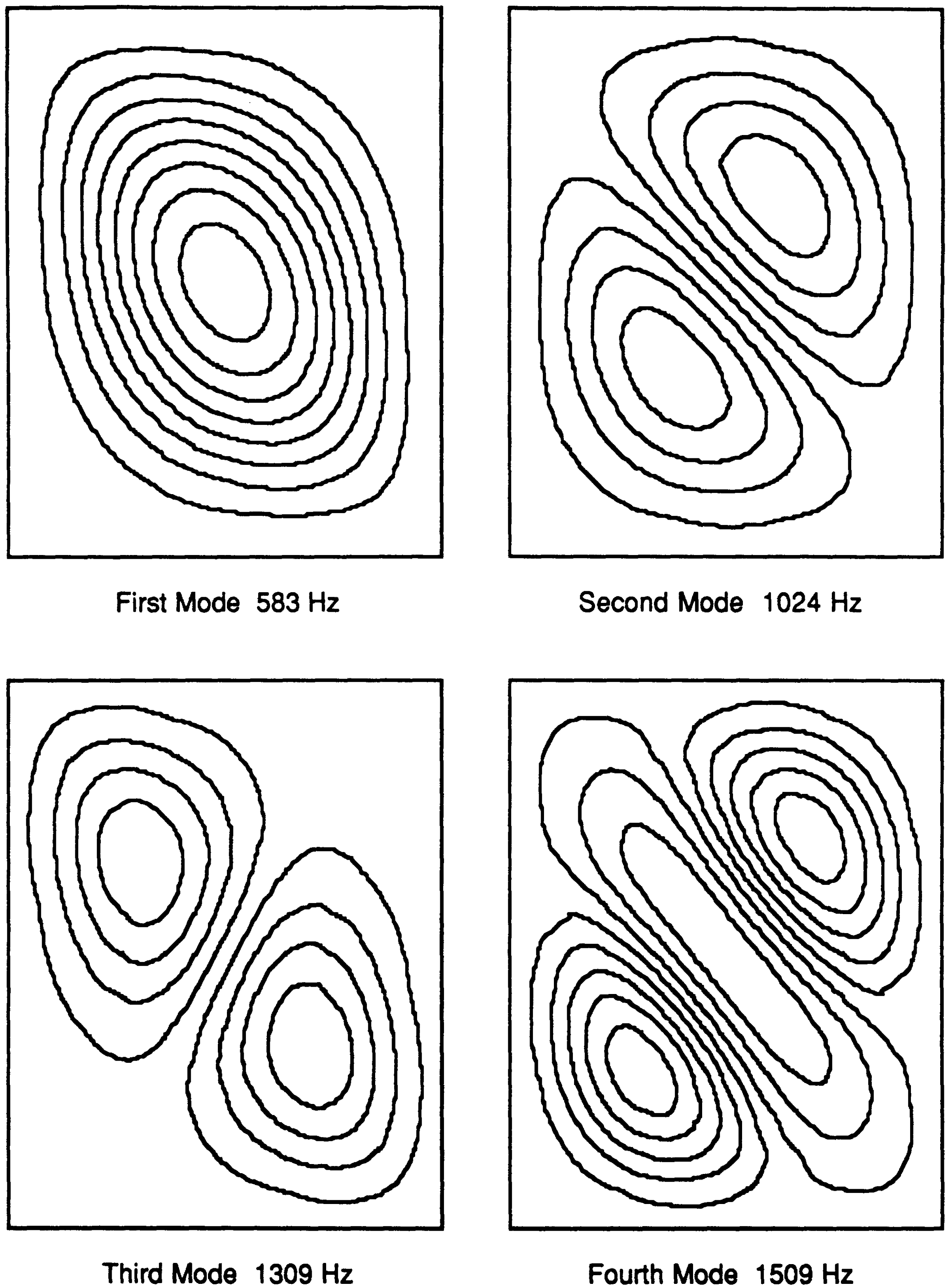

Figure 6.69 First four natural mode shapes and frequencies for Specimen A with all four edges clamped.

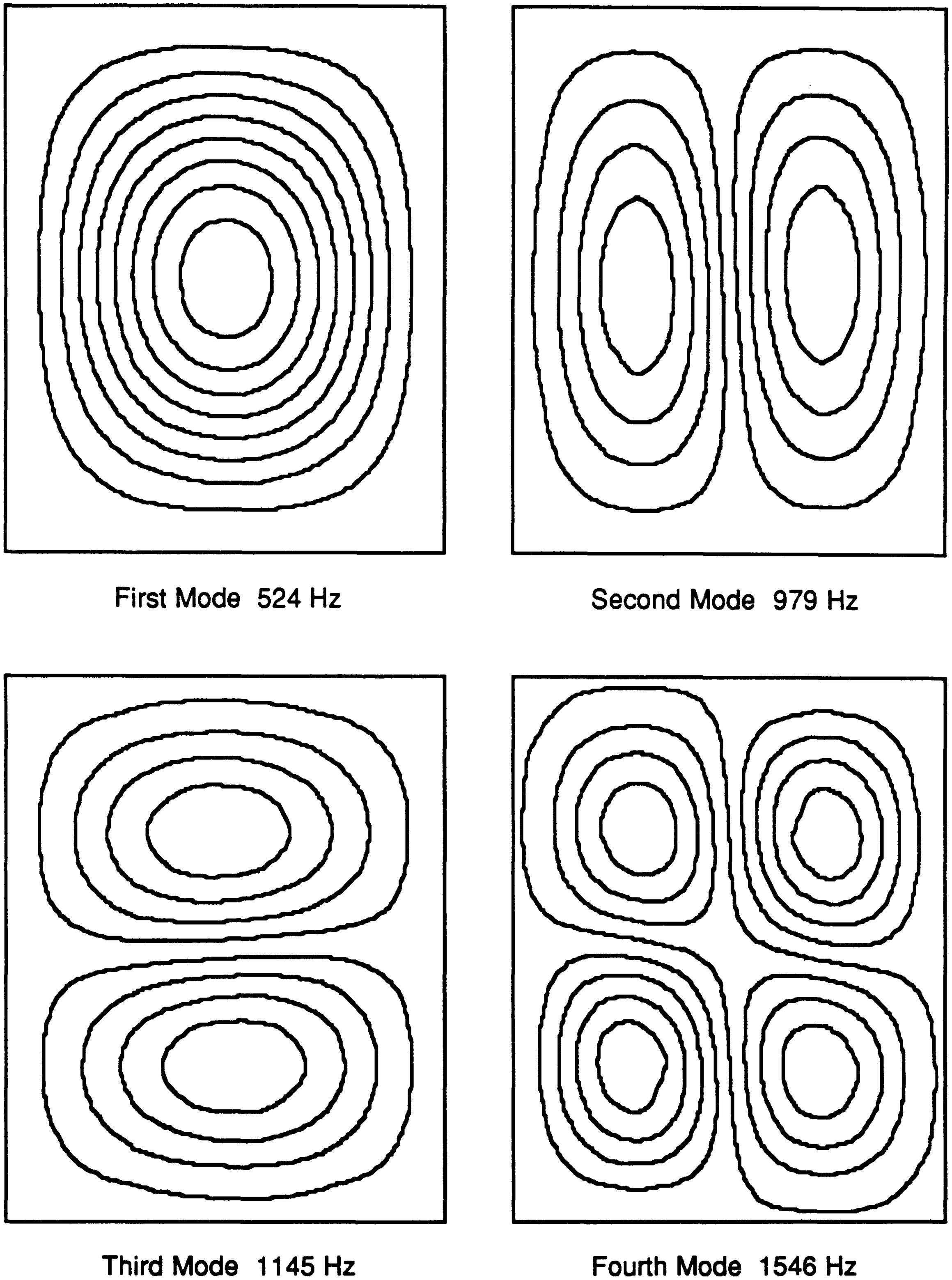

Figure 6.70 First four natural mode shapes and frequencies for Specimen B with all four edges clamped.

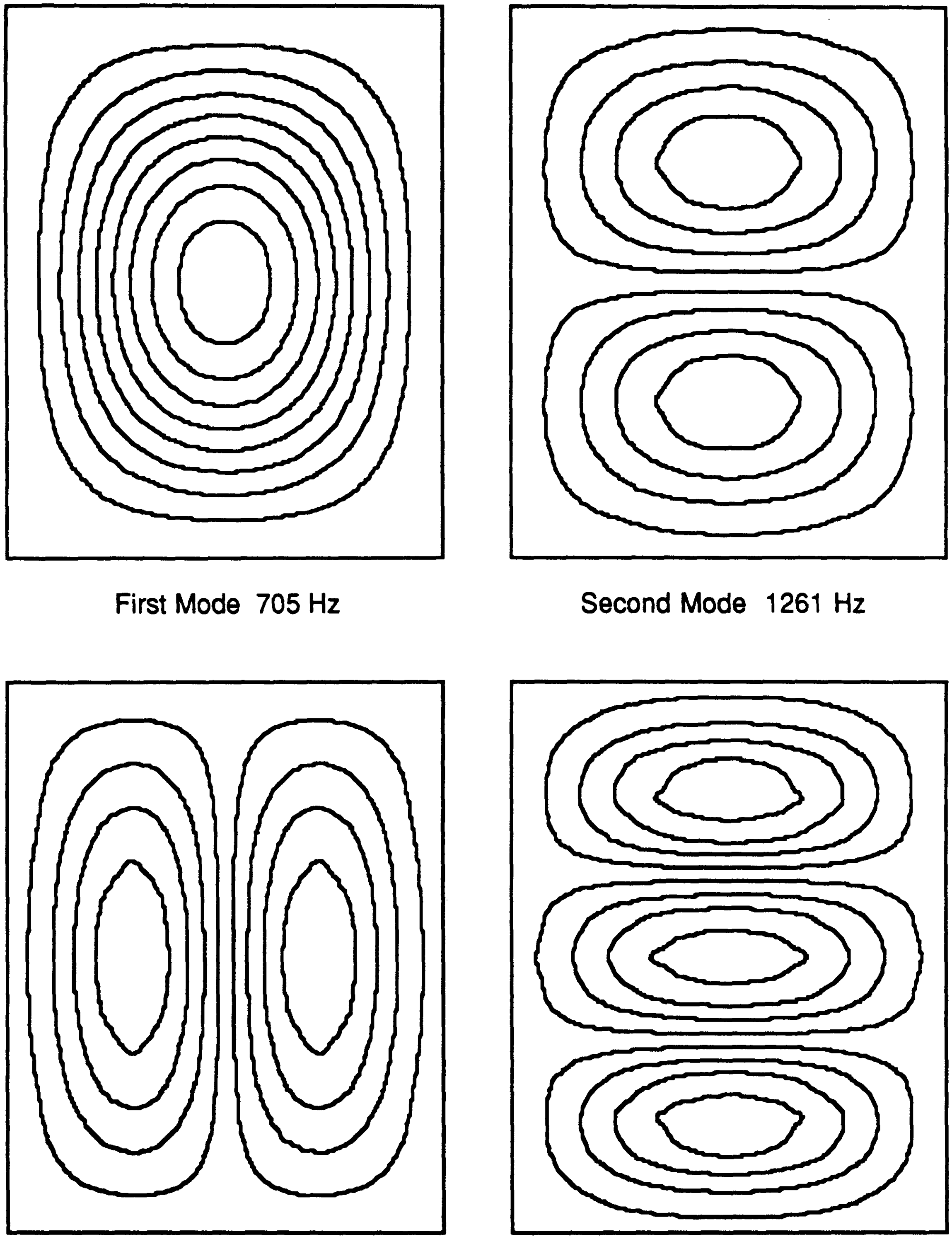

First Mode 705 Hz

Second Mode 1261 Hz

Third Mode 1551 Hz

Fourth Mode 2066 Hz

Figure 6.71 First four natural mode shapes and frequencies for Specimen C with all four edges clamped.

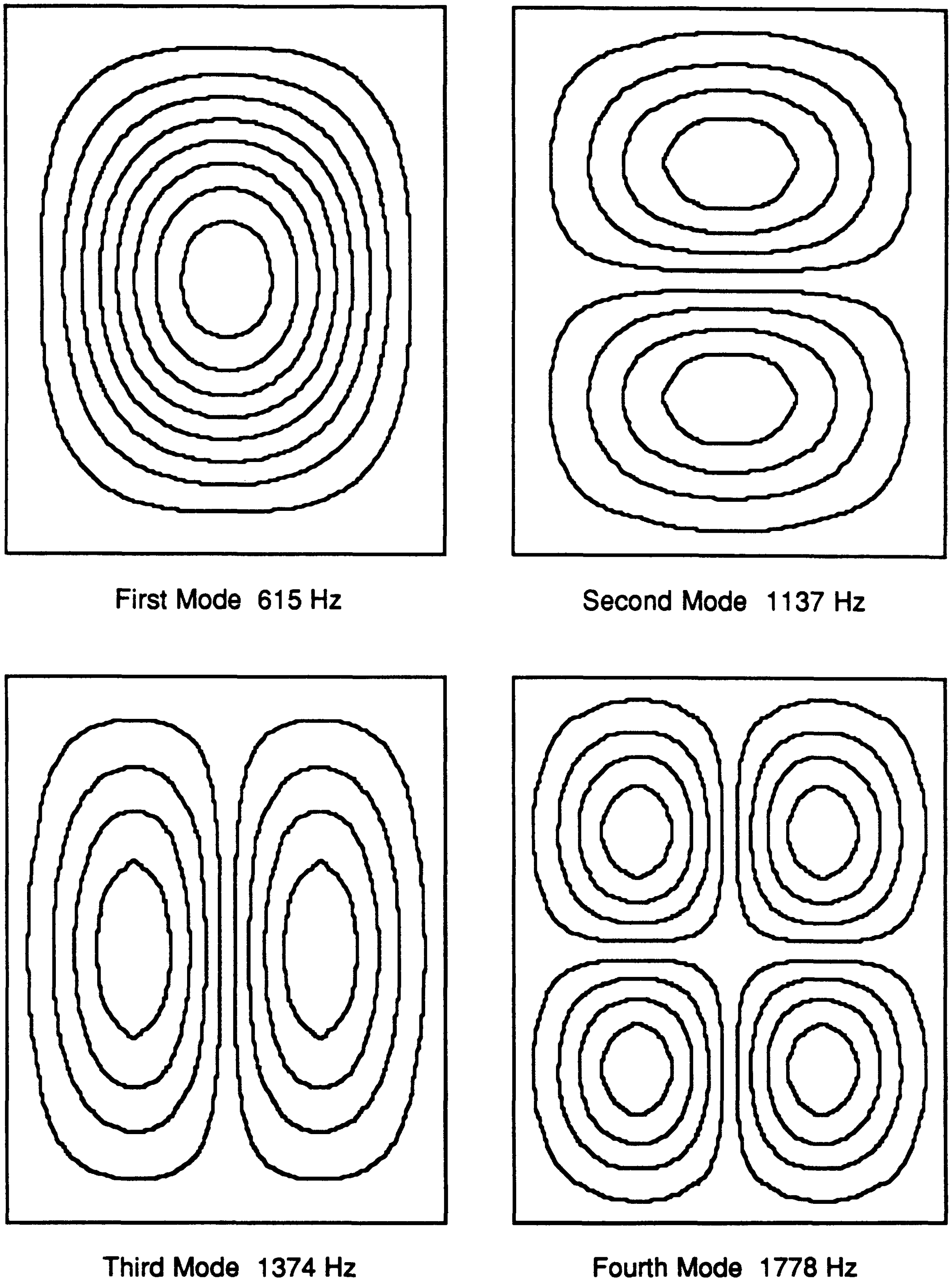

Figure 6.72 First four natural mode shapes and frequencies for Specimen D with all four edges clamped.

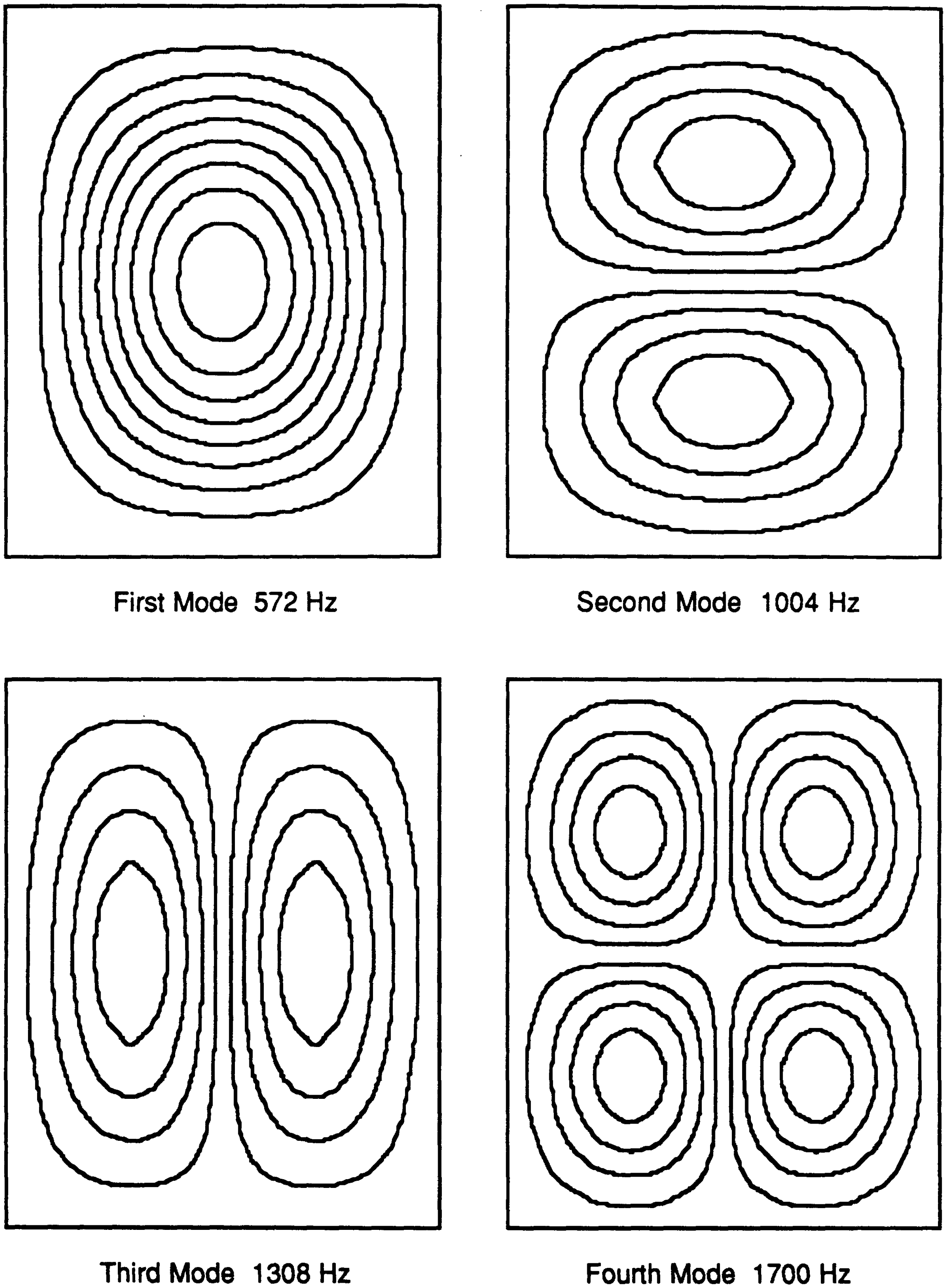

Figure 6.73 First four natural mode shapes and frequencies for Specimen I with all four edges clamped.

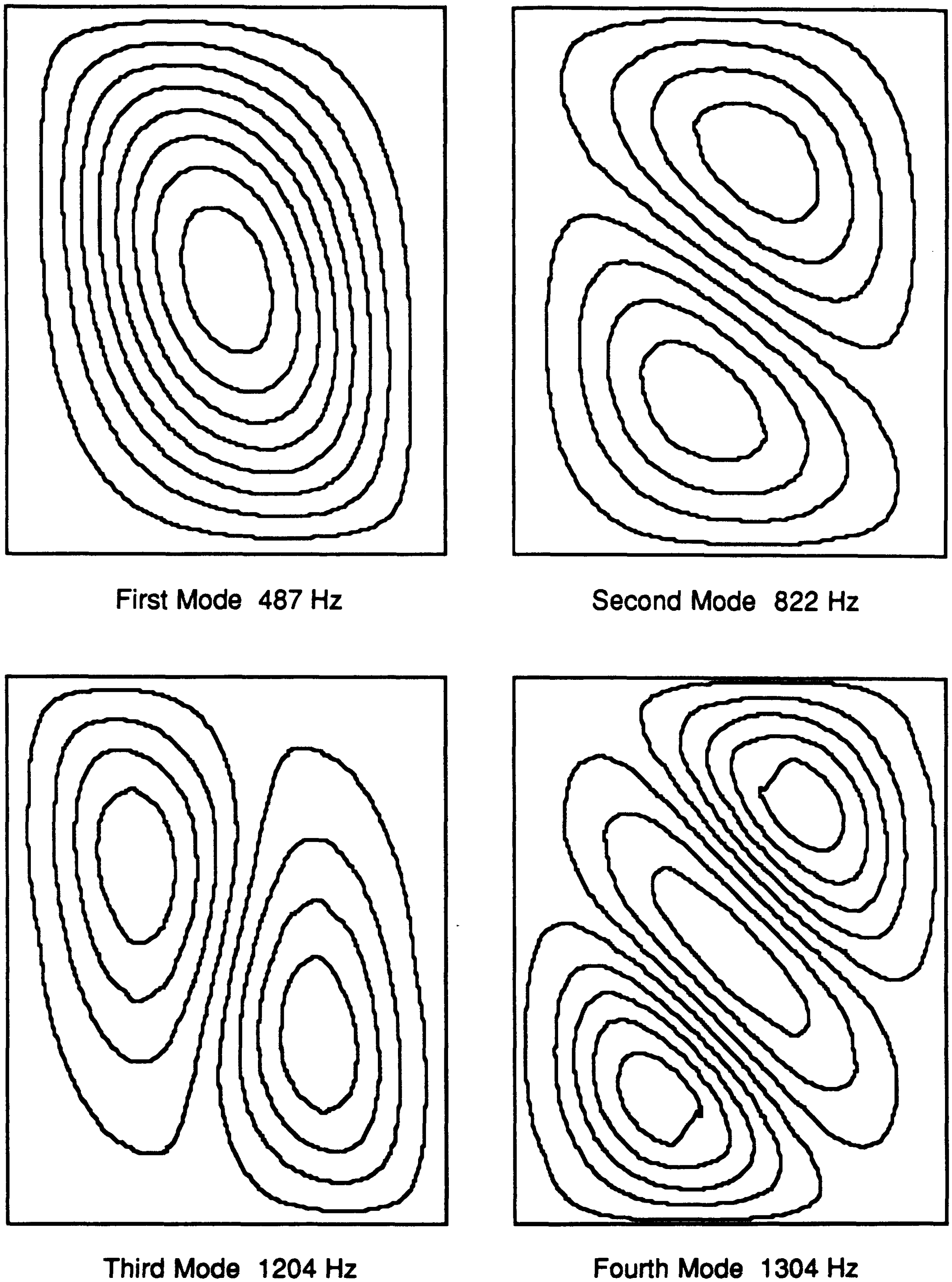

Figure 6.74 First four natural mode shapes and frequencies for Specimen A with x edges (short edges) simply supported and y edges (long edges) clamped.

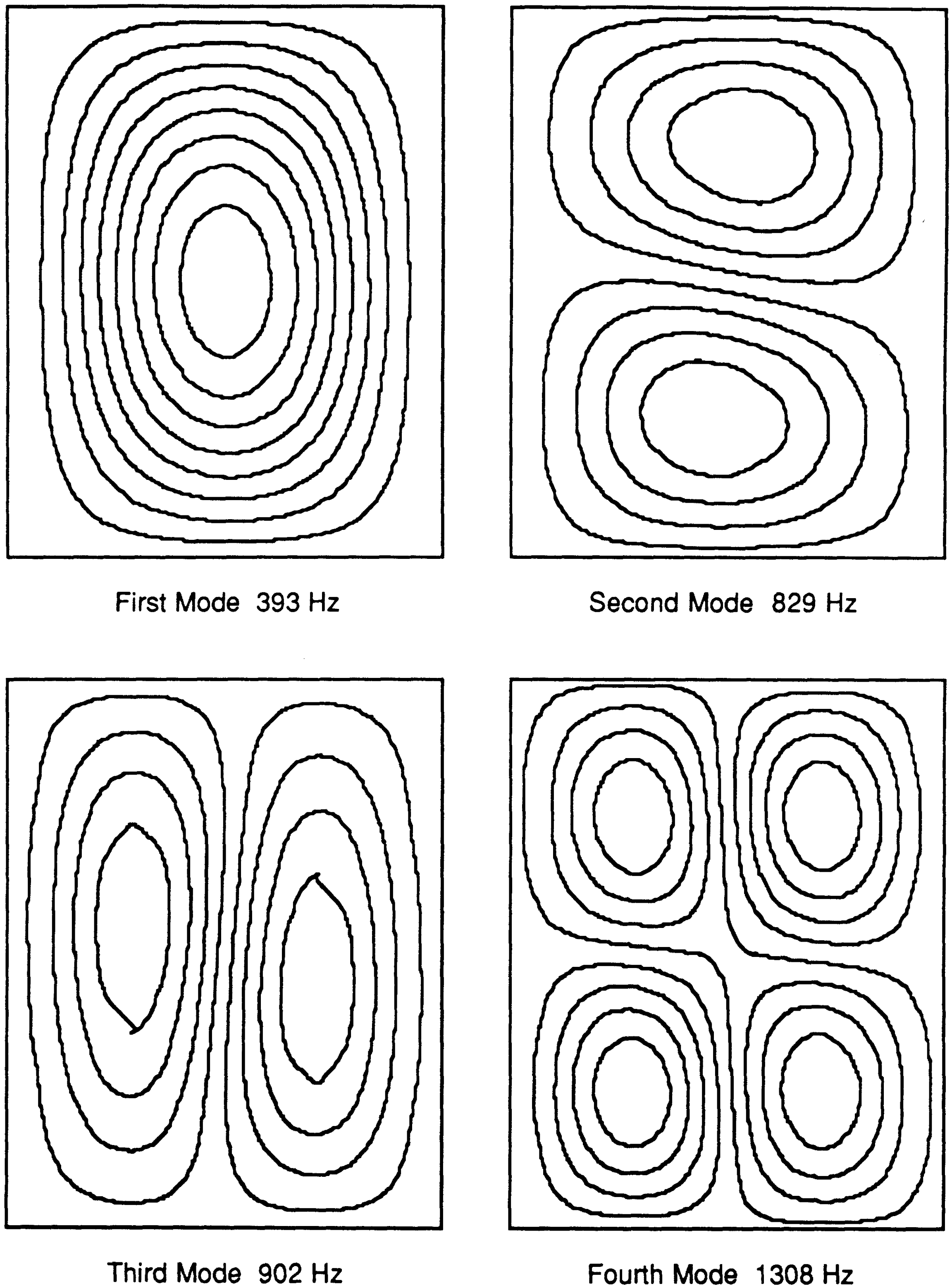

Figure 6.75 First four natural mode shapes and frequencies for Specimen B with x edges (short edges) simply supported and y edges (long edges) clamped.

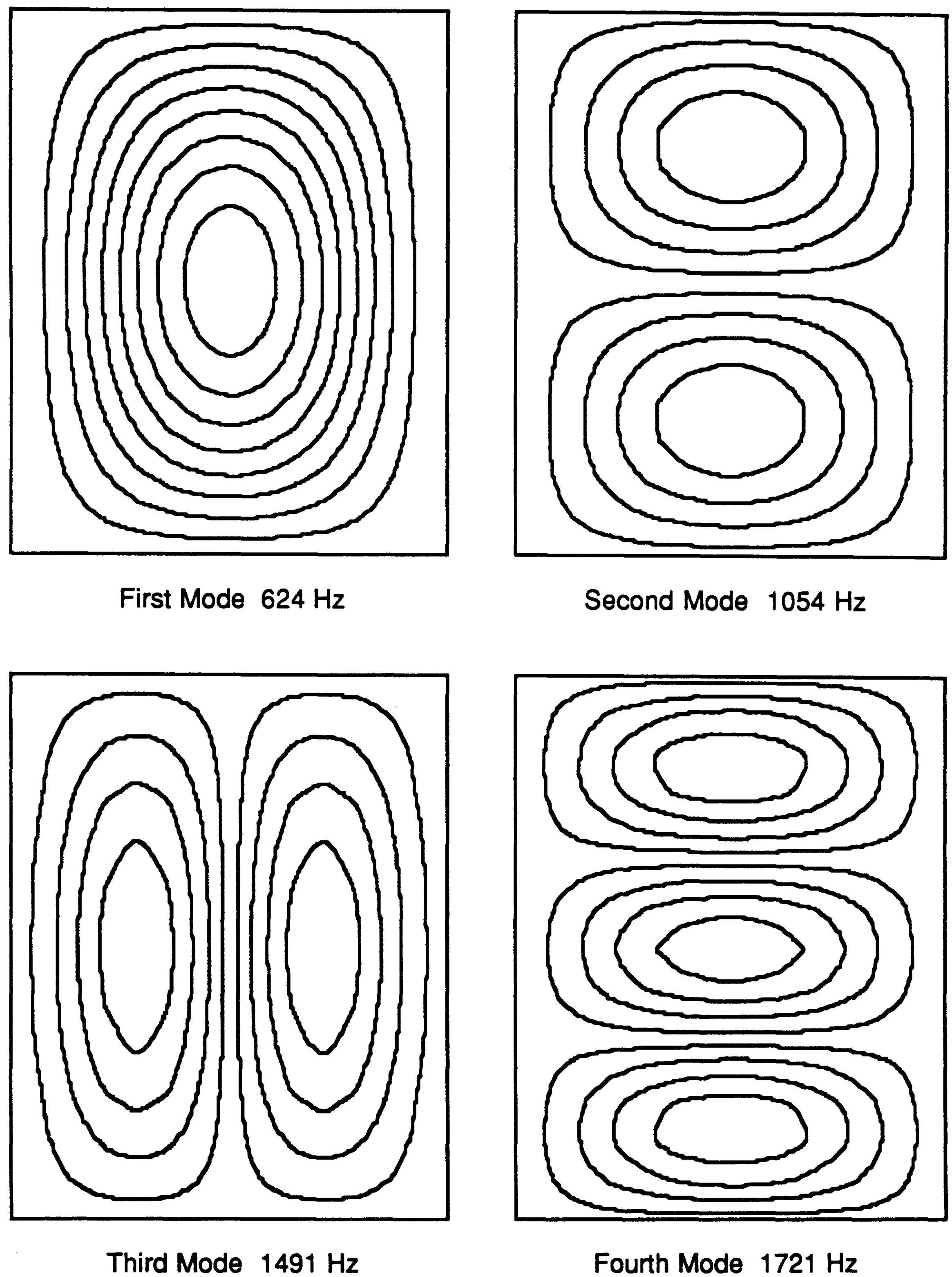

Figure 6.76 First four natural mode shapes and frequencies for Specimen C with x edges (short edges) simply supported and y edges (long edges) clamped.

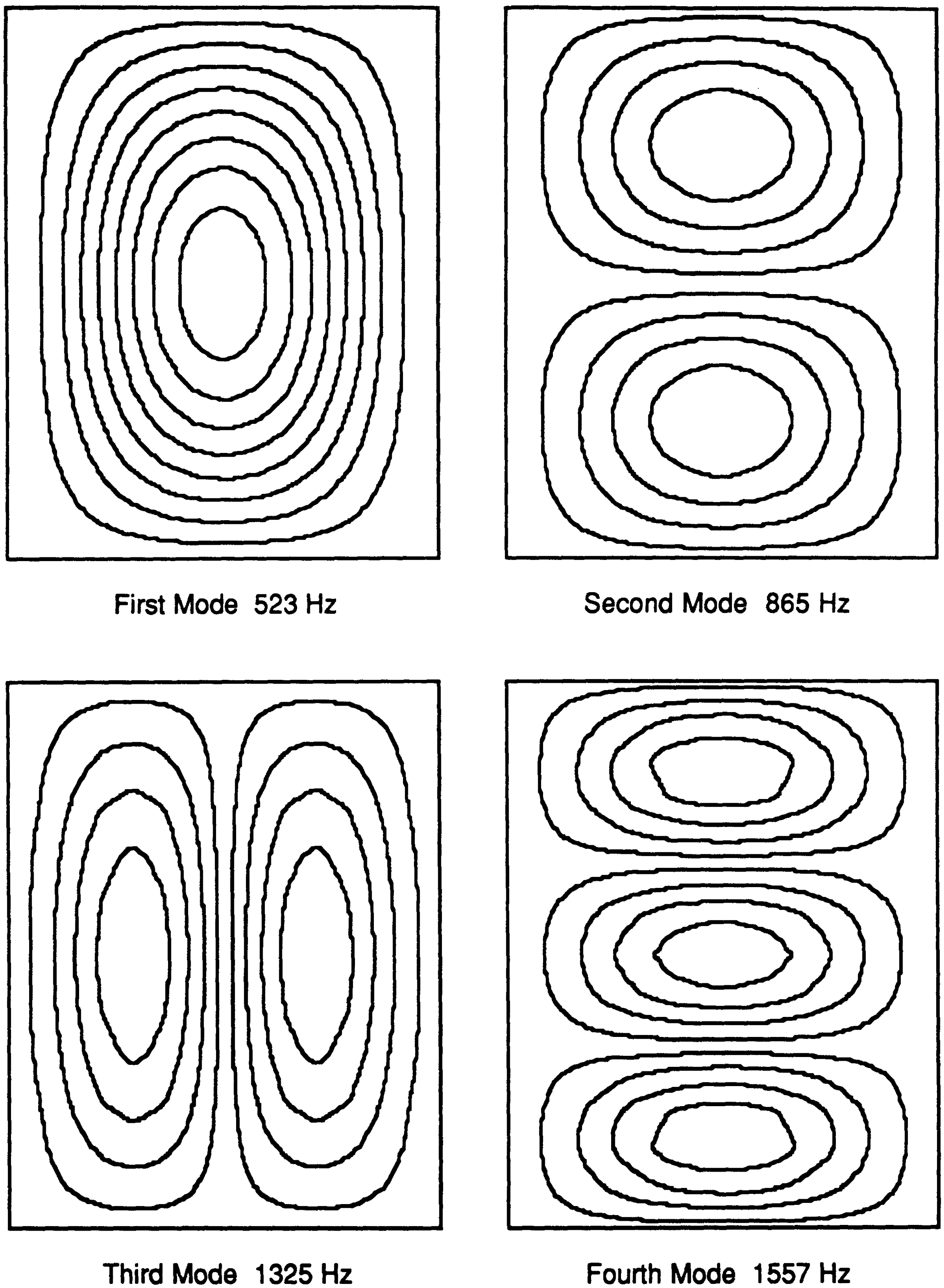

Figure 6.77 First four natural mode shapes and frequencies for Specimen D with x edges (short edges) simply supported and y edges (long edges) clamped.

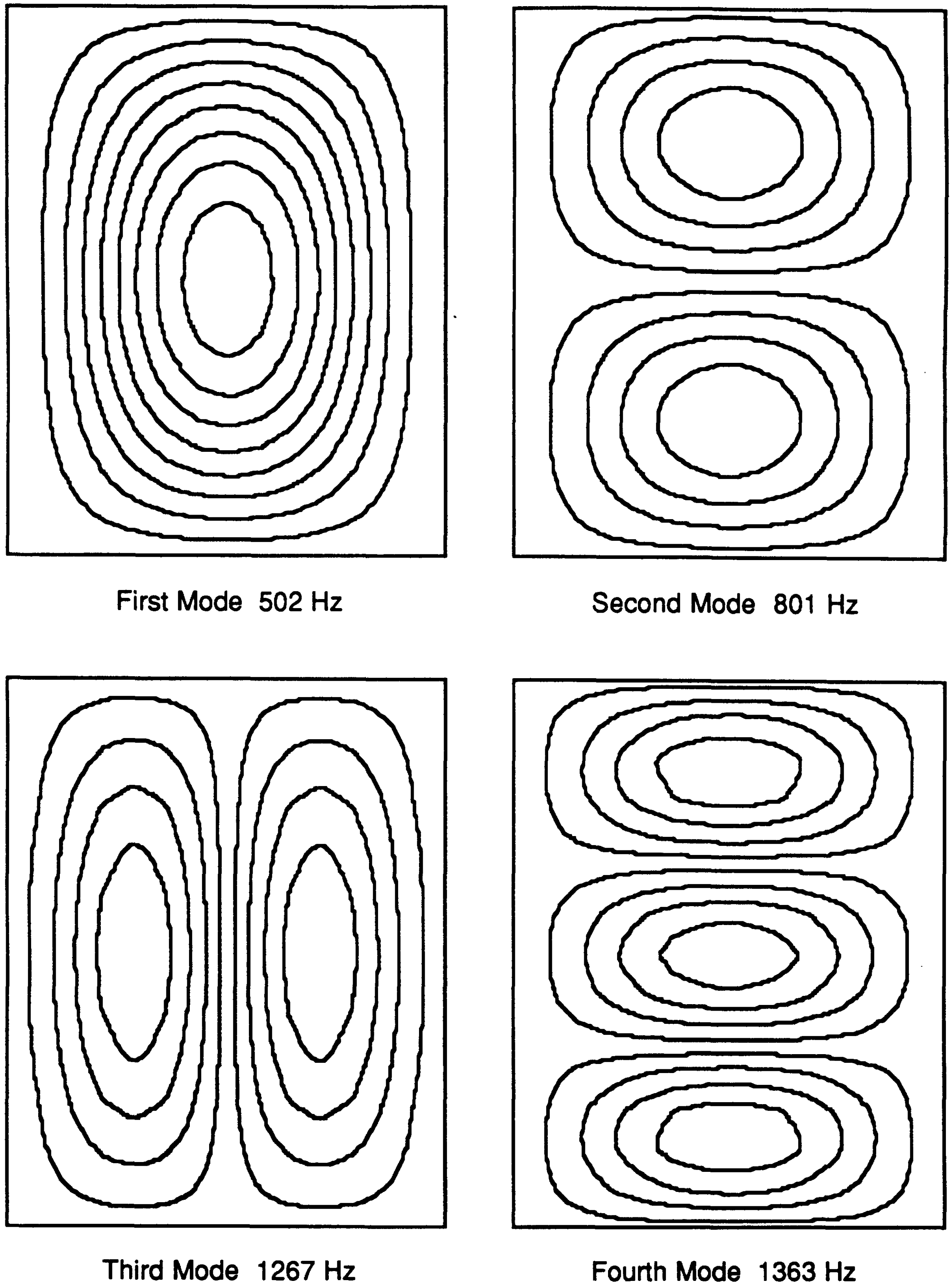

Figure 6.78 First four natural mode shapes and frequencies for Specimen I with x edges (short edges) simply supported and y edges (long edges) clamped.

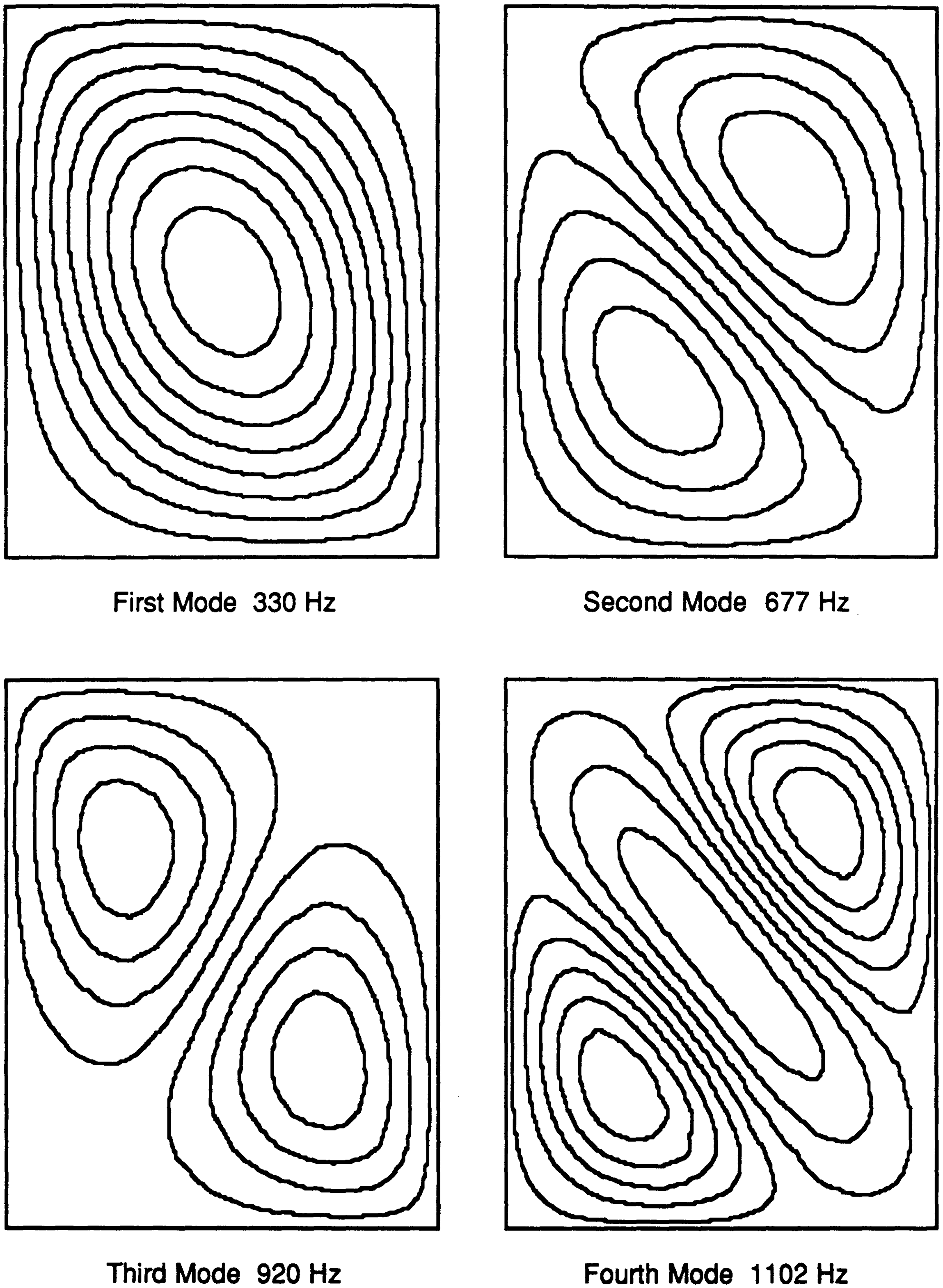

Figure 6.79 First four natural mode shapes and frequencies for Specimen A with all four edges simply supported.

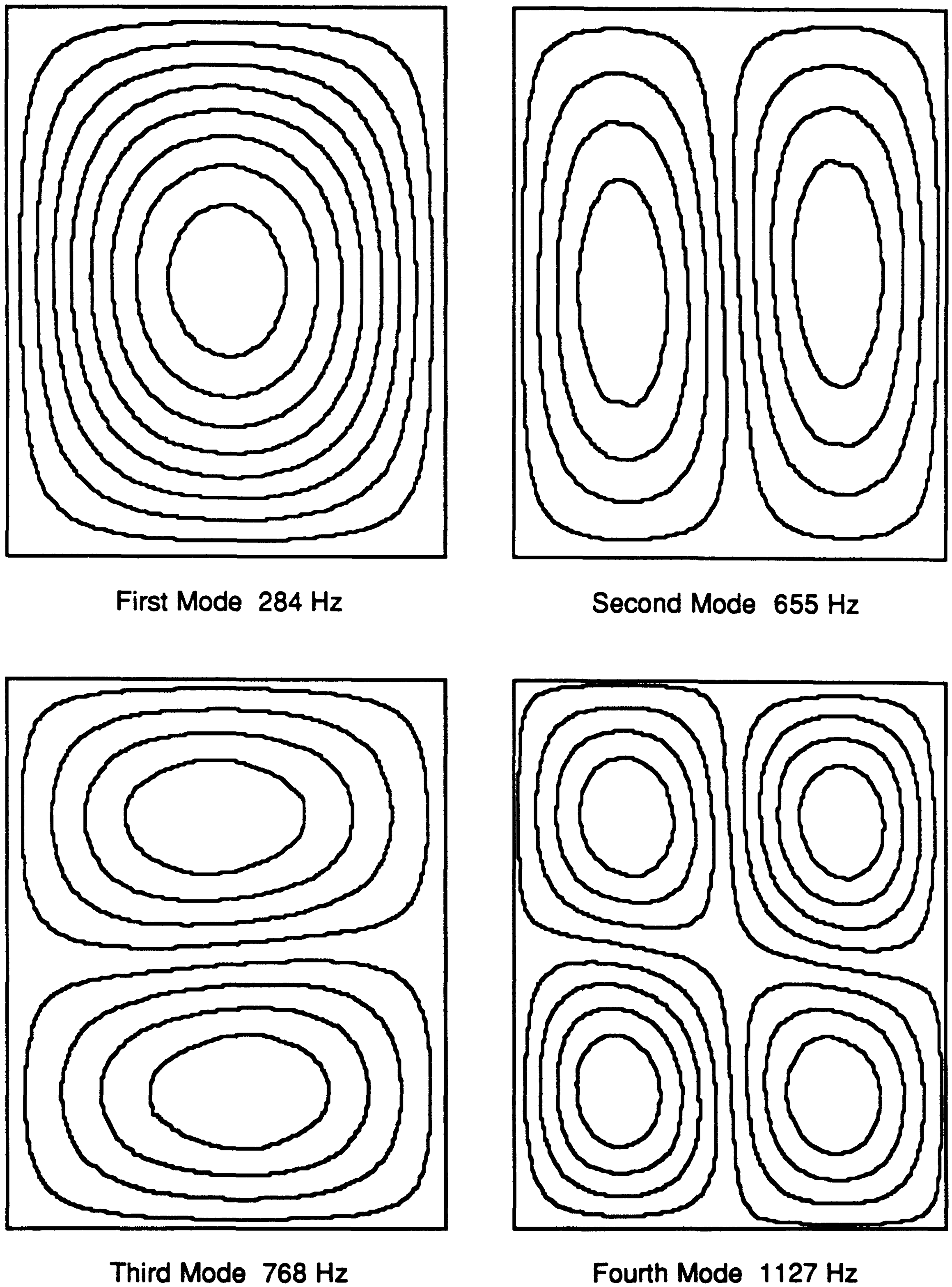

Figure 6.80 First four natural mode shapes and frequencies for Specimen B with all four edges simply supported.

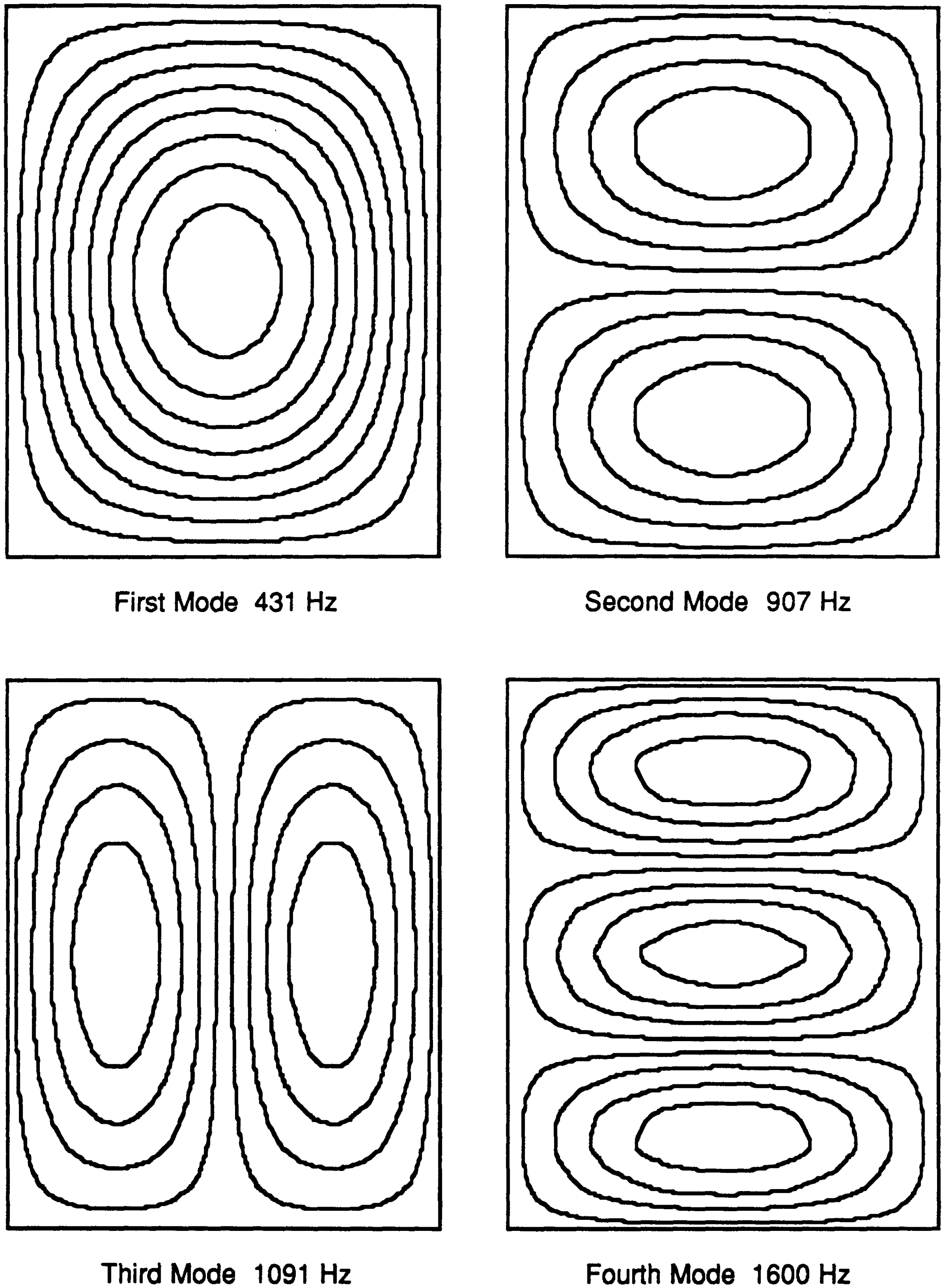

Figure 6.81 First four natural mode shapes and frequencies for Specimen C with all four edges simply supported.

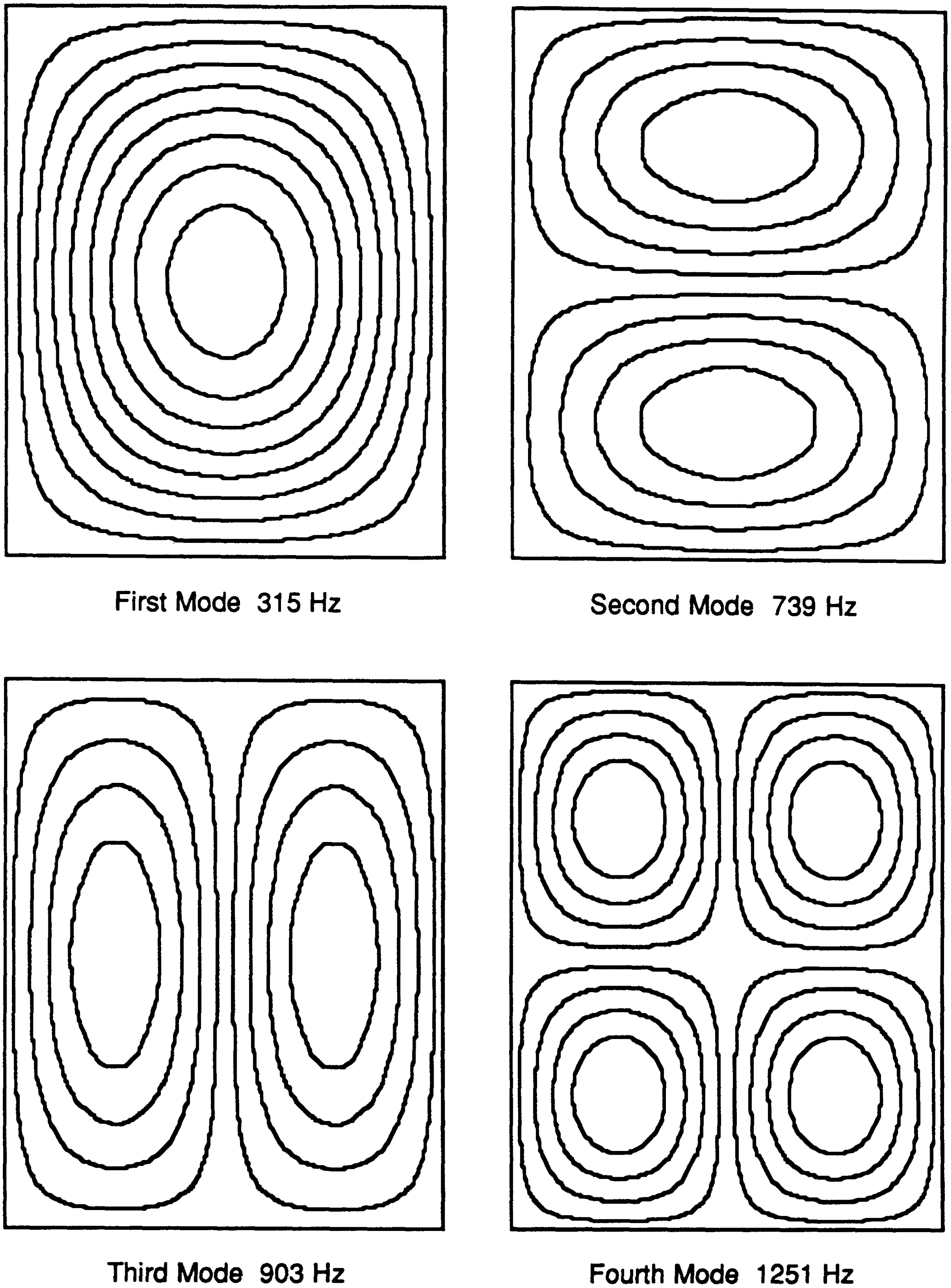

Figure 6.82 First four natural mode shapes and frequencies for Specimen D with all four edges simply supported.

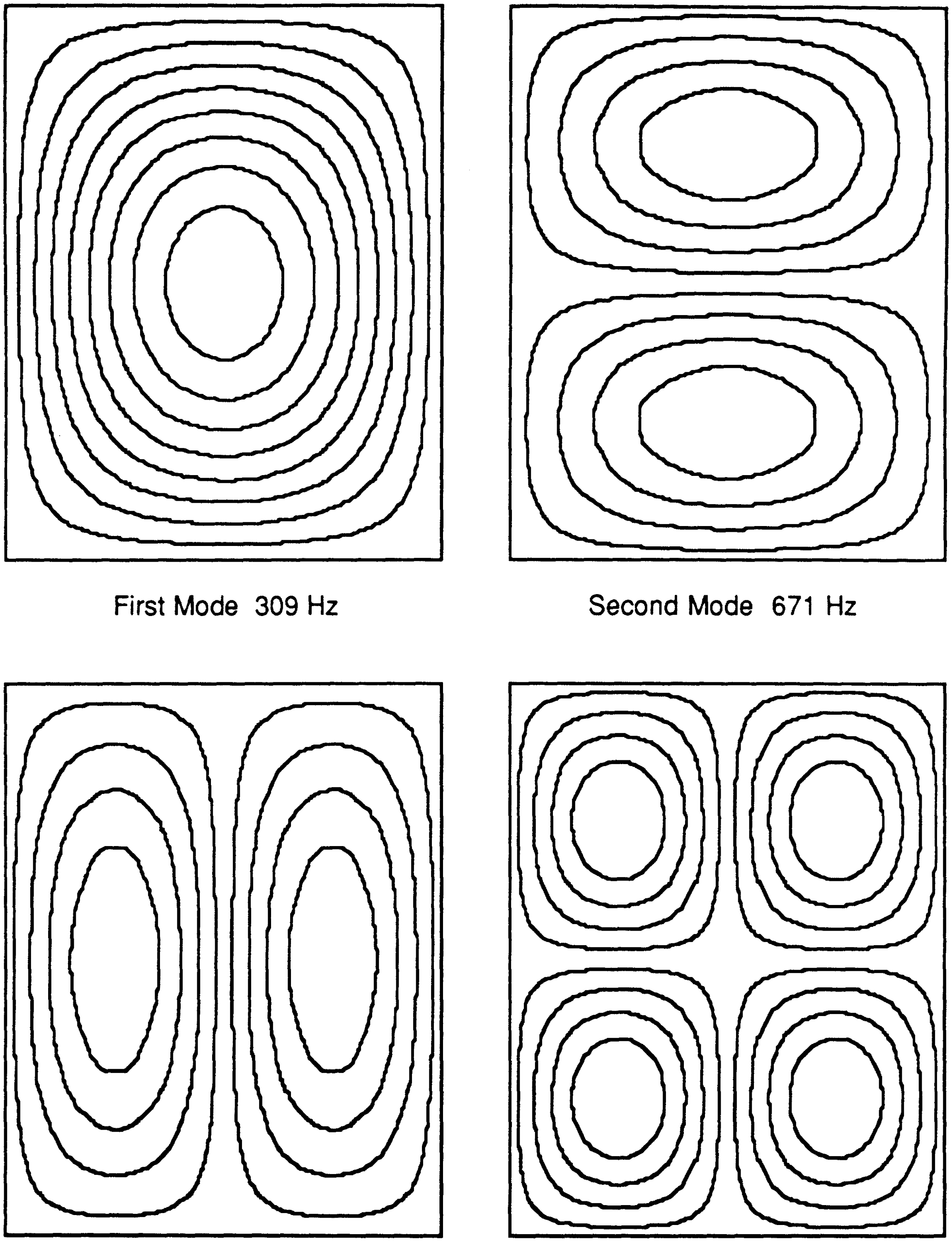

First Mode 309 Hz

Second Mode 671 Hz

Third Mode 874 Hz

Fourth Mode 1234 Hz

Figure 6.83 First four natural mode shapes and frequencies for Specimen I with all four edges simply supported.

Chapter 7
Comparison of Results

This chapter compares the experimental and analytical results for both the static loadings and the dynamic vibrations. Plots are presented comparing experimental and analytical deflections for the static loadings. Percentage differences between experimental and analytical stiffness and natural frequencies are summarized.

7.1 General Observations Regarding Experimental Results

In all cases, the experimental clamped condition was under constrained compared to the analysis, resulting in more deflection than analytically predicted. The increase in boundary flexibility may be attributed to either the sponginess of the teflon tape that was used to lubricate the boundary, the failure of the boundary condition to properly enforce the zero rotation condition, or a combination of the two effects. The two effects can not be separated from the experimental data available.

The error in the experimental clamped boundary condition appears to be proportional to the edge moment, which also indicates boundary condition stiffness as the problem. In general, off center loads have a larger error than centered loads and the URPP loads have a larger error than the point loads, while uniform pressure also exhibits a large error.

The simple supports were also slightly under constrained in most cases, however, the difference was almost always within the experimental error which was estimated at ± 8%. This error was composed of ± 2% from the measurement devices, ± 2% from the regressions, and ± 4% from the stiffness averaging. For some cases the simple supports are over constrained, as indicated in Table 7.1.

Table 7.1 summarizes the difference between the experimental stiffnesses and the Rayleigh-Ritz stiffness predictions. The stiffnesses at the first and third transducer locations have been compared because these points are closest to the center of loading for the centered and off-center loadings respectively. The transducers further from the loading show similar trends but slightly more error. For these transducers the error constitutes a larger percentage of the reading, because the displacements being measured are an order of magnitude smaller than the center displacements.

Negative values in Table 7.1 indicate that the experimental stiffness was less than the predicted analytical stiffness. The last column gives an average of the absolute values of the error over all five specimen types for each loading and boundary condition combination. These averages assist in deciphering trends in the stiffness differences.

Table 7.1 Difference of Experimental Stiffness from Rayleigh-Ritz Prediction

		Point	Percent Difference from Rayleigh-Ritz					
Loading	B.C.'s	#	A	B	C	D	I	Avg.
Centered Point Load	CL–CL	1	−11	−9	−15	−13	−10	12
		3	−13	−13	−19	−15	−17	15
	SS–SS	1	−7	8	−8	0	−7	6
		3	−8	8	−8	−1	−7	6
Off-Center Point Load	CL–CL	1	−27	−29	−33	−23	−31	29
		3	−38	−28	−30	−21	−30	29
	SS–CL	1	−21	−12	−24	−22	−22	20
		3	−15	−11	−21	−19	−17	17
	SS–SS	1	−8	−1	−7	−2	1	4
		3	−6	−1	−7	−3	2	4
Centered URPP	CL–CL	1	−12	−11	−20	−17	−12	14
		3	−16	−13	−21	−18	−15	17
	SS–SS	1	−6	8	−9	1	1	5
		3	−7	8	−9	0	1	5
Off-Center URPP	CL–CL	1	−23	−31	−29	−25	−37	29
		3	−19	−27	−25	−24	−41	27
	SS–CL	1	−19	−23	−25	−25	−22	23
		3	−13	−18	−22	−21	−17	18
	SS–SS	1	−8	−8	−11	−5	−4	7
		3	−5	−6	−11	−5	−2	6
Uniform Pressure	CL–CL	1	−23	−18	−30	−30	−30	26
		3	−24	−17	−31	−32	−33	27
	SS–CL	1	−17	4	−26	−20	−25	18
		3	−19	4	−28	−21	−24	19
	SS–SS	1	3	37	−10	14	6	14
		3	1	35	−11	13	5	13

7.2 Comparison of Results for Centered Point Load

The centered point load tests are fairly consistent. The excessive flexibility of the four sides clamped boundary condition results in 15% more deflection than analytically predicted by the Rayleigh-Ritz solution. The simply supported tests generally exhibit 5% more deflection than analytically predicted by the Rayleigh-Ritz solution, but this is within the ±8 % experimental error. In general, there is good agreement between the data and the Rayleigh-Ritz analysis.

In general, the single mode potential functions for four edges clamped and four edges simply supported are not sufficient to adequately describe the deformations caused by the centered point load. Additional modes need to be added to the single mode solution to obtain a converged answer.

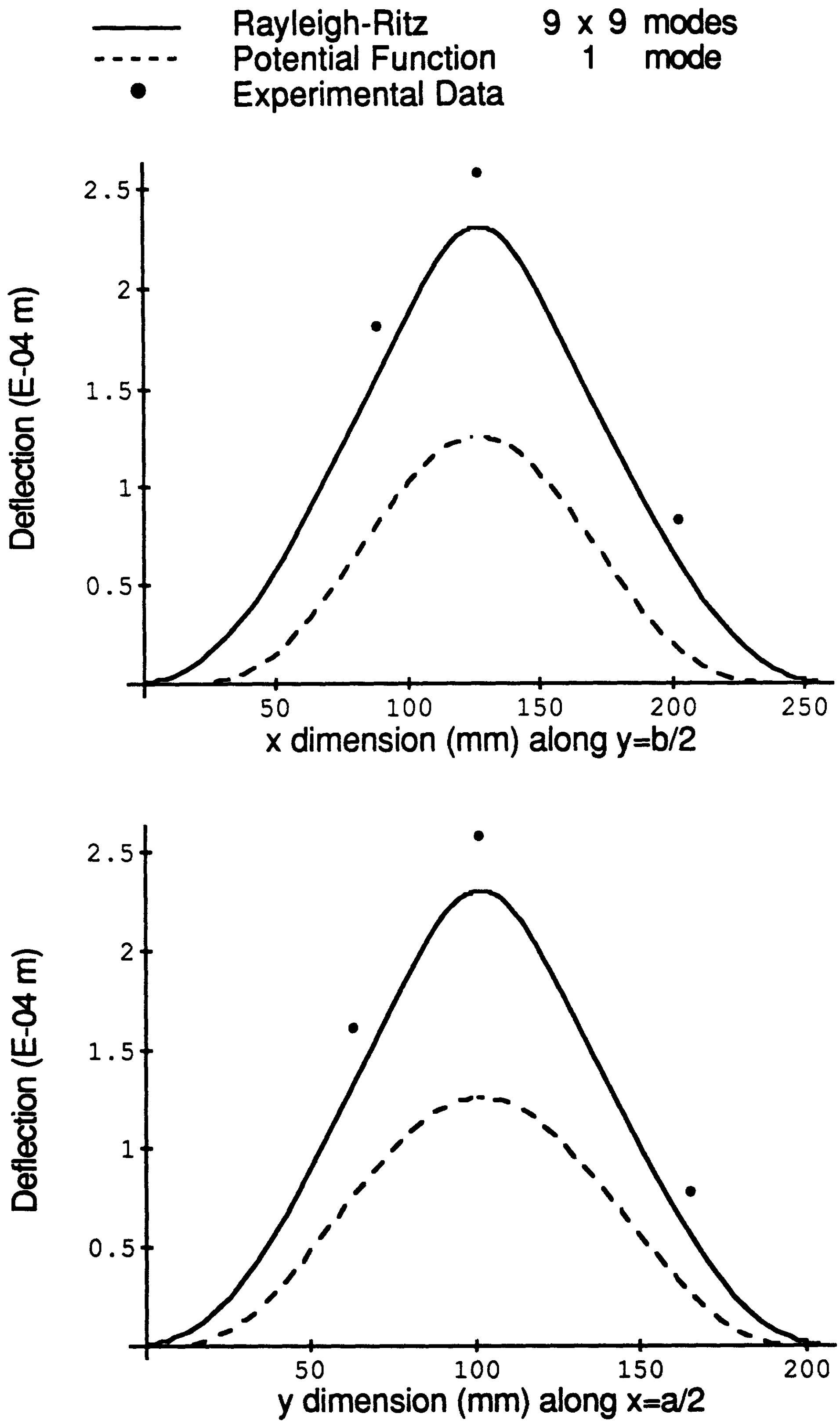

Figure 7.1 Transverse deflection for Specimen A, under a centered point load of 100 Newtons, with all four sides clamped.

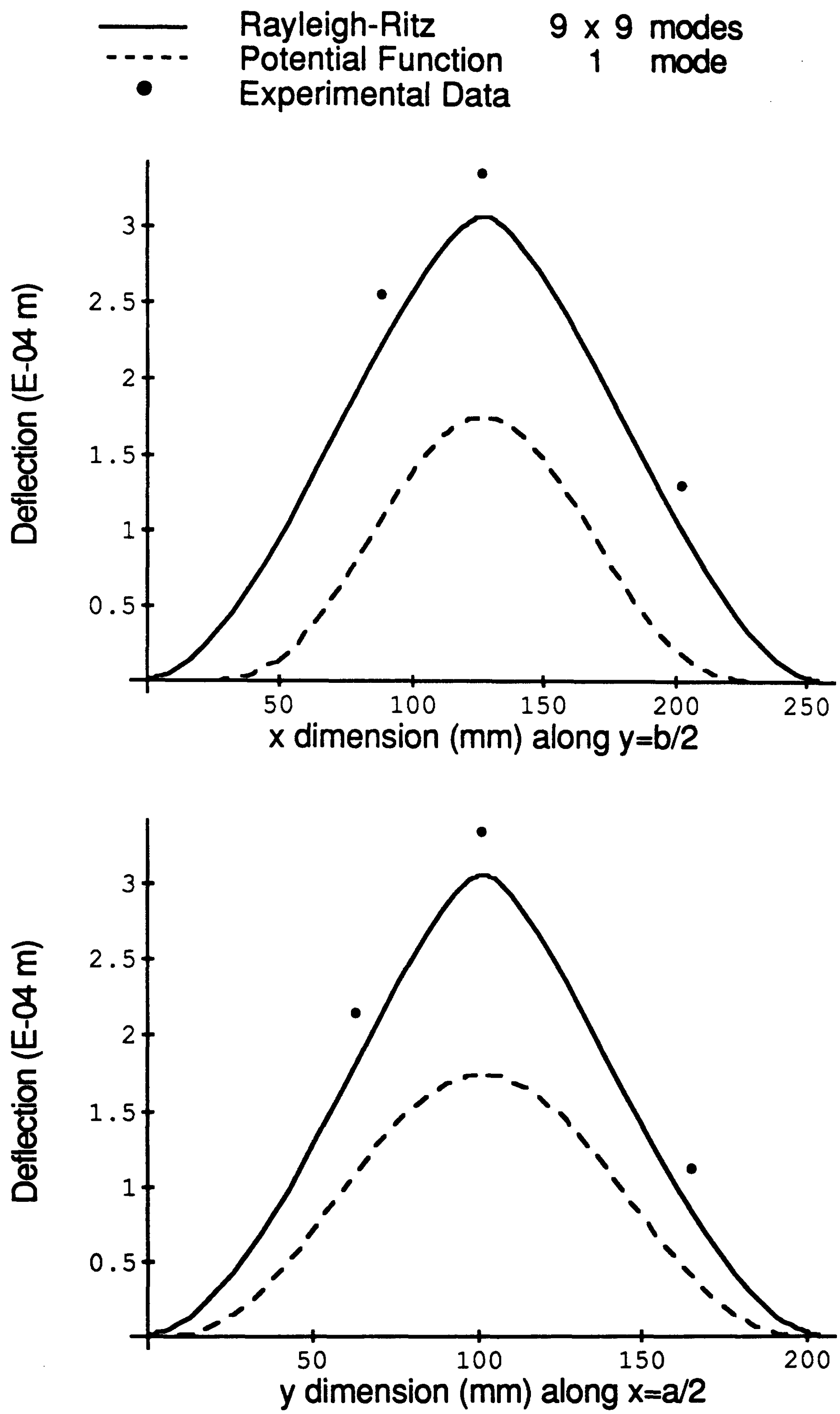

Figure 7.2 **Transverse deflection for Specimen B, under a centered point load of 100 Newtons, with all four sides clamped.**

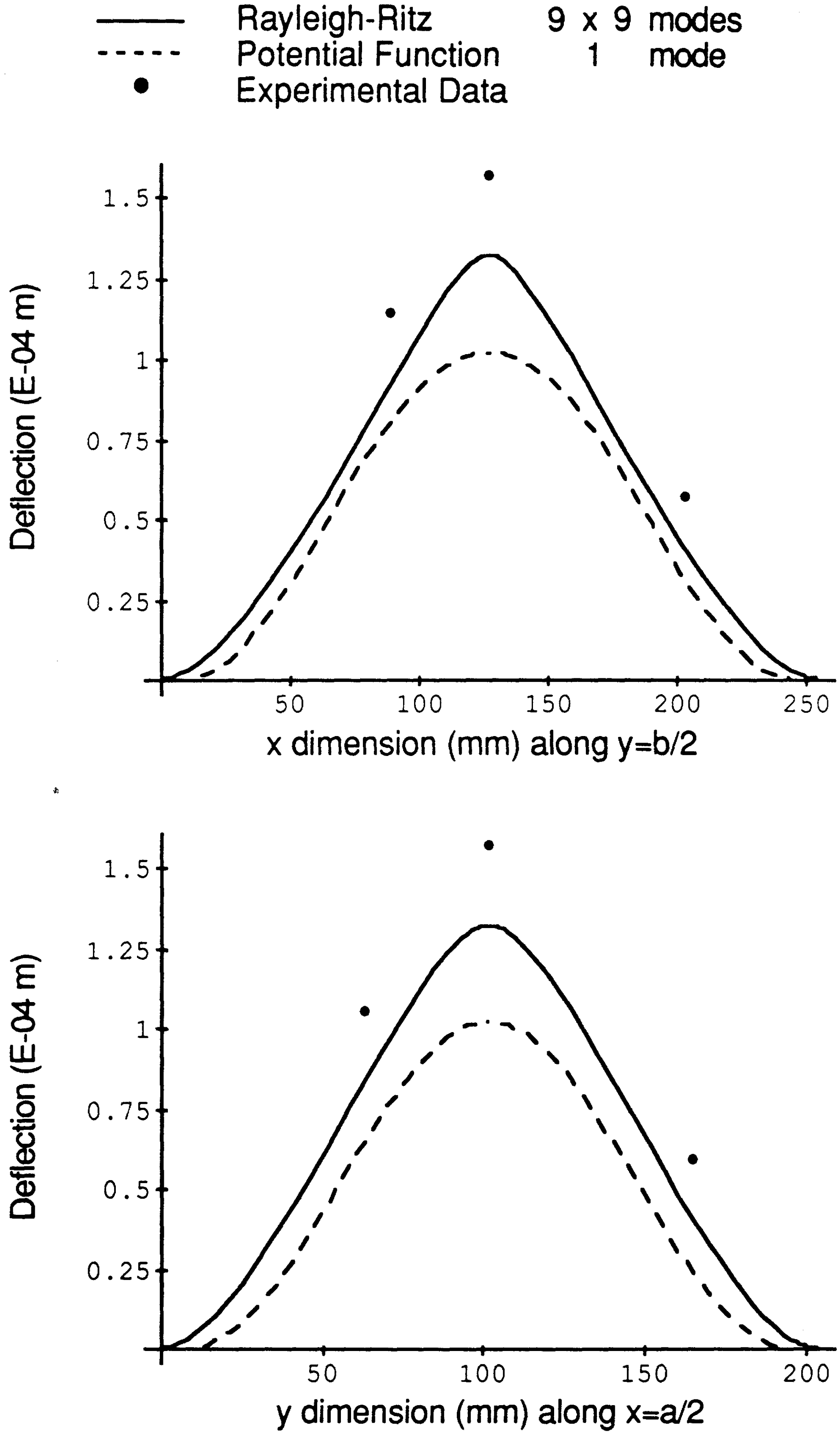

Figure 7.3 Transverse deflection for Specimen C, under a centered point load of 100 Newtons, with all four sides clamped.

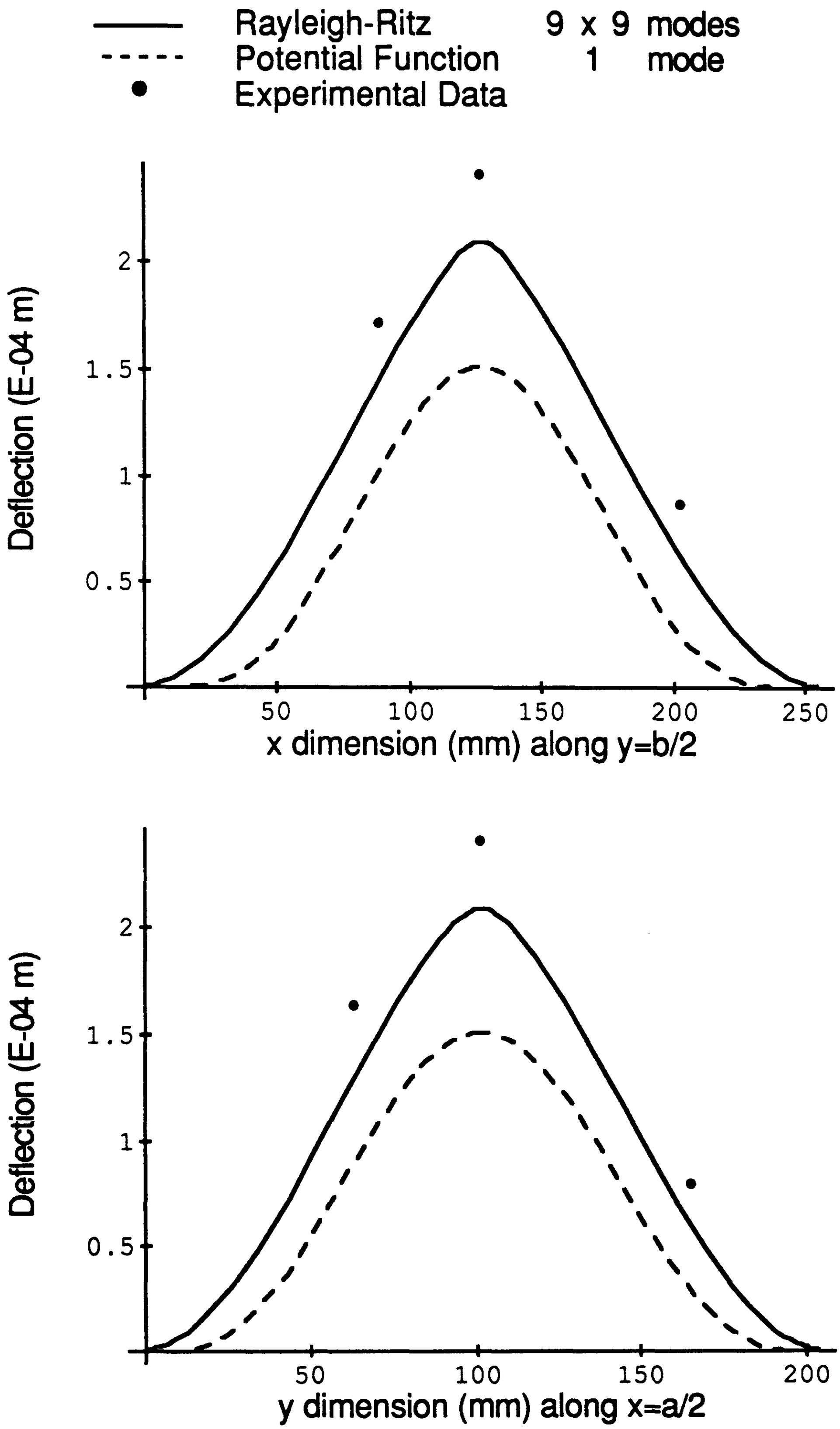

Figure 7.4 Transverse deflection for Specimen D, under a centered point load of 100 Newtons, with all four sides clamped.

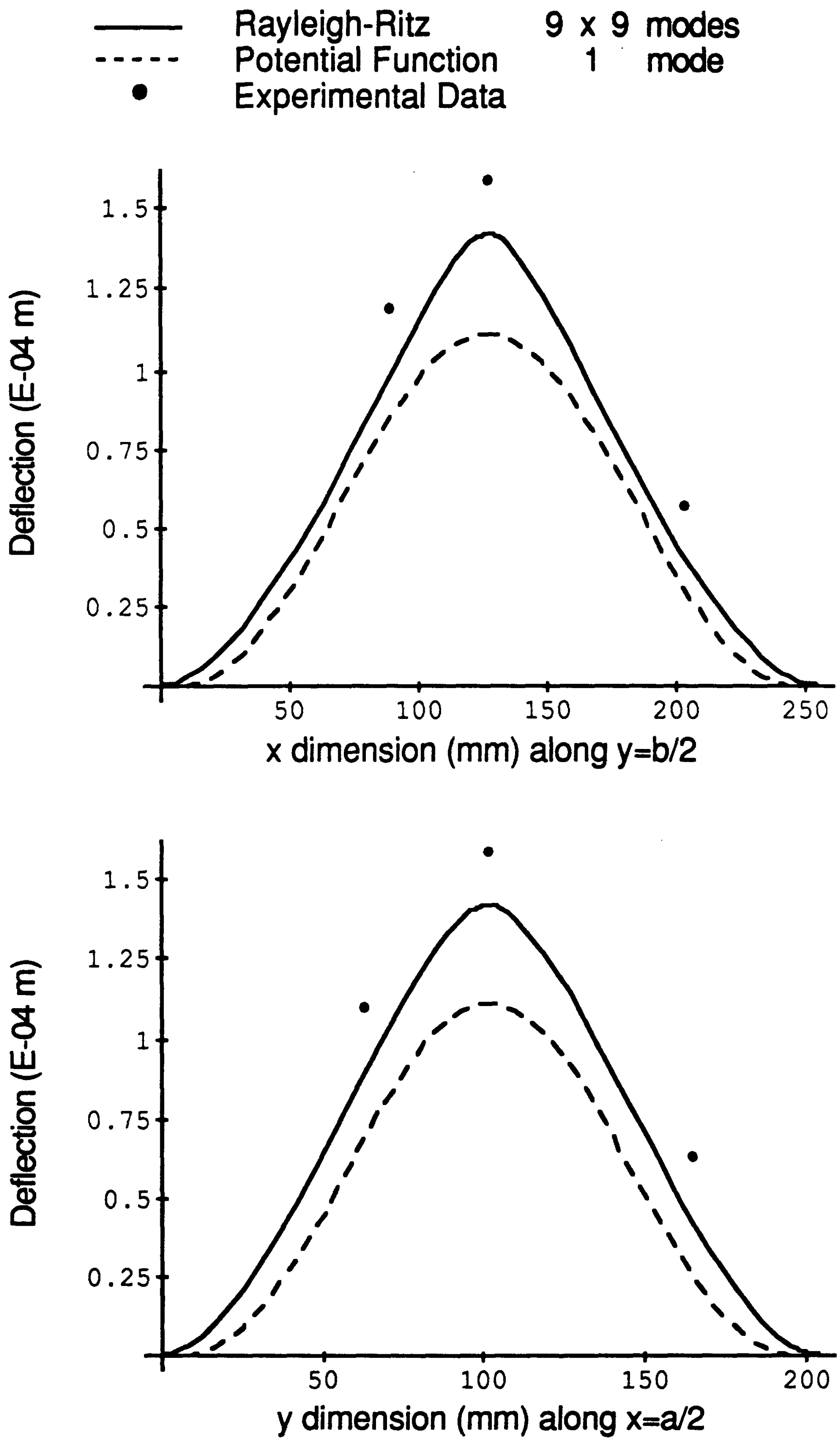

Figure 7.5 Transverse deflection for Specimen I, under a centered point load of 100 Newtons, with all four sides clamped.

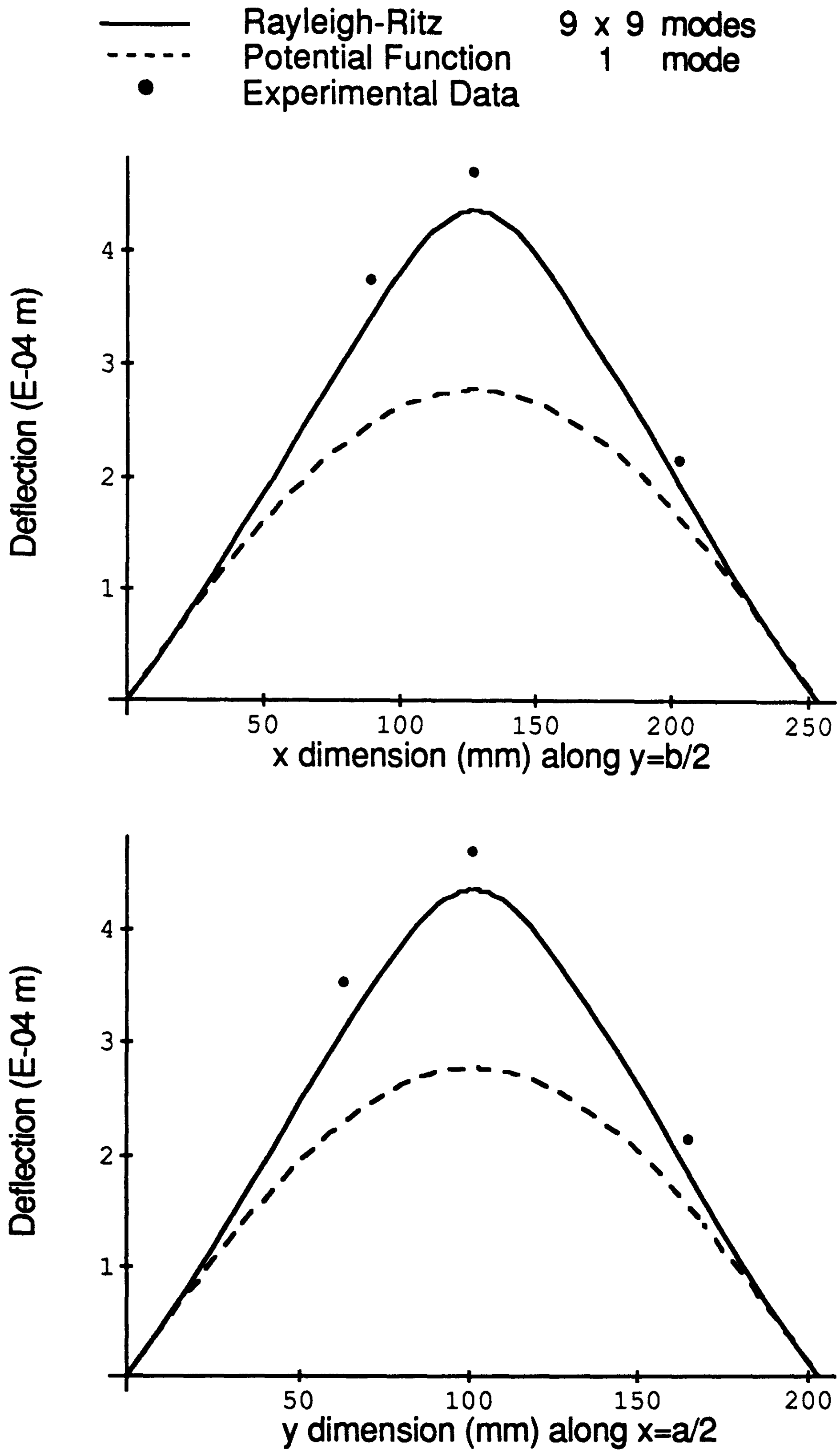

Figure 7.6 Transverse deflection for Specimen A, under a centered point load of 100 Newtons, with all four sides simply supported.

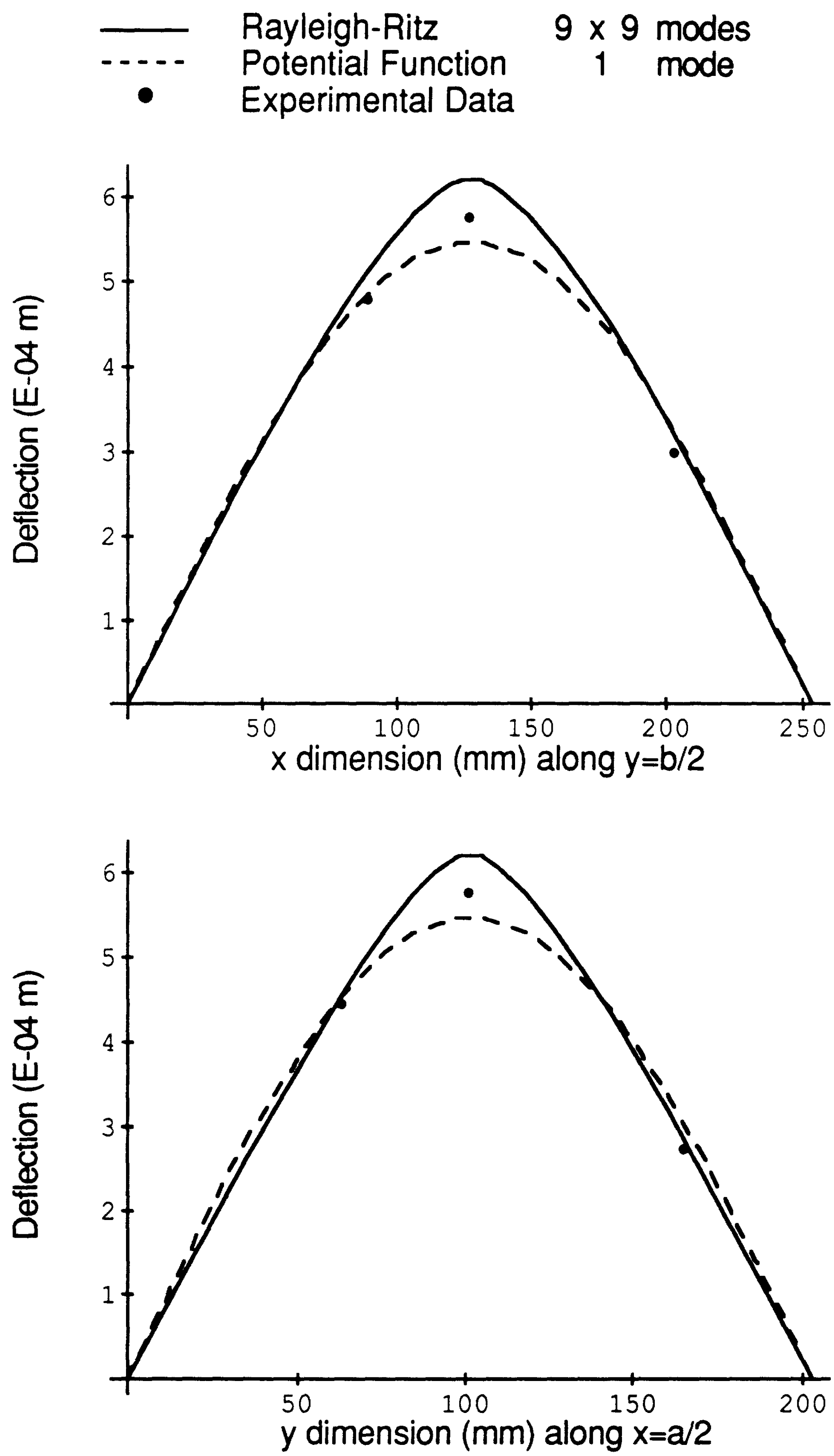

Figure 7.7 Transverse deflection for Specimen B, under a centered point load of 100 Newtons, with all four sides simply supported.

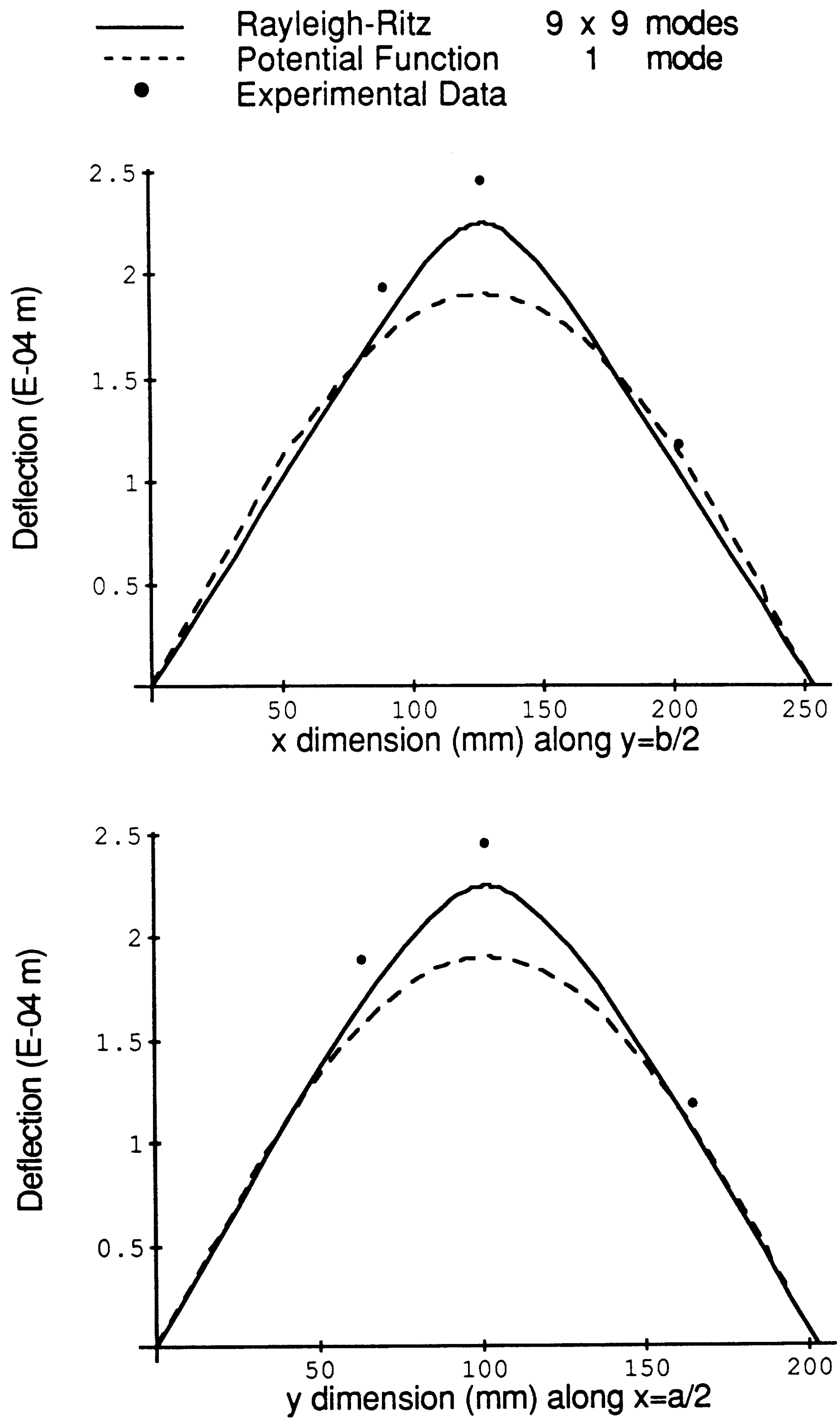

Figure 7.8 Transverse deflection for Specimen C, under a centered point load of 100 Newtons, with all four sides simply supported.

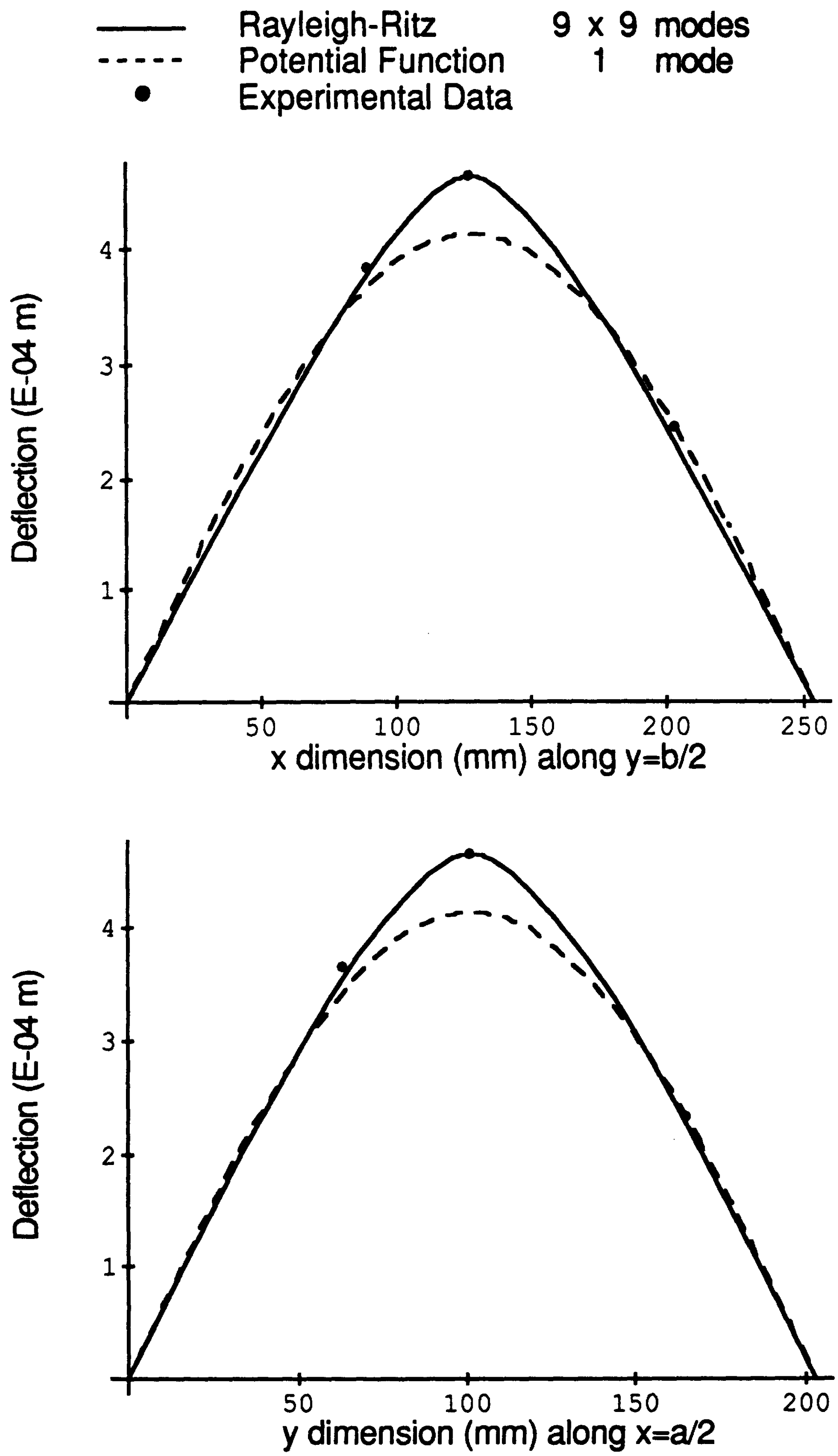

Figure 7.9 Transverse deflection for Specimen D, under a centered point load of 100 Newtons, with all four sides simply supported.

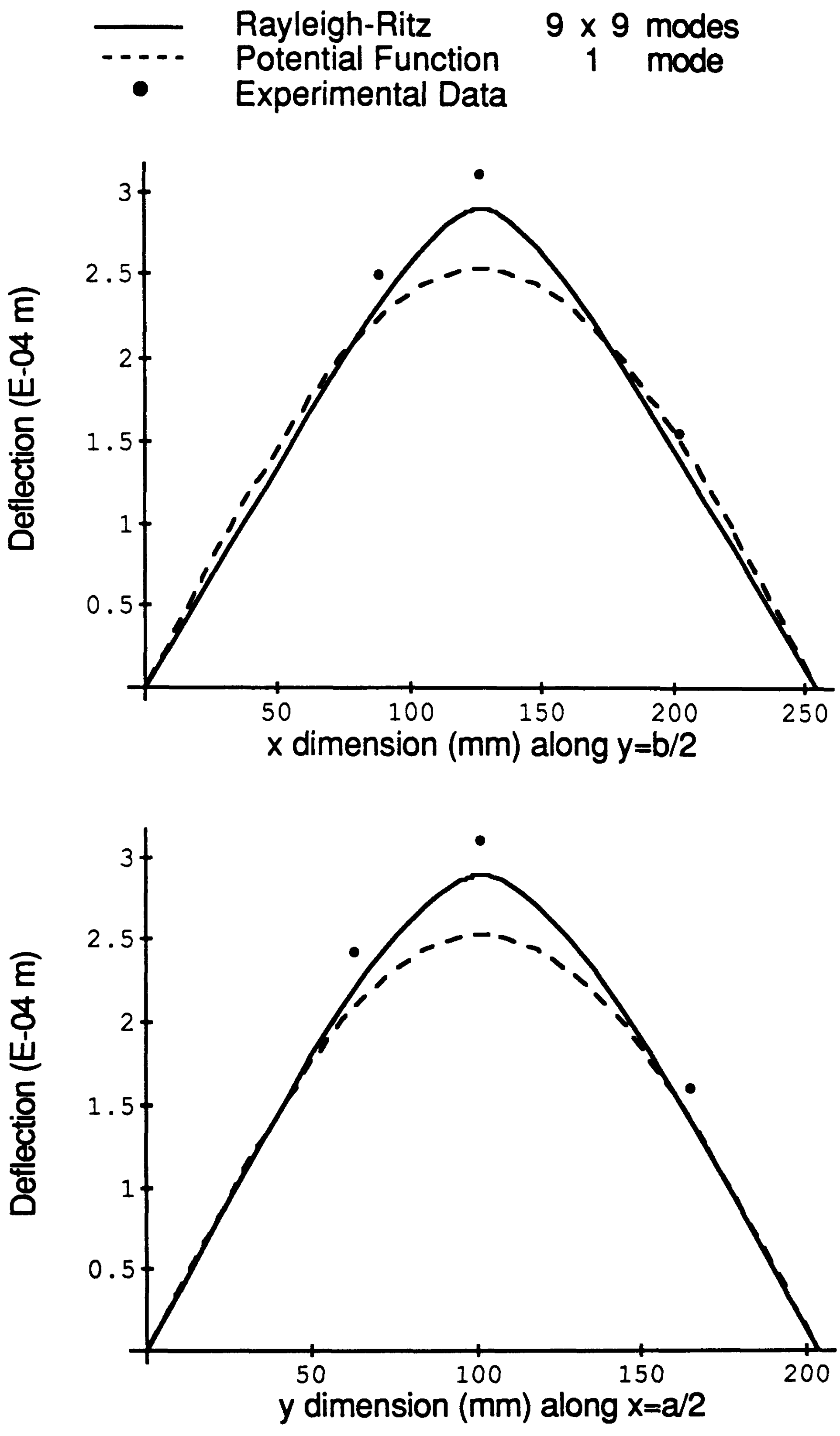

Figure 7.10 Transverse deflection for Specimen I, under a centered point load of 100 Newtons, with all four sides simply supported.

7.3 Comparison of Results for Off-Center Point Load

The off-center point load tests are also fairly consistent, however, additional error results from the experimental clamped boundary conditions due to the increased edge moment. The excessive flexibility of the four sides clamped boundary condition results in 30% more deflection than analytically predicted by the Rayleigh-Ritz solution. Even when only the y edges are clamped, the boundary condition results in 20% more deflection than predicted. The simply supported tests generally exhibit 5% more deflection than analytically predicted by the Rayleigh-Ritz solution, but again this is within the ±8 % experimental error. In general, there is good agreement between the data and the Rayleigh-Ritz analysis.

No comparisons were made with the single mode potential functions since the potential functions are symmetric, and would be unable to account for the off-center loading.

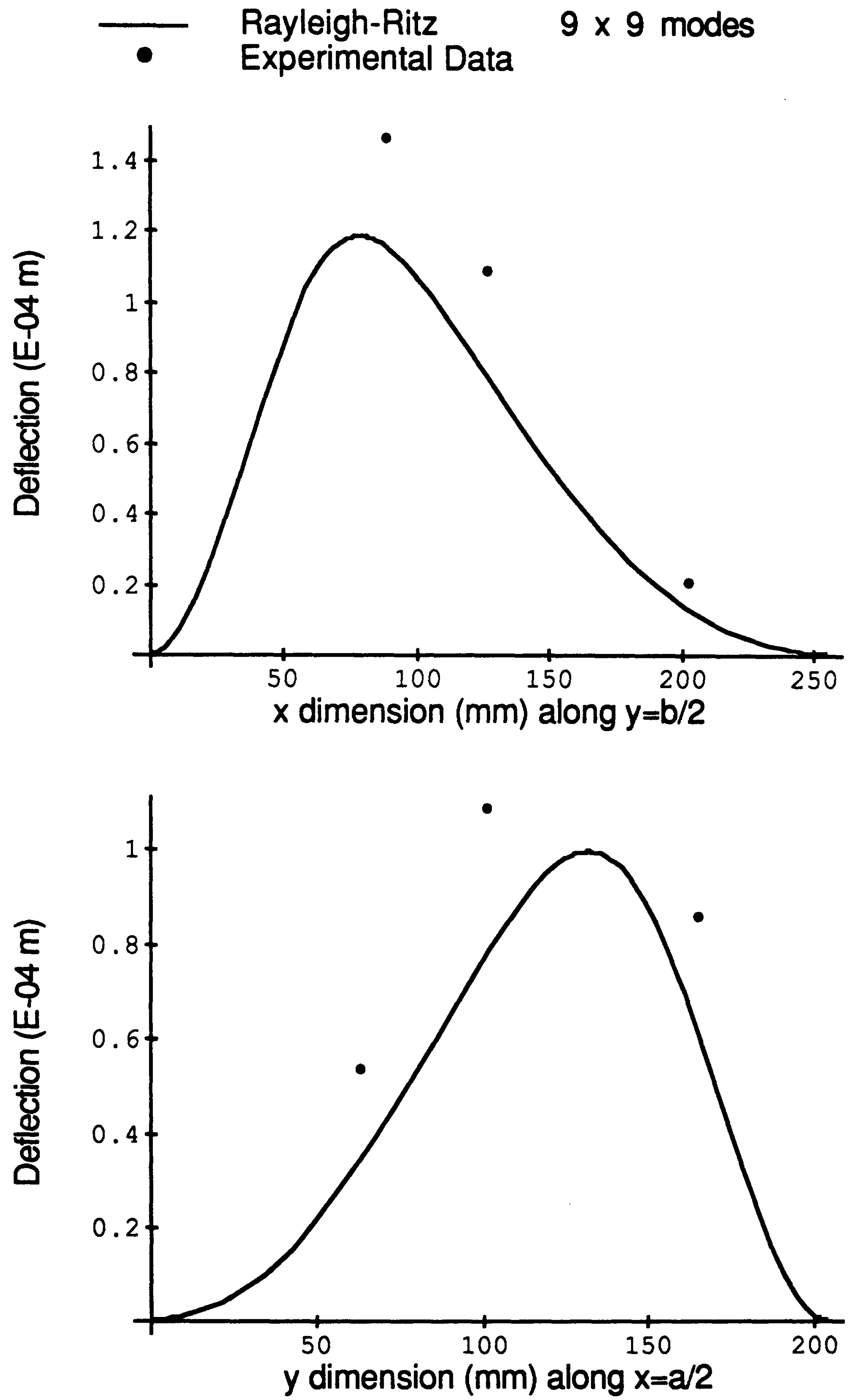

Figure 7.11 Transverse deflection for Specimen A, under an off-center point load of 100 Newtons, with all four sides clamped.

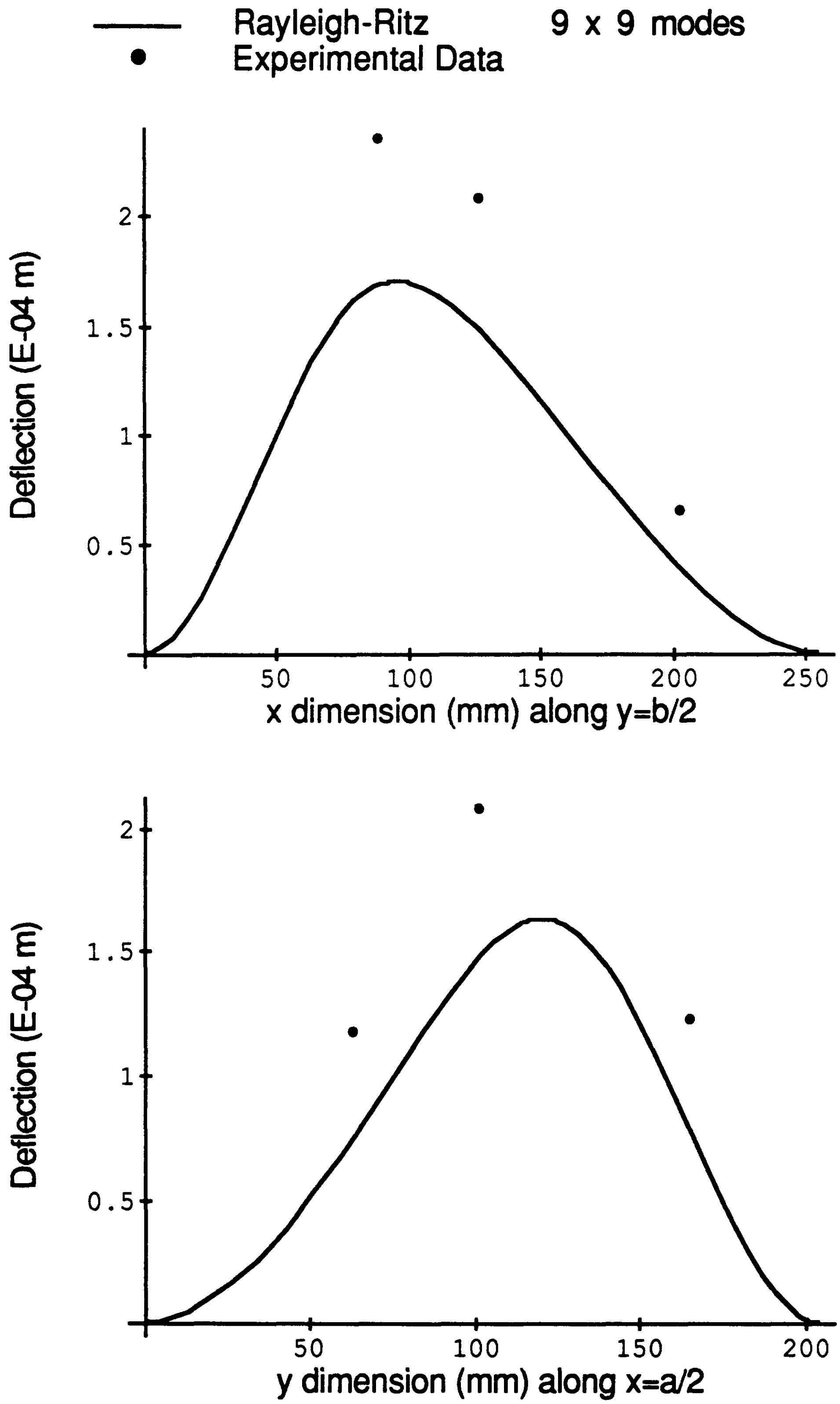

Figure 7.12 Transverse deflection for Specimen B, under an off-center point load of 100 Newtons, with all four sides clamped.

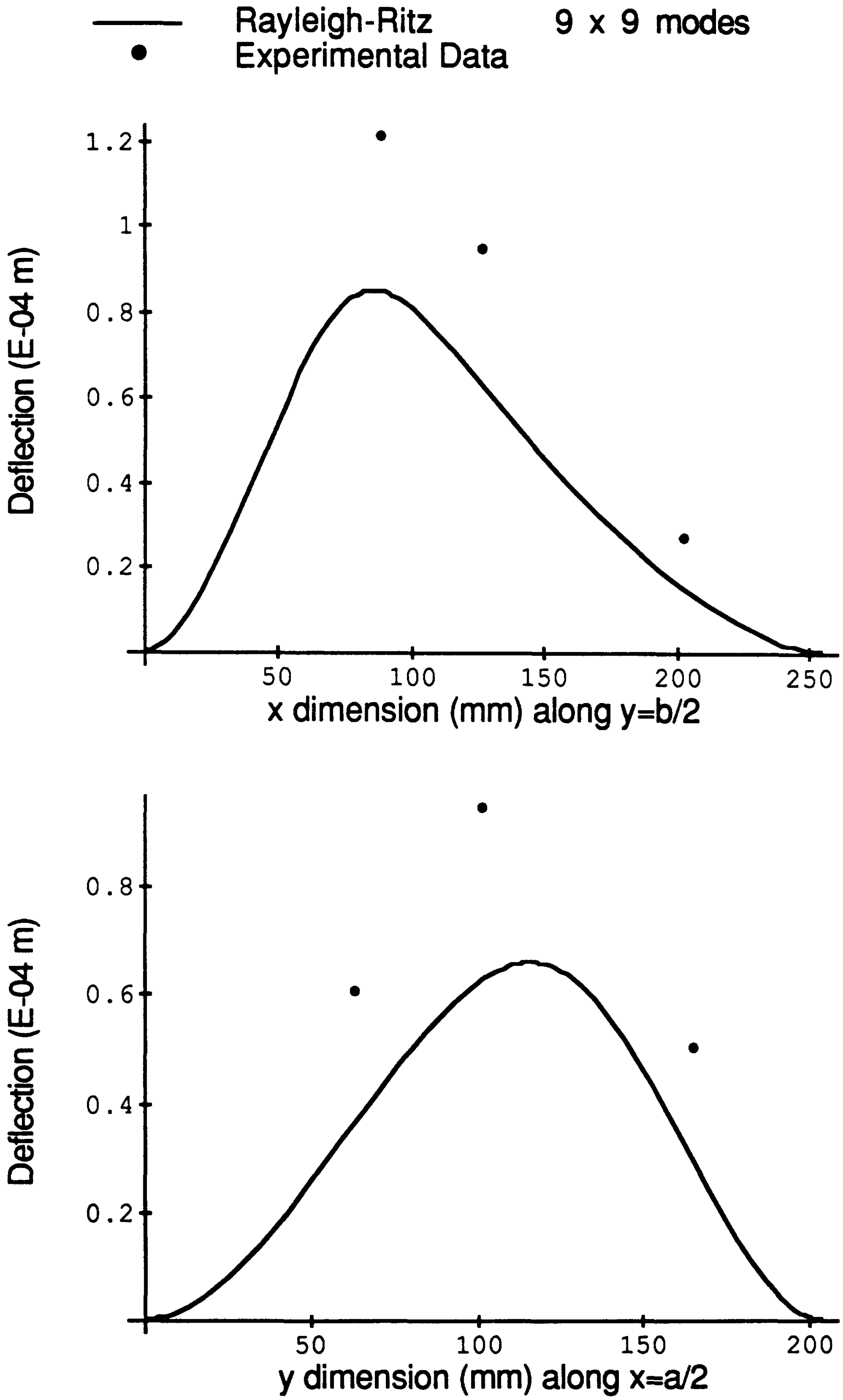

Figure 7.13 Transverse deflection for Specimen C, under an off-center point load of 100 Newtons, with all four sides clamped.

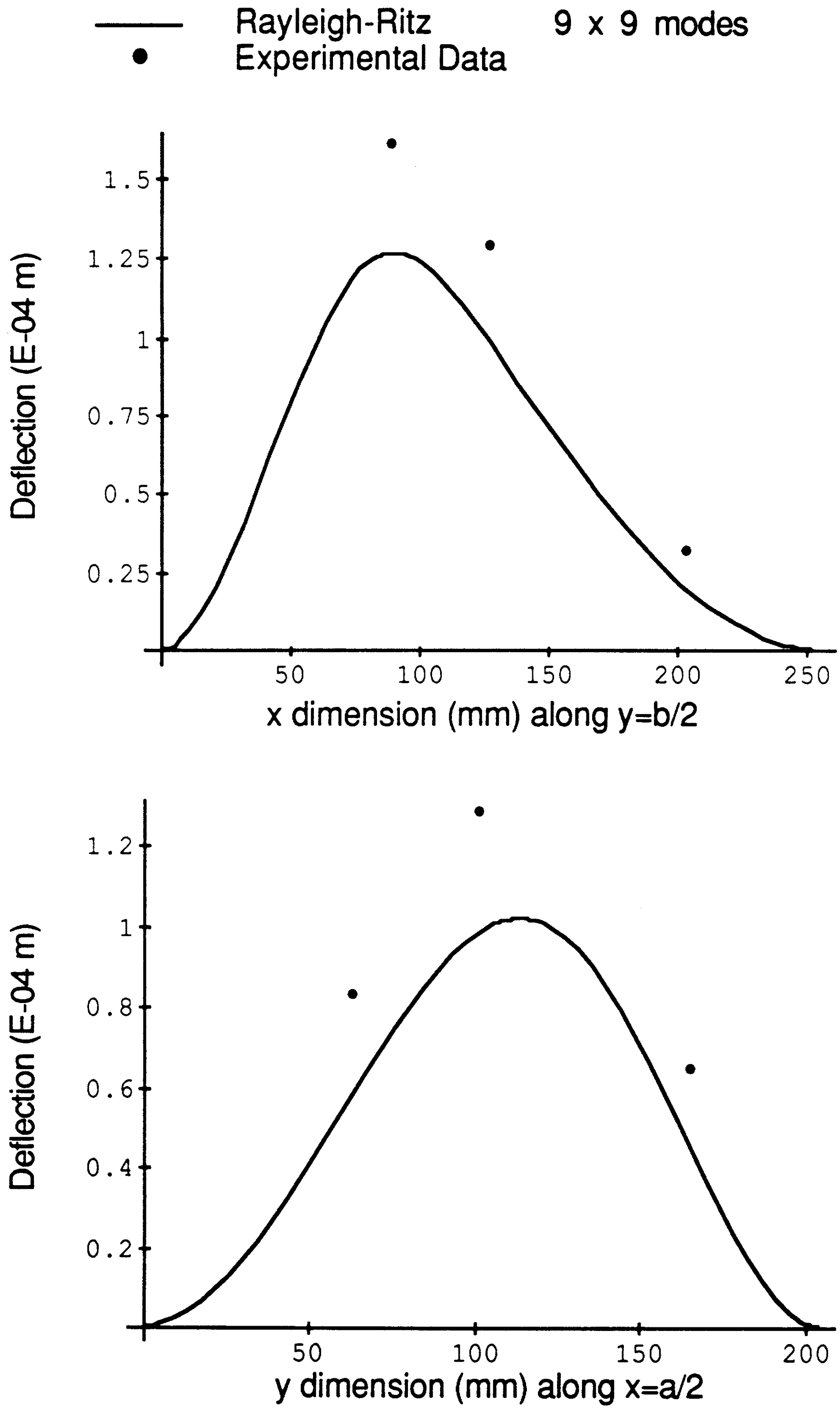

Figure 7.14 Transverse deflection for Specimen D, under an off-center point load of 100 Newtons, with all four sides clamped.

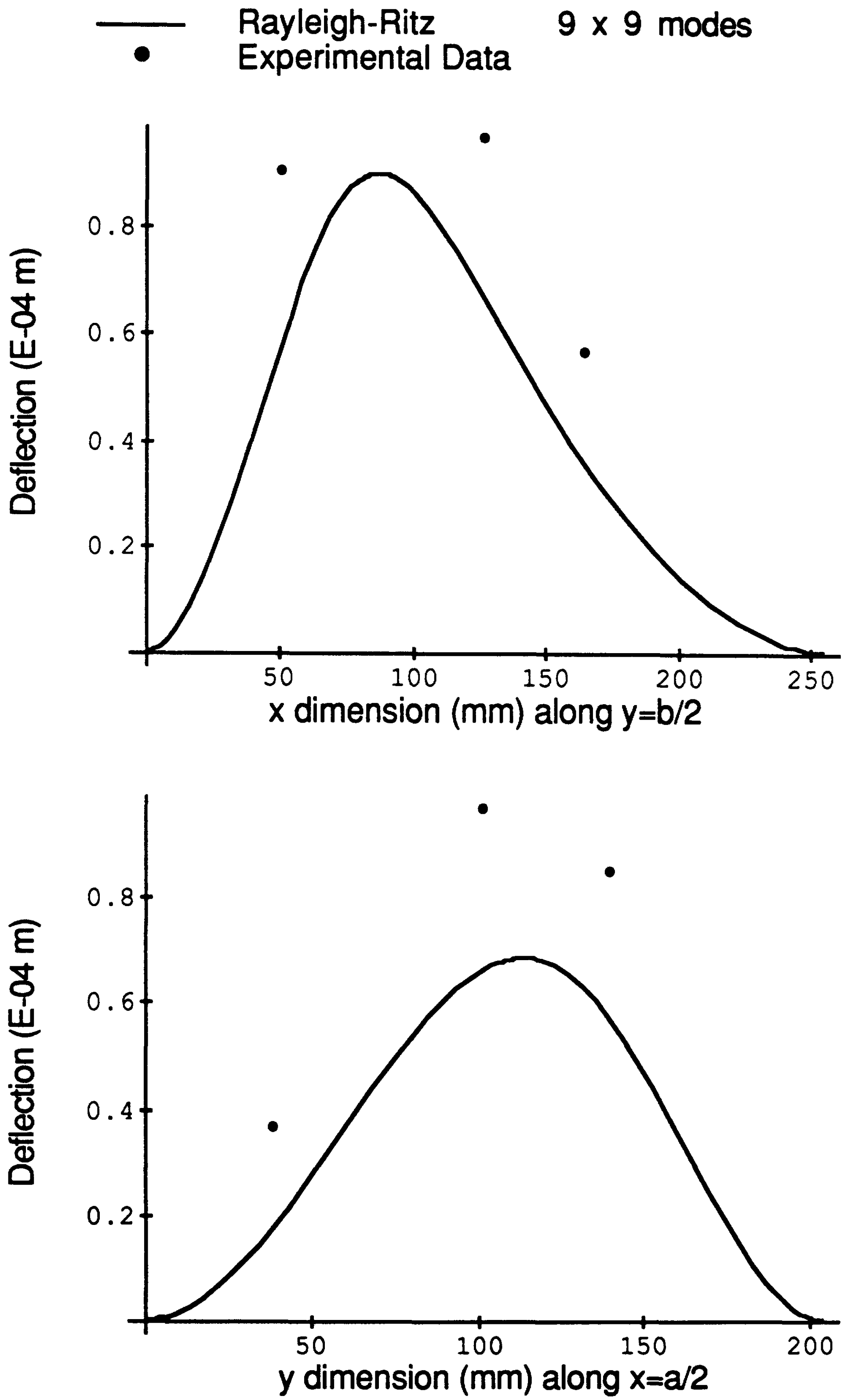

Figure 7.15 Transverse deflection for Specimen I, under an off-center point load of 100 Newtons, with all four sides clamped.

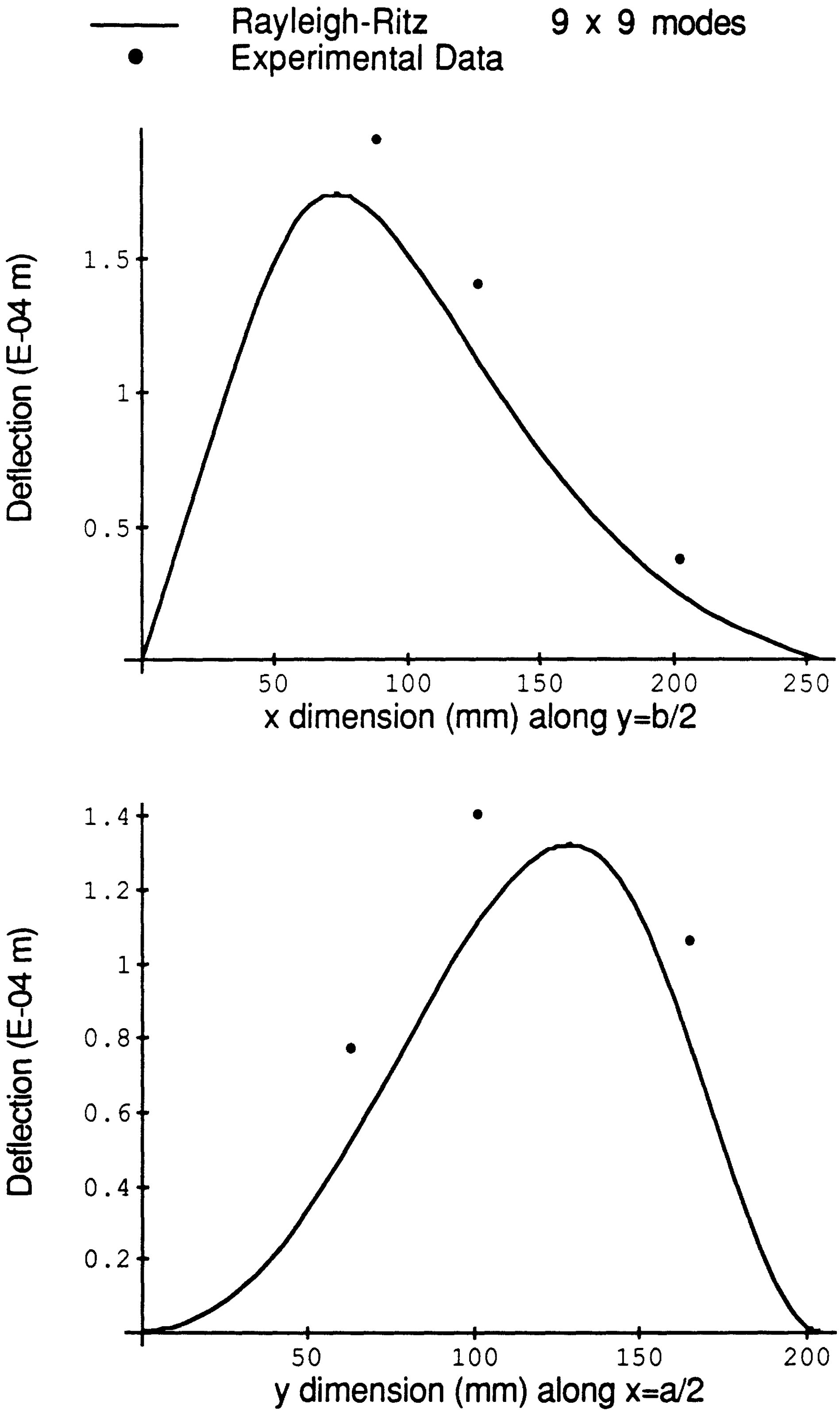

Figure 7.16 Transverse deflection for Specimen A, under an off-center point load of 100 Newtons, with x edges (short edges) simply supported and y edges (long edges) clamped.

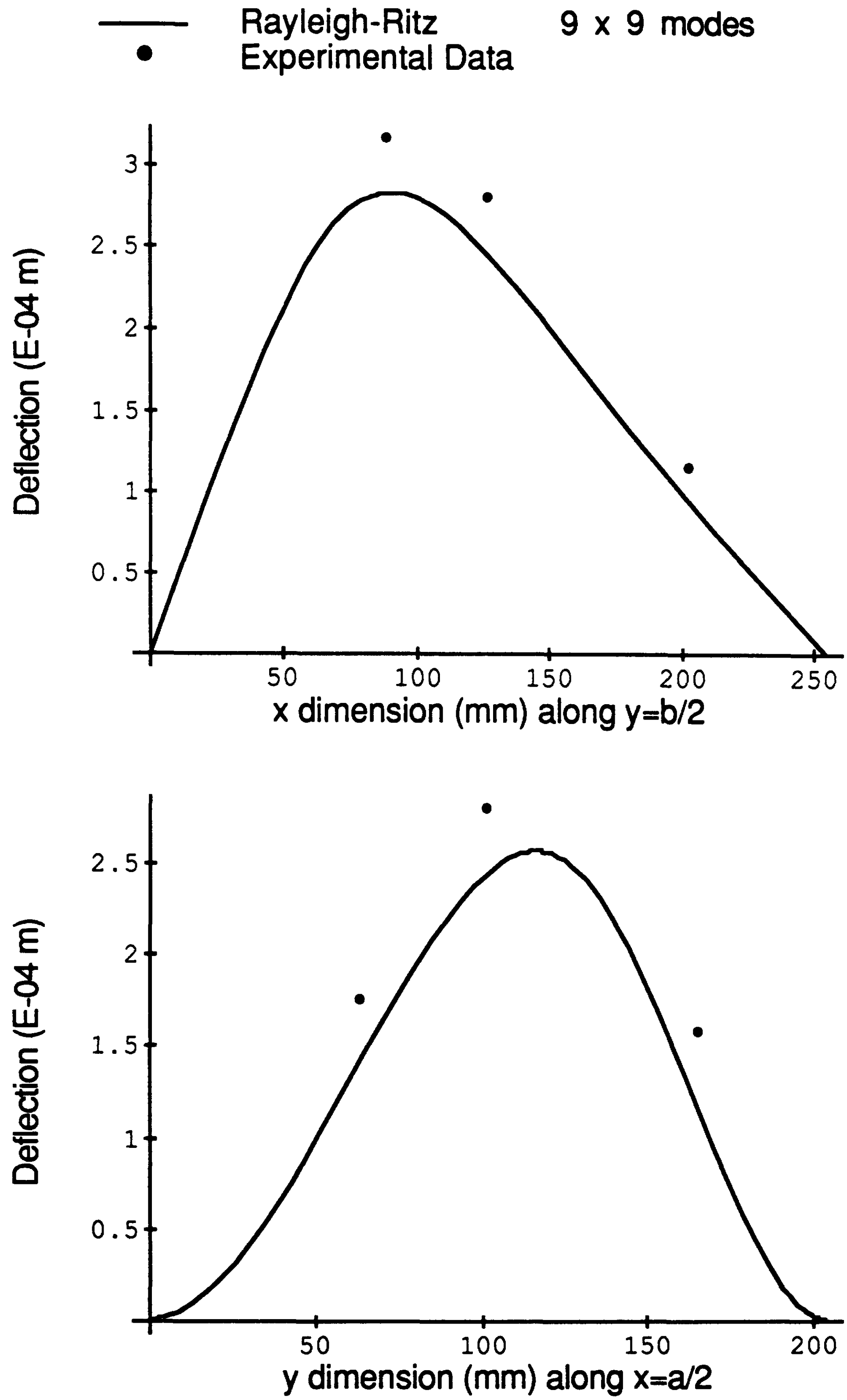

Figure 7.17 Transverse deflection for Specimen B, under an off-center point load of 100 Newtons, with x edges (short edges) simply supported and y edges (long edges) clamped.

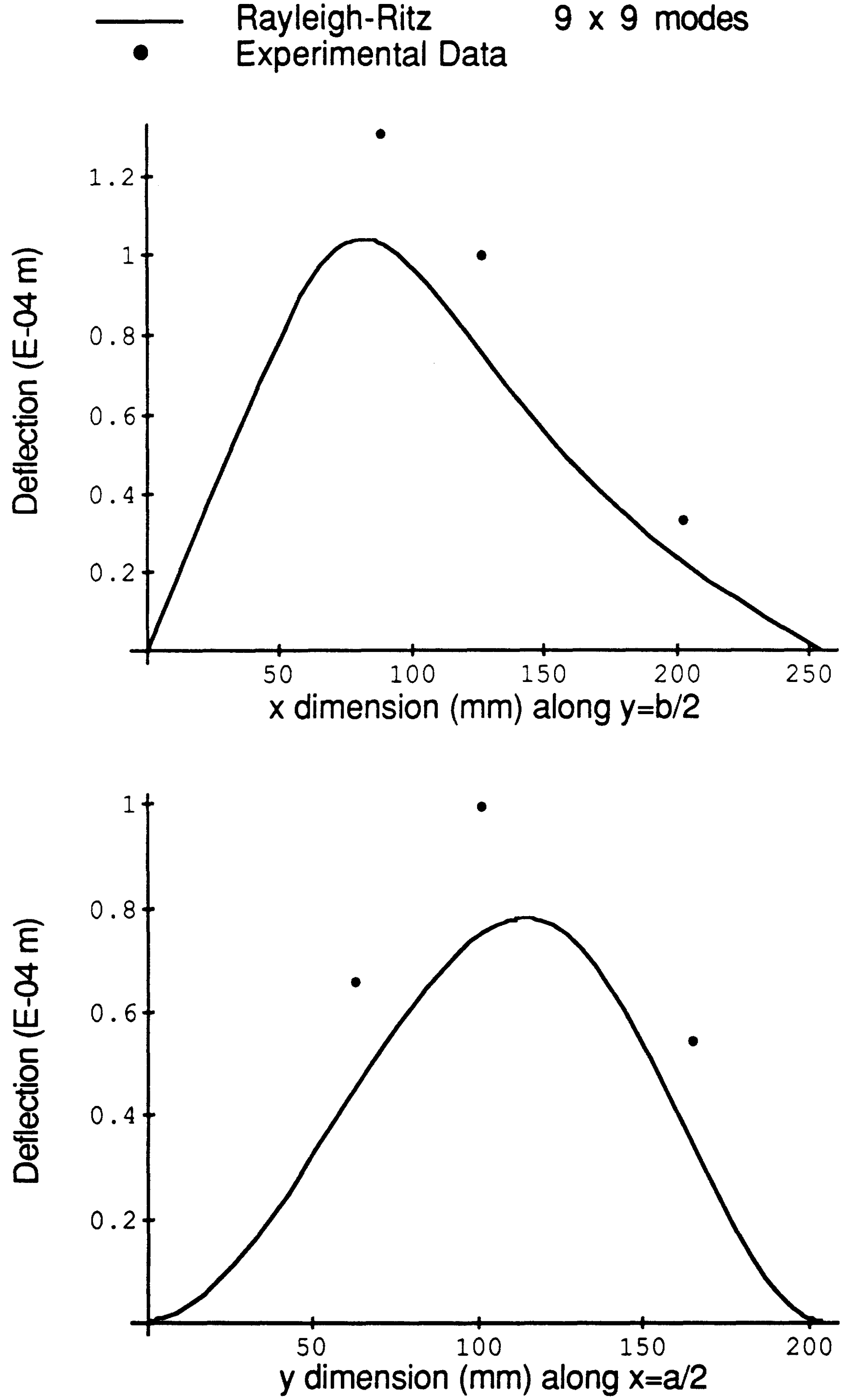

Figure 7.18 Transverse deflection for Specimen C, under an off-center point load of 100 Newtons, with x edges (short edges) simply supported and y edges (long edges) clamped.

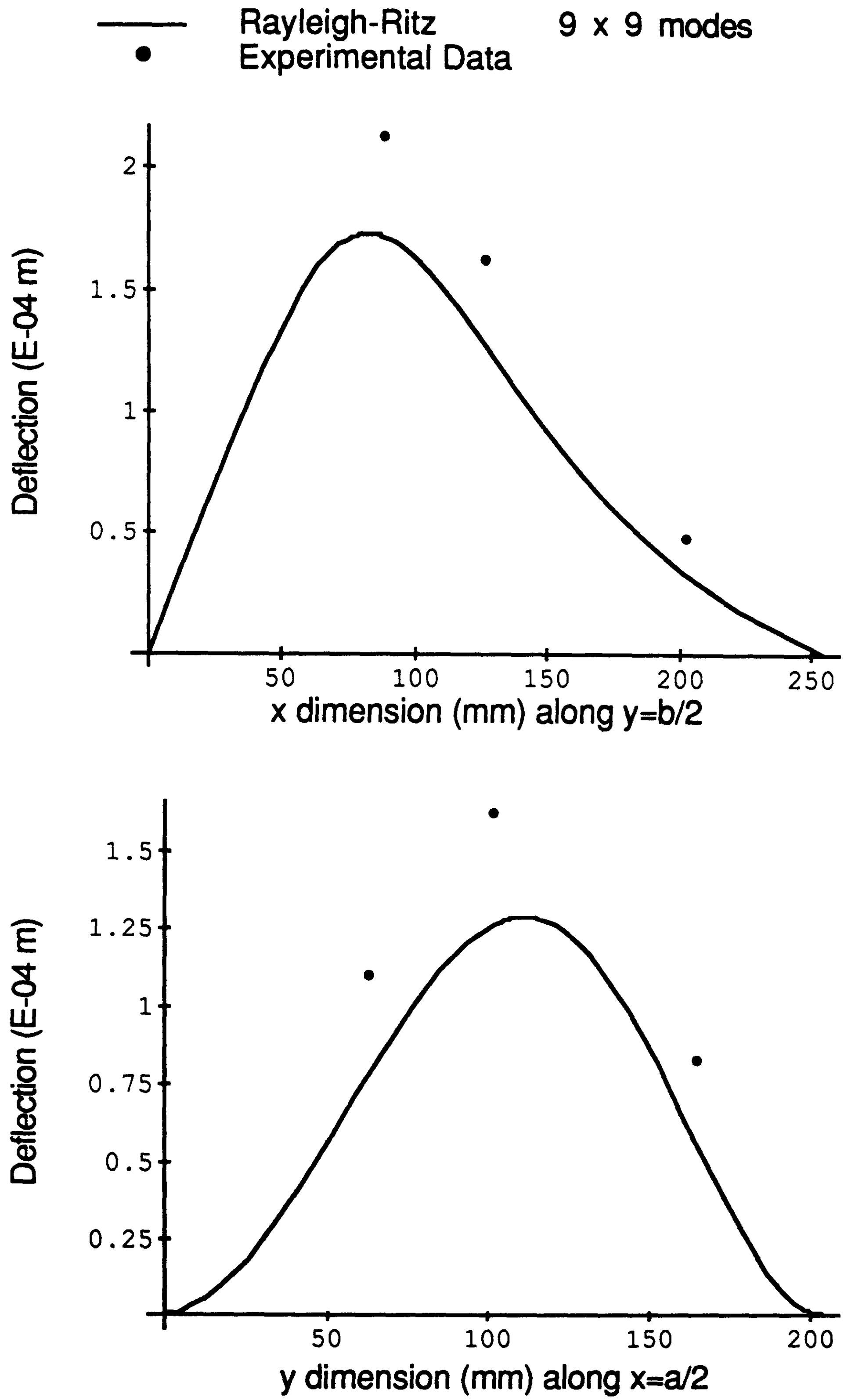

Figure 7.19 Transverse deflection for Specimen D, under an off-center point load of 100 Newtons, with x edges (short edges) simply supported and y edges (long edges) clamped.

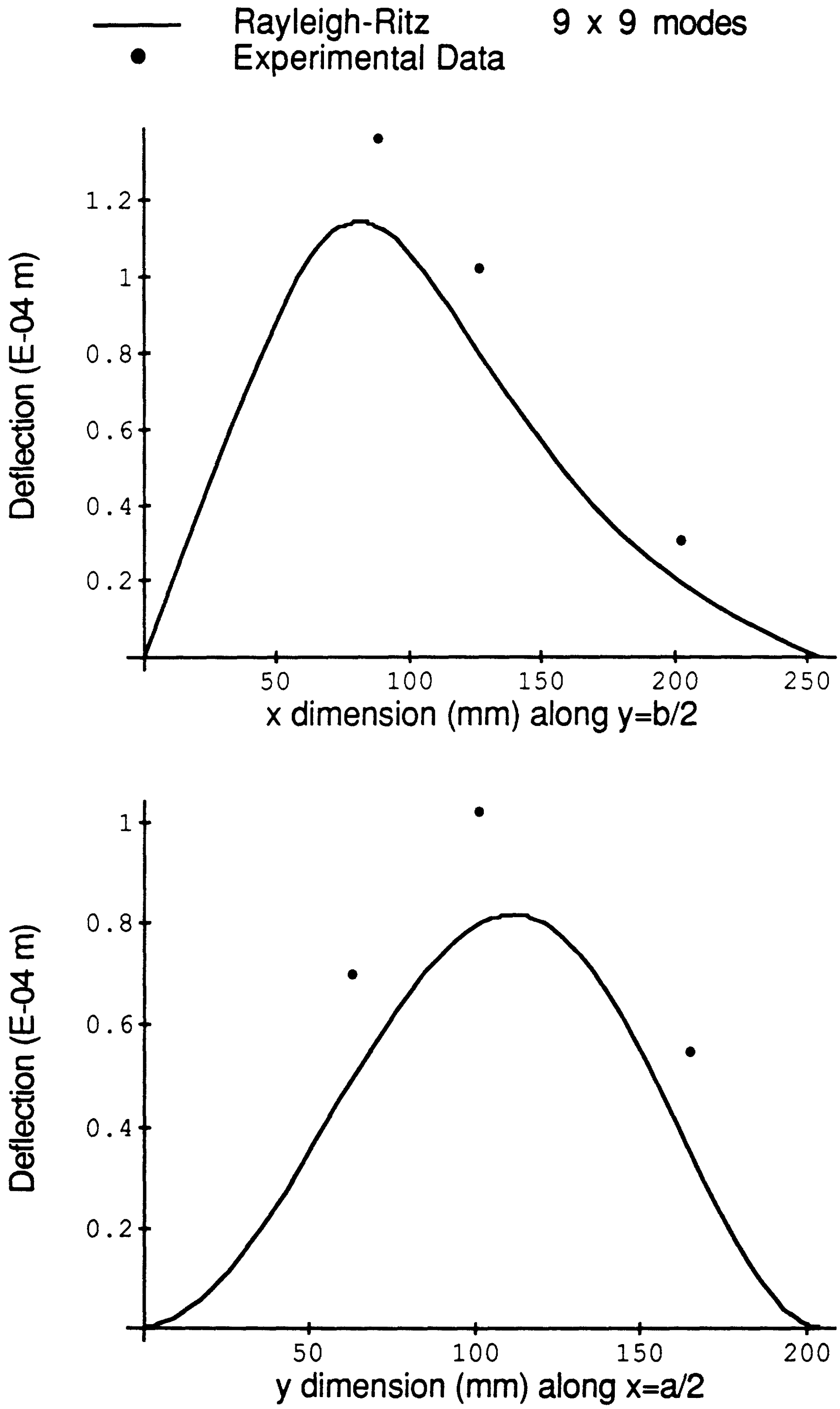

Figure 7.20 Transverse deflection for Specimen I, under an off-center point load of 100 Newtons, with x edges (short edges) simply supported and y edges (long edges) clamped.

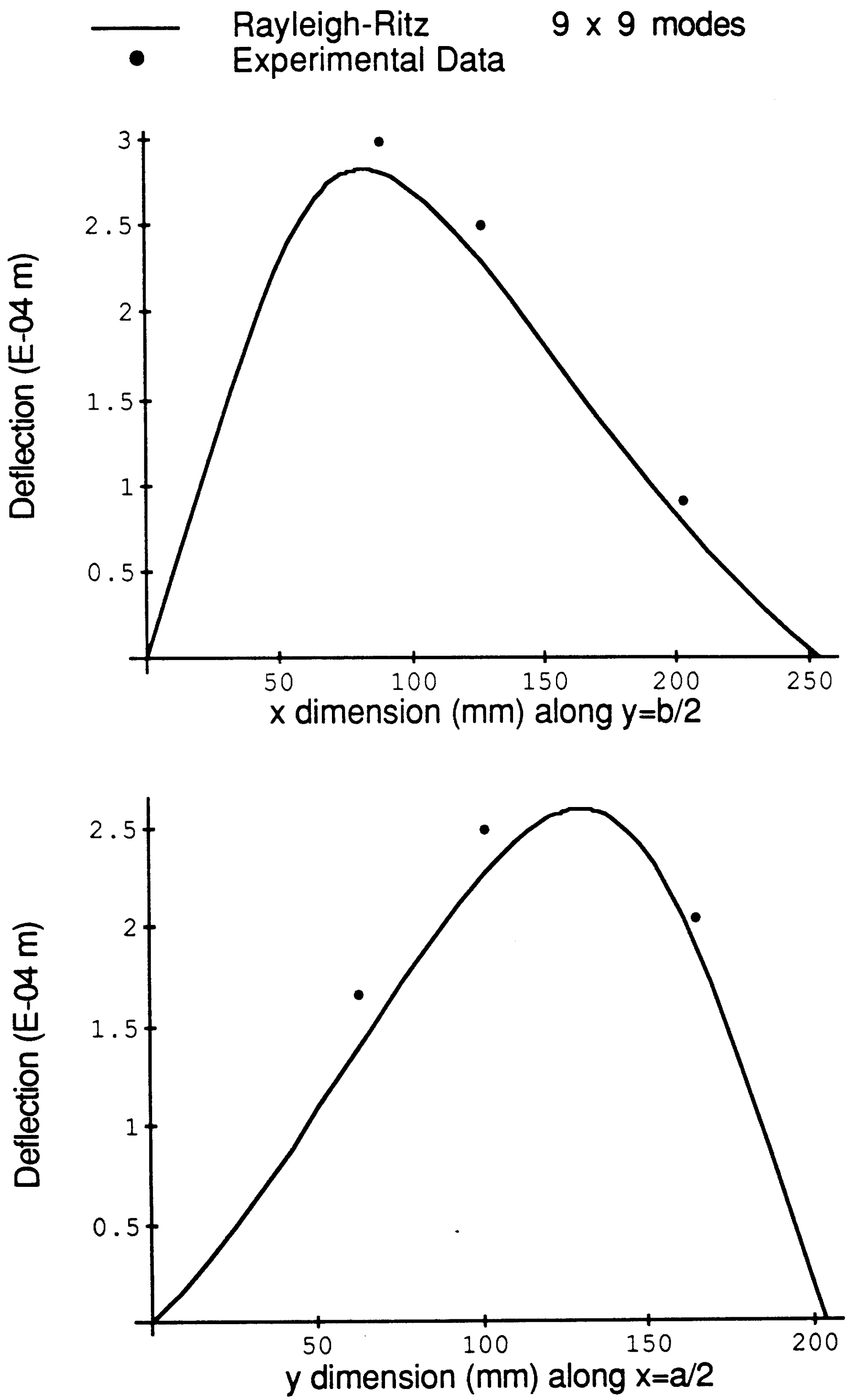

Figure 7.21 Transverse deflection for Specimen A, under an off-center point load of 100 Newtons, with all four sides simply supported.

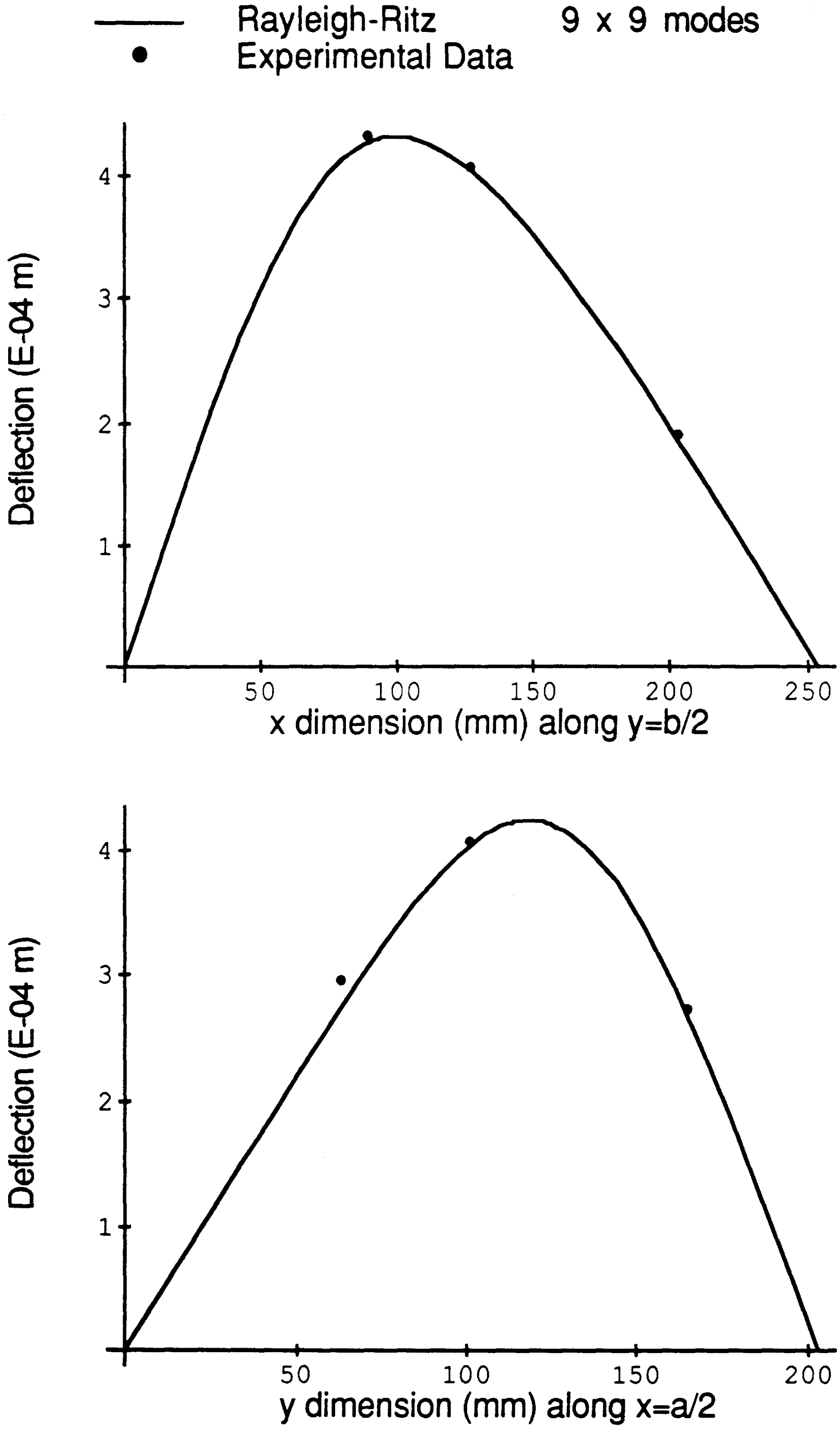

Figure 7.22 Transverse deflection for Specimen B, under an off-center point load of 100 Newtons, with all four sides simply supported.

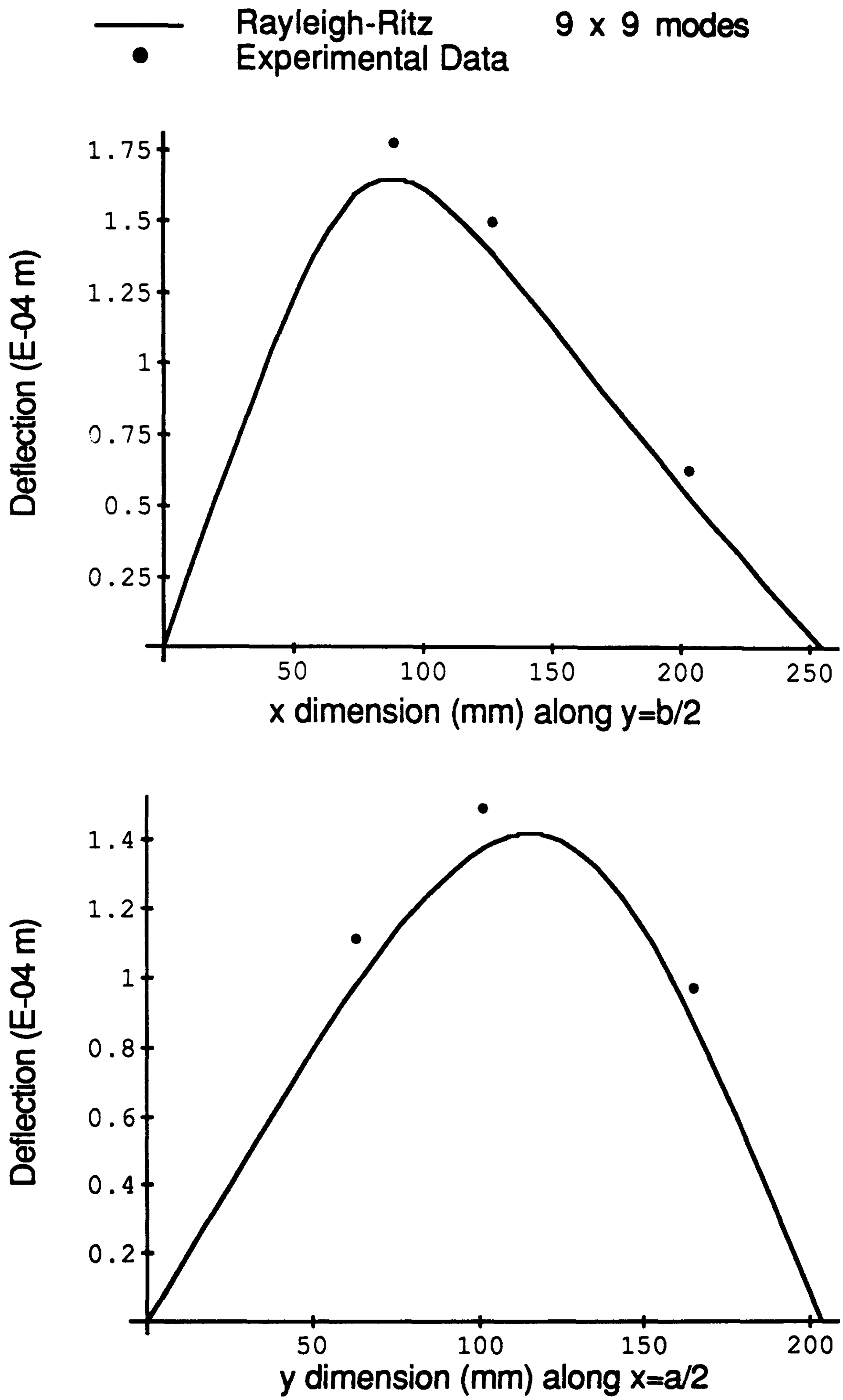

Figure 7.23 Transverse deflection for Specimen C, under an off-center point load of 100 Newtons, with all four sides simply supported.

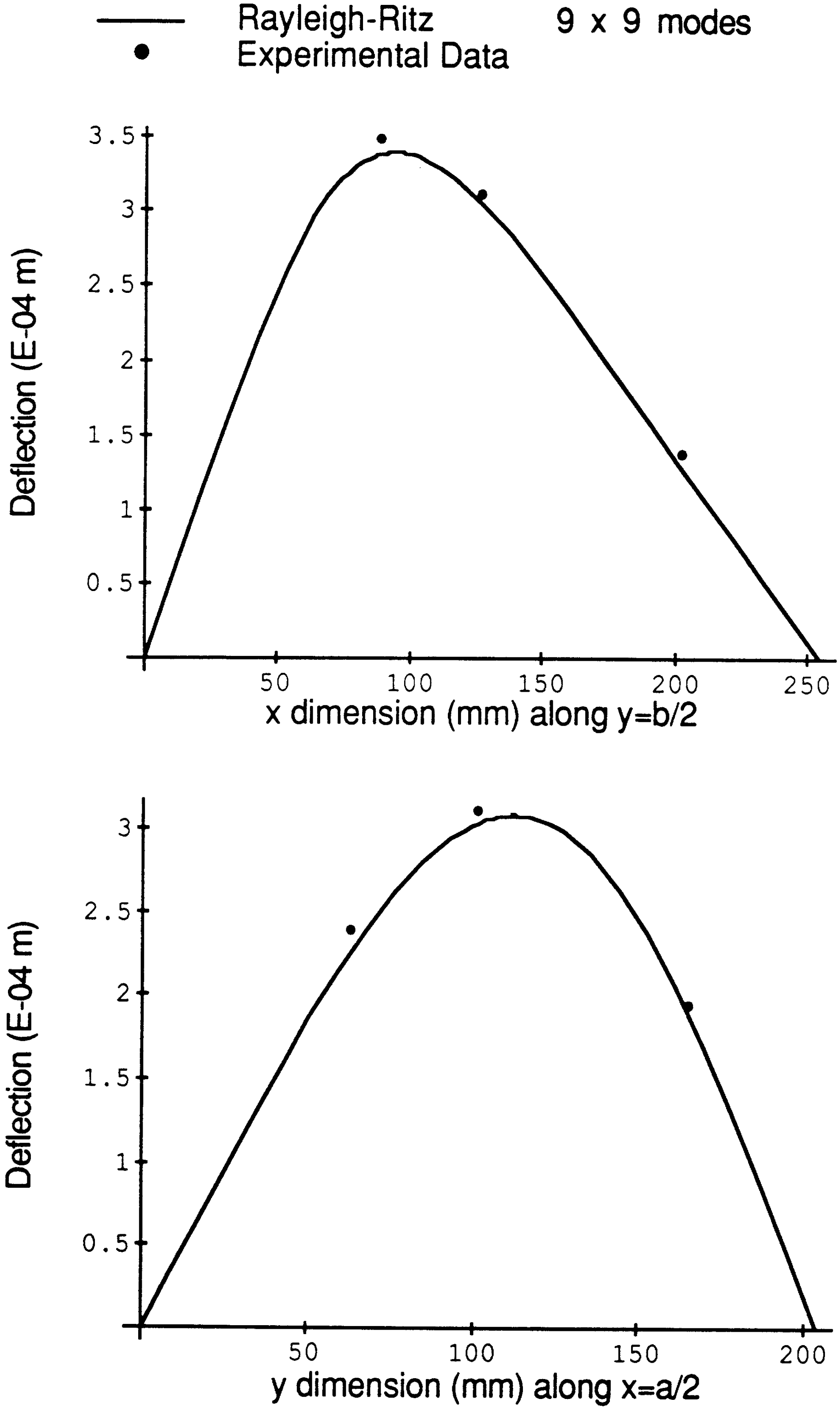

Figure 7.24 Transverse deflection for Specimen D, under an off-center point load of 100 Newtons, with all four sides simply supported.

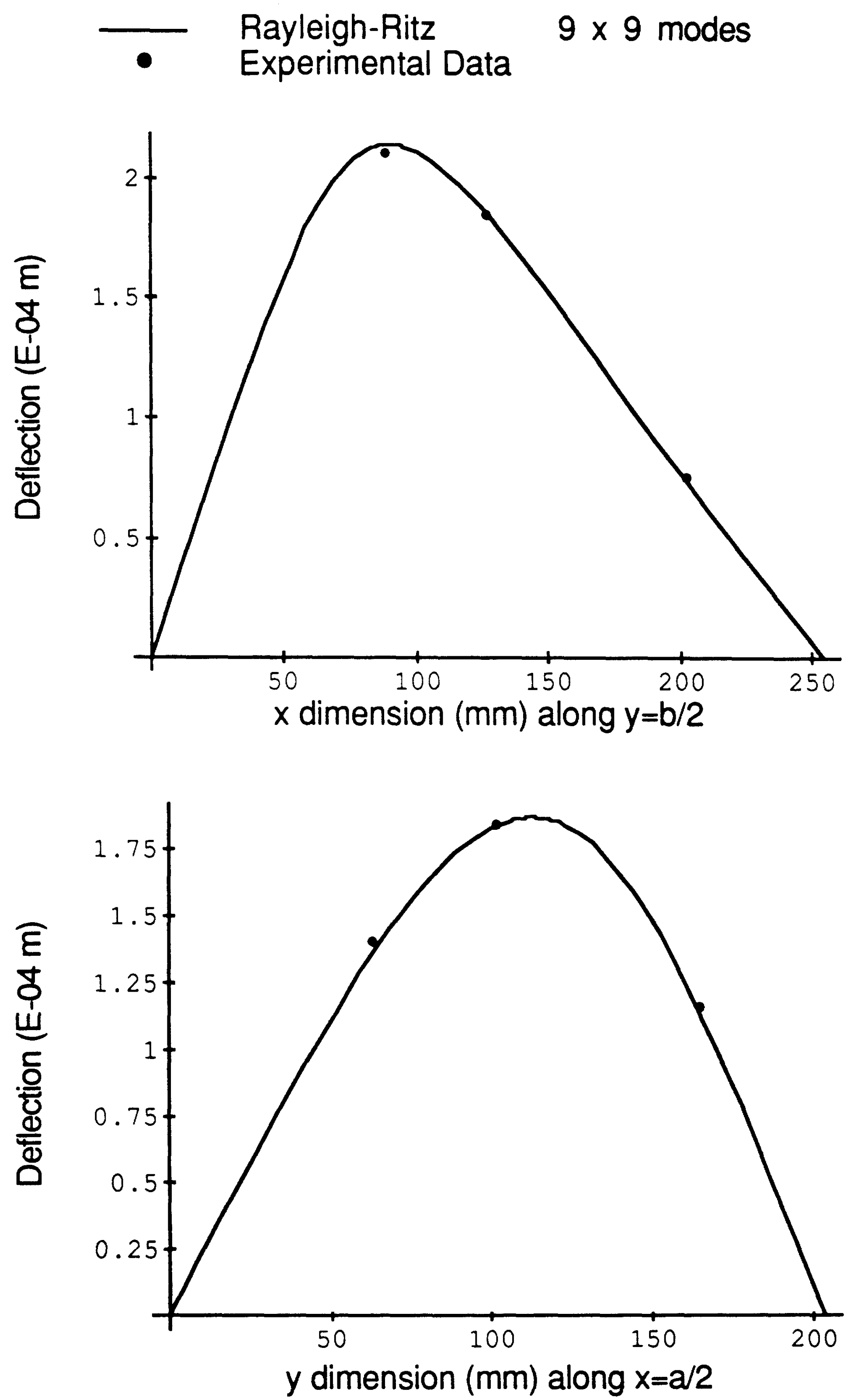

Figure 7.25 Transverse deflection for Specimen I, under an off-center point load of 100 Newtons, with all four sides simply supported.

7.4 Comparison of Results for Centered URPP

The centered URPP tests follow the same pattern as the centered point load tests. The four edges clamped case is 15% overly flexible and the four edges simply supported case is 5% overly flexible when compared to the Rayleigh-Ritz analysis. One interesting exception is specimen B with four edges simply supported. For this case the experimental stiffness is 8% stiffer than the Rayleigh-Ritz analysis. This over constraint comes close to exceeding the estimated experimental error of ±8 %. All the other specimens are under constrained or just marginally over constrained.

Again, the single mode potential functions for four edges clamped and four edges simply supported are not sufficient to adequately describe the deformations caused by the centered URPP. Additional modes need to be added to the single mode solution to obtain a converged answer.

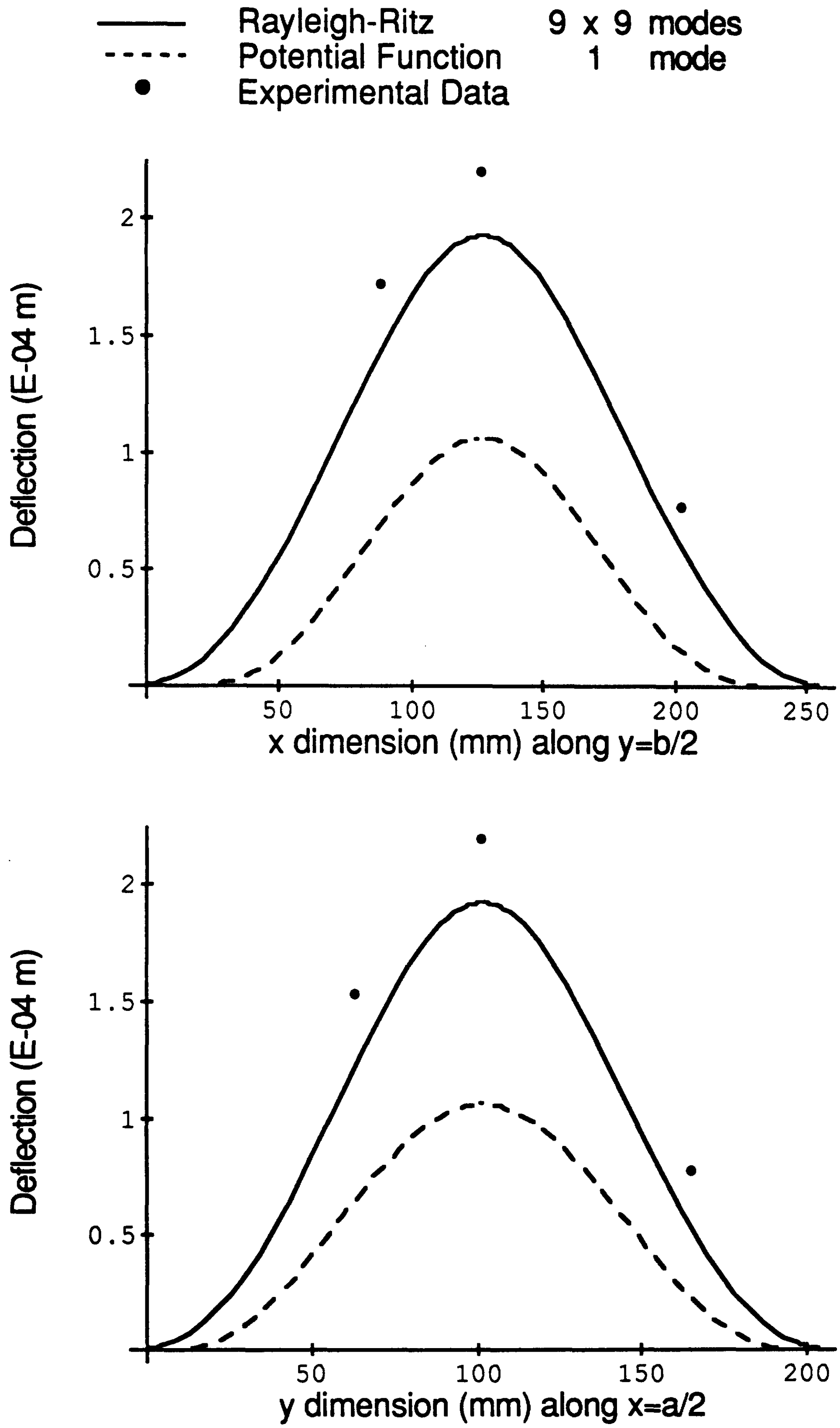

Figure 7.26 Transverse deflection for Specimen A, under a centered URPP load of 100 Newtons, with all four sides clamped.

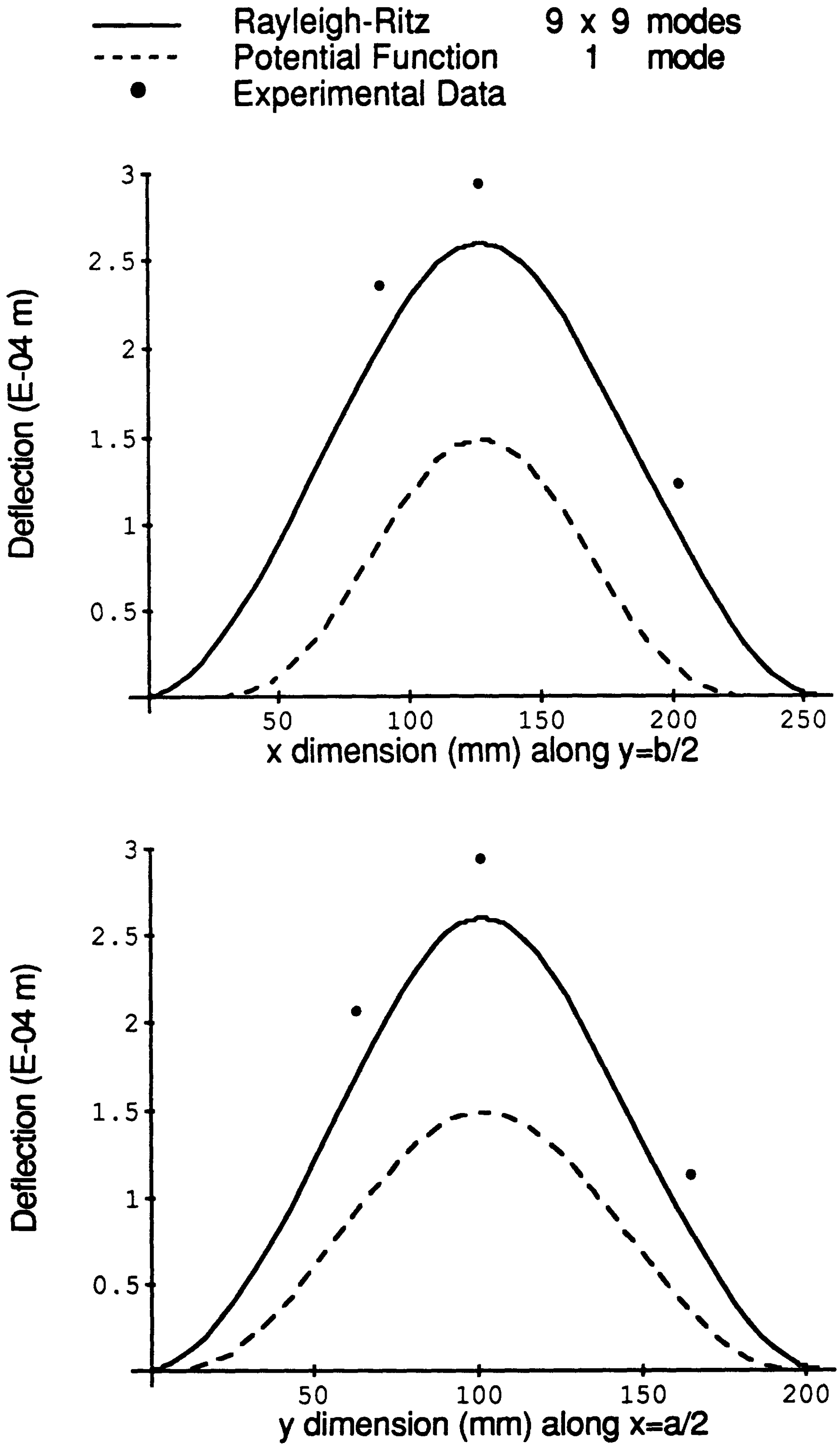

Figure 7.27 Transverse deflection for Specimen B, under a centered URPP load of 100 Newtons, with all four sides clamped.

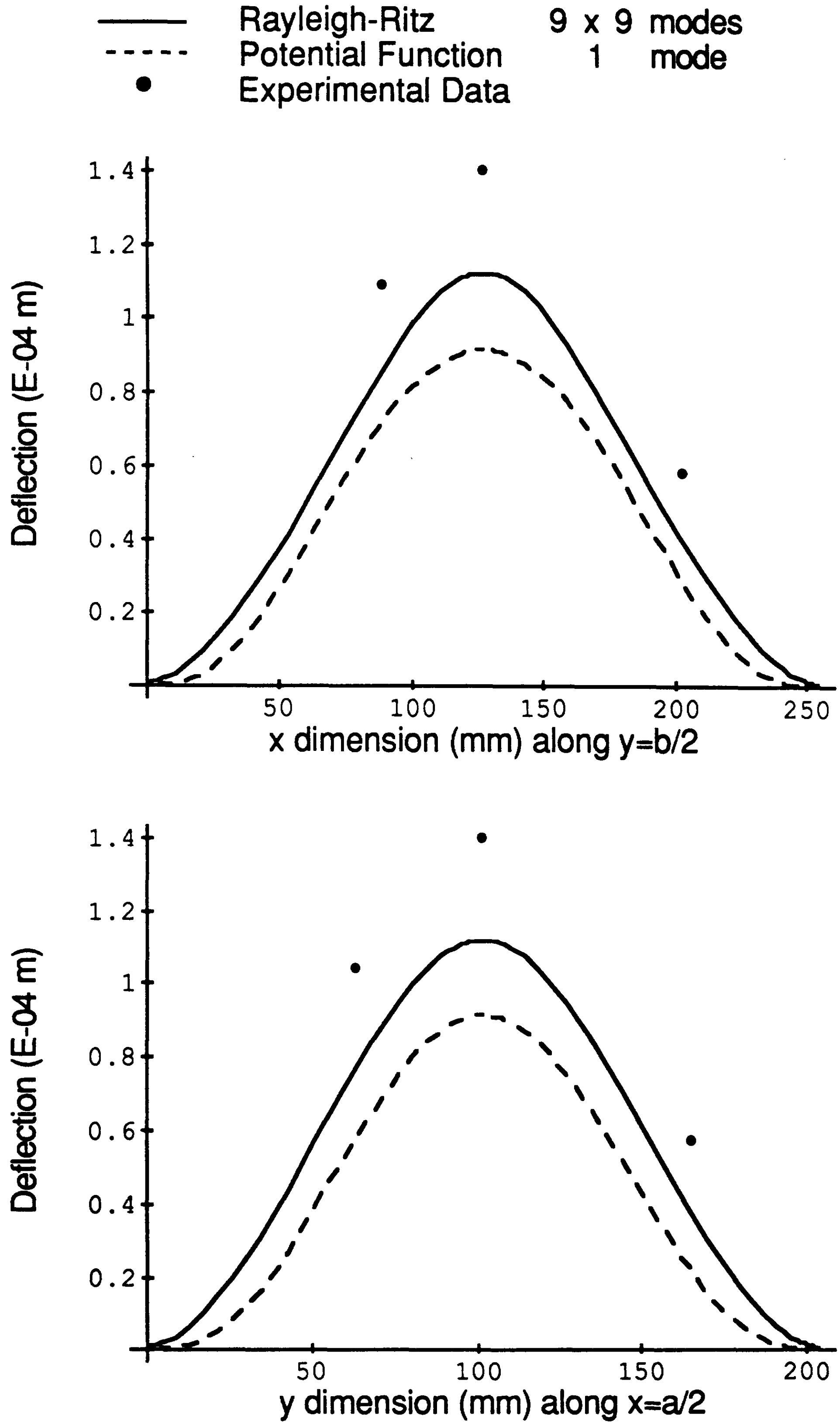

Figure 7.28 Transverse deflection for Specimen C, under a centered URPP load of 100 Newtons, with all four sides clamped.

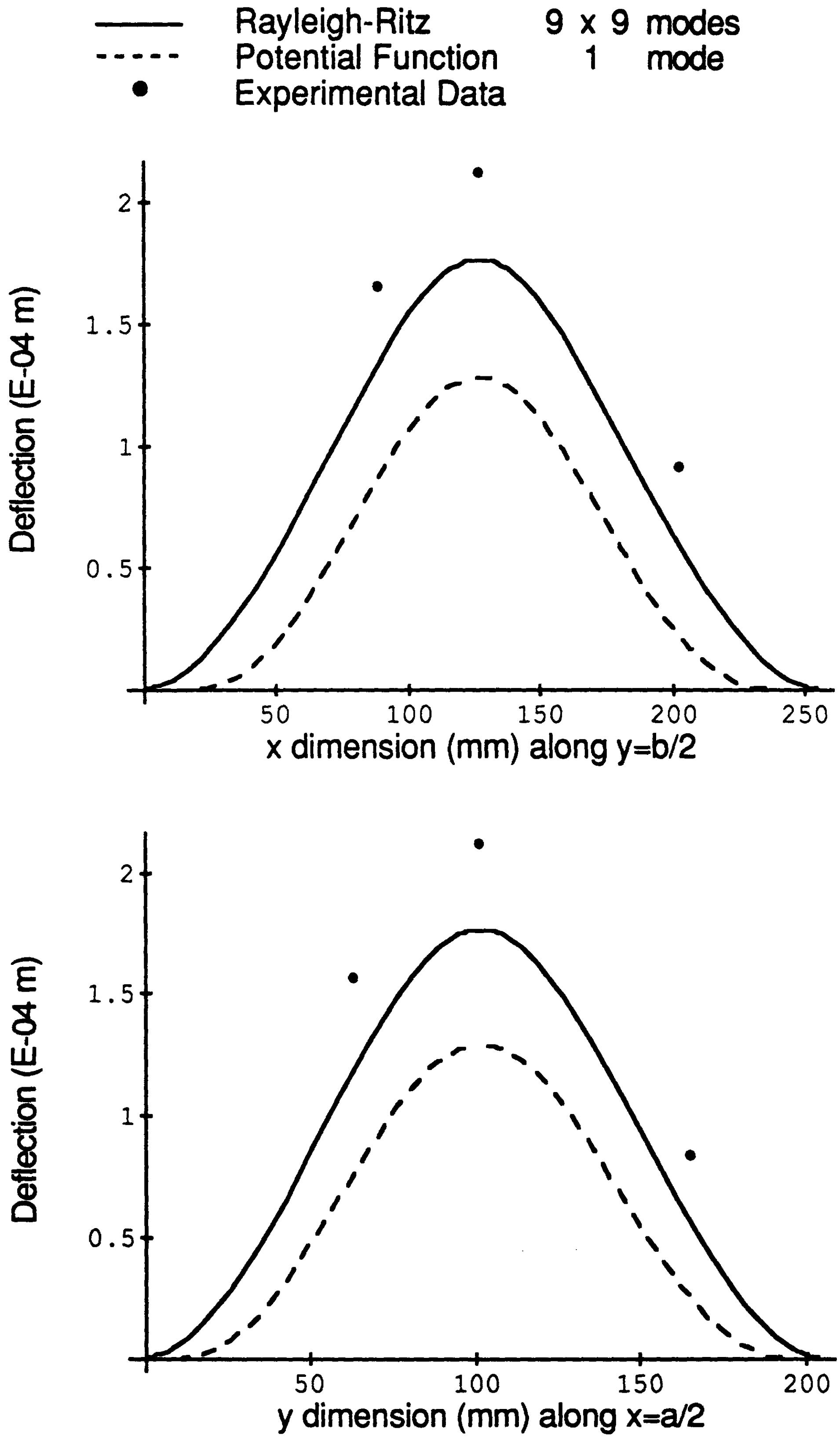

Figure 7.29 Transverse deflection for Specimen D, under a centered URPP load of 100 Newtons, with all four sides clamped.

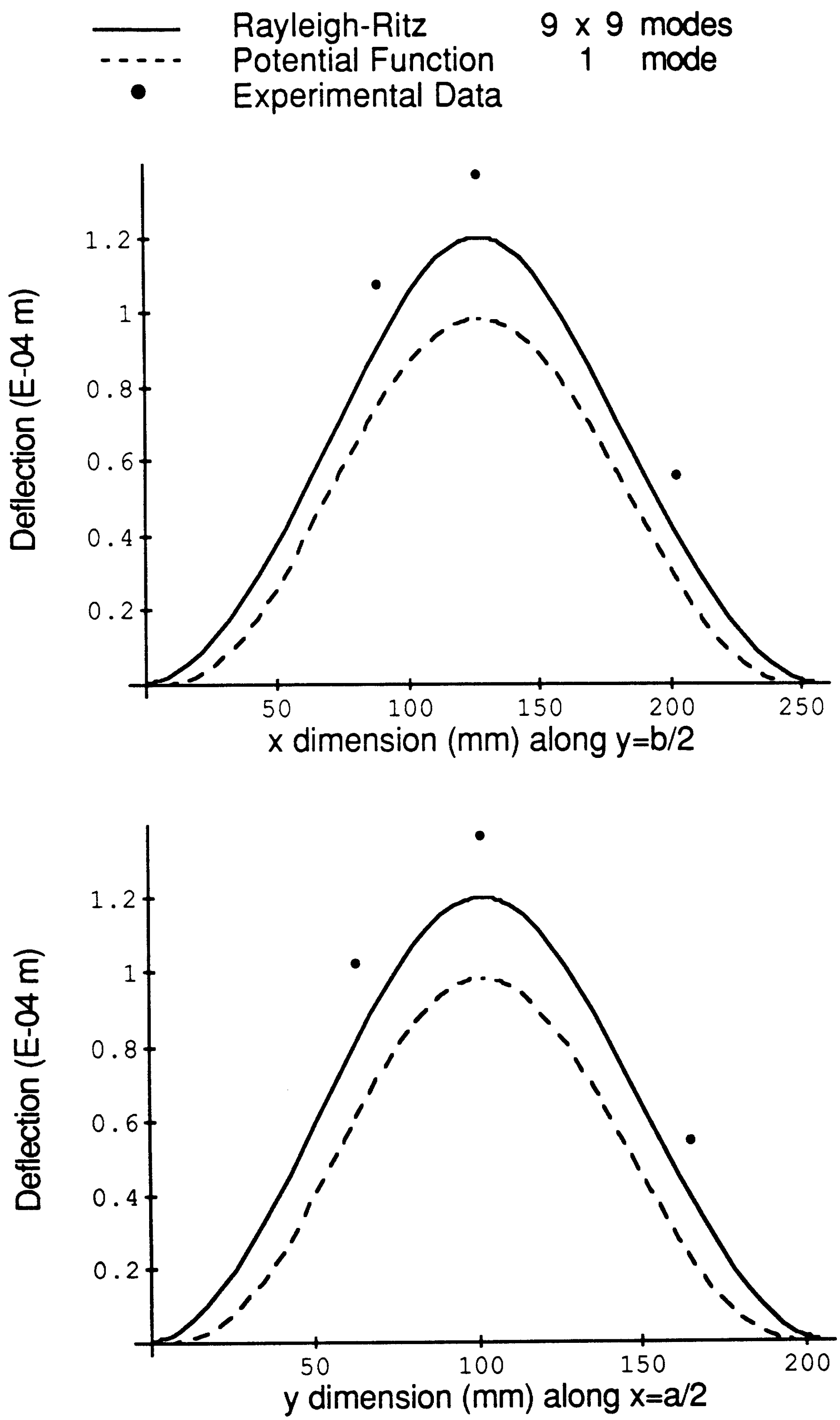

Figure 7.30 Transverse deflection for Specimen I, under a centered URPP load of 100 Newtons, with all four sides clamped.

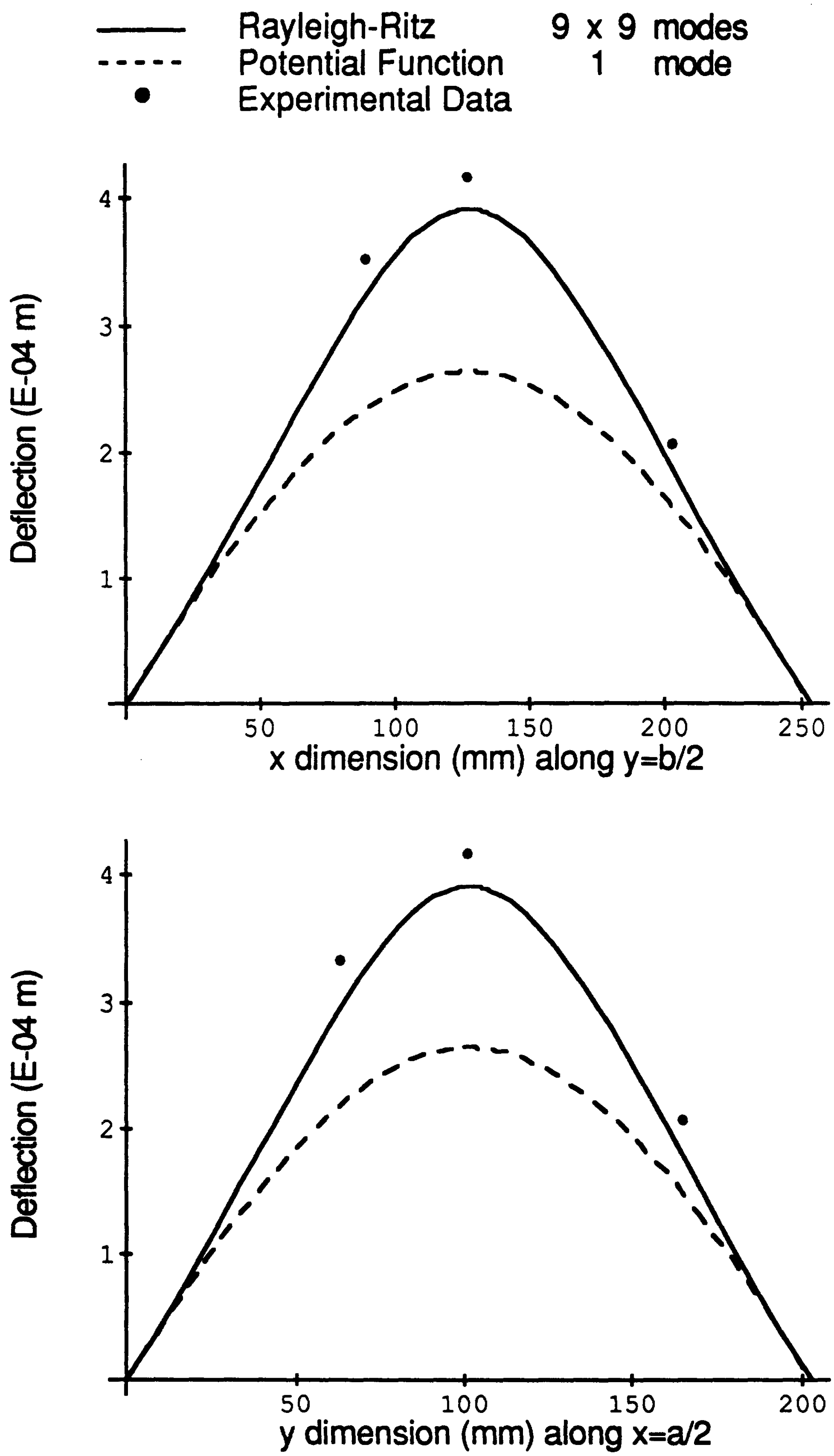

Figure 7.31 Transverse deflection for Specimen A, under a centered URPP load of 100 Newtons, with all four sides simply supported.

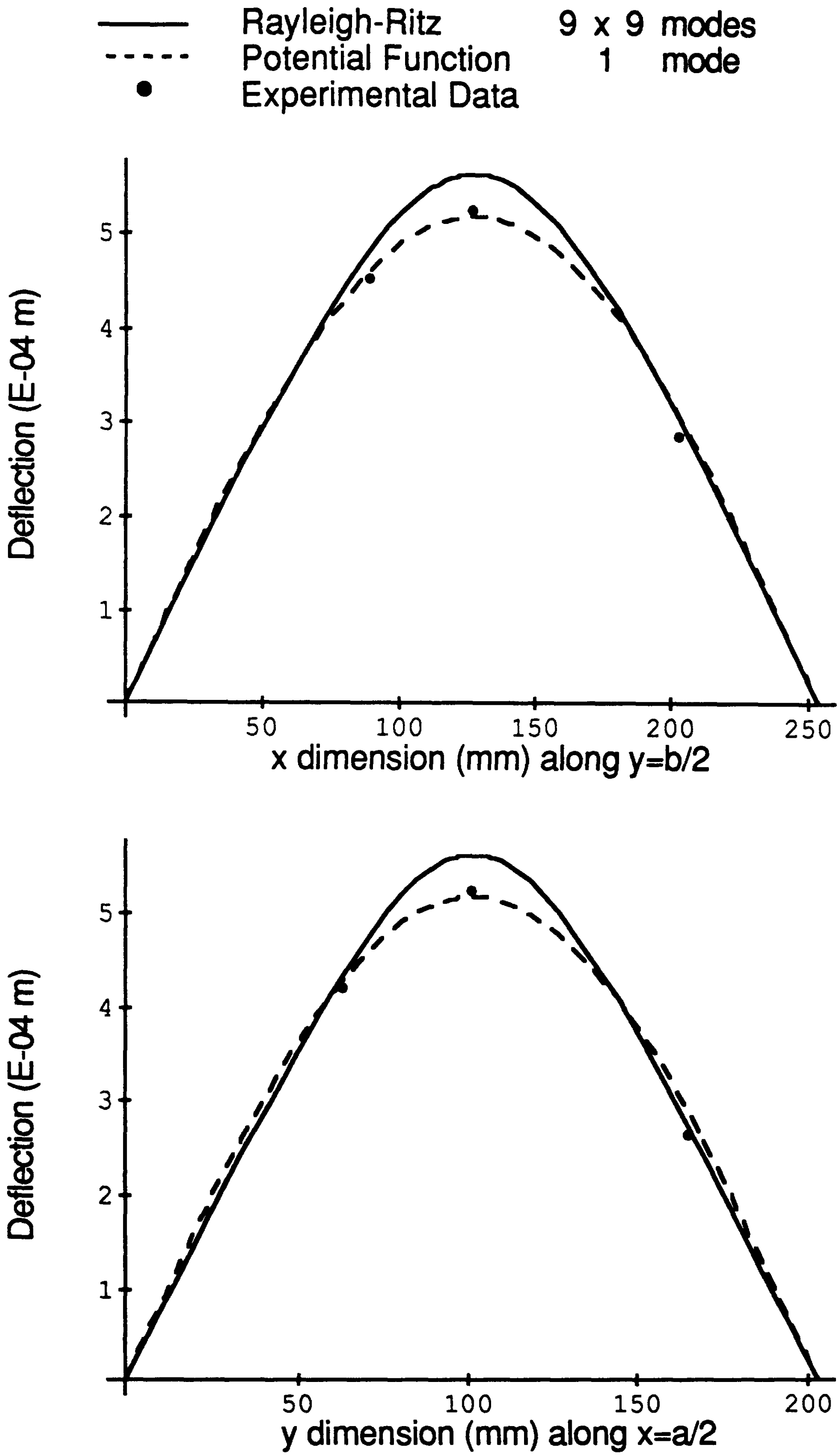

Figure 7.32 Transverse deflection for Specimen B, under a centered URPP load of 100 Newtons, with all four sides simply supported.

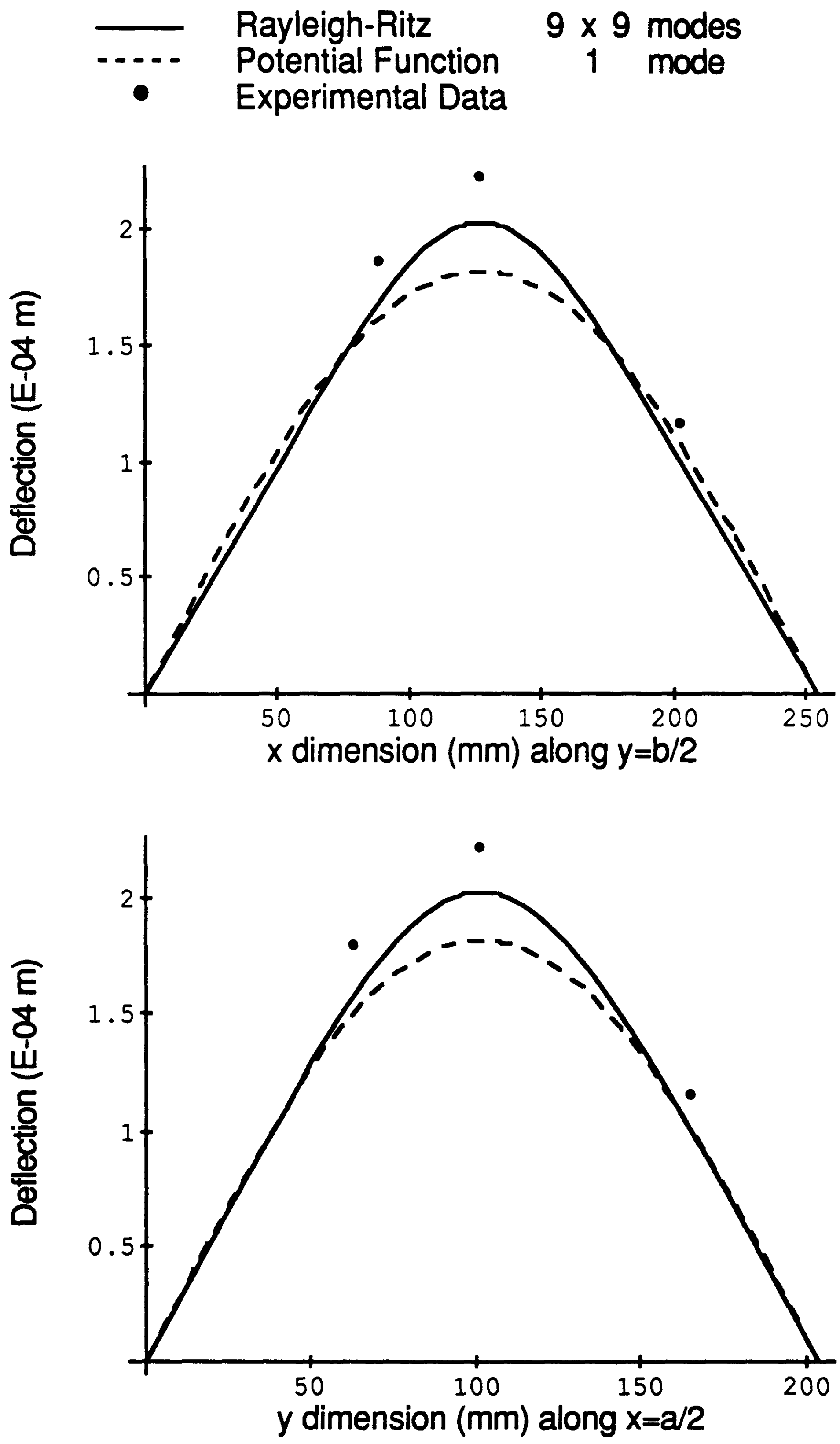

Figure 7.33 Transverse deflection for Specimen C, under a centered URPP load of 100 Newtons, with all four sides simply supported.

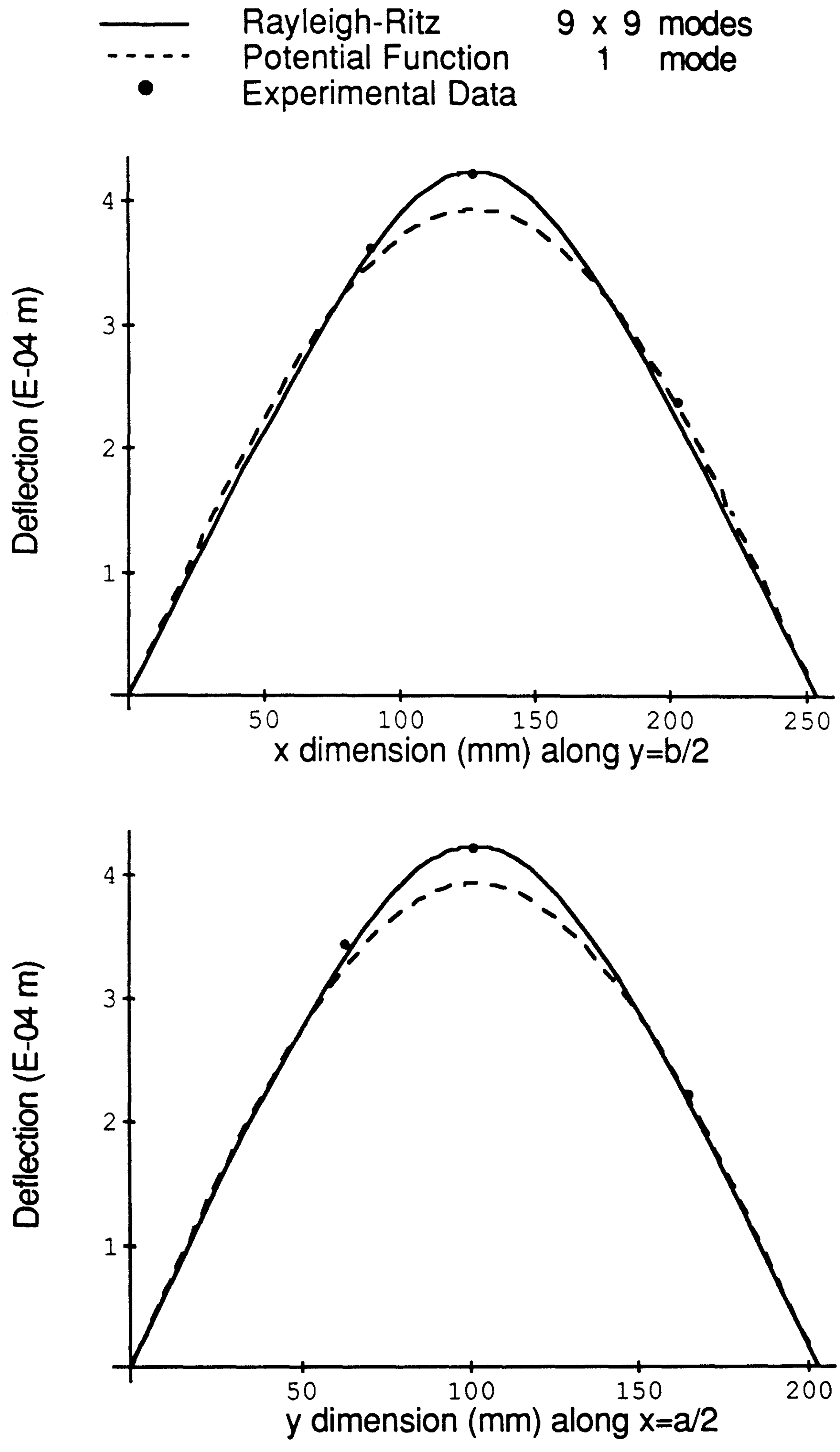

Figure 7.34 Transverse deflection for Specimen D, under a centered URPP load of 100 Newtons, with all four sides simply supported.

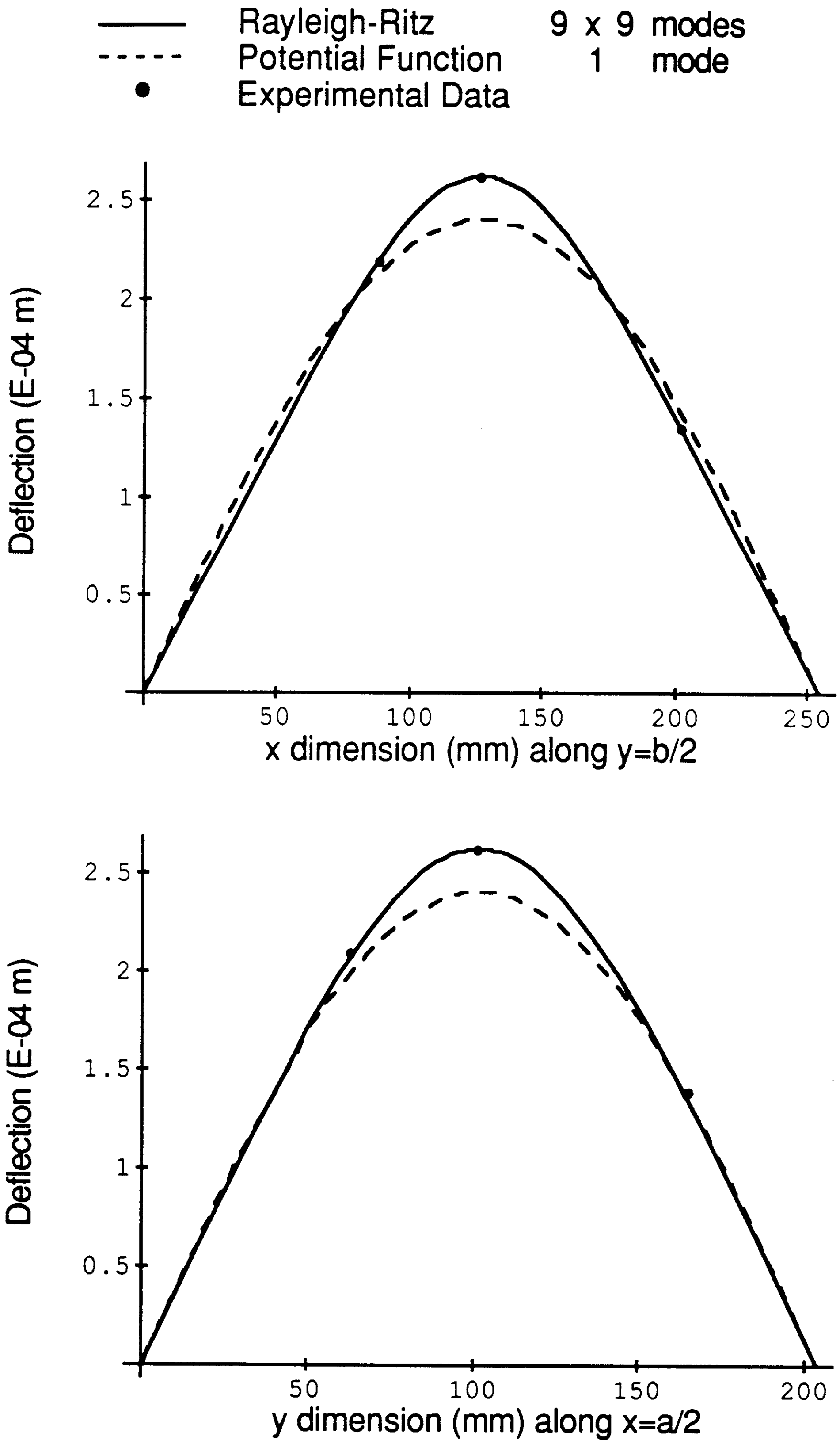

Figure 7.35 Transverse deflection for Specimen I, under a centered URPP load of 100 Newtons, with all four sides simply supported.

7.5 Comparison of Results for Off-Center URPP

The off-center URPP tests are slightly less consistent than the off-center point load tests, however, they follow the same pattern. The excessive flexibility of the four edges clamped boundary condition again results in 30% more deflection for four edges clamped, 20% more deflection for two edges clamped and two edges simply supported, and 5% more deflection for four edges simply supported, than analytically predicted by the Rayleigh-Ritz solution.

Again no comparisons were made with the single mode potential functions for four edges clamped and four edges simply supported since both potential functions are symmetric, and would be unable to account for the off-center loading.

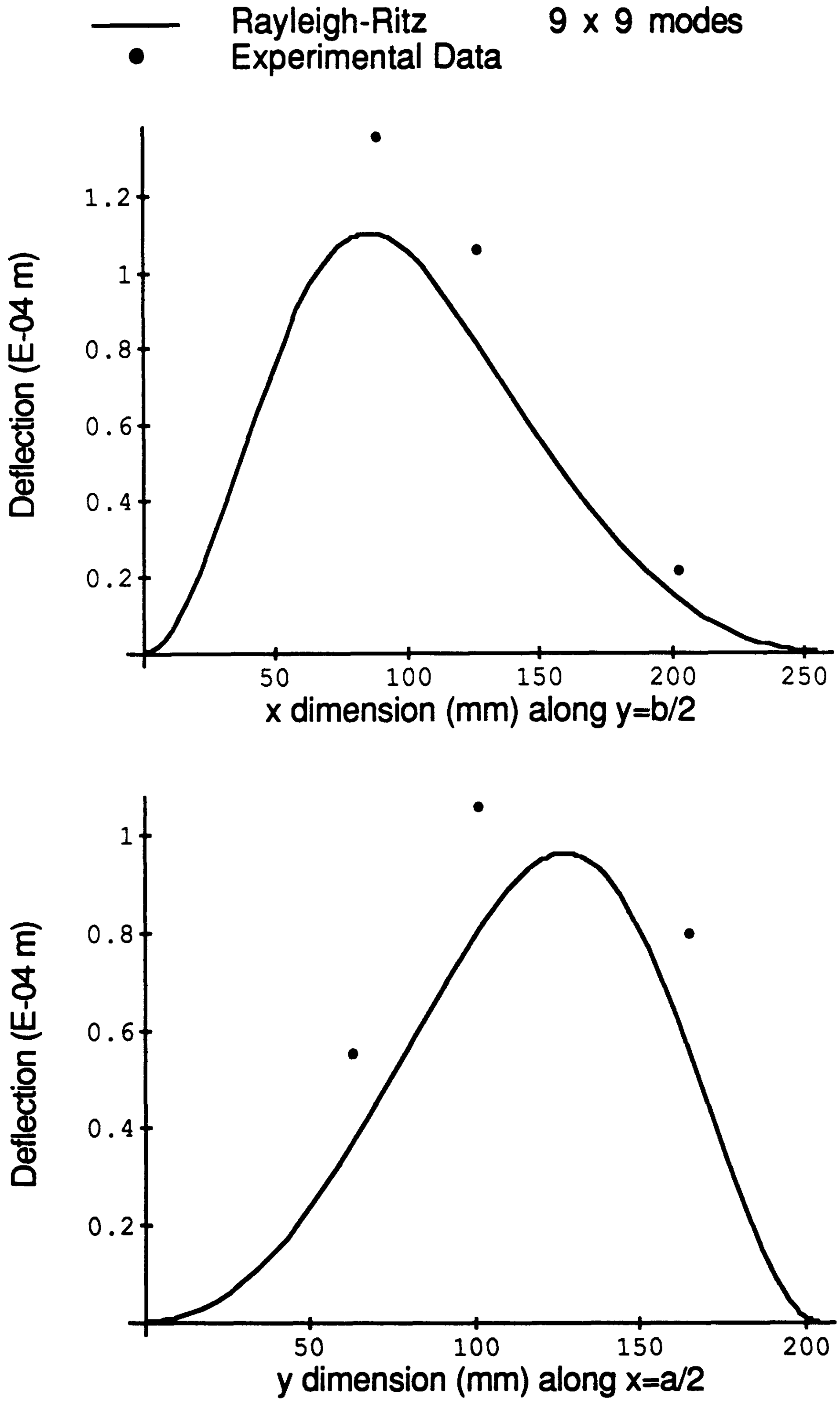

Figure 7.36 Transverse deflection for Specimen A, under an off-center URPP load of 100 Newtons, with all four sides clamped.

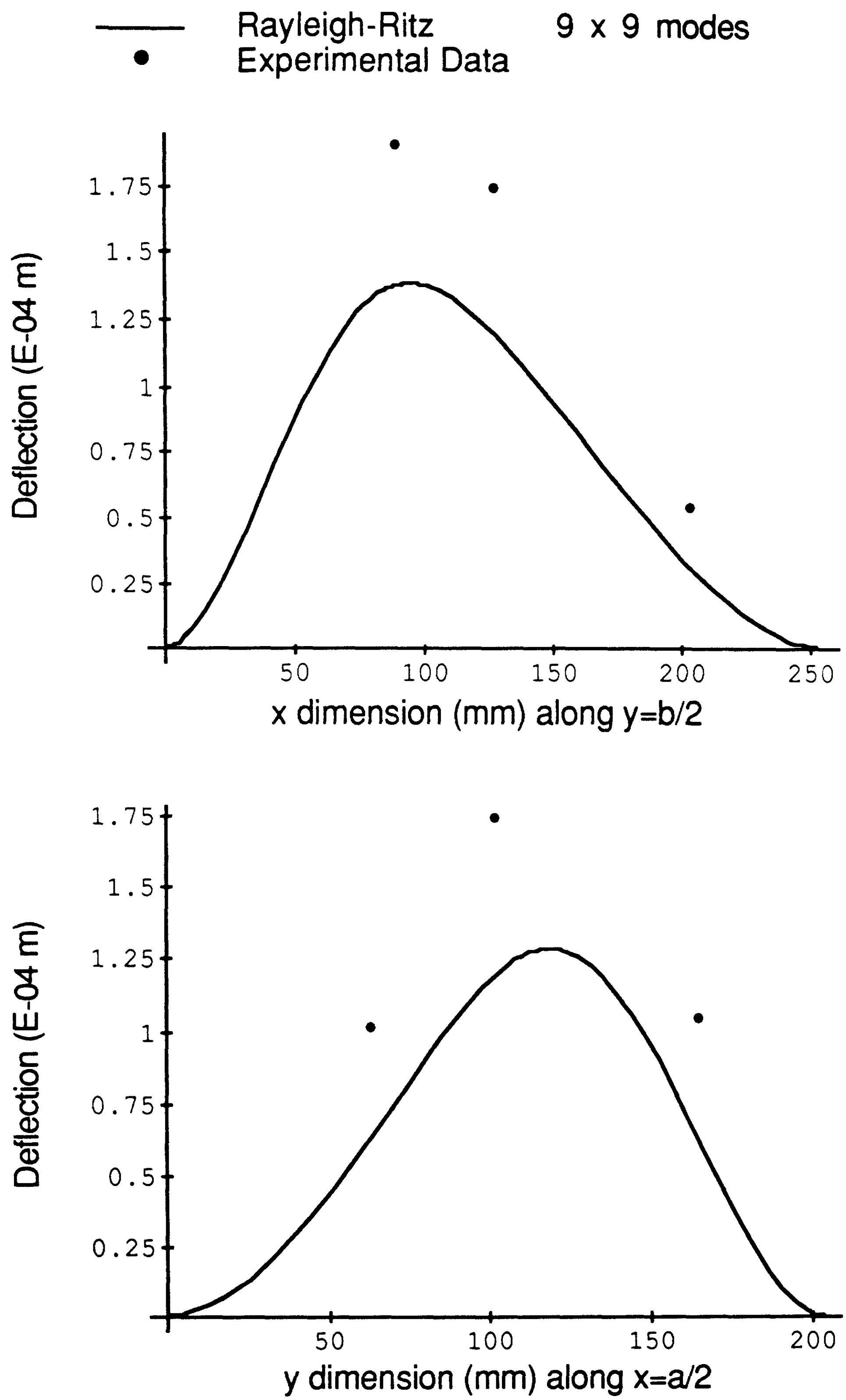

Figure 7.37 Transverse deflection for Specimen B, under an off-center URPP load of 100 Newtons, with all four sides clamped.

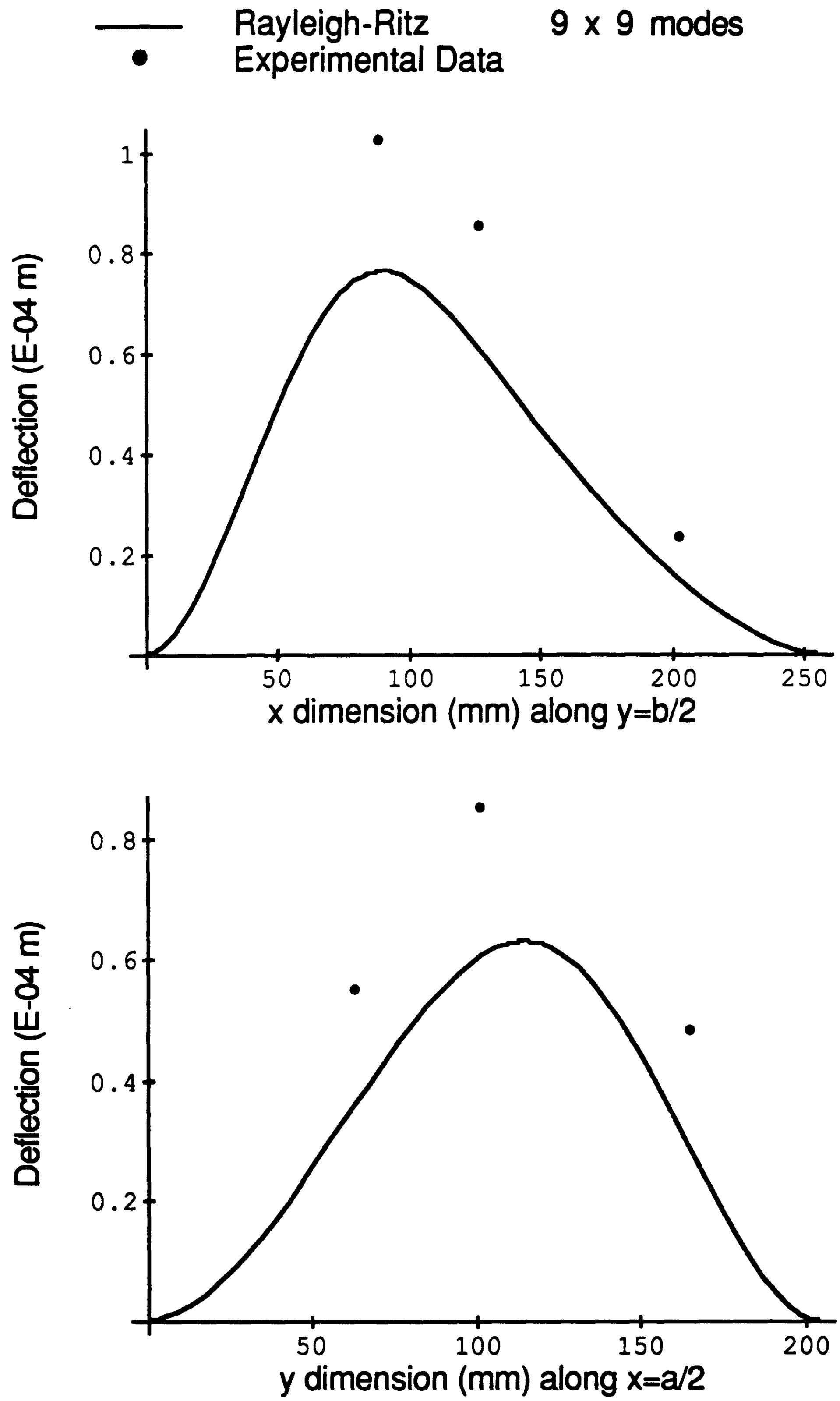

Figure 7.38 Transverse deflection for Specimen C, under an off-center URPP load of 100 Newtons, with all four sides clamped.

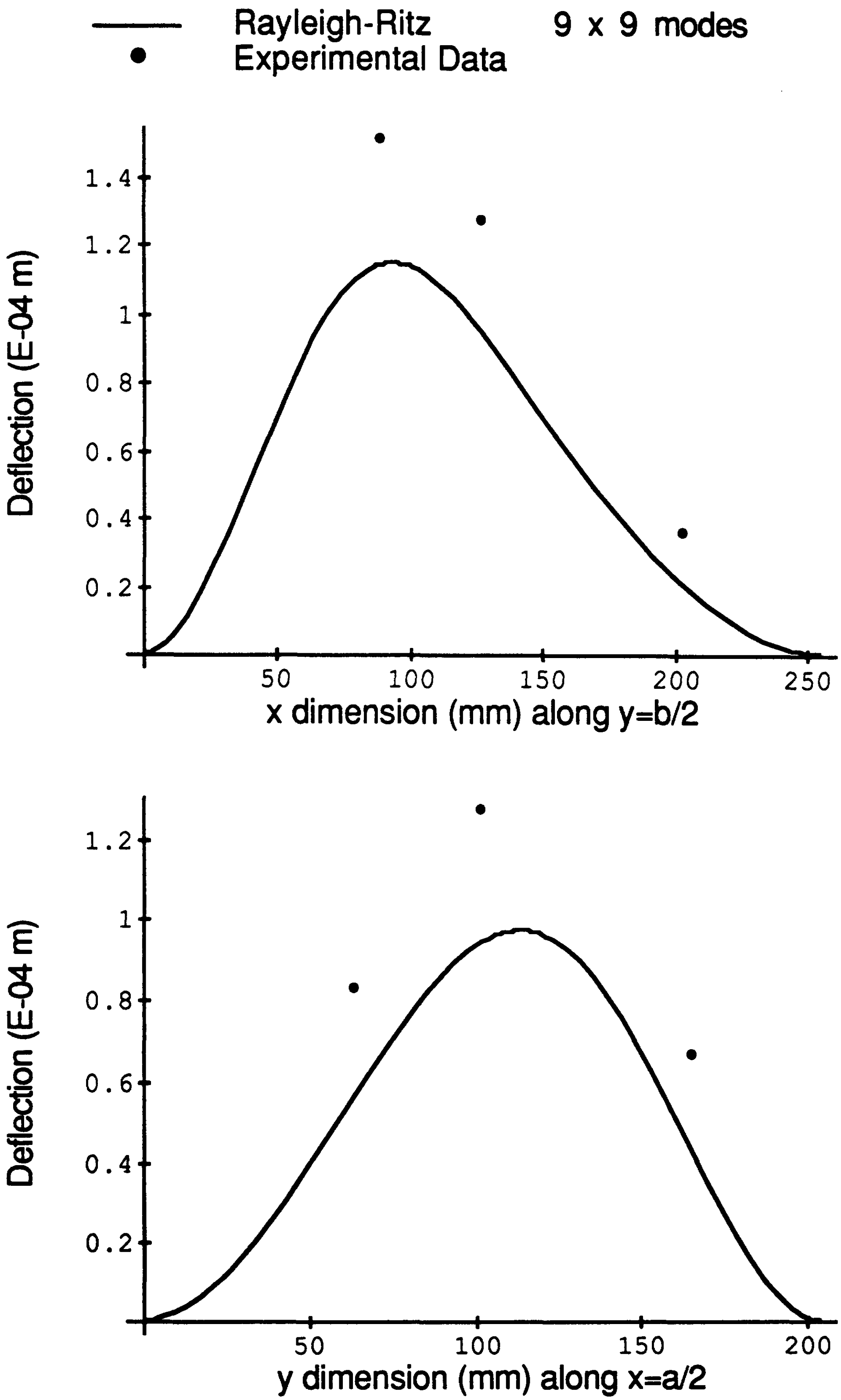

Figure 7.39 Transverse deflection for Specimen D, under an off-center URPP load of 100 Newtons, with all four sides clamped.

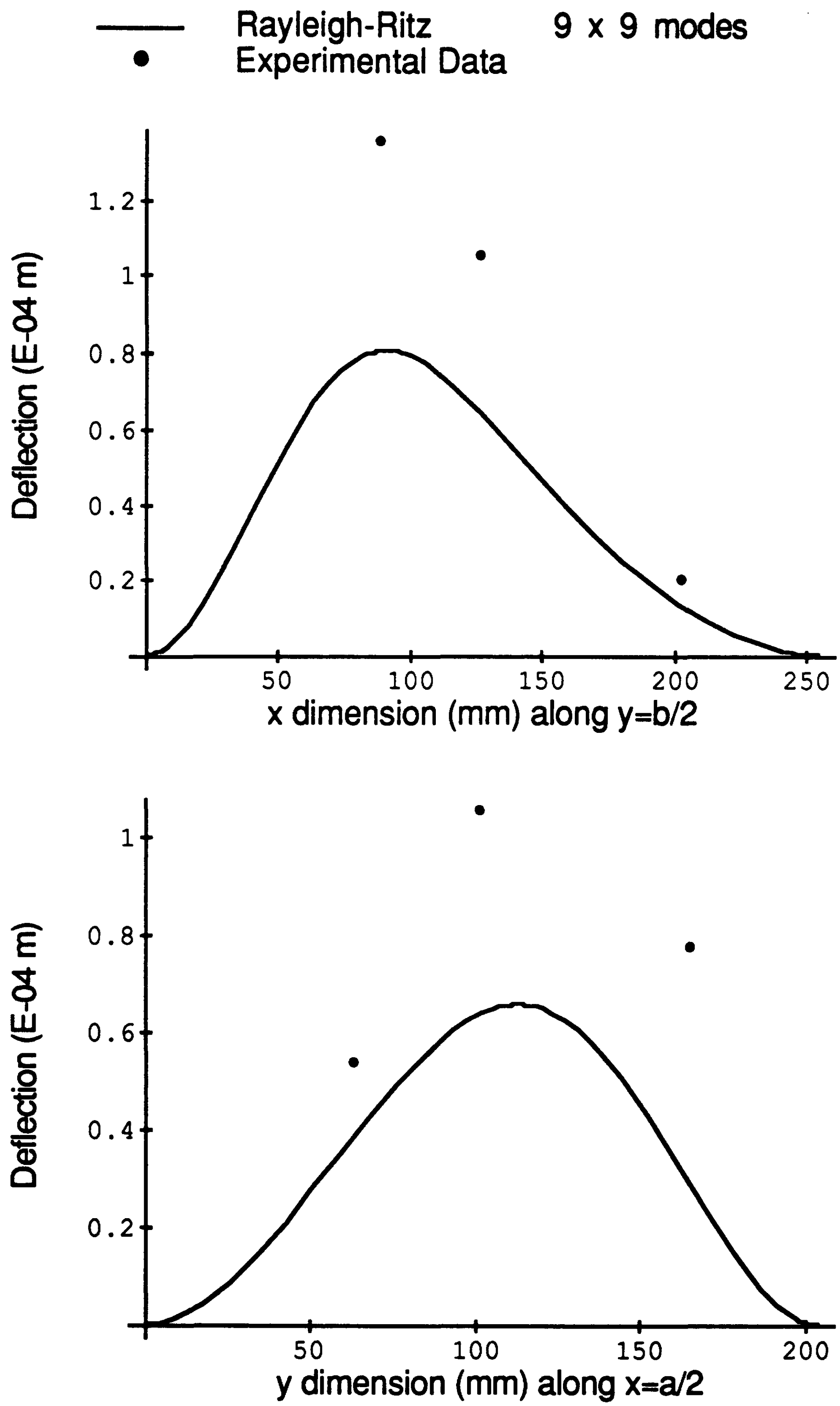

Figure 7.40 Transverse deflection for Specimen I, under an off-center URPP load of 100 Newtons, with all four sides clamped.

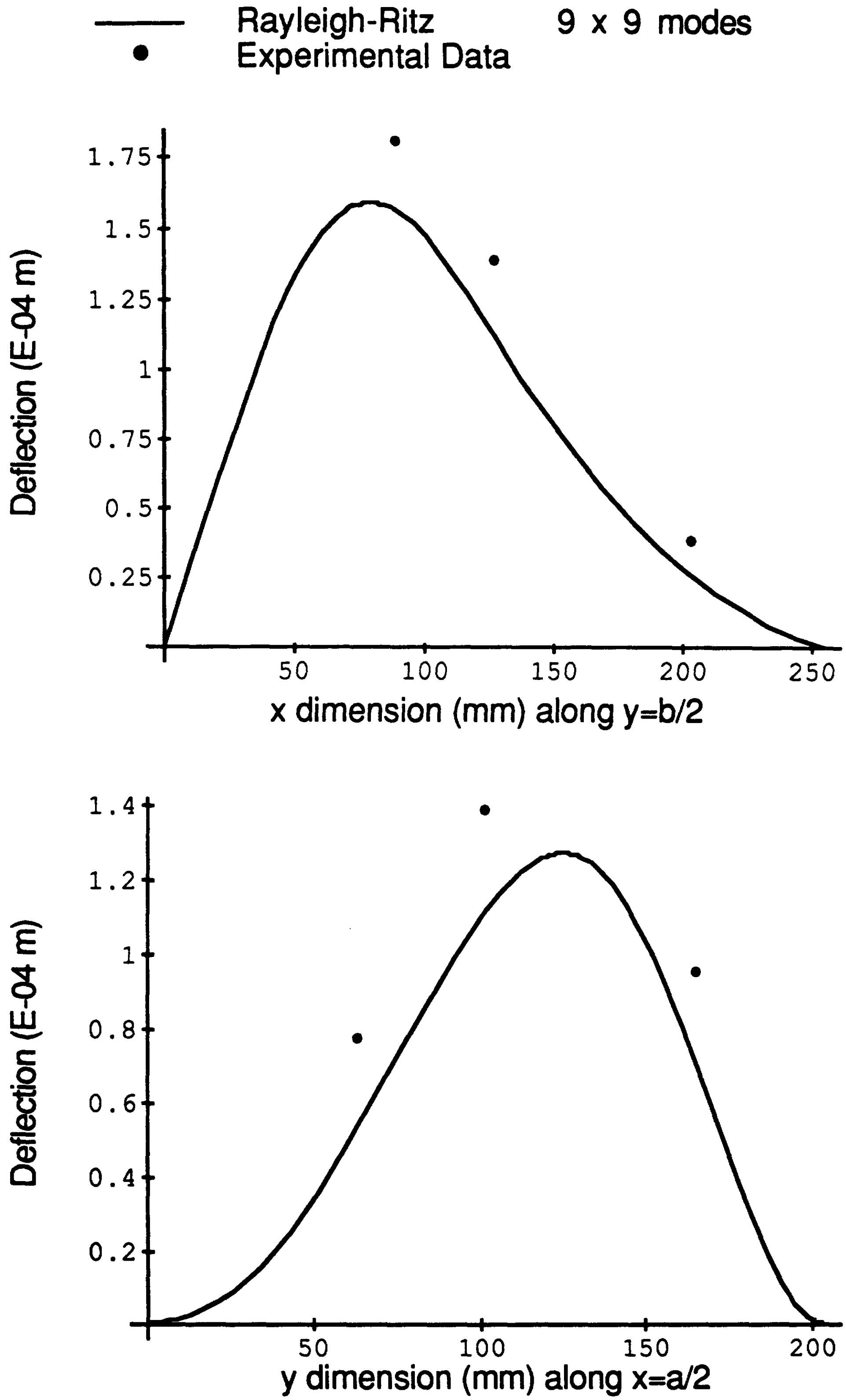

Figure 7.41 Transverse deflection for Specimen A, under an off-center URPP load of 100 Newtons, with x edges (short edges) simply supported and y edges (long edges) clamped.

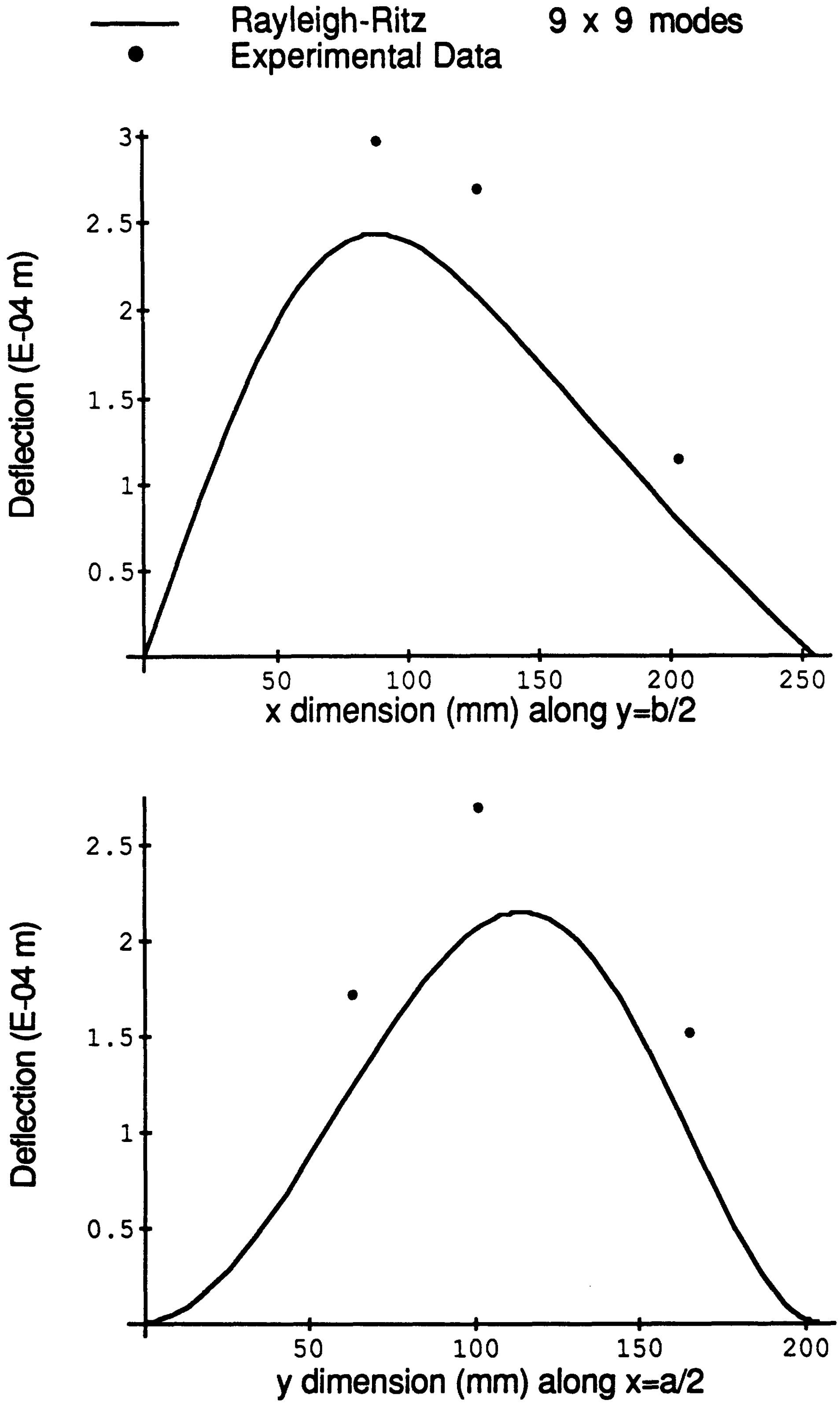

Figure 7.42 Transverse deflection for Specimen B, under an off-center URPP load of 100 Newtons, with x edges (short edges) simply supported and y edges (long edges) clamped.

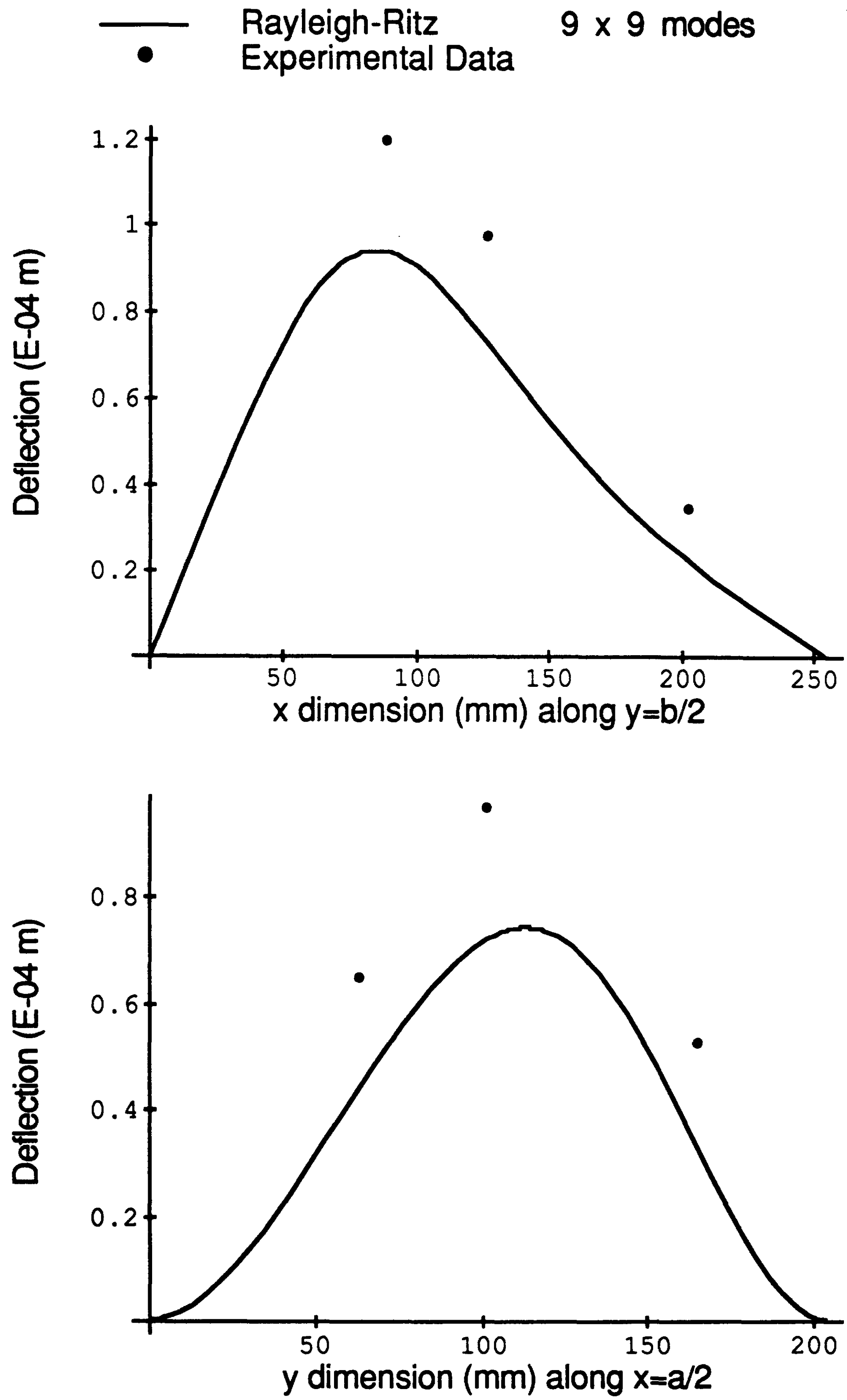

Figure 7.43 Transverse deflection for Specimen C, under an off-center URPP load of 100 Newtons, with x edges (short edges) simply supported and y edges (long edges) clamped.

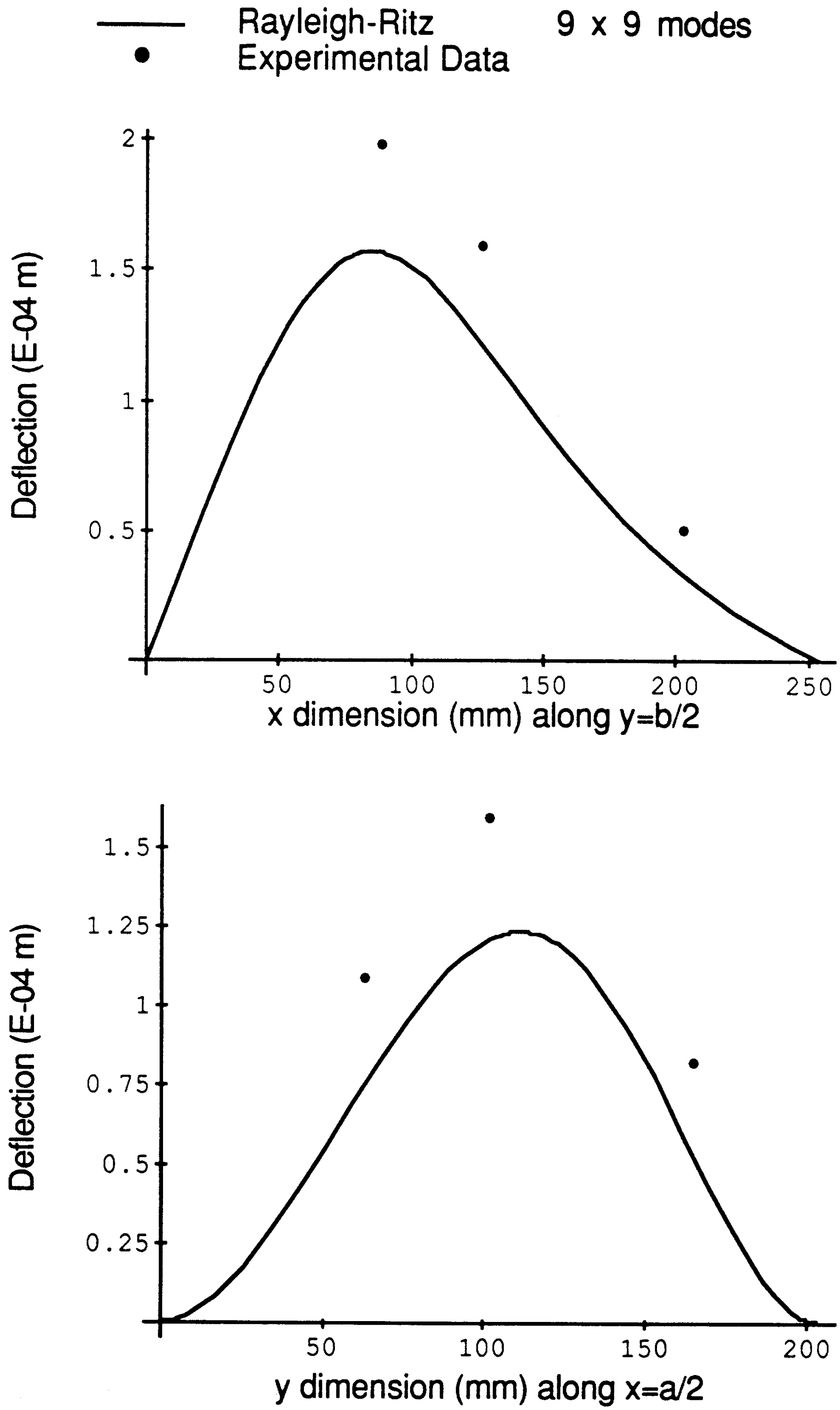

Figure 7.44 Transverse deflection for Specimen D, under an off-center URPP load of 100 Newtons, with x edges (short edges) simply supported and y edges (long edges) clamped.

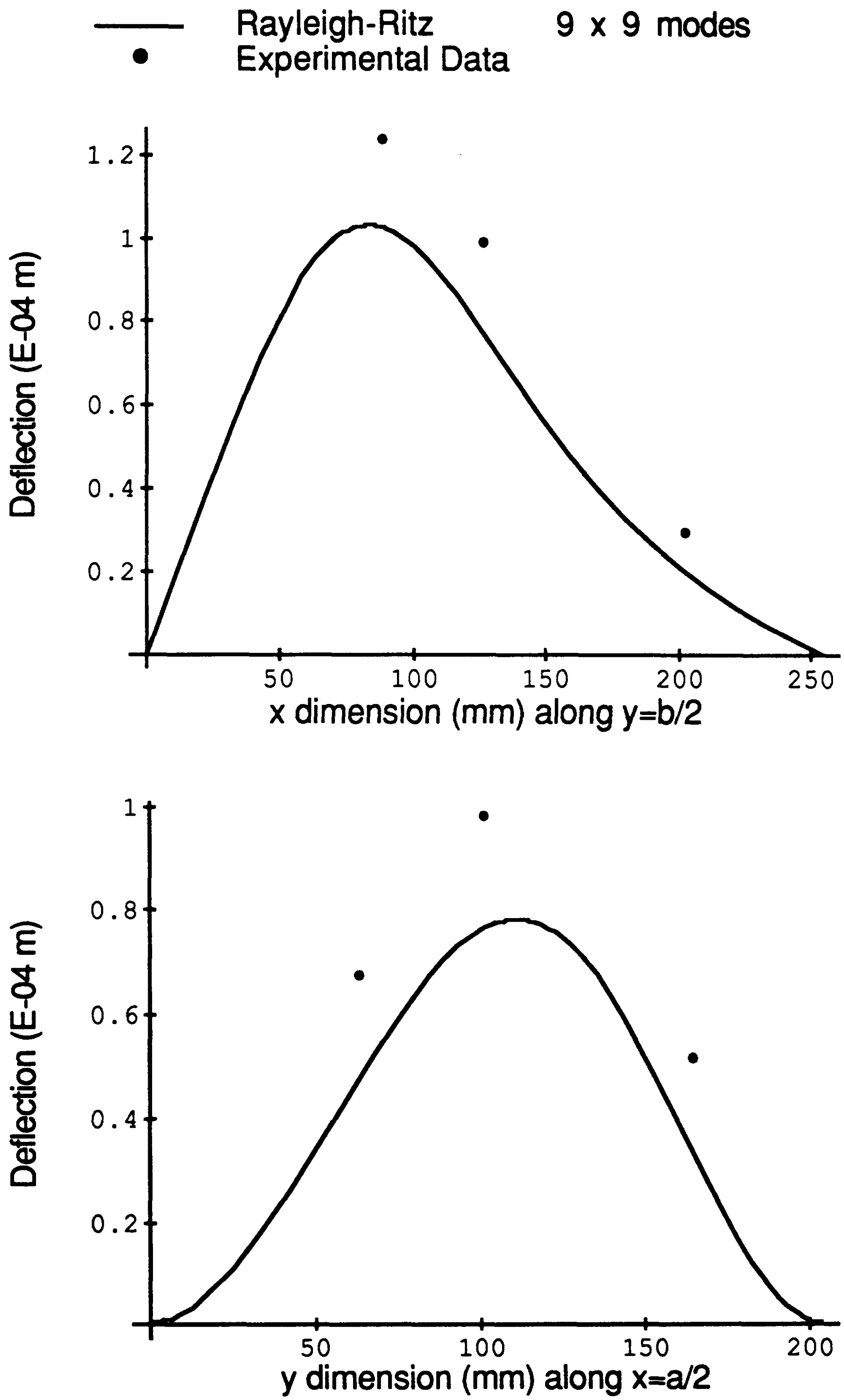

Figure 7.45 Transverse deflection for Specimen I, under an off-center URPP load of 100 Newtons, with x edges (short edges) simply supported and y edges (long edges) clamped.

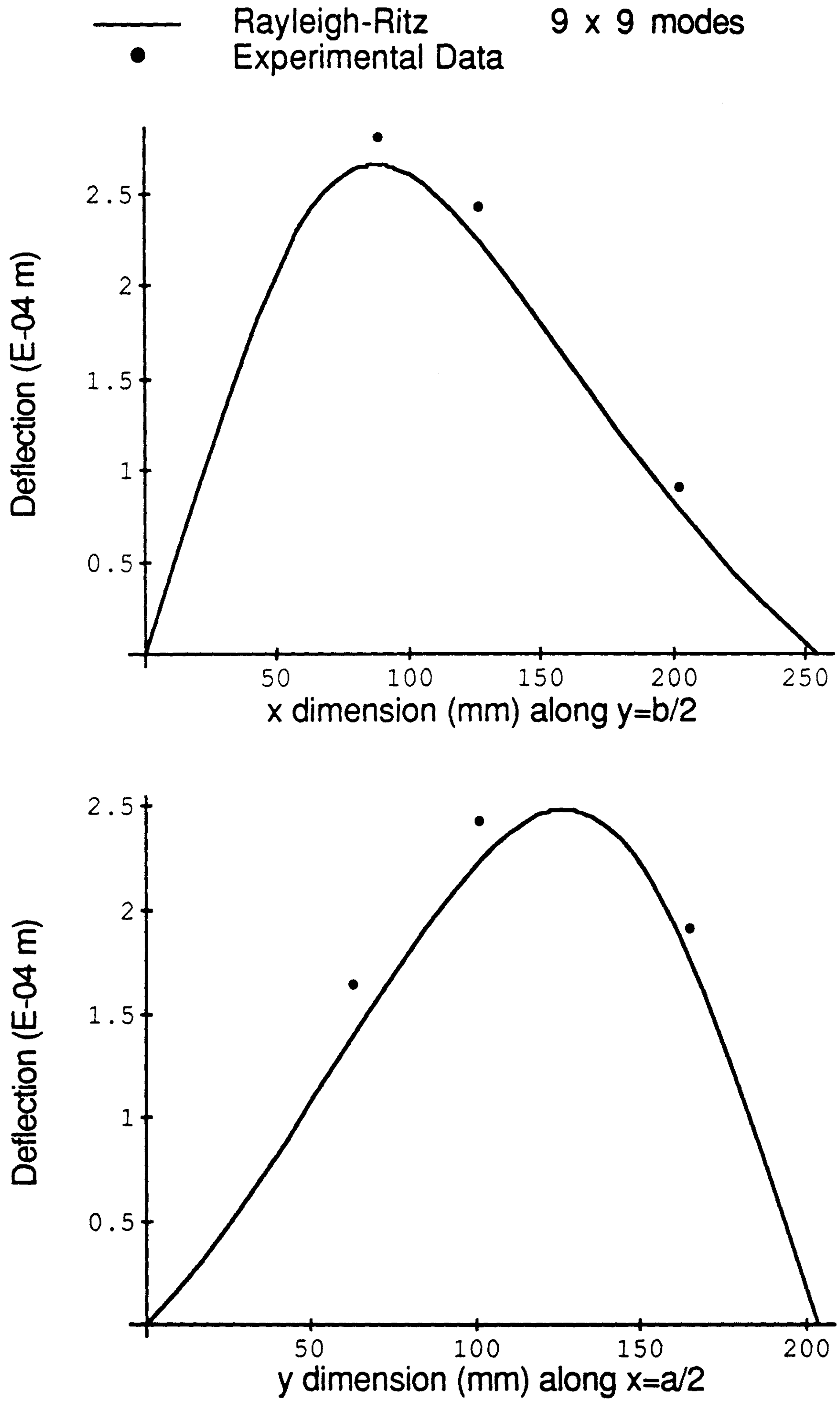

Figure 7.46 Transverse deflection for Specimen A, under an off-center URPP load of 100 Newtons, with all four sides simply supported.

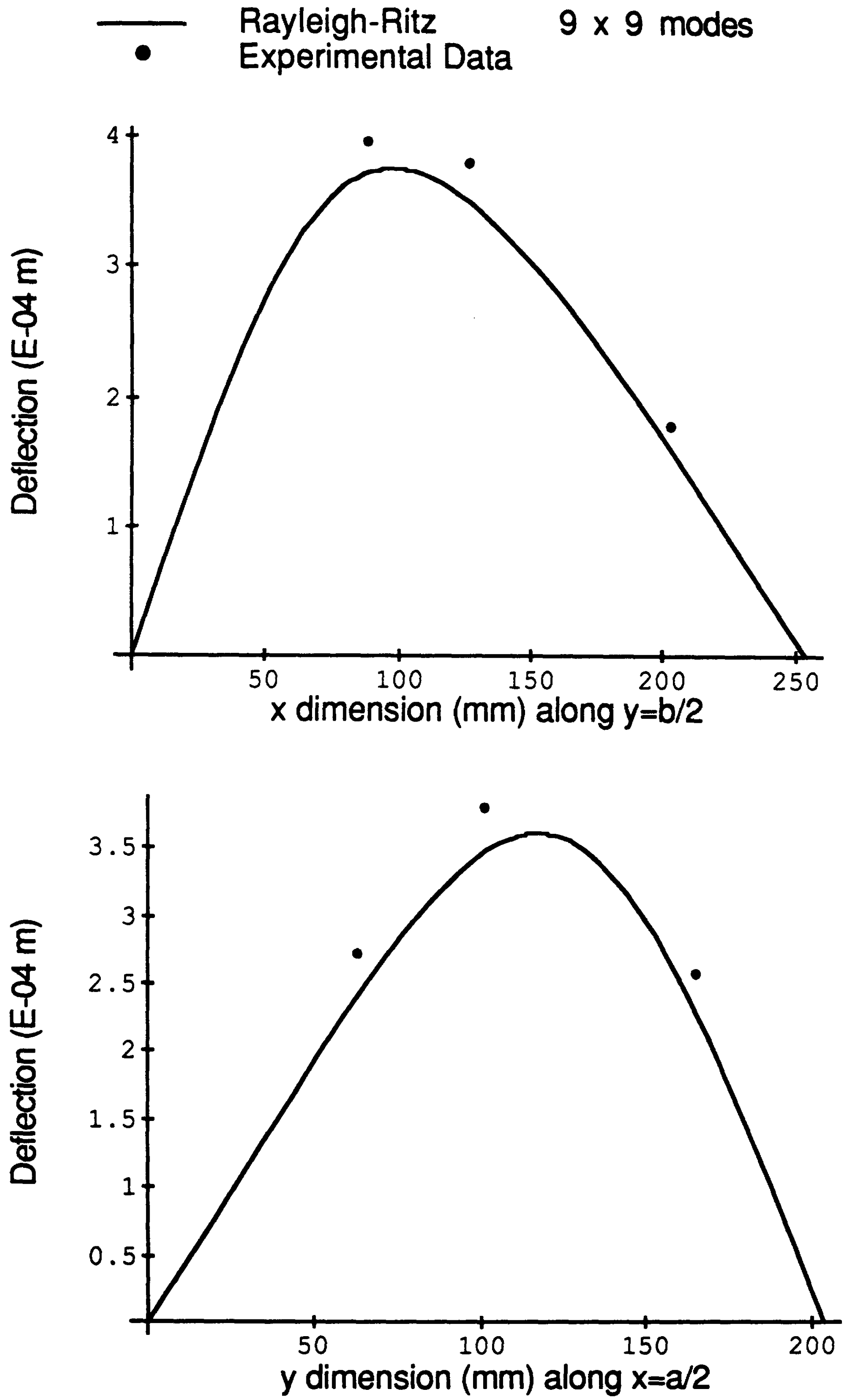

Figure 7.47 Transverse deflection for Specimen B, under an off-center URPP load of 100 Newtons, with all four sides simply supported.

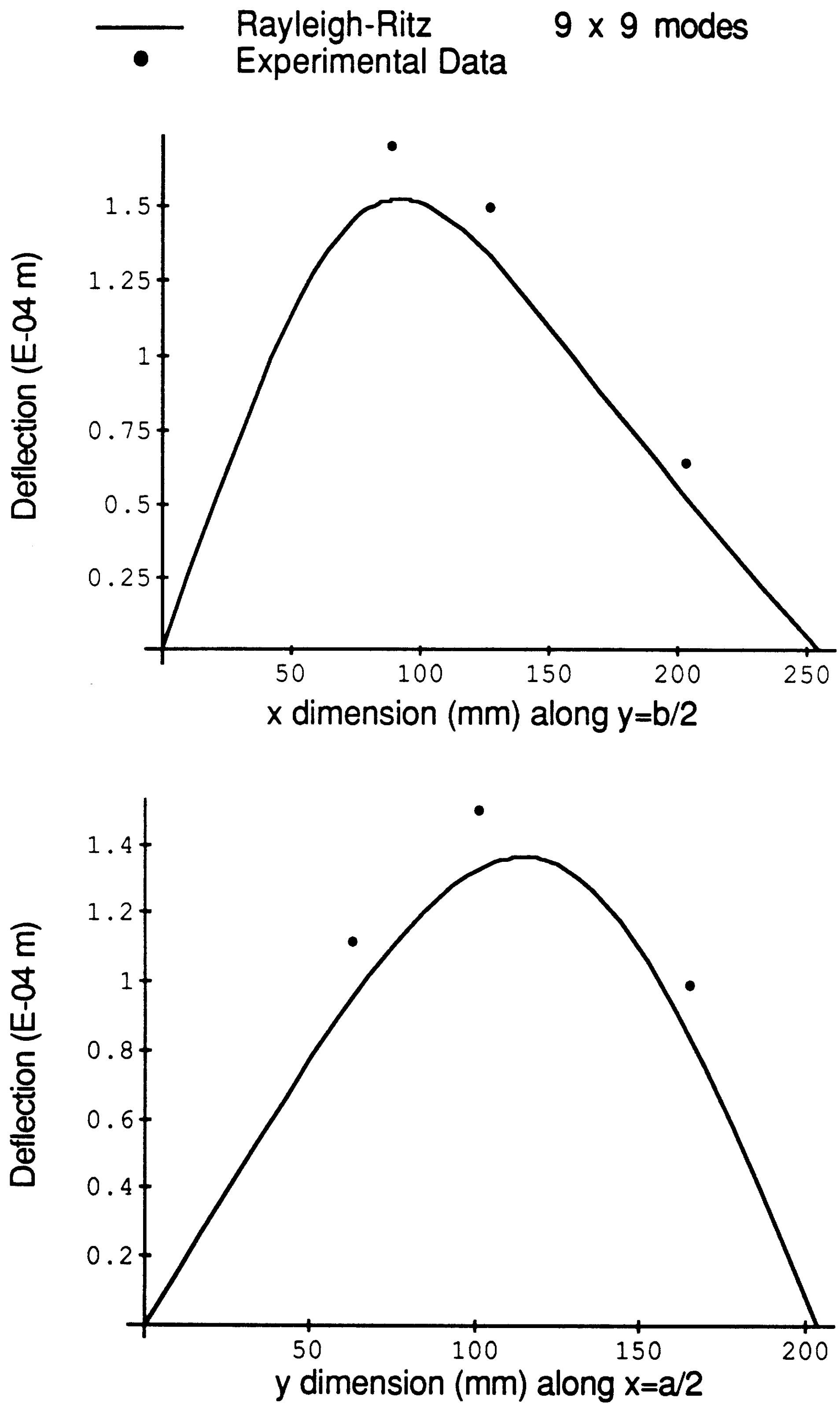

Figure 7.48 Transverse deflection for Specimen C, under an off-center URPP load of 100 Newtons, with all four sides simply supported.

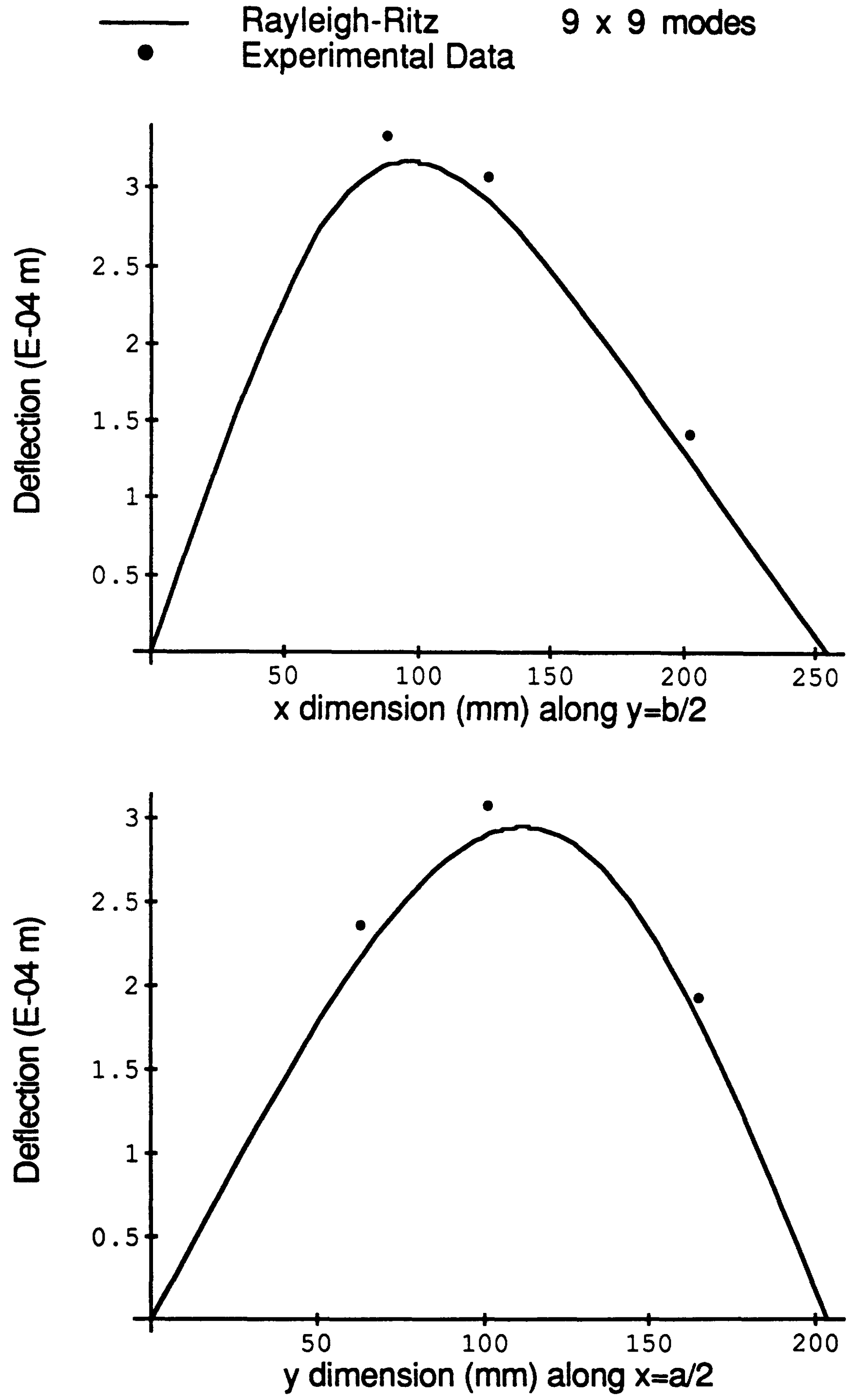

Figure 7.49 Transverse deflection for Specimen D, under an off-center URPP load of 100 Newtons, with all four sides simply supported.

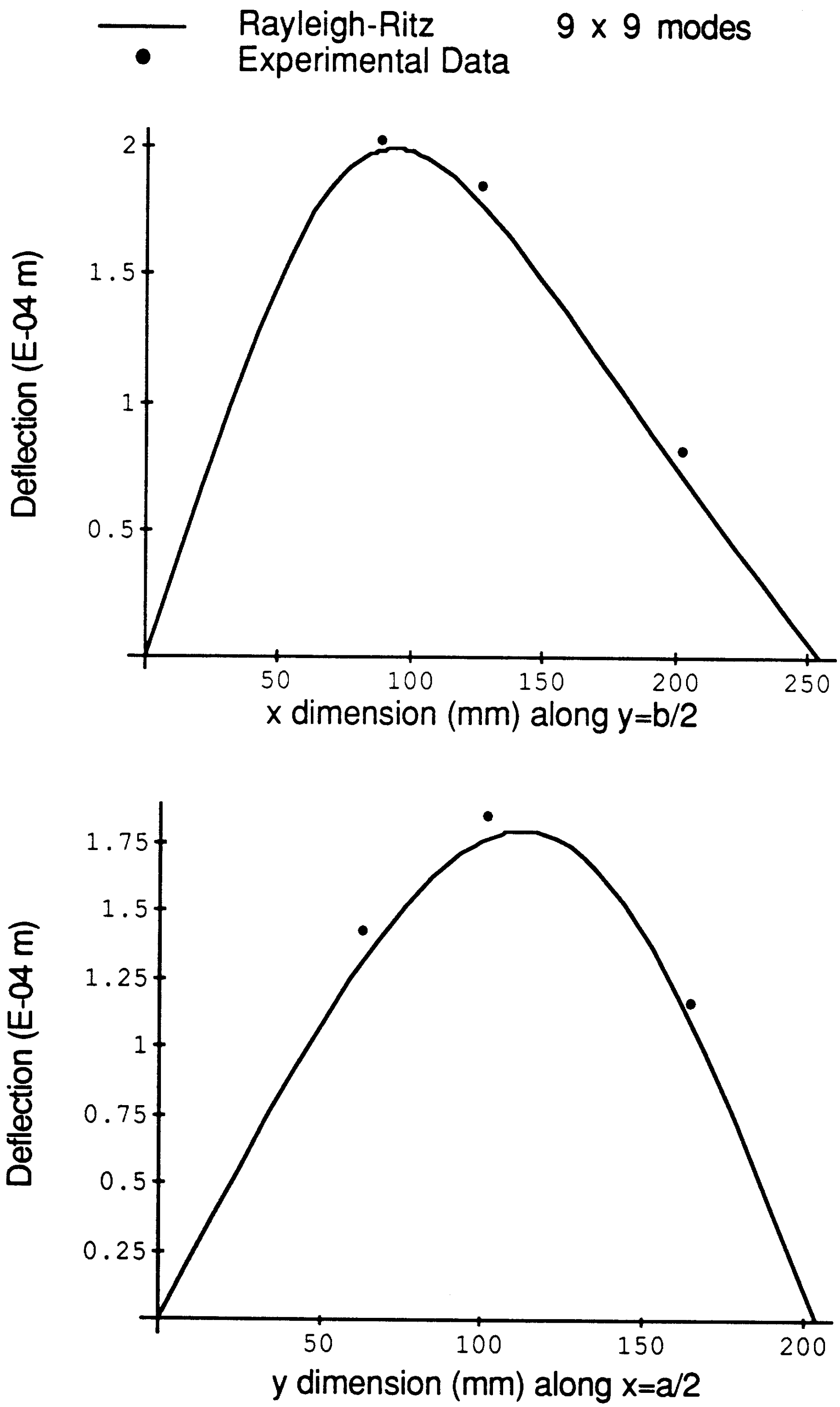

Figure 7.50 Transverse deflection for Specimen I, under an off-center URPP load of 100 Newtons, with all four sides simply supported.

7.6 Comparison of Results for Uniform Pressure

The uniform pressure results are the least consistent and therefore the most difficult to interpret. In general, the four edges clamped condition again results in 30% more deflection, the two edges clamped and two edges simply supported results in 20-25% more deflection, and the four edges simply supported condition results in 5-10% less deflection than predicted by the Rayleigh-Ritz prediction. Once again the B specimens are the furthest from the norm resulting in 20% more deflection, 5% more deflection, and 35% less deflection respectively, for the three boundary conditions compared to the Rayleigh-Ritz prediction. This is significantly more deviation from predicted stiffness than is observed in the A specimens which exhibit a much stronger bending-twisting coupling.

The single mode potential function for four edges simply supported yields surprisingly excellent results in the case of the uniform pressure loading. In fact, the single mode potential function solution, which has only 16 terms in its polynomial, is 2-4% more converged than the 81 term double sine Rayleigh-Ritz solution. This example illustrates the level of efficiency possible with potential functions.

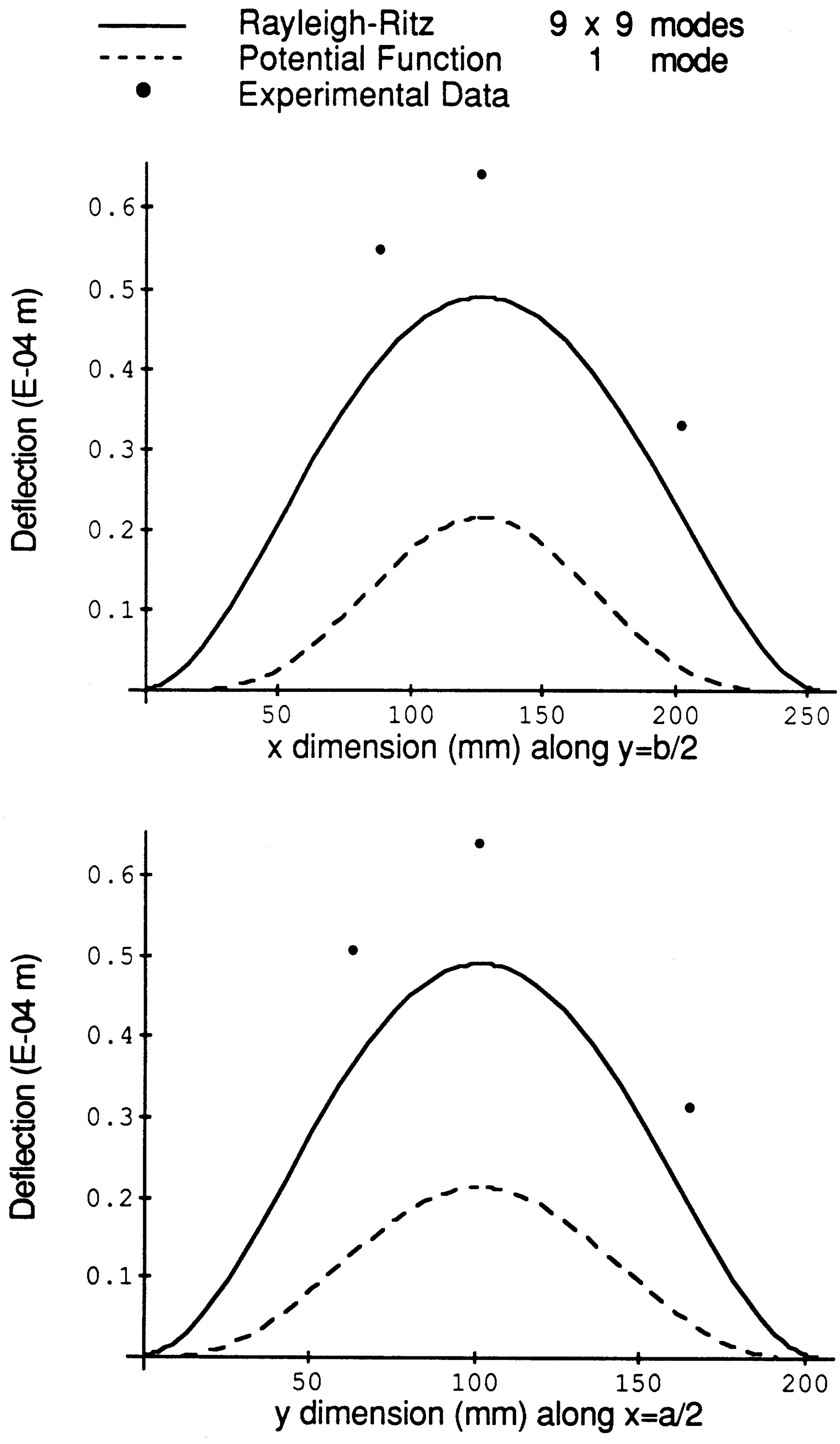

Figure 7.51 Transverse deflection for Specimen A, under a uniform pressure load of 100 Newtons, with all four sides clamped.

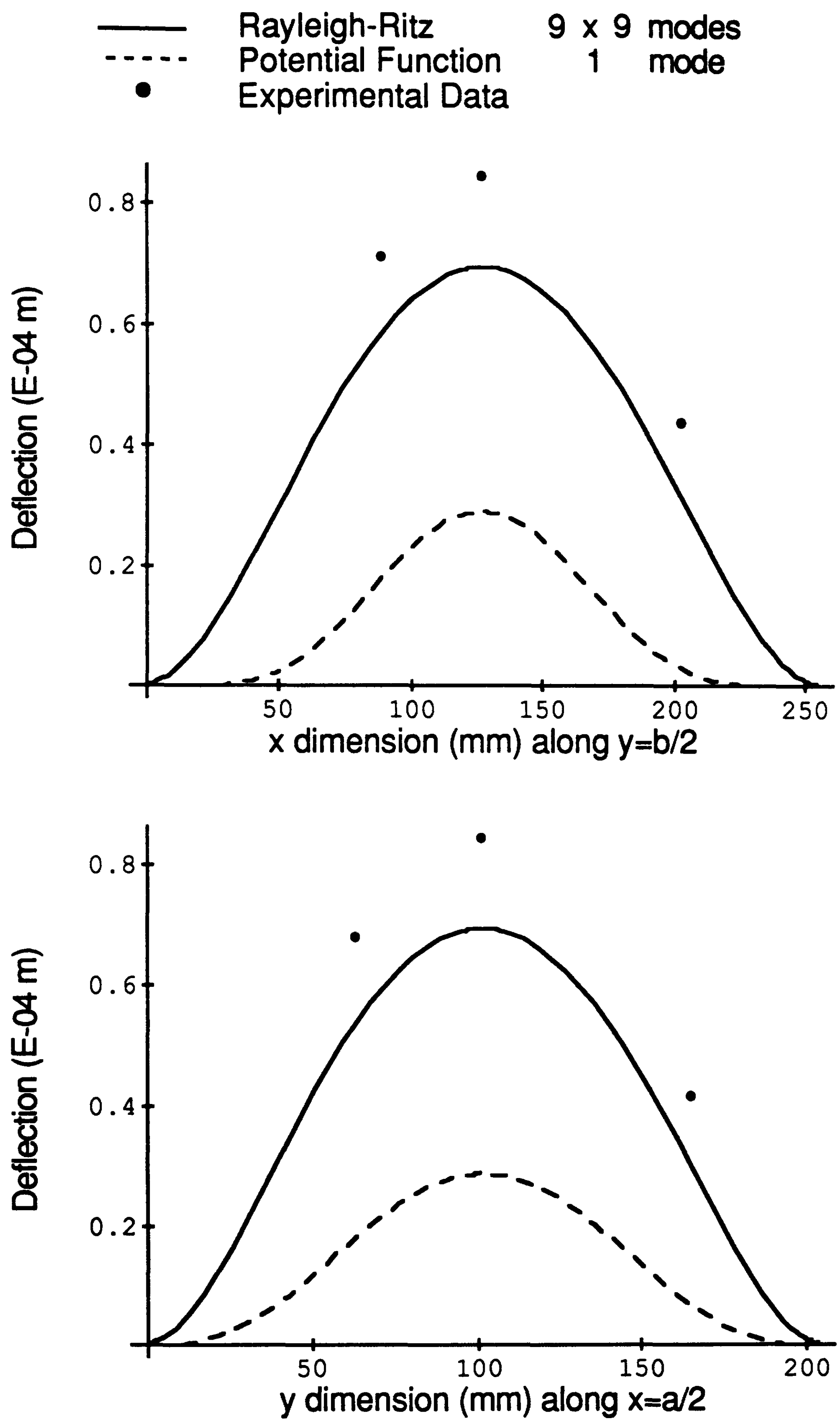

Figure 7.52 Transverse deflection for Specimen B, under a uniform pressure load of 100 Newtons, with all four sides clamped.

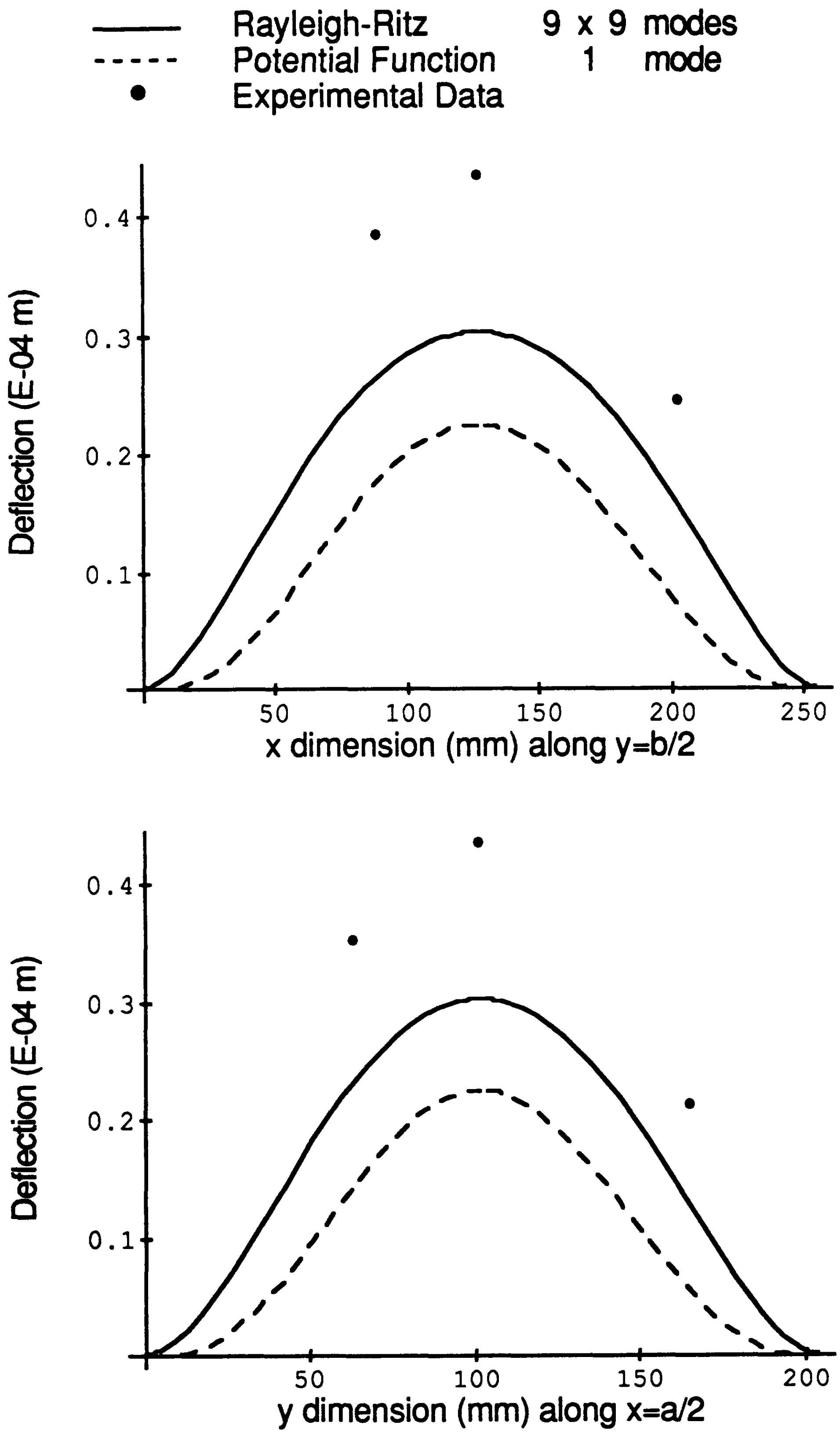

Figure 7.53 Transverse deflection for Specimen C, under a uniform pressure load of 100 Newtons, with all four sides clamped.

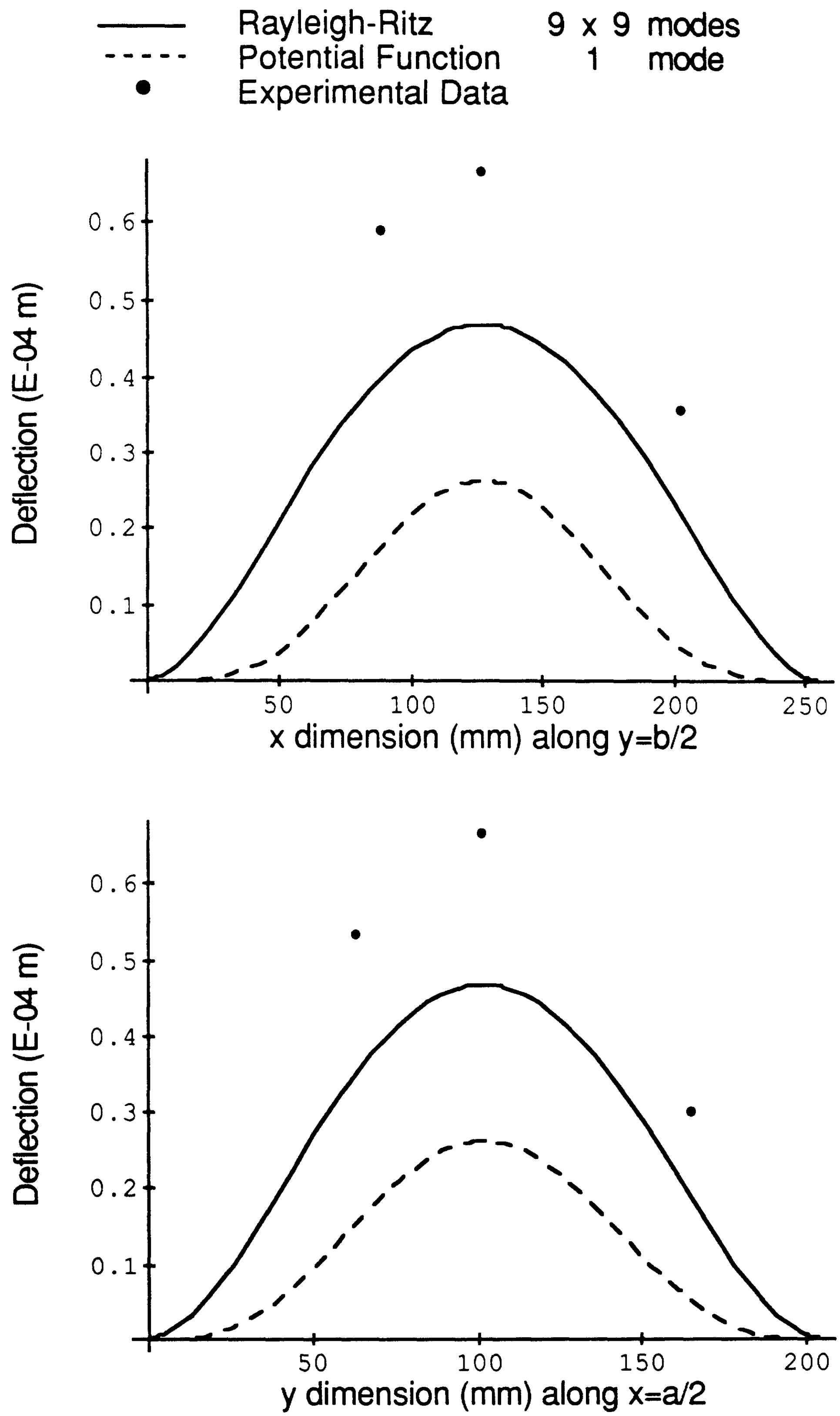

Figure 7.54 Transverse deflection for Specimen D, under a uniform pressure load of 100 Newtons, with all four sides clamped.

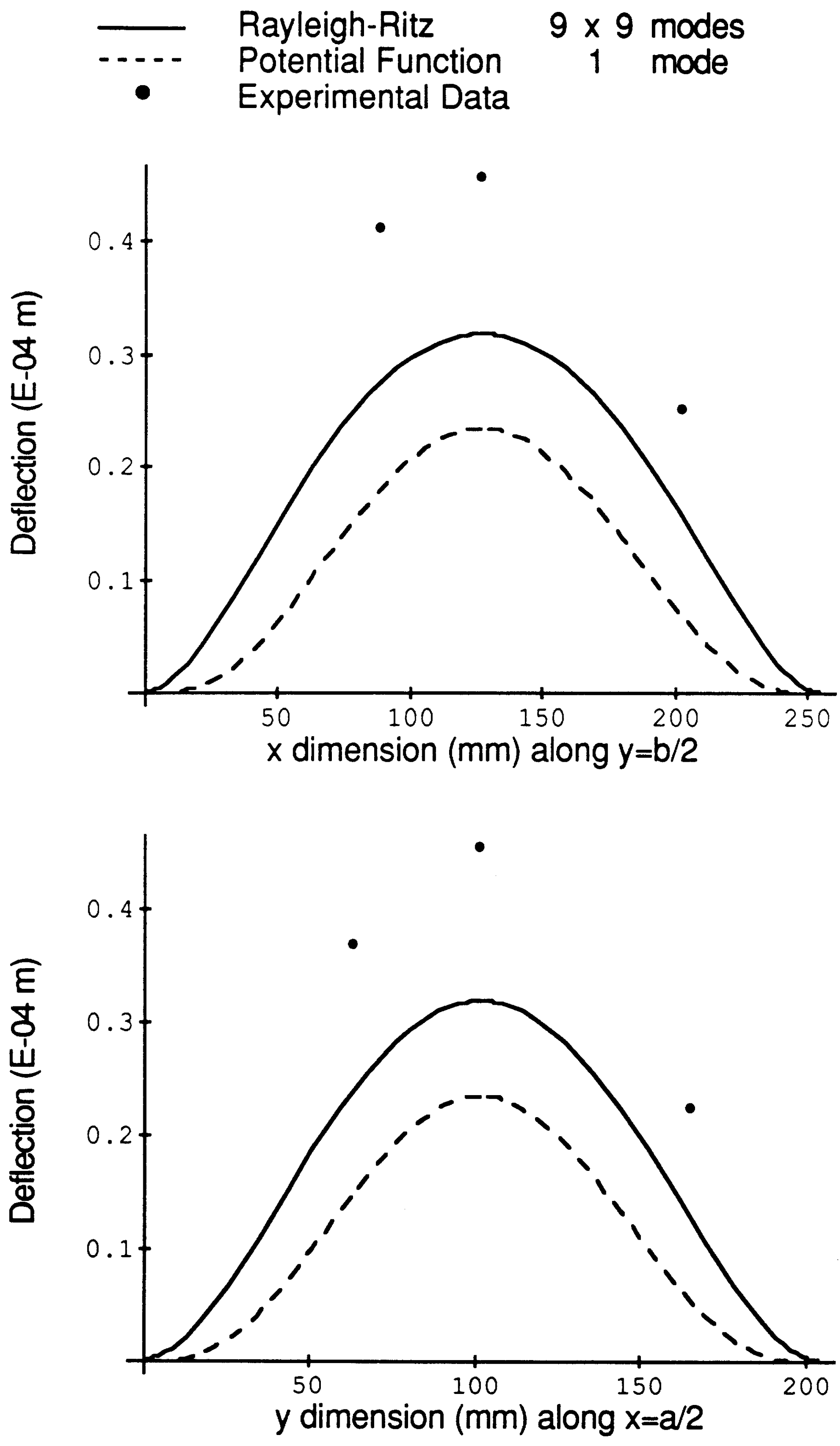

Figure 7.55 Transverse deflection for Specimen I, under a uniform pressure load of 100 Newtons, with all four sides clamped.

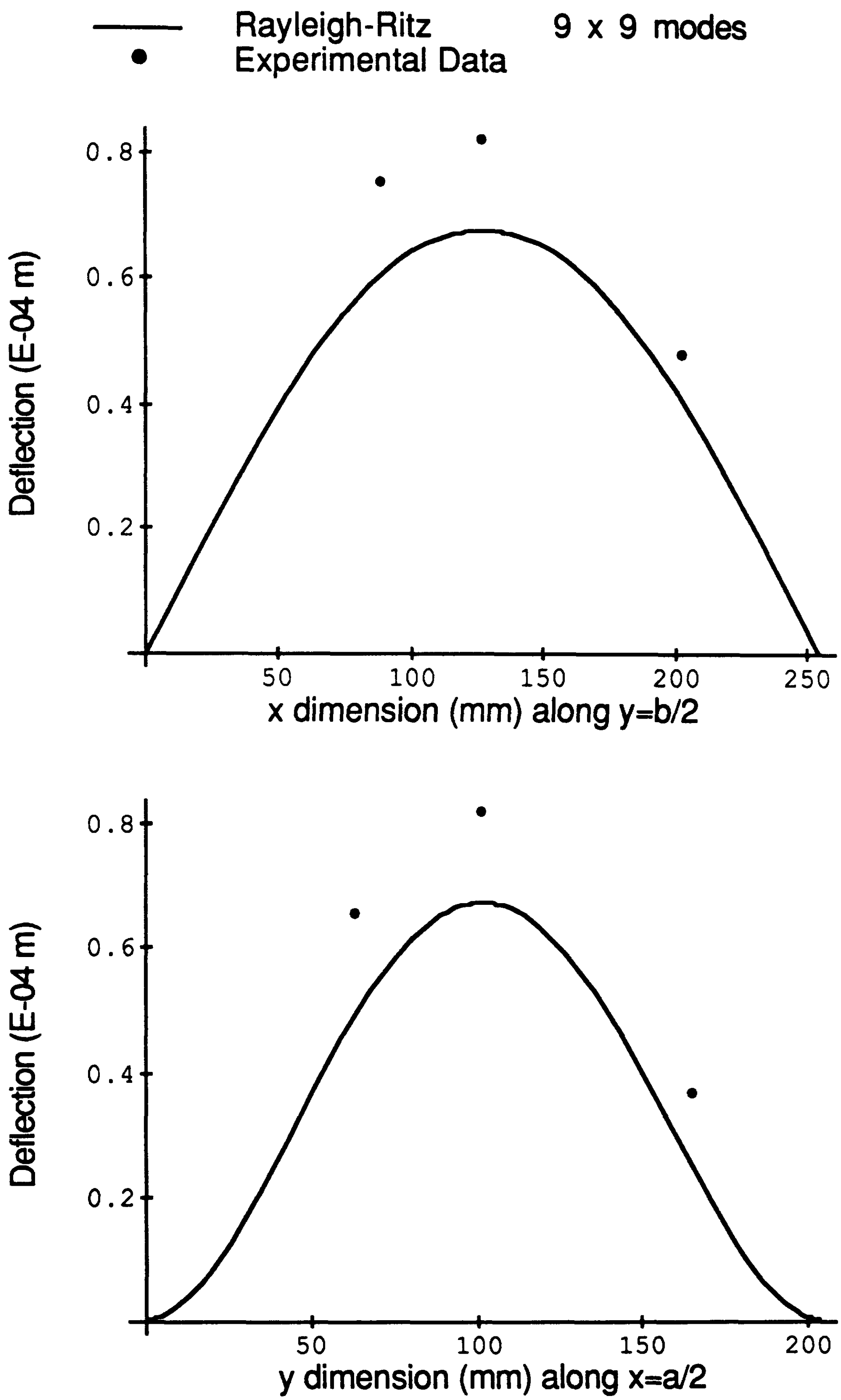

Figure 7.56 Transverse deflection for Specimen A, under a uniform pressure load of 100 Newtons, with x edges (short edges) simply supported and y edges (long edges) clamped.

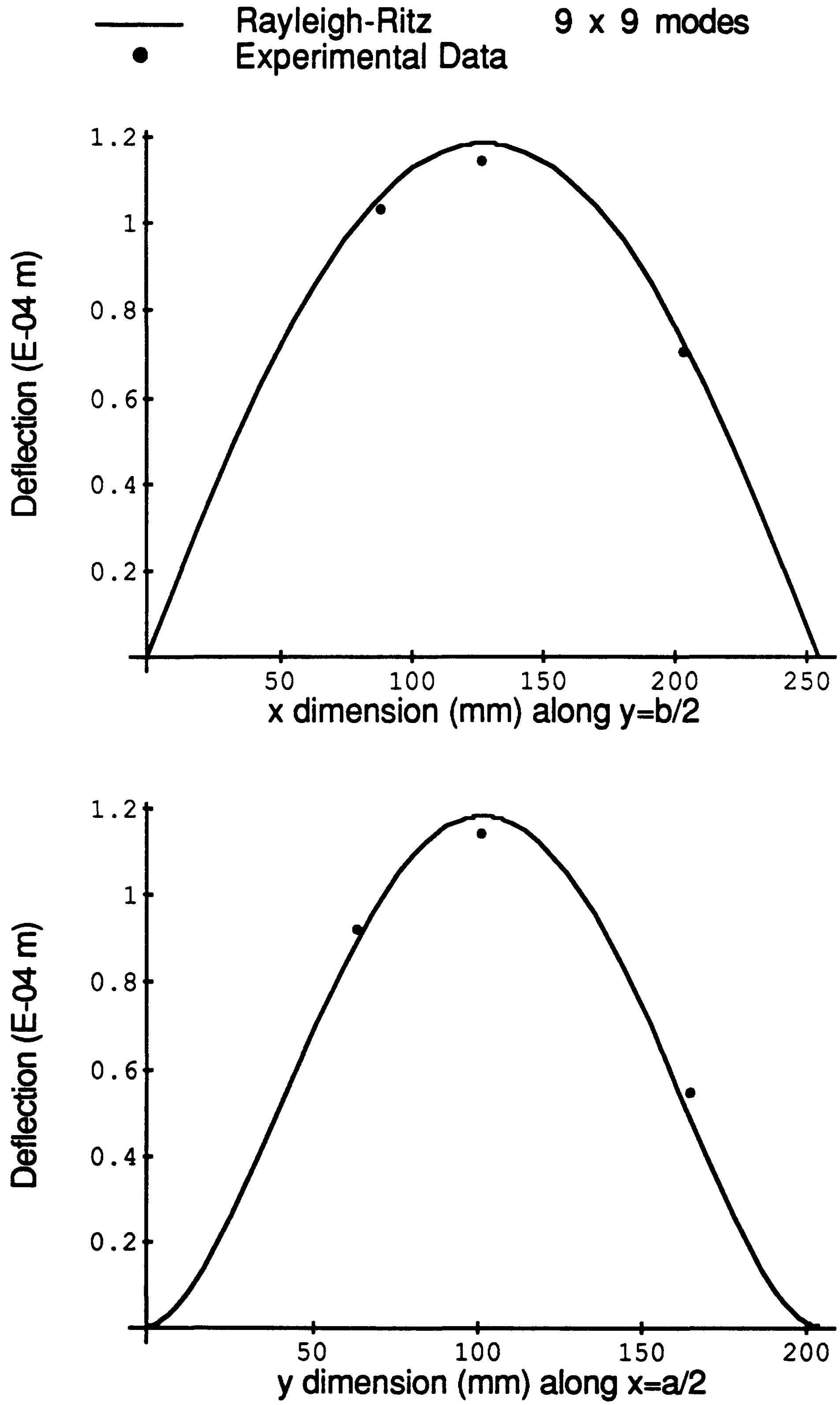

Figure 7.57 Transverse deflection for Specimen B, under a uniform pressure load of 100 Newtons, with x edges (short edges) simply supported and y edges (long edges) clamped.

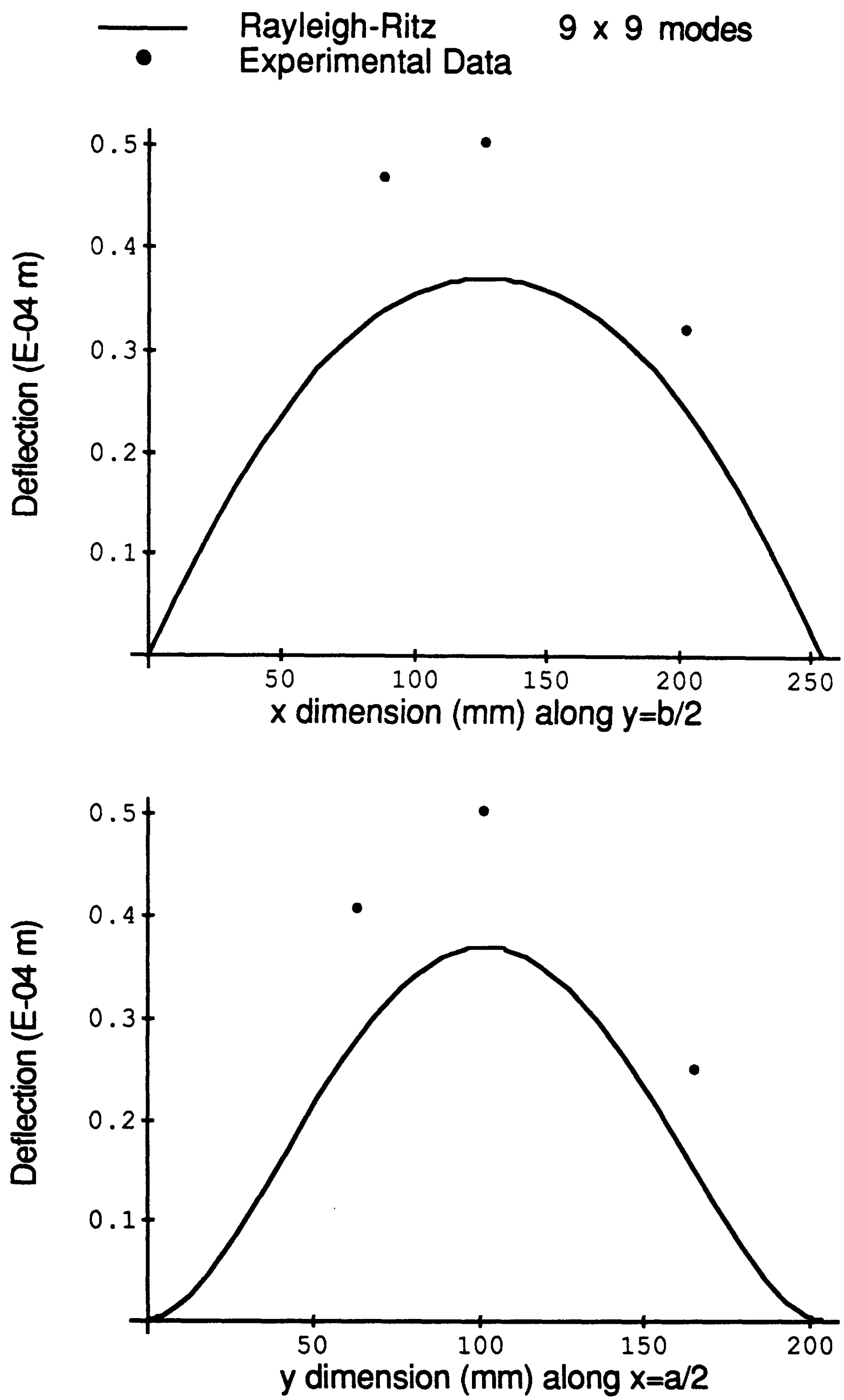

Figure 7.58 **Transverse deflection for Specimen C, under a uniform pressure load of 100 Newtons, with x edges (short edges) simply supported and y edges (long edges) clamped.**

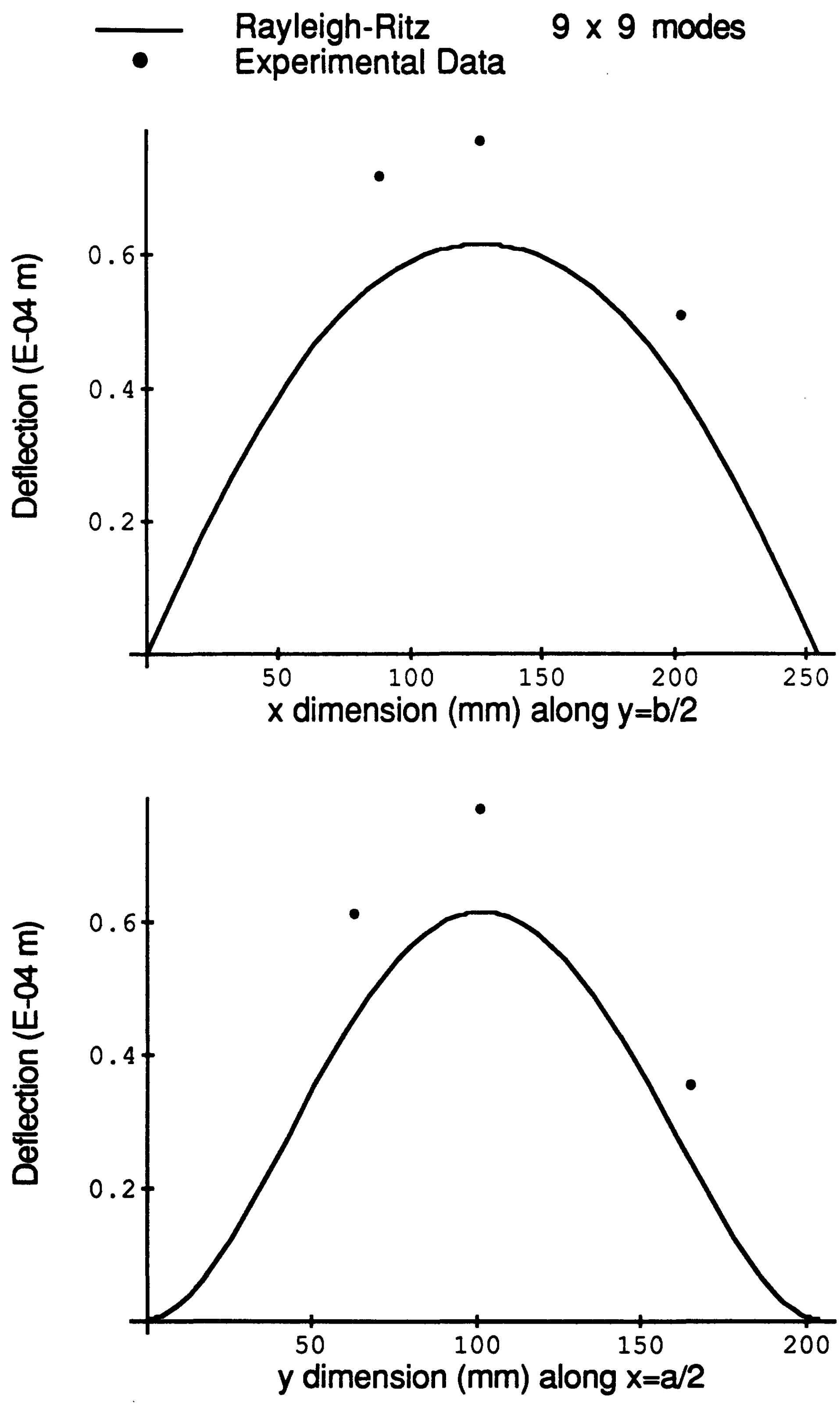

Figure 7.59 Transverse deflection for Specimen D, under a uniform pressure load of 100 Newtons, with x edges (short edges) simply supported and y edges (long edges) clamped.

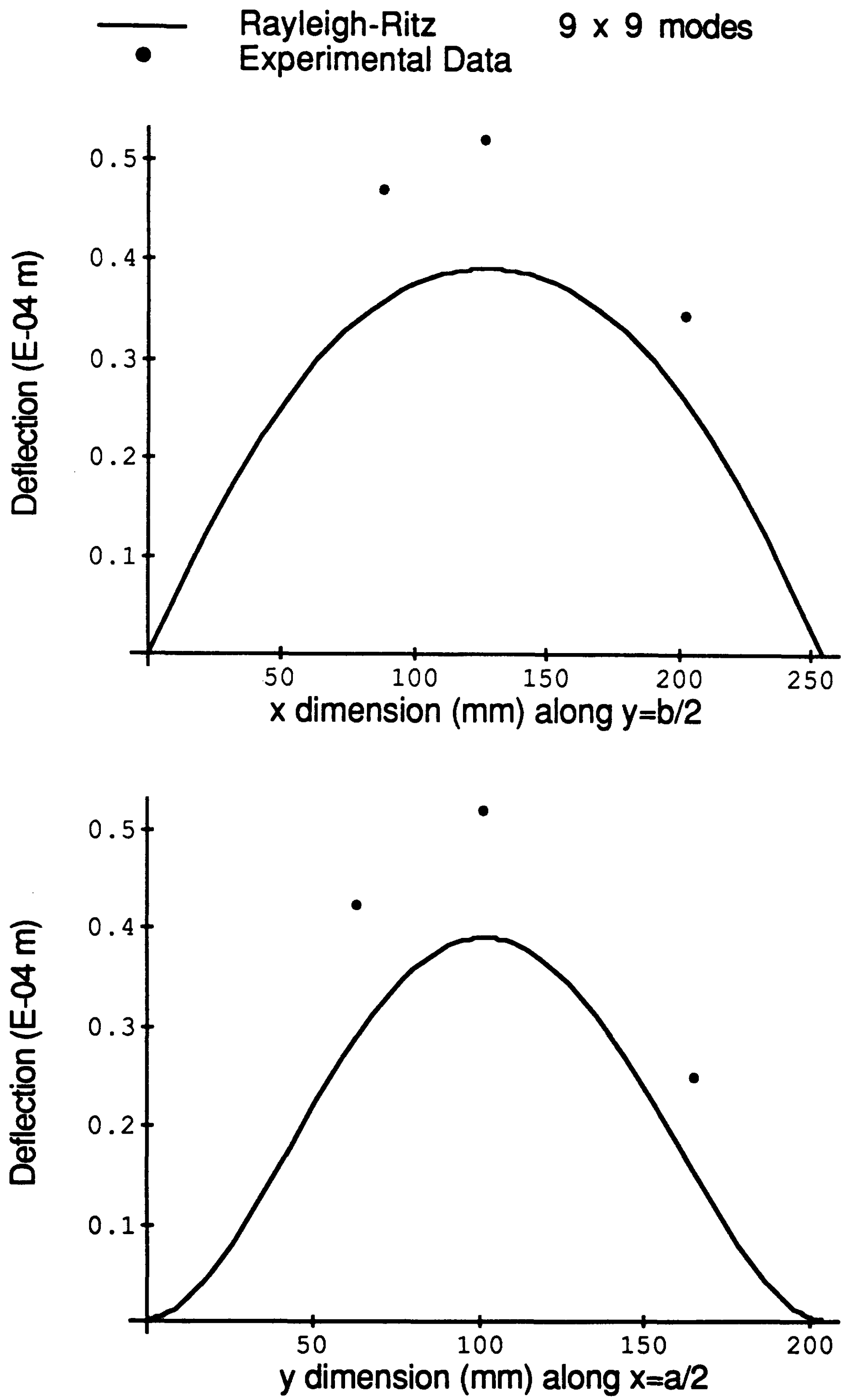

Figure 7.60 Transverse deflection for Specimen I, under a uniform pressure load of 100 Newtons, with x edges (short edges) simply supported and y edges (long edges) clamped.

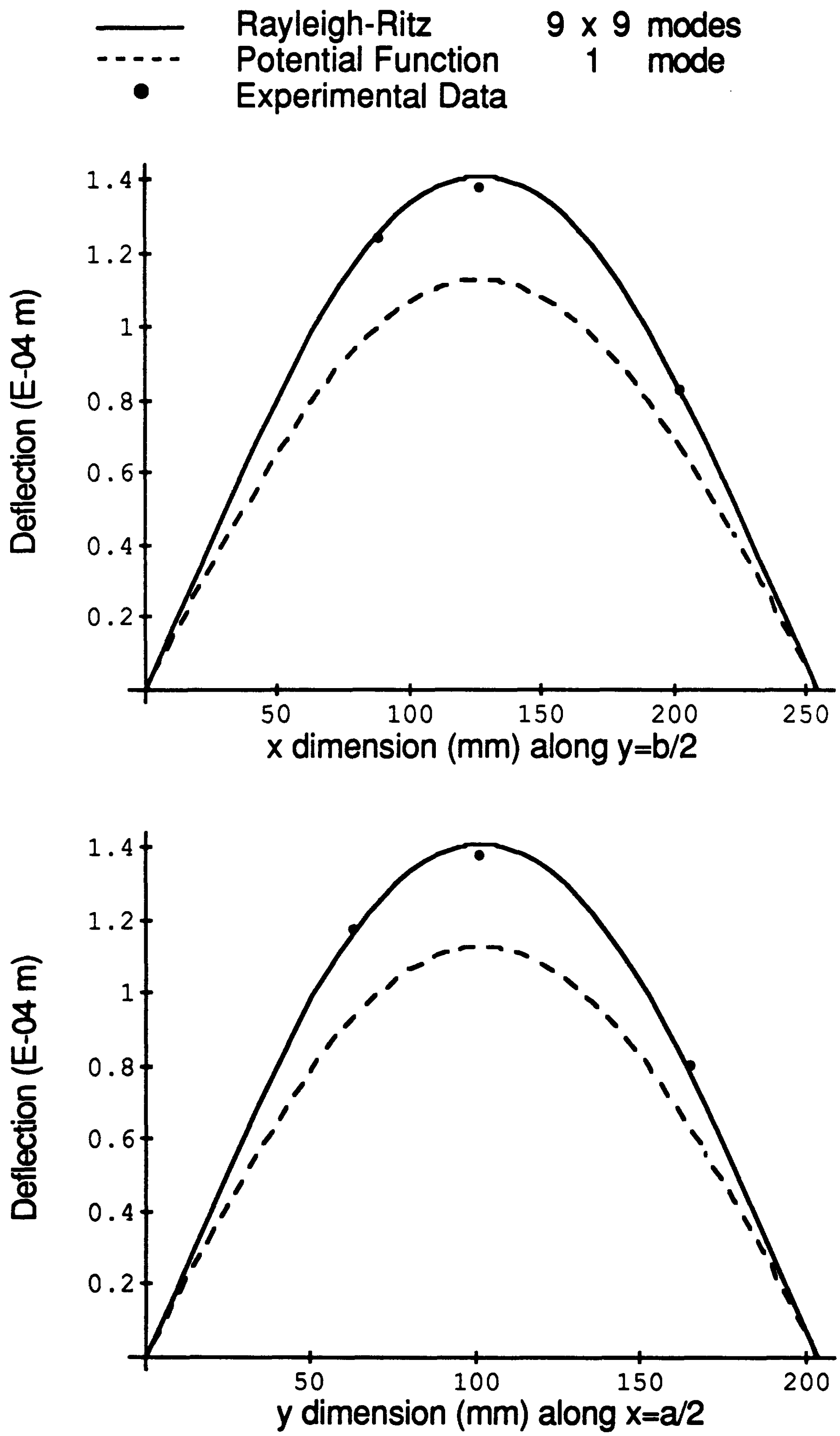

Figure 7.61 Transverse deflection for Specimen A, under a uniform pressure load of 100 Newtons, with all four sides simply supported.

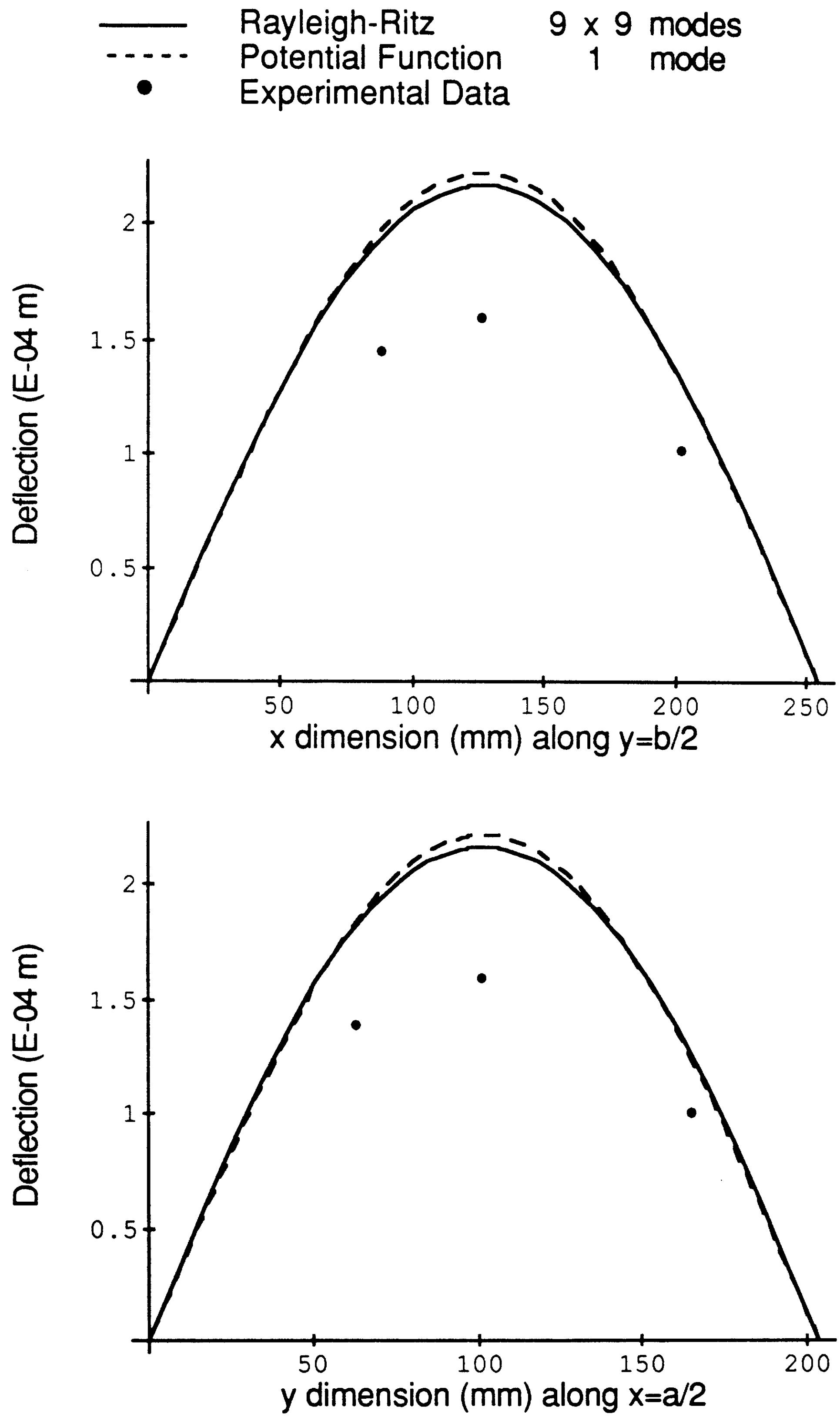

Figure 7.62 Transverse deflection for Specimen B, under a uniform pressure load of 100 Newtons, with all four sides simply supported.

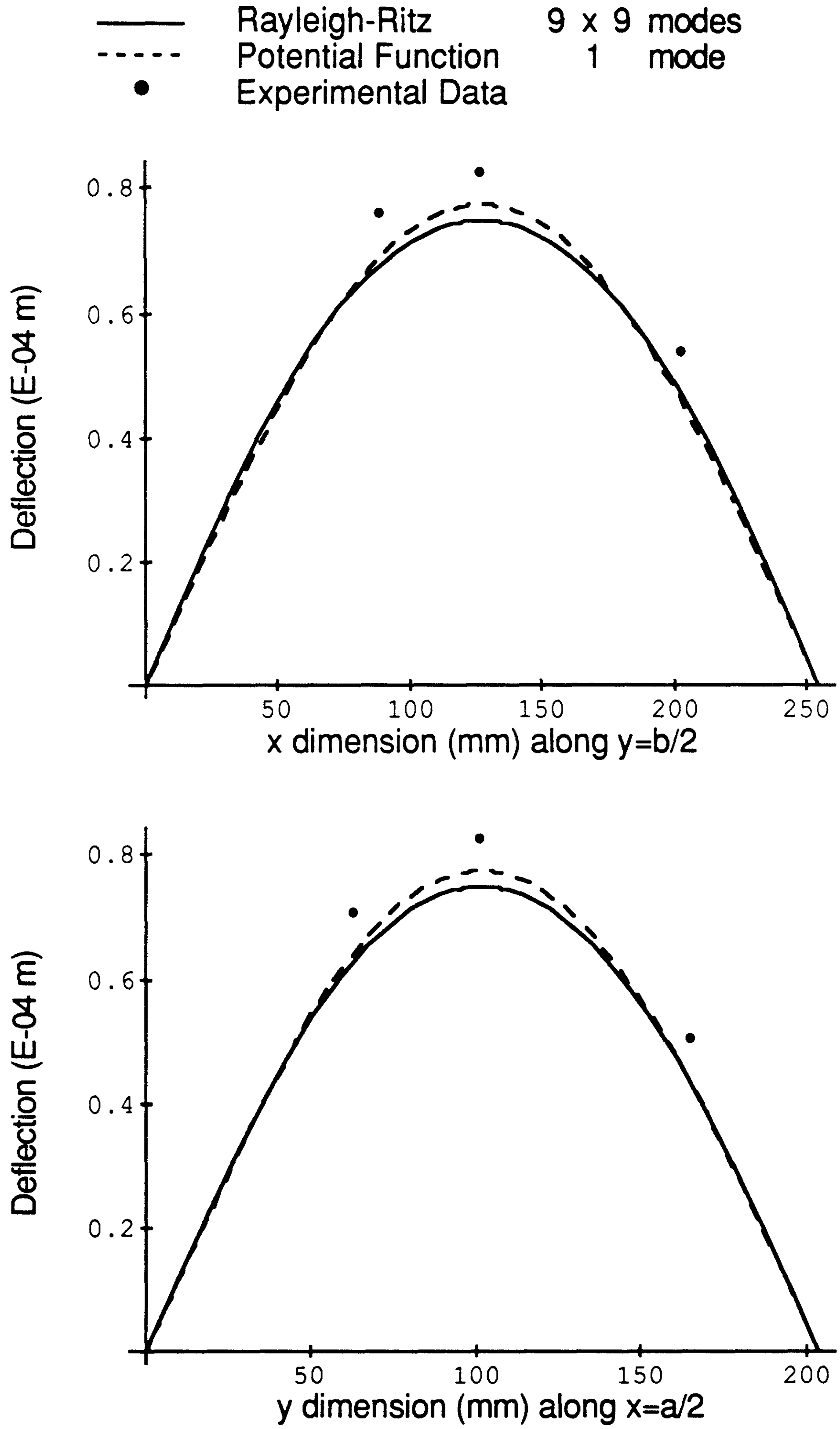

Figure 7.63 Transverse deflection for Specimen C, under a uniform pressure load of 100 Newtons, with all four sides simply supported.

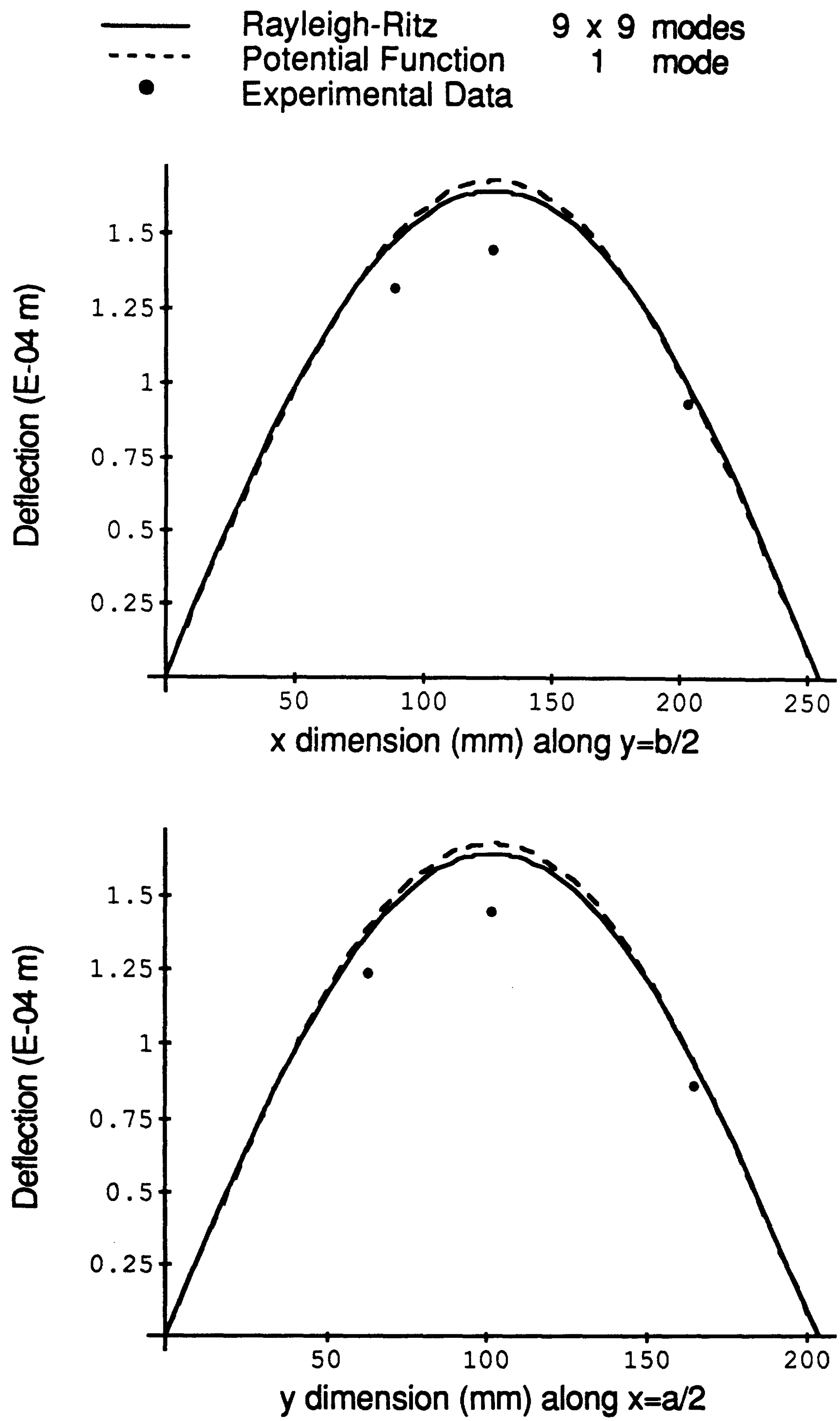

Figure 7.64 **Transverse deflection for Specimen D, under a uniform pressure load of 100 Newtons, with all four sides simply supported.**

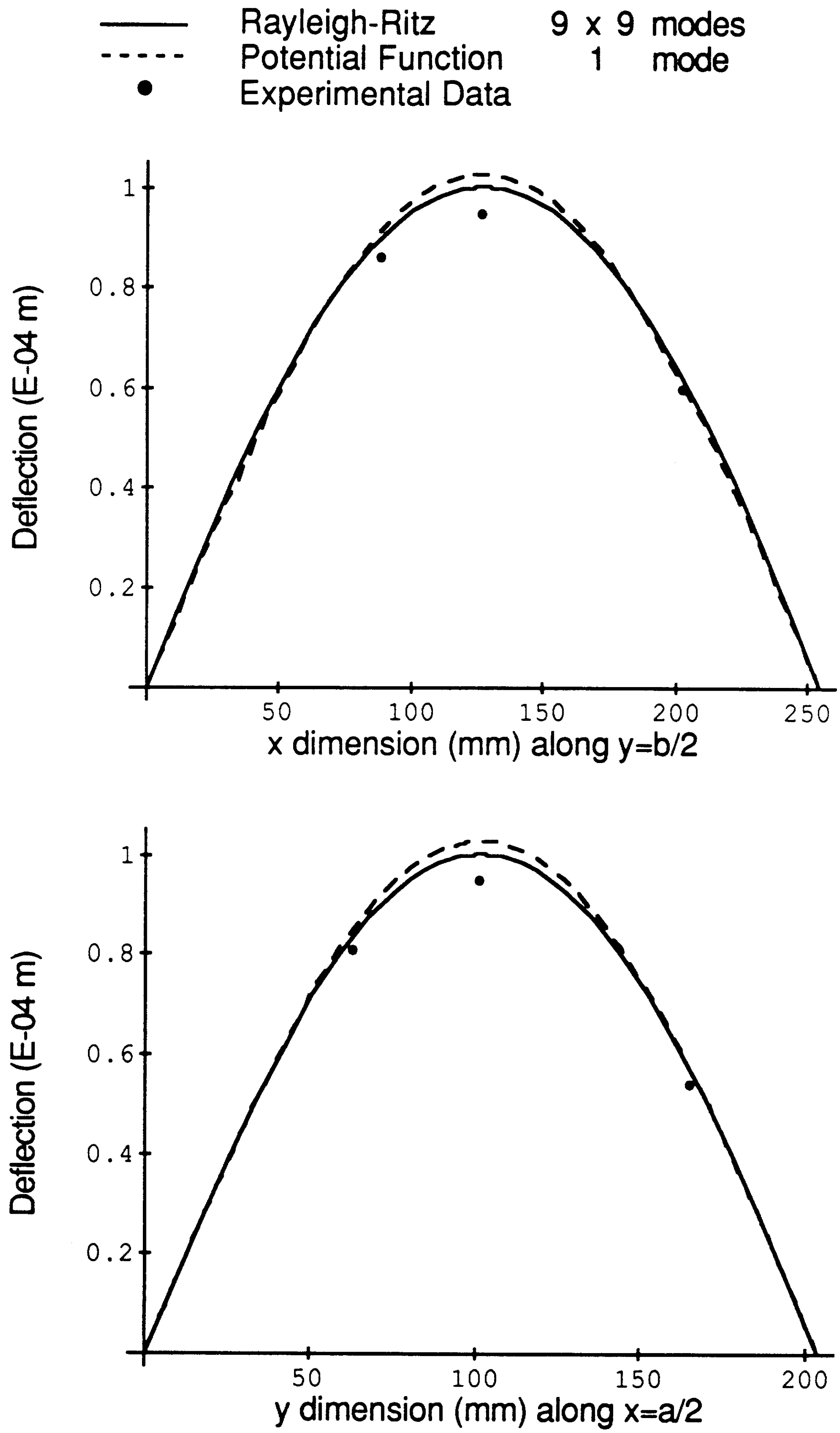

Figure 7.65 Transverse deflection for Specimen I, under a uniform pressure load of 100 Newtons, with all four sides simply supported.

7.7 Comparison of Results for Forced Vibration

The vibration tests also correlate well with the Rayleigh-Ritz predictions, both for natural frequency and mode shape. The experimental and analytical mode shapes were presented in Chapters 5 and 6 along with their respective frequencies. The two lowest modes were always found experimentally and the difference in frequency between experiment and Rayleigh-Ritz prediction is summarized in Table 7.2. Again, an average of the absolute values of the errors for each boundary condition was calculated. The four edges clamped condition exhibits the largest difference, two edges clamped and two edges simply supported is slightly better, and four edges simply supported is almost within experimental error. The average differences in frequency compare favorably with the largest differences in stiffness since frequency is proportional to the square root of stiffness.

Table 7.2 Difference of Experimental Frequency from Rayleigh-Ritz Prediction

		Percentage Difference form Rayleigh-Ritz					
B.C.'s	Mode	A	B	C	D	I	Average
CL–CL	First	−19	−17	6	22	−17	16
	Second	−14	−14	−17	−19	−12	15
SS–CL	First	−17	−8	−21	−5	−2	11
	Second	−5	−8	−26	−15	−3	11
SS–SS	First	−3	−3	−15	−3	10	7
	Second	−2	−3	−14	6	14	8

In some cases, the third and fourth lowest modes found experimentally match higher analytical modes, indicating that modes were missed in the experiments or that the mechanical shaker was not powerful enough to excite these modes. All the experimental modes presented in Chapter 5 can be correlated to analytical modes, however, not all correlate to the lowest four analytical modes presented in Chapter 6. In many cases the fourth and fifth analytical modes occur at frequencies very close to one another and in the experiments these modes occurred in the reverse order. Thus in several cases, the fourth lowest experimental mode is often the fifth lowest analytical mode. The first four analytical modes have been presented in Chapter 6. An example of the comparison between experimental and analytical mode shapes and frequencies is given in Figures 7.66 and 7.67, where Specimen B with four edges simply supported is contrasted. Note that the fourth experimental mode corresponds to the fifth analytical mode, which is presented in Figure 7.67.

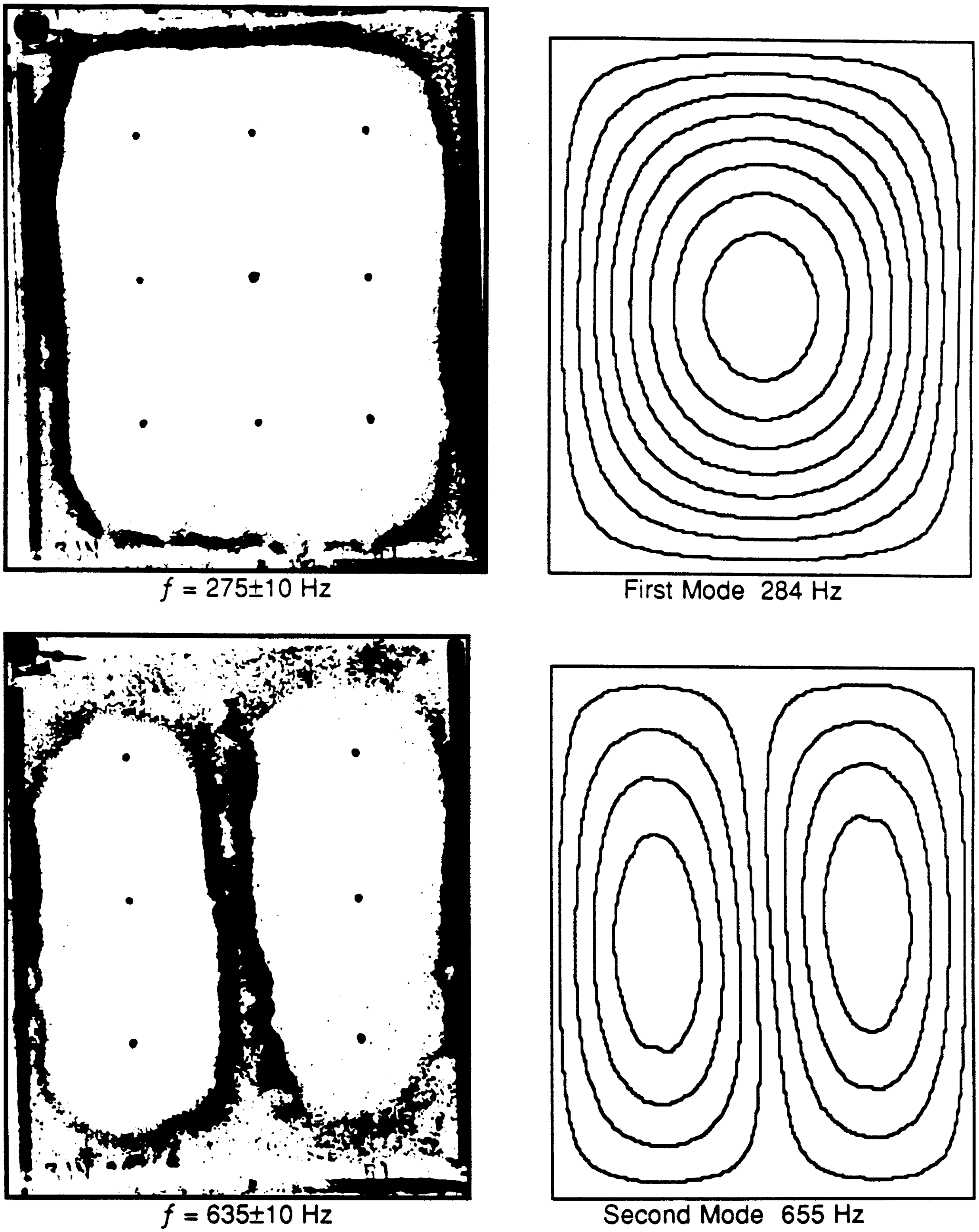

Figure 7.66 Comparison of first and second experimental and analytical modes for Specimen B with all four edges simply supported.

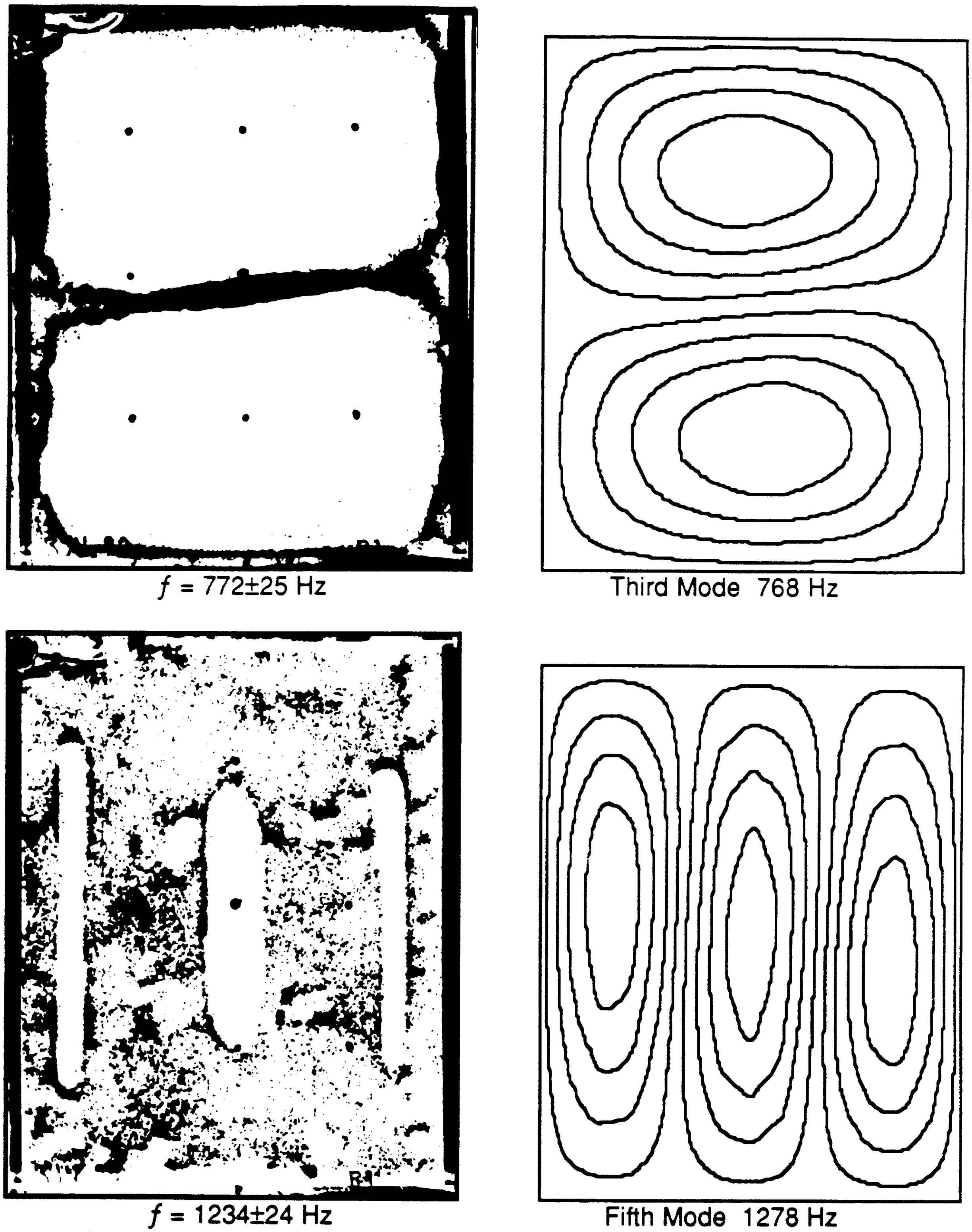

Figure 7.67 Comparison of third and fourth experimental and matching analytical modes for Specimen B with all four edges simply supported.

Chapter 8

Conclusions and Recommendations

The following conclusions were drawn considering the experimental and analytical results:

1. The theoretical simply supported boundary conditions were well modeled by the experimental jig. Almost all disagreement, for both static and dynamic loadings, between the experimental and analytical results for the simply supported cases was within experimental accuracy.

2. The clamped boundary conditions allowed more experimental static deflection, and caused lower natural frequencies than was analytically predicted. This lack of proper boundary condition stiffness is attributed to one of the following:
    1) the teflon tape that was used to lubricate the boundary conditions and allow in-plane sliding of the laminate
    2) the failure of the clamped boundary condition to properly enforce the zero rotation constraint
    3) a combination of the teflon tape and unenforced zero rotation constraint.

3. From the difficulty in modeling the clamped boundary condition, it may be assumed that a true clamped boundary condition will rarely occur in an aerospace structure. Understanding the range over which structure behaves, however, is of concern, and requires an understanding of both

the clamped and simply supported boundary conditions which represent two extremes of structural response.

4. The constrained Navier solution exhibits poor convergence, but does properly predict the displacement when bending-twisting coupling is neglected. The moment applied to the plate by the boundary conditions is not given explicitly by the solution, but may be reconstructed from the Lagrange multipliers.

5. The Rayleigh-Ritz solution correctly models all consistently observed experimental behavior, including the bending-twisting coupling. The one exception is the experimentally clamped boundary condition as discussed above.

6. The bending-shearing coupling, which was not modeled by any of the analysis, did not appear to influence plate deformation in the cases tested, where the plate was allowed to slide in-plane. In general, disagreement between the experimental and analytical results was no worse for specimen D, which had bending-shearing coupling, than for the other specimens.

7. The single mode potential function solution for plates with all four sides simply supported, under a uniform pressure loading, is less stiff (more converged) than the 9 x 9 Rayleigh-Ritz solution. The sixteen polynomial terms give a better solution for this boundary condition and loading than the 81 term double sine series, thus illustrating the efficiency that may be obtained with potential function solutions.

8. The current single mode potential function solution for four sides clamped is not capable of providing a converged solution for any of the three loading cases investigated. Either a new mode must be formulated or additional modes must be added to allow convergence for these solutions.

The following items are recommended for further investigation:

1. Improved modeling of the clamped boundary condition should be possible and would allow better understanding of the range of boundary condition response. Further work should be performed to experimentally create a truly clamped boundary condition.

2. Although bending-shearing coupling seemed to have no effect on plate deformation for the cases tested, this may be due to the flexibility of the plate to slide in-plane. Further tests should be conducted in which the plate is prevented from sliding in-plane to evaluate the effect of bending-shearing coupling with this additional constraint.

3. The single mode potential function solutions need to be expanded into sets of modes to allow proper modeling of all loading conditions. In addition, the single mode potential function for the all edges clamped case should be reexamined to evaluate whether a more suitable first mode shape exists.

4. Although experimental data was obtained for cases with free edges, no analysis has been performed for these boundary conditions. These cases should be analyzed to insure that they are correctly modeled by Rayleigh-Ritz or potential function solutions.

5. All of the cases studied in this investigation had symmetric boundary conditions. Further experimental and analytical results should be generated to confirm proper understanding of unsymmetric combinations of boundary conditions.

References

1. Timoshenko, S. P., and Woinowsky-Krieger, S., "Theory of Plates and Shells," 2nd Ed., McGraw-Hill, New York, 1959.

2. Jones, Robert M., "Mechanics of Composite Materials," Hemisphere Publishing Corp., New York, 1975.

3. Yang, P. C., Norris, C. H., and Stavsky, Y., "Elastic Wave Propagation in Heterogeneous Plates," International Journal of Solids and Structures, Vol. 2, 1966, pp. 665-684.

4. Mindlin, R. D., "Influence of Rotary Inertia and Shear on Flexural Motions of Isotropic, Elastic Plates," Journal of Applied Mechanics, Vol. 18, 1951, pp. 31-38.

5. Dobyns, A. L., "The Analysis of Simply-Supported Orthotropic Plates Subjected to Static and Dynamic Loads," AIAA Journal, Vol. 19, 1981, pp. 642-650.

6 Sun, Chang-Tsan and Whitney, J. M., "Forced Vibrations of Laminated Composite Plates in Cylindrical Bending," Journal of the Acoustical Society of America, Vol. 55, No. 5, 1974, pp. 1003-1008.

7. Enie, R. B. and Rizzo, R. R., "Three-Dimensional Laminate Moduli," Journal of Composite Materials, Vol. 4, 1970, pp. 150-154.

8. Sun, C. T. and Sijian, Li, "Three-Dimensional Effective Elastic Constants for Thick Laminates," Journal of Composite Materials, Vol. 22, 1988, pp. 629-639.

9. Whitney, J. M. and Pagano, N. J., "Shear Deformation in Heterogeneous Plates," Journal of Applied Mechanics, Vol. 92, 1970, pp. 1031-1036.

10. Reddy, J. N., "A Simple Higher-Order Theory for Laminated Composite Plates," Journal of Applied Mechanics, Vol. 51, 1984, pp. 745-752.

11. Vlasov, V. Z., "General Theory of Shells and It's Applications in Engineering," NASA TT-F-99, 1964.

12. Bisplinghoff, R. L., Mar, J. W., and Pian, T. H. H., "Statics of Deformable Solids," Dover Publications, New York, 1990.

13. Ambartsumyan, S. A., "Theory of Anisotropic Shells, "NASA TT-F-118, 1964.

14. Graves, M. J., "The Catastrophic Failure of Pressurized Graphite/Epoxy Cylinders," TELAC Report 82-10, MIT, Cambridge, MA, 02139, 1982.

15. Vinson, J. R., and Sierakowski, R. L., "The Behavior of Structures Composed of Composite Materials," Martinus Nijhoff Publishers, Boston, 1987.

16. Whitney, J. M., "Structural Analysis of Laminated Anisotropic Plates," Technomic Publishing Company, Stanford, CT, 1987.

17. Chen, P. C., and Ramkumar, R. L., "Static and Dynamic Analysis of Clamped Orthotropic Plates Using the Lagrangian Multiplier Method," AIAA Journal, Vol. 25, No. 2, 1987, pp. 316-323.

18. Ramkumar, R. L., Chen, P. C., and Sanders, W. J., "Free Vibration Solution for Clamped Orthotropic Plates Using Lagrangian Multiplier Technique," AIAA Journal, Vol. 25, No. 1, 1987, pp. 146-151.

19. Dugundji, John, "Simple Expressions for Higher Vibration Modes of Uniform Euler Beams," AIAA Journal, Vol. 26, No. 8, 1988, pp. 1013-1014.

20. Minguet, Pierre J., "Buckling of Graphite/Epoxy Sandwich Plates," TELAC Report 86-16, MIT, Cambridge, MA, 1986.

21. Lagace, P. A., Brewer, J. C., and Varnerin, C. F., "TELAC Manufacturing Class Notes," TELAC Report 88-4, MIT, Cambridge, MA, 1988.

22. G W Instruments, "MacADIOS II Hardware Series Instruction Manual," Cambridge, MA.

23. National Instruments Corp., "LABVIEW 2 User Manual," Austin, TX, 1990.

24. Cook, Robert D., "Concepts and Applications of Finite Element Analysis," Wiley & Sons, New York, 1981.

25. Wolfram, Stephen, "Mathematica, A System for Doing Mathematics by Computer," Addison-Wesley, New York, 1988.

Appendix A

Specimen Thickness Measurements

This appendix contains the thickness measurements of the composite plate specimens. Each specimen was measured at 25 points with a micrometer. The average of these measurements is also given for each plate. The average thickness for each layup, and the thickness of the aluminum specimens are given in Chapter 4.

Table A.1 Thickness Measurements for A and B Specimens (mm)

Location	A-1	A-2	A-3	B-1	B-2	B-3
1	3.03	3.05	3.20	2.70	2.66	2.65
2	3.03	3.12	3.27	2.79	2.80	2.76
3	3.05	3.06	3.32	2.81	2.80	2.76
4	3.02	3.03	3.22	2.82	2.79	2.76
5	2.90	2.92	3.08	2.70	2.68	2.71
6	3.26	3.28	3.27	2.84	2.84	2.81
7	3.26	3.30	3.34	2.93	2.90	2.89
8	3.28	3.25	3.39	2.90	2.87	2.90
9	3.31	3.25	3.37	2.95	2.92	2.96
10	3.21	3.23	3.30	2.81	2.84	2.87
11	3.19	3.28	3.31	2.83	2.83	2.84
12	3.30	3.28	3.33	2.86	2.97	2.95
13	3.36	3.36	3.44	2.92	2.95	2.92
14	3.34	3.30	3.46	2.96	2.98	2.94
15	3.25	3.34	3.34	2.86	2.85	2.86
16	3.10	3.17	3.18	2.78	2.78	2.80
17	3.21	3.23	3.31	2.88	2.90	2.92
18	3.30	3.30	3.40	2.86	2.91	2.88
19	3.28	3.32	3.40	2.99	2.91	2.90
20	3.21	3.27	3.28	2.84	2.82	2.84
21	3.00	3.05	3.00	2.67	2.74	2.70
22	3.12	3.14	3.20	2.75	2.85	2.80
23	3.21	3.14	3.28	2.82	2.84	2.82
24	3.20	3.20	3.25	2.86	2.80	2.80
25	3.16	3.17	3.17	2.68	2.77	2.74
Average	3.18	3.20	3.28	2.83	2.84	2.83

Table A.2 Thickness Measurements for C and D Specimens (mm)

Location	C-1	C-2	C-3	D-1	D-2	D-3
1	3.50	3.52	3.46	2.90	2.90	2.91
2	3.56	3.51	3.48	3.08	3.05	3.06
3	3.51	3.56	3.53	3.18	3.14	3.19
4	3.55	3.60	3.48	3.08	3.10	3.08
5	3.58	3.51	3.44	2.80	2.82	2.77
6	3.52	3.52	3.56	3.00	2.94	3.00
7	3.54	3.56	3.54	3.20	3.07	3.09
8	3.57	3.58	3.58	3.23	3.15	3.14
9	3.57	3.56	3.57	3.14	3.10	3.09
10	3.54	3.54	3.53	2.93	2.84	3.87
11	3.52	3.57	3.50	3.07	2.94	2.96
12	3.60	3.61	3.57	3.25	3.14	3.11
13	3.63	3.61	3.60	3.28	3.19	3.22
14	3.60	3.60	3.53	3.18	3.13	3.18
15	3.57	3.57	3.52	2.91	2.88	2.89
16	3.59	3.53	3.49	3.03	2.93	2.95
17	3.55	3.61	3.51	3.17	3.06	3.11
18	3.60	3.59	3.51	3.24	3.18	3.15
19	3.58	3.56	3.56	3.20	3.12	3.11
20	3.51	3.51	3.53	2.91	2.92	2.85
21	3.50	3.46	3.48	2.87	2.82	2.82
22	3.52	3.53	3.51	3.14	3.01	3.03
23	3.52	3.54	3.50	3.13	3.09	3.08
24	3.52	3.55	3.49	3.15	3.09	3.03
25	3.48	3.48	3.44	2.79	2.80	2.86
Average	3.55	3.55	3.52	3.07	3.02	3.06

Appendix B

Computer Code for Laminated Plate Stiffnesses

This code calculates the stiffnesses for a laminated plate according to the equations presented in Chapter 2. The program is written in the Mathematica™ programming language [25] and runs on a Macintosh. Two input files are required and one output file is created. The first input file is a material property data file, "mat.dat". The second file contains the laminate specific information, "lam.dat". Examples of these files along with an output file, "stiff.out" are included.

Copyright ©1991 Massachusetts Institute of Technology

Permission to use, copy, and modify this software and its documentation for internal purposes only and without fee is hereby granted provided that the above copywrite notice and this permission appear on all copies of the code and supporting documentation. For any other use of this software, in original or modified form, including but not limited to, adaptation as the basis of a commercial software or hardware product, or distribution in whole or in part, specific prior permission and/or the appropriate license must be obtained from MIT. This software is provided "as is" without any warranties whatsoever, either expressed or implied, including but not limited to the implied warranties of merchantability and fitness for a particular purpose. This software is a research program, and MIT does not represent that it is free of errors or bugs or suitable for any particular task.

Code Listing: Plate Stiffnesses

```
nmatmax = 12; (* max number of materials to be read *)
nplymax = 25  (* max number of plies in a laminate *)
small = 10^-16 (* check against to zero numerical error *)
matname = Array[m1,{nmatmax}];
matdat = Array[m2,{nmatmax,10}];

(* Reading material data from mat.dat *)
(* Reading: e1,e2,e3,g23,g31,g12,nu23,nu13,nu12,tply *)
OpenRead["mat.dat"];
        Do[Read["mat.dat",String];,{2}];
        Do[
                matname[[i]] = Read["mat.dat",String];
                Do[
                        matdat[[i,j]] = Read["mat.dat",Number];
                ,{j,10}];
                Read["mat.dat",String];
        ,{i,nmatmax}];
Close["mat.dat"];

(* Reading laminate data from lam.dat *)
(* Reading: nply, mat #, tply *)
nlam = Input["Number of laminates?"];
lamname = Array[l1,{nlam}];        lamdat = Array[l2,{nlam,3}];
lamangle = Array[l3,{nlam,nplymax}];
OpenRead["lam.dat"];
        Do[Read["lam.dat",String];,{3}];
        Do[
                lamname[[i]] = Read["lam.dat",String];
                Do[
                        lamdat[[i,j]] = Read["lam.dat",Number];
                ,{j,3}];
                If[lamdat[[i,3]] == 0, lamdat[[i,3]] =
                        matdat[[lamdat[[i,2]],10]]];
                Do[
                        lamangle[[i,k]] = Read["lam.dat",Number];
                ,{k,lamdat[[i,1]]}];
                Read["lam.dat",String];
        ,{i,nlam}];
Close["lam.dat"];

q = Array[q1,9]; r = Array[r1,3]; s = Array[s1,3];
a = Array[a1,9]; b = Array[b1,6]; d = Array[d1,6];
OpenWrite["stiff.out"];
```

```
Do[
        mn = lamdat[[i,2]]; tp = lamdat[[i,3]]; zt = tp lamdat[[i,1]]/2;
        qbdn = 1 - matdat[[mn,9]]^2 matdat[[mn,2]]/matdat[[mn,1]];
        qb11 = matdat[[mn,1]]/qbdn;
        qb12 = matdat[[mn,9]] matdat[[mn,2]]/qbdn;
        qb22 = matdat[[mn,2]]/qbdn;
        qb66 = matdat[[mn,6]];
        Do[a[[k]] = 0;,{k,9}];
        Do[{b[[k]] = 0;d[[k]] = 0;},{k,6}];
        Do[s[[k]] = 0;,{k,3}];
        Do[
                th = lamangle[[i,j]] Degree;
                q[[1]] = qb11 Cos[th]^4 + 2 (qb12+2qb66) Sin[th]^2 Cos[th]^2 +
                                qb22 Sin[th]^4;
                q[[6]] = (qb11 + qb22 - 4 qb66) Sin[th]^2 Cos[th]^2 +
                                qb12 (Sin[th]^4 + Cos[th]^4);
                q[[2]] = qb11 Sin[th]^4 + 2 (qb12+2qb66) Sin[th]^2 Cos[th]^2 +
                                qb22 Cos[th]^4;
                q[[5]] = (qb11 - qb12 - 2 qb66) Sin[th] Cos[th]^3 +
                                (qb12 - qb22 + 2 qb66) Sin[th]^3 Cos[th];
                q[[4]] = (qb11 - qb12 - 2 qb66) Sin[th]^3 Cos[th] +
                                (qb12 - qb22 + 2 qb66) Sin[th] Cos[th]^3;
                q[[3]] = (qb11 + qb22 - 2 qb12 - 2 qb66) Sin[th]^2 Cos[th]^2 +
                                qb66 (Sin[th]^4 + Cos[th]^4);
                                        (* transverse terms traditional plate *)
                q[[7]] = matdat[[mn,4]] Cos[th]^2 + matdat[[mn,5]] Sin[th]^2;
                q[[8]] = matdat[[mn,4]] Sin[th]^2 + matdat[[mn,5]] Cos[th]^2;
                q[[9]] = (-matdat[[mn,4]] + matdat[[mn,5]]) Cos[th] Sin[th];
                                        (* transverse terms 3-D elasticity *)
                r[[1]] = 1/matdat[[mn,4]] Cos[th]^2 + 1/matdat[[mn,5]] Sin[th]^2;
                r[[2]] = 1/matdat[[mn,4]] Sin[th]^2 + 1/matdat[[mn,5]] Cos[th]^2;
                r[[3]] = (-1/matdat[[mn,4]] + 1/matdat[[mn,5]]) Cos[th] Sin[th];
                Do[
                        a[[k]] = a[[k]] + q[[k]] tp//N;
                ,{k,9}];
                Do[
                        s[[k]] = s[[k]] + r[[k]]/lamdat[[i,1]]//N;
                ,{k,3}];
                Do[
                        b[[k]] = b[[k]] + q[[k]](tp^2 (1 - 2 j) + 2 tp zt)/2//N;
                        d[[k]] = d[[k]] + q[[k]]((zt-(j-1)tp)^3-(zt-j tp)^3)/3//N;
                ,{k,6}];
        ,{j,lamdat[[i,1]]}];
        {{r[[1]],r[[3]]},{junk,r[[2]]}} =
                2 zt Inverse[{{s[[1]], s[[3]]},{s[[3]], s[[2]]}}]//N;
        Do[ If[Abs[a[[k]]] < small,a[[k]]=0,],{k,9}];
```

```
        Do[ If[Abs[r[[k]]] < small,r[[k]]=0,],{k,3}];
        Do[ If[Abs[b[[k]]] < small,b[[k]]=0,],{k,6}];
        Do[ If[Abs[d[[k]]] < small,d[[k]]=0,],{k,6}];
        Write["stiff.out",lamname[[i]]];          (* header for laminate *)
        Write["stiff.out",N[a,3]];                (* classical A's in 10^6 N/m *)
        Write["stiff.out",N[r,3]];                (* 3-D transverse A's in 10^6 N/m *)
        Write["stiff.out",N[b,3]];                (* B's in 10^3 N *)
        Write["stiff.out",N[d,3]];                (* D's in N-m *)
,{i,nlam}];
Close["stiff.out"];
```

Input File: mat.dat

```
Entries ordered:  E1  E2  E3  G23  G31  G12
                  Nu23  Nu13  Nu12  Tply
AS4/3501-6
 .14200000E+03   .98100000E+01   .98100000E+01   .3770000E+01   .60000000E+01
.60000000E+01
 .34000000E+00  .30000000E+00  .30000000E+00  .13400000E+00
A370-5H/3501-6 (fabric)
 .72500000E+02   .72600000E+02   .98100000E+01   .27200000E+02   .27200000E+02
.44300000E+01
 .33300000E+00  .33300000E+00  .59000000E-01  .34300000E+00
Aluminum
 .69030000E+02   .69030000E+02   .69030000E+02   .26550000E+02   .26550000E+02
.26550000E+02
 .30000000E+00  .30000000E+00  .30000000E+00  .10000000E+01
```

Input File: lam.dat

```
laminate information:   label
                        number of plies, material #, tply (0=default)
                        ply angles ...
A's
 25 1 .129
 45 45 45 45 0 0 0 45 45 45 45 0 0 0 45 45 45 45 0 0 0 45 45 45 45
B's
 22 1 .129
 0 0 45 -45 0 0 45 -45 90 90 0 0 90 90 -45 45 0 0 -45 45 0 0
C's
 11 2 .322
 45 -45 45 -45 45 -45 45 -45 45 -45 45
D's
 24 1 .127
 -15 -15 -15 75 75 75 75 75 75 -15 -15 -15 15 15 15 -75 -75 -75 -75 -75 -75 15 15 15
I's
 1 3 3.16
 0
```

Output File: stiff.out

```
"A's"                                              {label}
{260., 106., 82.7, 68.6, 68.6, 72.9, 14.5, 17., 2.3} {A11, A22, A66, A26, A16, A12, A55, A44, A45}
{14.1, 16.6, 2.24}                                 {A44, A55, A45}
{0., 0., 0., 0., 0., 0.}                           {B11, B22, B66, B26, B16, B12}
{190., 105., 82.8, 71.5, 71.5, 74.3}               {D11, D22, D66, D26, D16, D12}
"B's"
{237., 134., 48.7, 0., 0., 40.1, 13., 14.7, 0.}
{12.4, 14., 0.}
{0., 0., 0., 0., 0., 0.}
{200., 48.5, 32.7, 3.43, 3.43, 26.9}
"C's"
{152., 152., 121., -0.00808, -0.00808, 121., 96.3, 96.3, 0.}
{96.3, 96.3, 0.}
{0., 0., 0., 0., 0., 0.}
{159., 159., 127., -0.0252, -0.0252, 126.}
"D's"
{209., 209., 41.7, 0., 0., 32.4, 14.9, 14.9, 0.}
{14.1, 14.1, 0.}
{0., 0., 0., 30.9, -30.9, 0.}
{188., 137., 32.3, 0., 0., 25.1}
"I's"
{240., 240., 83.9, 0., 0., 71.9, 83.9, 83.9, 0.}
{83.9, 83.9, 0.}
{0., 0., 0., 0., 0., 0.}
{199., 199., 69.8, 0., 0., 59.8}
```

Appendix C

Constant Coefficients for Anisotropic Plate Bending

This appendix lists the constant coefficients for the bending of a midplane symmetric anisotropic Mindlin plate. The sixth order partial differential equation in terms of a potential function, Φ, to which these coefficients belong, is given in Chapter 4.

$$P_1 = \kappa A_{55}\left(D_{11} D_{66} - D_{16}^2\right)$$

$$P_2 = 2\,\kappa A_{45}\left(D_{11} D_{66} - D_{16}^2\right) + 2\,\kappa A_{55}\left(D_{11} D_{26} - D_{12} D_{16}\right)$$

$$P_3 = \kappa A_{44}\left(D_{11} D_{66} - D_{16}^2\right) + 4\,\kappa A_{45}\left(D_{11} D_{26} - D_{12} D_{16}\right) + \kappa A_{55}\left(D_{11} D_{22} - D_{12}^2 + 2\,D_{16} D_{26} - 2\,D_{12} D_{66}\right)$$

$$P_4 = 2\,\kappa A_{44}\left(D_{11} D_{26} - D_{12} D_{16}\right) + 2\,\kappa A_{55}\left(D_{22} D_{16} - 2\,D_{12} D_{26}\right) + 2\,\kappa A_{45}\left(D_{11} D_{22} - D_{12}^2 + 2\,D_{16} D_{26} - 2\,D_{12} D_{66}\right)$$

$$P_5 = \kappa A_{44}\left(D_{11} D_{22} - D_{12}^2 + 2\,D_{16} D_{26} - 2\,D_{12} D_{66}\right) + 4\,\kappa A_{45}\left(D_{22} D_{16} - D_{12} D_{26}\right) + \kappa A_{55}\left(D_{22} D_{66} - D_{26}^2\right)$$

$$P_6 = 2\,\kappa A_{44}\left(D_{22} D_{16} - D_{12} D_{26}\right) + 2\,\kappa A_{45}\left(D_{22} D_{66} - D_{26}^2\right)$$

$$P_7 = \kappa A_{44}\left(D_{22} D_{66} - D_{26}^2\right)$$

$$P_8 = -R_0 R_2^2$$

$$P_9 = \kappa A_{55} R_2^2 + R_0 R_2\left(D_{11} + D_{66}\right)$$

$$P_{10} = 2\,\kappa A_{45} R_2^2 + 2\,R_0 R_2\left(D_{16} + D_{26}\right)$$

$$P_{11} = \kappa A_{44} R_2^2 + R_0 R_2\left(D_{22} + D_{66}\right)$$

$$P_{12} = -\kappa A_{55} R_2\left(D_{11} + D_{66}\right) - R_0\left(D_{11} D_{66} - D_{16}^2\right)$$

$$P_{13} = -2\,\kappa A_{45}\,R_2\,(D_{11} + D_{66}) - 2\,\kappa A_{55}\,R_2\,(D_{16} + D_{26}) +$$
$$2\,R_0\,(D_{12}\,D_{16} - D_{11}\,D_{26})$$

$$P_{14} = -\,\kappa A_{44}\,R_2\,(D_{11} + D_{66}) - 4\,\kappa A_{45}\,R_2\,(D_{16} + D_{26}) -$$
$$\kappa A_{55}\,R_2\,(D_{22} + D_{66}) + R_0\left(D_{12}^2 - D_{11}\,D_{22} + 2\,D_{12}\,D_{66} - 2\,D_{16}\,D_{26}\right)$$

$$P_{15} = -2\,\kappa A_{44}\,R_2\,(D_{16} + D_{26}) - 2\,\kappa A_{45}\,R_2\,(D_{22} + D_{66}) +$$
$$2\,R_0\,(D_{12}\,D_{26} - D_{22}\,D_{16})$$

$$P_{16} = -\,\kappa A_{44}\,R_2\,(D_{22} + D_{66}) - R_0\left(D_{22}\,D_{66} - D_{26}^2\right)$$

$$P_{17} = -\,D_{11}\,\kappa^2\left(A_{44}\,A_{55} - A_{45}^2\right) - K\left(D_{11}\,D_{66} - D_{16}^2\right)$$

$$P_{18} = -4\,D_{16}\,\kappa^2\left(A_{44}\,A_{55} - A_{45}^2\right) - 2\,K\,(D_{11}\,D_{26} - D_{12}\,D_{16})$$

$$P_{19} = -2\,D_{12}\,\kappa^2\left(A_{44}\,A_{55} - A_{45}^2\right) - 4\,D_{66}\,\kappa^2\left(A_{44}\,A_{55} - A_{45}^2\right) +$$
$$K\left(D_{12}^2 - D_{11}\,D_{22} + 2\,D_{12}\,D_{66} - 2\,D_{16}\,D_{26}\right)$$

$$P_{20} = -4\,D_{26}\,\kappa^2\left(A_{44}\,A_{55} - A_{45}^2\right) - 2\,K\,(D_{22}\,D_{16} - D_{12}\,D_{26})$$

$$P_{21} = -\,D_{22}\,\kappa^2\left(A_{44}\,A_{55} - A_{45}^2\right) - K\left(D_{22}\,D_{66} - D_{26}^2\right)$$

$$P_{22} = -\,R_0\,R_2\,\kappa\,(A_{44} + A_{55}) - K\,R_2^2$$

$$P_{23} = R_0\,\kappa\,(A_{44}\,D_{11} - 2\,A_{45}\,D_{16} + A_{55}\,D_{66}) +$$
$$R_2\,\kappa^2\left(A_{44}\,A_{55} - A_{45}^2\right) + K\,R_2\,(D_{11} + D_{66})$$

$$P_{24} = 2\,R_0\,\kappa\,(A_{44}\,D_{16} - A_{45}\,(D_{12} + D_{66}) + A_{55}\,D_{26}) + 2\,K\,R_2\,(D_{16} + D_{26})$$

$$P_{25} = R_0\,\kappa\,(A_{44}\,D_{66} - 2\,A_{45}\,D_{26} + A_{55}\,D_{22}) + R_2\,\kappa^2\left(A_{44}\,A_{55} - A_{45}^2\right) +$$
$$K\,R_2\,(D_{22} + D_{66})$$

$$P_{26} = K\,\kappa\,(A_{44}\,D_{11} - 2\,A_{45}\,D_{16} + A_{55}\,D_{66})$$

$$P_{27} = 2\,K\,\kappa\,(A_{44}\,D_{16} - A_{45}\,(D_{12} + D_{66}) + A_{55}\,D_{26})$$

$$P_{28} = K\,\kappa\,(A_{44}\,D_{66} - 2\,A_{45}\,D_{26} + A_{55}\,D_{22})$$

$$P_{29} = -\,R_0\,\kappa^2\,(A_{44}\,A_{55} - A_{45}) - K\,R_2\,\kappa\,(A_{44} + A_{55})$$

$$P_{30} = -\,K\,\kappa^2\left(A_{44}\,A_{55} - A_{45}^2\right)$$

Appendix D

Computer Code for Polynomial Potential Function

This code calculates the coefficients for a potential function that is complete in even powers of x and y through the tenth. Having satisfied the boundary conditions explicitly, the amplitude may be determined through the Galerkin method.

The analysis used is limited to symmetric loadings, and is only approximate. Either a point load or a rectangular patch of uniform pressure may be applied. The program is written in the Mathematica™ programming language [25] and runs on a Macintosh.

Copyright ©1991 Massachusetts Institute of Technology

Permission to use, copy, and modify this software and its documentation for internal purposes only and without fee is hereby granted provided that the above copywrite notice and this permission appear on all copies of the code and supporting documentation. For any other use of this software, in original or modified form, including but not limited to, adaptation as the basis of a commercial software or hardware product, or distribution in whole or in part, specific prior permission and/or the appropriate license must be obtained from MIT. This software is provided "as is" without any warranties whatsoever, either expressed or implied, including but not limited to the implied warranties of merchantability and fitness for a particular purpose. This software is a research program, and MIT does not represent that it is free of errors or bugs or suitable for any particular task.

Code Listing: Polynomial Potential Function

```
(* Written by M.J. Graves & R.J. Notestine *)
(* M.I.T. TELAC - 1991*)
(* This is an experimental one mode solution *)
(* Warning: Use ONLY for SYMMETRIC loadings *)
Share[];
conv = 254/10;                                      (* english to SI *)
a = 10 conv; b = 8 conv;                            (* x & y plate dimensions *)
K = 822467/1000000;                                 (* shear correction factor *)
{A44, A55} = {141/10,166/10} 1000;
{D11, D22, D66, D12} = {190,105,828/10,743/10} 1000;
P1 = -K A55 D11 D66;
P2 = -K A44 D11 D66 - K A55 (D11 D22 - D12^2 - 2 D12 D66);
P3 = -K A55 D22 D66 - K A44 (D11 D22 - D12^2 - 2 D12 D66);
P4 = -K A44 D22 D66;
P5 = K^2 A44 A55 D11;
P6 = 2 K^2 A44 A55 (D12 + 2 D66);
P7 = K^2 A44 A55 D22;
d131 = K A55 D66;
d132 = K A55 D22 - K A44(D12 + D66);
d133 = -K^2 A44 A55;
d231 = K A44 D66;
d232 = K A44 D11 - K A55(D12 + D66);
d233 = -K^2 A44 A55;
d331 = D11 D66;
d332 = D11 D22 - D12^2 - 2 D12 D66;
d333 = D22 D66;
d334 = -K (A44 D11 + A55 D66);
d335 = -K (A44 D66 + A55 D22);
d336 = K^2 A44 A55;
phi = 1 + a2 x^2 + a3 x^4 + a4 x^6 + a5 x^8 + a6 x^10 + a7 y^2 + a8 x^2 y^2 + a9 x^4 y^2 +
        a10 x^6 y^2 + a11 x^8 y^2 + a12 x^10 y^2 + a13 y^4 + a14 x^2 y^4 + a15 x^4 y^4 +
        a16 x^6 y^4 + a17 x^8 y^4 + a18 x^10 y^4 + a19 y^6 + a20 x^2 y^6 + a21 x^4 y^6 +
        a22 x^6 y^6 + a23 x^8 y^6 + a24 x^10 y^6 + a25 y^8 + a26 x^2 y^8 + a27 x^4 y^8 +
        a28 x^6 y^8 + a29 x^8 y^8 + a30 x^10 y^8 + a31 y^10 + a32 x^2 y^10 + a33 x^4 y^10 +
        a34 x^6 y^10 + a35 x^8 y^10 + a36 x^10 y^10;
psix = Expand[d131 D[phi,{x,3}] + d132 D[phi,x,{y,2}] +
        d133 D[phi,x]];
psiy = Expand[d231 D[phi,{y,3}] + d232 D[phi,{x,2},y] +
        d233 D[phi,y]];
w = Expand[d331 D[phi,{x,4}] + d332 D[phi,{x,2},{y,2}] +
        d333 D[phi,{y,4}] + d334 D[phi,{x,2}] +
        d335 D[phi,{y,2}] + d336 phi];
mx = Expand[D11 D[psix,x] + D12 D[psiy,y]];
```

```
my = Expand[D12 D[psix,x] + D22 D[psiy,y]];
mxy = Expand[D66 (D[psix,y] + D[psiy,x])];
qx = Expand[K A55 (D[w,x] + psix)];
qy = Expand[K A44 (D[w,y] + psiy)];
pde = Expand[P1 D[phi,{x,6}] + P2 D[phi,{x,4},{y,2}] +
P3 D[phi,{x,2},{y,4}] + P4 D[phi,{y,6}] + P5 D[phi,{x,4}] +
P6 D[phi,{x,2},{y,2}] + P7 D[phi,{y,4}]];
equationwx = w/.x->a/2;
equationwy = w/.y->b/2;
equationpsixx = psix/.x->a/2;
equationpsixy = psix/.y->b/2;
equationpsiyx = psiy/.x->a/2;
equationpsiyy = psiy/.y->b/2;
eq1 = equationwx/.y->0;
eq2 = Coefficient[equationwx,y^2];
eq3 = Coefficient[equationwx,y^4];
eq4 = Coefficient[equationwx,y^6];
eq5 = Coefficient[equationwx,y^8];
eq6 = Coefficient[equationwx,y^10];
eq7 = equationwy/.x->0;
eq8 = Coefficient[equationwy,x^2];
eq9 = Coefficient[equationwy,x^4];
eq10 = Coefficient[equationwy,x^6];
eq11 = Coefficient[equationwy,x^8];
eq12 = Coefficient[equationwy,x^10];
eq13 = equationpsixx/.y->0;
eq14 = Coefficient[equationpsixx,y^2];
eq15 = Coefficient[equationpsixx,y^4];
eq16 = Coefficient[equationpsixx,y^6];
eq17 = Coefficient[equationpsixx,y^8];
eq18 = Coefficient[equationpsixx,y^10];
eq19 = Coefficient[equationpsixy,x];
eq20 = Coefficient[equationpsixy,x^3];
eq21 = Coefficient[equationpsixy,x^5];
eq22 = Coefficient[equationpsixy,x^7];
eq23 = Coefficient[equationpsixy,x^9];
eq24 = Coefficient[equationpsiyx,y];
eq25 = Coefficient[equationpsiyx,y^3];
eq26 = Coefficient[equationpsiyx,y^5];
eq27 = Coefficient[equationpsiyx,y^7];
eq28 = Coefficient[equationpsiyx,y^9];
eq29 = equationpsiyy/.x->0;
eq30 = Coefficient[equationpsiyy,x^2];
eq31 = Coefficient[equationpsiyy,x^4];
eq32 = Coefficient[equationpsiyy,x^6];
eq33 = Coefficient[equationpsiyy,x^8];
```

```
eq34 = Coefficient[equationpsiyy,x^10];
Solve[{eq1==0,eq2==0,eq3==0,eq4==0,eq5==0,eq6==0,eq7==0,eq8==0,eq9==0,eq10==0,
      eq11==0,eq12==0,eq13==0,eq14==0,eq15==0,eq16==0,eq17==0,eq18==0,eq19==0,
      eq20==0,eq21==0,eq22==0,eq23==0,eq24==0,eq25==0,eq26==0,eq27==0,eq28==0,
      eq29==0,eq30==0,eq31==0,eq32==0,eq33==0,eq34==0},{a2,a3,a4,a5,a6,a7,a8,a9,a10,
      a11,a12,a13,a14,a15,a16,a17,a18,a19,a20,a21,a22,a23,a24,a25,a26,a27,a28,a29,a30,
      a31,a32,a33,a34,a35,a36}]
(* Uniform Pressure *)
ao = 10 conv; bo = 8 conv;                                  (* x & y patch dimensions *)
po = 1/ao/bo;                                               (* distributed load->N/mm^2 *)
A1 = Integrate[po w,{x,-ao/2,ao/2},{y,-bo/2,bo/2}]/Integrate[pde w,{x,-a/2,a/2},{y,-b/2,b/2}];
1/{A1 w/.{x->0, y->0}, A1 w/.{x->0, y->-1.5 conv},A1 w/.{x->1.5 conv, y->0}, A1 w/.{x->0, y->2.5 conv},
      A1 w/.{x->3 conv, y->0}}//N
(* Uniform Pressure Patch *)
ao = 25/10 conv; bo = 2 conv;                               (* x & y patch dimensions *)
po = 1/ao/bo;                                               (* distributed load->N/mm^2 *)
A2 = Integrate[po w,{x,-ao/2,ao/2},{y,-bo/2,bo/2}]/Integrate[pde w,{x,-a/2,a/2},{y,-b/2,b/2}];
1/{A2 w/.{x->0, y->0}, A2 w/.{x->0, y->-1.5 conv},A2 w/.{x->1.5 conv, y->0}, A2 w/.{x->0, y->2.5 conv},
      A2 w/.{x->3 conv, y->0}}//N
(* Point Load *)
po = 1;                                                     (* point load->N *)
A3 = {po w/.{x->0, y->0}}/Integrate[pde w,{x,-a/2,a/2},{y,-b/2,b/2}];
1/{A3 w/.{x->0, y->0}, A3 w/.{x->0, y->-1.5 conv},A3 w/.{x->1.5 conv, y->0}, A3 w/.{x->0, y->2.5 conv},
      A3 w/.{x->3 conv, y->0}}//N
```

Appendix E

Computer Codes for Lagrange Multiplier Solutions

The first code calculates the transverse deflections for an orthotropic plate with all four sides clamped. By stripping off the lagrange multipliers the four sides simply supported solution is also obtained in the final lines. The second code is for an orthotropic plate with two opposite edges clamped and the other pair of edges simply supported.

The analysis used has been modified from that of Ramkumar and Chen [17, 18]. Either a point load or a rectangular patch of uniform pressure may be applied. The programs are written in the Mathematica™ programming language [25] and run on a Macintosh.

Copyright ©1991 Massachusetts Institute of Technology

Permission to use, copy, and modify this software and its documentation for internal purposes only and without fee is hereby granted provided that the above copywrite notice and this permission appear on all copies of the code and supporting documentation. For any other use of this software, in original or modified form, including but not limited to, adaptation as the basis of a commercial software or hardware product, or distribution in whole or in part, specific prior permission and/or the appropriate license must be obtained from MIT. This software is provided "as is" without any warranties whatsoever, either expressed or implied, including but not limited to the implied warranties of merchantability and fitness for a particular purpose. This software is a research program, and MIT does not represent that it is free of errors or bugs or suitable for any particular task.

Code Listing: Four Sides Clamped

```
(* This program is based on work done by R. L. Ramkumar *)
(* Written by R. J. Notestine - M.I.T. TELAC - 1991*)
(* This version uses even and odd modes *)
conv = 25.4;
mu = 50; nu = 50;                      (* number of modes *)
l1 = 10 conv; l2 = 8 conv;             (* x & y plate dimensions *)
xo = 3 conv; yo = 5 conv;              (* loading center location *)
patch = False                          (* rectagular pressure patch rather than point load *)
l1o = 2.5 conv; l2o = 2 conv;          (* x & y patch dimensions *)
po = 1;                                (* distributed load->N/mm^2 OR point load->N *)
K = Pi^2/12;                           (* shear correction factor *)
kk = Table[0,{2(mu+nu)},{2(mu+nu)}];
qq = Table[0,{2(mu+nu)}];
a = {0,0,0,0,0,0,14.1,16.6,2.24} 1000;
d = {190,105,82.8,71.5,71.5,74.3} 1000;
Share[]
If[patch,
        pz = 4 po/(Pi^2 m n) (Cos[Pi m (-l1o/2 + xo)/l1] -
                Cos[Pi m (l1o/2 + xo)/l1]) (Cos[Pi*n*(-l2o/2 + yo)/l2] - Cos[Pi*n*(l2o/2 + yo)/l2])//N,
        pz = 4 po/l1/l2 Sin[m Pi xo/l1] Sin[n Pi yo/l2]//N];
l11 = K (a[[8]] (m Pi/l1)^2 + a[[7]] (n Pi/l2)^2)//N;
l12 = K a[[8]] (m Pi/l1)//N;
l13 = K a[[7]] (n Pi/l2)//N;
l22 = (K a[[8]] + d[[1]] (m Pi/l1)^2 + d[[3]] (n Pi/l2)^2)//N;
l23 = (d[[6]] + d[[3]]) (m Pi/l1) (n Pi/l2)//N;
l33 = (K a[[7]] + d[[3]] (m Pi/l1)^2 + d[[2]] (n Pi/l2)^2)//N;
det = Det[{{l11,l12,l13},{l12,l22,l23},{l13,l23,l33}}]//N;
Do[     qq[[n]]  = Sum[-pz (l13 l23 - l33 l12)/det,{m,mu}];
        kk[[n,n]]    = Sum[(l11 l33 - l13^2)/det,{m,mu}];
        kk[[n,nu+n]] = Sum[(-1)^m (l11 l33 - l13^2)/det,{m,mu}];
        Do[     kk[[n,2nu+m]]    = (l12 l13 - l11 l23)/det;
                kk[[n,2nu+mu+m]] = (-1)^n (l12 l13 - l11 l23)/det;
        ,{m,mu}];
,{n,nu}];
Do[     qq[[nu+n]] = Sum[-(-1)^m pz (l13 l23 - l33 l12)/det,{m,mu}];
        kk[[nu+n,n]]    = Sum[(-1)^m (l11 l33 - l13^2)/det,{m,mu}];
        kk[[nu+n,nu+n]] = Sum[(-1)^(2m) (l11 l33 - l13^2)/det,{m,mu}];
        Do[     kk[[nu+n,2nu+m]]    = (-1)^m (l12 l13 - l11 l23)/det;
                kk[[nu+n,2nu+mu+m]] = (-1)^(m+n) (l12 l13 - l11 l23)/det;
        ,{m,mu}];
,{n,nu}];
Do[     qq[[2nu+m]] = Sum[-pz (l12 l23 - l22 l13)/det,{n,nu}];
        Do[     kk[[2nu+m,n]]    = (l12 l13 - l11 l23)/det;
```

```
                kk[[2nu+m,nu+n]] = (-1)^m (l12 l13 - l11 l23)/det;
        ,{n,nu}];
        kk[[2nu+m,2nu+m]]    = Sum[(l11 l22 - l12^2)/det,{n,nu}];
        kk[[2nu+m,2nu+mu+m]] = Sum[(-1)^n (l11 l22 - l12^2)/det,{n,nu}];
,{m,mu}];
Do[     qq[[2nu+mu+m]] = Sum[-(-1)^n pz (l12 l23 - l22 l13)/det,{n,nu}];
        Do[     kk[[2nu+mu+m,n]]    = (-1)^n (l12 l13 - l11 l23)/det;
                kk[[2nu+mu+m,nu+n]] = (-1)^(n+m) (l12 l13 - l11 l23)/det;
        ,{n,nu}];
        kk[[2nu+mu+m,2nu+m]]    = Sum[(-1)^n (l11 l22 - l12^2)/det,{n,nu}];
        kk[[2nu+mu+m,2nu+mu+m]] = Sum[(-1)^(2n) (l11 l22 - l12^2)/det,{n,nu}];
,{m,mu}];
alpha = LinearSolve[kk,qq]
ClearAll[kk,qq];
w = Sum[(pz (l22 l33 - l23^2) + (alpha[[n]] + (-1)^m alpha[[nu+n]]) (l13 l23 - l33 l12) +
        (alpha[[2nu+m]] + (-1)^n alpha[[2nu+mu+m]]) *
        (l12 l23 - l22 l13))/det Sin[m Pi x/l1] Sin[n Pi y/l2], {m,mu},{n,nu}];
1/{w/.{x->5 conv,y->4 conv},w/.{x->5 conv,y->2.5 conv},
        w/.{x->3.5 conv,y->4 conv},w/.{x->5 conv,y->6.5 conv}, w/.{x->8 conv,y->4 conv}}//N
ClearAll[w];
wss  = Sum[pz (l22 l33 - l23^2)/det * Sin[m Pi x/l1] Sin[n Pi y/l2],{m,mu},{n,nu}];
1/{wss/.{x->5 conv,y->4 conv},wss/.{x->5 conv,y->2.5 conv},
        wss/.{x->3.5 conv,y->4 conv},wss/.{x->5 conv,y->6.5 conv}, wss/.{x->8 conv,y->4 conv}}//N
```

Code Listing: Two Sides Clamped & Two Sides Simply Supported

```
(* This program is based on work done by R. L. Ramkumar *)
(* Written by R. J. Notestine - M.I.T. TELAC - 1991*)
(* This version uses even and odd modes *)
conv = 25.4;
mu = 9; nu = 50;                      (* number of modes *)
l1 = 10 conv; l2 = 8 conv;            (* x & y plate dimensions *)
xo = 3 conv; yo = 5 conv;             (* loading center location *)
patch = False                         (* rectagular pressure patch rather than point load *)
l1o = 2.5 conv; l2o = 2 conv;         (* x & y patch dimensions *)
po = 1;                               (* distributed load->N/mm^2 OR point load->N *)
K = Pi^2/12;                          (* shear correction factor *)
kk = Table[0,{2 mu},{2 mu}];
qq = Table[0,{2 mu}];
a = {0,0,0,0,0,0,14.1,16.6,2.24} 1000;
d = {190,105,82.8,71.5,71.5,74.3} 1000;
Share[]
If[patch,
        pz = 4 po/(Pi^2 m n) (Cos[Pi m (-l1o/2 + xo)/l1] -
                Cos[Pi m (l1o/2 + xo)/l1]) (Cos[Pi*n*(-l2o/2 + yo)/l2] - Cos[Pi*n*(l2o/2 + yo)/l2])//N,
        pz = 4 po/l1/l2 Sin[m Pi xo/l1] Sin[n Pi yo/l2]//N];
l11 = K (a[[8]] (m Pi/l1)^2 + a[[7]] (n Pi/l2)^2)//N;
l12 = K a[[8]] (m Pi/l1)//N;
l13 = K a[[7]] (n Pi/l2)//N;
l22 = (K a[[8]] + d[[1]] (m Pi/l1)^2 + d[[3]] (n Pi/l2)^2)//N;
l23 = (d[[6]] + d[[3]]) (m Pi/l1) (n Pi/l2)//N;
l33 = (K a[[7]] + d[[3]] (m Pi/l1)^2 + d[[2]] (n Pi/l2)^2)//N;
det = Det[{{l11,l12,l13},{l12,l22,l23},{l13,l23,l33}}]//N;
Do[     qq[[m]] = Sum[-pz (l12 l23 - l22 l13)/det,{n,nu}];
        kk[[m,m]]   = Sum[(l11 l22 - l12^2)/det,{n,nu}];
        kk[[m,mu+m]] = Sum[(-1)^n (l11 l22 - l12^2)/det,{n,nu}];
,{m,mu}];
Do[     qq[[mu+m]] = Sum[-(-1)^n pz (l12 l23 - l22 l13)/det,{n,nu}];
        kk[[mu+m,m]]   = Sum[(-1)^n (l11 l22 - l12^2)/det,{n,nu}];
        kk[[mu+m,mu+m]] = Sum[(-1)^(2n) (l11 l22 - l12^2)/det,{n,nu}];
,{m,mu}];
alpha = LinearSolve[kk,qq]
w = Sum[(pz (l22 l33 - l23^2) + (alpha[[m]] + (-1)^n alpha[[mu+m]])*
          (l12 l23 - l22 l13))/det Sin[m Pi x/l1] Sin[n Pi y/l2],{m,mu},{n,nu}];
1/{w/.{x->5 conv,y->4 conv},w/.{x->5 conv,y->2.5 conv},
        w/.{x->3.5 conv,y->4 conv},w/.{x->5 conv,y->6.5 conv}, w/.{x->8 conv,y->4 conv}}//N
```

Appendix F

Computer Codes for Lagrange Multiplier Solutions

This code was written by Wilson Tsang in TELAC at MIT. A brief description of the code is supplied in chapters two and four. The code was modified to solve static loading problems in addition to finding the natural frequencies. Note: The modifications are quick and dirty and do not reflect good programing or efficient computing. The program is written in Fortran and runs on a Macintosh.

A Mathematica™ [25] postprocessor was written to create the extensive graphics used in this report. A listing of the postprocessor follows the source code listing.

Copyright ©1991 Massachusetts Institute of Technology

Permission to use, copy, and modify this software and its documentation for internal purposes only and without fee is hereby granted provided that the above copywrite notice and this permission appear on all copies of the code and supporting documentation. For any other use of this software, in original or modified form, including but not limited to, adaptation as the basis of a commercial software or hardware product, or distribution in whole or in part, specific prior permission and/or the appropriate license must be obtained from MIT. This software is provided "as is" without any warranties whatsoever, either expressed or implied, including but not limited to the implied warranties of merchantability and fitness for a particular purpose. This software is a research program, and MIT does not represent that it is free of errors or bugs or suitable for any particular task.

Code Listing: Rayleigh-Ritz Source Code

```
      PROGRAM SFREQ
C
C   NATURAL FREQUENCIES OF
C   A SANDWICH PANEL
C
C   WRITTEN BY : WILSON TSANG - MIT TELAC
C   MODIFIED : TO SOLVE STATIC LOADINGS AND PROVIDE
C          MATHEMATICA COMPATABLE OUTPUT
C   MODIFIED BY: R. NOTESTINE - MIT TELAC
C
      IMPLICIT REAL*4 (A-H,O-Z)
      REAL*4 MASS
C
      INCLUDE SFREQ.INC
C
      DIMENSION PSI(3,3,M1,M1),PHI(3,3,M2,M2),FV1(M3),FV2(M3)
      DIMENSION MASS(M3),STIFF(M4),EVALUE(M3),EVECTOR(M3,M3)
      COMMON/COEFX/ XBETA(M1),XB(M1),XA,XTHETA
      COMMON/COEFY/ YBETA(M2),YB(M2),YA,YTHETA
      COMMON /MATL/ TC,TF,RHOC,RHOF,A,B,D11,D12,D16,D22,D26,D66,
     &         A44,A45,A55,S
      COMMON /INVSE/ WORK(M3),KP(M3),DET(2),INERT(3)
C
C   UNIT    FILE       TYPE
C   1       SINPT.DAT    INPUT
C   2       FREQ.DAT     OUTPUT
C
      PI=3.141592654
C
      OPEN(UNIT=1,FILE='SINPT.DAT',STATUS='OLD')
      OPEN(UNIT=2,FILE='FREQ.DAT',STATUS='NEW')
C
      CALL INDAT (NX,NY,IX,IY,IFC,IFM,PO,PX,PY,PA,PB)
      CALL BCONS (XBETA,XTHETA,XA,XB,IX,NX,IFM)
      CALL BCONS (YBETA,YTHETA,YA,YB,IY,NY,IFM)
C
      IF (NX.EQ.4) THEN
       CALL INTGL1 (XBETA,XTHETA,XA,XB,IX,PSI)
      ELSE
       CALL INTGL (XBETA,XTHETA,XA,XB,IX,PSI)
      ENDIF
C
      IF (NY.EQ.4) THEN
       CALL INTGL1 (YBETA,YTHETA,YA,YB,IY,PHI)
```

```
      ELSE
       CALL INTGL (YBETA,YTHETA,YA,YB,IY,PHI)
      ENDIF
C
      CALL MATRIX (MASS,STIFF,IX,IY,PSI,PHI)
      N=3*IX*IY
C
      IF(NX.EQ.4.OR.NY.EQ.4) THEN
       CALL ARRAN(STIFF,MASS,N,NLIST)
      ELSE
       NLIST=0
      ENDIF
C
      IF(IFC.EQ.0) THEN
C
      CALL RCOND(MASS,STIFF,N,NLIST)
C
      WRITE(9,*)'INVERTING MASS MATRIX...'
      DO 10 I=1,N
       MASS(I)=1./MASS(I)
 10   CONTINUE
C
      WRITE(9,*)'CALCULATING MASS-1*STIFF...'
      NV=N*(N+1)/2
      NN=0
      DO 14 I=1,N
       DO 12 J=1,I
        NN=NN+1
        STIFF(NN)=STIFF(NN)*MASS(I)
 12    CONTINUE
 14   CONTINUE
C
      WRITE(9,*)'SOLVING FOR E-VALUES'
      CALL RSP(M3,N,NV,STIFF,EVALUE,1,EVECTOR,FV1,FV2,IERR)
      DO 16 I=1,N
       EVALUE(I)=SQRT(EVALUE(I))/2./PI
 16   CONTINUE
C
      ELSE
C
      CALL QVECT(EVECTOR,IX,IY,IFC,PO,PX,PY,PA,PB)
      DO 18 I=1,N
       EVALUE(I)=EVECTOR(I,1)
 18   CONTINUE
      CALL SSPFA(STIFF,N,KP,ICHECK)
      CALL SSPSL(STIFF,N,KP,EVECTOR)
```

```
C
   ENDIF
C
   IF(IFC.GT.0)IFC=1
   WRITE(2,*)A,B
   WRITE(2,*)NX,NY,IX,IY,IFC,IFM
   WRITE(2,*)XA,XTHETA,YA,YTHETA
   DO 24 I=1,IX
    WRITE(2,*)XB(I),XBETA(I)
 24  CONTINUE
   DO 26 I=1,IY
    WRITE(2,*)YB(I),YBETA(I)
 26  CONTINUE
   DO 30 I=1,N
    WRITE(2,*)I,EVALUE(I)
 30  CONTINUE
   NN=(1-N)*IFC+N
   DO 40 I=1,NN
    DO 35 J=1,N
     WRITE(2,*)EVECTOR(J,I)
 35   CONTINUE
 40  CONTINUE
C
   STOP
   END
C-----------------------------------------------
   SUBROUTINE INDAT(NX,NY,IX,IY,IFC,IFM,PO,PX,PY,PA,PB)
   IMPLICIT REAL*4 (A-H,O-Z)
   CHARACTER*70 TITLE1,TITLE2,TITLE3
   COMMON /MATL/ TC,TF,RHOC,RHOF,A,B,D11,D12,D16,D22,D26,D66,
  &         A44,A45,A55,S
C
C   INDEX NO.S FOR B.C.S:
C   1 FOR SS-SS
C   2 FOR CL-FR
C   3 FOR CL-CL
C   4 FOR FR-FR
C   5 FOR SS-CL
C   6 FOR SS-FR
C
   READ(1,10) TITLE1
   READ(1,10) TITLE2
   READ(1,10) TITLE3
   READ(1,*) NX
   READ(1,*) NY
   READ(1,*) IX
```

```
      READ(1,*) IY
      READ(1,*) IFC,IFM,PO,PX,PY,PA,PB
      READ(1,*) TC,TF,RHOC,RHOF,A,B,D11,D22,D66,D26,D16,D12,
     &        A44,A55,A45,S
C
 10   FORMAT(A)
      RETURN
      END
C-----------------------------------------
      SUBROUTINE BCONS (BETA,THETA,A,B,I,N,IFM)
      IMPLICIT REAL*4 (A-H,O-Z)
      DIMENSION BETA(*),B(*)
      WRITE (9,*) 'SETTING UP B.C.S'
C
      IF (N.EQ.1) THEN
       DO 10 J=1,I
        IF(IFM.EQ.1) THEN
         M=2*J-1
        ELSE
         M=J
        ENDIF
         BETA(J)=M*3.141592654
        B(J)=0.
 10    CONTINUE
       THETA=0.
       A=0.
       RETURN
      ENDIF
C
      IF (N.EQ.2) THEN
       DO 20 J=1,I
        IF(IFM.EQ.1) THEN
         M=2*J-1
        ELSE
         M=J
        ENDIF
         BETA(J)=(M-.5)*3.141592654
        B(J)=2*MOD(M,2)-1
 20    CONTINUE
       THETA=-.785398163
       A=1.
       RETURN
      ENDIF
C
      IF (N.EQ.3) THEN
       DO 30 J=1,I
```

```
    IF(IFM.EQ.1) THEN
     M=2*J-1
    ELSE
     M=J
    ENDIF
     BETA(J)=(M+.5)*3.141592654
     B(J)=2*MOD(M,2)-1
30   CONTINUE
     THETA=-.785398163
    A=1.
    RETURN
   ENDIF
C
   IF (N.EQ.4) THEN
    IF(IFM.EQ.1) THEN
     BETA(1)=0.
      BETA(2)=1.5*3.141592654
     B(1)=0.
     B(2)=1.
    ELSE
     BETA(1)=0.
     BETA(2)=0.
     B(1)=0.
     B(2)=0.
    ENDIF
    DO 40 J=3,I
     IF(IFM.EQ.1) THEN
      M=2*J-1
     ELSE
      M=J
     ENDIF
      BETA(J)=(M-2.+.5)*3.141592654
      B(J)=2*MOD(M-2,2)-1
40   CONTINUE
     THETA=2.35619449
    A=1.
    RETURN
   ENDIF
C
   IF (N.EQ.5) THEN
    DO 50 J=1,I
     IF(IFM.EQ.1) THEN
      M=2*J-1
     ELSE
      M=J
     ENDIF
```

```
      BETA(J)=(M+.25)*3.141592654
      B(J)=2*MOD(M,2)-1
50    CONTINUE
     THETA=0.
     A=0.
     RETURN
    ENDIF
C
    IF (N.EQ.6) THEN
     DO 60 J=1,I
      IF(IFM.EQ.1) THEN
       M=2*J-1
      ELSE
       M=J
      ENDIF
      BETA(J)=(M+.25)*3.141592654
      B(J)=2*MOD(M+1,2)-1
60    CONTINUE
     THETA=0.
     A=0.
     RETURN
    ENDIF
C
    END
C------------------------------------------------------------
     SUBROUTINE INTGL (BETA,THETA,A,B,II,F)
     IMPLICIT REAL*4 (A-H,O-Z)
     INTEGER P,Q
C
     INCLUDE SFREQ.INC
C
     DIMENSION BETA(*),B(*),F(3,3,M1,M1)
     WRITE (9,*) 'CALCULATING INTEGRALS OF BEAM FUNCTIONS'
     PI=3.141592654
     DO 10 I=1,3
      DO 10 J=1,3
       DO 10 M=1,II
        DO 10 N=1,II
        IF(I.GT.J) THEN
          F(I,J,M,N)=F(J,I,N,M)
          GOTO 10
        ENDIF
        P=I-1
        Q=J-1
         D1=BETA(M)-BETA(N)
         D2=BETA(M)+BETA(N)
```

```
      D3=BETA(M)*BETA(M)+BETA(N)*BETA(N)
      D4=2*MOD(P+1,2)-1
      D5=2*MOD(Q+1,2)-1
      D6=THETA+P*PI/2.
      D7=THETA+Q*PI/2.
     IF(M.EQ.N) THEN
       D8=COS(D6-D7)
     ELSE
        D8=(SIN(D1+D6-D7)-SIN(D6-D7))/D1
     ENDIF
      D9=(SIN(D6+D7)-SIN(D2+D6+D7))/D2
      D10=D4*A*(BETA(N)*COS(D7)+BETA(M)*SIN(D7))
      D11=B(M)*(BETA(M)*SIN(BETA(N)+D7)-BETA(N)*COS(BETA(N)+D7))
      D12=D5*A*(BETA(M)*COS(D6)+BETA(N)*SIN(D6))
      D13=B(N)*(BETA(N)*SIN(BETA(M)+D6)-BETA(M)*COS(BETA(M)+D6))
      D14=(D4*D5*A*A+B(M)*B(N))/D2
      F(I,J,M,N)=(BETA(M)**P)*(BETA(N)**Q)*(D8+D9+D14+1.414213562
   &          *(D10+D11+D12+D13)/D3)
 10 CONTINUE
C
   RETURN
   END
C-----------------------------------------------
   SUBROUTINE INTGL1 (BETA,THETA,A,B,II,F)
   IMPLICIT REAL*4 (A-H,O-Z)
   INTEGER P,Q
C
   INCLUDE SFREQ.INC
C
   DIMENSION BETA(*),B(*),F(3,3,M1,*)
   WRITE (9,*) 'CALCULATING INTEGRALS OF BEAM FUNCTIONS'
   PI=3.141592654
   R2=1.414213562
   R3=1.732050808
   DO 10 I=1,3
    DO 10 J=1,3
     DO 20 M=1,2
      DO 20 N=1,II
       F(I,J,M,N)=0.
 20   CONTINUE
     DO 30 M=1,II
      DO 30 N=1,2
       F(I,J,M,N)=0.
 30   CONTINUE
     DO 10 M=3,II
      DO 10 N=3,II
```

```
      IF(I.GT.J) THEN
        F(I,J,M,N)=F(J,I,N,M)
        GOTO 10
      ENDIF
      P=I-1
      Q=J-1
       D1=BETA(M)-BETA(N)
       D2=BETA(M)+BETA(N)
       D3=BETA(M)*BETA(M)+BETA(N)*BETA(N)
       D4=2*MOD(P+1,2)-1
       D5=2*MOD(Q+1,2)-1
       D6=THETA+P*PI/2.
       D7=THETA+Q*PI/2.
      IF(M.EQ.N) THEN
        D8=COS(D6-D7)
      ELSE
        D8=(SIN(D1+D6-D7)-SIN(D6-D7))/D1
      ENDIF
       D9=(SIN(D6+D7)-SIN(D2+D6+D7))/D2
       D10=D4*A*(BETA(N)*COS(D7)+BETA(M)*SIN(D7))
       D11=B(M)*(BETA(M)*SIN(BETA(N)+D7)-BETA(N)*COS(BETA(N)+D7))
       D12=D5*A*(BETA(M)*COS(D6)+BETA(N)*SIN(D6))
       D13=B(N)*(BETA(N)*SIN(BETA(M)+D6)-BETA(M)*COS(BETA(M)+D6))
       D14=(D4*D5*A*A+B(M)*B(N))/D2
       F(I,J,M,N)=(BETA(M)**P)*(BETA(N)**Q)*(D8+D9+D14+R2*
     &        (D10+D11+D12+D13)/D3)
 10  CONTINUE
C
     DO 40 I=3,II
       D1=SIN(BETA(I)+THETA)+SIN(THETA)
       D2=SIN(BETA(I)+THETA)-SIN(THETA)
       D3=COS(BETA(I)+THETA)-COS(THETA)
       F(1,2,1,I)=R2*D2+B(I)-A
       F(2,1,I,1)=F(1,2,1,I)
       F(1,2,2,I)= R3*(-R2*D1-B(I)-A+2./BETA(I)*(-R2*D3+A+B(I)))
       F(2,1,I,2)=F(1,2,2,I)
       F(2,1,2,I)=2.*R3/BETA(I)*(R2*D3-A-B(I))
       F(1,2,I,2)=F(2,1,2,I)
       F(1,3,1,I)=BETA(I)*(R2*D3+A+B(I))
       F(3,1,I,1)=F(1,3,1,I)
       F(1,3,2,I)=R3*F(1,3,1,I)-2.*R3*(BETA(I)*(R2*COS(BETA(I)+
     &        THETA)+B(I))-R2*D2-B(I)+A)
       F(3,1,I,2)=F(1,3,2,I)
       F(2,3,2,I)=-2.*R3*BETA(I)*(R2*D3+A+B(I))
       F(3,2,I,2)=F(2,3,2,I)
       F(2,2,2,I)=2.*R3*(-R2*D2-B(I)+A)
```

```
      F(2,2,I,2)=F(2,2,2,I)
 40   CONTINUE
C
      F(1,1,1,1)=1.
      F(1,1,2,2)=1.
      F(1,2,1,2)=-2.*R3
      F(2,1,2,1)=-2.*R3
      F(2,2,2,2)=12.
C
      RETURN
      END
C-------------------------------------------------------
      SUBROUTINE MATRIX(MASS,STIFF,IX,IY,PSI,PHI)
      IMPLICIT REAL*4 (A-H,O-Z)
      REAL*4 MASS
C
      INCLUDE SFREQ.INC
C
      DIMENSION PHI(3,3,M2,M2),PSI(3,3,M1,M1)
      DIMENSION MASS(M3),STIFF(M4)
C
      COMMON /MATL/ TC,TF,RHOC,RHOF,A,B,D11,D12,D16,D22,D26,D66,
     &          A44,A45,A55,S
      H=TC+2.*TF
      RHO=RHOC/RHOF
      RT=TC/H
C
      WRITE (9,*) 'SETTING UP STIFFNESS MATRIX'
      II=IX*IY
      DO 10 I=1,II
       DO 10 J=1,II
        M=(I-1)/IY+1
        N=I-IY*(M-1)
        K=(J-1)/IY+1
        L=J-IY*(K-1)
C
C     KAC(I,J)=
       STIFF((J+2*II)*(J+2*II-1)/2+I)=
     & S*S*(A55*B*PSI(2,2,M,K)*PHI(1,1,N,L)
     & +A45*A*PSI(2,1,M,K)*PHI(1,2,N,L))
C
C     KAB(I,J)=
       STIFF((J+II)*(J+II-1)/2+I)=
     & D12*PSI(3,1,M,K)*PHI(1,3,N,L)
     & +D16*B/A*PSI(3,2,M,K)*PHI(1,2,N,L)
     & +D26*A/B*PSI(2,1,M,K)*PHI(2,3,N,L)
```

```
     & +D66*PSI(2,2,M,K)*PHI(2,2,N,L)
     & +S*S*A45*A*B*PSI(2,1,M,K)*PHI(1,2,N,L)
C
C     KBC(I,J)=
      STIFF((J+2*II)*(J+2*II-1)/2+I+II)=
     & S*S*(A45*B*PSI(1,2,M,K)*PHI(2,1,N,L)
     & +A44*A*PSI(1,1,M,K)*PHI(2,2,N,L))
C
      IF (I.GT.J) GOTO 10
C
C     KAA(I,J)=
      STIFF(J*(J-1)/2+I)=
     & D11*B/A*PSI(3,3,M,K)*PHI(1,1,N,L)
     & +D16*PSI(3,2,M,K)*PHI(1,2,N,L)
     & +D16*PSI(2,3,M,K)*PHI(2,1,N,L)
     & +D66*A/B*PSI(2,2,M,K)*PHI(2,2,N,L)
     & +S*S*A55*B*A*PSI(2,2,M,K)*PHI(1,1,N,L)
C
C     KBB(I,J)=
      STIFF((J+II)*(J+II-1)/2+I+II)=
     & D22*A/B*PSI(1,1,M,K)*PHI(3,3,N,L)
     & +D26*PSI(1,2,M,K)*PHI(3,2,N,L)
     & +D26*PSI(2,1,M,K)*PHI(2,3,N,L)
     & +D66/A*B*PSI(2,2,M,K)*PHI(2,2,N,L)
     & +S*S*A44*A*B*PSI(1,1,M,K)*PHI(2,2,N,L)
C
C     KCC(I,J)=
      STIFF((J+2*II)*(J+2*II-1)/2+I+2*II)=
     & S*S*(A55*B/A*PSI(2,2,M,K)*PHI(1,1,N,L)
     & +A44*A/B*PSI(1,1,M,K)*PHI(2,2,N,L)
     & +A45*PSI(2,1,M,K)*PHI(1,2,N,L)
     & +A45*PSI(1,2,M,K)*PHI(2,1,N,L))
C
 10   CONTINUE
C
      WRITE(9,*) 'SETTING UP MASS MATRIX'
      DO 30 I=1,II
       M=(I-1)/IY+1
       N=I-IY*(M-1)
C     MA(I)=
      MASS(I)=RHOF*H*H*H/12.*(1.-RT*RT*RT+RHO*RT*RT*RT)
     & *B*A*PSI(2,2,M,M)
C     MB(I)=
      MASS(II+I)=RHOF*H*H*H/12.*(1.-RT*RT*RT+RHO*RT*RT*RT)
     & *A*B*PHI(2,2,N,N)
C     MC(I)=
```

```
      MASS(2*II+I)=RHOF*H*(1.-RT+RHO*RT)*A*B
   30 CONTINUE
C
      RETURN
      END
C-----------------------------------------
      SUBROUTINE RCOND(MASS,STIFF,N,NLIST)
      IMPLICIT REAL*4(A-H,O-Z)
      REAL*4 MASS
C
      INCLUDE SFREQ.INC
C
      DIMENSION MASS(*),STIFF(*)
      DIMENSION H(M5)
      COMMON /INVSE/ WORK(M3),KP(M3),DET(2),INERT(3)
      N2=(N+NLIST)/3
      N1=N-N2
C
      WRITE(9,*) 'INVERTING K2'
      WRITE(9,*)
      CALL SSPFA(STIFF,N1,KP,INFO)
      CALL SSPDI(STIFF,N1,KP,DET,INERT,WORK,001)
C
      WRITE(9,*) 'K1T*K2-1*K1'
      WRITE(9,*)
      DO 10 J=1,N2
       WRITE(9,90) J
       DO 20 K=1,N1
        WORK(K)=0.
        DO 20 L=1,N1
         IF(K.LE.L) WORK(K)=WORK(K)+STIFF((L-1)*L/2+K)
     &               *STIFF((J+N1)*(J+N1-1)/2+L)
         IF(K.GT.L) WORK(K)=WORK(K)+STIFF((K-1)*K/2+L)
     &               *STIFF((J+N1)*(J+N1-1)/2+L)
   20   CONTINUE
        DO 30 I=J,N2
        DUM=0.
        DO 40 K=1,N1
         DUM=DUM+STIFF((I+N1)*(I+N1-1)/2+K)*WORK(K)
   40    CONTINUE
        H((I-1)*I/2+J)=DUM
   30   CONTINUE
   10  CONTINUE
C
       WRITE(9,*) 'CONDENSING STIFF'
       DO 50 I=1,N2
```

```
      DO 50 J=I,N2
       STIFF((J-1)*J/2+I)=
   &   STIFF((J+N1-1)*(J+N1)/2+I+N1)-H((J-1)*J/2+I)
 50    CONTINUE
C
      WRITE(9,*) 'CONDENSING MASS...'
      DO 60 I=1,N2
       MASS(I)=MASS(I+N1)
 60    CONTINUE
      N=N2
 90    FORMAT('+',I4)
C
      RETURN
      END
C-----------------------------------------------------------
      SUBROUTINE ARRAN(STIFF,MASS,N,NLIST)
      IMPLICIT REAL*4(A-H,O-Z)
      REAL*4 MASS
C
      INCLUDE SFREQ.INC
C
      DIMENSION STIFF(*),MASS(*),ILIST(M1)
C
      DO 5 I=1,N
       IF(MASS(I).EQ.0.) THEN
        NLIST=NLIST+1
        ILIST(NLIST)=I
       ENDIF
 5    CONTINUE
      WRITE(9,*)
      WRITE(9,*) 'NLIST=',NLIST
      DO 7 I=1,NLIST
       WRITE(9,*) 'ILIST(',I,')=',ILIST(I)
 7    CONTINUE
C
      WRITE(9,*) 'REARRANGING MASS'
      IND1=1
      I=1
      IDUM=ILIST(IND1)
 10   CONTINUE
      IF(I.EQ.IDUM) THEN
       IND1=IND1+1
       DO 20 J=I,N+1-IND1
        MASS(J)=MASS(J+1)
 20     CONTINUE
       DO 30 K=IND1,NLIST
```

```
      IDUM=ILIST(K)-1
30    CONTINUE
     I=I-1
    ENDIF
C
    IF(IND1.EQ.NLIST+1) THEN
     GOTO 15
    ENDIF
C
    I=I+1
    GOTO 10
C
 15  WRITE(9,*) 'REARRANGING STIFF'
    IND1=1
    IND2=1
    IND3=1
    IND4=1
    DO 40 I=1,N
     IF(I.EQ.ILIST(IND3)) THEN
      IND3=IND3+1
      IND2=IND2+I
      GOTO 40
     ENDIF
     DO 50 J=1,I
      IF(J.EQ.ILIST(IND4)) THEN
       IND2=IND2+1
       IND4=IND4+1
       GOTO 50
      ENDIF
      STIFF(IND1)=STIFF(IND2)
      IND1=IND1+1
      IND2=IND2+1
 50    CONTINUE
      IND4=1
 40   CONTINUE
C
    IF(IND1.EQ.NLIST+1) THEN
     GOTO 25
    ENDIF
C
    I=I+1
C
 25  CONTINUE
    N=N-NLIST
    RETURN
    END
```

```
C---------------------------------------
   SUBROUTINE QVECT(Q,IX,IY,IFC,PO,PX,PY,PA,PB)
   IMPLICIT REAL*4(A-H,O-Z)
   REAL Q(*)
C
   INCLUDE SFREQ.INC
C
   COMMON/COEFX/ XBETA(M1),XB(M1),XA,XTHETA
   COMMON/COEFY/ YBETA(M2),YB(M2),YA,YTHETA
   COMMON /MATL/ TC,TF,RHOC,RHOF,A,B,D11,D12,D16,D22,D26,D66,
  &        A44,A45,A55,S
   NN = 2*IX*IY
   DO 10 I=1,NN
    Q(I)=0.
10  CONTINUE
   IF(IFC.EQ.1) THEN
    DO 30 I=1,IX
     DO 20 J=1,IY
          QX=SQRT(2.)*SIN(XBETA(I)*PX/A+XTHETA)+XA*EXP(-XBETA(I)*
  &       PX/A)+XB(I)*EXP(-XBETA(I)*(1.-PX/A))
        QY=SQRT(2.)*SIN(YBETA(J)*PY/B+YTHETA)+YA*EXP(-YBETA(J)*
  &       PY/B)+YB(J)*EXP(-YBETA(J)*(1.-PY/B))
      Q(NN+IX*(I-1)+J)=QX*QY*PO
20     CONTINUE
30    CONTINUE
   ELSE
    DO 50 I=1,IX
     DO 40 J=1,IY
          QX1=XA*A/XBETA(I)*(EXP(-XBETA(I)*(PX-PA/2)/A)-
  &        EXP(-XBETA(I)*(PX+PA/2)/A))
          QX2=XB(I)*A/XBETA(I)*(EXP(-XBETA(I)*(1-(PX-PA/2)/A))-
  &        EXP(-XBETA(I)*(1-(PX+PA/2)/A)))
          QX3=SQRT(2.)*A/XBETA(I)*(COS(XBETA(I)*(PX-PA/2)/A+XTHETA)-
  &        COS(XBETA(I)*(PX+PA/2)/A+XTHETA))
          QY1=YA*B/YBETA(J)*(EXP(-YBETA(J)*(PY-PB/2)/B)-
  &        EXP(-YBETA(J)*(PY+PB/2)/B))
          QY2=YB(J)*B/YBETA(J)*(EXP(-YBETA(J)*(1-(PY-PB/2)/B))-
  &        EXP(-YBETA(J)*(1-(PY+PB/2)/B)))
          QY3=SQRT(2.)*B/YBETA(J)*(COS(YBETA(J)*(PY-PB/2)/B+YTHETA)-
  &        COS(YBETA(J)*(PY+PB/2)/B+YTHETA))
      Q(NN+IX*(I-1)+J)=(QX1-QX2+QX3)*(QY1-QY2+QY3)*PO
40     CONTINUE
50    CONTINUE
   ENDIF
   RETURN
   END
```

```
C*****************************************************************************
C
C THIS IS THE INCLUDE FILE FOR THE PROGRAM SFREQ.FOR
C
C*****************************************************************************
C
C  THE PARAMETERS USED IN DIMENSIONING THE ARRAYS ARE:
C
C     M1 = MAXIMUM NUMBER OF MODES IN X-DIRECTION
C     M2 = MAXIMUM NUMBER OF MODES IN Y-DIRECTION
C     M3 = (M1 * M2 * 3) + 1
C     M4 = (M3 * (M3 + 1)) / 2
C     M5 = (M1 * M2)*(M1 * M2 +1) / 2
C     M6 = (M1 * M2)
C
C-----------------------------------------------------
C     17 MODES(X) BY 17 MODES(Y):
C
      PARAMETER(M1 = 10, M2 = 10,
     &        M3 = (M1 * M2 * 3) + 1. ,
     &        M4 = (M3 * (M3 + 1)) / 2. ,
     &        M5 = (M1 * M2)*(M1 * M2 + 1.) / 2. ,
     &        M6 = (M1 * M2) )
C*****************************************************************************
```

Code Listing: Postprocessor to Rayleigh-Ritz

```
(* Written by R. J. Notestine - M.I.T. TELAC - 1991*)
(* Plots Natural Mode Shapes from Ritz Fortran Code *)
kk = 4;          (* number of modes to plot *)
OpenRead["FREQ.DAT"];
        l1 = Read["FREQ.DAT",Number] 1000;
        l2 = Read["FREQ.DAT",Number] 1000;
        nx = Read["FREQ.DAT",Number];
        ny = Read["FREQ.DAT",Number];
        ix = Read["FREQ.DAT",Number];
        iy = Read["FREQ.DAT",Number];
        ifc = Read["FREQ.DAT",Number];
        ifm = Read["FREQ.DAT",Number];
        evect = Table[0,{i,ix iy}, {j,ix iy}];
        xb = Table[0,{i,ix}];
        xbeta = Table[0,{i,ix}];
        yb = Table[0,{i,iy}];
        ybeta = Table[0,{i,iy}];
        xa = Read["FREQ.DAT",Number];
        xtheta = Read["FREQ.DAT",Number];
        ya = Read["FREQ.DAT",Number];
        ytheta = Read["FREQ.DAT",Number];
        Do[
                xb[[i]] = Read["FREQ.DAT",Number];
                xbeta[[i]] = Read["FREQ.DAT",Number];
        ,{i,ix}];
        Do[
                yb[[i]] = Read["FREQ.DAT",Number];
                ybeta[[i]] = Read["FREQ.DAT",Number];
        ,{i,iy}];
        Do[Read["FREQ.DAT",Number];,{2 (1+3 ifc) ix iy}];
        Do[
                evect[[i,j]] = Read["FREQ.DAT",Number];
        ,{i,ix iy},{j,(1-ix iy) ifc+ix iy}];
Close["FREQ.DAT"];
If[ifc == 0,
Do[
        f = Sum[evect[[k,ix(i-1)+j]] (Sqrt[2] Sin[xbeta[[i]] x/l1 +
        xtheta] + xa Exp[-xbeta[[i]] x/l1] + xb[[i]] Exp[-xbeta[[i]]*
        (1-x/l1)])*(Sqrt[2] Sin[ybeta[[j]] y/l2 + ytheta] +
        ya Exp[-ybeta[[j]] y/l2] + yb[[j]] Exp[-ybeta[[j]]*
        (1-y/l2)]),{i,ix},{j,iy}];
        ff = ContourPlot[f,{y,0,l2},{x,0,l1}];
```

```
        Show[ff,AspectRatio->l1/l2, Framed->True, Axes->None];
,{k,kk}],
f = Sum[evect[[ix(i-1)+j,1]] (Sqrt[2] Sin[xbeta[[i]] x/l1 +
        xtheta] + xa Exp[-xbeta[[i]] x/l1] + xb[[i]] Exp[-xbeta[[i]]*
        (1-x/l1)])*(Sqrt[2] Sin[ybeta[[j]] y/l2 + ytheta] +
        ya Exp[-ybeta[[j]] y/l2] + yb[[j]] Exp[-ybeta[[j]]*
        (1-y/l2)]),{i,ix},{j,iy}];
  (* Plot[f/.y->l2/2,{x,0,l1},AspectRatio->.75]; *)
  (* Plot[f/.x->l1/2,{y,0,l2},AspectRatio->.75]; *)
        100/{f/.{x->.5 l1, y->.5 l2},f/.{x->.5 l1,y->.6875 l2},f/.{x->.35 l1,y->.5 l2},f/.{x->.5 l1,
                y->.1875 l2},f/.{x->.8 l1, y->.5 l2}}//N]
```

Appendix G

Experimental Stiffness Regressions

This appendix contains the regressed stiffnesses, force per unit deflection (N/mm), for all the static tests. The stiffnesses represent the magnitude of force that must be applied, through the appropriate mechanism, to achieve one mm of deflection at the transducer location. A stiffness was regressed for each transducer location per test. Only the linear portions of each displacement curve were used in the regressions. Initial contact effects and any large deflection non-linearities were removed.

The regressed stiffnesses are labeled as K, and the goodness of fit values for the individual regressions are labeled as R. The average stiffness, calculated from the three specimens tested at each condition, is labeled as K Avg., and the maximum percentage deviation from the average stiffness is labeled as Dev. Only one aluminum plate was tested for each condition.

The regressed stiffness information for all the tests conducted in this study is contained in Tables G.1 through G.17. Three plates were accidentally tested in the incorrect orientation. These cases have been marked with an '*' and have not been included in the averages.

Table G.1 Experimental Stiffnesses for Centered Point Load (CL–CL)

Transducer		#1	#2	#3	#4	#5
A-1	K	382	621	537	1239	1169
	R	0.989	0.989	0.989	0.988	0.99
A-2	K	402	646	574	1361	1255
	R	0.991	0.989	0.991	0.99	0.991
A-3	K	383	611	552	1281	1251
	R	0.995	0.994	0.995	0.995	0.992
	K Avg.	389	625	554	1292	1224
	Dev.	0.03	0.03	0.03	0.05	0.05
B-1	K	303	470	396	902	792
	R	0.988	0.988	0.988	0.988	0.988
B-2	K	301	468	391	879	769
	R	0.988	0.988	0.988	0.989	0.988
B-3	K	295	459	388	901	755
	R	0.992	0.992	0.992	0.99	0.994
	K Avg.	299	466	392	894	772
	Dev.	0.02	0.01	0.01	0.02	0.03
C-1	K	652	969	890	1715	1792
	R	0.998	0.998	0.998	0.997	0.997
C-2	K	650	967	892	1709	1790
	R	0.997	0.997	0.998	0.997	0.997
C-3	K	618	922	844	1638	1696
	R	0.998	0.997	0.997	0.997	0.997
	K Avg.	639	952	875	1686	1758
	Dev.	0.04	0.03	0.04	0.03	0.04
D-1	K	438	644	615	1336	1224
	R	0.995	0.995	0.995	0.995	0.994
D-2	K	410	601	570	1193	1122
	R	0.995	0.995	0.994	0.994	0.993
D-3	K	403	590	566	1245	1162
	R	0.995	0.995	0.995	0.995	0.995
	K Avg.	416	611	583	1255	1168
	Dev.	0.05	0.05	0.05	0.06	0.05
I-2	K	633	917	845	1597	1758
	R	0.998	0.999	0.998	0.998	0.997

Table G.2 Experimental Stiffnesses for Centered Point Load (SS–SS)

Transducer		#1	#2	#3	#4	#5
A-1	K	203	271	254	445	448
	R	0.981	0.981	0.98	0.979	0.981
A-2	K	209	276	263	457	454
	R	0.984	0.683	0.984	0.983	0.98
A-3	K	227	306	288	505	503
	R	0.992	0.992	0.992	0.992	0.991
	K Avg.	213	284	267	468	467
	Dev.	0.06	0.07	0.07	0.07	0.07
B-1	K	181	239	219	385	347
	R	0.972	0.973	0.972	0.973	0.973
B-2	K	179	234	215	382	344
	R	0.97	0.968	0.969	0.968	0.967
B-3	K	163	207	196	343	318
	R	0.969	0.968	0.97	0.969	0.97
	K Avg.	174	226	209	369	336
	Dev.	0.07	0.09	0.07	0.08	0.06
C-1	K	403	520	510	829	843
	R	0.997	0.997	0.997	0.997	0.996
C-2	K	403	523	511	826	848
	R	0.995	0.995	0.995	0.996	0.995
C-3	K	419	540	531	875	868
	R	0.995	0.995	0.995	0.995	0.995
	K Avg.	408	528	517	843	853
	Dev.	0.03	0.02	0.03	0.04	0.02
D-1	K	216	276	265	431	402
	R	0.982	0.982	0.982	0.984	0.981
D-2	K	207	263	251	414	390
	R	0.982	0.982	0.982	0.981	0.981
D-3	K	222	283	269	450	441
	R	0.986	0.986	0.987	0.986	0.986
	K Avg.	215	274	261	431	410
	Dev.	0.04	0.04	0.04	0.04	0.07
I-2	K	323	414	401	628	650
	R	0.993	0.993	0.994	0.992	0.993

Table G.3 Experimental Stiffnesses for Off-Center Point Load (CL–CL)

Transducer		#1	#2	#3	#4	#5
A-1*	K	495	745	459	1497	1980
	R	0.981	0.981	0.981	0.978	0.982
A-2*	K	567	850	518	1642	2176
	R	0.986	0.985	0.984	0.983	0.985
A-3	K	921	1864	685	1168	4846
	R	0.994	0.995	0.994	0.994	0.981
	K Avg.	921	1864	685	1168	4846
B-1	K	496	885	440	851	1586
	R	0.988	0.986	0.989	0.987	0.983
B-2	K	480	833	422	831	1520
	R	0.996	0.996	0.996	0.996	0.996
B-3	K	470	836	417	770	1513
	R	0.989	0.989	0.989	0.989	0.986
	K Avg.	482	851	426	816	1539
	Dev.	0.03	0.04	0.03	0.06	0.03
C-1	K	1094	1705	856	2011	3695
	R	0.998	0.997	0.998	0.998	0.991
C-2	K	1033	1628	808	1899	3719
	R	0.998	0.998	0.998	0.997	0.997
C-3	K	1055	1613	816	2017	3726
	R	0.999	0.999	0.999	0.999	0.998
	K Avg.	1060	1648	826	1974	3713
	Dev.	0.03	0.03	0.03	0.04	0.01
D-1	K	820	1277	663	1650	3174
	R	0.993	0.993	0.993	0.993	0.989
D-2	K	738	1127	590	1411	3058
	R	0.994	0.995	0.994	0.995	0.989
D-3	K	777	1202	619	1621	3255
	R	0.994	0.993	0.993	0.993	0.991
	K Avg.	777	1198	622	1553	3160
	Dev.	0.05	0.06	0.06	0.10	0.03
I-2	K	1035	1177	1773	2703	1106
	R	0.998	0.998	0.998	0.997	0.998

Table G.4 Experimental Stiffnesses for Off-Center Point Load (SS–CL)

Transducer		#1	#2	#3	#4	#5
A-1	K	718	1312	518	983	2740
	R	0.996	0.996	0.996	0.997	0.993
A-2	K	708	1280	510	934	2667
	R	0.995	0.995	0.995	0.995	0.993
A-3	K	715	1300	518	926	2674
	R	0.995	0.994	0.995	0.995	0.989
	K Avg.	713	1297	515	947	2693
	Dev.	0.01	0.01	0.01	0.04	0.02
B-1	K	377	602	332	662	920
	R	0.99	0.99	0.99	0.989	0.988
B-2	K	355	568	316	644	854
	R	0.992	0.993	0.992	0.993	0.992
B-3	K	343	546	303	594	849
	R	0.994	0.994	0.994	0.994	0.994
	K Avg.	358	571	316	632	873
	Dev.	0.05	0.05	0.05	0.06	0.05
C-1	K	1013	1519	773	1817	3082
	R	0.996	0.994	0.995	0.994	0.993
C-2	K	988	1500	753	1825	2959
	R	0.995	0.994	0.995	0.995	0.991
C-3	K	1018	1554	773	1895	3148
	R	0.993	0.993	0.993	0.99	0.991
	K Avg.	1006	1524	766	1845	3061
	Dev.	0.02	0.02	0.02	0.03	0.03
D-1	K	657	978	510	1333	2194
	R	0.983	0.983	0.984	0.982	0.985
D-2	K	596	875	451	1108	2078
	R	0.993	0.992	0.993	0.992	0.983
D-3	K	605	889	458	1193	2056
	R	0.98	0.976	0.98	0.98	0.974
	K Avg.	618	912	472	1204	2108
	Dev.	0.06	0.07	0.07	0.10	0.04
I-2	K	981	1439	736	1842	3325
	R	0.999	0.999	0.999	0.999	0.997

Table G.5 Experimental Stiffnesses for Off-Center Point Load (SS–SS)

Transducer		#1	#2	#3	#4	#5
A-1	K	379	570	320	468	1057
	R	0.991	0.991	0.991	0.991	0.99
A-2	K	407	612	339	495	1103
	R	0.991	0.992	0.992	0.992	0.992
A-3	K	423	643	352	516	1155
	R	0.992	0.993	0.993	0.993	0.993
	K Avg.	402	607	337	492	1103
	Dev.	0.06	0.06	0.05	0.05	0.04
B-1	K	258	362	242	383	559
	R	0.981	0.981	0.981	0.982	0.98
B-2	K	245	343	230	365	521
	R	0.977	0.976	0.977	0.976	0.977
B-3	K	236	319	223	360	499
	R	0.985	0.986	0.985	0.985	0.984
	K Avg.	246	340	231	369	525
	Dev.	0.05	0.07	0.04	0.04	0.06
C-1	K	670	900	570	1032	1611
	R	0.998	0.998	0.998	0.997	0.997
C-2	K	675	906	567	1026	1632
	R	0.997	0.997	0.997	0.997	0.997
C-3	K	666	897	563	1025	1582
	R	0.998	0.997	0.998	0.998	0.996
	K Avg.	670	901	567	1028	1608
	Dev.	0.01	0.01	0.01	0.00	0.02
D-1	K	323	421	292	518	719
	R	0.989	0.988	0.988	0.988	0.987
D-2	K	331	432	297	526	735
	R	0.983	0.983	0.982	0.983	0.982
D-3	K	311	405	276	501	731
	R	0.984	0.984	0.984	0.983	0.984
	K Avg.	322	419	288	515	728
	Dev.	0.03	0.03	0.04	0.03	0.01
I-2	K	544	713	478	859	1344
	R	0.996	0.996	0.996	0.996	0.996

Table G.6 Experimental Stiffnesses for Off-Center Point Load (FR–CL)

Transducer		#1	#2	#3	#4
A-1	K	555	1112	349	786
	R	0.984	0.986	0.986	0.982
A-2	K	521	1026	328	741
	R	0.982	0.985	0.983	0.985
A-3*	K	209	320	1561	282
	R	0.975	0.969	0.974	0.969
	K Avg.	538	1069	339	764
	Dev.	0.03	0.04	0.03	0.03
B-1	K	326	511	248	672
	R	0.954	0.953	0.953	0.949
B-2	K	288	457	222	602
	R	0.983	0.981	0.981	0.983
B-3	K	303	486	230	634
	R	0.965	0.961	0.965	0.963
	K Avg.	305	484	233	634
	Dev.	0.06	0.06	0.06	0.06
C-1	K	749	1131	544	1515
	R	0.996	0.996	0.996	0.995
C-2	K	745	1123	553	1498
	R	0.998	0.998	0.998	0.997
C-3	K	715	1082	523	1419
	R	0.996	0.996	0.996	0.994
	K Avg.	736	1112	540	1476
	Dev.	0.03	0.03	0.03	0.04
D-1	K	644	985	441	1361
	R	0.991	0.993	0.992	0.99
D-2	K	597	885	410	1265
	R	0.991	0.992	0.993	0.993
D-3	K	609	901	420	1313
	R	0.991	0.991	0.991	0.988
	K Avg.	616	922	423	1312
	Dev.	0.04	0.06	0.04	0.04
I-2	K	908	1288	645	1808
	R	0.997	0.997	0.998	0.994

Table G.7 Experimental Stiffnesses for Off-Center Point Load (FR–SS)

Transducer		#1	#2	#3	#4
A-1	K	169	258	126	219
	R	0.98	0.98	0.98	0.98
A-2	K	170	259	128	220
	R	0.976	0.977	0.977	0.977
A-3	K	163	251	123	212
	R	0.992	0.992	0.992	0.992
	K Avg.	167	256	125	217
	Dev.	0.02	0.02	0.02	0.02
B-1	K	81	106	70	134
	R	0.976	0.976	0.976	0.975
B-2	K	79	102	68	129
	R	0.974	0.974	0.974	0.973
B-3	K	81	105	70	133
	R	0.979	0.979	0.98	0.979
	K Avg.	80	104	69	132
	Dev.	0.02	0.02	0.02	0.02
C-1	K	230	295	199	382
	R	0.994	0.994	0.994	0.993
C-2	K	226	291	194	372
	R	0.994	0.994	0.994	0.994
C-3	K	221	285	191	368
	R	0.099	0.993	0.993	0.993
	K Avg.	226	290	194	374
	Dev.	0.02	0.02	0.02	0.02
D-1	K	193	249	150	319
	R	0.992	0.992	0.991	0.991
D-2	K	181	231	140	298
	R	0.985	0.985	0.985	0.984
D-3	K	178	227	138	298
	R	0.989	0.989	0.989	0.989
	K Avg.	184	235	142	305
	Dev.	0.05	0.05	0.05	0.04
I-2	K	315	402	254	521
	R	0.996	0.996	0.996	0.996

Table G.8 Experimental Stiffnesses for Centered URPP (CL–CL)

Transducer		#1	#2	#3	#4	#5
A-1	K	440	639	560	1277	1250
	R	0.997	0.997	0.997	0.997	0.997
A-2	K	460	664	589	1311	1328
	R	0.996	0.996	0.995	0.995	0.995
A-3	K	465	657	596	1293	1319
	R	0.997	0.997	0.997	0.997	0.995
	K Avg.	455	653	581	1294	1298
	Dev.	0.03	0.02	0.04	0.01	0.04
B-1	K	355	502	447	953	848
	R	0.993	0.994	0.994	0.993	0.992
B-2	K	347	489	439	919	807
	R	0.994	0.994	0.995	0.993	0.993
B-3	K	324	465	395	815	819
	R	0.985	0.984	0.984	0.984	0.983
	K Avg.	341	485	426	892	824
	Dev.	0.05	0.04	0.08	0.09	0.03
C-1	K	734	976	950	1780	1681
	R	0.997	0.997	0.997	0.997	0.992
C-2	K	718	978	926	1718	1781
	R	0.997	0.997	0.997	0.998	0.997
C-3	K	699	936	888	1721	1684
	R	0.996	0.995	0.996	0.996	0.995
	K Avg.	717	963	921	1739	1714
	Dev.	0.03	0.03	0.04	0.02	0.04
D-1	K	496	680	644	1301	1201
	R	0.998	0.998	0.998	0.998	0.997
D-2	K	455	608	584	1083	962
	R	0.995	0.995	0.996	0.992	0.995
D-3	K	469	633	595	1225	1145
	R	0.994	0.993	0.994	0.993	0.992
	K Avg.	473	639	607	1196	1093
	Dev.	0.05	0.06	0.06	0.10	0.14
I-2	K	733	979	934	1838	1783
	R	0.997	0.997	0.997	0.997	0.995

Table G.9 Experimental Stiffnesses for Centered URPP (SS–SS)

Transducer		#1	#2	#3	#4	#5
A-1	K	232	290	276	472	473
	R	0.981	0.98	0.98	0.98	0.982
A-2	K	252	319	300	516	508
	R	0.987	0.987	0.986	0.986	0.986
A-3	K	236	298	281	482	487
	R	0.986	0.985	0.986	0.986	0.985
	K Avg.	240	302	285	489	489
	Dev.	0.05	0.05	0.05	0.05	0.04
B-1	K	210	266	244	411	385
	R	0.971	0.97	0.97	0.971	0.97
B-2	K	194	241	223	381	356
	R	0.967	0.967	0.968	0.967	0.968
B-3	K	173	213	202	341	318
	R	0.974	0.974	0.974	0.974	0.971
	K Avg.	191	238	222	376	351
	Dev.	0.10	0.12	0.10	0.10	0.10
C-1	K	454	561	542	875	861
	R	0.995	0.995	0.994	0.994	0.995
C-2	K	455	562	541	854	876
	R	0.996	0.996	0.996	0.996	0.995
C-3	K	449	552	533	870	843
	R	0.996	0.996	0.996	0.995	0.996
	K Avg.	452	558	539	866	860
	Dev.	0.01	0.01	0.01	0.01	0.02
D-1	K	235	288	274	444	403
	R	0.985	0.985	0.985	0.984	0.984
D-2	K	243	297	283	460	428
	R	0.982	0.982	0.982	0.983	0.983
D-3	K	235	287	274	449	427
	R	0.988	0.988	0.987	0.989	0.986
	K Avg.	238	291	277	451	419
	Dev.	0.02	0.02	0.02	0.02	0.04
I-2	K	384	479	458	725	744
	R	0.993	0.992	0.993	0.992	0.993

Table G.10 Experimental Stiffnesses for Off-Center URPP (CL–CL)

Transducer		#1	#2	#3	#4	#5
A-1	K	956	1854	750	1306	4791
	R	0.997	0.997	0.997	0.996	0.981
A-2	K	915	1751	713	1208	4473
	R	0.996	0.996	0.997	0.996	0.993
A-3	K	977	1846	761	1278	4836
	R	0.998	0.997	0.998	0.998	0.993
	K Avg.	949	1816	741	1262	4694
	Dev.	0.04	0.04	0.04	0.05	0.05
B-1	K	588	1008	544	976	1914
	R	0.997	0.997	0.997	0.997	0.996
B-2	K	581	995	537	981	1861
	R	0.998	0.998	0.998	0.997	0.997
B-3	K	558	961	504	921	1793
	R	0.999	0.998	0.998	0.999	0.998
	K Avg.	575	988	527	959	1855
	Dev.	0.03	0.03	0.05	0.04	0.03
C-1	K	1198	1869	1007	2121	4422
	R	0.998	0.996	0.997	0.997	0.989
C-2	K	1191	1847	990	2085	4470
	R	0.996	0.996	0.996	0.997	0.993
C-3	K	1140	1736	941	2036	4007
	R	0.998	0.998	0.998	0.998	0.997
	K Avg.	1176	1816	978	2080	4289
	Dev.	0.03	0.05	0.04	0.02	0.07
D-1	K	863	1324	725	1658	3187
	R	0.998	0.998	0.998	0.998	0.995
D-2	K	727	1100	616	1344	2373
	R	0.998	0.998	0.998	0.998	0.997
D-3	K	774	1198	650	1511	3014
	R	0.996	0.995	0.996	0.995	0.994
	K Avg.	784	1201	661	1494	2811
	Dev.	0.09	0.09	0.09	0.11	0.18
I-2	K	950	1852	737	1293	4891
	R	0.992	0.991	0.991	0.991	0.968

Table G.11 Experimental Stiffnesses for Off-Center URPP (SS–CL)

Transducer		#1	#2	#3	#4	#5
A-1	K	734	1335	558	1069	2732
	R	0.995	0.996	0.995	0.995	0.992
A-2	K	703	1248	543	1028	2536
	R	0.998	0.998	0.998	0.998	0.996
A-3	K	728	1296	563	1035	2659
	R	0.994	0.994	0.994	0.994	0.994
	K Avg.	722	1292	555	1044	2640
	Dev.	0.03	0.04	0.02	0.02	0.04
B-1	K	379	591	343	673	887
	R	0.991	0.991	0.991	0.99	0.99
B-2	K	377	589	342	683	889
	R	0.995	0.995	0.995	0.995	0.994
B-3	K	361	569	328	625	877
	R	0.991	0.991	0.991	0.991	0.989
	K Avg.	372	583	338	659	884
	Dev.	0.03	0.02	0.03	0.05	0.01
C-1	K	1061	1569	859	1897	3039
	R	0.994	0.992	0.994	0.992	0.995
C-2	K	1006	1524	820	1884	2881
	R	0.996	0.996	0.995	0.994	0.993
C-3	K	1030	1540	834	1893	2902
	R	0.996	0.997	0.997	0.996	0.988
	K Avg.	1032	1544	837	1891	2939
	Dev.	0.03	0.02	0.03	0.00	0.03
D-1	K	661	957	533	1307	2040
	R	0.996	0.996	0.996	0.996	0.995
D-2	K	619	911	497	1161	1945
	R	0.997	0.997	0.997	0.997	0.997
D-3	K	611	898	491	1216	2008
	R	0.996	0.997	0.996	0.996	0.995
	K Avg.	630	921	506	1225	1997
	Dev.	0.05	0.04	0.05	0.06	0.03
I-2	K	1017	1490	811	1941	3397
	R	0.997	0.998	0.997	0.997	0.998

Table G.12 Experimental Stiffnesses for Off-Center URPP (SS–SS)

Transducer		#1	#2	#3	#4	#5
A-1	K	394	590	342	505	1071
	R	0.996	0.996	0.996	0.996	0.996
A-2	K	418	615	362	530	1111
	R	0.996	0.996	0.996	0.995	0.995
A-3	K	424	632	366	540	1162
	R	0.992	0.991	0.992	0.991	0.993
	K Avg.	412	612	357	525	1113
	Dev.	0.04	0.04	0.04	0.04	0.04
B-1	K	278	391	265	409	596
	R	0.985	0.985	0.984	0.985	0.986
B-2	K	258	359	247	380	552
	R	0.99	0.99	0.99	0.99	0.988
B-3	K	257	357	247	378	542
	R	0.989	0.99	0.99	0.989	0.99
	K Avg.	264	368	253	388	563
	Dev.	0.05	0.06	0.05	0.05	0.06
C-1	K	671	898	590	1018	1554
	R	0.998	0.997	0.998	0.997	0.996
C-2	K	681	920	597	1025	1647
	R	0.998	0.998	0.998	0.997	0.998
C-3	K	655	880	577	1001	1530
	R	0.997	0.997	0.998	0.997	0.996
	K Avg.	669	899	588	1015	1575
	Dev.	0.02	0.02	0.02	0.01	0.04
D-1	K	337	442	314	539	728
	R	0.986	0.985	0.986	0.984	0.986
D-2	K	319	417	294	505	680
	R	0.987	0.988	0.987	0.987	0.986
D-3	K	324	420	294	516	728
	R	0.994	0.995	0.995	0.995	0.994
	K Avg.	326	426	300	520	711
	Dev.	0.03	0.04	0.04	0.04	0.05
I-2	K	543	701	495	862	1240
	R	0.997	0.996	0.996	0.996	0.995

Table G.13 Experimental Stiffnesses for Off-Center URPP (FR–CL)

Transducer		#1	#2	#3	#4
A-1	K	537	1064	348	798
	R	0.998	0.998	0.998	0.998
A-2	K	513	1020	338	771
	R	0.996	0.995	0.996	0.996
A-3	K	524	1045	345	769
	R	0.998	0.997	0.998	0.998
	K Avg.	525	1043	344	779
	Dev.	0.02	0.02	0.02	0.02
B-1	K	291	450	227	595
	R	0.997	0.997	0.997	0.997
B-2	K	286	445	224	591
	R	0.996	0.996	0.996	0.996
B-3	K	280	433	220	580
	R	0.996	0.996	0.996	0.996
	K Avg.	286	443	223	588
	Dev.	0.02	0.02	0.02	0.01
C-1	K	784	1165	589	1624
	R	0.998	0.997	0.998	0.997
C-2	K	771	1154	580	1550
	R	0.996	0.995	0.996	0.997
C-3	K	786	1174	588	1648
	R	0.995	0.995	0.996	0.995
	K Avg.	780	1164	586	1606
	Dev.	0.01	0.01	0.01	0.04
D-1	K	653	968	449	1385
	R	0.994	0.994	0.994	0.993
D-2	K	597	879	415	1248
	R	0.998	0.998	0.999	0.998
D-3	K	611	900	425	1311
	R	0.996	0.996	0.996	0.995
	K Avg.	619	914	429	1312
	Dev.	0.05	0.06	0.04	0.05
I-2	K	959	1406	699	1875
	R	0.997	0.997	0.998	0.997

Table G.14 Experimental Stiffnesses for Off-Center URPP (FR–SS)

Transducer		#1	#2	#3	#4
A-1	K	169	255	128	224
	R	0.988	0.989	0.988	0.988
A-2	K	166	251	127	221
	R	0.989	0.99	0.989	0.989
A-3	K	189	285	144	249
	R	0.976	0.976	0.976	0.976
	K Avg.	174	263	133	231
	Dev.	0.08	0.08	0.08	0.07
B-1	K	88	114	77	144
	R	0.981	0.981	0.981	0.981
B-2	K	90	116	78	145
	R	0.981	0.981	0.981	0.981
B-3	K	89	115	78	146
	R	0.971	0.971	0.97	0.97
	K Avg.	89	115	78	145
	Dev.	0.01	0.01	0.01	0.01
C-1	K	230	295	201	379
	R	0.995	0.995	0.995	0.995
C-2	K	222	285	193	361
	R	0.996	0.996	0.996	0.997
C-3	K	224	285	194	373
	R	0.995	0.995	0.995	0.995
	K Avg.	225	288	196	371
	Dev.	0.02	0.02	0.02	0.03
D-1	K	205	261	163	344
	R	0.996	0.996	0.995	0.995
D-2	K	189	241	151	315
	R	0.999	0.999	0.999	0.998
D-3	K	190	241	151	318
	R	0.997	0.997	0.997	0.997
	K Avg.	195	247	155	325
	Dev.	0.05	0.05	0.05	0.05
I-2	K	350	449	285	570
	R	0.981	0.981	0.983	0.981

Table G.15 Experimental Stiffnesses for Uniform Pressure (CL–CL)

Transducer		#1	#2	#3	#4	#5
A-1	K	1519	1920	1743	3140	2839
	R	0.999	0.999	0.999	0.997	0.999
A-2	K	1553	1978	1838	3140	3040
	R	0.999	0.999	0.998	0.998	0.999
A-3	K	1623	2056	1924	3374	3192
	R	0.999	0.999	0.999	0.999	0.999
	K Avg.	1564	1983	1832	3214	3017
	Dev.	0.04	0.04	0.05	0.05	0.06
B-1	K	1226	1523	1434	2526	2344
	R	0.999	0.999	0.999	0.999	0.999
B-2	K	1185	1464	1409	2479	2344
	R	0.999	0.999	0.999	0.999	0.999
B-3	K	1147	1425	1378	2234	2211
	R	0.999	0.999	0.999	0.998	0.998
	K Avg.	1185	1470	1406	2406	2298
	Dev.	0.03	0.03	0.02	0.08	0.04
C-1	K	2331	2834	2663	4792	4096
	R	0.999	0.999	0.999	0.999	0.999
C-2	K	2288	2951	2541	4540	4106
	R	0.999	0.999	0.999	0.999	0.999
C-3	K	2273	2731	2587	4833	4058
	R	0.999	0.999	0.999	0.999	0.999
	K Avg.	2297	2836	2596	4718	4087
	Dev.	0.01	0.04	0.03	0.04	0.01
D-1	K	1560	1944	1752	3555	2946
	R	0.999	0.997	0.998	0.999	0.997
D-2	K	1437	1819	1637	3072	2731
	R	0.999	0.999	0.999	0.998	0.999
D-3	K	1509	1866	1710	3414	2748
	R	0.999	0.999	0.999	0.999	0.999
	K Avg.	1500	1875	1698	3334	2805
	Dev.	0.04	0.04	0.04	0.09	0.05
I-2	K	2200	2722	2440	4469	3973
	R	0.998	0.998	0.998	0.999	0.999

Table G.16 Experimental Stiffnesses for Uniform Pressure (SS–CL)

Transducer		#1	#2	#3	#4	#5
A-1	K	1198	1497	1330	2779	2096
	R	0.999	0.999	0.999	0.999	0.999
A-2	K	1212	1520	1322	2692	2098
	R	0.998	0.998	0.999	0.999	0.998
A-3	K	1258	1563	1359	2663	2075
	R	0.999	0.999	0.999	0.999	0.999
	K Avg.	1222	1526	1337	2711	2090
	Dev.	0.03	0.02	0.02	0.02	0.01
B-1	K	881	1087	971	1870	1400
	R	0.999	0.999	0.999	0.999	0.999
B-2	K	914	1118	998	1860	1482
	R	0.999	0.999	0.999	0.996	0.999
B-3	K	842	1073	947	1777	1378
	R	0.999	0.999	0.999	0.999	0.999
	K Avg.	878	1092	972	1835	1418
	Dev.	0.04	0.02	0.03	0.03	0.04
C-1	K	1942	2396	2140	3823	3094
	R	0.999	0.999	0.999	0.999	0.999
C-2	K	1998	2501	2164	4010	3163
	R	0.999	0.999	0.999	0.999	0.999
C-3	K	2022	2479	2098	4156	3111
	R	0.997	0.998	0.998	0.999	0.999
	K Avg.	1987	2458	2134	3992	3123
	Dev.	0.02	0.03	0.02	0.04	0.01
D-1	K	1333	1687	1446	2858	2019
	R	0.999	0.999	0.999	0.999	0.999
D-2	K	1257	1564	1342	2692	1878
	R	0.999	0.999	0.998	0.998	0.998
D-3	K	1323	1665	1430	2935	2021
	R	0.999	0.999	0.999	0.999	0.999
	K Avg.	1303	1637	1404	2825	1971
	Dev.	0.04	0.05	0.05	0.05	0.05
I-2	K	1924	2370	2129	4010	2906
	R	0.999	0.999	0.999	0.998	0.999

Table G.17 Experimental Stiffnesses for Uniform Pressure (SS–SS)

Transducer		#1	#2	#3	#4	#5
A-1	K	715	838	786	1224	1198
	R	0.999	0.999	0.999	0.999	0.999
A-2	K	740	863	824	1252	1212
	R	0.999	0.999	0.999	0.999	0.999
A-3	K	730	853	814	1278	1232
	R	0.999	0.999	0.999	0.999	0.999
	K Avg.	728	851	808	1251	1214
	Dev.	0.02	0.02	0.03	0.02	0.01
B-1	K	638	729	700	1008	991
	R	0.997	0.998	0.997	0.998	0.998
B-2	K	659	753	715	1032	1019
	R	0.998	0.998	0.998	0.999	0.998
B-3	K	600	699	666	961	956
	R	0.996	0.996	0.996	0.997	0.996
	K Avg.	631	726	693	999	988
	Dev.	0.05	0.04	0.04	0.04	0.03
C-1	K	1171	1360	1268	1895	1800
	R	0.999	0.999	0.999	0.999	0.999
C-2	K	1277	1462	1368	2111	1912
	R	0.999	0.999	0.999	0.999	0.999
C-3	K	1194	1427	1314	1982	1862
	R	0.999	0.999	0.999	0.999	0.999
	K Avg.	1212	1415	1315	1992	1857
	Dev.	0.05	0.04	0.04	0.06	0.03
D-1	K	700	814	767	1180	1067
	R	0.996	0.997	0.997	0.998	0.998
D-2	K	675	792	744	1139	1052
	R	0.997	0.998	0.998	0.998	0.999
D-3	K	711	825	772	1192	1097
	R	0.997	0.997	0.997	0.997	0.998
	K Avg.	695	810	761	1170	1072
	Dev.	0.03	0.02	0.02	0.03	0.02
I-2	K	1060	1241	1164	1856	1672
	R	0.999	0.999	0.999	0.999	0.999

Appendix H
Analytical Stiffnesses

This appendix contains the stiffnesses, force per unit deflection (N/mm), obtained from the Navier and constrained Navier, Rayleigh-Ritz, and potential function analyses for the first three boundary conditions: CL–CL, SS–CL, and SS–SS. The stiffness represents the magnitude of force that must be applied, through the appropriate mechanism, to achieve one mm of deflection at the point of interest. The stiffnesses have been calculated at five points which correspond to the five points at which transducer measurements were taken in the laboratory tests.

The Navier and constrained Navier stiffnesses in Tables H.1 through H.5 are based on 50 modes in directions with constrained, clamped boundary conditions and 9 modes in directions with simply supported boundary conditions. This results in 2500, 450, and 81 modes for the three boundary conditions, CL–CL, SS–CL, and SS–SS respectively. The Navier analyses do not include bending-twisting coupling.

The Rayleigh-Ritz stiffnesses in Tables H.6 through H.10 are based on the 81 mode Rayleigh-Ritz solution discussed in Chapter 4, which includes bending-twisting coupling.

The stiffnesses from the polynomial potential functions are listed in Tables H.11 through H.13. These polynomial functions were also discussed in Chapter 4.

Table H.1 Navier Stiffnesses for Centered Point Load Cases

B. C.'s	Spec.	Stiffnesses (N/mm) for Points of Interest #1	#2	#3	#4	#5
CL – CL	A	557	913	801	1990	1860
	B	335	574	469	1310	1090
	C	768	1210	1110	2610	2590
	D	492	812	727	1830	1800
	I	728	1160	1070	2580	2650
SS – SS	A	309	417	385	671	649
	B	161	218	194	353	317
	C	444	593	563	949	976
	D	215	282	264	444	438
	I	346	453	430	715	731

Table H.2 Navier Stiffnesses for Off–Center Point Load Cases

B. C.'s	Spec.	Stiffnesses (N/mm) for Points of Interest #1	#2	#3	#4	#5
CL – CL	A	1200	2130	954	2570	5230
	B	709	1400	625	1440	2870
	C	1670	2880	1230	3710	7590
	D	1090	1860	838	2470	5920
	I	1610	2710	1180	3710	9050
SS–CL	A	892	1500	695	2020	2830
	B	417	718	362	934	1100
	C	1380	2300	996	3170	4800
	D	829	1350	607	1980	3400
	I	1310	2140	919	3140	5700
SS – SS	A	490	694	434	776	1190
	B	245	358	233	381	539
	C	724	1010	608	1150	1880
	D	329	441	296	534	793
	I	542	729	468	880	1390

Table H.3 Navier Stiffnesses for Centered URPP Cases

		Stiffnesses (N/mm) for Points of Interest				
B. C.'s	Spec.	#1	#2	#3	#4	#5
CL – CL	A	670	990	869	2120	1950
	B	402	613	516	1370	1160
	C	915	1330	1200	2820	2700
	D	594	884	785	1940	1870
	I	868	1280	1150	2770	2740
SS – SS	A	344	441	407	701	675
	B	177	229	206	366	332
	C	495	632	594	1000	1010
	D	236	297	278	465	455
	I	381	480	453	751	756

Table H.4 Navier Stiffnesses for Off–Center URPP Cases

		Stiffnesses (N/mm) for Points of Interest				
B. C.'s	Spec.	#1	#2	#3	#4	#5
CL – CL	A	1250	2180	1050	2680	5280
	B	746	1420	681	1520	2930
	C	1730	2930	1370	3830	7630
	D	1140	1920	930	2590	5810
	I	1670	2790	1310	3850	8840
SS–CL	A	934	1540	759	2110	2870
	B	441	743	391	990	1140
	C	1430	2350	1100	3270	4850
	D	868	1400	667	2080	3350
	I	1360	2210	1010	3260	5590
SS – SS	A	512	717	465	810	1230
	B	257	370	248	400	558
	C	752	1040	657	1200	1920
	D	344	459	317	560	814
	I	565	757	504	919	1420

Table H.5 Navier Stiffnesses for Uniform Pressure Cases

B. C.'s	Spec.	Stiffnesses (N/mm) for Points of Interest #1	#2	#3	#4	#5
CL – CL	A	2520	3280	2940	6090	5360
	B	1530	1980	1820	3640	3520
	C	3460	4530	3960	8500	6880
	D	2290	3050	2690	5880	5030
	I	3350	4450	3890	8610	7030
SS–CL	A	1830	2420	2010	4600	2890
	B	874	1160	969	2210	1420
	C	2790	3690	3040	7050	4270
	D	1700	2290	1860	4510	2650
	I	2670	3580	2910	7040	4080
SS – SS	A	912	1080	1010	1580	1490
	B	462	546	515	797	766
	C	1340	1580	1480	2320	2150
	D	609	726	676	1070	1000
	I	999	1190	1110	1760	1620

Table H.6 Rayleigh-Ritz Stiffnesses for Centered Point Load Cases

		Stiffnesses (N/mm) for Points of Interest				
B. C.'s	Spec.	#1	#2	#3	#4	#5
CL – CL	A	435	752	640	1830	1680
	B	329	546	449	1220	1020
	C	755	1180	1080	2480	2460
	D	478	769	689	1690	1660
	I	705	1110	1020	2400	2460
SS – SS	A	229	320	291	545	525
	B	161	218	194	353	316
	C	444	593	563	949	976
	D	215	282	264	444	438
	I	346	453	430	715	731

Table H.7 Rayleigh-Ritz Stiffnesses for Off–Center Point Load Cases

		Stiffnesses (N/mm) for Points of Interest				
B. C.'s	Spec.	#1	#2	#3	#4	#5
CL – CL	A	1270	2870	865	1650	8150
	B	675	1320	593	1300	2610
	C	1590	2700	1180	3430	6780
	D	1010	1700	788	2240	5030
	I	1500	2490	1110	3370	7710
SS–CL	A	897	1900	604	1290	4170
	B	409	698	354	866	1080
	C	1330	2190	971	2970	4540
	D	790	1260	584	1830	3130
	I	1250	2010	886	2910	5250
SS – SS	A	439	712	357	529	1310
	B	247	363	234	377	546
	C	724	1010	608	1150	1880
	D	329	441	296	534	793
	I	542	729	468	879	1390

Table H.8 Rayleigh-Ritz Stiffnesses for Centered URPP Cases

		Stiffnesses (N/mm) for Points of Interest				
B. C.'s	Spec.	#1	#2	#3	#4	#5
CL – CL	A	519	808	693	1910	1730
	B	385	582	492	1270	1090
	C	891	1290	1160	2680	2560
	D	567	836	744	1800	1730
	I	833	1220	1100	2580	2550
SS – SS	A	256	337	308	566	544
	B	177	229	206	366	331
	C	495	632	594	1000	1010
	D	236	297	278	465	455
	I	381	480	453	751	756

Table H.9 Rayleigh-Ritz Stiffnesses for Off–Center URPP Cases

		Stiffnesses (N/mm) for Points of Interest				
B. C.'s	Spec.	#1	#2	#3	#4	#5
CL – CL	A	1240	2680	911	1820	7310
	B	835	1560	726	1620	3220
	C	1650	2750	1310	3530	6820
	D	1050	1750	872	2350	4970
	I	1560	2560	1240	3500	7590
SS–CL	A	893	1830	640	1420	3850
	B	482	799	411	1030	1280
	C	1380	2240	1070	3070	4590
	D	826	1310	640	1920	3090
	I	1300	2070	976	3030	5160
SS – SS	A	447	713	377	570	1300
	B	287	412	269	440	636
	C	752	1040	657	1200	1920
	D	344	459	317	560	814
	I	565	757	504	919	1420

Table H.10 Rayleigh-Ritz Stiffnesses for Uniform Pressure Cases

		Stiffnesses (N/mm) for Points of Interest				
B. C.'s	Spec.	#1	#2	#3	#4	#5
CL – CL	A	2040	2720	2420	5310	4660
	B	1440	1850	1700	3350	3240
	C	3300	4290	3770	7920	6460
	D	2130	2820	2500	5360	4610
	I	3140	4150	3630	7880	6480
SS–CL	A	1480	2010	1650	4010	2470
	B	845	1110	936	2090	1370
	C	2700	3550	2950	6680	4150
	D	1630	2180	1780	4210	2540
	I	2560	3410	2790	6590	3910
SS – SS	A	710	854	798	1290	1220
	B	461	545	514	796	765
	C	1340	1580	1480	2320	2150
	D	609	726	676	1070	1000
	I	999	1190	1110	1760	1620

Table H.11 Potential Function Stiffnesses for Centered Point Load Cases

B. C.'s	Spec.	Stiffnesses (N/mm) for Points of Interest #1	#2	#3	#4	#5
CL – CL	A	797	1300	1230	3900	6160
	B	571	901	931	2540	6150
	C	975	1520	1240	4200	3190
	D	663	1100	980	3500	4190
	I	901	1420	1180	4030	3250
SS – SS	A	360	432	404	647	611
	B	183	220	205	329	311
	C	524	630	588	942	891
	D	242	291	271	435	411
	I	395	475	443	710	672

Table H.12 Potential Function Stiffnesses for Centered URPP Cases

B. C.'s	Spec.	Stiffnesses (N/mm) for Points of Interest #1	#2	#3	#4	#5
CL – CL	A	936	1520	1440	4570	7230
	B	675	1060	1100	3000	7270
	C	1090	1700	1380	4700	3570
	D	774	1290	1140	4090	4890
	I	1020	1610	1330	4550	3670
SS – SS	A	379	455	425	681	644
	B	193	231	216	346	327
	C	552	663	619	992	938
	D	255	306	286	458	433
	I	416	500	467	748	707

Table H.13 Potential Function Stiffnesses for Uniform Pressure Cases

		Stiffnesses (N/mm) for Points of Interest				
B. C.'s	Spec.	#1	#2	#3	#4	#5
CL – CL	A	4680	7620	7210	22900	36200
	B	3460	5460	5640	15400	37300
	C	4430	6920	5620	19100	14500
	D	3800	6330	5610	20100	24000
	I	4240	6710	5550	19000	15300
SS – SS	A	887	1070	994	1590	1500
	B	451	542	506	810	766
	C	1290	1550	1450	2320	2190
	D	596	716	669	1070	1010
	I	974	1170	1090	1750	1660